

ULTIMATE LOAD ANALYSIS AND DESIGN
OF STIFFENED PLATES IN COMPRESSION

A thesis submitted for the degree of Doctor of Philosophy
in the Faculty of Engineering of the University
of London

by

S. Chatterjee, B.E., D.I.C., M.Sc., M.I.C.E., M.I.Struct.E.

Imperial College of Science and Technology
London

January 1978

ABSTRACT

The thesis begins with a review of the stability requirements in the Merrison Rules for stiffened plates in box girders, and identifies particular aspects that need further research. The rest of the thesis is devoted to theoretical and experimental investigations into the collapse behaviour of box girder compression flanges and to their design. The special features of the stiffened flange are identified, and several recently proposed design methods are critically examined for their treatment of these features. From the non-linear behaviour of its various components, an analysis model of the whole flange is assembled. The large-deflection plate theory is used to obtain the influence of initial imperfections and welding stresses on the behaviour of plate panels up to their collapse. The orthotropic response of the whole stiffened flange is quantified by extending the large-deflection theory to orthotropic plates. The effect of varying axial load due to bending moment gradient is derived from energy considerations of a Fourier Series deflected shape of stiffener. Eccentricity of axial loading, transverse loading and random patterns of imperfections in adjacent spans, are analysed from the moment-rotation compatibility of continuous beam-columns. Limitations to avoid premature torsional buckling of flat stiffeners are derived from plate theory, and extended to cover other types of stiffeners, flexural restraint from the flange plate, and a non-uniform stress distribution over the depth of the stiffeners.

A series of box girder tests at Imperial College is described and complete details are given for four tests related to failure of the compression flange. Good correlation is obtained between measured and predicted longitudinal welding stresses. Complete behaviour of the models and their critical components up to the ultimate load and the post-peak unloading characteristics are described and explained.

Using measured dimensions, properties, imperfections and residual stresses, the collapse loads of the boxes are calculated by the theory developed in this thesis, and are shown to compare

very satisfactorily with test observations. Further verification of the theory is provided by its application to thirty six tests on single-span stiffened panels of a wide range of geometries conducted at Manchester. Good correlation with regard to not only collapse loads, but also in-plane and out-of-plane deformations in these tests confirm the various hypotheses developed in this thesis.

Finally, simple rules are given for design of stiffened compression flanges, and compatible fabrication tolerances on imperfections of plates and stiffeners are also recommended. These design rules and tolerances have been adopted as the basis of the relevant clauses in the new British Standard Specifications for steel bridge design.

ACKNOWLEDGEMENTS

The investigations reported in this thesis were carried out under the supervision of Dr. P.J. Dowling. The author is deeply grateful for his advice and guidance throughout the study.

The experimental work was sponsored at Imperial College by the author's employers, the Department of Transport. The author is indebted to the Department of Transport for permission to undertake the subsequent theoretical investigations as part of his official duties.

Thanks are also due to:

Dr. P.A. Frieze, Dr. F.M. Moolani, Mr. J. Neale and other members of the Engineering Structures Laboratories for their co-operation and team effort in the experimental programme;

Mr. J.J. Lewkowicz (of D.Tp) and Miss Susan Webb (of Imperial College) for compiling the data in Table 2 of Chapter 11;

Mrs. Maxine Frieze and Mrs. Hazel Guile for their high standard of typing and drafting of the figures, respectively.

Finally, the author is most grateful to his wife Isabella, but for whose patience this work would never have been completed.

CONTENTS

| | Page No. |
|--|----------|
| ABSTRACT | 2 |
| ACKNOWLEDGEMENTS | 4 |
| NOTATION | 6 |
| CHAPTER 1 Background and a Review of the Stability Clauses in the Merrison Rules | 10 |
| CHAPTER 2 Box Girder Compression Flange - Introduction and Literature Survey | 28 |
| CHAPTER 3 Non-linear Behaviour of Stiffener Components | 51 |
| CHAPTER 4 Elastic Buckling Behaviour of Initially Flat Orthotropic Plates | 68 |
| CHAPTER 5 Buckling Behaviour of Initially Imperfect Plate Constrained to Remain Straight Along Longitudinal Edges | 89 |
| CHAPTER 6 Buckling Behaviour of Initially Imperfect Orthotropic Plate with Longitudinal Edges Free to Pull-in | 112 |
| CHAPTER 7 Effect of Bending Moment Gradient in Box Girder on Strength of Compression Flange | 120 |
| CHAPTER 8 Effect of Continuity on Strength of Flange Stiffeners | 133 |
| CHAPTER 9 Torsional Buckling of Stiffener Outstands | 146 |
| CHAPTER 10 Box Girder Tests for Behaviour of Stiffened Compression Flange | 177 |
| CHAPTER 11 Comparison of Experimental Observations with Theory | 201 |
| CHAPTER 12 Design Rules and Tolerances for Longitud- inal Stiffeners in Box Girder Compression Flange | 217 |
| CHAPTER 13 Conclusions | 231 |
| REFERENCES | 234 |
| FIGURES | 240 |

NOTATION

| | |
|-----------------------|---|
| a | - length of plate |
| a | - distance of shear centre of stiffener from connected edge |
| A | - area of cross-section |
| A | - amplitude of plate deflection |
| A_e, A_g | - effective and gross area of strut respectively |
| A_o, A_R | - amplitude of initial imperfection of stress-free and welded plates respectively |
| A_s | - area of stiffening rib; (A_{sx}, A_{sy} relate to ribs in $x-x$ and $y-y$ direction) |
| A_w | - area of weld |
| b | - width of plate or spacing of stiffener |
| b_1 | - width of flange of tee stiffener |
| B | - width of orthotropic plate |
| B | - width of compression flange between webs |
| c | - coefficient of weld shrinkage force |
| C_1, C_2, C_3 | - design coefficient for varying axial load |
| d | - depth of tee stiffener |
| D | - flexural rigidity of isotropic plate |
| D_x, D_y, D, D_{xy} | - bending rigidities of orthotropic plate |
| e | - strain |
| E | - Young's modulus |
| F | - Airy stress function |
| F | - effective eccentricity factor for continuous struts |
| F_1, F_2, F_3 | - coefficients for torsional buckling critical stress |
| G | - Coulomb's modulus |
| H | - twisting rigidity of orthotropic plate |
| I | - second moment of area |

| | |
|------------|---|
| I_e, I_g | - second moment of area of effective and gross section respectively |
| I_p | - polar moment of inertia |
| J_x, J_y | - St. Venants' torsion constant in $x-x$ and $y-y$ directions |
| K_s | - secant stiffness |
| K_{su} | - secant stiffness of plate at its ultimate load |
| K_t | - tangent stiffness |
| l | - half-wave length |
| L | - span of stiffener |
| m, n | - no. of half-waves of critical buckling |
| m | - magnification factor for initial imperfection |
| M | - bending moment |
| N | - no. of stiffeners |
| P | - axial load |
| P_e | - Euler critical load for struts |
| q | - distributed axial load per unit length |
| r | - radius of gyration |
| r | - residual stress parameter σ_R/σ_{ys} |
| r_e | - radius of gyration of effective section |
| R | - radius of curvature |
| S | - slenderness parameter of plate $\frac{b}{t} \sqrt{\frac{\sigma_{ys}}{E}}$ |
| t | - thickness of flange plate |
| t_e | - smeared thickness of flange $= t + \frac{NA_s}{B}$ |
| t_1, t_2 | - thickness of flange and web respectively of tee stiffener |
| T | - total potential energy |

| | |
|----------------------------|--|
| T_b | - potential energy of bending |
| u, v | - displacement in $x-x$ and $y-y$ directions respectively |
| u | - stability parameter $\frac{L}{2} \sqrt{\frac{P}{EI}}$ |
| U | - strain energy |
| U_b, U_m | - strain energy of bending and membrane forces respectively |
| w | - deflection of plate |
| w | - leg length of fillet weld |
| W | - warping constant |
| x, y | - co-ordinate directions |
| y_o, y_p | - initial and final deflections |
| z | - co-ordinate direction normal to plane of plate |
| Z | - section modulus |
| δ | - offset of stiffener centroid with respect to axial force |
| δ_o | - initial imperfection parameter $= \frac{A_o}{t}$ for flange plate $= \frac{A_o}{a} \sqrt{\frac{E}{\sigma_{ys}}}$ for flat outstand |
| δ_R | - imperfection parameter for welded flange plate = $\frac{A_R}{t}$ |
| Δ | - total stiffener eccentricity |
| Δ_p | - initial imperfection of plate |
| Δ_s | - initial imperfection of stiffener |
| Δ_{sx}, Δ_{sy} | - initial imperfection of stiffener perpendicular and parallel to plane of flange plate respectively |
| η | - ratio of width of yielded strip to thickness of welded plate |

| | |
|----------------------|---|
| η | - imperfection factor in Perry's strut equation = $\frac{\Delta sx}{r^2}$ times maximum fibre distance |
| θ | - slope of unloading curve in plate behaviour |
| θ | - slope of continuous beam-columns at support |
| λ_b | - factor against elastic critical buckling |
| ν | - Poisson's ratio |
| σ | - direct stress |
| σ_a | - applied stress or nominal stress |
| σ_{au} | - ultimate stress for plate in direct compression |
| σ_{cr} | - elastic critical stress |
| σ_{cr}^* | - elastic critical stress of orthotropic panel |
| σ_{eq} | - Hencky-Mises equivalent stress |
| σ_E | - Euler critical stress for struts |
| σ_R | - welding residual compressive stress |
| σ_{su} | - ultimate stress on strut |
| σ_x, σ_y | - stresses in $x-x$ and $y-y$ directions |
| σ_{ys} | - yield stress |
| τ | - shear stress |
| τ_a | - applied shear stress |
| τ_u | - ultimate stress in shear |
| τ_{ys} | - shear yield stress = $\sigma_{ys}/\sqrt{3}$ |
| ϕ | - aspect ratio |
| $\phi(u)$ | - stability function, $\frac{3}{u} \left[\frac{1}{\sin 2u} - \frac{1}{2u} \right]$ |
| $\Psi(u)$ | - stability function, $\frac{3}{2u} \left[\frac{1}{2u} - \frac{1}{\tan 2u} \right]$ |

CHAPTER 1

BACKGROUND AND A REVIEW OF THE STABILITY CLAUSES
IN THE MERRISON RULES

1. BACKGROUND

Following the collapses of three steel box girder bridges during construction (The Danube Bridge on 6 November, 1969, the Milford Haven Bridge on 2 June, 1970, and the West Gate Bridge on 15 October, 1970), the Merrison Committee of Enquiry was set up in December 1970 to investigate into the design and construction of such bridges. Another steel box girder bridge collapsed during these investigations, viz. the Koblenz Bridge on 10 November, 1971. This Committee produced an Interim Report^[1] in September 1971 and a Final Report^[2] in February 1973. These reports were accompanied by a very comprehensive set of rules^[3] for checking and designing steel box girder bridge construction. It was assumed in the development of these rules that initial geometrical imperfections and welding residual stresses have very significant influence on the unserviceability and collapse strength of stiffened plate construction. However, the Committee discovered that sufficient theoretical and experimental evidence did not exist at that time regarding the quantitative influence of these imperfections, particularly in regions of complex stress patterns; hence these rules had to be based on various assumptions and hypotheses. This Committee also initiated a comprehensive programme of experimental investigations involving collapse tests on stiffened panels, support diaphragms, quarter-scale models of box girders, and also two almost full-scale models of box girder bridges. The immediate objective of this programme was to validate or improve the various assumptions and hypotheses made in the design rules. The results of this extensive testing programme could not, however, be fully analysed in the time that was available before the final report of the Merrison Committee. Subsequently, a Working Group on Long-Term Research in Steel Box Girders was set up by the Department of Transport (then the Department of the Environment). The brief of this Working Group was to sponsor a further programme of theoretical and experimental research, including complete analysis of the results already available. The author was personally

associated with this Working Group, and on its behalf undertook an independent review of the stability clauses of the Merrison Rules as a first step towards identifying the most important areas for further research.

This review was completed in 1973 and its results are described in the following section of this chapter. Some of the observations may now appear out-of-date, as several gaps identified as then existing in the understanding of stiffened plate behaviour have since been covered by the extensive research in several institutions which followed from this review. In the subsequent stage the author had to perform the dual role of

- (i) sponsoring and managing research in various areas of stiffened plate construction in various institutions on behalf of the Working Group, and
- (ii) undertaking an in-depth investigation into the behaviour of stiffened compression flanges, which formed the subject of this thesis.

2. BASIC DESIGN CRITERIA USED IN THE MERRISON RULES

The Merrison Rules^[3] stipulate that the adequacy of the whole structure is to be checked by examining the adequacy of its component parts. These parts have been identified for this purpose as:

- (a) individual plate panels, i.e. areas of plate bounded by stiffeners or other stiff members capable of preventing out-of-plane movement of the plate panel edges,
- (b) stiffened panels, i.e. areas of stiffened plates bounded by diaphragms, cross-frames and/or other walls of the box, each capable of preventing out-of-plane movement of the stiffened panel edges.

The component parts are to be checked for the two limit states of unserviceability and collapse. The unserviceability limit state need not, however, be checked for stocky plate panels that are capable of developing their full squash strength as per the criteria given; otherwise, unserviceability is deemed to occur when, due to applied edge stresses and the presence of initial imperfections, yield stress is reached over a localised area.

3. PLATE PANELS

3.1 Plate Panels Subjected to Uniaxial Compression

3.1.1 *Calculation of unserviceability and collapse limit states -*

Unserviceability: The unserviceability criterion is calculated using a method based on the large-deflection theory of plates. The maximum surface stress occurring in the plate, which is assumed to have initial out-of-plane deformations in the critical buckling mode, is estimated using this approach. When this stress causes yield the limit of unserviceability is reached. Although the unserviceability limit state is not the controlling design criterion for all plate panels, (the collapse criterion for the plate panel and adequacy of the entire stiffened panel being usually more critical), large-deflection analysis is also involved in the calculation of collapse strength of the plate panel as explained in the next paragraph.

Collapse: The correct collapse strength of a plate panel can be assessed analytically only by large-deflection elasto-plastic analysis. Because tools for such analysis were not available to cover the range of initial geometric imperfections, welding residual stresses and various boundary conditions normally met in practice, the Merrison Rules resorted to the following formula:

$$\sigma_{eu} = \left[1 - \frac{\sigma_{ys}}{8\alpha\sigma_{ecr}} \right] \dots\dots (1)$$

where σ_{eu} = ultimate equivalent stress due to applied edge loading,

σ_{ys} = yield stress,

σ_{ecr} = elastic critical buckling value of σ_{eu} ,

$\alpha = \frac{\text{the value of } \sigma_{eu} \text{ causing local yielding in the plate}}{\sigma_{ys}}$

The value of the factor α above is obtained from graphs based on the results of elastic large-deflection analysis of plates, and hence is dependent on plate slenderness, imperfections, and boundary conditions.

This equation is very similar in form to the strut formula, given below, which was recommended by the American Column Research Council^[4] for hot-rolled wide-flange sections of low to medium slender-

ness ratio (L/r), for which it was shown that the effects of residual stress due to differential cooling were as important in considering column strength as those due to initial curvatures or accidental eccentricities. It would further appear to reflect the narrower margin observed between measured and calculated strengths for plates of intermediate slenderness than is the case for columns of intermediate slenderness. This it attempts to do by the use of the term 8α rather than 4 in the denominator. For comparison, the relevant column formula is:

$$\sigma_{su} = \sigma_{ys} \left[1 - \frac{\sigma_{ys}}{4\sigma_E} \right] \dots\dots (2)$$

The effects of welding residual stresses in the plate panel are allowed for in the Merrison Rules by:

- (a) adding the welding residual compressive stress to the applied stresses, or
- (b) assuming an increased out-of-flatness of the plate panel from the given equations.

The second alternative had been adopted in the Part II Design Rules, and has also been used later in this chapter. This empirical manner of dealing with welding residual stresses has not been quantitatively verified by any theoretical or experimental work.

3.1.2 *Validity of the empirical method for calculating panel collapse strength* - It can be seen from the above that the assessment of

the collapse strength of plate panels was empirically based. The research programme commissioned by the Merrison Committee did not include tests on individual plate panels. In this report test results obtained by Moxham^[5] on "exceedingly flat" plate panels with various magnitudes of welding residual stresses are compared with the results predicted by the use of the Merrison Rules, Part III, for ideally flat plates with the same magnitudes of welding residual stresses.

The unloaded longitudinal edges of the plate panel both in Moxham's tests and in the Merrison calculations have been taken as unrestrained against rotation and in-plane movement. The comparison, shown in Fig. 1, shows two important features:

- (a) For a typical value of $\eta = 3$ (ηt being the width of tensile yielded strips), the Merrison Rules under-estimate the ultimate strength of the plate panels by approximately 15 per cent,
- (b) Moxham's tests indicate a significant fall in ultimate strength with increase in welding residual stresses, whereas the results calculated using the Merrison Rules are relatively insensitive to the magnitude of welding residual stresses.
(This aspect will be examined in more detail in Section 3.1.3.)

No test results could be traced for plate panels with unloaded edges either restrained fully against in-plane movement, or constrained to remain straight though free to pull in. In the absence of test results, Merrison values may be compared with those obtained by other theoretical methods. Though theoretical results based on large-deflection elasto-plastic analysis are now available, it was found at that time that only Ractliffe's work was relevant. Ractliffe^[6] developed a theoretical method for plates with unloaded edges free to pull in but constrained to remain straight, allowing for initial out-of-flatness in the preferred buckling mode and also for welding residual stresses. Results theoretically obtained by Ractliffe have been compared with those predicted by the Merrison Rules, Part III, for initial out-of-flatness up to $b/1000$ in Fig. 2. It can be seen that,

- (a) Values predicted by the Merrison method are higher than those predicted by Ractliffe by approximately 20 - 30 per cent for out-of-flatness equal to $b/1000$; the comparable Merrison tolerance for out-of-flatness varies from approximately $b/320$ for 12 mm plate to $b/600$ for plates 25 mm thick and over;
- (b) Ractliffe's method indicates a fall in the strength of plate panels with increase in plate imperfection, whereas results from Merrison Rules are insensitive to plate out-of-flatness of this order.

Although it was not possible to come to any general conclusion from this limited study, it is worth noting that the Merrison empirical method does not predict the fall in strength due to increase in welding residual stresses that has been exhibited in the Moxham tests, and also the fall due to increased out-of-flatness and/or welding stresses

predicted by the theoretical methods developed by both Ractliffe^[6] and Moxham^[7]. For this reason, and also because there are important implications with regard to tolerances, it was considered essential to investigate the imperfection sensitivity of panel strength as given by the Merrison Rules.

3.1.3 *Imperfection sensitivity given by Merrison Rules* - Part III of the Merrison Rules has been used to assess the sensitivity of ultimate strengths and unserviceability limit loads for plate panels, the unloaded edges of which are (i) free to pull in, and (ii) constrained to remain straight. The results are shown in Figs 3 and 4. It can be noticed, that for plates with in-plane restraints on the edges, Fig. 3, the ultimate stress is not adversely affected by increase in the level of imperfections; in fact the strength seems to improve, though marginally, for slender plates beyond a critical b/t ratio; for unrestrained plates the fall in the ultimate stress is only marginal. The fall in the unserviceability limit loads, Fig. 4, is by comparison bigger for both boundary conditions, but for restrained panels there is in fact substantial improvement with bigger initial imperfections beyond the critical b/t ratio. *Thus it would seem that if the Merrison Rules are accepted as a valid basis for calculating the strength of plate panels, then so far as ultimate stress is concerned, strict limitations on out-of-flatness tolerances and the requirement to allow for welding residual stresses may be superfluous.*

The accuracy with which the attainment of first surface yield can be calculated by the method adopted in the Merrison Rules is very much open to question, particularly as the maximum stress is calculated on the assumption that the initial out-of-flatness is in the most critical buckling mode and also because of the empirical nature of the treatment of the welding residual stresses as described in Section 3.1.1. The relevance of such a criterion may also be questioned as, at the stage where first surface yield is reached no significant change in behaviour was discernible in much of the recent testing - certainly no visible damage necessitating major repair was seen to occur.

3.1.4 *Summary of study on compression plate panels* - This pilot investigation into the Merrison Design Rules for plates in uniaxial compression leads the author to the following important observations, viz.:

- (a) A main underlying presumption of the Merrison Rules is that initial geometric imperfections and welding residual stresses play a significant part in the strength of plate panels. Despite this, when the Merrison Rules, Part III, are applied to investigate the sensitivity of plate panel strengths to initial imperfections, the results seem to indicate that the strength of a panel in compression is practically insensitive to the variation in panel tolerances and residual stresses.
- (b) There were, however, experimental and other theoretical evidences, available at the time when the Merrison Rules were produced, to suggest that plate panel strength was more sensitive to imperfections than the Merrison Rules predict.
- (c) Unserviceability limit loads, as defined in the Merrison Rules, were found to be more significantly affected by plate panel imperfections.

3.2 Plate Panels in Pure Shear

3.2.1 *Calculation of unserviceability and collapse limit states* - In the Merrison Rules the collapse strength and the unserviceability limit load for plate panels in shear are calculated in much the same way as panels in compression. However, an empirical formula has been given for calculating the factor α in equation (1), and hence the maximum plate stress due to initial imperfections; this formula was derived from the results of a number of elastic large-deflection analyses^[8] of initially imperfect plates subject to various combinations of applied shear and longitudinal stresses.

The validity of the extension of the collapse strength formula referred to in Section 3.1.1 to plates subjected to shear is not obvious. Moreover, this empirical formula has been used to cover both plates with in-plane edge restraints and plates without such edge restraints, on the basis that the incorporation of the factor α (see Section 3.1.1) will account for the difference in strength of unrestrained and restrained panels. It is further postulated in Part III of the Rules that this calculated difference in strength constitutes the reserve of strength due to tension field action. (In the context of the Merrison Rules, full in-plane restraint is synonymous to edges constrained to remain straight.)

3.2.2 *Comparison of Merrison predicted tension field strength for fully restrained webs with that given by other theories* - To investigate this postulation the results for plates subjected to pure shear, as given by the Merrison Rules, have been compared with those given by other theories of tension field action in webs, viz. Rockey^{[9]*} et al. and Ostapenko^[10] et al.

Edge Restraints: In the Merrison approach and also in the tension field model suggested by Rockey^[9], the flexural stiffness of the horizontal boundary members on the top and bottom edges of the web plate panel provide the necessary in-plane restraint, whereas in the tension field model suggested by Ostapenko the in-plane restraint to the panel edges is assumed to be provided by the flexural stiffness of the vertical stiffeners. The flexural stiffness of the horizontal boundary members in the plane of the web therefore determines the degree of in-plane restraint and consequently the magnitude of diagonal tension in both the Merrison and the Rockey approach. But the flexural stiffness of neither vertical stiffeners nor horizontal boundary members play any part in the calculation of diagonal tension in the Ostapenko approach; presumably it was assumed in the latter that intermediate vertical stiffeners, with substantial width of web plates acting in conjunction, would invariably have almost infinite flexural stiffness in the plane of the web. The additional contribution of vierendeel frame action between flanges and vertical stiffeners has been ignored in this study when both the Rockey^[9] and the Ostapenko^[10] methods are used.

Fully Restrained Edges: In the Merrison and the Rockey approach, for box girders as opposed to plate girders, there still remains the uncertainty of exactly what constitutes the horizontal boundary member and what are the forces to which it is subjected. In order to eliminate this uncertainty from the scope of the present study, the webs are first considered to be "fully restrained" in their plane at the horizontal edges (without worrying at this stage about how this restraint is

* The Rockey theory referred to in this review is the earlier Rockey-Skaloud model of diagonal tension; the various discrepancies between this and the Ostapenko model identified in this review were largely removed in a unified diagonal tension model that has since been proposed by Rockey[11].

achieved), and secondly, to be completely unrestrained in their plane at the horizontal edges. The out-of-plane (i.e. flexural) restraint on the edges of the web is ignored in this study on all edges. For "fully restrained" webs, Fig. 5 gives the comparison between the values calculated by the Merrison and the Rockey methods. It can be seen that *the empirical method of the Merrison Rules under-estimates the ultimate shear capacities of fully restrained webs as given by the full tension field in the Rockey model*^[9] by 10 - 20 per cent throughout the common b/t and a/b ratios.

Unrestrained Edges: For webs completely unrestrained in plane along their horizontal edges, the Rockey model limits the ultimate strength to the elastic critical value, whereas the Merrison Rules, Part II, limit it to 80 per cent of the elastic critical value. Merrison Rules, Part III, however, allow the ultimate strength to be as high as the elastic critical value. The stated reason for limiting the ultimate strength to 80 per cent of the elastic critical value is to avoid the situation where both the local web panels and the overall stiffened webs reach their critical stresses simultaneously^[12]. Theoretical studies^[12] have indicated that in such cases the actual stresses in the stiffener increase very substantially when the applied loading approached the critical loading. However, the separation of local and overall buckling of a stiffened web can be achieved with more economical use of steel if the web plate is utilised to its full critical buckling strength and the stiffeners increased in size.

One other interesting feature of the study on webs unrestrained in their plane on longitudinal edges is that the Ostapenko model which does not depend on flexural stiffness of the horizontal boundary members still provides an alternative tension field mechanism to carry very significantly higher shear. Figures 6a and 6b show that the Merrison values are only 25 - 50 per cent of the Ostapenko values for b/t ratios in the region of 120 - 180.

3.2.3 *Sensitivity of ultimate shear strength to initial imperfections -*

The Merrison Rules stipulate tolerances on web panel initial out-of-flatness and also require the calculation of welding residual stresses in such panels. The Part II rules are only applicable when the welding residual compressive stresses are less than 10 per cent of the yield

stress. The sensitivity of plate strengths in pure shear as given by the Part III rules for various assumed values of initial imperfections and welding stresses are studied in this section. The results are shown in Figs 7 and 8. *Within the imperfection range stated no change in strength or unserviceability loads was observed for restrained panels, and a very small variation was found for the unserviceability limit load of unrestrained web panels for low b/t 's.*

These results support the frequently stated view that initial out-of-flatness or welding residual stresses do not affect shear carrying capacity of web panels. The various tension field theories take no account of these imperfections and are still reported to produce satisfactory estimates of ultimate shear strength. It has been observed in tests at Imperial College^[13] and at Cardiff^[11,9,14] that there was no significant variation in shear capacity of comparable panels despite the presence of different magnitudes of welding stresses and out-of-plane deformations. This can be attributed to the fact that initial geometric imperfections are highly unlikely to follow the preferred buckling mode in shear.

3.2.4 *Summary of study on shear plate panels* - The following points emerged from the pilot study of shear plate panels:

- (a) The Merrison Rules method for estimating the strength of plate panels in shear under-estimates the strength of a fully restrained panel compared to other tension field theories by as much as 20 per cent.
- (b) The Merrison Rules can be used to show that both the collapse and unserviceability limit state loads are almost insensitive to the level of initial out-of-plane deformations and residual stresses.

3.3 Plate Panels Subjected to Complex Patterns of Edge Stresses

3.3.1 *Calculation of collapse loads* - The previous sections of this review have referred to the problems of using an empirical formula for collapse strength for plates subjected to the simple stress pattern of uniaxial compression or pure shear. Though, at the time this review was undertaken, test data or theoretical work on the strength of plates subjected to complex or combined stress patterns, i.e. compression plus

shear, were not available for comparison with results calculated from the Merrison method, one can assume that the degree of uncertainty will be at least as much as, if not more than, that for the simple compression or shear case.

3.3.2 *Sensitivity of limit loads to imperfections* - Another difficulty is encountered in attempting to assess the effects of various levels of imperfections on the ultimate strength of these complex or combined stress cases. It has already been noted that, according to Moxham^[7] and Ractliffe^[6], strength of plates in pure compression are likely to be susceptible to initial imperfections, but test results^[13,14] indicate that plates in pure shear are not. Though Merrison rules governing tolerances are based on the assumption that all plate strengths are dependent on initial imperfections, calculations using Merrison rules rather surprisingly indicate a general insensitivity to levels of imperfection. Tension field theories of Rockey^[9] and Ostapenko^[10] have been extended to cover combined shear and bending stresses on webs without longitudinal stiffeners; and similar theoretical work is in progress for horizontally stiffened webs. But such theories cannot predict any sensitivity on initial imperfections of the strength of plate panels subject to these complex stresses. However, this review has subsequently led to the development of powerful elasto-plastic large-deflection computer programs^[15,16], which have since been used to study this problem.

4. STIFFENED PANELS

4.1 Stiffened Compression Flanges

4.1.1 *Calculation of limit state loads* - The method for checking the adequacy of stiffened panels in the Merrison Rules is based on a consideration of the individual stiffeners and associated widths of flange plate. The formulae given in Part III for calculating maximum stresses are derived from the well-known strut formula:

$$\text{Max. stress in the strut} = \frac{P}{A} + \frac{P \Delta_{sx}}{Z} \frac{P_{cr}}{P_{cr} - P} \quad \dots \quad (3)$$

where P = axial load at ends

P_{cr} = elastic critical load

A = area

Z = section modulus

Δ_{sx} = initial imperfection and/or end eccentricity.

The ratio $\frac{P_{cr}}{P_{cr}-P}$, which can also be expressed as $\frac{\lambda_b}{\lambda_b-1}$ (when λ_b is the factor by which the applied stresses must be increased to cause elastic critical buckling), is to be calculated for:

- (a) the whole orthotropic stiffened panel containing the stiffener, when the stiffening system and the loading pattern is fairly regular (e.g. flanges), taking into account coexistent shear, transverse compression, etc., or
- (b) the individual stiffener, but taking into account the destabilising effects of shear or transverse compression on the flange plate, when the stiffening system or the loading pattern is irregular, e.g. in diaphragms.

Failure Criteria: The resultant stress in the stiffener outstand is limited to either the yield stress or two-thirds of the elastic critical torsional buckling stress of the outstand. The resultant mean stress in the flange plate is limited to that value that would cause *onset of surface yield in the plate panel*, as obtained from graphs based on large-deflection analysis of initially imperfect flange plate panels. These graphs are based on the same elastic large-deflection analysis of plates that were used for obtaining the α -values referred to in the preceding sections. The reason for not going beyond the stage of first surface yield in flange plate initiated failure is that the load-end deformation behaviour of plate panels in the post-elastic range had not at that time been established for the various combinations of geometric imperfections, welding residual stresses and boundary conditions met in actual practice.

4.1.2 *A study of the Merrison failure criterion for flange initiated failure* - It would appear to be quite justified to limit the strength of the stiffener in the case of outstand initiated failure to the value corresponding to attainment of yield stress on the stiffener outstand, as the flexural stiffness of the whole stiffener will fall very sharply in the post-elastic range. A similar failure criterion has been used successfully for the collapse of columns for many years, viz. the Perry-Robertson approach. However, the use of the first sur-

face yield criteria for flange initiated failure, when the stresses deemed to cause surface yield include the local stresses due to bending of the plate panel caused by panel out-of-plane movement, seems questionable. With the onset of surface yield on the flange plate, the tangent stiffness (i.e. slope of the load-end deformation behaviour) of the flange plate panel, and so the flexural stiffness of the stiffened section as a whole, should not fall dramatically. With respect to the flange panel alone, the margin between the load that causes first surface yielding and that causing collapse of the flange panel may be quite substantial in the higher b/t range. *In the Merrison approach for flange initiated failure for stiffeners this margin is ignored.*

To calculate the reserve capacity left in the plate in the post-elastic range, a knowledge of the post-elastic load-end shortening behaviour of the plate is essential. Theoretical work done by Moxham^[7] in this field is not strictly applicable to this particular problem, as Moxham analysed only plates with unloaded edges free to pull in - whereas in stiffened flanges having several longitudinal stiffeners, in-plane restraint is a more appropriate boundary condition for the panels between the stiffeners. However, computer programs for elasto-plastic analysis of plate panels have been developed recently at the Transport and Road Research Laboratory, Crowthorne^[15], and also at Imperial College^[16,17], which can provide the necessary information. Before these data were available a preliminary study was made, based primarily on an extension of the method currently contained within the Merrison Rules. The following is an outline of the method adopted for this study:

Method Used to Calculate Capacity Beyond First Yield: Using the Merrison Rules for stiffeners, the value of the axial load, and the total mean plate stress (i.e. applied stress and flexural stress due to stiffener buckling) have been calculated for the first onset of yield in the plate, signifying the end of the elastic phase. Beyond this stage hypothetical load-end shortening graphs for the plate panel of the type shown in Fig. 9 have been used. The stress range for this elasto-plastic phase has been taken as the difference between the collapse strength of the plate panel as given by the Merrison Rules for plate panels (taking account of the initial imperfections in the pres-

cribed manner) and the total mean plate stress at the end of the elastic phase. Different values of the total end shortening - from the end of the elastic phase to the peak collapse stress - have been tried, as shown by the three curves, by taking different values of the index Ψ in the equation given in Fig. 9. The steep curve given by $\Psi = 1.25$ is intended to represent a 'brittle' type of plate behaviour, likely to be typical for plates with low residual stresses and of slenderness ratio in the region of $\sqrt{\frac{E}{\sigma_{ys}}}$; the curve given by $\Psi = 3$ represents a 'ductile' type of plate behaviour, possibly with a gradual reduction in the load carried after the peak load has been reached; and the curve given by $\Psi = 6$ represents a very stable type of load-end deformation behaviour with a wide flat plateau. An incremental type of analysis was adopted. The reduced plate effectiveness, given by the slope of the assumed load-deformation graphs, was calculated at certain intervals of the total mean plate stress; the actual applied mean longitudinal stress at the ends of the stiffener that would produce this particular total mean plate stress was calculated by successive approximation, making allowance for the reduced stiffener properties when calculating the flexural stresses.

Results of Pilot Study: Figure 10 shows the variation in stiffener collapse stress in a particular stiffener design (plate $b/t = 40$) due to the different assumed post-elastic load-end shortening graphs. It can be noticed that in each case the maximum stiffener stress σ_{su} was reached before the calculated plate collapse stress of 295 N/mm^2 was reached in the plate; this is due to the accelerated reduction in stiffener inertia caused by the reduced plate effectiveness K_t . It can be noted that the 'brittle' type of load-deformation behaviour ($\Psi = 1.25$, see also Fig. 9) enables a higher stiffener stress σ_{su} to be reached, because the plate stiffness K_t is maintained at higher values for most of the elasto-plastic phase; but after the maximum stiffener load σ_{su} is reached, the fall in the load is more drastic with such 'brittle' plate behaviour. In this example the maximum stiffener applied stress achieved is 8 per cent higher with $\Psi = 1.25$, and 1½ per cent lower with $\Psi = 6$, compared with the value obtained for $\Psi = 3$. This difference is not considered quantitatively significant, and hence for the rest of the exercise the load-deformation

graph given by $\Psi = 3$ was used. The purpose of this preliminary exercise was to indicate the salient features that govern the behaviour of the stiffener in the post-elastic phase of the flange response.

4.1.3 *Sensitivity of stiffener strength to plate imperfections* - A previous study by Edwards^[18] indicated that according to the Merrison Rules, stiffener strengths are very sensitive to flange plate out-of-flatness. (This would follow from conclusion (c), Section 3.1.4, and the failure criteria discussed in Section 4.1.1.) In this section a number of stiffener designs of various combinations of plate panel slenderness, ratio of stiffener to plate area and stiffener slenderness are examined. This study covered the behaviour up to the elastic limit in accordance with the Merrison Rules, and was extended into the post-elastic phase of the flange panel in accordance with the method outlined in Section 4.1.2. The results of this examination are seen in Figs 11a to 11d to confirm Edward's findings. However, it was felt that *this sensitivity of stiffener behaviour to flange panel out-of-plane deformations and welding residual stresses, would be less pronounced if the post-elastic behaviour of the flange plate panel were taken into account in the assessment of stiffener strength. The graphs in Figs 11a to 11d confirm this conjecture.*

4.1.4 *Outstand initiated failures* - For outstand initiated failure of stiffeners the sensitivity of stiffener strength to welding residual stress can be estimated using an exact column analysis of the type used in the Imperial College^[19] and Cambridge^[20] studies of stiffened flanges. The likely nature and magnitude of the residual stress at the tip of the outstand due to welding are still not fully understood. If this stress is tensile, which may be the case in some situations due to the eccentricity of the weld position with respect to the effective stiffener cross-section, then residual stress may in fact increase the stiffener strength! On the other hand, compressive residual stresses will reduce the capacity of the flange in outstand initiated collapse.

4.2 Stiffened Webs

No systematic examination of the design of such elements was made within this study. However, the following observations on the existing rules may be made.

At the time of this review little was known about the large-deflection behaviour of stiffened web systems subjected to shear and longitudinal stresses. Very recently some theoretical work^[21] has become available, and some experimental work is also now in progress in Cardiff. The treatment of longitudinal web stiffeners in the Merrison Rules is basically similar to that of the compression flange longitudinal stiffeners, and hence the comments made on the latter in the earlier section also apply. For the vertical web stiffeners, the Merrison Rules specify that they must be designed for axial compression caused by any assumed tension field action in the web panels. This stipulation is considered to be satisfactory in principle. But the fact that only 32 times the web thickness is allowed to act in conjunction with the stiffeners, whereas the compressive forces in the stiffener arise from a wider tension field in the web, leads to very heavy vertical stiffeners, when these are placed on only one side of the web. The only practical way to cope with the prescribed eccentricity of this loading on the assumed strut section is to provide stiffening area as near to the plane of the web as possible, viz. an angle section turned the "wrong" way round, with one leg attached to the plate (as used to be the practice in rivetted construction). This problem appeared to demand further investigation. As a result of these observations, further studies were subsequently commissioned to investigate into the behaviour of vertical web stiffeners.

5. CONCLUSIONS OF STUDY ON MERRISON RULES

- (1) Although the requirements for estimating welding residual stresses and for the construction tolerances on plate panels in the workmanship clauses of the Merrison Rules presuppose that initial imperfections affect the strength of plate panels significantly, application of the rules governing panel strength suggest that plate panel strengths are almost insensitive to imperfections.
- (2) There are both theoretical and experimental evidences to suggest that plate panel strength in compression is more sensitive to initial imperfection of welding residual stresses and out-of-flatness than the Merrison Rules indicate.

- (3) The limit of unserviceability, when defined as the attainment of first surface yield is, however, relatively sensitive to the level of imperfections in a plate panel subjected to compression.
- (4) As the failure criterion used for the collapse of stiffened panels in compression is the attainment of first surface yield, it follows from conclusion (3) that the collapse of compression flanges due to plate initiated failure is also sensitive to plate panel imperfections.
- (5) The results of this study suggest that the present out-of-plane tolerances required by the Merrison Rules are needed almost entirely to satisfy the restrictions implied by defining unserviceability as the attainment of first surface yield in the case of plate panels and using a collapse criteria for stiffened flanges which is too conservative.
- (6) A procedure which extends the Merrison elastic column approach for stiffened compression panels beyond the range where first surface yield in the plate panel occurs, shows that the existing design method is conservative (by as much as 13 per cent with slender plate panels), and that furthermore, it exaggerates the sensitivity of stiffened flange collapse to plate panel imperfections.
- (7) The arguments used for the retainment of the definition of unserviceability quoted above, are that it represents the maximum degree to which current knowledge can be reliably extended. However, it is highly doubtful if the current procedures used to predict surface yield could be accurate in view of the degree of empiricism introduced in the method, i.e. it is doubtful if the calculated unserviceability loads bear any relation to the actual loads causing first surface yield. Moreover, the attainment of first surface yield in a plate has little obvious effect on the overall behaviour of the plate panel.
- (8) There is a definite need to improve the design procedure for stiffened compression flanges as the failure criteria used for plate initiated failure is clearly too conservative in many cases.

- (9) The existing rules can be used to show that both the unserviceability and collapse limit states for web plate panels are insensitive to plate panel imperfections.
- (10) The strength of fully restrained shear web panels as predicted by the Merrison Rules are significantly less (up to 80 per cent) than those predicted by tension field theories.
- (11) For unrestrained web panels under shear, the Ostapenko tension field model predicts a substantially higher shear capacity than the Merrison Rules.

6. FURTHER RESEARCH

The above review of the stability clauses of the Merrison Rules established the need for further research in the behaviour of both stiffened compression flanges and stiffened webs of box girders. However, it was felt that priority should be given to the compression flange, rather than the web, as a larger proportion of the total material requirement is used here.

The main part of the research carried out by the author and reported in this thesis was thus devoted to the behaviour of stiffened compression flanges of box girders.

CHAPTER 2

BOX GIRDER COMPRESSION FLANGES
INTRODUCTION AND LITERATURE SURVEY

1. GENERAL

This chapter reviews most of the methods recently developed for the design of box girder compression flanges. Because of the wide scope of some of these approaches it has not been possible to include all the necessary design formulae here; instead, this chapter concentrates on the basic principles underlying each of the methods and discusses their scope and limitations. All of the methods attempt to determine the ultimate load carrying capacities of compression flanges, even though in many cases the basic theory on which they are founded is non-linear elastic theory.

1.1 Flange Layout

Compression flanges of stiffened steel box girders are usually comprised of a steel flange plate stiffened longitudinally by either open (i.e. flat, bulb-flat, tee or angle), or closed (i.e. trough, vee) stiffeners spanning between transverse frames. In small or medium span bridges, the top flange is often covered with structural reinforced concrete decking which, after hardening, acts compositely with the steel flange through shear connectors. Typical details of a box girder compression flange are illustrated in Fig. 12.

1.2 Stress Systems

Such compression flanges may be subjected to the stress systems described below and shown in Fig. 13:

- (a) Longitudinal stresses associated with overall bending moment and axial force on the box girder caused by applied vertical and horizontal loading; these stresses may vary across the width of the box girder due to shear lag, and also along the length of the flange following the gradient of the bending moment diagram; additional longitudinal stresses may be caused by restrained warping of the box girder.

- (b) In-plane shear stresses in the flange plate; these may be due partly to the applied torsion on the box girder, and partly to the vertical and horizontal shear force associated with the overall bending moment gradients.
- (c) Top flange bending stresses caused by locally applied wheel loading; these stresses are the cumulative stresses due to local plate bending and flexure of the longitudinal and transverse stiffeners.
- (d) Other in-plane transverse stresses in the flange plate may be caused by distortion of the box cross-section due to asymmetrical loading, or in-plane bending of diaphragms in the vicinity of piers or abutments.

2. SPECIAL PROBLEMS FOR ANALYSIS AND DESIGN

A stiffened compression flange is often idealised as a series of disconnected pin-ended struts spanning between transverse frames and subjected to combined axial and transverse loads. This simple idealisation may not adequately cope with the following complications:

- (a) The stiffened cross-section is unsymmetrical about the horizontal centroidal plane - the centroid usually being considerably nearer the flange plate than the stiffener tip. For a given out-of-plane deflection the compressive flexural stress will be much higher when the deflection is towards the plate rather than towards the stiffener. For stiffeners with high slenderness ratio L/r , failure may be initiated by tensile yielding at the outstand tip rather than by the maximum compressive stress. Hence not only the magnitude of the deflection, but also its direction is important in determining the ultimate load of the strut.
- (b) Stiffeners are normally continuous over transverse frames. Though continuity generally tends to improve the behaviour of the stiffeners, in some cases there may be weakening effects, e.g. an inward deflection produces hogging moment over the transverse supports and because of (a) above the compressive stresses produced in this region may be higher than those at midspan.

- (c) Adjacent stiffeners are connected in real flanges and do, therefore, interact. Transverse continuity between stiffeners has a restraining effect on the deflections of heavily loaded individual stiffeners; the entire flange between the box girder webs will act as an orthotropic plate supported on its longitudinal edges by the webs and transversely by the intermediate cross-frames provided they are adequately stiff.
- (d) In the region of significant gradient in the overall bending moment the axial loading on the stiffeners will vary along their length; the magnitude of this variation may be significant even within one span between the transverse frames.
- (e) Because of the overall curvature of the box girder in the vertical plane the axial load will tend to act eccentrically with respect to the centroid of the stiffener section, i.e. higher applied stresses on the flange plate than at the stiffener tip.
- (f) In-plane shear stresses τ and transverse stresses σ_y which are present in the flange plate and discussed in Section 1.2(b) and (d), may reduce the load at which first yield occurs in the flange plate, and also reduce the resistance of the flange to longitudinal destabilising forces.
- (g) There are four independent buckling modes associated with stiffened compression flanges of normal layout, viz.,
- (i) local buckling of the flange plate panels between the longitudinal stiffeners;
 - (ii) local buckling of the outstand of an open stiffener or of the walls of a closed stiffener;
 - (iii) buckling of the longitudinally stiffened plate between transverse frames;
 - (iv) overall buckling of the orthogonally stiffened flange between the girder webs.

The possibility of the fourth mode occurring is often eliminated by designing the transverse frames to be sufficiently stiff to act as non-deflecting supports.

Any two or all of the above buckling modes may interact with each other.

- (h) For flanges of normal proportions the elastic critical buckling loads for each of the above modes are usually much higher than the highest factored design loads; very often they are also higher than the squash loads, i.e. loads required to produce uniform yield stress in an ideally perfect structure. However, structures invariably have initial geometrical imperfections, and when these imperfections have a significant component in any one or more of the above buckling modes the behaviour of the structure will be influenced by the level of the initial geometric imperfections right from the onset of loading. The stiffness of the structure will gradually reduce with increasing applied load until the maximum load is attained when the stiffness reduces to zero.
- (i) Locked up residual stresses present in the structure may produce early yielding in certain regions and consequently an acceleration in loss of stiffness. Since the compression flange is primarily subjected to compressive applied stresses, which are superimposed over the residual stresses, both the magnitude and the distribution of *compressive* residual stresses are important. While the nature and the level of residual stresses caused by handling, fabrication and transportation are not clearly understood, some data are available for residual stresses caused by rolling and welding processes.

3. RECENT DEVELOPMENTS

Several accidents during construction of steel box girder bridges in the last six years have led to a considerable amount of experimental and theoretical research into the behaviour of stiffened steel box girders, and as a result several methods are now available for the analysis and design of the stiffened compression flanges. A brief description will be given here of the following published methods, followed by a discussion on the main features of each method. Finally, the scope of the methods with regard to the various problems referred to in Section 2 is summarised in Table 1.

4. MERRISON RULES [3]

4.1 Description

In this method, plate panels between the stiffening ribs are assumed to have initial geometrical imperfections Δ_p (i.e. out-of-flatness) in the elastic critical buckling mode. The magnitude of the assumed imperfections for analysis is related to the specified fabrication tolerances, but account has been taken of the unlikelihood of all adjacent plate panels having equal and alternately up and down imperfections at a particular cross-section. The longitudinal stiffeners (composed of the stiffening ribs and an effective width of the flange plate) are also assumed to have initial out-of-straightness Δ_{sx} in the elastic critical buckling mode, i.e. a sinusoidal pattern alternating in direction in adjacent spans.

An approximate elastic analysis of the non-linear behaviour of an initially imperfect plate panel subjected to longitudinal compression has been used to produce the following:

- (i) the ratio of average stress to edge stress called the secant stiffness K_s ;
- (ii) the ratio of incremental average stress to incremental edge stress called the tangent stiffness K_t ; and
- (iii) the level of edge stress σ_{BL} in the initially imperfect plate that produces yielding on the surface of the plate.

The secant stiffness K_s is used to calculate the associated plate width of the stiffener for all purposes except as mentioned later. For this analysis of the plate panel, the internal longitudinal edges of all panels have been assumed to remain straight but free to pull in, but the longitudinal edge of an outer panel adjacent to the girder web has been assumed to be free to pull in without any restriction.

Individual stiffeners are analysed as a single span strut, with the initial stiffener imperfection Δ_{sx} assumed to be magnified under an applied stress σ_a to a value

$$\Delta_{sx} \frac{\sigma_{cr}^*}{\sigma_{cr}^* - \sigma_a} ,$$

where σ_{cr}^* is the elastic critical buckling stress of an *orthotropic plate* bounded by the girder webs and the transverse stiffeners. In calculating σ_{cr}^* the gradually reducing longitudinal stiffness of the associated plate panel is taken into account by using the tangent stiffness K_t in calculating the effective width of the flange plate. The reason for using K_t , instead of K_s , is that the instantaneous flexural stiffness of the orthotropic plate, valid for the particular level of applied stresses, was considered more appropriate for calculating the magnified deflection of the strut. Since the orthotropic plate σ_{cr}^* is always higher than the isolated strut critical stress the method does, therefore, recognise some of the beneficial effects of plate continuity.

The effect of coincident in-plane shear stress τ and transverse stress σ_y in the flange plate is accounted for by using a reduced elastic critical stress for the individual plate panels when calculating K_s , K_t and σ_{BL} , and in addition a reduced effective yield stress calculated from the Mises-Hencky yield criterion has been used. The stiffened flange critical stress, σ_{cr}^* , is also reduced to allow for the destabilising effects of these stresses.

Formulae are given for calculating longitudinal residual compressive stresses in the flange caused by welding the stiffeners and the girder webs to the flange plate. These stresses are added to the stresses due to applied loading. However, when checking the local strength of the flange plate these residual stresses may be neglected, or a reduced value taken, if the width-thickness ratio of the flange plate between stiffeners is less than 20, or between 20 - 40 respectively. This is intended to reflect the diminishing influence of residual stress on the local strength of plate panels as they become more stocky.

The total stresses occurring in the mid-plane of the flange plate and the outstand tip due to the combined effects of applied stress σ_a , welding compressive stresses, flexure of the flange both due to magnification of the initial imperfection and initial eccentricity of flange loading due to overall curvature of the whole girder, are respectively limited to the following:

- (i) σ_{BL} , i.e. the average stress in the effective flange plate that produces yielding on the surface.
- (ii) Yield stress, or two-thirds of the elastic critical torsional buckling stress, calculated for a combined half wave length of buckling of the open-type stiffener outstand and the plate panel between stiffeners.

The above theory has been used to produce tables of coefficients and graphs, from which the limiting applied stress σ_{su} for any stiffened panel geometry and stress pattern can be obtained directly.

It is assumed that shear lag effects and secondary stresses due to restrained warping, etc. can be ignored in the calculation of ultimate strength, owing to the likely plastic redistribution of longitudinal stresses, except when torsional buckling of the outstand is critical. In checking the unserviceability limit state (which has been taken to occur with the spread of yielding over an area of sides equal to 5 times the plate thickness), due account must be taken of shear lag and secondary stresses. (Different load and material factors have been specified for the ultimate and the unserviceability limit states.)

When the applied longitudinal stresses vary along the length of the flange, the maximum value within the middle-third has to be used as the average stress for checking the stiffener as a strut, and the end at which the maximum stress occurs also has to be checked to ensure that local buckling or yielding does not limit the flange strength. An empirical formula discussed in Section 3, Chapter 1, has been used to obtain the local buckling strength of plate panels.

For locally applied wheel loading, flexural stresses calculated for this loading only are magnified by a factor $\frac{\sigma_{cr}^*}{\sigma_{cr}^* - \sigma_a}$ and superimposed on the stresses due to longitudinal loading.

For ultimate strength calculations it is permissible to redistribute the applied longitudinal stress over the width of the flange in such a manner that the stiffener subjected to high local bending moment carries less or no longitudinal stress.

4.2 Discussion

- (a) The Merrison Rules cover all the special features of stiffened compression flanges discussed in Section 2; indeed, most of these features were first identified and defined in the earlier version of the Merrison appraisal rules^[54]. As has already been noted in Chapter 1, Section 4.1.2, the main defect of the rules relating to the design of stiffened flanges is the criterion chosen for flange plate initiated failure of a stiffened plate. Failure is assumed to occur when the surface of the plate panel yields as predicted by an approximate elastic large-deflection analysis of initially imperfect plates. The stated reason for not going beyond the stage of surface yield was that the behaviour of plates in the post-elastic range had not been fully established at the time the rules were formulated. Recent large-deflection elasto-plastic studies show that there is no sudden fall-off in stiffnesses K_s or K_t on reaching surface yield; rapid deterioration in stiffness only occurs after yield is reached on the longitudinal edges. These studies show that the margin between the load causing surface yield and the load causing yield on the edges may be substantial.
- (b) This method involves the use of both the secant and the tangent effective width factors K_s and K_t of the flange plate panels. In Chapter 3 the theoretical justification for the use of both of these factors will be examined in the light of a non-linear analysis from the first principles of an initially imperfect strut made up of materials having non-linear stress-strain response.
- (c) Another shortcoming of the Merrison Rules is their complexity for design office use. Even the simplified version of the Rules given in Part II and related to specific fabrication tolerances of Part IV, also involves the use of several tables and graphs, for a particular check.

5. LIEGE METHOD

5.1 Description

This method^[22] takes account of initial geometrical imperfections and of large deformations. The non-linearity of the material is considered by using a collapse criterion, which extends fictitiously the elastic range. Extensional and flexural rigidities, including shear rigidity and out-of-plane torsional rigidity are considered. Effects of stiffener eccentricities with respect to the mid-plane of the flange sheet are accounted for by modifying the flexural rigidities. The design is carried out in two steps.

In the first step, the rigidities are uniformly spread to obtain a substitute orthotropic plate, bounded by the webs and the transverse frames, the latter being sufficiently rigid to constitute nodal lines for buckling. This orthotropic plate is assumed to have a sinusoidal pattern of initial geometrical imperfections in both directions. The edges are all assumed to be simply supported and, in addition, the loaded ones are assumed to be deformed uniformly whilst the unloaded edges adjacent to the webs are assumed to be free to pull in.

The generalised non-linear (large-deflection) equations for orthotropic plates are solved and lead to a magnification of the initial imperfections due to applied longitudinal compression load and to a non-uniform distribution of longitudinal stresses on the loaded edges, with a maximum membrane stress at the edges adjacent to the webs. The ultimate strength of the orthotropic plate is assumed to be reached when the mean membrane longitudinal stress along the unloaded edges is equal to the yield stress σ_{ys} ; this constitutes the collapse criterion. It is then possible to define an efficiency of the substitute orthotropic plate as the ratio:

$$\rho_t = \frac{\text{mean longitudinal stress over the loaded edge}}{\text{mean stress along the longitudinal edge } (\sigma_{ys} \text{ at collapse)}}$$

In the second step, allowance is made for the discontinuous character of the stiffening which is reflected by a loss of efficiency of the isotropic plate of breadth b between longitudinal stiffeners. For this purpose, use is made of the following effective width factor, proposed originally by Winter^[23] for thin walls of light-gauge cold-

formed members (see equation (4), Section 7), and later slightly modified by Faulkner^[24] to provide the best fit to experimental results on welded stiffened plates:

$$\frac{b_e}{b} = \frac{2t}{b} \sqrt{\frac{E}{\sigma_e}} - \frac{t^2 E}{b^2 \sigma_e} \leq 1 \quad \dots \quad (1)$$

where b_e is the effective width

E the Young's modulus

t the thickness of the isotropic plate

σ_e the maximum stress at the edge of the plate panel.

In the above formula, σ_e is taken as the already calculated value of $\rho_t \sigma_{ys}$ which represents a mean stress, and is the same for all the panels. Finally, the partial efficiency is calculated as:

$$\rho' = \frac{b_e t + A_s}{b t + A_s}$$

A_s being the area of one longitudinal stiffener.

The global efficiency is given by the product of the two above efficiencies:

$$\rho = \rho_t \rho'$$

and thus, the ultimate average stress of the whole flange is given by:

$$\sigma_{su} = \rho \sigma_{ys}$$

In fact, there is a progressive loss of efficiency of the plate between the panels with increase in loading, so that, to be rigorous, an incremental procedure would be needed. A computer program has been developed to increment loading and to substitute for Faulkner's formula, more theoretically exact values taking account of initial imperfections of the plate panels and residual stresses and considering, for the evaluation of the partial efficiency, all the panels separately with their own stress distribution. Numerical simulation shows, however, that the use of Faulkner's formula is justified for current values of imperfections and residual stresses and

that there is close agreement between values of the global efficiency obtained by the direct or by the incremental procedure.

The value of the average ultimate stress is meaningful only if the ultimate strength of the webs is not reached before that of the compressed flange and the flange stiffeners do not collapse prematurely by local instability.

5.2 Discussion

- (a) This is the first method to deal with the orthotropic behaviour of the entire stiffened flange panel in a comprehensive manner, and is particularly suitable for flanges where orthotropic behaviour is dominant, viz., stiffeners with high slenderness ratio.
- (b) In the compression flange of practical box girder construction, longitudinal stiffeners usually have low to medium slenderness ratio between the transverse frames - in order to make an efficient use of the steel material. In such construction orthotropic behaviour of the whole flange contributes very little to the strength of the flange and hence this design method is unsuitable.
- (c) The only failure criteria used is a limit on the average mid-plane longitudinal stress along the edges to the yield stress; the possibility of failure by outstand yielding or buckling is ignored. Neither the combined effect of the mid-plane stresses and additional flexural stresses in the stiffeners due to further deflections is considered.
- (d) In this method no recognition is made of the nature of the initial stiffener imperfections and the mode of buckling, i.e. whether the imperfections/buckling mode is inwards, i.e. producing additional compression in the flange plate, or outwards, producing additional compression in the stiffener outstand. It has been found experimentally^[13] that the direction of the stiffener imperfections has a significant influence on the buckling behaviour of stiffened compression flanges.
- (e) In the direct method orthotropic plate stiffnesses are calculated for the total plate and stiffener cross-section. No

allowance is made, therefore, for reduction in plate width for slender plate panels. However, any effective width that might be adopted at this stage of calculation could only be a first guess, as the stresses in the plate are not known. These guessed effective widths would then have to be verified after the stresses are known.

- (f) The formula relating the mean edge stress of the orthotropic flange to the magnification factor of the initial imperfection is an equation involving the third power of the magnification factor. Hence solution of this equation in the absence of charts or tables is time-consuming in design.

6. CAMBRIDGE METHOD

6.1 Description

In this method [25] individual stiffeners are checked as isolated struts. A modified version of the Perry formula given below has been used to represent the proposed European column curves:-

$$(\sigma_{ys} - \sigma_{su}) (\sigma_E - \sigma_{su}) = \eta \sigma_E \sigma_{su} \quad \dots \quad (2)$$

where σ_{ys} = yield stress

σ_E = Euler stress

σ_{su} = collapse stress of strut

η = an imperfection parameter $\frac{y \Delta_{sx}}{r^2}$, when y is the maximum fibre distance.

Dwight recommended the following formula for η :

$$\eta = 0 \text{ when } \frac{L}{r} \leq \frac{\pi}{5} \sqrt{\frac{E}{\sigma_{ys}}} \quad \dots \quad (3)$$

$$= \alpha \left[\frac{L}{r} - \frac{\pi}{5} \sqrt{\frac{E}{\sigma_{ys}}} \right] \text{ when } \frac{L}{r} > \frac{\pi}{5} \sqrt{\frac{E}{\sigma_{ys}}}$$

Curves generated by using the following α -values correspond to the European column curves applicable to the particular types of struts described below:

$\alpha = .0020$ for hollow sections and universal beams bending about major axis

$\alpha = .0035$ for universal beams bending about minor axis and universal columns bending about major axis

$\alpha = .0055$ for universal columns bending about minor axis.

In addition, $\alpha = .0015$ has been proposed specifically for use with stiffened plating.

Stiffeners have to be checked for buckling in two different modes, i.e. inward failure of the stiffener between transverse frames, with collapse occurring when the stress in the plate panel reaches a limiting value for local buckling, and outward column failure triggered by compressive yield at the tip of the outstand. In the former mode, σ_{ys} in the above equation is replaced by σ_{au} , the local plate buckling stress; whereas, in the latter mode σ_{ys} = yield stress of the outstand. The plate strength σ_{au} has been derived partly from tests and partly from the elasto-plastic large-deflection analysis developed by Moxham. Two sets of plate strengths have been given, one for plates with continuously welded stiffeners and the other for plates with intermittently welded stiffeners. The appropriate set of column curves to be used for the strut check depends primarily upon a cross-sectional parameter, viz. the ratio of maximum fibre distance to the radius of gyration of strut section; the value of α that defines the column curve is higher for higher values of this ratio. The effect of shear is allowed for by assuming a reduced effective yield stress when obtaining σ_{au} . Orthotropic action of the entire flange between the webs and the transverse stiffeners is catered for assuming a slightly reduced effective length of the strut in using the column curves. Torsional buckling of the outstand is prevented by limiting the geometrical proportions of the cross-section; but these limits have not been specified. When the flange is subjected to a varying moment the applied stress at a distance $0.4 \times$ effective length from the heavily stressed end is used for the column check, whereas the maximum load at one end must be checked against $\Sigma (\sigma_{au} bt + \sigma_{ys} A_s)$ where A_s is the area of an individual stiffening rib. Shear lag effects are ignored for flanges with up to three longitudinal stiffeners. For flanges with a higher number of stiffeners the maximum stress is calculated in a plate

panel adjacent to the web, taking shear lag into account, but using reduced load factors appropriate to the limit state of unserviceability. This stress should not exceed the local buckling stress σ_{au} of the plate.

6.2 Discussion

- (a) This method is less demanding on design time than the previous two methods and is simple to comprehend.
- (b) In this method the buckling behaviour of a slender welded flange plate is taken into account by substituting its ultimate strength for yield stress in the Perry formula. But no account is taken of the loss of axial stiffness of the flange plate at its ultimate strength, which is reached at an axial strain significantly higher than the ratio σ_{au}/E would indicate. This loss of axial stiffness of the flange plate causes reduction in the flexural stiffness of the flange plate/stiffener assembly, and the high strain involved may cause yielding of the outstand near its connected edge. This method is thus likely to over-estimate the buckling strength of the stiffener on these accounts.
- (c) The plate strength curves have been derived partially from test results and partially from the theoretical work by Moxham. Both the tests and the theoretical work relate to plate panels free to pull in at the unloaded edges. In a stiffened flange with many longitudinal stiffeners, all the internal panels are likely to behave like a plate with unloaded edges restrained to remain straight and subjected to a net force in the transverse direction over a half-wave length of buckling equal to zero. Thus on this account this method is likely to be somewhat conservative for plate initiated failure of the stiffeners.
- (d) The European column curves and the modified Perry-type formula adopted in this method to represent these curves do not allow for a situation when failure of an unsymmetrical strut may actually be triggered by tensile yielding on the extreme fibre of the outstand. Such situations can develop when the distance

of the extreme tensile fibre is several times the distance of the extreme compression fibre and the slenderness ratio of the strut is high.

7. KARLSRUHE METHOD

7.1 Description

This method^[26] is basically an elastic large-deflection analysis of an initially imperfect plate-stiffener assembly under uniform compression. The pattern of both initial and final out-of-plane deflections is assumed to be sinusoidal along the length, but the transverse distribution pattern may be varied and is solved for minimum total potential energy; hence several possible transverse patterns of the deflected shape are investigated and the critical one established. Bending in both directions, twisting of the flange plate, and membrane forces in the longitudinal direction are taken into account in the energy calculations; the torsional stiffness of stiffeners, membrane shear stress and transverse stress are ignored.

In the calculation of the stiffener properties, an effective width of the plate between the stiffeners, given by Winter^[23] and quoted below, is taken into account:

$$\frac{b_e}{b} = 1 - \left(1 - 0.95 \frac{t}{b} \sqrt{\frac{E}{\sigma_e}} \right)^2, \quad \text{if } 0.95 \frac{t}{b} \sqrt{\frac{E}{\sigma_e}} < 1$$

..... (4)

$$= 1, \quad \text{if } 0.95 \frac{t}{b} \sqrt{\frac{E}{\sigma_e}} > 1$$

σ_e being the average value of the edge stresses of all the plate panels.

The method involves calculating three basic non-dimensional parameters from the properties of the stiffened panel, viz.:

a stiffness parameter ,

$$\alpha^* = \frac{L}{B} \sqrt[4]{\frac{bt^3}{12(1-\nu^2) I_e}}$$

a stress parameter , $\bar{\sigma}_R = \frac{\sigma_B}{\sigma_{cr}^*}$

an imperfection parameter, $\bar{u} = \frac{\pi}{2L} \sqrt{\frac{E}{\sigma_B}} \cdot \Delta_{sx}$

where I_e is the second moment of area of one effective stiffener section

σ_B is the stress along the longitudinal edges which in the first instance may be assumed to be the yield stress.

From the given graphs, and using the above three parameters, the efficiency factor ρ , additional deflection of the stiffened panel and the variation of the membrane longitudinal stress across the width of the stiffened flange may be obtained. From these, the stresses in the extreme fibres of the central longitudinal stiffener due to membrane compression and flexure can be calculated. The average ultimate stress on the effective compression flange is then $\rho\sigma_B$, provided the extreme fibre stresses do not exceed a limiting value, e.g. yield stress. Otherwise another lower value of σ_B has to be assumed and the process repeated.

7.2 Discussion

This method is similar to the Liege Method in the basic approach, i.e. it is an elastic large-deflection analysis of stiffened plates. The main difference between the two are as follows:

- (a) The Karlsruhe Method takes into account discreet stiffeners acting in conjunction with the continuous flange plate, whereas in the Liege Method stiffener properties are 'smeared' over the entire width to produce an idealised orthotropic plate.
- (b) The Karlsruhe Method has not been extended to closed longitudinal stiffeners, as torsion of the stiffeners is neglected in the energy formulation.
- (c) The method includes a separate failure criterion on the basis of the maximum fibre stress of central stiffeners, and is thus more comprehensive than the Liege Method. However, this check

involves a series of cycles of trial and error, - solving for orthotropic action first and then checking for yielding at extreme fibres of stiffeners or at edges of stiffened panel; this cycle to be repeated till maximum stress equals yield stress.

- (d) A reduced effective width of flange is assumed for stiffener properties; but as it depends upon the edge stresses of individual panels, it has to be a trial value at first, to be checked later with the calculated stresses.

8. MONASH METHOD

8.1 Description

In this method^[27] the flange stiffeners are analysed as individual single-span struts in the classical Perry manner, but allowance is made for loss of effectiveness of flange plate panels between stiffeners. If the elastic critical buckling stress σ_{cr} of the plate panels is less than the Euler buckling stress σ_E of the strut, then a reduced effective width of the flange plate panel is taken for the effective cross-section of the strut. The shift in the centre of gravity of the effective section relative to that of the gross section is expressed as an additional initial eccentricity Δ'_s as follows:

$$\Delta'_s = \Delta \left[1 - \frac{\sigma_{cr} (A_s + bt)}{\sigma'_E (A_s + b_e t)} \right]$$

where Δ is the shift of centroid

σ'_E is the Euler stress of the effective strut.

This additional initial eccentricity is added algebraically to the tolerance of out-of-straightness of the stiffener to obtain the maximum axial stress from the Perry formula:

$$\frac{\sigma'_{su}}{\sigma_{ys}} = \frac{1}{2} \left[1 + (1 + \eta) \frac{\sigma'_E}{\sigma_{ys}} \right] - \sqrt{\frac{1}{4} \left[1 + (1 + \eta) \frac{\sigma'_E}{\sigma_{ys}} \right]^2 - \frac{\sigma'_E}{\sigma_{ys}}}$$

..... (5)

$$\text{where } \eta = \frac{y' (\Delta_{sx} + \Delta'_s)}{(r')^2}$$

σ'_{su} and σ'_E are the ultimate axial stress and Euler stress of the effective stiffener

y' = maximum fibre distance from the centroid of effective section

r' = radius of gyration of effective section.

The ultimate stress σ_{su} on the gross section is given by:

$$\sigma_{su} = \sigma'_{su} \frac{A_s + b \cdot e \cdot t}{A_s + bt}$$

It is pointed out [59] that although theoretical non-linear elastic analysis is available for initially imperfect residual-stress-free compression plate panels with the unloaded edges either free to pull in or restrained to remain straight, test results are only available for plates with unloaded edges free to pull in. For plates with stress-free longitudinal edges a formula relating the average stress to the maximum longitudinal membrane stress along the unloaded edge is given. By assuming the ultimate load to be reached when this maximum edge stress equals yield stress an expression is given for the ultimate stress σ_{au} in terms of an initial imperfection parameter:

$$\frac{\Delta_p}{t} = \alpha \left[\frac{\sigma_{ys}}{\sigma_{cr}} \right]^{1/2}$$

where Δ_p = initial geometrical imperfection in the critical mode

$$\sigma_{cr} = \frac{\pi^2 E t^2}{3(1-\nu^2) b^2}$$

α = a coefficient for imperfections.

The value of the coefficient α is then determined from available test results for such plates; it is found that $\alpha = 0.4$ gives good correlation between the theoretical and the lower bound test results for welded plates, whereas $\alpha = 0.3$ provides a good comparison with the median of the scatter of test results. An expression is developed for the average plate stress σ_{au} on a plate with edges held

straight, such that the membrane stresses in the two directions on the longitudinal edge just reach the Tresca yield criterion. By using the value of the imperfection coefficient $\alpha = 0.4$, a curve is drawn for the ratio $\frac{\sigma_{au}}{\sigma_{ys}}$ against $\left[\frac{\sigma_{ys}}{\sigma_{cr}} \right]^{\frac{1}{2}}$. The effective width is then given by:

$$b_e = \frac{\sigma_{au}}{\sigma_{ys}} b$$

For combined axial and bending loading specific design rules have not been given due to lack of sufficient experimental evidence, but the following recommendations are offered:

- (i) If the local lateral loading produces compression on the outstand, gross section may be used for stiffener properties.
- (ii) If the local loading produces tension on the outstand, then a reduced effective width of the flange plate should be taken when the plastic neutral axis of the cross-section, taking into account axial and flexural stresses, lies within the outstand.

It is suggested that if there is any tensile zone in the plate, it will stabilise the plate against buckling.

- (iii) Extreme fibre yield due to axial forces, applied bending moment and magnified deflections may be adopted as the failure criterion.

8.2 Discussion

- (a) This method is simple to use and comprehend.
- (b) It assumes that the flange plate panel is fully effective, i.e. it is capable of resisting a compressive force of $bt \sigma_{ys}$, if its elastic critical buckling stress σ_{cr} is higher than the Euler buckling stress σ_E of the strut. According to the Perry formula, the maximum axial load on the strut for flange plate initiated collapse occurs with the attainment of yield stress in the flange plate, whatever is the actual value of the Euler stress. Hence if $\sigma_{cr} > \sigma_E$, this method implies that the flange plate, irrespective of its width/thickness ratio, is capable of resisting its squash load $bt \sigma_{ys}$. This assumption

must be optimistic, and contradicts the strength/effectiveness graph of plates incorporated in the method. A more rational approach would be to use in all cases an effective width of the plate given by the above graph.

9. MANCHESTER METHOD

9.1 Description

This method^[28] analyses flange stiffeners as axially loaded individual single-span struts in the Perry manner, with an allowance made for loss of effectiveness of the flange plate panels. Secant effective width factor K_s is defined as the ratio of mean stress to longitudinal stress at the unloaded edges and is derived from a large-deflection elastic analysis of plates with initial geometrical imperfections in the critical buckling mode. The longitudinal edges of the plate are assumed to be held straight, with zero net transverse stress over a half-wave length.

It is assumed that the plate reaches maximum strength when the longitudinal membrane stress on the unloaded edges equals yield stress, and graphs are given for K_s at maximum plate strength for various levels of initial imperfections. The levels of this imperfection Δ_p to be taken for this purpose is given by:

$$\Delta_p = \left(\Delta_m + \frac{1}{2} \Delta_t \right) \frac{b}{30t} \sqrt{\frac{\sigma_{ys}}{245}} \quad \dots \quad (6)$$

where Δ_m is the measured imperfection in the plate panel

Δ_t is the fabrication tolerance for out-of-plane imperfection of the plate panel given in the Merrison Rules^[3]

σ_{ys} is in N/mm².

The part $\frac{1}{2} \Delta_t$ above is meant to cover the following aspects that are ignored in the derivation for K_s :

- (a) residual stresses due to welding, etc.,
- (b) onset of plasticity due to flexural stresses,
- (c) influence of transverse membrane stresses on yielding at longitudinal edges.

With the above effective width of flange, the strength of the strut is then calculated from the Perry formula (see equation (2) Section 6.1), but with the following modifications:

- (a) 1.2 times the shift of centroidal axis of the effective section relative to that of the gross section is added to initial out-of-straightness of the strut.
- (b) The total out-of-straightness of the strut is then reduced by a factor $\frac{L-L_0}{L}$, in order to avoid any reduction in the strength of a strut of very low L/r' ratio, where $L_0 = \frac{\pi}{5} r' \sqrt{\frac{E}{\sigma_{ys}}}$ and r' is the radius of gyration of the effective cross-section.
- (c) For plate initiated failure, the maximum stress is calculated at the mid-plane of the plate instead of the outer surface.

9.2 Discussion

- (a) The method deals with the mode of stiffener failure initiated by flange plate in compression only, though it would appear quite simple to extend it to cover the other modes, i.e. stiffener outstand reaching yield stress either in compression or in tension, by taking in the Perry equation:
 - (i) the distance of the tip of the outstand from the centroidal axis;
 - (ii) algebraic sum of the stiffener out-of-straightness and the shift of centroidal axis.
- (b) The empirical treatment for welding residual stresses in the flange plate, i.e. adding half of the plate imperfection tolerance in equation (6), does not take any account of the level of the welding stresses. This treatment is also restricted by being related to the Merrison tolerance on plate flatness which may be changed in future rules.
- (c) It is not clear whether the values of Δ_m and Δ_t to be used in equation (6) are those measured over twice the half-wave-length of critical buckling (which is the procedure for measuring imperfections in the Merrison Rules), or whether the values measured in this fashion should be reduced to some equivalent values effective over the half-wave-length.

- (d) The ratio $\frac{b}{30t}$ incorporated in equation (6) substantially alters the initial imperfection magnitude; it is reduced for plates with $\frac{b}{t}$ ratio less than 30, and increased for $\frac{b}{t} > 30$. Since the plate strength/stiffness curves are derived from sophisticated large-deflection analyses, such arbitrary and drastic alteration in the most important parameter is open to question.

| Aspects of Stiffened Compression Flange, Covered in the Different Methods | Method | | | | | |
|---|----------------|--------------|------------------|------------------|---------------|-------------------|
| | Merrison Rules | Liege Method | Cambridge Method | Karlsruhe Method | Monash Method | Manchester Method |
| 1. Asymmetry of cross-section about horizontal axis | ✓ | - | ✓ | ✓ | ✓ | ✓ |
| 2. Buckling of plate between stiffeners | ✓ | ✓ | ✓ | ✓ | ✓ | ✓ |
| 3. Torsional buckling of stiffener outstand | ✓ | - | - | - | - | - |
| 4. In-plane transverse stresses in flange plate | ✓ | - | - | - | - | - |
| 5. In-plane shear stresses in flange plate | ✓ | - | ✓ | - | - | - |
| 6. Locally applied lateral loading | ✓ | - | - | - | ? | - |
| 7. Varying axial load | ✓ | - | ✓ | - | - | - |
| 8. Overall curvature of box girder | ✓ | - | - | - | - | - |
| 9. Orthotropic behaviour of flange | ? | ✓ | ? | ✓ | - | - |
| 10. Continuity over transverse frames | - | - | - | - | - | - |
| 11. Welding residual stresses | ✓ | - | ✓ | - | - | ✓ |
| 12. Other residual stresses | - | - | - | - | - | - |
| 13. Shear lag | ✓ | - | ✓ | - | - | - |
| 14. Composite action of concrete | ✓ | - | - | - | - | - |

TABLE 1

CHAPTER 3

NON-LINEAR BEHAVIOUR OF STIFFENER COMPONENTS

1. INTRODUCTION

1.1 The stiffened compression flange of a box girder can be visualised in a simplified form as a series of unconnected parallel struts each made up of one stiffening rib and half the width of the flange plate panel on either side. Though the stress-strain behaviour of the materials will be assumed to be linearly elastic up to the yield stress and ideally plastic afterwards, the load-end shortening behaviour under longitudinal compression of each of these two individual components may not be linear, due to initial geometric imperfections and welding residual stresses, etc.

1.2 The stress analysis of such a strut will thus have to deal with the following two separate and distinct non-linear effects:

- (i) the non-linear response of the whole strut due to initial geometric imperfections of the nature of an overall bow or an eccentricity of applied loading at the ends or both;
- (ii) the non-linear response of the individual components, viz. the flange plate or the stiffener outstand, due to the presence of residual stresses and/or out-of-flatness.

1.3 The buckling analysis of a perfectly straight and concentrically loaded strut made of perfectly elastic material was first done by Euler (1744). This concept of critical buckling was extended to the Double Modulus and the Tangent Modulus theories by Considere (1889), Engesser (1895) and Shanley (1947), in order to deal with perfect concentrically loaded struts made of inelastic materials. The stress analysis of initially imperfect struts made of perfectly elastic material was carried out by many investigators; the well-known Perry Formula for concentrically loaded sinusoidally crooked struts and the Secant Formula for eccentrically loaded initially straight struts belong to this category of strut analysis. The present author has not been able to locate any suitable set of explicit formulae for the combination of an overall bow (and/or end

eccentricity) and non-linear material response. Several computer programs are, however, available [19,29] for the analysis of such struts; these programs are based on dividing the length of the strut into a large number of segments and establishing equilibrium between the internal stresses and applied forces and moments for each of these segments. In this chapter explicit equations will be derived, linking stresses and applied longitudinal loads for such struts, and a design method will be developed from these basic equations.

2. BASIC EQUATIONS FOR COMPOSITE STRUTS OF NON-LINEAR MATERIALS

First consider a beam-column of any arbitrary cross-section, which is symmetrical about the plane of bending and is made up of a series of horizontal strips of different materials like F-F shown in Fig. 14(a) - each strip possessing different non-linear stress-strain characteristics as shown typically in Fig. 14(b). Assuming plane cross-sections remain plane and normal to the longitudinal axis after bending, the strain e of any fibre FG , under the action of axial force P and bending moment M at any cross-section, is equal to y/R , when R is the radius of curvature and y is the distance of the fibre from the neutral plane MM , i.e. the plane of zero strain.

If the actual non-linear stress-strain behaviour of a strip like FF is as shown typically by the thick continuous line in Fig. 14(b) (and not the linear material behaviour shown by the dotted line) the stress at fibre FF is given by

$$\sigma = eEK_s = EK_s y/R \quad \dots \quad (1)$$

where K_s is the ratio σ/eE corresponding to strain e , obtained from Fig. 14(b). Let $K_s b$ be called the effective width of any strip of actual width b .

$$\begin{aligned} P &= \int \sigma b dy = \int \frac{E}{R} b K_s y dy \\ &= \frac{E}{R} \quad [\text{first moment of all the effective strips in the} \\ &\quad \text{cross-section about } MM] \\ &= \frac{E}{R} A_e y_o \quad \dots \quad (2) \end{aligned}$$

where A_e = the total effective area of the cross-section = $\int K_s b dy$
 y_o = the distance of the centroid of the effective area
 from neutral plane MM .

In equation (1) y may be replaced by $(\bar{y} + y_o)$, where \bar{y} is the distance of the fibre from the centroid of the effective area, with all distances taken as positive downwards. Hence,

$$\begin{aligned}\sigma &= \frac{E}{R} K_s (\bar{y} + y_o) \\ &= K_s \left[\frac{E\bar{y}}{R} + \frac{P}{A_e} \right], \text{ from (2)} \quad \dots\dots (3)\end{aligned}$$

We shall now take P to be acting through the centroid of the effective section and adjust the magnitude of M to allow for any offset between this centroid and the actual line of action of the axial force. This adjusted value of M will be given by:

$$\begin{aligned}M &= \int \sigma \cdot \bar{y} b dx \\ &= \int \frac{yEK_s}{R} \bar{y} b dx, \text{ from (1)} \\ &= \frac{E}{R} \int (\bar{y} + y_o) K_s \bar{y} b dx \\ &= \frac{E}{R} \left[\int \bar{y}^2 K_s b dx + y_o \int \bar{y} K_s b dx \right] \\ &= \frac{E}{R} [I_e + \text{zero}],\end{aligned}$$

where I_e is the second moment of area of the effective section about its centroidal axis.

Hence $\frac{M}{I_e} = \frac{E}{R}$

and, from (3)

$$\sigma = K_s \left[\frac{M\bar{y}}{I_e} + \frac{P}{A_e} \right] \quad \dots\dots (4)$$

In the above expression for stress σ at any fibre, K_s must correspond to the calculated stress σ at the fibre, and the cross-sectional properties I_e and A_e of the effective section must be calculated by taking effective widths of each strip in the cross-section appropriate to the calculated stress there.

3. APPLICATION OF THE BASIC EQUATIONS TO A STIFFENED FLANGE

The stiffened compression flange of box girders between cross-frames consists of two components, i.e. the flange plate panel and the stiffening rib. Hence the K_s -factors under consideration are related to the load-shortening behaviour of these two components. However, due to the various reasons explained in Chapter 9, the geometric proportions on the cross-section and the tolerances on initial imperfections of the stiffening ribs may be chosen such that there is no significant non-linearity in the load-shortening behaviour of the stiffening ribs. Thus in applying expression (4) to the stiffened flange problem, only one K_s , i.e. that of the flange plate panel need to be considered in this formulation. Thus from (4)

$$\left. \begin{aligned} \sigma_p &= K_s \left[\frac{P}{A_e} + \frac{My_p}{I_e} \right] \\ \sigma_o &= \frac{P}{A_e} + \frac{My_o}{I_e} \end{aligned} \right\} \dots\dots (5)$$

where σ_p = stress in the mid-plane of the flange plate
 σ_o = stress at any point on the stiffening rib
 y_p, y_o = distance of the mid-plane of the flange plate and of the point on the stiffening rib from the centroid of the effective section comprising the stiffening rib and K_s -times the actual width of the flange plate
 K_s = the effectiveness factor of the flange plate relating to stress σ_p , which is obtained from the load-shortening curve of the flange plate.

It should be noted that the formulae in (5) are valid only if σ_o does not exceed yield stress at any point on the outstand.

4. A STRUT DESIGN APPROACH FOR A STIFFENED FLANGE

Formula (5) may be used to analyse stresses for given values of P and M by the method of successive approximations. A value of σ_p , say σ_1 , may be assumed at first; with an appropriate value of K_s corresponding to this assumed value of σ_p , another value of σ_p , say σ_2 , may be calculated from (5) and compared with σ_1 ; this process may be repeated until $\sigma_2 = \sigma_1$. This iterative method of successive approximations will be time-consuming and cannot be considered suitable for design purposes. It should, however, be noted that:

- (i) if $\sigma_2 > \sigma_1$, the first assumed value of K_s is too high and the correct value σ_p will be higher than σ_2 ;
- (ii) if $\sigma_2 < \sigma_1$, the first assumed value of K_s is too low and the correct value of σ_p will be less than σ_2 .

Based on the above observations it is possible to derive a safe design method that will not require a series of successive approximations. One point from the load-shortening curve of the flange plate panel may be chosen, and the design method will be aimed to produce in the plate panel, when subjected to the design loading, the conditions of stress and shortening represented by this point. This point should normally correspond to the peak stress in the load-shortening curve as shown in Fig. 15(a); but if there is no clear peak, or if the peak occurs at a strain much higher than yield strain, the point may have to correspond to an arbitrarily set strain limit as indicated in Fig. 15(b). The object of setting such a limit in the latter case is to avoid excessive deformation of the stiffener as a whole and also to prevent strains on the upper part of the stiffening rib greatly exceeding yield strain and thus producing premature lateral instability. Also, if the load-shortening behaviour indicates a sharp fall-off after the peak load, the design point should be chosen well below the peak in order to avoid a very unstable state. For the chosen point on the load-shortening curve of the flange plate let σ_{au} denote the stress and $K_{su} = \sigma_{au}/n\sigma_{ys}$ denote the effectiveness factor. Hence, from equation (5), the design of the stiffener can now be checked to satisfy the following conditions:

$$\left. \begin{aligned} \sigma_p &= K_{su} \left[\frac{P}{A_e} + \frac{My_p}{I_e} \right] \} \sigma_{au} \\ \sigma_o &= \frac{P}{A_e} + \frac{My_o}{I_e} \} \sigma_{ys} \end{aligned} \right\} \dots \quad (6)$$

It may be argued that when the plate stress σ_p , calculated from equations (6), is significantly less than σ_{au} , e.g. when the bending moment M produces tension in the plate, the adopted effective width of the flange plate is unduly low. But in such a situation, the design is not sensitive to the effective width of the flange plate, as the stress in the plate is obviously not critical, and the maximum compressive stress in the stiffening rib is slightly overestimated by any conservative assumption regarding flange plate effective width.

In the above design approach one can identify two effectiveness factors, i.e.

- (i) a strength effectiveness factor = σ_{au}/σ_{ys} , and
- (ii) a stiffness effective width factor K_s which reduces with increase in the stress level and which is equal to $\sigma_{au}/n\sigma_{ys}$ when the limiting stress σ_{au} is reached at strain $n\sigma_{ys}/E$.

K_s has been termed the secant effective width factor in the Merrison Interim Design Rules for Box Girders.

A further simplification of the design method is possible when $n = 1$, i.e. either the peak stress occurs at a strain of σ_{ys}/E or the stress corresponding to this strain is arbitrarily chosen as a limit for the plate. In this case the two effectiveness factors are equal, i.e. $K_{su} = \sigma_{au}/\sigma_{ys}$, and the design method will simply consist of taking one effective width of flange equal to $K_{su}b$ for an effective strut section and then checking that the yield stress is not exceeded anywhere on this effective section. Such a simple effective width approach has been the basis for many of the recommended methods for compression flange design, but strictly speaking this approach is theoretically correct only when $n = 1$, i.e. the peak stress occurs or is assumed to occur, at yield strain.

5. FACTORS INFLUENCING THE BUCKLING OF THE STRUT

It has been shown in Section 2 that when a composite beam-column of non-linear materials is subjected to axial load and flexure, the magnitude of the bending moment and the curvature at any section of the beam-column is related by equation (4), i.e. $M/I_e = E/R$, where I_e is the second moment of area of the effective cross-section about its centroidal axis, in which an effective width of all the strips equal to $K_s b$ has been taken - K_s being related to the stress in the particular strip at this cross-section calculated from equation (4). The bending moment M is calculated with respect to the centroid of this effective cross-section. For small deflections the reciprocal of R can be approximately taken as dy^2/dx^2 when y represents deflections due to flexure, and with the sign convention of downward deflection and sagging bending moment positive, we get for any cross-section,

$$M_x = - EI_e \frac{d^2 y}{dx^2} .$$

Consider now the case of an initially imperfect composite strut subjected to a longitudinal load P applied eccentrically at its ends. If y_0 and y represent the initial and the final deflected shapes of the centroidal axis of the effective section A_e respectively, then at any cross-section,

$$M_x = - EI_e \frac{d^2 (y - y_0)}{dx^2} .$$

Equating this internal moment to the externally applied moment at the section, leads to:

$$- EI_e \frac{d^2 (y - y_0)}{dx^2} = P\delta \quad \dots \quad (7)$$

where δ is the distance of the centroid of the effective section A_e in its deflected position measured normal to and from the line of action of P . This is the governing equation for the deflected shape of the strut.

Equation (7) is identical to that for an initially imperfect and eccentrically loaded strut of a perfectly elastic material, except that I_e replaces the constant second moment of area. For the box girder stiffened flange problem I_e depends upon K_s and hence the stress in the flange plate. The total stress in the flange plate is the sum of that due to the axial load P and that due to the bending moment M_x , and as M_x varies along the length of the strut, I_e is not theoretically constant. If the bending stresses are small compared to the axial stress, then the variation in K_s will not be large. Moreover, any change in K_s causes a comparatively small variation in I_e , as can be seen from the following expressions for I_e :

$$I_e = I_o - \frac{A_o^2}{A_s + K_s bt}$$

In this expression A_o and I_o are the first and the second moments of area about the flange mid-plane of the stiffening rib section A_s , and b and t are the width and thickness of the flange plate. Taking as an example a 300 mm \times 12 mm flange plate stiffened by a 200 mm \times 15 mm rib, the ratio of the second moment of area of the effective section I_e to that of the gross section I_g are given below for different values of K_s :

| | | | | |
|-----------|-----|------|------|-----|
| K_s | 1.0 | 0.8 | 0.6 | 0.5 |
| I_e/I_g | 1.0 | 0.93 | 0.85 | 0.8 |

Furthermore, the effect of increased second moment of area away from the mid-span has comparatively little effect on the deflected shape of the strut. This can be illustrated by taking the example of a simple beam of sinusoidally varying second moment of area, the minimum being at the mid-span, and subjected to a sinusoidal bending moment pattern with maximum value at mid-span. If the maximum deflection is calculated with the assumption of uniform second moment of area equal to the minimum value, it will be overestimated, compared with the exact value, by only 4½% and 11½% for the ratio of minimum to maximum second moment of area equal to 0.75 and 0.5 respectively.

From the above considerations it is reasonable, and safe, to assume a constant value of I_e corresponding to the maximum stress in the flange plate. In Section 7 of this chapter, the bending moment expression in equation (7) is used in conjunction with an assumed initial deflection pattern, to obtain the solution for the final deflections and bending moments along the length of the strut. This solution, i.e. equation (10) is very similar to the design equation given in the Merrison Rules^[3], except that in the latter, for critical buckling stress, I_e is calculated on the basis of the tangent stiffness K_t of the flange plate (i.e. the slope of the tangent to the load-shortening behaviour of the plate at the appropriate stress level), instead of the secant stiffness K_s as derived in Section 2. The author understands that this approach in the Merrison Rules owes its origin to the theories of inelastic buckling of straight struts, i.e. the Tangent-modulus theory of Engesser or the Double-modulus theory of Considere, in which the buckling stress of straight struts of inelastic material is derived in terms of the slope of the tangent to the stress-strain curve at the appropriate point. To explain this anomaly the origin of the tangent modulus concept will be traced back by reference to its use in the inelastic buckling of straight struts, and its validity to the analysis model adopted in the Merrison Rules examined in the following section.

6. INELASTIC BUCKLING OF STRAIGHT STRUTS

Consider a straight composite strut compressed by an applied load P without any deflection. If e_p is the uniform axial strain, stress σ at any strip is equal to $K_s E e_p$; K_s and hence σ may vary from strip to strip, depending upon the shape of the stress-strain curve of the strips.

$$P = \int K_s E e_p b dy = E e_p \int K_s b dy = E e_p A_e$$

where A_e is the effective area consisting of strips of effective widths $K_s b$. It is obvious that for no flexure P must act through the centroid of the effective area A_e , i.e. the line of action of P must change with the magnitude of P .

Now apply a very small deflection to the strut. In every cross-section there will be one axis MM perpendicular to the plane of bending in which the stress and the strain developed prior to deflection does not change. See Fig. 16.

On the concave side of this line the compressive stresses will be increased, the relationship between the incremental stress to incremental strain being $d\sigma/de = EK_t$, when K_t is the slope of the tangent to the load-shortening diagram at stress σ . On the convex side of the line the compressive stresses will be reduced by flexure and as unloading follows a linear relationship between stress and strain with constant modulus E , $d\sigma/de = E$.

Denoting the incremental strains and stresses due to flexure at distance y from MM by e_b and σ_b , and noting that $e_b = y/R$, we get:

$$\sigma_b = EK_t e_b = EK_t \frac{y}{R} \text{ on the concave side;}$$

$$\sigma_b = Ee_b = E \frac{y}{R} \text{ on the convex side.}$$

As these additional stresses do not alter the total axial load,

$$\int_0^{y_c} EK_t \frac{y}{R} b \, dy - \int_0^{y_t} E \frac{y}{R} b \, dy = 0$$

or,

$$\int_0^{y_c} K_t b y \, dy - \int_0^{y_t} b y \, dy = 0$$

Imagine a tangent effective area A_{et} , with $K_t b$ for each strip on the concave side and the actual widths of strips on the convex side of the line MM . Since from the above equation the first moment of area of this section about MM is zero, MM must be the centroidal axis of this section A_{et} .

The bending moment M_x at the cross-section is given by:

$$\begin{aligned}
 M_x &= \int_0^{y_c} EK_t \frac{y}{R} by dy + \int_0^{y_t} E \frac{y}{R} by dy \\
 &= \frac{E}{R} \int_0^{y_c} K_t by^2 dy + \int_0^{y_t} by^2 dy \\
 &= \frac{E}{R} I_{et}
 \end{aligned}$$

where I_{et} is the second moment of area of the tangent effective section A_{et} . Denoting the deflection of the centroidal axis of A_{et} by y , and noting that for small deflections $1/R = -d^2y/dx^2$, we get:

$$-EI_{et} \frac{d^2y}{dx^2} = Py \quad \dots \quad (8)$$

Equation (8) represents the differential equation of the centroidal axis of a composite strut in the state of unstable equilibrium and is of the same form as that for the deflected shape of a perfectly elastic strut. Thus, for a simply supported strut of composite section and length L we can get the smallest buckling load P_{cr} by following the approach of the Double-modulus theory:

$$P_{cr} = \frac{\pi^2 EI_{et}}{L^2} \quad \dots \quad (9)$$

According to the Tangent Modulus theory, the ratio of incremental stress and strain is taken as EK_t for the whole cross-section and not just on the concave side, and thus I_{et} is calculated for a tangent-effective section in which the actual widths of all the strips are multiplied by corresponding K_t .

It can be seen that

- (i) equation (7), involving secant stiffness K_s , relates to the equilibrium condition for the deflected position of an initially imperfect composite strut;
- (ii) equation (8), involving tangent stiffness K_t , relates to the position of an initially straight composite strut when subjected to a small lateral disturbance.

Thus the tangent stiffness K_t is the appropriate factor for the analysis of inelastic buckling of composite straight struts. It

will also be appropriate for an *incremental* analysis of initially imperfect composite struts, i.e. for its complete load-shortening behaviour. But the secant stiffness K_s is appropriate for the effective cross-sectional properties in the single-step design approach developed in Section 4.

7. IMPERFECTIONS AND A DESIGN METHOD FOR BOX GIRDER STIFFENED COMPRESSION FLANGES

For the design of box girder compression flange stiffeners, it will be assumed that they may have both initial misalignments and eccentricity of applied load as shown in Fig. 17(a). Equation (7) governs the deflected shape:

$$- EI_e \frac{d^2(y - y_0)}{dx^2} = P\delta$$

As explained in Section 5, y_0 and y represent the initial and the final position of the centroid of the effective section A_e ; δ is the offset of the deflected centroid of the effective section from the line of action of P ; and I_e shall be taken as constant. Denoting the eccentricity of applied loading at each end with respect to the centroid of the effective section by e_1 , we get $\delta = e_1 + y$, and

$$- EI_e \frac{d^2(y - y_0)}{dx^2} = P(e_1 + y)$$

Assuming the initial shape to be given by $y_0 = e_2 \sin \pi x/L$, the solution to the above differential equation is:

$$y = -e_1 + e_1 \frac{\sin ux + \sin u(L-x)}{\sin uL} + e_2 \frac{\pi^2}{\pi^2 - u^2 L^2} \sin \frac{\pi x}{L}$$

where $u^2 = \frac{P}{EI_e}$. The bending moment at any section is then:

$$M_x = P(e_1 + y) = P \left[e_1 \frac{\sin ux + \sin u(L-x)}{\sin uL} + e_2 \frac{\pi^2}{\pi^2 - u^2 L^2} \sin \frac{\pi x}{L} \right]$$

The maximum bending moment occurs at the centre and is given by:

$$M = P \left[e_1 \sec \frac{\pi}{2} \sqrt{\frac{P}{P_E}} + e_2 \frac{P_E}{P_E - P} \right]$$

where $P_E = \frac{\pi^2 EI}{L^2} e =$ Euler load of an elastic strut of section A_e and length L between hinged ends.

In the Merrison Rules Section 20, the tangent effective width factor K_t is stipulated for the effective cross-section for the purpose of calculating the Euler load P_E and the bending moment due to initial imperfection; subsequently, however, the secant effective width factor K_s is used to calculate the stresses in the cross-section due to the axial force and the bending moment. But from the derivations in this and the previous sections it should be apparent that the secant effective width factor K_s is theoretically more appropriate for the entire analysis of an initially imperfect inelastic strut; this conclusion also leads to considerable simplification in the strut analysis as only one effective width factor for the plate is involved.

$$M \text{ can be written as } M = P m (e_2 + \frac{m^1}{m} e_1),$$

$$\text{where } m = \frac{P_E}{P_E - P} \text{ and } m^1 = \sec \frac{\pi}{2} \sqrt{\frac{P}{P_E}}$$

The ratio m^1/m for different values of P/P_E is shown in the following table. For compression flange stiffeners, factored applied load is not expected to be more than two-thirds of the Euler load P_E , and hence for the sake of simplicity it is reasonable to take the ratio m^1/m equal to unity.

| | | | | | |
|---------|-------|-------|-------|-------|-------|
| P/P_E | 0.2 | 0.4 | 0.6 | 0.8 | 0.9 |
| m^1/m | 1.048 | 1.099 | 1.154 | 1.212 | 1.242 |

Thus the maximum bending moment in the strut is given by:

$$M = P \cdot (e_1 + e_2) \frac{P/E}{P/E - P}, \quad \dots \quad (10)$$

$$= \frac{\pi^2 EI}{L^2} e (e_1 + e_2) (m - 1)$$

It should be noted that e_1 is the eccentricity of applied loading with respect to the centroid of the effective section A_e ; hence if the actual eccentricity is given with respect to the centroid of the gross cross-section, the shift of the centroid of the effective section must be allowed for in calculating e_1 .

In a steel box girder it is difficult to identify the exact distribution of stresses in the various stiffened elements at different cross-sections of the girder, since plates are liable to buckle between longitudinal stiffeners, which in their turn are liable to buckle between the transverse stiffeners. It is, however, reasonable to assume that a global analysis based on linear elastic theory will predict satisfactorily the stress distribution on the box girder cross-section at the locations of adequately designed cross-frames. The loading pattern at the ends of each span of longitudinal compression flange stiffeners can be obtained by applying Engineers' Bending Theory, in conjunction with shear lag effective width ratios, to the gross cross-section of the box girder and the calculated girder bending moment at the section. The end loading for the compression flange stiffeners will thus be represented by a stress gradient on their gross cross-section, as shown in Fig. 17(b).

The stress block shown shaded, acting on the flange stiffener can be represented by superimposing an axial force P and a bending moment M_e , given by:

$$P = A_g \sigma_a$$

$$\frac{M_e}{I_g} = \text{stress gradient} = \frac{\sigma_a}{h}$$

where A_g is the gross area of cross-section of the stiffener
 σ_a is the stress calculated by Engineers' Bending Theory at the centroid of the gross stiffener section
 I_g is the second moment of area of the gross stiffener section
 h is the distance between the centroid of the gross stiffener section and the neutral axis, i.e. the level of zero stress, of the box girder.

Instead of a moment M_e and a force P acting through the centroid of the gross section, we can take P acting with an eccentricity e'_1 with respect to the centroid of the gross section, given by:

$$e'_1 = \frac{M_e}{P} = \frac{I_g \sigma_a}{h A_g \sigma_a} = \frac{r_g^2}{h}$$

where r_g is the radius of gyration of the gross-section.

To apply equation (10) for the maximum bending moment on the flange stiffener, the shift e''_1 of the centroid of the effective section must be added algebraically to e'_1 ; e''_1 is given by:

$$e''_1 = A_o \left[\frac{1}{A_s + K_s bt} - \frac{1}{A_s + bt} \right]$$

where A_s = area of the stiffening rib

A_o = the first moment of area of the stiffening rib about the mid-plane of the flange plate.

e_1 in equation (10) is therefore given by:

$$e_1 = e'_1 + e''_1 = \frac{r_g^2}{h} + A_o \left[\frac{1}{A_s + K_s bt} - \frac{1}{A_s + bt} \right] \dots \dots (11)$$

8. STIFFENED COMPRESSION FLANGE DESIGN AND THE EUROPEAN STRUT CURVES

Extensive theoretical studies and corroboration with test data^[30], undertaken on behalf of the European Convention for Constructional Steelwork, on the flexural buckling of axially loaded

struts of compact cross-sections, with initial imperfections, residual stresses and variable yield stresses in the strut have led to a set of three basic European column curves. The selection of a particular curve for a specific column depends upon section geometry, axis of buckling and the process of fabrication, i.e. as-rolled, welded, annealed, flame-cut edges, etc. Unfortunately, the stiffened compression flange of box girders has certain features that have not been adequately covered in this study. These are:

- (i) Though the investigation covered welded box sections and tee sections separately, the stiffened compression flange has a combination of the worst features of both, i.e. the adverse geometry of the tee section buckling with the web on the concave side and the unfavourable welding residual stress pattern of fairly uniform compression in the flange plate.
- (ii) The flange plate and the outstand may be more slender than the limits of compactness of cross-section, and hence local buckling can be critical.
- (iii) The European column curves were based on an assumed sinusoidal initial bow of 1/1000 of the column length. Though it was shown that any eccentricity of applied loading of up to 1/20 times the radius of gyration was likely to be covered by the assumed initial bow, it was considered unnecessary to cover the possibility of a combination of a bow and an eccentricity of these magnitudes in the case of ordinary struts. As shown in the previous section, the loading on the stiffened compression flange acts with an end eccentricity which depends upon the geometry of not only the stiffened flange but the whole box.

Dwight^[31] has shown that these European column curves can be represented by the well-known Perry strut formulae:

$$\sigma_{su} = \frac{1}{2} \{ \sigma_{ys} + (\eta + 1) \sigma_E \} - \sqrt{\frac{1}{4} \{ \sigma_{ys} + (\eta + 1) \sigma_E \}^2 - \sigma_{ys} \sigma_E}$$

where σ_{su} = ultimate axial stress

σ_E = Euler stress

$$\eta = \frac{\Delta_{sx} y_f}{r^2}$$

Δ_{sx} = amplitude of a sinusoidal initial bow
 y_f = maximum compressive fibre distance from the centroidal axis.

The theoretical basis of the Perry formula is that the maximum load on the strut is attained when the total compressive stress due to axial load and flexure reaches yield stress at the extreme fibre. Robertson expressed the imperfection parameter η as $C \cdot L/r$; and by taking different values for C for different column types and introducing a lower limit of L/r below which η may be taken as zero, the three European column curves can be fairly accurately represented by the Perry equation.

It can be easily shown that the Perry equation is analogous to equating the maximum compressive stress either in the flange or in the outstand to the limiting values, in the same way as done in equations (6), with the bending moment calculated from equation (10). Because of the reasons already advanced, no assumptions shall be made regarding the Perry factor η or the Robertson constant C , but instead a calculated value for the eccentricity e_1 and a tolerance limit for the initial bow e_2 shall be used in equation (10). σ_{au} and K_{su} in equation (6) shall be derived from the load-shortening behaviour of the flange plate for which initial out-of-flatness and welding residual stresses in the plate shall be taken into account.

CHAPTER 4

ELASTIC INITIAL AND POST-BUCKLING BEHAVIOUR OF
FLAT ORTHOTROPIC PLATES

1. INTRODUCTION

In this chapter the elastic buckling behaviour of initially flat orthotropic plates under uniaxial in-plane compression, including post-buckling behaviour, will be analysed. Following from this analysis, the next two chapters will deal with the buckling behaviour of initially imperfect isotropic and orthotropic plates, leading respectively to:

- (a) the load-end shortening characteristics of flange plate panels between the stiffening ribs, which can be incorporated in the stress analysis of flange stiffeners as indicated in Chapter 3;
- (b) the influence of adjacent longitudinal stiffeners on each other, i.e. the orthotropic action of the entire stiffened flange between girder webs.

The differential equation for equilibrium at any point in an *isotropic* plate is:

$$\frac{\partial^4 w}{\partial x^4} + \frac{2\partial^4 w}{\partial x^2 \partial y^2} + \frac{\partial^4 w}{\partial y^4} = \frac{t}{D} \left[\frac{q}{t} + \sigma_x \frac{\partial^2 w}{\partial x^2} + \sigma_y \frac{\partial^2 w}{\partial y^2} + 2\tau_{xy} \frac{\partial^2 w}{\partial x \partial y} \right]$$

where t is the thickness of the plate

D is the flexural rigidity of the plate, given by $\frac{Et^3}{12(1-\nu^2)}$

q is the intensity of lateral loading per unit area at (x, y)

w is the deflection at (x, y)

σ_x, σ_y are the tensile membrane stresses in the respective directions at (x, y)

τ_{xy} is the shear stress in x - y plane at (x, y)

The above equation was originally derived by St. Venant (1883) for small deflections of *isotropic* plates in which the membrane stresses were due entirely to applied in-plane loads on the edges and were not affected by the plate deflections. This equation may also be used for larger deflections of *isotropic* plates, provided changes in the membrane stresses at different points caused by the stretching of the mid-plane are taken into account, and also provided the deflections are still small

enough compared to the length of the sides to justify the conventional approximation that curvature is equal to the second derivative of the deflection. Further assumptions involved are:

- (a) the thickness of the plate is small compared to the sides; hence stresses between adjacent horizontal layers in the plate are negligible, and also the effect of vertical shearing stresses on deflection of the plate is negligible;
- (b) plane sections remain plane and normal to the neutral surface.

Similar equations have been derived by several authors for anisotropic plates; because of the different assumptions made by them regarding the flexural rigidities, the basic properties relevant to our case and a suitable form of the equilibrium equation are given below for the convenience of the reader.

An anisotropic plate has different elastic properties, and hence flexural rigidities, in different directions. Assuming three planes of symmetry with respect to elastic properties, and taking them as the coordinate planes, the following five extensional constants are involved in the analysis of an 'orthotropic' (i.e. orthogonally anisotropic) plate in plane stress:

E_x = ratio of stress to strain in x -direction when there is no stress in the y -direction

E_y = ratio of stress to strain in y -direction when there is no stress in the x -direction

ν_x = $-E_x$ times the strain in x -direction due to unit stress in y -direction, with no stress in x -direction

ν_y = $-E_y$ times the strain in y -direction due to unit stress in x -direction, with no stress in y -direction

G = shear modulus.

From Hooke's Law of elasticity the relationship between stresses and strains in an orthotropic plate are:

$$\left. \begin{aligned} e_x &= \frac{1}{E_x} (\sigma_x - \nu_x \sigma_y) \\ e_y &= \frac{1}{E_y} (\sigma_y - \nu_y \sigma_x) \\ e_{xy} &= \frac{1}{G} \tau_{xy} \end{aligned} \right\} \dots\dots (1)$$

From Maxwell's reciprocal theorem, the strain in x -direction due to unit stress in y -direction must be equal to the strain in y -direction due to unit stress in x -direction. Hence, from the above definitions of the elastic constants:

$$\frac{\nu_x}{E_x} = \frac{\nu_y}{E_y}$$

An ideal orthotropic plate is defined to be such that the variation in flexural rigidities in the orthogonal directions is due entirely to the varying extensional elastic properties, and that the geometry is uniform in all directions, i.e. it is a plate of uniform thickness throughout.

Taking the curvature in each direction as the partial second derivative of the deflection and integrating the stresses over the thickness, it can be shown that the bending and twisting moments per unit length at any section are given by:

$$\left. \begin{aligned} M_x &= - \left[D_x \frac{\partial^2 w}{\partial x^2} + D_1 \frac{\partial^2 w}{\partial y^2} \right] \\ M_y &= - \left[D_y \frac{\partial^2 w}{\partial y^2} + D_1 \frac{\partial^2 w}{\partial x^2} \right] \\ M_{xy} &= M_{yx} = + 2D_{xy} \frac{\partial^2 w}{\partial x \partial y} \end{aligned} \right\} \dots \quad (2)$$

where the bending rigidities D_x , D_y , D_1 and D_{xy} are defined as:

$$\left. \begin{aligned} D_x &= \frac{E_x t^3}{12(1-\nu_x \nu_y)} \\ D_y &= \frac{E_y t^3}{12(1-\nu_x \nu_y)} \\ D_1 &= \nu_y D_x = \nu_x D_y \\ D_{xy} &= \frac{Gt^3}{12} \end{aligned} \right\} \dots \quad (3)$$

Taking $H = 2D_{xy} + \frac{1}{2}(\nu_x D_y + \nu_y D_x)$, the modified form of St. Venant's equilibrium equation for an orthotropic plate takes the form:

$$D_x \frac{\partial^4 w}{\partial x^4} + 2H \frac{\partial^4 w}{\partial x^2 \partial y^2} + D_y \frac{\partial^4 w}{\partial y^4} = q + \sigma_x t \frac{\partial^2 w}{\partial x^2} + \sigma_y t \frac{\partial^2 w}{\partial y^2} + 2\tau_{xy} t \frac{\partial^2 w}{\partial x \partial y} \dots \quad (4)$$

2. ELASTIC CRITICAL BUCKLING OF ORTHOTROPIC PLATES IN UNIAXIAL COMPRESSION

The elastic critical buckling stress for orthotropic plates in uniaxial compression has been derived by many authors in various different ways. As its magnitude is an important factor in the post-buckling behaviour of ideally flat plates and also in the whole behaviour of an initially imperfect plate, a technique (originally due to Timoshenko) for calculating it will be presented here for the convenience of the reader as an introduction. Figure 18 shows such a plate.

In this method the plate is given a very small lateral deflection, consistent with its edge conditions, at various levels of applied compressive forces. Consider the increment of strain energy of bending ΔU_b due to this small deflection and the increment of work ΔT_b done by the forces due to the in-plane movement of the loaded edges as a consequence of this small lateral deflection. At a critical level of σ_x , ΔU_b and ΔT_b will be equal and the plate will be in neutral equilibrium. The lowest critical load obtained by equating ΔU_b and ΔT_b for all possible modes of lateral deflection is the elastic critical buckling load.

In the case of uniaxial compression, as a very small deflection is being considered, σ_x may be considered to be constant everywhere in the plate and equal to the applied edge stress σ_α ; and $q = \sigma_y = \tau_{xy} = 0$. Hence the equilibrium equation (4) reduces to:

$$D_x \frac{\partial^4 w}{\partial x^4} + 2H \frac{\partial^4 w}{\partial x^2 \partial y^2} + D_y \frac{\partial^4 w}{\partial y^4} = -\sigma_\alpha t \frac{\partial^2 w}{\partial x^2} \dots \quad (5)$$

The boundary conditions for deflection are:

$$(i) \quad w = 0 \text{ when } x = \pm \frac{a}{2} \text{ and also when } y = \pm \frac{b}{2}$$

We shall assume that the plate is free to rotate at all the edges; hence,

$$(ii) \quad M_x = 0 \text{ when } x = \pm \frac{a}{2}$$

$$(iii) \quad M_y = 0 \text{ when } y = \pm \frac{b}{2}$$

The above boundary conditions are satisfied if we assume the deflected shape as:

$$w = A \cos \frac{m\pi x}{a} \cos \frac{n\pi y}{b} \quad \dots \quad (6)$$

since both w and the second derivatives $\frac{\partial^2 w}{\partial x^2}$ and $\frac{\partial^2 w}{\partial y^2}$ are zero when either $x = \pm \frac{a}{2}$ or $y = \pm \frac{b}{2}$.

If the effects of shear forces and stretching of mid-plane are neglected, then the bending strain energy stored in any element of the plate dx by dy is the sum of the work done by the bending moments $M_x dy$ and $M_y dx$, and by the twisting moments $M_{xy} dy$ and $M_{yx} dx$.

Hence, from (2)

$$\begin{aligned} d(\Delta U_b) &= \frac{1}{2} D_x \left[\left(\frac{\partial^2 w}{\partial x^2} \right)^2 + \nu_y \frac{\partial^2 w}{\partial y^2} \frac{\partial^2 w}{\partial x^2} \right] dx dy \\ &+ \frac{1}{2} D_y \left[\left(\frac{\partial^2 w}{\partial y^2} \right)^2 + \nu_x \frac{\partial^2 w}{\partial x^2} \frac{\partial^2 w}{\partial y^2} \right] dx dy \\ &+ 2D_{xy} \left[\frac{\partial^2 w}{\partial x \partial y} \right]^2 dx dy \end{aligned}$$

Using equation (6) and integrating $d(\Delta U_b)$ over the whole area, one gets:

$$\Delta U_b = \frac{\pi^4 A^2}{4} \left[\frac{1}{2} D_x m^4 \frac{b}{a^3} + \frac{1}{2} D_y n^4 \frac{a}{b^3} + H \frac{m^2 n^2}{ab} \right] \quad \dots \quad (7)$$

The work ΔT_b done by the applied forces can be obtained by considering the amount by which the loaded edges approach each other; from simple geometry this amount is equal to $\int \frac{1}{2} \left(\frac{\partial w}{\partial x} \right)^2 dx$, if powers of $\frac{\partial w}{\partial x}$ greater than 2 are neglected. Hence:

$$\Delta T_b = \sigma_a t \int_{-b/2}^{+b/2} \int_{-a/2}^{+a/2} \frac{1}{2} \left(\frac{\partial w}{\partial x} \right)^2 dx dy .$$

Substituting for w gives:

$$\Delta T_b = \frac{1}{8} \sigma_a t \pi^2 m^2 A^2 \frac{b}{a} \quad \dots \quad (8)$$

Equating (7) and (8), the critical value of σ_a is obtained as:

$$\sigma_{cr} = \frac{\pi^2}{tb^2} \left[D_x \frac{m^2 b^2}{a} + D_y \frac{n^4}{m^2} \frac{a^2}{b^2} + 2Hn^2 \right]$$

It is obvious that σ_{cr} will be minimum when $n=1$, i.e. there will be only one halfwave across the width b .

Taking $\phi = \frac{a}{mb}$:

$$\sigma_{cr} = \frac{\pi^2}{tb^2} \left[\frac{D_x}{\phi^2} + D_y \phi^2 + 2H \right] \quad \dots \quad (9)$$

For minimum value of σ_{cr} , $\frac{d\sigma_{cr}}{d\phi} = 0$, i.e. $\phi^4 = \frac{D_x}{D_y}$. Hence, the critical value of the longitudinal stress is given by:

$$\sigma_{cr} = \frac{2\pi^2}{tb^2} \left[\sqrt{\frac{D_x D_y}{x y}} + H \right] \quad \dots \quad (10)$$

and the half wave length of buckling, in the longitudinal direction, is given by:

$$l = \frac{a}{m} = b\phi = b \left[\frac{D_x}{D_y} \right]^{\frac{1}{4}} \quad \dots \quad (11)$$

For long isotropic plates $D_x = D_y = H = \frac{Et^3}{12(1-\nu^2)}$, and equations (10) and (11) reduce to the well-known Bryan's (1891) formula:

$$\sigma_{cr} = \frac{4\pi^2 E}{12(1-\nu^2)} \left(\frac{t}{b} \right)^2 \quad \dots \quad (12)$$

and $\phi = 1$, i.e. $l = \frac{a}{m} = b$.

The stiffened compression flange of a box girder differs from an ideal orthotropic plate in that discrete stiffeners are connected to the surface of the flange plate. However, equation (10) for critical stress may still be used as a good approximation, provided the flexural rigidities D_x , D_y and H are calculated taking the stiffening into account in the following manner:

From equations (2), considering curvature in one direction only at a time and smearing the rigidities uniformly,

$$D_x = \frac{EI_x}{b'} \quad \text{and} \quad D_y = \frac{EI_y}{L}$$

where I_x is the second moment of area of longitudinal stiffeners taking an effective width of flange plate equal to $b' K_s$; - K_s being the secant effective width factor of the flange plate discussed in Chapter 3,

I_y is the second moment of area of transverse stiffeners taking an effective width of flange plate equal to L ,

b' and L are the spacing of longitudinal and transverse stiffeners respectively as shown in Fig. 19.

From the definitions v_x and v_y given in Section 1, they may be assumed as follows:

$$v_x = v \frac{b't}{b't + A_{sx}}$$

$$v_y = v \frac{Lt}{Lt + A_{sy}}$$

where A_{sx} and A_{sy} are the area of each stiffening rib in the x and y direction respectively.

For the ideal orthotropic plate of uniform and continuous thickness t , the rigidity H is given by:

$$H = \frac{Gt^3}{6} + \frac{1}{2} v_y D_x + \frac{1}{2} v_x D_y .$$

In a stiffened compression flange, however, the plate has discrete stiffeners, and the contribution of flexural rigidities D_x and D_y towards the torsional rigidity H is not certain; so it is safe to ignore the latter two terms. The first term is equal to half the torsional rigidity of the orthotropic plate; hence we may add half the torsional rigidities of the stiffening ribs in each direction, thus resulting in the following expression for H for stiffened flanges:

$$H = \frac{Gt^3}{6} + \frac{GJ_x}{2b'} + \frac{GJ_y}{2L}$$

where J_x and J_y are the torsional constraints of the stiffening rib sections in x and y direction respectively and are given by:

- (i) $\Sigma \frac{dt^3}{3}$ for open type sections, when d and t are the width and thickness of each element in the section;
- (ii) $\frac{4A_{en}^2}{\Sigma \frac{d}{t}}$ for closed type sections, when A_{en} is the area enclosed by the middle planes of the elements, and d and t are as defined above.

However, for the following reasons, it is recommended that the transverse stiffeners should be designed to be sufficiently stiff so as not to buckle before the longitudinal stiffeners:

- (i) Transverse stiffeners often form part of the internal cross-frames of box girders resisting angular distortion of the box section when subjected to torsion;
- (ii) interactive buckling between longitudinal and transverse stiffeners will be highly sensitive to initial imperfections [32,33];
- (iii) top flange transverse stiffeners must support lateral loading on the deck.

Thus, for such designs, instead of overall buckling of the whole flange involving one or more transverse stiffeners in one half-wave-length, local buckling of the flange between adjacent transverse stiffeners is going to be a more important consideration. In this case the orthotropic plate is represented by the longitudinally stiffened panel between the cross-frames. Since the transverse stiffeners do not contribute to the flexural rigidities D_x , D_y and H in this mode of buckling, these can be taken as follows:

$$D_x = \frac{EI_x}{b'}$$

$$D_y = \frac{Et^3}{12(1-\nu^2)}$$

$$H = \frac{Gt^3}{6} + \frac{1}{2} \nu_y D_x + \frac{1}{2} \nu_x D_y + \frac{GJ_x}{2b'}$$

where t is the thickness of the flange plate,

$$\nu_x = \nu \frac{b't}{b't + A_{sx}}$$

I_x , J_x and A_{sx} are as defined above for longitudinal stiffeners,

$$\nu_y = \nu.$$

For an ideal orthotropic plate, $\nu_y D_x = \nu_x D_y$. In the case of a discretely stiffened compression flange between transverse stiffeners, D_y will be much smaller than D_x and this equality will not usually be satisfied. Moreover, as argued before, contribution of D_x towards torsional rigidity H is uncertain. Hence, it will be prudent to take

$$H = \frac{Gt^3}{6} + \nu_x D_y + \frac{GJ_x}{2b^3}.$$

From equation (9), replacing b by B , total critical load on the entire compression flange is given by:

$$P_{cr} = \sigma_{cr} Bt = \frac{\pi^2}{B} \left[\frac{D_x}{\phi^2} + D_y \phi^2 + 2H \right]$$

The average critical stress on the flange is then:

$$\sigma_{cr} = \frac{\pi^2}{B^2 t_e} \left[\frac{D_x}{\phi^2} + D_y \phi^2 + 2H \right]$$

where $t_e = t + \frac{NA_{sx}}{B}$ = smeared thickness of flange.

From equation (11), the natural half-wave-length of buckling should be $B (D_x/D_y)^{1/4}$; but as D_x/D_y will be very large, the actual half-wave-length will be limited to the spacing L between transverse stiffeners; hence, ϕ must be taken as L/B , leading to:

$$\sigma_{cr} = \frac{\pi^2}{t_e} \left[\frac{D_x}{L^2} + \frac{D_y L^2}{B^4} + \frac{2H}{B^2} \right] \dots \dots (13)$$

provided $\frac{D_x}{D_y} > \left(\frac{L}{B}\right)^4$

For torsionally weak longitudinal stiffeners, i.e. open stiffeners, D_y and H are negligible compared to D_x for buckling between transverse stiffeners. For overall buckling H is negligible but $D_y = \frac{EI_y}{L}$.

The minimum value of the second moment of area I_y of transverse stiffeners, necessary to ensure that overall buckling is not more critical than local buckling, may be obtained by using equations (10) and (13), i.e.:

$$\frac{2\pi^2}{t_e B^2} \sqrt{D_x D_y} > \frac{\pi^2}{t_e} \frac{D_x}{L^2}$$

leading to:

$$I_y > \frac{B^4 I_x}{4b' L^3} .$$

The above result is only true for elastic critical buckling of ideally flat stiffened panels; however, if I_y is only just above this limiting value, interactive buckling between the local and the overall modes is likely to render the system highly sensitive to initial imperfections, and buckling, when it occurs, will be characterised by a sudden unloading^[32,33]. Hence, I_y should be several times the above theoretical value in order to ensure that overall buckling involving deflection of transverse stiffeners will not be as critical as buckling of longitudinal stiffeners between the transverse stiffeners, i.e. that the latter may be assumed to provide non-deflecting support to the former. Hereafter it shall be assumed that transverse stiffeners shall always be designed to satisfy the above requirements.

3. POST-BUCKLING BEHAVIOUR OF ORTHOTROPIC PLATES IN UNIAXIAL COMPRESSION

In Section 2, the critical stress for initial elastic buckling of flat orthotropic plates in uniaxial compression has been derived. The plate can, however, continue to carry higher stresses in a buckled, but still stable form, due to the stretching of the middle plane of the plate. In this section the post-buckling behaviour of orthotropic plates will be analysed by generally following the method given by Bulson^[34] for isotropic plates.

If u , v and w denote the three components of displacements, in the longitudinal, transverse and lateral directions respectively, of any

point in the neutral plane of the plate, then the following relationships between strains and displacements can be derived by geometry:

$$\left. \begin{aligned} e_x &= \frac{\partial u}{\partial x} + \frac{1}{2} \left(\frac{\partial w}{\partial x} \right)^2 \\ e_y &= \frac{\partial v}{\partial y} + \frac{1}{2} \left(\frac{\partial w}{\partial y} \right)^2 \\ e_{xy} &= \frac{\partial u}{\partial y} + \frac{\partial v}{\partial x} + \frac{\partial w}{\partial x} \frac{\partial w}{\partial y} \end{aligned} \right\} \dots \quad (14)$$

By differentiating these expressions, the following compatibility condition between strains and deflection can be obtained:

$$\frac{\partial^2 e_x}{\partial y^2} + \frac{\partial^2 e_y}{\partial x^2} - \frac{\partial^2 e_{xy}}{\partial x \partial y} = \left[\frac{\partial^2 w}{\partial x \partial y} \right]^2 - \frac{\partial^2 w}{\partial x^2} \frac{\partial^2 w}{\partial y^2}$$

Considering a small element dx by dy of the plate and the membrane forces acting on it, the following partial differential equations of equilibrium can be obtained:

$$\frac{\partial \sigma_x}{\partial x} + \frac{\partial \tau_{xy}}{\partial y} = 0$$

$$\frac{\partial \sigma_y}{\partial y} + \frac{\partial \tau_{xy}}{\partial x} = 0$$

We shall use Airy's stress function F , such that:

$$\sigma_x = \frac{\partial^2 F}{\partial y^2} ; \quad \sigma_y = \frac{\partial^2 F}{\partial x^2} ; \quad \tau_{xy} = - \frac{\partial^2 F}{\partial x \partial y} \quad \dots \quad (15)$$

where σ_x , σ_y and τ_{xy} are the membrane stresses at (x, y) .

It can easily be shown that such a stress function automatically satisfies the above membrane equilibrium conditions.

Using Hooke's Law relationships of equations (1), the compatibility condition for orthotropic plates takes the following form:

$$\frac{1}{E_x} \frac{\partial^4 F}{\partial y^4} + \frac{1}{E_y} \frac{\partial^4 F}{\partial x^4} + \left[\frac{1}{G} - \frac{\nu_x}{E_x} - \frac{\nu_y}{E_y} \right] \frac{\partial^4 F}{\partial x^2 \partial y^2} = \left[\frac{\partial^2 w}{\partial x \partial y} \right]^2 - \frac{\partial^2 w}{\partial x^2} \cdot \frac{\partial^2 w}{\partial y^2} \quad \dots \quad (16)$$

This compatibility equation and the equilibrium equation (4) govern the elastic behaviour of orthotropic plates. These are fourth order non-linear equations and few rigorous solutions exist for the various stress patterns and boundary conditions. Marguerre and Trefftz (1937) analysed the post-buckling behaviour of flat rectangular isotropic plates under uniaxial compression by the Rayleigh-Ritz procedure, i.e. first assuming a pattern of deflections and then using the extremum principle of minimum total potential energy - an extremely powerful concept introduced into the theory of elasticity originally by Kirchhoff (1850). This method shall now be extended to orthotropic plates in uniaxial compression.

In the previous section it was shown that the critical buckling mode of an orthotropic plate in uniaxial compression is given by:

$$w = A \cos \frac{\pi x}{l} \cos \frac{\pi y}{b} \quad \dots \quad (17)$$

where b is the width, and

l is the natural half-wave-length of buckling.

We shall now assume that when the applied stress σ_a exceeds the critical value σ_{cr} , the plate buckles in the above mode with an amplitude A which is no longer very small.

The objective is to obtain a relationship between the deflection amplitude A and the applied stress σ_a when $\sigma_a > \sigma_{cr}$. Bending energy of the plate may be obtained either from equation (7), taking $m = n = 1$ and $a = l$, or from a definition of the critical stress which states that a deflected shape with any value of the amplitude A is possible under the action of σ_{cr} . U_b is thus equal to $\sigma_{cr} b t$ times the average shortening of the longitudinal strips due to deflection w . Shortening of any strip is given by:

$$\int_{-l/2}^{+l/2} \frac{1}{2} \left(\frac{\partial w}{\partial x} \right)^2 dx$$

Average shortening over the width b is thus given by:

$$\frac{1}{b} \int_{-b/2}^{+b/2} \int_{-l/2}^{+l/2} \frac{1}{2} \left(\frac{\partial w}{\partial x} \right)^2 dx dy$$

$$= \frac{1}{8} \frac{A^2 \pi^2}{L} , \quad \text{on substitution from equation (15).}$$

Hence, bending energy:

$$U_b = \sigma_{cr} b t \frac{A^2 \pi^2}{8L} \quad \dots\dots \quad (18)$$

After buckling the pattern of membrane stresses σ_x , σ_y and τ_{xy} will no longer remain the same. These membrane stresses and the strain energy due to them depend upon the in-plane boundary conditions along the edges (in addition to the out-of-plane boundary conditions which we already assumed to be free to rotate about the supported edges). In the following two sections, two different types of in-plane boundary conditions along the longitudinal edges will be examined.

4. POST-BUCKLING BEHAVIOUR - LONGITUDINAL EDGES HELD STRAIGHT

For the first set of possible boundary conditions, we shall assume that all the edges remain straight and the plate retains its rectangular outline as it deflects. For the stress function F , an expression similar to the one Bulson^[34] used for isotropic plates may be used, as follows:

$$F = - \left[\frac{1}{2} \sigma_m y^2 + \frac{1}{2} \sigma_n x^2 + \frac{A^2}{32} \left\{ E_x \left(\frac{b}{L} \right)^2 \cos \frac{2\pi y}{b} + E_y \left(\frac{L}{b} \right)^2 \cos \frac{2\pi x}{L} \right\} \right]$$

where σ_m and σ_n are two constant values in units of stress.

The left-hand side of the compatibility equation (16) becomes:

$$- \frac{\pi^4 A^2}{2b^2 L^2} \left\{ \cos \frac{2\pi y}{b} + \cos \frac{2\pi x}{L} \right\}$$

Using equation (17), the right-hand side of the compatibility equation (16) can also be shown to be the same and hence the assumed stress function satisfies the condition of compatibility at all points in the plate. The membrane stresses σ_x , σ_y and τ_{xy} at any point (x, y) can then be obtained from equations (15) by differentiating F , as follows:

$$\left. \begin{aligned}
 \sigma_x &= \frac{\partial^2 F}{\partial y^2} = -\sigma_m + \frac{E_x A^2 b^2}{32l^2} \left[\frac{2\pi}{b} \right]^2 \cos \frac{2\pi y}{b} \\
 \sigma_y &= \frac{\partial^2 F}{\partial x^2} = -\sigma_n + \frac{E_y A^2 l^2}{32b^2} \left[\frac{2\pi}{b} \right]^2 \cos \frac{2\pi x}{l} \\
 \tau_{xy} &= -\frac{\partial^2 F}{\partial x \partial y} = 0
 \end{aligned} \right\} \dots \quad (19)$$

Since $\int_{-b/2}^{+b/2} \cos \frac{2\pi y}{b} dy = \int_{-l/2}^{+l/2} \cos \frac{2\pi x}{l} dx = 0$, we can note the

following interesting features of the stress field in the plate from the above expressions:

- $-\sigma_m$ is the average compressive stress in the x -direction over width b and hence must be identical with the applied loading σ_a ;
- σ_n is the average tensile stress in the y -direction over length l ;
- σ_x depends only on y , and not on x , and hence is constant along any longitudinal strip;
- σ_y depends only on x , and not on y , and hence is constant along any transverse strip;
- τ_{xy} is zero everywhere in the plate.

If we now assume one more boundary condition of no net transverse force along the longitudinal edges, i.e. $\sigma_n = 0$, the stress function F becomes:

$$F = - \left[\frac{1}{2} \sigma_a y^2 + \frac{A^2}{32} \left\{ E_x \left(\frac{b}{l} \right)^2 \cos \frac{2\pi y}{b} + E_y \left(\frac{l}{b} \right)^2 \cos \frac{2\pi x}{l} \right\} \right] \dots (20)$$

Strain energy U_m due to membrane stresses is given by:

$$\begin{aligned}
 U_m &= \frac{t}{2} \int_{-l/2}^{+l/2} \int_{-b/2}^{+b/2} (\sigma_x e_x + \sigma_y e_y + \tau_{xy} e_{xy}) dx dy \\
 &= \frac{t}{2} \int_{-l/2}^{+l/2} \int_{-b/2}^{+b/2} \left[\frac{\sigma_x^2}{E_x} + \frac{\sigma_y^2}{E_y} - \sigma_x \sigma_y \left(\frac{\nu_x}{E_x} + \frac{\nu_y}{E_y} \right) + \frac{\tau_{xy}^2}{G} \right] dx dy
 \end{aligned}$$

Substitution from equation (19), and noting that the integration of the third and the fourth terms are both zero, leads to:

$$U_m = \frac{\sigma_a^2 b l t}{2E_x} + \frac{\pi^4 A^4 b l t}{256} \left[\frac{E_x}{l^4} + \frac{E_y}{b^4} \right] \dots \quad (21)$$

Total internal energy U is the sum of the strain energy due to bending and membrane stresses. Hence from equations (18) and (21):

$$\dot{U} = U_b + U_m = \frac{\pi^2 A^2 b t \sigma_{cr}}{8l} + \frac{\sigma_a^2 b l t}{2E_x} + \frac{\pi^4 A^4 b l t}{256} \left[\frac{E_x}{l^4} + \frac{E_y}{b^4} \right] \dots \quad (22)$$

Potential energy T of the applied loads is the negative product of the external forces and the displacements of their points of application in the direction of the forces; the negative sign arises from the principle of conservation of energy, i.e. any work done by the forces causes a reduction in their potential energy.

From equations (1) and (14):

$$\frac{\partial u}{\partial x} = \frac{\sigma_x}{E_x} - \frac{\nu_x \sigma_y}{E_x} - \frac{1}{2} \left[\frac{\partial w}{\partial x} \right]^2$$

Substitution for w from equation (17), for σ_x and σ_y from equations (19) with $\sigma_m = \sigma_a$ and $\sigma_n = 0$, and integrating over length l , total change of length Δl is obtained as:

$$\Delta l = \int_{-l/2}^{+l/2} \frac{\partial u}{\partial x} dx = -\frac{\sigma_a l}{E_x} - \frac{\pi^2 A^2}{8l}$$

where negative sign indicates shortening.

It is evident that the total shortening of the longitudinal strips does not depend on y , i.e. loaded edges are displaced uniformly. Similarly, it can be shown that the total shortening Δb of the transverse strips is also uniform and is equal to $-\frac{\pi^2 A^2}{8b}$. Hence:

$$\begin{aligned} T &= (-) (-\sigma_a b t) \left[-\frac{\sigma_a l}{E_x} - \frac{\pi^2 A^2}{8l} \right] \dots \quad (23) \\ &= -\frac{\sigma_a^2 l b t}{E_x} - \frac{\pi^2 A^2 \sigma_a b t}{8l} \end{aligned}$$

From the principles of stationary total potential energy, for stable equilibrium, the first derivative of total potential energy ($U+T$) with respect to the unknown deflection parameter A must be zero, i.e. from equations (22) and (23):

$$\frac{\pi^2 A b t \sigma_{cr}}{4l} + \frac{\pi^4 A^3 b l t}{64} \left[\frac{E_x}{l^4} + \frac{E_y}{b^4} \right] - \frac{\pi^2 A \sigma_a b t}{4l} = 0$$

or

$$(\sigma_a - \sigma_{cr}) = \frac{\pi^2 A^2 l^2}{16} \left[\frac{E_x}{l^4} + \frac{E_y}{b^4} \right] \quad \dots \quad (24)$$

Apparent longitudinal strain e_a is given by:

$$\begin{aligned} e_a &= -\frac{\Delta l}{l} = \frac{\sigma_a}{E_x} + \frac{\pi^2 A^2}{8l^2} \\ &= \frac{1}{E_x} \left[\sigma_a + 2 (\sigma_a - \sigma_{cr}) \frac{E_x b^4}{E_x b^4 + E_y l^4} \right] \end{aligned}$$

For an isotropic plate the natural half-wave-length of buckling l is equal to b and $E_x = E_y$. For an ideal orthotropic plate of uniform thickness, the orthotropy is due to varying Young's modulus in the orthogonal directions; using equations (11) and (3) the natural half-wave-length of buckling l is given by:

$$l = b \left(\frac{D_x}{D_y} \right)^{\frac{1}{4}} = b \left(\frac{E_x}{E_y} \right)^{\frac{1}{4}}$$

Hence, in either of the above two cases, apparent compressive longitudinal strain is:

$$\begin{aligned} e_a &= -\frac{\Delta l}{l} = \frac{1}{E_x} \left[\sigma_a + (\sigma_a - \sigma_{cr}) \right] \\ &= \frac{1}{E_x} \left[\sigma_{cr} + 2 (\sigma_a - \sigma_{cr}) \right] \quad \dots \quad (25) \end{aligned}$$

This shows that the post-buckling stiffness of an isotropic or ideally orthotropic plate is half of that of the unbuckled plate. This

is in agreement with results obtained by Marguerre and Trefftz [35], Yamaki [36], and Stein [37]. The relationship between applied stress and deflection can be obtained from equation (24) as:

$$\begin{aligned}\sigma_a &= \sigma_{cr} + \frac{\pi^2 A^2 l^2}{16} \left[\frac{E_x}{l^4} + \frac{E_y}{b^4} \right] \\ &= \sigma_{cr} + \frac{\pi^2 A^2 E_x}{8l^2}\end{aligned}$$

for isotropic or ideally orthotropic plate. The longitudinal stresses at any point are given from equations (19) and (24) by:

$$\begin{aligned}-\sigma_x &= \sigma_{cr} + \frac{\pi^2 A^2 l^2}{16} \left[\frac{E_x}{l^4} + \frac{E_y}{b^4} \right] - \frac{\pi^2 A^2 E_x}{8l^2} \cos \frac{2\pi y}{b} \\ &= \sigma_{cr} + \frac{\pi^2 A^2 E_x}{8l^2} \left[1 - \cos \frac{2\pi y}{b} \right]\end{aligned}$$

for isotropic or ideally orthotropic plates.

5. POST-BUCKLING BEHAVIOUR - LONGITUDINAL EDGES FREE TO PULL-IN

The boundary condition for longitudinal edges completely free for in-plane displacement, i.e. $\sigma_y = 0$ when $y = \pm b/2$, is much more difficult to solve, as a simple form of stress function satisfying the equilibrium and compatibility conditions everywhere and boundary conditions on the edges is not available. Hemp [38], Coan [39], Yamaki [36], and Cox [40] solved the case of square isotropic plates, and Massonnet and Maquoi [22] (1973) solved the general case of an orthotropic plate; but these solutions are too complex for design purposes. Walker [41,42] produced approximate explicit functions relating deflections to applied edge loading for isotropic square plates.

In order to obtain a simple approximate solution applicable to both isotropic and orthotropic plates, it shall be assumed that σ_y is zero everywhere in the plate and not just on the longitudinal edges; this assumption is borne out by some experimental evidence as well [43].

From equilibrium equations for membrane forces and from the condition that shear stresses along the edges are zero, it follows from this

assumption that τ_{xy} is also zero everywhere and σ_x is constant along any longitudinal strip. Falconer and Chapman^[44] analysed the large-deflection behaviour of an infinitely long orthogonally stiffened panel with the assumptions of zero transverse and shear stresses everywhere in the panel. They, however, took the half-wave-length of buckling ' l ' in the longitudinal direction to be a variable quantity; the "gravest" half-wave-length was calculated by minimising the average compressive force σ_a with respect to l . This, however, led to a series of rather complicated expressions. As has already been explained in Section 2, if the stiffened panel is provided with substantial transverse stiffeners then the critical half-wave-length of buckling will be the spacing L between such transverse stiffeners. In the following analysis the post-buckled deflected shape is assumed to be the same as the mode of critical buckling, i.e.:

$$w = A \cos \frac{\pi x}{l} \cos \frac{\pi y}{b}$$

It is now necessary to establish the relationship between deflection amplitude A and applied stress σ . The bending strain energy will be given by equation (18), i.e.:

$$U_b = \sigma_{cr} b t \frac{A^2 \pi^2}{8l}$$

Since σ_y and τ_{xy} are assumed zero everywhere, strain energy due to membrane forces will be given by:

$$\begin{aligned} U_m &= \frac{t}{2} \int_{-b/2}^{+b/2} \int_{-l/2}^{+l/2} \frac{\sigma_x^2}{E_x} dx dy \\ &= \frac{lt}{2E_x} \int_{-b/2}^{+b/2} \sigma_x^2 dy \end{aligned}$$

since σ_x is independent of x . Total strain energy $U = U_b + U_m$.

Rate of change of U with respect to deflection amplitude A is given by:

$$\frac{dU}{dA} = \sigma_{cr} b t \frac{A \pi^2}{4l} + \frac{lt}{E_x} \int_{-b/2}^{+b/2} \sigma_x \frac{d\sigma_x}{dA} dy \quad \dots \quad (26)$$

From equations (1) and (14), since $\sigma_y = 0$:

$$\begin{aligned}\frac{\partial u}{\partial x} &= \frac{\sigma_x}{E_x} - \frac{1}{2} \left[\frac{\partial w}{\partial x} \right]^2 \\ &= \frac{\sigma_x}{E_x} - \frac{1}{2} \frac{\pi^2 A^2}{l^2} \sin^2 \frac{\pi x}{l} \cos^2 \frac{\pi y}{b}\end{aligned}$$

Total change of length ΔL is:

$$\Delta L = \int_{-l/2}^{+l/2} \frac{\partial u}{\partial x} dx = \frac{\sigma_x l}{E_x} - \frac{A^2 \pi^2}{4l} \cos^2 \frac{\pi y}{b} \quad \dots \quad (27)$$

Potential energy T of applied loads = (-) work done by loads:

$$\begin{aligned}&= - \int_{-b/2}^{+b/2} \sigma_x t dy \Delta L \\ &= - \frac{t l}{E_x} \int_{-b/2}^{+b/2} \sigma_x^2 dy + \frac{A^2 \pi^2 t}{4l} \int_{-b/2}^{+b/2} \sigma_x \cos^2 \frac{\pi y}{b} dy\end{aligned}$$

Rate of change of T with respect to deflection amplitude A is given by:

$$\begin{aligned}\frac{dT}{dA} &= - \frac{t l}{E_x} \int_{-b/2}^{+b/2} 2\sigma_x \frac{\partial \sigma_x}{\partial A} dy + \frac{A^2 \pi^2 t}{4l} \int_{-b/2}^{+b/2} \frac{\partial \sigma_x}{\partial A} \cos^2 \frac{\pi y}{b} dy \\ &\quad + \frac{A \pi^2 t}{2l} \int_{-b/2}^{+b/2} \sigma_x \cos^2 \frac{\pi y}{b} dy \quad \dots \quad (28)\end{aligned}$$

From (27):

$$\sigma_x = \frac{\Delta L E_x}{l} + \frac{E_x A^2 \pi^2}{4l^2} \cos^2 \frac{\pi y}{b}$$

Hence

$$\begin{aligned}\frac{t l}{E_x} \int_{-b/2}^{+b/2} \sigma_x \frac{\partial \sigma_x}{\partial A} dy &= \int_{-b/2}^{+b/2} t \Delta L \frac{\partial \sigma_x}{\partial A} dy \\ &\quad + \frac{t A^2 \pi^2}{4l} \int_{-b/2}^{+b/2} \frac{\partial \sigma_x}{\partial A} \cos^2 \frac{\pi y}{b} dy\end{aligned}$$

The loaded edges are assumed to approach each other uniformly. Hence, Δl is not a function of y . Taking Δl outside the integral sign, the first integral above is the change in the total applied load, which is zero.

The second term above is identical to the second term in equation (28). The third term in equation (28):

$$\begin{aligned} &= \frac{A\pi^2 t}{2l} \int_{-b/2}^{+b/2} \left[\frac{\Delta l E_x}{l} + \frac{E_x A^2 \pi^2}{4l^2} \cos^2 \frac{\pi y}{b} \right] \cos^2 \frac{\pi y}{b} dy \\ &= \frac{A\pi^2 t}{2l} \left[\frac{\Delta l E_x}{l} \frac{b}{2} + \frac{E_x A^2 \pi^2}{4l^2} \frac{3}{8} b \right] \end{aligned}$$

Hence:

$$\frac{dT}{dA} = - \frac{t l}{E_x} \int_{-b/2}^{+b/2} \sigma_x \frac{d\sigma_x}{dA} dy + \frac{A\pi^2 t}{2l} \left[\frac{\Delta l b E_x}{2l} + \frac{E_x A^2 \pi^2 b}{l^2} \frac{3}{32} \right] \quad \dots \quad (29)$$

From the principle of minimum total potential energy:

$$\frac{d}{dA} (U + T) = \frac{dU}{dA} + \frac{dT}{dA} = 0$$

Hence from (26) and (29):

$$\sigma_{cr} b t \frac{A\pi^2}{4l} + \frac{A\pi^2 t}{2l} \left[\frac{\Delta l b E_x}{2l} + \frac{E_x A^2 \pi^2 b}{l^2} \frac{3}{32} \right] = 0$$

wherefrom:

$$-\Delta l = \sigma_{cr} \frac{l}{E_x} + \frac{3}{16} \frac{A^2 \pi^2}{l} \quad \dots \quad (30)$$

Substituting for Δl from (30) in (27):

$$-\sigma_x = \sigma_{cr} + \frac{3}{16} \frac{E_x A^2 \pi^2}{l^2} - \frac{E_x A^2 \pi^2}{4l^2} \cos^2 \frac{\pi y}{b}$$

the negative sign for σ_x indicating compression.

Maximum longitudinal stress occurs at $y = \pm b/2$ and is given by:

$$\sigma_{max} = \sigma_{cr} + \frac{3}{16} \frac{E_x A^2 \pi^2}{l^2}$$

Minimum longitudinal stress occurs at $y = 0$ and is given by:

$$\sigma_{min} = \sigma_{cr} - \frac{1}{16} \frac{E_x A^2 \pi^2}{l^2}$$

Integrating over width b , the average longitudinal stress is given by:

$$\sigma_a = \sigma_{cr} + \frac{1}{16} \frac{A^2 \pi^2 E_x}{l^2}$$

(31)

This equation gives the relationship between applied load and deflection of the plate.

The apparent strain:

$$e_a = -\frac{\Delta l}{l} = \frac{\sigma_{cr}}{E_x} + \frac{3}{16} \frac{A^2 \pi^2}{l^2} = \frac{\sigma_{max}}{E_x} \quad \dots \quad (32)$$

From (31) and (32), denoting $\frac{\sigma_{cr}}{E_x}$ by e_{cr} :

$$(\sigma_a - \sigma_{cr}) = \frac{E_x}{3} (e_a - e_{cr})$$

i.e. the post-buckling stiffness of the plate is one-third of that of the unbuckled plate.

The above fairly simple expressions are valid for both isotropic and orthotropic plates and their derivation has been possible because of the simplifying assumption of σ_y as zero everywhere in the plate. More exact solutions have been obtained for isotropic plates [36,38,40]; these indicate that the post-buckling stiffness is 0.41 times that of the unbuckled plate. Hence the simpler solutions given above are conservative.

CHAPTER 5

BUCKLING BEHAVIOUR OF AN INITIALLY IMPERFECT PLATE CONSTRAINED
TO REMAIN STRAIGHT ALONG LONGITUDINAL EDGES - ITS
APPLICATION TO PLATE PANEL BEHAVIOUR

1. PLATES WITH INITIAL GEOMETRIC IMPERFECTIONS

We shall assume both initial and final deflections to be in the preferred buckling mode of the orthotropic plate, i.e.

$$\left. \begin{aligned} \text{Initial deflection } w_0 &= A_0 \cos \frac{\pi x}{l} \cos \frac{\pi y}{b} \\ \text{Final deflection } w &= A \cos \frac{\pi x}{l} \cos \frac{\pi y}{b} \end{aligned} \right\} \dots \quad (1)$$

where l is the natural half wave length of the elastic critical buckling mode.

The flexure of the plate will be associated with the change of shape given by:

$$(A - A_0) \cos \frac{\pi x}{l} \cos \frac{\pi y}{b}$$

Hence equation (18) of Chapter 4 must be modified as given below for the bending energy U_b :

$$U_b = \sigma_{cr} bt \frac{\pi^2}{8l} (A - A_0)^2 \quad \dots \quad (2)$$

The relationships between strains, displacements and stresses given in equations (1) and (14) of Chapter 4 for flat plates become:

$$\left. \begin{aligned} e_x &= \frac{\partial u}{\partial x} + \frac{1}{2} \left(\frac{\partial w}{\partial x} \right)^2 - \frac{1}{2} \left(\frac{\partial w_0}{\partial x} \right)^2 = \frac{1}{E_x} (\sigma_x - \nu_x \sigma_y) \\ e_y &= \frac{\partial v}{\partial y} + \frac{1}{2} \left(\frac{\partial w}{\partial y} \right)^2 - \frac{1}{2} \left(\frac{\partial w_0}{\partial y} \right)^2 = \frac{1}{E_y} (\sigma_y - \nu_y \sigma_x) \\ e_{xy} &= \frac{\partial u}{\partial y} + \frac{\partial v}{\partial x} + \frac{\partial w}{\partial x} \frac{\partial w}{\partial y} - \frac{\partial w_0}{\partial x} \frac{\partial w_0}{\partial y} = \frac{\tau_{xy}}{G} \end{aligned} \right\} \dots \quad (3)$$

The compatibility equation (16) of Chapter 4 becomes:

$$\frac{1}{E_x} \frac{\partial^4 F}{\partial y^4} + \frac{1}{E_y} \frac{\partial^4 F}{\partial x^4} + \left[\frac{1}{G} - \frac{\nu_x}{E_x} - \frac{\nu_y}{E_y} \right] \frac{\partial^4 F}{\partial x^2 \cdot \partial y^2} = \dots \quad (4)$$

$$\left[\frac{\partial^2 w}{\partial x \partial y} \right]^2 - \left[\frac{\partial^2 w_0}{\partial x \partial y} \right]^2 - \frac{\partial^2 w}{\partial x^2} \cdot \frac{\partial^2 w}{\partial y^2} + \frac{\partial^2 w_0}{\partial x^2} \cdot \frac{\partial^2 w_0}{\partial y^2}$$

For individual flange plate panels between the stiffening ribs it shall be assumed that the net transverse force along the longitudinal edges is zero; then the stress function F given by equation (20), Chapter 4, is modified as follows:

$$F = - \left[\frac{1}{2} \sigma_a y^2 + \frac{A^2 - A_0^2}{32} \left\{ E_x \left(\frac{b}{l} \right)^2 \cos \frac{2\pi y}{b} + E_y \left(\frac{l}{b} \right)^2 \cos \frac{2\pi x}{l} \right\} \right] \dots \quad (5)$$

Similarly, the strain energy U_m due to membrane stresses will be given by the following:

$$U_m = \frac{\sigma_a^2 b l t}{2 E_x} + \frac{(A^2 - A_0^2)^2 \pi^4 b l t}{256} \left[\frac{E_x}{l^4} + \frac{E_y}{b^4} \right] \dots \quad (6)$$

The total internal energy U will be the sum of (2) and (6).

From equation (3):

$$\frac{\partial u}{\partial x} = \frac{\sigma_x}{E_x} - \frac{\nu_x \sigma_y}{E_x} - \frac{1}{2} \left[\frac{\partial w}{\partial x} \right]^2 + \frac{1}{2} \left[\frac{\partial w_0}{\partial x} \right]^2$$

σ_x and σ_y may be obtained by differentiating F ; substituting these expressions we get:

$$\text{Shortening } \Delta l = \int_{-l/2}^{+l/2} \frac{\partial u}{\partial x} dx = - \frac{\sigma_a l}{E_x} - \frac{\pi^2}{8l} (A^2 - A_0^2)$$

$$\text{and potential energy } T = \sigma_a b t \cdot \Delta l = - \left[\frac{\sigma_a^2 b l t}{E_x} + \frac{\pi^2 (A^2 - A_0^2) \sigma_a b t}{8l} \right] \dots \quad (7)$$

From the condition $\frac{\partial}{\partial A} (U + T) = 0$,

$$\frac{\pi^2 (A - A_0) b t \sigma_{cr}}{4l} + \frac{\pi^4 b l t}{64} \left[\frac{E_x}{l^4} + \frac{E_y}{b^4} \right] (A^2 - A_0^2) A - \frac{\pi^2 A \sigma_a b t}{4l} = 0 \dots \quad (8)$$

The above equation gives the final deflection amplitude A for any given initial deflection amplitude A_0 and applied stress σ_a .

For a long isotropic plate $E_x = E_y = E$ and $l = b$. Taking $A = mA_0$, when m is the magnification factor A/A_0 of the deflections, equation (8) reduces to:

$$\sigma_a = \sigma_{cr} \left(1 - \frac{1}{m}\right) + \frac{\pi^2 EA_0^2}{8b^2} (m^2 - 1) \quad \dots \quad (9)$$

The stress function F given in equation (5) reduces to the following for isotropic plates:

$$F = - \left[\frac{1}{2} \sigma_a y^2 + \frac{(m^2 - 1) A_0^2 E}{32} \left\{ \cos \frac{2\pi y}{b} + \cos \frac{2\pi x}{b} \right\} \right]$$

Differentiating F in accordance with equations (15), Chapter 4:

$$\left. \begin{aligned} \sigma_x &= \frac{\partial^2 F}{\partial y^2} = - \left[\sigma_{cr} \left(1 - \frac{1}{m}\right) + \frac{\pi^2 EA_0^2}{8b^2} (m^2 - 1) \left(1 - \cos \frac{2\pi y}{b}\right) \right] \\ \sigma_y &= \frac{\partial^2 F}{\partial x^2} = + \frac{\pi^2 (m^2 - 1) A_0^2 E}{8b^2} \cos \frac{2\pi x}{b} \\ \tau_{xy} &= 0 \end{aligned} \right\} \quad (10)$$

The above results are summarised by the following equations:

$$\left. \begin{aligned} \text{Average stress, } - \sigma_a &= \sigma_{cr} \left(1 - \frac{1}{m}\right) + \frac{3}{8} (1 - \nu^2) \sigma_{cr} \left[\frac{A_0}{t}\right]^2 (m^2 - 1) \\ \text{Longitudinal edge stress, } - \sigma_e &= \sigma_{cr} \left(1 - \frac{1}{m}\right) + \frac{3}{4} (1 - \nu^2) \sigma_{cr} \left[\frac{A_0}{t}\right]^2 (m^2 - 1) \\ \text{Apparent strain, } - e_a &= -\frac{\Delta l}{l} = \frac{1}{E} \left[\sigma_{cr} \left(1 - \frac{1}{m}\right) + \frac{3}{4} (1 - \nu^2) \sigma_{cr} \left[\frac{A_0}{t}\right]^2 (m^2 - 1) \right] \\ &= -\frac{\sigma_e}{E} \end{aligned} \right\} \quad (11)$$

Secant stiffness, $K_s = \frac{\text{Average stress}}{\text{Apparent strain} \times E} =$

$$\begin{aligned}
 &= \frac{1 + \frac{3}{8} (1 - \nu^2) \left[\frac{A_0}{t} \right]^2 m(m+1)}{1 + \frac{3}{4} (1 - \nu^2) \left[\frac{A_0}{t} \right]^2 m(m+1)} \\
 \text{Tangent stiffness } K_t &= \frac{d\sigma_a}{d\left(\frac{\Delta L}{L}\right)} \times \frac{1}{E} = \frac{d\sigma_a}{dm} \cdot \frac{dm}{d\left(\frac{\Delta L}{L}\right)} \times \frac{1}{E} \\
 &= \frac{1 + \frac{3}{4} (1 - \nu^2) \left[\frac{A_0}{t} \right]^2 m^3}{1 + \frac{3}{2} (1 - \nu^2) \left[\frac{A_0}{t} \right]^2 m^3}
 \end{aligned} \tag{11}$$

From equation (10) it may be noticed that the transverse stresses vary from maximum tensile at $x = 0$ to maximum compressive at $x = \pm b/2$, these maximum values being:

$$\frac{\pi^2 (m^2 - 1) A_0^2 E}{8b^2} = \frac{3}{8} \sigma_{cr} (1 - \nu^2) \left[\frac{A_0}{t} \right]^2 (m^2 - 1) \dots \tag{12}$$

Using the Hencky - von Mises formula for equivalent stress, i.e.

$$\sigma_{eq}^2 = \sigma_x^2 + \sigma_y^2 - \sigma_x \sigma_y + 3 \tau^2$$

and neglecting flexural stresses, the maximum equivalent stress $\sigma_{eq_{max}}$ in the mid-plane of the plate will occur at $x = 0$, $y = \pm b/2$, and is given by:

$$\begin{aligned}
 \sigma_{eq_{max}}^2 &= \left[\sigma_{cr} \left(1 - \frac{1}{m} \right) \right]^2 + \left[\frac{3}{4} (1 - \nu^2) \sigma_{cr} \left(\frac{A_0}{t} \right)^2 (m^2 - 1) \right]^2 \\
 &+ 2 \sigma_{cr} \left(1 - \frac{1}{m} \right) \frac{3}{4} (1 - \nu^2) \sigma_{cr} \left[\frac{A_0}{t} \right]^2 (m^2 - 1) \\
 &+ \left[\frac{3}{8} \sigma_{cr} (1 - \nu^2) \left(\frac{A_0}{t} \right)^2 (m^2 - 1) \right]^2 \\
 &+ \sigma_{cr} \left(1 - \frac{1}{m} \right) \frac{3}{8} \sigma_{cr} (1 - \nu^2) \left(\frac{A_0}{t} \right)^2 (m^2 - 1) \\
 &+ \frac{3}{4} \cdot \frac{3}{8} \left[\sigma_{cr} (1 - \nu^2) \left(\frac{A_0}{t} \right)^2 (m^2 - 1) \right]^2
 \end{aligned}$$

$$\begin{aligned}
&= \left\{ \sigma_{cr} \left(1 - \frac{1}{m} \right) \right\}^2 + \left\{ (1 - \nu^2) \sigma_{cr} \left(\frac{A_o}{t} \right)^2 (m^2 - 1) \right\}^2 \left\{ \frac{9}{16} + \frac{9}{64} + \frac{9}{32} \right\} \\
&\quad + 2 \sigma_{cr} \left(1 - \frac{1}{m} \right) (1 - \nu^2) \sigma_{cr} \left(\frac{A_o}{t} \right)^2 (m^2 - 1) \left\{ \frac{3}{4} + \frac{3}{16} \right\} \\
&= \left\{ \sigma_{cr} \left(1 - \frac{1}{m} \right) \right\}^2 + \left\{ (1 - \nu^2) \sigma_{cr} \left(\frac{A_o}{t} \right)^2 (m^2 - 1) \frac{\sqrt{63}}{8} \right\}^2 \\
&\quad + 2 \sigma_{cr} \left(1 - \frac{1}{m} \right) (1 - \nu^2) \sigma_{cr} \left(\frac{A_o}{t} \right)^2 (m^2 - 1) \frac{15}{16}
\end{aligned}$$

Since $\frac{15}{16}$ and $\frac{\sqrt{63}}{8}$ are approximately equal to one, σ_{eqmax} can be conservatively approximated as:

$$\sigma_{cr} \left(1 - \frac{1}{m} \right) + \sigma_{cr} (1 - \nu^2) \left[\frac{A_o}{t} \right]^2 (m^2 - 1)$$

It shall now be assumed that the plate behaves elastically until σ_{eqmax} reaches the yield stress σ_{ys} , i.e.

$$\sigma_{cr} \left(1 - \frac{1}{m_e} \right) + \sigma_{cr} (1 - \nu^2) \left[\frac{A_o}{t} \right]^2 (m_e^2 - 1) = \sigma_{ys}$$

$$\text{or, } 0.91 \left[\frac{A_o}{t} \right]^2 m_e^2 - \frac{1}{m_e} = \frac{\sigma_{ys}}{\sigma_{cr}} + 0.91 \left[\frac{A_o}{t} \right]^2 - 1 \quad \dots \quad (13)$$

where m_e is the magnification of initial deflections at the limit of the primarily elastic phase, and

ν is taken as 0.3.

It is further postulated that the ultimate strength of the plate is reached when the average mid-plane equivalent stress at the edges $y = \pm \frac{b}{2}$ reaches yield stress. Transverse stresses σ_y vary from tension to compression and the average value in either the tensile or the compressive zone is:

$$\frac{2}{\pi} (\text{max value}) = \frac{\pi}{4b^2} (m^2 - 1) A_o^2 E = \frac{3}{4\pi} \sigma_{cr} \left[\frac{A_o}{t} \right]^2 (1 - \nu^2) (m^2 - 1)$$

In the tensile zone of transverse stress the average equivalent stress is given by the square root of:

$$\sigma_{cr}^2 \left(1 - \frac{1}{m} \right)^2 + \left[\frac{3}{4} \sigma_{cr} (1 - \nu^2) \left(\frac{A_o}{t} \right)^2 (m^2 - 1) \right]^2 +$$

$$\begin{aligned}
& + 2\sigma_{cr} \left(1 - \frac{1}{m}\right) \frac{3}{4} \sigma_{cr} (1 - \nu^2) \left[\frac{A_0}{t}\right]^2 (m^2 - 1) \\
& + \left[\frac{3}{4\pi} \sigma_{cr} \left(\frac{A_0}{t}\right)^2 (1 - \nu^2) (m^2 - 1)\right]^2 \\
& + \left[\sigma_{cr} \left(1 - \frac{1}{m}\right) + \frac{3}{4} \sigma_{cr} (1 - \nu^2) \left(\frac{A_0}{t}\right)^2 (m^2 - 1)\right] \\
& \quad \left[\frac{3}{4\pi} \sigma_{cr} \left(\frac{A_0}{t}\right)^2 (1 - \nu^2) (m^2 - 1)\right]
\end{aligned}$$

In the compressive zone of transverse stress the average equivalent stress is given by the square root of the same expression except that the last term is negative.

As an approximation, the average equivalent stress along the whole edge may be taken as the square root of the above expression but ignoring the last term, i.e. square root of:

$$\begin{aligned}
& \sigma_{cr}^2 \left(1 - \frac{1}{m}\right)^2 + \left[\frac{3}{4} \sigma_{cr} (1 - \nu^2) \left(\frac{A_0}{t}\right)^2 (m^2 - 1)\right]^2 \\
& + 2\sigma_{cr} \left(1 - \frac{1}{m}\right) \frac{3}{4} \sigma_{cr} (1 - \nu^2) \left(\frac{A_0}{t}\right)^2 (m^2 - 1) \\
& + \left[\frac{3}{4\pi} \sigma_{cr} \left(\frac{A_0}{t}\right)^2 (1 - \nu^2) (m^2 - 1)\right]^2 \\
& = \sigma_{cr}^2 \left(1 - \frac{1}{m}\right)^2 + \left[\sigma_{cr} \left(\frac{A_0}{t}\right)^2 (1 - \nu^2) (m^2 - 1) 0.787\right]^2 \\
& + 2\sigma_{cr} \left(1 - \frac{1}{m}\right) 0.75 \sigma_{cr} (1 - \nu^2) \left(\frac{A_0}{t}\right)^2 (m^2 - 1)
\end{aligned}$$

Since 0.787 is approximately equal to 0.75, the average equivalent stress on the edge may be further simplified to:

$$\sigma_{eq_{av}} = \sigma_{cr} \left(1 - \frac{1}{m}\right) + 0.77 \sigma_{cr} (1 - \nu^2) \left(\frac{A_0}{t}\right)^2 (m^2 - 1)$$

Equating the above to yield stress and denoting the magnification factor at the ultimate state by m_u , the expression needed to calculate the ultimate strength is:

$$\sigma_{cr} \left(1 - \frac{1}{m_u}\right) + 0.77 \sigma_{cr} (1 - \nu^2) \left(\frac{A_0}{t}\right)^2 (m_u^2 - 1) = \sigma_{ys}$$

or, taking $\nu = 0.3$,

$$0.7 \left(\frac{A_o}{t}\right)^2 m_u^2 - \frac{1}{m_u} = \frac{\sigma_{ys}}{\sigma_{cr}} + 0.7 \left(\frac{A_o}{t}\right)^2 - 1 \quad \dots \quad (14)$$

By solving the cubical equations (13) and (14), m_e and m_u can be evaluated. Using these values for m the average stresses σ_{ae} and σ_{au} , and apparent strains e_{ae} and e_{au} , for the elastic limit and ultimate states respectively may be obtained from equations (11). However, because of the gradual spread of plasticity after reaching m_e , it shall be postulated that in the post-elastic phase, i.e. when the average stress increases from σ_{ae} to σ_{au} , the apparent strain will increase at twice the rate predicted by the above elastic theory, i.e. apparent strain at the ultimate stage will be increased by $(e_{au} - e_{ae})$ to a value $(2e_{au} - e_{ae})$.

The above postulations were verified against results of elasto-plastic plate analysis based on a finite difference/dynamic relaxation method^[17]. For the following examples of mild steel plates ($\sigma_{ys} = 245 \text{ N/mm}^2$), stresses and deformations are calculated using the above theory and shown in the table below:

| b/t | A_o/t | m_e | σ_{ae}/σ_{ys} | Ee_{ae}/σ_{ys} | m_u | σ_{au}/σ_{ys} | Ee_{au}/σ_{ys} |
|-------|---------|--------|---------------------------|-----------------------|--------|---------------------------|-----------------------|
| 20 | .167 | 1.1422 | .96 | .98 | 1.1444 | .9765 | 1.0176 |
| 30 | .375 | 1.2768 | .83 | .9316 | 1.2985 | .883 | 1.0556 |
| 40 | .667 | 1.3116 | .656 | .863 | 1.3595 | .743 | 1.1110 |
| 60 | 1.5 | 1.2217 | .47 | .7877 | 1.2726 | .580 | 1.1723 |

TABLE 1: STRESSES AND STRAINS OF PLATES AT ELASTIC LIMIT AND ULTIMATE STATE ($\sigma_{ys} = 245 \text{ N/mm}^2$)

When the two crucial points $\left[\frac{\sigma_{ae}}{\sigma_{ys}}, \frac{Ee_{ae}}{\sigma_{ys}} \right]$ and $\left[\frac{\sigma_{au}}{\sigma_{ys}}, \frac{Ee_{au}}{\sigma_{ys}} \right]$, - representing the elastic limit and the ultimate state respectively - are plotted on the load-shortening curves obtained by Frieze, et al.^[17], as shown by points (1) and (2) in Figs 20a to 20d, very close agreement is found. This comparison illustrates good correlation between the approximate theory just presented and the more rigorous elasto-plastic theory.

Solution of the cubic equations (13) and (14) for m involves successive approximation. The right hand side of the equations can be evaluated for the given data of plate dimensions and the magnitude of initial imperfection A_0 . If the right hand side is designated J , then:

$$\frac{dJ}{dm_e} = 1.82 \left(\frac{A_0}{t} \right)^2 m_e + \frac{1}{m_e^2}; \quad \frac{dJ}{dm_u} = 1.4 \left(\frac{A_0}{t} \right)^2 m_u + \frac{1}{m_u^2}$$

For any guessed value of m_e , say m_{e1} , the left hand side of the equation (13) and $\frac{dJ}{dm_e}$, say J_1 and $\frac{dJ}{dm_{e1}}$ respectively, can be calculated. The next approximation for m_e is given by:

$$m_{e2} = m_{e1} - \frac{J_1 - J}{dJ/dm_{e1}}, \quad \text{and so on.}$$

Similarly for m_u . Normally close agreement is obtained between J and J_n within three or four cycles.

2. EFFECTS OF WELDING RESIDUAL STRESSES

Experimental and analytical work at Cambridge by Dwight and others^[45] (1960-70) has shown that residual stresses in a plate caused by welding longitudinal stiffeners can be represented by a stress pattern of the type shown in Fig. 21, which consists of one fairly uniform compressive zone in the middle, flanked by two tensile yielded strips adjacent to the stiffener. From equilibrium considerations, the width ηt of each tensile yielded strip is given by:

$$\eta t = \frac{\sigma_R}{\sigma_R + \sigma_{ys}} \frac{b}{2} \quad \dots \quad (15)$$

where σ_R is the compressive residual stress in the middle zone.

For analytical purposes, we can replace this pattern by a combination of:

- (i) uniform compression σ_R over the whole width b , and
- (ii) fictitious tensile stress of magnitude $(\sigma_{ys} + \sigma_R)$ in two edge strips.

It is now postulated that σ_R can simply be added to the applied uniform compressive stresses σ_a for the analysis of the plate behaviour described in Section 1, and that since the tensile blocks are adjacent to the supported edges of the plate they do not affect its stability. However, after the full strength of the plate is reached under the action of $(\sigma_a + \sigma_R)$ (which is assumed to occur when the average equivalent stress on the edge reaches yield stress), the tensile blocks near the edges continue to resist further applied compressive forces till compressive yield is reached there. This additional compressive force is obviously given by:

$$2nt^2 (\sigma_{ys} + \sigma_R) = tb\sigma_R, \quad \text{from equation (15)}$$

During this stage the middle part of the plate will not offer any resistance though it will continue to be strained along with the edge strips. The strain absorbed in this phase is equal to $\frac{1}{E} (\sigma_{ys} + \sigma_R)$.

Thus from equation (11):

$$(\sigma_a + \sigma_R) = \sigma_{cr} \left(1 - \frac{1}{m}\right) + \frac{3}{8} (1 - \nu^2) \sigma_{cr} \left(\frac{A_o}{t}\right)^2 (m^2 - 1)$$

or

$$\sigma_a = \sigma_{cr} \left(1 - \frac{1}{m}\right) + \frac{3}{8} (1 - \nu^2) \sigma_{cr} \left(\frac{A_o}{t}\right)^2 (m^2 - 1) - \sigma_R \quad \dots \quad (16)$$

where σ_a and σ_R are applied average compressive stress and residual compressive stress in the mid-portion of the plate respectively.

The value of A_o relates to the initial imperfection in a stress-free state. If the initial imperfection A_R is given for the welded condition, then $A_o < A_R$ and from equation (11) they are related as follows:

$$\sigma_R = \sigma_{cr} \left(1 - \frac{A_o}{A_R}\right) + \frac{3}{8} (1 - \nu^2) \sigma_{cr} \frac{A_R^2 - A_o^2}{t^2}$$

By rearranging,

$$A_o = \left[\frac{4\sigma_{cr} b^2}{\pi^2 EA_R} \right]^2 + A_R^2 + (\sigma_{cr} - \sigma_R) \frac{8b^2}{\pi^2 E} \Bigg]^{1/2} - \frac{4\sigma_{cr} b^2}{\pi^2 EA_R} \quad \dots \quad (17)$$

From equations (11), the apparent strain e_{at} under the action of $(\sigma_a + \sigma_R)$ is given by:

$$e_{at} = \frac{1}{E} \left[(\sigma_a + \sigma_R) + \frac{3}{8} (1 - \nu^2) \sigma_{cr} \left(\frac{A_o}{t} \right)^2 (m^2 - 1) \right]$$

The apparent strain e_{ar} due to residual stress σ_R alone is given by:

$$e_{ar} = \frac{1}{E} \left[\sigma_R + \frac{3}{8} (1 - \nu^2) \sigma_{cr} \left(\frac{A_o}{t} \right)^2 (m_r^2 - 1) \right]$$

where $m_r = \frac{A_R}{A_o}$.

Hence the apparent strain e_a due to applied stress alone is given by:

$$\begin{aligned} e_a &= e_{at} - e_{ar} = \frac{1}{E} \left[\sigma_a + \frac{3}{8} (1 - \nu^2) \sigma_{cr} \left(\frac{A_o}{t} \right)^2 (m^2 - m_r^2) \right] \\ &= \frac{1}{E} \left[\sigma_{cr} \left(1 - \frac{1}{m} \right) + \frac{3}{8} (1 - \nu^2) \sigma_{cr} \left(\frac{A_o}{t} \right)^2 (2m^2 - m_r^2 - 1) - \sigma_R \right] \\ &\dots\dots (18) \end{aligned}$$

by substitution for σ_a from equation (16).

We shall retain our postulation that the ultimate strength of the plate is reached when the average mid-plane equivalent stress on the edges $y = \pm \frac{b}{e}$ is equal to σ_{ys} ; but this phase will be followed by further squash of the tensile yielded edge strips. The magnification m_u will still, therefore, be given by equation (14).

Knowing m_u , the values of σ_a and e_a can be calculated by equations (16) and (18) respectively.

In order to estimate the additional load that can be carried by the tensile yielded strips, it must be examined whether the substantial additional strain of $\frac{1}{E} (\sigma_{ys} + \sigma_R)$ can be absorbed by the remainder of the plate without shedding off some of the load it is already carrying. Residual-stress-free plates of certain geometries and certain levels of initial imperfections show a stable and horizontal load-shortening curve after the peak load is reached, whereas certain other plates show a falling load-shortening behaviour after the peak load. From the extensive

computer studies of plates available^[17], the following approximate pattern of post-peak behaviour can be established for residual-stress-free plates with initial imperfection amplitude A_0 of the order of $\frac{1}{400}$ to $\frac{1}{100}$ times the plate width b :

$$\begin{aligned} \Theta &= 0, & \text{when } S < 0.7 : \\ &0.2 (S - 0.7), & \text{" } 0.7 < S < 1.4 ; \quad \dots \quad (19) \\ &0.14, & \text{" } S > 1.4. \end{aligned}$$

where Θ is the downward slope of the graph, of average stress-apparent strain times E , after peak load.

S is the slenderness parameter of the plate given by:

$$\frac{b}{t} \sqrt{\frac{\sigma_{ys}}{E}}$$

Thus the nett additional load carried during the squash stage of the yielded strips is:

$$bt \sigma_R - \frac{1}{E} (\sigma_{ys} + \sigma_R) E \Theta bt$$

i.e. an average stress of $\sigma_R - \Theta (\sigma_{ys} + \sigma_R)$

The entire behaviour of the plate can thus be split into two distinct phases:

- (i) A predominantly elastic phase up to the attainment of m_u of the magnification factor, given by equation (14), i.e.

$$0.7 \left(\frac{A_0}{t} \right)^2 m_u^2 - \frac{1}{m_u} = \frac{\sigma_{ys}}{\sigma_{cr}} + 0.7 \left(\frac{A_0}{t} \right)^2 - 1 \quad \dots \quad (14)$$

The average stress σ_{ae} and apparent strain e_{ae} at the end of this stage are respectively given by equations (16) and (18), i.e.

$$\sigma_{ae} = \sigma_{cr} \left(1 - \frac{1}{m_u} \right) + \frac{3}{8} (1 - \nu^2) \sigma_{cr} \left(\frac{A_0}{t} \right)^2 (m_u^2 - 1) - \sigma_R$$

$$e_{ae} = \frac{1}{E} \left[\sigma_{cr} \left(1 - \frac{1}{m_u} \right) + \frac{3}{8} (1 - \nu^2) \sigma_{cr} \left(\frac{A_0}{t} \right)^2 (2m_u^2 - m_r^2 - 1) - \sigma_R \right]$$

..... (20)

- (ii) A squash stage of the yielded strips, at the end of which are reached the ultimate stress σ_{au} and apparent strain e_{au} given by the following equations:

$$\begin{aligned}\sigma_{au} &= \sigma_{ae} + \sigma_R - \theta (\sigma_{ys} + \sigma_R) \\ &= \sigma_{cr} \left(1 - \frac{1}{m_u}\right) + \frac{3}{8} (1 - \nu^2) \sigma_{cr} \left(\frac{A_0}{t}\right)^2 (m_u^2 - 1) - \theta (\sigma_{ys} + \sigma_R) \\ e_{au} &= e_{ae} + \frac{1}{E} (\sigma_{ys} + \sigma_R) \\ &= \frac{1}{E} \left[\sigma_{cr} \left(1 - \frac{1}{m_u}\right) + \frac{3}{8} (1 - \nu^2) \sigma_{cr} \left(\frac{A_0}{t}\right)^2 (2m_u^2 - m_r^2 - 1) + \sigma_{ys} \right] \\ &\dots\dots (21)\end{aligned}$$

where θ is given in equation (19).

The following interesting aspects emerge from a study of the above equations as well as from the exact curves of reference [17]:

- (i) If θ is zero, i.e. if the load-shortening behaviour of a residual-stress-free plate does not show any fall-off after peak load, the ultimate strength σ_{au} of a welded plate will be identical to the ultimate strength of a residual-stress-free plate with the same dimensions and initial geometric imperfections.
- (ii) Comparing equation (21) for e_{au} with the equation (14), and noting that m_r is only marginally above unity for moderate values of σ_R , e_{au} is only marginally below $\frac{2\sigma_{ys}}{E}$; that is, the ultimate strength of a welded plate is reached at approximately twice the yield strain.
- (iii) The initial elastic phase of the plate behaviour ends when the applied average stress reaches the ultimate stress for a residual-stress-free plate minus σ_R .
- (iv) The squash stage of the yielded strips is characterised by a linear relationship between average stress and apparent strain, the gradient being equal to:

$$E \left[\frac{\sigma_R}{\sigma_R + \sigma_{ys}} - \theta \right]$$

- (v) Since the departure from linearity is not found to be very considerable in the initial elastic phase, the entire load-shortening behaviour of a welded plate may be described by two straight lines, i.e. a bi-linear relationship stretching between the origin and the points (σ_{ae}, e_{ae}) and (σ_{au}, e_{au}) , as shown in Fig. 22.

3. FORMULAE FOR LOAD-SHORTENING CURVES OF PLATE PANELS

An examination of the formulae given in the previous section will indicate that the following are the three vital parameters:

$$(i) \quad S = \frac{b}{t} \sqrt{\frac{\sigma_{ys}}{E}}$$

$$(ii) \quad \delta_R = \frac{A_R}{t}, \quad \text{where } A_R \text{ is the amplitude of initial imperfection of the welded plate.}$$

$$(iii) \quad r = \frac{\sigma_R}{\sigma_{ys}}, \quad \text{where } \sigma_R \text{ is the compressive welding residual stress.}$$

Taking Poisson's ratio $\nu = 0.3$, the relevant formulae can be expressed as follows:

- (a) *Plates with residual stresses, i.e. $r > 0$:*

Equation (17):

$$\delta_o = \frac{A_o}{t} = \left[\left(\frac{1.4652}{\delta_R} \right)^2 + \sigma_R^2 + 2.9304 - 0.8106 r S^2 \right]^{1/2} - \frac{1.4652}{\delta_R}$$

$$m_R = \frac{\delta_R}{\delta_o}$$

Equation (14):

$$0.7 \delta_o^2 m_u^2 - \frac{1}{m_u} = 0.2766 S^2 + 0.7 \delta_o^2 - 1$$

Equation (20) for point A, Fig. 26:

$$\frac{\sigma_{ae}}{\sigma_{ys}} = \frac{3.6152}{S^2} \left(1 - \frac{1}{m_u} \right) + \frac{1.2337}{S^2} \delta_o^2 (m_u^2 - 1) - r$$

$$\frac{Ee_{ae}}{\sigma_{ys}} = \frac{\sigma_{ae}}{\sigma_{ys}} + \frac{1.2337}{S^2} \delta_o^2 (m_u^2 - m_r^2)$$

$$K_{se} = \frac{\sigma_{ae}}{\sigma_{ys}} \cdot \frac{\sigma_{ys}}{Ee_{ae}}$$

Equation (19):

$$\begin{aligned} \Theta &= 0, & \text{when } S < 0.7 \\ &= 0.2 (S - 0.7), & \text{" } 0.7 < S < 1.4 \\ &= 0.14, & \text{" } S > 1.4 \end{aligned}$$

Equation (21) for point B, Fig. 26:

$$\frac{\sigma_{au}}{\sigma_{ys}} = \frac{\sigma_{ae}}{\sigma_{ys}} + r - \Theta (1 + r)$$

$$\frac{Ee_{au}}{\sigma_{ys}} = \frac{Ee_{ae}}{\sigma_{ys}} + 1 + r$$

$$K_{su} = \frac{\sigma_{au}}{\sigma_{ys}} \frac{\sigma_{ys}}{Ee_{au}}$$

(b) *Plates without residual stresses, i.e. $r = 0$:*

Equation (13):

$$0.91 \delta_o^2 m_e^2 - \frac{1}{m_e} = 0.2766 S^2 + 0.91 \delta_o^2 - 1$$

Equation (11):

$$\frac{Ea_e}{\sigma_{ys}} = \frac{3.6152}{S^2} \left(1 - \frac{1}{m_e}\right) + \frac{2.4674}{S^2} \delta_o^2 (m_e^2 - 1)$$

Equation (14):

$$0.7 \delta_o^2 m_u^2 - \frac{1}{m_u} = 0.2766 S^2 + 0.7 \delta_o^2 - 1$$

Equation (11):

$$\frac{\sigma_{au}}{\sigma_{ys}} = \frac{3.6152}{S^2} \left(1 - \frac{1}{m_u}\right) + \frac{1.2337}{S^2} \delta_o^2 (m_u^2 - 1)$$

$$\frac{Ee_{au}}{\sigma_{ys}} = 2 \left[\frac{\sigma_{au}}{\sigma_{ys}} + \frac{1.2337}{S^2} \delta_o^2 (m_u^2 - 1) \right] - \frac{Ea_e}{\sigma_{ys}}$$

$$K_{su} = \frac{\sigma_{au}}{\sigma_{ys}} \frac{\sigma_{ys}}{Ee_{au}}$$

4. IMPLICATIONS OF THE PLATE BEHAVIOUR ON FLANGE STIFFENER DESIGN

For welded flanges, stress and strain for either point A or point B of Fig. 22, or any intermediate point between them, may be used for the analysis of the flange stiffener comprised of the flange plate and the stiffening rib in accordance with Chapter 3. As the strain for point B is nearly equal to twice the yield strain, part of the stiffening rib near its attachment with the flange plate will also have to undergo a strain higher than yield, to develop in the flange plate the stress corresponding to point B. Hence the formulae for stresses given in Chapter 3 will not strictly be valid when using point B, as they are based on the assumption that yield strain is not exceeded in the outstand. The exact solution can only be obtained by assuming trial strain patterns over the whole section and equating the resultant moment and axial load to the applied values. An approximate solution may, however, be to ignore the calculated stresses above yield stress over the area of the outstand undergoing higher than yield strain. For example, in Fig. 23, the amount to be deducted from the axial load is equal to:

$$\frac{1}{2} h t_s (\sigma_t - \sigma_{ys}) = \frac{1}{2} t_s (\sigma_t - \sigma_{ys})^2 \frac{I_e}{M}$$

where I_e is the moment of inertia of the effective section, and M is the bending moment at the section.

5. LEVELS OF WELDING STRESSES AND INITIAL IMPERFECTIONS

5.1 Welding Stresses

The compressive welding residual stress σ_R in the flange plate may be calculated from the following formula developed in Cambridge^[45] (1960-70):

$$\sigma_R = \frac{c A_w}{A_g - \frac{c A_w}{\sigma_{ys}}}$$

where A_w is the area of the weld

A_g is the area of the plate-stiffener assembly

c is a coefficient for shrinkage force in the weld.

c has been experimentally found^[46] to vary from 7.7 kN/mm² for manual welding to 12.5 kN/mm² for submerged arc welding, and hence may be taken as 10 kN/mm² as a mean value for design rule purposes.

A_w may be taken approximately as $0.6 w^2$, when w is the leg length of fillet weld. For intermittent welding on each face of the stiffening rib, the above formula reduces to:

$$\frac{\sigma_R}{\sigma_{ys}} = \frac{1}{\frac{\sigma_{ys}}{12000} \left(\frac{b}{t}\right) \left(1 + \frac{A_s}{bt}\right) \left(\frac{t}{w}\right)^2 \left(\frac{L_m + L_w}{L_w}\right) - 1} \quad \dots \quad (22)$$

where L_m and L_w are the missed and the welded lengths respectively shown in Fig. 24.

In practical stiffened compression flanges of box girders stiffener welding is usually intermittent and σ_R hardly ever exceeds $0.1 \sigma_{ys}$.

This is also illustrated in the following table showing calculated welding compressive stresses for a few compression flange geometries with intermittent welding and ratio $L_m/L_w = 2$. These geometries are the extreme examples of the practical range so far as welding stress level is concerned. For higher values of b/t ratio, equation (22) clearly shows that σ_R will be less than for the examples included in the table.

| b/t | t mm | b mm | Stiffener size mm | A_s/bt | w mm | w/t | σ_R/σ_{ys} for $\sigma_{ys} =$ | |
|-------|-----------|-----------|----------------------|----------|-----------|-------|--|-----------------------|
| | | | | | | | 245 N/mm ² | 355 N/mm ² |
| 16 | 12 | 192 | 150 × 6 | 0.33 | 4.5 | 0.375 | .121 | .080 |
| | 18 | 288 | 150 × 8 | 0.23 | 6.0 | 0.33 | .101 | .068 |
| | 25 | 400 | 150 × 10 | 0.15 | 8.0 | 0.32 | .100 | .067 |
| | 40 | 640 | 225 × 18 | 0.16 | 10.0 | 0.25 | .058 | .040 |
| 20 | 12 | 240 | 125 × 8 | 0.35 | 5.0 | 0.417 | .118 | .078 |
| | 18 | 360 | 150 × 8 | 0.185 | 6.0 | 0.333 | .083 | .056 |
| | 25 | 500 | 150 × 10 | 0.12 | 8.0 | 0.320 | .081 | .054 |
| | 40 | 800 | 225 × 18 | 0.13 | 10.0 | 0.25 | .047 | .032 |

TABLE 2: CALCULATED WELDING STRESSES IN TYPICAL GEOMETRIES OF BOX GIRDER COMPRESSION FLANGES

It is suggested that an assumed value for σ_R equal to 10% of σ_{ys} will cover almost all design situations for compression flanges.

The condition that the compressive residual stress σ_R does not exceed 0.1 σ_{ys} can be then conveniently expressed as:

$$\frac{\sigma_R}{\sigma_{ys}} = \frac{c A_w}{\sigma_{ys} A_g - c A_w} \} 0.1$$

or,

$$p \} 0.91 \times 10^{-3} \sigma_{ys}$$

$$\text{say, } 1 \times 10^{-3} \sigma_{ys} \quad \dots \quad (23)$$

where p is the percentage of weld volume to steel volume in the stiffened compression flange.

5.2 Geometrical Imperfections

Merrison fabrication tolerance Δ_p for out-of-flatness of flange plates is given by:

$$\Delta_p = \frac{G}{30t} \left(1 + \frac{b}{5000} \right) \left[\frac{t}{25} \right],$$

measured over a gauge length of $G = 2b$; the term within the brackets [] is applicable only when $t > 25$. (All dimensions are in mm.)

The related design amplitude for imperfection A_R is given by:

$$A_R = \frac{b}{25t} \left(1 + \frac{b}{5000} \right) \left(\frac{1}{N+1} \right)^{1/3} \left[\frac{t}{25} \right]$$

where N is the number of longitudinal stiffeners in the compression flange between girder webs, and as before the term within the brackets [] is applicable when $t > 25$.

It can be seen that the design amplitude has been taken to be:

$$1.2 \left(\frac{1}{N+1} \right)^{1/3}$$

times the fabrication tolerance, when both are related to the same measuring length. The first factor 1.2 is a safety factor to allow for inaccuracies in measurement; the second factor involving N is a reduction factor to allow for the fact that parallel flange plate panels

between stiffening ribs are not likely to have initial imperfections in complete phase with each other, i.e. at any cross-section alternately up and down across the width and at the adjacent cross-sections at a distance b , alternatively down and up again across the width.

If imperfection measurements for individual flange panels do not satisfy the tolerance Δ_p , Merrison gives a complicated procedure for calculating effective imperfections from measurements on adjacent panels, but this time the tolerance is reduced by the factor $(\frac{1}{N+1})^{1/3}$.

Extensive measurements of imperfections on existing bridges and their analysis^[47] suggest that:

- (i) calculation of effective imperfections is an unduly arduous task;
- (ii) effective imperfections can sometimes be more critical than the criterion for individual panel measurements, particularly when the imperfection mode in adjacent panels is similar to the natural buckling mode, i.e. sinusoidally up and down, and because of the factor $(\frac{1}{N+1})^{1/3}$; and
- (iii) it is more difficult to satisfy the fabrication tolerances for thicker plates than for thinner plates.

To meet these criticisms it is proposed that:

- (i) tolerance levels could be increased for thicker plates; and
- (ii) the concept of effective imperfection can be discarded for tolerance requirements.

The following expressions for fabrication tolerances and design imperfection are therefore suggested to be appropriate:

$$\text{Fabrication tolerance } \Delta_p = \frac{G}{250} \sqrt{\frac{\sigma_{ys}}{245}} \quad , \quad \text{measured over} \\ \text{gauge length } G = 2b \quad \dots \dots \quad (24)$$

$$\text{Imperfection parameter } \delta_R = \frac{A_R}{t} = \frac{b}{200t} \sqrt{\frac{\sigma_{ys}}{245}} = 0.145 S \quad \dots \quad (25)$$

where S is the slenderness parameter $\frac{b}{t} \sqrt{\frac{\sigma_{ys}}{E}}$

and σ_{ys} is in N/mm^2 .

Introduction of the factor $\sqrt{\frac{\sigma_{ys}}{245}}$ enables one set of curves to be used for plates of all yield stresses. A comparison between the magnitudes of Merrison fabrication tolerances and of those suggested in (24) above is given below for mild steel plates. It is clear from this table that the suggested tolerance levels should be more easily acceptable to steel fabricators than the Merrison tolerances. This comparison will be still more favourable to the newly suggested tolerances for higher grades of steel. Considerable simplicity is achieved in relating the tolerance to the gauge length only for any given quality of steel. The measurement procedure does not entail the recording and analysis of measurements on adjacent panels, and so should reduce the cost of measurements significantly.

| <i>b</i> <i>mm</i> | <i>G</i> <i>mm</i> | <i>t</i> <i>mm</i> | <i>Merrison</i> Δ_p <i>mm</i> | <i>Suggested</i> Δ_p <i>for</i> <i>mild steel</i> <i>mm</i> |
|-----------------------|-----------------------|-----------------------|--|--|
| 200 | 400 | 10 | 1.39 | 1.60 |
| | | 12 | 1.16 | |
| | | 15 | 0.92 | |
| 400 | 800 | 12 | 2.40 | 3.20 |
| | | 15 | 1.92 | |
| | | 20 | 1.44 | |
| | | 25 | 1.15 | |
| 600 | 1200 | 12 | 3.73 | 4.80 |
| | | 20 | 2.24 | |
| | | 30 | 1.79 | |
| | | 40 | 1.79 | |
| 800 | 1600 | 15 | 4.12 | 6.40 |
| | | 20 | 3.09 | |
| | | 30 | 2.47 | |
| | | 40 | 2.47 | |

TABLE 3: COMPARISON BETWEEN MERRISON AND PROPOSED TOLERANCES FOR PLATES

6. SENSITIVITY OF PLATE STRENGTH TO INITIAL IMPERFECTION LEVELS

The governing equations for the strength of residual stress-free plates are given in Section 3 of this chapter.

For chosen values of the plate slenderness parameter $S = \frac{b}{t} \sqrt{\frac{\sigma_{ys}}{E}}$, plate strength ratio $\frac{\sigma_{au}}{\sigma_{ys}}$ may be calculated for various values of δ_o . However, m_u must be obtained by solving a cubic equation before $\frac{\sigma_{au}}{\sigma_{ys}}$ can be calculated. An alternative method is described below.

By substituting δ_o from equation (14), equation (11) may be written as:

$$\frac{\sigma_{au}}{\sigma_{ys}} = \frac{1.8528}{S^2} \left(1 - \frac{1}{m_u}\right) + 0.4875 \quad \dots \quad (26)$$

We have already concluded in Section 5, equation (25), that δ_o may be taken as a simple function of S , i.e.

$$\delta_o = \frac{A_o}{t} = C' S$$

where C' is a coefficient for imperfection; its exact value will give the magnitude of initial imperfection to be assumed in design.

A tentative value of $C' = 0.145$ was found to be more advantageous for fabrication tolerances than the Merrison Rules. Substitution for δ_o converts the equation (14) to:

$$C' = \left[\frac{0.3951}{m_u^2 - 1} - \frac{1.4286}{S^2 m_u (m_u + 1)} \right]^{1/2} \quad \dots \quad (27)$$

For any particular value of S , pairs of values of strength ratio $\frac{\sigma_{au}}{\sigma_{ys}}$ and imperfection coefficient C' may be obtained from equations (26) and (27), through a range of values of m_u , thus enabling a graph of $\frac{\sigma_{au}}{\sigma_{ys}}$ against C' to be drawn.

Such graphs are shown in Fig. 25 for three values of $S = 0.7, 1.3, 1.9$, corresponding to b/t ratio of 20.2, 37.6 and 55.0 for mild steel ($\sigma_{ys} = 245 \text{ N/mm}^2$) and 16.8, 31.2 and 45.7 for high yield steel ($\sigma_{ys} = 355 \text{ N/mm}^2$) respectively.

For the purpose of choosing the optimum value of C' , i.e. optimum tolerances, these graphs must be complemented by data for cost of fabric-

ation to various levels of tolerances. Edwards^[18] carried out such a study; he used the empirical equations in the Merrison Rules for the plate strengths. Cost data obtained by Edwards from the fabricators related to Merrison tolerances, and twice and half of Merrison tolerances. The tolerances now being suggested are higher than Merrison values, but, as can be seen from the table in Section 5, they are not in a particular proportion for all geometries. Hence it is not possible to extend Edwards' cost data to the present exercise.

Reliable cost data could not be obtained from the industry at the present time. However, an examination of Fig. 25 will indicate that the strength starts to fall rather sharply around the suggested imperfection levels for $S = 0.7$ and 1.3 . For $S = 1.9$, i.e. very slender plate not often used in compression flanges, there is a very sharp fall in strength for very small imperfections, followed by a continuous steady fall around the suggested imperfection level. Hence it would appear that the chosen imperfection levels are reasonable.

7. DESIGN DATA FOR PLATE PANEL BEHAVIOUR

From the equations in Section 3 plate curves can be drawn for initial imperfection parameter δ_R equal to $0.145 S$, and residual stress parameter ρ equal to either zero or 0.1 .

For $\rho = 0.1$, the design of the combined plate-stiffening rib assembly may be checked by taking the plate stress and secant stiffness corresponding to either point A or point B of Fig. 22. However, as explained in Section 4, if the values for point B are chosen the axial load must be reduced to allow for the high strains in the stiffening rib. The gradient of the portion A-B of Fig. 22 is $(0.09-0)$. Since this gradient is rather small and can even be negative, and in order to avoid the complications of reducing the calculated load, a simple design approach is postulated by taking the relevant values for point A only. The following table and the graphs in Figs 26a and 26b give the two required parameters for plate behaviour related to point A, i.e.

- (i) the maximum stress parameter $\frac{\sigma_{au}}{\sigma_{ys}}$;

(ii) the secant stiffness parameter $K_{su} = \frac{\sigma_{au}}{\sigma_{ys}} \cdot \frac{\sigma_{ys}}{Ee_{au}}$

both against slenderness parameter $b/t \sqrt{\frac{\sigma_{ys}}{E}}$.

For plates without residual stresses only point A is relevant; it is found that K_{su} values are marginally smaller than $\frac{\sigma_{au}}{\sigma_{ys}}$, but they are close enough to justify only one graph. Thus the values for K_{su} were plotted against $b/t \sqrt{\frac{\sigma_{ys}}{E}}$ to give both the parameters of maximum stress and secant stiffness, i.e. $\frac{\sigma_{au}}{\sigma_{ys}}$ and K_{su} . The concept of a single effective width of plate for an effective stiffener section, with stresses calculated for the effective section limited to yield stress, is thus valid for residual-stress-free stiffeners.

Such a simple concept is, however, not strictly valid for welded stiffeners, as the residual stresses produce a bi-linear load-shortening pattern of the flange plate. The first part of this pattern ends with a stress level less than the maximum stress of a residual-stress-free plate by the magnitude of the residual compressive stress, but with the secant stiffness virtually the same as for the latter. The second part is characterised by very high strains and the secant stiffness at the peak of this part is less than half the secant stiffness of a residual-stress-free plate at its maximum stress. Hence it is suggested that the two separate parameters for maximum stress and secant stiffness be retained for welded flanges.

| $S = \frac{b}{t} \sqrt{\frac{\sigma_{ys}}{E}}$ | b/t for σ_{ys} | | welded plates | | Residual-stress-free plates; $\frac{\sigma_{au}}{\sigma_{ys}}$ and K_s |
|--|--------------------------|--------------------------|---------------------------|----------|--|
| | 355 N/mm ² | 245 N/mm ² | σ_{au}/σ_{ys} | K_{su} | |
| 0.5 | 12.01 | 14.46 | .8965 | .9960 | .9875 |
| 0.7 | 16.82 | 20.25 | .8905 | .9935 | .9935 |
| 1.0 | 24.03 | 28.93 | .8779 | .9783 | .9648 |
| 1.3 | 31.24 | 37.60 | .8503 | .9499 | .9221 |
| 1.6 | 38.45 | 46.28 | .7976 | .8946 | .8463 |
| 1.9 | 45.66 | 54.96 | .7272 | .8199 | .7562 |
| 2.2 | 52.87 | 63.64 | .6617 | .7501 | .6797 |
| 2.5 | 60.08 | 72.32 | .6099 | .6946 | .6225 |
| 2.8 | 67.29 | 80.99 | .5706 | .6523 | .5803 |

TABLE 4: PLATE PANEL PARAMETERS FOR DESIGN OF STIFFENED FLANGE

CHAPTER 6

BUCKLING BEHAVIOUR OF INITIALLY IMPERFECT ORTHOTROPIC PLATES
WITH LONGITUDINAL EDGES FREE TO PULL-IN - ITS APPLICATION
TO OVERALL FLANGE BEHAVIOUR

1. APPROXIMATE SOLUTION

It is assumed that the longitudinal edges are completely free to move in-plane, i.e. $\sigma_y = 0$ when $y = \pm b/2$. The further simplifying assumption, originally proposed in Ref. [44], and made in Chapter 4, for post-buckling behaviour of initially flat plates, i.e. σ_y , and hence τ_{xy} , are zero everywhere in the plate, shall also be retained. The initial and the final deflections w_0 and w respectively are assumed to follow the critical buckling mode, i.e.

$$\begin{aligned} w_0 &= A_0 \cos \frac{\pi x}{l} \cos \frac{\pi y}{B} \\ w &= A \cos \frac{\pi x}{l} \cos \frac{\pi y}{B} \end{aligned} \quad \dots \quad (1)$$

where l is the natural half-wave-length of elastic critical buckling of the orthotropic plate in the x -direction, and B is its width.

Since flexure of the plate is associated with the change of shape given by $(w - w_0)$, the bending energy U_b will now be given by the following equation, instead of (18) of Chapter 4:

$$U_b = \sigma_{cr}^* Bt \frac{\pi^2}{8l} (A - A_0)^2,$$

where σ_{cr}^* is the critical buckling stress of the orthotropic plate.

Since σ_y and τ_{xy} are zero and σ_x is independent of x , the strain energy U_m associated with the membrane forces is given by:

$$U_m = \frac{lt}{2E_x} \int_{-B/2}^{+B/2} \sigma_x^2 dy$$

The total strain energy $U = U_b + U_m$.

The rate of change of total strain energy with respect to amplitude of deflection is given by:

$$\frac{dU}{dA} = \sigma_{cr}^* B t \frac{\pi^2}{4l} (A - A_0) + \frac{t}{E_x} \int_{-B/2}^{+B/2} \sigma_x \frac{d\sigma_x}{dA} dy \dots (2)$$

From equations (1) and (14), Chapter 4, since σ_y is zero:

$$\frac{\partial u}{\partial x} = \frac{\sigma_x}{E_x} - \frac{1}{2} \left(\frac{\partial w}{\partial x} \right)^2 + \frac{1}{2} \left(\frac{\partial w_0}{\partial x} \right)^2$$

The total change of length Δl is given by:

$$\Delta l = \int_{-l/2}^{+l/2} \frac{\partial u}{\partial x} dx = \frac{\sigma_x l}{E_x} - \frac{\pi^2 (A^2 - A_0^2)}{4l} \cos^2 \frac{\pi y}{B} \dots (3)$$

The potential energy T of applied loads = (-) work done by applied loads, i.e.

$$T = - \frac{t l}{E_x} \int_{-B/2}^{+B/2} \sigma_x^2 dy + \frac{(A^2 - A_0^2) \pi^2 t}{4l} \int_{-B/2}^{+B/2} \sigma_x \cos^2 \frac{\pi y}{B} dy$$

The rate of change of T with respect to A is:

$$\begin{aligned} \frac{dT}{dA} = & - \frac{2t l}{E_x} \int_{-B/2}^{+B/2} \sigma_x \left(\frac{d\sigma_x}{dA} \right) dy + \frac{(A^2 - A_0^2) \pi^2 t}{4l} \times \\ & \int_{-B/2}^{+B/2} \left(\frac{d\sigma_x}{dA} \right) \cos^2 \frac{\pi y}{B} dy + \frac{A \pi^2 t}{2l} \int_{-B/2}^{+B/2} \sigma_x \cos^2 \frac{\pi y}{B} dy \\ & \dots (4) \end{aligned}$$

From (3):

$$\sigma_x = \frac{\Delta l \cdot E_x}{l} + \frac{E_x (A^2 - A_0^2) \pi^2}{4l^2} \cos^2 \frac{\pi y}{B} \dots (5)$$

Following the procedure in Chapter 4, it can be shown that:

$$\begin{aligned} \frac{dT}{dA} = & - \frac{t l}{E_x} \int_{-B/2}^{+B/2} \sigma_x \frac{d\sigma_x}{dA} dy + \frac{A \pi^2 t}{2l} \left[\frac{\Delta l E_x B}{2l} + \frac{E_x (A^2 - A_0^2) \pi^2 B}{l^2} \frac{3}{32} \right] \\ & \dots (6) \end{aligned}$$

Taking $A = m A_0$, and applying the condition $(dU/dA + dT/dA) = 0$ for minimum total potential energy, leads to:

$$-\Delta l = \sigma_{cr}^* \frac{l}{E_x} \left(\frac{m-1}{m} \right) + \frac{3}{16} \frac{(m^2-1) A_0^2 \pi^2}{l} \quad \dots \quad (7)$$

Putting this in (5):

$$-\sigma_x = \sigma_{cr}^* \left(\frac{m-1}{m} \right) + \frac{3}{16} \frac{E_x (m^2-1) A_0^2 \pi^2}{l^2} - \frac{E_x (m^2-1) A_0^2 \pi^2}{4l^2} \times \cos^2 \frac{\pi y}{B} \quad \dots \quad (8)$$

(The negative sign for σ_x indicating compression.)

The mean longitudinal compressive stress σ_a can be obtained by integrating over width B ; thus

$$\sigma_a = \sigma_{cr}^* \left(\frac{m-1}{m} \right) + \frac{1}{16} \frac{E_x (m^2-1) \pi^2 A_0^2}{l^2} \quad \dots \quad (9)$$

The above equation embodies the important relationship between the applied compressive stress σ_a and the amplitude of the final deflected shape $m A_0$.

The maximum and the minimum longitudinal stresses occur at $y = \pm b/2$ and $y = 0$ respectively and they are:

$$\left. \begin{aligned} \sigma_{max} &= \sigma_{cr}^* \left(\frac{m-1}{m} \right) + \frac{3}{16} \frac{E_x (m^2-1) \pi^2 A_0^2}{l^2} \\ \sigma_{min} &= \sigma_{cr}^* \left(\frac{m-1}{m} \right) - \frac{1}{16} \frac{E_x (m^2-1) \pi^2 A_0^2}{l^2} \end{aligned} \right\} \dots \quad (10)$$

It may be noted from equations (7) and (10) that σ_{max} is equal to $-\Delta l \cdot E_x/l$.

For given magnitudes of initial perfection A_0 and applied average stress σ_a , the equations (8) to (10) will give the variation of longitudinal stress across the width and also the deflected shape. Equation (9) is a cubic equation, and hence a successive approximation method such as one described below will have to be used to obtain m :

$$\frac{d\sigma_a}{dm} = \frac{\sigma_{cr}^*}{m^2} + \frac{E_x \pi^2 A_o^2 m}{8L^2} \dots\dots (11)$$

For a trial value of m , say m_1 , calculate σ_{a1} and $\frac{d\sigma_a}{dm_1}$ from equations (9) and (11) respectively. A suitable next approximation for m is:

$$m_2 = m_1 + \frac{(\sigma_a - \sigma_{a1})}{\frac{d\sigma_a}{dm_1}} ; \text{ and so on.}$$

The bending moments in the orthotropic plate per unit width are given by:

$$M_x = - \left[D_x \frac{\partial^2 (w - w_o)}{\partial x^2} + D_1 \frac{\partial^2 (w - w_o)}{\partial y^2} \right]$$

$$M_y = - \left[D_y \frac{\partial^2 (w - w_o)}{\partial y^2} + D_1 \frac{\partial^2 (w - w_o)}{\partial x^2} \right]$$

where $D_1 = \nu_y D_x = \nu_x D_y$ for an ideal orthotropic plate.

For buckling of the stiffened flange between transverse stiffeners, from Section 2, Chapter 4:

$$D_x = \frac{EI_x}{b'}$$

where I_x is the second moment of area of longitudinal stiffener, and b' is its spacing.

$$D_y = \frac{Et^3}{12(1 - \nu^2)}$$

where t is the flange plate thickness.

Since D_y is very small compared with D_x , both D_1 and D_y may be neglected, giving:

$$M_x = \frac{EI_x \pi^2}{b' L^2} (m - 1) A_o \cos \frac{\pi x}{L} \cos \frac{\pi y}{B}$$

The maximum bending moment in any stiffener at distance y from the longitudinal centre-line of the orthotropic panel is given by:

$$M_s = \frac{EI_x \pi^2}{L^2} (m - 1) A_o \cos \frac{\pi y}{B} \dots (12)$$

The highest bending moment will occur at the mid-span of a stiffener along or nearest to the longitudinal centre-line, and is given by:

$$\frac{EI_x \pi^2}{L^2} (m - 1) A_o \dots (13)$$

Stiffeners near the longitudinal edges will have very little bending moment as they will hardly deflect.

Equation (13) is identical in form to the expression for bending moment in an initially imperfect or eccentrically loaded isolated strut, i.e. equation (10) in Chapter 3.

Hence the orthotropic action of the whole stiffened flange can be taken into account in checking individual stiffeners by:

- (a) taking the applied longitudinal stress on the stiffener from equations (8), i.e. less than the average stress on a central stiffener, but a higher value on an edge stiffener;
- (b) calculating the bending moment due to buckling on the basis of a magnification factor m for the entire orthotropic plate obtained from equation (9).

2. INITIAL IMPERFECTIONS

As discussed in Chapter 3 for isolated struts, the equivalent initial imperfection in the orthotropic plate may be due to:

- (i) an initial bow in the buckling length l ,
- (ii) an eccentricity of applied loading due to the curvature of the whole box girder, and
- (iii) an eccentricity of applied loading due to loss of stiffness of a slender flange plate.

Imperfection (ii) and (iii) will be uniform across the whole width B of the flange. Imperfection (i) can also be the maximum permitted tolerance Δ_{sx} on all or most of the stiffeners. Hence the worst pattern of initial imperfection at a cross-section may not be the sinusoidal

type $w_0 = A_0 \cos \frac{\pi y}{B}$, assumed in the preceding analysis of the orthotropic plate, but a constant value of say A_c across the whole width B .

A_c can be represented by a Fourier Series, i.e.

$$A_c = \sum_{n=1}^{\infty} A_n \cos \frac{n\pi y}{B}$$

$$\text{where } A_n = \frac{2A_c}{B} \int_{-B/2}^{+B/2} \cos \frac{n\pi y}{B} dy$$

It can be shown that the even terms A_2, A_4, A_6 , etc. are zero,

$$\text{and } A_1 = \frac{4A_c}{\pi}; \quad A_3 = -\frac{4A_c}{3\pi}; \quad A_5 = +\frac{4A_c}{5\pi}, \text{ etc.}$$

Taking the first term of the Fourier Series, the initial imperfection pattern may be taken as:

$$w_0 = \frac{4}{\pi} A_c \cos \frac{\pi y}{B} \cos \frac{\pi x}{L}$$

i.e. the amplitude of the assumed double sinusoidal initial imperfection shape should be taken as $\frac{4}{\pi}$ times the maximum imperfection of an individual stiffener.

3. COMPARISON WITH MORE EXACT THEORY

It has already been explained that the derivation of the fairly simple equations (8) to (10) has been possible only because of the simplifying assumption of zero transverse membrane stress everywhere in the plate. Maquoi^[48] found that for his assumed stress function F , the assumed deflection shape given by equations (1) did not exactly satisfy the equilibrium equation (4) in Chapter 4. He adopted an approximate variational procedure, due to Bubnov-Galerkin, to obtain the amplitude of additional deflection w by stipulating that the error represented by the inequality of the two sides in equation (4), Chapter 4, must be orthogonal to w .

His solution may be considered to be more exact, although it can be criticised for being far too complex for design purposes. The relationship between the average longitudinal stress σ_e along the unloaded edges and the magnification m of initial deflections that Maquoi obtained can be expressed as:

$$\frac{\sigma_e}{\sigma_{cr}^*} = \frac{m-1}{m} + Q' (m^2 - 1) \delta_o^2 \quad \dots\dots \quad (14)$$

where $\delta_o = \frac{\text{Initial Deflection } A_o}{\text{Thickness } t}$

Q' is a dimensional property of the stiffened panel, derived by a series of very lengthy computations.

The equation (10) for the maximum longitudinal membrane stress, occurring along the unloaded edges, may also be expressed exactly as equation (14), with the dimensional factor Q' being given by:

$$Q' = \frac{3}{16} \frac{\pi^2 E_x t^2}{\sigma_{cr}^* L^2} \quad \dots\dots \quad (15)$$

The values of Q' obtained by applying Maquoi's method and the above formula (15) are compared below for the three box models 2, 4 and 8 tested at Imperial College under constant bending moment and reported in detail in Chapter 10. Very close agreement between the two sets of values of Q' is obtained.

| Box No. | Value of Q' | |
|---------|---------------|---------------|
| | Maquoi | Equation (15) |
| 2 | 0.02224 | 0.02160 |
| 4 | 0.01577 | 0.01539 |
| 8 | 0.03354 | 0.02982 |

Maquoi defined the efficiency ρ_t of the orthotropic plate as the ratio of the mean stress σ_a to the maximum membrane stress σ_e along the edges $y = \pm b/2$. His expression for ρ_t can be transformed to:

$$\rho_t = 1 - \frac{1}{\left[\frac{8L^2 \sigma_{cr}^*}{\pi^2 m (m+1) A_o^2 E} \right] + Q''} \quad \dots\dots \quad (16)$$

where Q'' is a dimensional property of the stiffened panel.

Using equations (9) and (10), the efficiency ρ_t can also be expressed as:

$$\rho_t = 1 - \frac{1}{\left[\frac{8L^2 \sigma_{cr}^*}{\pi^2 E_x m (m+1) A_o^2} \right] + 1.5} \quad \dots \quad (17)$$

The second term in the denominator, i.e. Q'' or 1.5, is usually much smaller than the first term within the brackets [**], and hence the two expressions for ρ_t are very similar. For example, for the geometry of the box models 2, 4 and 8, Q'' worked out, after a lengthy series of computations, as 1.544, 1.537 and 2.537 respectively. The first two values agree closely with the value 1.5 derived in equation (17). Though agreement for the value of Q'' for box 8 was not so close, the term within bracket [**] worked out, for the most critical case, to be 46 (see Chapter 10). Since this is much larger than Q'' , the value of the efficiency ρ_t was almost identical from the two equations.

The close agreement between the formulae derived from the simplified analysis in this chapter and the more accurate theory developed by Maquoi confirms the usefulness of the present analysis for design rule purposes.

CHAPTER 7

EFFECT OF BENDING MOMENT GRADIENT IN BOX GIRDER ON
STRENGTH OF COMPRESSION FLANGE

1. INTRODUCTION

The applied axial stress in a longitudinal stiffener in the compression flange of a box girder varies according to the shape of the bending moment diagram of the box girder. When the gradient of the bending moment diagram is steep, e.g. near an intermediate support of a continuous box girder, the applied longitudinal stress at the two ends of a flange stiffener span may differ considerably from each other, and it may be too conservative to design the stiffener on the basis of a uniform axial stress equal to the higher end stress. The Merrison Rules^[2] and Dwight^[25] stipulated that such a stiffener may be checked, first, as a uniformly compressed strut with an applied axial stress equal to that occurring at a certain distance from the heavily stressed end (0.33 L according to Merrison, 0.4 L according to Dwight); secondly, the load at the heavily stressed end should not be more than that to cause squashing of the stiffener cross-section. Though the basis of the second check is quite obvious, that of the first one is believed to be mainly intuitive. In this chapter the basis of the first check will be examined by means of a theoretical analysis of the behaviour of a non-uniformly compressed strut.

2. ANALYSIS OF A NON-UNIFORMLY COMPRESSED STRUT

The strut will be assumed to be pin-ended and subjected to a linearly varying axial load, as shown in Fig. 27. The axial compressive force on the strut is P at one end and $(P + qL)$ at the other, the difference between these two values being balanced by a distributed axial loading of magnitude q per unit length. This loading pattern will be assumed to be invariable, i.e. P and qL will be in identical proportion throughout the loading history.

In any deflected state of the strut, statical equilibrium will require vertical reactions V at each pinned end given by:

$$V = \frac{q}{L} \int_0^L y \, dx \quad \dots \quad (1)$$

where y is the deflection of the strut at distance x as shown in

Fig. 27.

The critical buckling load and the natural buckling mode of the strut will be obtained by applying the Ritz^[49] method in conjunction with the energy method due to Timoshenko^[50]. In this procedure, we shall assume a small deflection of the strut given by the first two terms of the Fourier Series:

$$y = \delta_1 \sin \frac{\pi x}{L} - \delta_2 \sin \frac{2\pi x}{L} \dots \dots \quad (2)$$

In the above equation δ_1 and δ_2 are two free parameters that will produce an unsymmetrical deflected shape of the type intuitively expected from the unsymmetrical axial loading on the strut. By equating the strain energy due to bending ΔU to the work done by the external loads ΔT due to movement arising from this flexure, an expression for the critical buckling value of the loads can be obtained in terms of the parameters δ_1 and δ_2 . Finally, the relative magnitudes of δ_1 and δ_2 are determined for the minimum values of the critical load, i.e. from the conditions:

$$\frac{\partial P}{\partial \delta_1} = 0 \qquad \frac{\partial P}{\partial \delta_2} = 0$$

Thus both the minimum critical buckling load and the natural buckling mode of the strut are obtained.

Since only two terms of the Fourier Series are included in equation (2), it is necessary to check the accuracy of the results; this is done by comparing the bending moments at several sections calculated (a) from the second derivative of the deflection equation (2), and (b) by simple statics, with respect to the derived deflections of the strut.

Taking the origin at end A , as shown in Fig. 27, bending moment at distance x is given by:

$$M_x = P.y + \int_0^x q d\xi (y - \eta) + V.x$$

where $y = \delta_1 \sin \frac{\pi x}{L} - \delta_2 \sin \frac{2\pi x}{L}$

$$\eta = \delta_1 \sin \frac{\pi\xi}{L} - \delta_2 \sin \frac{2\pi\xi}{L}$$

$$V = \frac{q}{L} \int_0^L y \, dx = \frac{2}{\pi} \delta_1 q$$

Substitution of the above and integration leads to:

$$\begin{aligned} M_x = \delta_1 \left[P \sin \frac{\pi x}{L} + q \left(x \sin \frac{\pi x}{L} + \frac{L}{\pi} \cos \frac{\pi x}{L} - \frac{L}{\pi} + \frac{2x}{\pi} \right) \right] \\ - \delta_2 \left[P \sin \frac{2\pi x}{L} + q \left(x \sin \frac{2\pi x}{L} + \frac{L}{2\pi} \cos \frac{2\pi x}{L} - \frac{L}{2\pi} \right) \right] \\ \dots \dots \dots \quad (3) \end{aligned}$$

The bending strain energy ΔU is given by:

$$\Delta U = \int_0^L \frac{M_x^2}{2EI} \, dx \quad \dots \dots \dots \quad (4)$$

The square of the expression in equation (3) contains a very large number of terms involving first or second powers of:

$$x, \sin \frac{\pi x}{L}, \cos \frac{\pi x}{L}, \sin \frac{2\pi x}{L} \text{ and } \cos \frac{2\pi x}{L}$$

Though integration of some of the terms will vanish because of the orthogonality relationship between the Fourier series terms, the equation (4) will still contain a large number of terms. Working through all these terms leads finally to:

$$\begin{aligned} EI(\Delta U) = 0.25 \delta_1^2 P^2 L + 0.25 \delta_1^2 P q L^2 + 0.06569 \delta_1^2 q^2 L^3 \\ + 0.28145 \delta_1 \delta_2 P q L^2 + 0.14072 \delta_1 \delta_2 q^2 L^3 \\ + 0.25 \delta_2^2 P^2 L + 0.25 \delta_2^2 P q L^2 + 0.11816 \delta_2^2 q^2 L^3 \\ \dots \dots \dots \quad (5) \end{aligned}$$

The work ΔT done by the axial loads during flexure of the strut will be calculated next. Assuming the end B of the strut to remain in its original position, the displacement u of concentrated load P at end A is given by:

$$u = \frac{1}{2} \int_0^L \left(\frac{dy}{dx} \right)^2 \, dx$$

Substitution for y from equation (2) and integration leads to the following result:

$$u = \frac{\pi^2}{4L} (\delta_1^2 + 4 \delta_2^2)$$

Work done by the load P is given by:

$$(\Delta T)_P = P \cdot u = \frac{\pi^2 P}{4L} (\delta_1^2 + 4 \delta_2^2) \quad \dots \quad (6)$$

For the work done by the distributed axial loading of intensity q per unit length, consider a small element ds at a distance x , as shown in Fig. 27. Due to the inclination of this element the load qx will move by a magnitude:

$$(ds - dx) \approx \frac{1}{2} \left(\frac{dy}{dx} \right)^2 dx$$

Hence the work done:

$$= \frac{1}{2} q x \left(\frac{dy}{dx} \right)^2 dx$$

The total work done by the distributed load due to flexure of the whole strut is:

$$(\Delta T)_q = \int_0^L \frac{1}{2} q x \left(\frac{dy}{dx} \right)^2 dx$$

Substitution for y from equation (2) and integration leads to:

$$(\Delta T)_q = \frac{1}{2} q \left[\frac{\pi^2 \delta_1^2}{4} + \pi^2 \delta_2^2 + \frac{40}{9} \delta_1 \delta_2 \right] \quad \dots \quad (7)$$

Adding expressions (6) and (7), the total work done by the applied axial loads is given by:

$$\begin{aligned} \Delta T = & 2.4674 \delta_1^2 \frac{P}{L} + 1.2337 \delta_1^2 q + 2.2222 \delta_1 \delta_2 q \\ & + 9.8696 \delta_2^2 \frac{P}{L} + 4.9348 \delta_2^2 q \quad \dots \quad (8) \end{aligned}$$

For the critical condition of buckling:

$$\Delta U = \Delta T$$

Equating expressions (5) and (8) and rearranging, the value of P_{cr} is obtained as:

$$P_{cr} = \frac{EI}{L} \left[\frac{\beta_1 + \frac{\delta_2}{\delta_1} \beta_2 + \left(\frac{\delta_2}{\delta_1}\right)^2 \beta_3}{\alpha_1 + \frac{\delta_2}{\delta_1} \alpha_2 + \left(\frac{\delta_2}{\delta_1}\right)^2 \alpha_3} \right] \dots \quad (9)$$

where $\alpha_1 = 0.25 + 0.25 \frac{qL}{P} + 0.06569 \left(\frac{qL}{P}\right)^2$

$$\alpha_2 = 0.28145 \frac{qL}{P} + 0.14072 \left(\frac{qL}{P}\right)^2$$

$$\alpha_3 = 0.25 + 0.25 \frac{qL}{P} + 0.11816 \left(\frac{qL}{P}\right)^2$$

$$\beta_1 = 2.4674 + 1.2337 \frac{qL}{P}$$

$$\beta_2 = 2.2222 \frac{qL}{P}$$

$$\beta_3 = 9.8696 + 4.9348 \frac{qL}{P}$$

The minimum value for P_{cr} will occur when:

$$\frac{\partial P_{cr}}{\partial \delta_1} = 0 \quad \dots \quad (10a)$$

$$\frac{\partial P_{cr}}{\partial \delta_2} = 0 \quad \dots \quad (10b)$$

Partial differentiation of expression (9) with respect to δ_1 and δ_2 leads to the following relationship:

$$\frac{2\delta_1\beta_1 + \delta_2\beta_2}{2\delta_1\alpha_1 + \delta_2\alpha_2} = \frac{\delta_1\beta_2 + 2\delta_2\beta_3}{\delta_1\alpha_2 + 2\delta_2\alpha_3}$$

This can be expressed in quadratic form as:

$$\left(\frac{\delta_2}{\delta_1}\right)^2 (\alpha_2\beta_3 - \alpha_3\beta_2) + 2\frac{\delta_2}{\delta_1} (\alpha_1\beta_3 - \alpha_3\beta_1) + (\alpha_1\beta_2 - \alpha_2\beta_1) = 0$$

Its solution is:

$$\frac{\delta_2}{\delta_1} = -\frac{\alpha_1\beta_3 - \alpha_3\beta_1}{\alpha_2\beta_3 - \alpha_3\beta_2} \pm \left[\left(\frac{\alpha_1\beta_3 - \alpha_3\beta_1}{\alpha_2\beta_3 - \alpha_3\beta_2} \right)^2 + \left(\frac{\alpha_2\beta_1 - \alpha_1\beta_2}{\alpha_2\beta_3 - \alpha_3\beta_2} \right) \right]^{1/2}$$

..... (11)

It is obvious that the strut will deflect more in the heavily stressed half of the span; hence for positive values of P and qL , from equation (2) and Fig. 27, only the positive value for (δ_2/δ_1) , i.e. the +ve sign in equation (11), needs to be considered. If, however, qL is negative, i.e. tensile in nature, then from the same reasoning, the negative value for (δ_2/δ_1) from equation (11) is valid. For any given ratio of (qL/P) , the coefficients $\alpha_1, \alpha_2, \alpha_3, \beta_1, \beta_2,$ and β_3 can be calculated from the expressions given in (9); the critical deflection ratio (δ_2/δ_1) can then be obtained from equation (11). Substitution of these values in equation (9) will yield the minimum critical value of P ; the coexisting critical value of distributed axial load qL for this combination of loading is obviously in the given ratio of (qL/P) . Equations (9) and (11) are valid for all cases when P and q are both greater than zero. For the limiting cases when either P or q is zero the following adjustments are necessary:

- (a) When $P = 0$, obtain α_1, β_1 etc. by taking the numerical coefficient of the last terms only, e.g. $\alpha_1 = 0.06569, \beta_1 = 1.2337$, etc. The ratio $(\frac{\delta_2}{\delta_1})$ works out to be 0.07129, and by equating expressions (5) and (8):

$$q_{cr} = \frac{EI}{L^3} (18.706) .$$

- (b) When $q = 0$, from symmetry $(\frac{\delta_2}{\delta_1})$ is obviously zero, and

$$P_{cr} = \frac{EI}{L^2} \frac{\beta_1}{\alpha_1} = \pi^2 \frac{EI}{L^2} , \quad \text{i.e.}$$

the well-known Euler load.

3. ACCURACY OF THE APPROXIMATE THEORETICAL RESULTS

As only the first two terms of the Fourier Series have been included in the deflection equation (2), the accuracy of the results

is verified by comparing the bending moments at several positions of the span calculated first from the curvature of the deflected shape, i.e.

$$M_x = -EI \frac{d^2y}{dx^2} = EI \frac{\pi^2}{L^2} \left[\delta_1 \sin \frac{\pi x}{L} - 4\delta_2 \sin \frac{2\pi x}{L} \right] \dots \quad (12)$$

and secondly, from statics, by equation (3).

Three loading patterns are investigated as follows:

- (i) $P = 0$ (i.e. a triangular axial load pattern)
- (ii) $P = qL$
- (iii) $P = 2qL$.

For each case, bending moments are calculated from the two formulae at three sections, i.e. two quarter-points C and E , and mid-span D , as shown in Fig. 27.

Denoting the bending moments M_x as $\frac{m' EI \delta_1}{L^2}$, where the coefficient m' is equal to m'_1 when formula (12) is used and m'_2 when formula (3) is used, the results are given in the following table:

| Loading Pattern | BM Coefficients | Sections | | |
|-----------------|-----------------|----------|--------|--------|
| | | C | D | E |
| $P = 0$ | m'_1 | 9.7932 | 9.8696 | 4.1644 |
| | m'_2 | 9.8995 | 9.7775 | 4.4189 |
| $P = qL$ | m'_1 | 7.9594 | 9.8696 | 5.9982 |
| | m'_2 | 7.9602 | 9.8474 | 6.0257 |
| $P = 2qL$ | m'_1 | 7.5702 | 9.8696 | 6.3874 |
| | m'_2 | 7.5679 | 9.8617 | 6.4000 |

It can be seen that the agreement between m'_1 and m'_2 is very good - within 1% in eight cases out of nine; in the ninth case, i.e. point E when $P = 0$, the agreement is within 6%; but as the bending moment at this section is not actually critical, this discrepancy may be discounted.

Thus it can be concluded that the deflection expression (2) using only two terms of the Fourier Series adequately represents the behaviour of struts subjected to linearly varying axial loads.

4. INITIALLY IMPERFECT STRUT CARRYING VARYING AXIAL LOAD

The initial and the final shapes of the deflection curve, y_0 and y_p respectively, are assumed to occur in the critical buckling mode obtained for the particular loading pattern in accordance with Section 2 of this chapter, viz.

$$\left. \begin{aligned} y_0 &= \delta_{10} \sin \frac{\pi x}{L} - \delta_{20} \sin \frac{2\pi x}{L} \\ y_p &= \delta_{1p} \sin \frac{\pi x}{L} - \delta_{2p} \sin \frac{2\pi x}{L} \end{aligned} \right\} \dots \quad (13)$$

where $\frac{\delta_{20}}{\delta_{10}} = \frac{\delta_{2p}}{\delta_{1p}}$

It shall also be assumed that the magnification of the initial deflections will be given by the same expression as for an axially loaded strut, i.e.

$$y_p = y_0 \frac{P_{cr}}{P_{cr} - P}$$

The bending moment at any section will then be given by:

$$\begin{aligned} M_x &= -EI \frac{d^2}{dx^2} (y_p - y_0) \\ &= EI \frac{P}{P_{cr} - P} \delta_{10} \frac{\pi^2}{L^2} \left[\sin \frac{\pi x}{L} - \frac{4\delta_{20}}{\delta_{10}} \sin \frac{2\pi x}{L} \right] \dots \quad (14) \end{aligned}$$

The fibre stress in the cross-section of the strut is then:

$$\sigma = \frac{P + qx}{A} + \frac{\pi^2 EI \delta_{10}}{L^2 Z} \frac{P}{P_{cr} - P} \left[\sin \frac{\pi x}{L} - \frac{4\delta_{20}}{\delta_{10}} \sin \frac{2\pi x}{L} \right] \dots \quad (15)$$

where A is the area, and

Z is the relevant section modulus of the cross-section of the strut. (Z should be taken as positive on the concave side of

the cross-section and negative on the convex side, i.e. -ve for tensile flexural stress.)

For maximum fibre stress:

$$\frac{d\sigma}{dx} = 0, \text{ i.e. from equation (15)}$$

$$\frac{q}{A} + \frac{m'' P}{P_{cr} - P} \frac{8\pi \delta_{20}}{L \delta_{10}} + \frac{m'' P}{P_{cr} - P} \frac{\pi}{L} \cos \frac{\pi x}{L} - \frac{m'' P}{P_{cr} - P} \frac{16\pi}{L} \times \frac{\delta_{20}}{\delta_{10}} \cos^2 \frac{\pi x}{L} = 0$$

where $m'' = \frac{EI \pi^2 \delta_{10}}{L^2 Z}$

This is a quadratic equation in $\cos \frac{\pi x}{L}$, the solution of which gives the position of the section for maximum stress. Though the maximum stress is generally expected to be compressive and occurs on the concave side, in some situations the stress on the convex side can be tensile and even larger than the maximum compressive stress on the concave side.

Substituting:

$$A = \frac{m'' P}{P_{cr} - P} \frac{16\pi}{L} \frac{\delta_{20}}{\delta_{10}}$$

$$B = \frac{m'' P}{P_{cr} - P} \frac{\pi}{L}$$

$$C = \frac{q}{A} + \frac{m'' P}{P_{cr} - P} \frac{8\pi}{L} \frac{\delta_{20}}{\delta_{10}}$$

the solution of the quadratic equation reduces to:

$$\cos \frac{\pi x}{L} = \frac{B \pm \sqrt{B^2 + 4AC}}{2A} \dots \dots (16)$$

Of the two solutions, one given by the -ve sign is valid for +ve values of P and qL , as x in this case must be greater than $L/2$; the other solution given by the +ve sign is valid if qL is -ve, i.e. tensile.

Equation (16) indicates that x , i.e. the position of the section for maximum fibre stress differs for maximum compressive and possible maximum tensile stress, and also that it depends on the ratio P/P_{cr} , i.e. the level of applied loading with respect to the elastic critical loading.

If a Perry-Robertson type design approach is envisaged for struts subjected to variable axial loading, with maximum fibre stress equal to the yield stress for the ultimate strength of the strut, then the above approach will be rather complicated for design office use.

An alternative simpler method is therefore suggested in which two cross-sections of the strut should be checked for maximum fibre stress, viz. one cross-section subjected to maximum bending moment and the other cross-section subjected to maximum axial loading. This approach will theoretically be marginally non-conservative, but should be adequate for design purposes. The second cross-section will obviously be at the heavily stressed end where bending moment is zero. For the position of the first cross-section, from equation (14):

$$\frac{dM_x}{dx} = EI \delta_{10} \frac{\pi^2}{L^2} \frac{P}{P_{cr} - P} \left[\frac{\pi}{L} \cos \frac{\pi x}{L} - \frac{4\delta_{20}}{\delta_{10}} \frac{2\pi}{L} \cos \frac{2\pi x}{L} \right] = 0$$

$$\text{or, } \cos \frac{\pi x}{L} = \frac{8\delta_{20}}{\delta_{10}} \left[2 \cos^2 \frac{\pi x}{L} - 1 \right]$$

The relevant solution of the above quadratic equation is:

$$\cos \frac{\pi x}{L} = \frac{1 \pm \sqrt{1 + 512 (\delta_{20}/\delta_{10})^2}}{32 (\delta_{20}/\delta_{10})} \dots \dots \quad (17)$$

When both P and qL are +ve, (i.e. compressive) x must be larger than $L/2$, and hence the solution given by taking the -ve sign is valid. When, however, qL is -ve, (i.e. tensile) x must be less than $L/2$, and the solution given by taking the +ve sign is valid.

5. DESIGN RULES FOR STRUTS WITH VARYING AXIAL LOAD

5.1 Basis for a Design Method

The basis for a design method can now be developed from the results of the previous sections as follows:

- (a) For any given ratio of the applied axial stresses at the ends $P/(P + qL)$, the maximum bending moment due to imperfection and further buckling is given by:

$$M_{max} = \frac{\pi^2 EI \Delta}{L^2} (m - 1) C_2 \quad \dots \quad (18)$$

where $m = \frac{\frac{\pi^2 EI}{L^2} C_3}{\frac{\pi^2 EI}{L^2} C_3 - (P + qL)}$

$$C_3 = \frac{1}{\pi^2} \frac{P + qL}{P} \left[\frac{\beta_1 + \frac{K}{32} \beta_2 + \frac{K^2}{1024} \beta_3}{\alpha_1 + \frac{K}{32} \alpha_2 + \frac{K^2}{1024} \alpha_3} \right]$$

$$K = 32 (\delta_2 / \delta_1), \text{ with } (\delta_2 / \delta_1) \text{ given by equation (11)}$$

$$C_2 = \sin \frac{\pi x}{L} - \frac{K}{8} \sin \frac{2\pi x}{L}, \text{ with } x \text{ given by:}$$

$$\cos \frac{\pi x}{L} = \frac{1}{K} - \sqrt{\frac{1}{K^2} + \frac{1}{2}}$$

Δ is the design tolerance on straightness of the strut.

Coefficients C_2 and C_3 have been plotted against the ratio of axial stresses at the two ends in Fig. 28 and can be used directly to obtain M_{max} from equation (18).

- (b) The co-existent axial load P_x at the cross-section with the maximum bending moment is given by:

$$P_x = P + C_1 qL \quad \dots \quad (19)$$

where $C_1 = \frac{x}{L}$, and

$$x \text{ is given by } \cos \frac{\pi x}{L} = \frac{1}{K} + \sqrt{\frac{1}{K^2} + \frac{1}{2}} .$$

Coefficient C_1 has been plotted in Fig. 28 against the axial stress ratio $P/(P + qL)$.

- (c) The strut cross-section should be checked for maximum fibre stress due to the combined effect of bending moment M_{max} and axial load P_x .
- (d) The strut cross-section should also be checked for squashing due to the maximum axial load at its end, i.e. $(P + qL)$.

5.2 A Simplified Design Approach

The design basis developed in Section 5.1 was further explored to examine if an alternative simplified design approach of treating the strut as subjected to an equivalent constant axial force would be reasonably safe as well as economic. Three formulae for the magnitude of this equivalent constant axial force P_{eq} were tried, viz. the value at a section at

- I Mid-span, i.e. $P_{eq} = P + \frac{1}{2} qL$.
 - II $0.4 L$ from the heavily stressed end, suggested by Dwight [25],
i.e. $P_{eq} = P + 0.6 qL$
 - III $0.33 L$ from the heavily stressed end, as stipulated in the Merrison Rules [3], i.e. $P_{eq} = P + 0.67 qL$
- } (20)

In this simplified approach the maximum bending moment in a strut with sinusoidal initial out-of-alignment would be given by:

$$M_{app} = \frac{\pi^2 EI \Delta}{L^2} \left[\frac{P_{eq}}{\frac{\pi^2 EI}{L^2} - P_{eq}} \right] \dots \dots (21)$$

The ratios of the approximate and the more exact values of (i) the bending moments, given by equations (21) and (18) respectively, and (ii) the co-existent axial forces, given by equations (20) and (19) respectively, i.e.

$$(i) \frac{M_{app}}{M_{max}} \quad \text{and} \quad (ii) \frac{P_{eq}}{P_x}$$

are shown in Figs 29a to 29c for different values of end stress ratios.

The bending moment ratio depends on the slenderness of the strut, i.e. the factor of safety against elastic critical buckling; Fig. 29a shows this ratio for a very stocky strut with a very large factor of safety against elastic critical buckling, and Fig. 29b shows this ratio for a very slender strut with a factor of safety against elastic critical buckling equal to 1.33. (Smaller values were not considered as they seldom occur in practice and bending moments tend to get very high.)

It can be noted from Figs 29a to 29c that none of the simplified approaches satisfies the dual criteria of safety and economy in the entire range of the slenderness of the struts and the ratio of end stresses. However, of the three methods, method II, i.e. the equivalent constant axial force equal to the value at a distance of $0.4 L$ from the heavily stressed end, is to be preferred. In the case of slender struts subjected to a substantial variation in the applied end stresses, it is obvious that the use of the design basis given in Section 5.1 will lead to significant economy.

CHAPTER 8

EFFECT OF CONTINUITY ON STRENGTH OF FLANGE STIFFENERS

1. INTRODUCTION

In the previous chapters the flange stiffeners have been treated as single-span pin-ended struts. The behaviour of each span of a continuous multi-span strut will not differ much from that of a single-span pin-ended strut, when

- (i) the strut cross-section is symmetrical about the centroidal axis normal to the plane of flexure;
- (ii) the initial geometrical imperfections are equal, and in the sinusoidal alternately up and down mode, in all the spans;
- (iii) the axial load is uniform and constant throughout all the spans and is applied through the centroidal axis.

In a continuous strut of the above description, first surface yield, followed soon by formation of a plastic hinge, will occur simultaneously at the centre of all the spans. No bending moment will develop over any intermediate support on account of the exact anti-symmetry on the two sides of these supports and hence plastic hinges do not form at these locations.

However, in the compression flanges of box girders, the strut cross-section, consisting of the flange plate panel and the stiffener, is not symmetrical about the centroidal axis perpendicular to the plane of flexure. It is also improbable that initial geometrical imperfections will be equal in magnitude and opposite in sign in adjacent spans. For design purposes, however, the worst possible situation with imperfections in this natural buckling mode must be considered. The magnitude of the applied axial load is fairly uniform in adjacent spans in the sagging moment zone of a continuous box girder bridge, but varies sharply in the hogging moment zone over piers. Due to the curvature of the box girder, the applied axial load acts on the flange stiffener with an eccentricity causing higher stress on the flange plate. This aspect has already been discussed in Chapter 3, Section 7. Hence the effects of continuity on the behaviour of longitudinal stiffeners in

the compression flange of box girders needs further consideration. This chapter deals with this problem.

2. ANALYSIS OF A CONTINUOUS BEAM-COLUMN

Timoshenko^[50] derived the three-moment equation for continuous beam-columns, with each span having a constant axial force and constant flexural rigidity, though these quantities may vary from span to span. Let 1, 2, 3 denote the consecutive supports; M_1, M_2, M_3, \dots the corresponding bending moments; L_1, L_2, L_3, \dots the span lengths. Consider any two consecutive spans between the supports $n - 1, n,$ and $n + 1,$ as shown in Fig. 30. The bending moments at the supports are assumed positive when they cause compression on the top of the beam, i.e. sagging; the angles of rotation at the supports are also taken as positive when they are in the same direction as the positive bending moments. The three-moment equation can be written as:

$$M_{n-1} \phi(u_{n-1}) + 2M_n \left[\Psi(u_{n-1}) + \frac{L_n}{L_{n-1}} \frac{I_{n-1}}{I_n} \Psi(u_n) \right] + M_{n+1} \frac{L_n}{L_{n-1}} \frac{I_{n-1}}{I_n} \phi(u_n) = - \frac{6 E I_{n-1}}{L_{n-1}} (\Theta_n + \Theta'_n) \dots \dots (1)$$

where u is the parameter $\frac{\pi}{2} \sqrt{\frac{P}{P/E}} = \frac{L}{2} \sqrt{\frac{P}{EI}}$ for any span,

$$\text{i.e. } u_n = \frac{L_n}{2} \sqrt{\frac{P_n}{EI_n}}$$

$\phi(u)$ and $\Psi(u)$ are stability functions given by:

$$\phi(u) = \frac{3}{u} \left[\frac{1}{\sin 2u} - \frac{1}{2u} \right]$$

$$\Psi(u) = \frac{3}{2u} \left[\frac{1}{2u} - \frac{1}{\tan 2u} \right]$$

Θ'_n is the angle of rotation at support n of span $n - 1,$ when this span is considered as simply supported at both ends.

Θ_n is the angle of rotation at support n of span $n,$ when this span is considered simply supported at both ends.

3. CONTINUOUS STRAIGHT COLUMN CARRYING ECCENTRICALLY APPLIED LOAD

3.1 Five-Span Continuous Beam-Column

The continuous longitudinal stiffeners in the flange of a box girder shall be analysed first as a continuous perfectly straight beam-column of five equal spans, of constant geometrical cross-section, subjected to an eccentric constant axial load throughout the five spans, as shown in Fig. 31a.

The end slopes Θ_n of a simply supported beam-column subjected to an eccentric axial load is derived by Timoshenko [50] as:

$$\Theta_n = \frac{PeL}{6EI} \left[2 \Psi(u) + \phi(u) \right] \dots\dots (2)$$

The mid-span bending moment M_f of such a simply supported beam-column is given by:

$$M_f = P.e \cdot \sec u \dots\dots (3)$$

From equations (1) and (2), the three-moment equations for this continuous beam are then:

$$\begin{aligned} 4 M_2 \Psi(u) + M_3 \phi(u) &= - 2 Pe [2 \Psi(u) + \phi(u)] \\ M_2 \phi(u) + M_3 [4 \Psi(u) + \phi(u)] &= - 2 Pe [2 \Psi(u) + \phi(u)] \end{aligned} \dots\dots (4)$$

The bending moments M_2 and M_3 at the respective supports are due to the continuity effect. For total bending moments over the supports the applied bending moment Pe must be added to these values. Additional mid-span deflections y_{12} , y_{23} and y_{34} in the spans 1-2, 2-3 and 3-4 due to the support moments can be obtained from Timoshenko's formula as:

$$\left. \begin{aligned} y_{12} &= \frac{M_2}{P} \left[\frac{\sin u}{\sin 2u} - \frac{1}{2} \right] \\ y_{23} &= \frac{M_2 + M_3}{P} \left[\frac{\sin u}{\sin 2u} - \frac{1}{2} \right] \\ y_{34} &= \frac{2M_3}{P} \left[\frac{\sin u}{\sin 2u} - \frac{1}{2} \right] \end{aligned} \right\} \dots\dots (5)$$

Additional mid-span bending moments due to continuity are:

$$\left. \begin{aligned} M_{12} &= \frac{M_2}{2} + P.y_{12} = M_2 \frac{\sin u}{\sin 2u}, \text{ from (3)} \\ M_{23} &= \frac{M_2 + M_3}{2} + P.y_{23} = (M_2 + M_3) \frac{\sin u}{\sin 2u}, \text{ from (3)} \\ M_{34} &= M_3 + P.y_{34} = M_3 \frac{2\sin u}{\sin 2u}, \text{ from (3)} \end{aligned} \right\} \dots (6)$$

For total mid-span bending moments, these quantities are to be added to the free mid-span bending moment M_f given in equation (3).

Effectiveness factor F for any section of the continuous beam-column may be defined as the ratio:

$$\frac{\text{B.M. at a particular section in continuous beam-column}}{\text{Max. B.M. in the simply supported beam-column}}$$

Thus if F_{12} , F_{23} and F_{34} represent the effectiveness factors for mid-span sections in spans 1-2, 2-3 and 3-4 respectively, and if F_2 and F_3 represent the effectiveness factors over supports 2 and 3, then:

$$F_{12} = \frac{M_{12} + M_f}{M_f}; \quad F_2 = \frac{Pe + M_2}{M_f}, \text{ etc.}$$

Solving the two simultaneous equations (4) for M_2 and M_3 leads to:

$$\begin{aligned} F_{12} &= \frac{8\Psi^2(u) - \phi^2(u)}{D}; \quad F_2 = - \frac{[\phi^2(u) + 4\Psi(u)\phi(u)] \cos u}{D} \\ F_{23} &= \frac{-2\Psi(u) \cdot \phi(u)}{D}; \quad F_3 = \frac{\phi^2(u) \cos u}{D} \quad \dots (7) \\ F_{34} &= \frac{\phi^2(u)}{D} \end{aligned}$$

where $D = 4\Psi(u) [4\Psi(u) + \phi(u)] - \phi^2(u)$

The value of u can range from 0 to $\frac{\pi}{2}$, corresponding to the value of axial load from 0 to the Euler load $\frac{\pi^2 EI}{L^2}$; however, when u approaches $\frac{\pi}{2}$ the flexural stiffness of the beam-column reduces to zero and the deflections tend to infinity. For various values of u in this range, the different effectiveness factors are given in the following table:

| <i>u</i> | <i>Effectiveness Factors</i> | | | | | <i>P/P_E</i> |
|----------|------------------------------|-----------------------|-----------------------|----------------------|----------------------|------------------------|
| | <i>in mid-span</i> | | | <i>over supports</i> | | |
| | <i>F₁₂</i> | <i>F₂₃</i> | <i>F₃₄</i> | <i>F₂</i> | <i>F₃</i> | |
| 0 | 0.3684 | -0.1053 | 0.0526 | -0.2632 | 0.0526 | 0 |
| 0.1 | 0.3681 | -0.1055 | 0.0528 | -0.2624 | 0.0525 | 0.0041 |
| 0.25 | 0.3666 | -0.1064 | 0.0539 | -0.2585 | 0.0522 | 0.2530 |
| 0.5 | 0.3608 | -0.1102 | 0.0580 | -0.2444 | 0.0509 | 0.1013 |
| 0.75 | 0.3498 | -0.1172 | 0.0661 | -0.2199 | 0.0484 | 0.2280 |
| 1.0 | 0.3308 | -0.1289 | 0.0807 | -0.1828 | 0.0436 | 0.4053 |
| 1.25 | 0.2974 | -0.1403 | 0.1084 | -0.1277 | 0.0342 | 0.6333 |
| 1.5 | 0.2314 | -0.1840 | 0.1691 | -0.0380 | 0.0120 | 0.9119 |
| 1.57 | 0.2000 | -0.1998 | 0.1996 | - | - | 0.999 |

TABLE 1: CONTINUITY EFFECT IN A FIVE-SPAN BEAM-COLUMN

It can be seen that the bending moments in the continuous beam-column vary between $+\frac{7}{19}$ to $-\frac{5}{19}$, i.e. + 0.3684 to - 0.2632 times the maximum bending moment in a single-span beam-column, except the extreme ends where the bending moment is obviously Pe . (In the compression flange of box girders, extreme ends do not carry any axial load, bending moment on the girder being zero.) It may, however, be noted that the bending moments in the interior regions changes from sagging to hogging, though the analysis of a simple span beam-column will not indicate any change in the sign of the bending moment.

If, however, the design rules for longitudinal stiffeners in the compression flange are based on the analysis of a single-span, the effective eccentricity should then be taken as + 0.3681 to - 0.2624 times the actual eccentricity e , shown in Fig. 31a, and due to overall curvature of the box girder and the shift of centroid of the effective strut section as discussed in Chapter 3, Section 7.

3.2 Influence of the Number of Spans

To get an idea of the effect of the total number of spans on the results obtained above, a three-span and a two-span continuous perfectly

straight beam-column of constant inertia and subjected to uniform axial load were analysed in a similar manner. The range of effectiveness factors obtained for the two cases, except at the extreme ends, are:

$$\begin{aligned} &+ 0.4 \quad \text{to} \quad - 0.3333 \quad \text{for three-span system} \\ &+ 0.25 \quad \text{to} \quad - 0.5 \quad \text{for two-span system.} \end{aligned}$$

3.3 Influence of Variation in Axial Load in Adjacent Spans

To find the effect of variation of axial load, a three-span constant section beam-column was analysed, in which the axial loads in the end spans were assumed to be half of that of the central span, as shown in Fig. 31b.

The three-moment equation for the continuous beam-column is:

$$2M_2 \left[\Psi\left(\frac{u}{\sqrt{2}}\right) + \Psi(u) \right] + M_3 \phi(u) = -\frac{6EI}{L} (\Theta_{2l} + \Theta_{2r}) \quad \dots (8)$$

and $M_2 = M_3$

where Θ_{2l} and Θ_{2r} are the angles of rotation of the right end of span 1-2, and the left end of span 2-3 respectively, each span being considered simply supported at its ends; Θ_{2l} and Θ_{2r} are given by:

$$\begin{aligned} \Theta_{2l} &= \frac{PeL}{12EI} \left[2 \Psi\left(\frac{u}{\sqrt{2}}\right) + \phi\left(\frac{u}{\sqrt{2}}\right) \right] \\ \Theta_{2r} &= \frac{PeL}{6EI} \left[2 \Psi(u) + \phi(u) \right] \end{aligned}$$

Substitution of the above in equation (8) leads finally to:

$$M_2 = M_3 = -P.e \frac{[\Psi(u/\sqrt{2}) + \frac{1}{2} \phi(u/\sqrt{2}) + 2\Psi(u) + \phi(u)]}{2\Psi(u/\sqrt{2}) + 2\Psi(u) + \phi(u)} \quad \dots (9)$$

The additional mid-span deflection y_{23} in span 2-3 due to the support moments is given by:

$$y_{23} = \frac{2M_2}{P} \left[\frac{\sin u}{\sin 2u} - \frac{1}{2} \right] \quad \dots (10)$$

The additional mid-span bending moment M_{23} due to continuity is given by:

$$M_{23} = M_2 + P.y_{23} = M_2 \sec u, \text{ from (10) } \dots\dots (11)$$

Effectiveness factors for mid-span section in span 2-3 and a section just on the right of support 2 are given by:

$$F_{23} = \frac{M_{23} + M_f}{M_f}; \quad F_{2R} = \frac{M_2 + P.e}{M_f}$$

where M_f is the mid-span bending moment in span 2-3, considered as a simple span, i.e. $M_f = P.e \sec u$.

Substituting for M_f , M_{23} and M_2 leads to:

$$\left. \begin{aligned} F_{23} &= \frac{\Psi(u/\sqrt{2}) - \frac{1}{2} \phi(u/\sqrt{2})}{2\Psi(u/\sqrt{2}) + 2\Psi(u) + \phi(u)} \\ F_{2R} &= \frac{\Psi(u/\sqrt{2}) - \frac{1}{2} \phi(u/\sqrt{2})}{2\Psi(u/\sqrt{2}) + 2\Psi(u) + \phi(u)} \cos u \end{aligned} \right\} \dots\dots (12)$$

The maximum value of the effectiveness factors F_{23} and F_{2R} for the whole range of $0 < u < \frac{\pi}{2}$ is + 0.1.

3.4 Simple Rules for Continuous Beam-Column

From the above results it is clear that in a multi-span continuous perfectly straight beam-column subjected to an eccentrically applied longitudinal load, the bending moment changes sign and the effective eccentricity is less than the actual eccentricity so far as the maximum bending moment is concerned. This change of sign of the bending moment cannot, however, be predicted from the analysis of a single span. From the cases considered, a simple design rule may be suggested: a continuous perfectly straight but eccentrically loaded strut may be treated as a single-span straight strut for design purposes, provided the effective eccentricity of the applied loading is taken as half the actual eccentricity; if the strut cross-section is not symmetrical about the centroidal axis normal to the plane of flexure, it shall be assumed that the effective eccentricity may occur on either side of the centroidal axis.

4. INITIAL OUT-OF-STRAIGHTNESS IN CONTINUOUS BEAM-COLUMNS

When the initial out-of-straightness imperfections in a multi-span continuous strut do not follow the natural buckling pattern of sinusoidal alternatively up and down mode in adjacent spans, their effects on the buckling of the continuous strut can be analysed by applying the three-moment equations (1).

Consider a three-span strut subjected to a uniform axial load. The effects on the bending moments in the central span due to initial imperfections in the central span only and in the end spans only will be separately analysed. It may be assumed that the initial imperfections further away from the span under consideration in a multi-span system will not have a very significant effect.

Imperfections in any particular span will be assumed to follow a sine curve with maximum amplitude δ_0 . For applying the three-moment equations (1), the end-slopes of a simply-supported span with this pattern of imperfection under the action of compressive load P is given by:

$$\frac{\pi \delta_0 P_E}{L P_E - P}$$

Following the same method as discussed in Section 3.1, it can be shown that:

- (a) for the case shown in Fig. 32a, i.e. only the central span having initial imperfections, the effectiveness factor F_{23} for mid-span moment in span 2-3 and factor F_2 for support moment can have maximum values of + 0.618 and - 0.382 respectively;
- (b) for the case shown in Fig. 32b, i.e. the adjacent spans having initial imperfections but the central span being straight, F_{23} ranges from - 0.382 to - 0.667 for $0 \leq u \leq \frac{\pi}{2}$, with a value of approximately 0.5 for $u = 1.11$ (i.e. $P = \frac{1}{2} P_E$). The maximum value of F_2 is - 0.382;
- (c) when all the three spans have initial imperfections in the same directions and of equal magnitude, i.e. a "hungry horse" pattern, the value of F_{23} ranges from + 0.236 to - 0.259 within the range $0 \leq u \leq 1.5$, the negative values occurring

for $u > 1.14$, i.e. for $P > 0.53 P_E$. The maximum value of F_2 is - 0.764.

It is not straight-forward to provide a simple formula for effective imperfection in a span in terms of the imperfections in the particular span and in the adjacent ones, as the maximum values of the different effectiveness factors occur at different values of u . However, if we assume that the load P is not expected to be greater than $\frac{1}{2} P_E$, then the following approximate formula may be suggested:

$$\delta_{n_{eq}} = -\frac{1}{4} \delta_{n-1} \pm \frac{1}{2} \delta_n - \frac{1}{4} \delta_{n+1} \quad \dots \quad (13)$$

where $\delta_{n_{eq}}$ is the equivalent imperfection in span n .

It should be noted that δ_n , etc. must be taken with their correct signs, i.e. say +ve when sagging. This formula is very similar to the one suggested for this purpose in the Merrison Rules^[3], but the necessity for the \pm sign for δ_n was not recognised there. This \pm sign for δ_n must, however, be taken in order to provide for the changing sign of the bending moment from the mid-span to the support regions due to continuity.

5. LOCAL TRANSVERSE LOADING ON CONTINUOUS BEAM-COLUMN

A continuous beam-column subjected to axial and local transverse loads can be analysed by the application of the three-moment equations (1). A three-span beam-column of constant section subjected to some local loading at the central span and a constant axial load throughout, as shown in Fig. 33a, is considered first.

5.1 The basic equation for the three-span beam column is:

$$4 M_2 \Psi(u) + M_2 \phi(u) = -\frac{6EI}{L} \theta_{2r} \quad \dots \quad (14)$$

where θ_{2r} is the slope on the right hand side of support 2 of the span 2-3 of the beam-column, when this span is considered simply supported.

θ_{2r} may be assumed to be approximately given by:

$$\frac{P_E}{P_E - P} \bar{\theta}_{2r}$$

where $\bar{\theta}_{2r}$ is the slope due to local loads at support 2 of span 2-3, assumed simply-supported and without any axial loading in the span.

Hence:

$$M_2 = - \frac{6EI}{L} \left[\frac{P}{P_E - P} \right] \frac{\bar{\theta}_{2r}}{4\Psi(u) + \phi(u)} \quad \dots \quad (15)$$

The additional mid-span deflection in span 2-3 caused by the continuity moments at supports 2 and 3 is given by:

$$2 \frac{M_2}{P} \left[\frac{\sin u}{\sin 2u} - \frac{1}{2} \right]$$

Hence total mid-span moment M_{23} is given by:

$$\begin{aligned} M_{23} &= \bar{M}_s \frac{P_E}{P_E - P} + M_2 + P \cdot \frac{2 M_2}{P} \left[\frac{\sin u}{\sin 2u} - \frac{1}{2} \right] \\ &= \bar{M}_s \frac{P_E}{P_E - P} + \frac{2 \sin u}{\sin 2u} M_2 \quad \dots \quad (16) \end{aligned}$$

where \bar{M}_s = mid-span moment in a simple span 2-3 due to wheel load, without any axial load

M_2 = support moment at 2, given by equation (15).

Similar expressions can be developed for the two-span beam-column shown in Fig. 33b; these are:

$$\left. \begin{aligned} M_2 &= - \frac{6EI}{L} \frac{P_E}{P_E - P} \frac{\bar{\theta}_{2L}}{4\Psi(u)} \\ M_{12} &= \bar{M}_s \frac{P_E}{P_E - P} + \frac{\sin u}{\sin 2u} M_2 \end{aligned} \right\} \dots \quad (17)$$

where $\bar{\theta}_{2L}$ and \bar{M}_s are the slope at support 2 and mid-span moment in span 1-2 due to local loading, when the span is considered simply-supported and without any axial load.

Formulae (15), (16) and (17) were applied for both single concentrated load and uniformly distributed load in span 2-3 of Fig. 33a and 1-2 of Fig. 33b respectively for the range of $0 \leq u \leq 1.5$, and the results are shown in Table 2.

5.2 It may be noticed that, for a given magnitude of the local loading W , as the ratio P/P_E increases, the span moments $M_{2,3}$ (Fig. 33a) and $M_{1,2}$ (Fig. 33b) increases rapidly, but the support moments M_2 increases only marginally. For example, when P/P_E increases from zero to 0.6333, the span moments increase by between 103 and 140 per cent, but the support moments increase by between 20 and 30 per cent. When the wheel loads produce significant bending stress, the ratio P/P_E is not expected to be higher than 0.4; hence the following simple design rules may be suggested:

- (i) Calculate bending moments in the mid-span regions and over the supports of the continuous beam due to local loads, ignoring the axial load.
- (ii) Take design span moments as the moments calculated in step (i), multiplied by the ratio $\frac{P_E}{P_E - P}$.
- (iii) Take design support moments as the moments calculated in step (i).

The above simple design rules are likely to over-estimate the span moments and under-estimate the support moments by not more than 15 per cent and hence can be considered satisfactory. It should be noted that the Merrison Rules stipulate multiplying both the span and the support moments by the ratio $\frac{P_E}{P_E - P}$, and hence over-estimate the support moments.

6. FAILURE CRITERION FOR CONTINUOUS STRUTS

In any theory for strength of single-span struts, the first yielding of an extreme fibre is generally taken as the criterion for failure. In a continuous multi-span strut, complete failure can only occur when sufficient numbers of plastic hinges at mid-spans and/or supports form a mechanism. However, it can be argued that the flexural stiffness of the continuous strut will fall at an accelerated rate once

| | | u | 0 | 0.1 | 0.25 | 0.5 | 0.75 | 1.0 | 1.25 | 1.50 |
|-----------------------------------|---------------|--------------------|--------|--------|--------|--------|--------|--------|--------|---------|
| | | P/P_E | 0 | .0041 | .0253 | .1013 | .2280 | .4053 | .6333 | .9119 |
| 3-Span Beam-Column Fig. 33a | Conc. Load | M_2/WL | -.0750 | -.0751 | -.0755 | -.0769 | -.0795 | -.0836 | -.0897 | -.0992 |
| | | M_{23}/WL | +.175 | +.1755 | +.1786 | +.1906 | +.2152 | +.2656 | +.3973 | +1.4353 |
| | | $M_{23}/M_{23u=0}$ | 1.0000 | 1.0029 | 1.0206 | 1.0891 | 1.2300 | 1.5177 | 2.2703 | 8.2017 |
| | Dist. Load | M_2/WL | -.0500 | -.0500 | -.0503 | -.0513 | -.0530 | -.0557 | -.0598 | -.0661 |
| | | M_{23}/WL | +.075 | +.0753 | +.0763 | +.0806 | +.0895 | +.1071 | +.1522 | +.4844 |
| | | $M_{23}/M_{23u=0}$ | 1.0000 | 1.0040 | 1.0173 | 1.0747 | 1.1933 | 1.4280 | 2.0293 | 6.4587 |
| 2-Span Beam-Column Fig. 33b | Conc. Load | M_2/WL | -.0937 | -.0939 | -.0946 | -.0972 | -.1019 | -.1097 | -.1225 | -.1448 |
| | | M_{12}/WL | +.2031 | +.2038 | +.2077 | +.2228 | +.2542 | +.3189 | +.4875 | +1.8142 |
| | | $M_{12}/M_{12u=0}$ | 1.00 | 1.0034 | 1.0226 | 1.0970 | 1.2516 | 1.5702 | 2.4003 | 8.9325 |
| | Dist. Load | M_2/WL | -.0625 | -.0626 | -.0630 | -.0648 | -.0679 | -.0732 | -.0817 | -.0965 |
| | | M_{12}/WL | +.0937 | +.0941 | +.0957 | +.1022 | +.1155 | +.1424 | +.2113 | +.7368 |
| | | $M_{12}/M_{12u=0}$ | 1.00 | 1.0037 | 1.0208 | 1.0901 | 1.2277 | 1.5189 | 2.2539 | 7.8592 |

TABLE 2: BENDING MOMENTS IN CONTINUOUS BEAM-COLUMNS
CARRYING LATERAL AND AXIAL LOADS

yielding starts at any cross-section, and hence even for continuous struts first yielding may be assumed to be a criterion for failure. The concept of effectiveness factors derived in this chapter, i.e. the ratio of maximum bending moment in a continuous strut to that in a single span strut with identical eccentricity, is dependent upon the validity of this assumption. To check this, twelve three-span straight continuous struts subjected to eccentrically applied longitudinal load were analysed for ultimate load by:

- (i) applying the three-moment theorem as described in this chapter, in conjunction with first yield as failure criterion, and
- (ii) an elasto-plastic computer program^[19], which divides the spans into a large number of segments and maintains compatibility of deformations and stresses in all the segments as increments of load are applied. This program can thus be considered to predict the true ultimate load.

The values of the main parameters in these twelve examples largely cover the range of practical geometries generally used in stiffened compression flanges, and are given below:

- (i) Three geometries with
 - (a) $\frac{\text{Stiffener area}}{\text{Flange plate area}}$ 0.35, 0.60, 0.90
 - (b) $\frac{\text{Extreme fibre distance to stiffener tip}}{\text{Extreme fibre distance of flange plate}}$... 3.25, 4.40, 6.80
- (ii) Slenderness ratio $\frac{L}{r}$ 50, 80
- (iii) $\frac{\text{Span}}{\text{Eccentricity of applied loading}}$ 500, 1000

The ultimate load obtained by the application of the three-moment theorem as described in this chapter, in conjunction with first yield as the failure criterion, were found to lie between 0.96 to 0.99 times the values given by the computer program. This comparison validates the hypothesis that first yield at any cross-section is a suitable failure criterion for continuous struts.

CHAPTER 9

TORSIONAL BUCKLING OF STIFFENER OUTSTANDS

1. INTRODUCTION

In Section 3 of Chapter 3 it has been stated that the geometry of the stiffener outstands and the tolerances on initial lateral misalignments of the stiffeners should be subjected to such restrictions as to ensure negligible non-linearity in the axial load-shortening behaviour of the stiffener outstands. There are several reasons for this cautionary approach and these are discussed below:

- (a) If both the flange plate panel and the stiffening rib are slender, then due to interactive buckling the combined strut will be highly sensitive to initial imperfections, and the load-shortening curve of this strut will show a violent fall-off after the peak load. This phenomenon has been demonstrated by, amongst others, Koiter^[32] and Thompson^[33] from theoretical considerations, and Horne and Narayanan^[51] experimentally.
- (b) With increasing axial load on the combined stiffener, as the flexure of the stiffener increases, the pattern of longitudinal stress on the stiffener outstand changes from a generally uniform one over the whole depth to a linearly varying one. The maximum stresses occur at the tip of the outstand if the flexure is towards the flange plate, or at the flange plate if the flexure is towards the stiffener tip. Thus, for a theoretical analysis for the combined stiffener, load-end shortening characteristics of a slender outstand will be required for a wide range of stress pattern. This will present some formidable difficulties in any theoretical analysis method, particularly when the stiffener outstand is other than a flat section, i.e. an angle or a bulb flat or tee.
- (c) For the load-shortening behaviour of the flange plate panels, large-deflection plate theory has been utilised on the assumption that the longitudinal edges of the plate are held against out-of-plane deflection. This is not strictly true in reality,

since flexure of the whole stiffener between transverse supports indicates that the longitudinal edges of the plate panel are not fully held against out-of-plane deflection. This assumption will be still more optimistic if the stiffener outstand geometries are made so slender as to significantly reduce the effective flexural rigidity of the combined strut.

- (d) Longitudinal stiffeners in box girders are often attached to flange plating by intermittent welding. Tests at Manchester^[51] have indicated that these gaps between welding, if too large, may have a damaging effect both on the magnitude of the maximum load and also on the behaviour of the stiffener at or past the maximum load, i.e. a sudden and drastic fall-off in the load. This type of failure was initiated by gross lateral deformation of the outstand in the region of the weld gaps, followed by a bursting of the welds. This phenomenon was found to be more serious with slender outstands. By ensuring a compact section of the stiffener outstands it is hoped that this undesirable effect of intermittent welding on the performance of stiffener outstands shall be removed.

In the Merrison Rules a safeguard against torsional buckling of the stiffener outstand has been incorporated in the form of a restriction that the maximum calculated stress in the stiffener outstand, due to applied longitudinal loading and flexure due to initial imperfections, end eccentricity, etc., must not exceed two-thirds of the elastic critical torsional buckling stress of the outstand. There are also certain tolerances on initial lateral imperfections of the stiffeners, but these tolerances are not theoretically related to the above stress limitation.

In the following sections this problem of torsional buckling of the stiffener outstand will be investigated in the following analytical sequences:

- (a) Large-deflection plate theory will be used to examine the sensitivity of strength and stiffness of plate outstands with respect to initial lateral imperfections.
- (b) Single large-deflection theory cannot be readily used for other types of open-type stiffener outstands, i.e. angles, tees and bulb flats, a suitable criterion will be developed for compact-

ness of outstand geometry based on elastic critical buckling stress only, but derived from the application of large-deflection theory to flat stiffeners.

- (c) Rotational restraint offered by the flange plate panels to the stiffener outstand will be examined.
- (d) The effect of variation of the longitudinal stress pattern over the depth of the stiffener outstand, due to the flexure of the combined strut section consisting of the flange plate and the stiffener outstand, will be investigated.

No explicit allowance for residual stresses shall be made in this analysis of stiffener outstands, as the magnitude, pattern and even the sign of the residual stresses due to welding of these stiffeners to the flange plate cannot be predicted with any degree of certainty. Field measurements^[52] have shown that residual stresses in the outstand seem to depend on the method of handling, assembling for fabrication and sequence of operations, etc., and thus they vary considerably in different fabricated panels.

2. LARGE-DEFLECTION PLATE THEORY APPLIED TO PLATE STIFFENER OUTSTAND

The St. Venant equation for equilibrium at any point in an isotropic plate is, from Section 1 of Chapter 4:

$$\frac{\partial^4 w}{\partial x^4} + \frac{2\partial^4 w}{\partial x^2 \partial y^2} + \frac{\partial^4 w}{\partial y^4} = \frac{t}{D} \left[\frac{q}{t} + \sigma_x \frac{\partial^2 w}{\partial x^2} + \sigma_y \frac{\partial^2 w}{\partial y^2} + 2\tau_{xy} \frac{\partial^2 w}{\partial x \partial y} \right]$$

where all the terms are as defined in Section 1, Chapter 4.

The elastic critical buckling stress of an ideally flat outstand subjected to uniaxial compression shall be evaluated first, then the post-buckling behaviour of the initially flat outstand, and finally the behaviour of an initially imperfect plate outstand, i.e. a plate with initial out-of-plane deflections, investigated.

2.1 Elastic Critical Buckling Stress of a Flat Outstand

This has been derived by several authors and Bulson^[34] gives a resume of the various methods adopted for this purpose. The same

energy method as already used in Chapter 4, and due originally to Timoshenko, will be used here, mainly to form the foundation for the subsequent sections of this Chapter. In this method the plate is given a very small out-of-plane deflection consistent with its edge conditions, at various levels of applied compressive forces. The increment of strain energy ΔU_b due to this small deflection is equated to the increment of work done ΔT_b due to the in-plane movement of the loaded edges as a consequence of the small deflection. Figure 34 shows the geometry of the plate.

Since the deflection considered is very small, (i) σ_x is constant everywhere in the plate, and (ii) $q = \sigma_y = \tau_{xy} = 0$; this reduces the St. Venant equation to:

$$\frac{\partial^4 w}{\partial x^4} + \frac{2\partial^4 w}{\partial x^2 \partial y^2} + \frac{\partial^4 w}{\partial y^4} = - \frac{\sigma_x t}{D} \frac{\partial^2 w}{\partial x^2} \quad \dots \quad (1)$$

The out-of-plane boundary conditions are:

$$\text{At } y = 0: \quad (\text{i}) \quad w = 0; \quad (\text{ii}) \quad M_y = D \left[\frac{\partial^2 w}{\partial y^2} + \nu \frac{\partial^2 w}{\partial x^2} \right] = 0$$

$$\text{At } y = b: \quad (\text{iii}) \quad M_y = D \left[\frac{\partial^2 w}{\partial y^2} + \nu \frac{\partial^2 w}{\partial x^2} \right] = 0;$$

$$(\text{iv}) \quad \text{Shear } V = D \left[\frac{\partial^3 w}{\partial y^3} + (2-\nu) \frac{\partial^3 w}{\partial x^2 \partial y} \right] = 0$$

$$\text{At } x = 0: \quad (\text{v}) \quad w = 0; \quad (\text{vi}) \quad M_x = D \left[\frac{\partial^2 w}{\partial x^2} + \nu \frac{\partial^2 w}{\partial y^2} \right] = 0$$

$$\text{At } x = a: \quad (\text{vii}) \quad w = 0; \quad (\text{viii}) \quad M_x = D \left[\frac{\partial^2 w}{\partial x^2} + \nu \frac{\partial^2 w}{\partial y^2} \right] = 0$$

All the above boundary conditions, except (iii) and (iv), are satisfied if we assume the deflected shape to be:

$$w = A \frac{y}{b} \text{Sin} \frac{n\pi x}{a}, \quad \text{when } A \text{ is very small} \quad \dots \quad (2)$$

$$\text{At } y = b, \quad M_y = -D \nu A \frac{n^2 \pi^2}{a^2} \text{Sin} \frac{n\pi x}{a}$$

$$V = -D (2-\nu) \frac{A}{b} \frac{n^2 \pi^2}{a^2} \text{Sin} \frac{n\pi x}{a}$$

From boundary conditions (iii) and (iv), the above two expressions should have been zero. Later on in this section, it will be found that, for critical buckling, $n = 1$. The length of the plate a is normally many times the width b and since the maximum amplitude of deflection A is small compared with b , these apparent reactive forces at the free edge for the above deflected shape will actually be very small. (This has also been numerically demonstrated in Section 4 of this chapter.) Hence the assumed deflected shape given by equation (2) will be retained.

The bending strain energy $d(\Delta U_b)$ in any element $dx \cdot dy$ is the sum of the work done by the bending moments $M_x dy$ and $M_y dx$, and by the twisting moments $M_{xy} dy$ and $M_{yx} dx$. The work done by each of these moments is $\frac{1}{2} \times \text{moment} \times \text{angle of distortion}$. Using equations (2) of Chapter 4, it can be shown that for isotropic plates:

$$d(\Delta U_b) = \frac{1}{2} D \left[\left(\frac{\partial^2 w}{\partial x^2} \right)^2 + \left(\frac{\partial^2 w}{\partial y^2} \right)^2 + 2\nu \frac{\partial^2 w}{\partial x^2} \frac{\partial^2 w}{\partial y^2} + 2(1-\nu) \left(\frac{\partial^2 w}{\partial x \partial y} \right)^2 \right] dx dy$$

and
$$\Delta U_b = \int_0^b \int_0^a d(\Delta U_b)$$

Using equation (2) and integration over the whole plate leads to:

$$\Delta U_b = \frac{D}{2} \frac{A^2 n^2 \pi^2}{ab} \left[\frac{n^2 \pi^2 b^2}{6a^2} + (1-\nu) \right] \dots \dots \quad (3)$$

The loaded edges approach each other by an amount:

$$\int_0^a \frac{1}{2} \left(\frac{\partial w}{\partial x} \right)^2 dx$$

Hence the work done ΔT_b by the external forces is:

$$\Delta T_b = \sigma_a t \int_0^a \int_0^b \frac{1}{2} \left(\frac{\partial w}{\partial x} \right)^2 dx dy$$

Using equation (2) leads to:

$$\Delta T_b = \frac{1}{2} \sigma_a t A^2 \frac{n^2 \pi^2 b}{6a} \dots \dots \quad (4)$$

Equating $\Delta U_b = \Delta T_b$, the critical stress is given by:

$$\sigma_{cr} = \frac{6Et^2}{12(1-\nu^2) b^2} \left[\frac{n^2 \pi^2 b^2}{6a^2} + (1-\nu) \right]$$

Obviously σ_{cr} will be minimum when $n = 1$.

Hence:

$$\sigma_{cr} = \left[\frac{1}{\phi^2} + \frac{6(1-\nu)}{\pi^2} \right] \frac{\pi^2 E}{12(1-\nu^2)} \left(\frac{t}{b} \right)^2 \quad \dots \quad (5a)$$

where $\phi = \frac{a}{b} =$ aspect ratio of the plate.

If a is very large compared to b , i.e. a long plate of narrow width, then $\frac{1}{\phi} \rightarrow 0$, and

$$\sigma_{cr} = \frac{E}{2(1+\nu)} \left(\frac{t}{b} \right)^2 = G \left(\frac{t}{b} \right)^2 \quad \dots \quad (5b)$$

2.2 Post-buckling Behaviour of an Ideally Flat Outstand

The post-buckled deflected shape shall be assumed to be in the elastic critical buckling mode, i.e.

$$w = A \frac{y}{b} \sin \frac{\pi x}{a} \quad \dots \quad (6)$$

where A is no longer very small.

The boundary condition for the longitudinal edges completely free for in-plane displacement is $\sigma_y = 0$ when $y = 0$ and b . A simple form of stress function satisfying the equilibrium and compatibility conditions everywhere, i.e. equations (4) and (16) respectively of Chapter 4 simplified for an isotropic plate, and also all the boundary conditions on the edges, is not known to exist. In order to obtain an approximate solution, it shall be assumed that σ_y is zero everywhere in the plate, and not just on the longitudinal edges. From equilibrium equations for membrane forces, i.e.

$$\frac{\partial \sigma_x}{\partial x} + \frac{\partial \tau_{xy}}{\partial y} = 0$$

$$\frac{\partial \sigma_y}{\partial y} + \frac{\partial \tau_{yx}}{\partial x} = 0$$

and from the condition that shear stresses along the edges are zero, it follows that τ_{xy} is also zero everywhere and σ_x is constant along any longitudinal strip. The relationship between the deflection amplitude A and the average applied stress σ_a will be derived from the principle of minimum total potential energy.

The bending strain energy U_b will be given by equation (3), with $n = 1$, which becomes, on simplification:

$$U_b = \sigma_{cr} bt \frac{\pi^2 A^2}{12a}$$

i.e. critical load times shortening.

The strain energy U_m due to membrane forces will be given by:

$$\begin{aligned} U_m &= \frac{t}{2E} \int_0^b \int_0^a \sigma_x^2 dx dy \\ &= \frac{ta}{2E} \int_0^b \sigma_x^2 dy \end{aligned}$$

since σ_x is a function of y only.

$$\text{Total strain energy } U = U_b + U_m.$$

The rate of change of U with respect to deflection amplitude A is given by:

$$\frac{dU}{dA} = \sigma_{cr} bt \frac{\pi^2 A}{6a} + \frac{ta}{E} \int_0^b \sigma_x \frac{\partial \sigma_x}{\partial A} dy \quad \dots \quad (7)$$

From equations (1) and (14), Chapter 4, since $\sigma_y = 0$

$$\begin{aligned} \frac{\partial u}{\partial x} &= \frac{\sigma_x}{E} - \frac{1}{2} \left(\frac{\partial w}{\partial x} \right)^2 \\ &= \frac{\sigma_x}{E} - \frac{1}{2} \left[\frac{\pi y A}{ab} \cos \frac{\pi x}{a} \right]^2 \end{aligned}$$

using equation (6).

The total change of length Δa is:

$$\Delta a = \int_0^a \frac{\partial u}{\partial x} dx = \frac{\sigma_x a}{E} - \frac{\pi^2 y^2 A^2}{4b^2 a} \quad \dots \quad (8)$$

The potential energy T of applied loads = (-) work done by the loads:

$$\begin{aligned} &= - \int_0^b \sigma_x t \Delta a \, dy \\ &= - \frac{at}{E} \int_0^b \sigma_x^2 \, dy + \frac{\pi^2 A^2 t}{4b^2 a} \int_0^b \sigma_x y^2 \, dy \end{aligned}$$

on substitution for Δa from (8).

The rate of change of T with respect to deflection amplitude A is given by:

$$\begin{aligned} \frac{dT}{dA} &= \int_0^b \frac{-2\sigma_x t a}{E} \frac{\partial \sigma_x}{\partial A} \, dy + \frac{A\pi^2 t}{2b^2 a} \int_0^b \sigma_x y^2 \, dy \\ &\quad + \frac{A^2 \pi^2 t}{4b^2 a} \int \frac{\partial \sigma_x}{\partial A} y^2 \, dy \quad \dots \quad (9) \end{aligned}$$

From (8):

$$\sigma_x = \frac{\Delta a E}{a} + \frac{A^2 y^2 \pi^2 E}{4a^2 b^2} \quad \dots \quad (10)$$

$$\text{Hence} \quad \frac{ta}{E} \int_0^b \sigma_x \frac{\partial \sigma_x}{\partial A} \, dy = \int_0^b \Delta a \cdot t \frac{\partial \sigma_x}{\partial A} \, dy + \int_0^b \frac{tA^2 \pi^2}{4b^2 a} \frac{\partial \sigma_x}{\partial A} y^2 \, dy$$

We shall assume at this stage that the loaded edges approach each other uniformly; hence Δa is not a function of y and can be taken outside the integral sign of the first term. The first integral on the right hand side then becomes the change in the total applied load, which must be zero, since we are investigating the buckled shape under a particular magnitude of the applied load. The second integral on the right hand side above is identical to the last term of equation (9). Hence

$$\frac{dT}{dA} = - \int_0^b \frac{\sigma_x t a}{E} \frac{\partial \sigma_x}{\partial A} \, dy + \frac{A\pi^2 t}{2b^2 a} \int_0^b \sigma_x y^2 \, dy \quad \dots \quad (9a)$$

From the principle of minimum total potential energy:

$$\frac{d(U+T)}{dA} = \frac{dU}{dA} + \frac{dT}{dA} = 0$$

Hence from equations (7) and (9a)

$$\sigma_{cr} b t \frac{\pi^2 A}{6a} + \frac{A \pi^2 t}{2b^2 a} \int_0^b \sigma_x y^2 dy = 0$$

Substitution for σ_x from equation (10) leads to:

$$\frac{\sigma_{cr} b^3}{3} = - \int_0^b \left[\frac{\Delta a E y^2}{a} + \frac{A^2 y^4 \pi^2 E}{4a^2 b^2} \right] dy = - \left[\frac{\Delta a E b^3}{3a} + \frac{EA^2 \pi^2 b^5}{20 a^2 b^2} \right]$$

$$\text{or, } - \Delta a = \frac{1}{E} \sigma_{cr} a + \frac{3\pi^2}{20} \frac{A^2}{a} \quad \dots \quad (11)$$

Putting this in equation (10):

$$- \sigma_x = \sigma_{cr} + \frac{3}{20} \frac{\pi^2 EA^2}{a^2} - \frac{EA^2 \pi^2 y^2}{4a^2 b^2}$$

the negative sign for σ_x indicating compression.

Mean longitudinal compressive stress σ_a is given by:

$$\sigma_a = \frac{1}{b} \int_0^b (-\sigma_x) dy = \sigma_{cr} + \frac{1}{15} \frac{E \pi^2 A^2}{a^2} \quad \dots \quad (12)$$

From equation (11), apparent compressive strain e_a is given by:

$$e_a = - \frac{\Delta a}{a} = e_{cr} + \frac{3\pi^2}{20} \frac{A^2}{a^2}$$

where $e_{cr} = \sigma_{cr}/E$

$$\text{Hence } (\sigma_a - \sigma_{cr}) = \frac{E \pi^2 A^2}{15a^2} = \frac{4}{9} (e_a - e_{cr})$$

i.e. the post-buckling stiffness of the plate is 4/9 times that of the unbuckled plate.

2.3 Buckling Behaviour of an Initially Imperfect Flat Outstand

The in-plane boundary conditions are that the longitudinal edges are completely free for in-plane movement, i.e. $\sigma_y = 0$ when $y = 0$ and b . The further simplifying assumption, made in Section 2.2 of

of this chapter for post-buckling behaviour of initially perfect flat outstand, that σ_y , and hence τ_{xy} , are zero everywhere in the flat outstand, shall also be retained. The initial and the final deflections shall be assumed in the natural buckling mode, i.e.

$$\left. \begin{aligned} \text{Initial deflection} \quad w_o &= A_o \frac{y}{b} \sin \frac{\pi x}{a} \\ \text{Final deflection} \quad w &= A \frac{y}{b} \sin \frac{\pi x}{a} \end{aligned} \right\} \dots \quad (13)$$

Since flexure of the plate is associated with the change of shape given by $(w - w_o)$, bending energy U_b , will now be given by:

$$U_b = \sigma_{cr} b t \frac{\pi^2 (A - A_o)^2}{12a}$$

where σ_{cr} is the elastic critical buckling stress.

Since σ_y and τ_{xy} are zero everywhere and σ_x is independent of x , strain energy U_m due to membrane forces is given by:

$$U_m = \frac{t a}{2E} \int_0^b \sigma_x^2 dy$$

Total strain energy $U = U_b + U_m$; and rate of change of total strain energy with respect to amplitude of deflection is given by:

$$\frac{dU}{dA} = \sigma_{cr} b t \frac{\pi^2 (A - A_o)}{6a} + \frac{t a}{E} \int_0^b \sigma_x \frac{\partial \sigma_x}{\partial A} dy \quad \dots \quad (14)$$

From equations (1) and (14), Chapter 4, since $\sigma_y = 0$

$$\begin{aligned} \frac{\partial u}{\partial x} &= \frac{\sigma_x}{E} - \frac{1}{2} \left(\frac{\partial w}{\partial x} \right)^2 + \frac{1}{2} \left(\frac{\partial w_o}{\partial x} \right)^2 \\ &= \frac{\sigma_x}{E} - \frac{1}{2} \frac{(A^2 - A_o^2) y^2 \pi^2}{a^2 b^2} \cos^2 \frac{\pi x}{a} \end{aligned}$$

using equation (13).

The total change of length Δa of a is:

$$\Delta a = \int_0^a \frac{\partial u}{\partial x} dx = \frac{\sigma_x a}{E} - \frac{(A^2 - A_o^2) y^2 \pi^2}{4b^2 a} \quad \dots \quad (15)$$

The potential energy T of applied loads = (-) work done by load:

$$= - \int_0^b \sigma_x t \Delta a. dy$$

$$= - \frac{\alpha t}{E} \int_0^b \sigma_x^2 dy + \frac{(A^2 - A_0^2) \pi^2 t}{4b^2 a} \int_0^b \sigma_x y^2 dy$$

Rate of change of T with respect to A is:

$$\frac{dT}{dA} = \int_0^b \frac{-2\sigma_x t a}{E} \frac{\partial \sigma_x}{\partial A} dy + \frac{A\pi^2 t}{2b^2 a} \int_0^b \sigma_x y^2 dy$$

$$+ \frac{(A^2 - A_0^2) \pi^2 t}{4b^2 a} \int_0^b \frac{\partial \sigma_x}{\partial A} y^2 dy \quad \dots \quad (16)$$

From equation (15):

$$\sigma_x = \frac{\Delta a \cdot E}{a} + \frac{(A^2 - A_0^2) y^2 \pi^2 E}{4a^2 b^2} \quad \dots \quad (17)$$

Following the procedure in the previous section, it can be shown that:

$$\frac{dT}{dA} = - \int_0^b \frac{\sigma_x t a}{E} \frac{\partial \sigma_x}{\partial A} dy + \frac{A\pi^2 t}{2b^2 a} \int_0^b \sigma_x y^2 dy \quad \dots \quad (18)$$

From the principle of minimum total potential energy:

$$\frac{dU}{dA} + \frac{dT}{dA} = 0$$

Hence from equations (14) and (18), and taking $A = mA_0$:

$$\sigma_{cr} b t \frac{\pi^2 A_0^{(m-1)}}{6a} + \frac{mA_0 \pi^2 t}{2b^2 a} \int_0^b \sigma_x y^2 dy = 0$$

or,

$$\frac{\sigma_{cr} b}{3} (m-1) + m \int_0^b \sigma_x y^2 dy = 0$$

Substituting for σ_x from equation (17), and integration leads to:

$$\frac{\sigma_{cr} b^3 (m-1)}{3} = -m \left[\frac{\Delta\alpha \cdot E}{a} \cdot \frac{b^3}{3} + \frac{A_o^2 (m^2-1) \pi^2 E}{4\alpha^2 b^2} \frac{b^5}{5} \right]$$

Hence $-\Delta\alpha = \sigma_{cr} \frac{(m-1)}{mE} + \frac{3\pi^2 A_o^2 (m^2-1)}{20\alpha} \dots \dots \dots (19)$

Putting this in equation (17):

$$-\sigma_x = \sigma_{cr} \frac{m-1}{m} + \frac{3\pi^2 EA_o^2 (m^2-1)}{20\alpha^2} - \frac{\pi^2 E (m^2-1) A_o^2 y^2}{4\alpha^2 b^2} \dots \dots \dots (20)$$

the negative sign for σ_x indicating compression.

Mean longitudinal compressive stress σ_α is given by:

$$\begin{aligned} \sigma_\alpha &= \frac{1}{b} \int_0^b (-\sigma_x) dy \\ &= \sigma_{cr} \frac{m-1}{m} + \frac{\pi^2 EA_o^2 (m^2-1)}{15\alpha^2} \dots \dots \dots (21) \end{aligned}$$

Maximum longitudinal compressive stress occurs at $y = 0$, and is given by:

$$\sigma_{max} = \sigma_{cr} \frac{m-1}{m} + \frac{3\pi^2 EA_o^2 (m^2-1)}{20\alpha^2} \dots \dots \dots (22)$$

From equation (19), the apparent compressive strain e_α is given by:

$$e_\alpha = \frac{-\Delta\alpha}{\alpha} = \sigma_{cr} \frac{m-1}{mE} + \frac{3\pi^2 A_o^2 (m^2-1)}{20\alpha^2} = \frac{\sigma_{max}}{E} \dots \dots \dots (23)$$

The secant stiffness K_s , defined as the ratio of average stress to E times apparent strain, is given by:

$$K_s = \frac{\sigma_\alpha}{\sigma_{max}} = \frac{\sigma_{cr} + \frac{\pi^2 EA_o^2 m (m+1)}{15\alpha^2}}{\sigma_{cr} + \frac{3\pi^2 EA_o^2 m (m+1)}{20\alpha^2}} \dots \dots \dots (24)$$

For plates simply supported on all four edges and subjected to longitudinal compression, maximum membrane stresses occur at the longitudinal edges, and in Chapter 5 it has been found that a satisfactory criterion for the ultimate strength of the plate is the attainment of membrane yield stress on these edges. For plates simply supported on three edges only, and subjected to longitudinal compression, it shall similarly be assumed that the ultimate strength of the plate is reached when the membrane stress on supported longitudinal edge reaches yield stress, i.e. from equation (22):

$$\sigma_{max} = \sigma_{cr} \frac{m-1}{m} + \frac{3\pi^2}{20} \frac{EA_o^2 (m^2-1)}{a^2} = \sigma_{ys}$$

For long plates, i.e. when $a \gg b$, σ_{cr} may be obtained from equation (5b).

Hence the above stipulation leads to:

$$\frac{Et^2 (m-1)}{2.6 \sigma_{ys} b^2 m} + \frac{3\pi^2 EA_o^2 (m^2-1)}{20 \sigma_{ys} a^2} = 1$$

Taking $\frac{b}{t} \sqrt{\frac{\sigma_{ys}}{E}} = S$, a slenderness parameter

$$\frac{A_o}{a} \sqrt{\frac{E}{\sigma_{ys}}} = \delta_o, \text{ an imperfection parameter}$$

the above equation may be expressed as:

$$3.849 S^2 \delta_o^2 m^2 - \frac{1}{m} = 2.6 S^2 + 3.849 S^2 \delta_o^2 - 1 \dots (25)$$

and equations (21) and (24) for mean stress σ_a and secant stiffness K_s for ultimate state may be expressed as:

$$K_{su} = \frac{\sigma_{au}}{\sigma_{ys}} = \frac{m-1}{2.6 S^2 m} + 0.658 \delta_o^2 (m^2-1) \dots (26)$$

For any plate of given slenderness parameter S and initial imperfection parameter δ_o , the magnification factor m at its ultimate load may be obtained from equation (25), and then the secant stiffness K_{su} , or the strength parameter $\frac{\sigma_{au}}{\sigma_{ys}}$, may be obtained from equation (26).

Equation (25) is cubical in terms of m and hence its solution will require a successive approximation approach. The right hand of the equation can be calculated from the given data; calling this J , the derivative $\frac{dJ}{dm}$ may be obtained for an assumed value of m , say m_1 , from:

$$\frac{dJ}{dm} = 7.698 S^2 \delta_o^2 m_1 - \frac{1}{m_1^2}$$

For this assumed value of m_1 , the left hand side of equation (25) may be calculated as J_1 say. Next approximation for m is:

$$m_2 = m_1 - \frac{J_1 - J}{(dJ/dm_1)}$$

and so on.

3. SENSITIVITY OF STRENGTH/STIFFNESS OF FLAT OUTSTAND TO INITIAL IMPERFECTIONS

Equations (25) and (26) have been used to draw curves of K_{su} ($= \frac{\sigma_{au}}{\sigma_{ys}}$) against slenderness parameter S ($= \frac{b}{t} \sqrt{\sigma_{ys}/E}$), for three values of initial imperfection parameter δ_o ($= \frac{A_o}{a} \sqrt{E/\sigma_{ys}}$) of 0.2, 0.1 and 0.05. These values of δ_o relate to design limits of lateral misalignments approximately equal to $\frac{a}{150}$, $\frac{a}{300}$ and $\frac{a}{600}$ respectively for steel of yield stress 245 N/mm². These curves are shown in Fig. 35.

It shall now be postulated that the secant stiffness K_{su} or strength parameter $\frac{\sigma_{au}}{\sigma_{ys}}$ shall not be allowed to drop to any value less than 0.975, i.e. a maximum fall in stiffness or strength of 2.5% shall be taken to be the limit for assuming a linear load-shortening behaviour of the outstand.

From the graphs in Fig. 35, the maximum permitted values of the slenderness parameter S then works out as follows for the three initial imperfection parameters δ_o :

| | | | |
|------------|-----|-------|-------|
| δ_o | 0.2 | 0.1 | 0.05 |
| S_{max} | 0.3 | 0.425 | 0.525 |

$S_{max} = 0.3$ is too severe a design restriction, as $\frac{b}{t}$ ratio has to be limited to 8.7 and 7.2 for steel of yield stress 245 and 355 N/mm² respectively. The other extreme of $S_{max} = 0.525$ will, however, have to be accompanied by a design tolerance of $\frac{a}{600}$ on lateral misalignment which is considered too severe for fabrication in the light of the Merrison fabrication tolerances, which can be as high as $\frac{1}{175}$ of the gauge length. Hence as a compromise, it seems that the best solution is to take the initial imperfection parameter $\delta_0 = 0.1$, coupled with a restriction on the slenderness parameter S as not more than 0.425.

From equation (5b), $S \leq 0.425$ leads to a factor of safety against elastic critical buckling of not less than 2.13, i.e.

$$\frac{\sigma_{cr}}{\sigma_{ys}} \geq 2.13$$

Rounding up this figure to 2.25, it shall now be postulated that for any type of open stiffener outstand, i.e. angles, bulb flats, tees or flats:

- (i) the ratio of elastic critical buckling stress σ_{cr} to the applied stress σ_a on the outstand at ultimate load shall not be less than 2.25;
- (ii) the fabrication tolerance on lateral misalignment of stiffener outstands shall be taken as 2/3 of the design limit on initial imperfection, i.e.

$$A_0 \leq \frac{1}{450} \sqrt{\frac{\sigma_{ys}}{E}} \text{ times the gauge length}$$

The above limitations are stricter than the Merrison Rules as the latter prescribes a minimum factor of 1.5 only for the ratio $\frac{\sigma_{cr}}{\sigma_a}$, and also the Merrison ratios of fabrication tolerance to gauge length of measurements are higher than the values stipulated here. But in view of the above results of the application of the large deflection plate theory to flat outstands, these stricter limitations are considered necessary and more rational.

4. BOUNDARY CONDITIONS AT THE FREE EDGE

It has already been noted in Section 2.1 that the assumed deflected shape does not satisfy the boundary condition that M_y is

zero at the free edge $y = b$. The maximum value of M_y at this edge occurs at $x = a/2$ and is equal to:

$$M_y = -D \nu (m-1) A_o \frac{\pi^2}{a^2}$$

and the maximum fibre stress due to this moment is given by:

$$\sigma_f = \frac{E \nu t}{2(1-\nu^2)} (m-1) A_o \frac{\pi^2}{a^2}$$

With the notations $\delta_o = \frac{A_o}{a} \sqrt{\frac{E}{\sigma_{ys}}}$ and $S = \frac{b}{t} \sqrt{\frac{\sigma_{ys}}{E}}$, σ_f may be expressed as:

$$\sigma_f = \frac{\pi^2 \nu}{2(1-\nu^2)} (m-1) \frac{\delta_o}{S} \frac{b}{a} \sigma_{ys}$$

It has already been decided that δ_o shall not exceed 0.1. With $\delta_o = 0.1$, the magnification factor m for different values of S works out from equation (25) as follows:

| | | | |
|-----------------|------|------|------|
| S | 0.4 | 0.5 | 0.6 |
| m | 1.68 | 2.50 | 3.87 |
| $\frac{m-1}{S}$ | 1.7 | 3.0 | 4.8 |

Thus the factor $\left(\frac{m-1}{S}\right)$ increases with higher values of S . The limiting value of S has already been taken as 0.425. For this value of S , the factor $\left(\frac{m-1}{S}\right)$ works out as 2.0. The ratio $\frac{b}{a}$, i.e. width to span of the outstand is of the order of $\frac{1}{10}$. Hence, taking $\nu = 0.3$, the maximum possible value of σ_f will be of the order of:

$$\frac{\pi^2 \nu}{2(1-\nu^2)} (0.02) \sigma_{ys} = 0.033 \sigma_{ys}$$

This value is considered small enough to justify the validity of the solutions derived from an assumed deflected shape which did not fully satisfy two out of the total eight boundary conditions.

5. ELASTIC CRITICAL BUCKLING OF TEE-TYPE OUTSTAND

Bleich^[53] and Timoshenko^[50] have given the solution for elastic critical stress for torsional buckling of Tee-type stiffener outstands attached to a thin sheet of plating. In the simplest case, the flexural rigidity of the plate is ignored. The problem of stiffeners unsymmetrical about the vertical plane, i.e. angle type of stiffeners, is dealt with by Timoshenko, but the correct solution is too complicated for simple design rules.

5.1 Outstand of Tee-Section

For Tee-type stiffeners shown in Fig. 36, the critical stress for torsional buckling is given by the following expression, when flexural rigidity of the flange plate is ignored:

$$\sigma_{cr} = \frac{1}{I_p} \left[EW \frac{\pi^2}{L^2} + EI_y a^2 \frac{\pi^2}{L^2} + GJ \right] \dots \quad (27)$$

where I_p = polar moment of inertia of outstand about its attachment to flange plate O

W = warping constant of outstand section

I_y = second moment of area of outstand section about Y-Y axis

a = distance between the shear centre of the outstand section and its attachment to flange plate O

J = St. Venant torsional constant of outstand section

L = span of stiffener between adjacent transverse supports.

For Tee-section:

$$W = \frac{t_1^3 b_1^3}{144} + \frac{t_2^3 d^3}{36}$$

$$I_y = \frac{t_1 b_1^3}{12}, \text{ ignoring the small contribution from the web}$$

$a = d$, since shear centre coincides with the intersection of the centre-line of the web and the flange of the outstand

$$J = \frac{d t_2^3 + b_1 t_1^3}{3}$$

$$I_p = \int_{web} (x^2 + y^2) dA + \int_{flg} (x^2 + y^2) dA$$

where dA is a small elemental area in the web or the flange at a distance of x and y from O along the respective axes.

Hence

$$I_p = \frac{t_2 d^3}{3} + \frac{t_1 b_1^3}{12} + t_1 b_1 d^2$$

For a flat section, all the above terms apply, except that b_1 and t_1 may be taken to be zero, and $a = \frac{d}{2}$, since the shear centre coincides with the centroid of the flat section.

Taking $t_1 = K_1 t_2$, and $b_1 = K_2 d$, the critical buckling stress σ_{cr} given by equation (27) can be expressed as follows:

$$\sigma_{cr} = \frac{E}{L^2} \left[t_2^2 F_1 + d^2 F_1 \right] + E F_3 \left[\frac{t_2}{d} \right]^2 \dots\dots (28)$$

where

$$F_1 = \frac{\pi^2}{12} \frac{4 + K_1^3 K_2^3}{4 + K_1 K_2^3 + 12 K_1 K_2}$$

$$F_2 = \pi^2 \frac{K_1 K_2^3}{4 + K_1 K_2^3 + 12 K_1 K_2}$$

$$F_3 = 1.5385 \frac{1 + K_1^3 K_2}{4 + K_1 K_2^3 + 12 K_1 K_2} \dots\dots (29)$$

Graphs for F_1 , F_2 and F_3 are given in Fig. 37.

6. EFFECT OF FLEXURAL RESTRAINT PROVIDED BY THE FLANGE PLATE

Assuming n numbers of half-waves of buckling in the length L between transverse supports, the differential equation of equilibrium at the critical buckling state has been given by Bleich^[53] as follows:

$$(GJ - \sigma I_p) \frac{\pi^2 n^2}{L^2} \Theta_o + E (W + a^2 I_y) \frac{\pi^4 n^4}{L^4} \Theta_o + C \Theta_o = 0 \dots\dots (30)$$

where θ_0 is the amplitude of rotation about point O, Fig. 36
 C = flexural stiffness of the flange plate measured in terms
of bending moment applied per unit length of stiffener
for unit rotation at O

all the other terms are as defined in Section 5.

Flexural stiffness C of the flange plate may be derived by assuming alternately up and down deflection of the flange plate in the adjacent panels, conforming to the buckling mode, as shown in Fig. 38.

Bending moment M on the flange plate on either side of each stiffener and the change of slope θ over each stiffener area related by:

$$\theta = \frac{M b}{2EI}$$

where I is the second moment of area of the flange plate per unit length.

Taking Poisson's effect into account, EI may be taken as

$D = \frac{Et^3}{12(1-\nu^2)}$ where t is the thickness and D is the flexural rigidity of the flange plate. Total bending moment on one stiffener is equal to $2M$, and hence

$$C = \frac{2M}{\theta} = \frac{4EI}{b} = \frac{4D}{b}$$

The above has been derived from the consideration of flexure only of the flange plate. When the flange plate is subjected to longitudinal in-plane compression as well, buckling due to the latter will reduce the flexural stiffness of the flange plate. It shall now be assumed that the above expression for C is valid when the longitudinal compressive stress σ on the flange plate is zero, but that C will reduce linearly from the above value to zero as the longitudinal compressive stress σ reaches the elastic critical buckling stress σ_{crp} of the flange plate, i.e.

$$C = \frac{4D}{b} \frac{\sigma_{crp} - \sigma}{\sigma_{crp}}$$

where $\sigma_{crp} = \frac{4 \pi^2 D}{b^2 t}$

Applying the above to equation (30):

$$E(W + a^2 I_y) \frac{\pi^4 n^4}{L^4} + GJ \frac{\pi^2 n^2}{L^2} + \frac{4D}{b} - \sigma \left[\frac{\pi^2 n^2 I_p}{L^2} + \frac{bt}{\pi^2} \right] = 0$$

Wherefrom the critical value of σ is given by:

$$\sigma_{cr} = \frac{E(W + a^2 I_y) \frac{\pi^4 n^4}{L^4} + GJ \frac{\pi^2 n^2}{L^2} + \frac{4D}{b}}{\frac{\pi^2 n^2 I_p}{L^2} + \frac{bt}{\pi^2}} \dots \dots \quad (31)$$

The lowest value of σ_{cr} shall be obtained by equating $\frac{d\sigma_{cr}}{dn} = 0$. Equation (31) is of the form AB^{-1} , where A is the numerator and B is the denominator of the expression in (31):

$$\frac{d\sigma_{cr}}{dn} = \frac{1}{B^2} \left[B \frac{dA}{dn} - A \frac{dB}{dn} \right] = 0$$

So the lowest value of σ_{cr} shall be given by:

$$\begin{aligned} \sigma_{cr} = \frac{A}{B} = \frac{dA/dn}{dB/dn} &= \frac{E(W + a^2 I_y) \frac{4 \pi^4 n^3}{L^4} + GJ \frac{2 \pi^2 n}{L^2}}{\frac{2 \pi^2 n I_p}{L^2}} \\ &= \frac{2E(W + a^2 I_y) \pi^2 n}{I_p L^2} + \frac{GJ}{I_p} \dots \dots \quad (32) \end{aligned}$$

where n is given by:

$$B \frac{dA}{dn} - A \frac{dB}{dn} = 0 ,$$

$$\begin{aligned} \text{or, } \left[I_p \frac{\pi^2 n^2}{L^2} + \frac{bt}{\pi^2} \right] \left[E(W + a^2 I_y) \frac{4 \pi^4 n^3}{L^4} + GJ \frac{2 \pi^2 n}{L^2} \right] \\ = \left[E(W + a^2 I_y) \frac{\pi^4 n^4}{L^4} + GJ \frac{\pi^2 n^2}{L^2} + \frac{4D}{b} \right] \left[I_p \frac{2 \pi^2 n}{L^2} \right] \end{aligned}$$

which, on simplification, leads to:

$$I_p E(W + a^2 I_y) \frac{\pi^6 n^4}{L^4} + \frac{2 \pi^2 bt E(W + a^2 I_y) n^2}{L^2} + bt GJ - 4 \pi^2 I_p \frac{D}{b} = 0$$

This is a quadratic equation in n^2 . Ignoring the negative solution, the valid solution for this equation is:

$$n^2 = - \frac{L^2 bt}{\pi^4 I_p} + \left[\frac{L^4 b^2 t^2}{\pi^8 I_p^2} + \frac{4 DL^4}{\pi^4 Eb(W + a^2 I_y)} - \frac{bt GJ L^4}{\pi^6 EI_p (W + a^2 I_y)} \right]^{1/2}$$

Taking $\nu = 0.3$, this leads approximately to:

$$n^2 = - 0.01 \frac{bt L^2}{I_p} + \left[0.0001 \frac{b^2 t^2 L^4}{I_p^2} + 0.00376 \frac{t^3 L^4}{b(W + a^2 I_y)} - 0.0004 \frac{bt J L^4}{I_p (W + a^2 I_y)} \right]^{1/2} \dots \quad (33)$$

The theoretically correct method for obtaining σ_{cr} will be:

- (i) Take a positive integer value of n nearest to the exact value of n from equation (33);
- (ii) Calculate σ_{cr} from equation (31) by substituting this positive integer value of n .

However, equation (32) is much simpler than equation (31) and will always give a slightly conservative value for σ_{cr} , since even fractional values of n are admitted for approximation purposes. Hence equation (32) is adopted.

If equation (33) produces a value of n less than 1, we can conclude that the effect of the flexural stiffness of the flange plate on the torsional buckling critical stress of the outstand is small, as the buckling half-wave-length is not altered; hence in this situation we can take for σ_{cr} the critical buckling stress of the outstand assumed hinged to the flange plate, i.e. from equation (27). We shall get an identical result if it is stipulated that in using equation (32), n^2 shall not be taken less than half. Equation (32) is very similar to the equation (27) for hinged outstand, except that the first two terms in equation (32) are multiplied by $2n^2$.

If the dimensional coefficients F_1 , F_2 and F_3 given in equation (29) are made use of, then equation (32) can be expressed as:

$$\sigma_{cr} = m E F_1 + m E F_2 \left(\frac{d}{t_2}\right)^2 + E F_3 \left(\frac{t_2}{d}\right)^2 \dots \quad (34)$$

$$\text{where } m = \frac{2 n^2 t_2^2}{L^2} = \frac{1}{50} [\{\alpha^2 + 40\beta - 4\gamma\}^{1/2} - \alpha],$$

but not less than $(t_2/L)^2$;

$$\text{where } \alpha = \frac{bt t_2^2}{I_p}$$

$$\beta = \frac{bt}{A_s} \left(\frac{t}{b}\right)^2 \frac{t_2^4}{d^2 r_y^2}$$

$$\gamma = \frac{bt}{A_s} \frac{J}{I_p} \frac{t_2^4}{d^2 r_y^2}$$

..... (35)

r_y = radius of gyration of outstand about Y-Y axis

A_s = area of outstand

$I_p = I_x + I_y$.

In equation (34) the three terms are respectively the contributions of the warping constant W , the lateral flexural inertia I_y and the St. Venant torsion constant J . It may be noted by comparing equations (28) and (34) that the third term is unaffected by the flexural restraint provided by the flange plate.

7. OTHER TYPES OF STIFFENER OUTSTANDS

7.1 Bulb-flat Outstand

Equation (34) is valid for tee-type stiffeners, and also for flat stiffeners as already discussed. Bulb-flat stiffeners may be assumed to be equivalent to a tee-section of the same overall depth, web thickness and flange width, with the flange thickness assumed to be the same as the average thickness of the bulb as indicated in Fig. 39a.

7.2 Angle Outstand

Equation (34) is strictly not valid for angle sections, due to asymmetry about the Y-Y axis, as discussed in Section 5. Since the correct solution given by Timoshenko for angle sections hinged to the flange plate is too complicated for design office use, it is recommended that equation (34) is used also for angle sections, except that I_p and r_y are taken for an equivalent tee-section of the same flange dimensions.

8. VARIATION OF STRESS IN THE DEPTH OF THE STIFFENER OUTSTAND

If the longitudinal loading on the stiffened compression flange is applied through its centroid, then the flange stiffener will have uniform compressive stress over its entire depth. But any eccentricity of this applied loading with respect to the centroid of the combined stiffener section, or flexure of the stiffener between its adjacent transverse supports due either to any locally applied transverse loading or to any initial out-of-straightness of the stiffener, will cause a variation of the longitudinal stress in its depth, with higher compressive stresses on the concave side and lower compressive stresses on the convex side of the deflected shape of the stiffener.

The previous sections of this chapter deal with a uniform compressive stress pattern over the entire stiffener. In this section, suitable modifications will be derived for application to the results of the previous sections, to allow for the variation of the longitudinal stress in the depth of the stiffener.

8.1 Flat Stiffener

For a flat stiffener outstand, hinged to the flange plate, the elastic critical buckling stress for uniform applied compressive stress on the flat section has been derived in Section 2.1 of this chapter. Consider the case when the applied compressive stress varies from a maximum value at the tip of the outstand to zero at its attachment to the flange plate, as shown in Fig. 40. The elastic critical magnitude of this linearly varying stress pattern will be derived here by applying the same principles as in Section 2.1. The deflected shape will be assumed to be given by equation (2). The bending strain energy ΔU_b will be identical to equation (3). The applied longitudinal stress σ_x varies with y , i.e.

$$\sigma_x = \sigma_b \frac{y}{b}$$

where σ_b is the maximum stress at $y = b$.

Hence the work done ΔT_b by the external forces is:

$$\Delta T_b = \frac{1}{2} t \int_0^b \int_0^a \sigma_x \left(\frac{\partial w}{\partial x} \right)^2 dx dy$$

$$= \frac{1}{2} t \sigma_b \int_0^b \int_0^a \frac{y}{b} A^2 \frac{y^2 n^2 \pi^2}{b^2 a^2} \cos^2 \frac{n\pi x}{a} dx dy$$

Integration over the plate leads to:

$$\Delta T_b = A^2 n^2 \pi^2 \sigma_b \frac{tb}{16a} \quad \dots \quad (37)$$

Equating $\Delta U_b = \Delta T_b$, the critical value of σ_b is given by:

$$\sigma_{bcr} = \frac{8 \pi^2 E}{12(1-\nu^2)} \left(\frac{t}{b}\right)^2 \left[\frac{n^2 b^2}{6a^2} + \frac{1-\nu}{\pi^2} \right]$$

The minimum value of σ_{bcr} will occur when $n = 1$ and is given by:

$$\sigma_{bcr} = \frac{\pi^2 E}{12(1-\nu^2)} \left(\frac{t}{b}\right)^2 \left[\frac{4b^2}{3a^2} + \frac{8(1-\nu)}{\pi^2} \right]$$

If a is very large compared with b , $\frac{b}{a} \rightarrow 0$, and

$$\sigma_{bcr} = \frac{2E}{3(1+\nu)} \left(\frac{t}{b}\right)^2 = \frac{4}{3} G \left(\frac{t}{b}\right)^2 \quad \dots \quad (38)$$

This is $\frac{4}{3}$ times the value obtained in equations (5a) and (5b) for the elastic critical buckling value for uniform compressive stress on the flat outstand.

The total stress on the stiffener outstand consists of a uniform pattern due to the centroidally applied longitudinal load and a linearly varying pattern due to the bending moment associated with the flexure. The centroid of the combined stiffener section is usually very near the inner surface of the flange plate and hence the two stress components may be approximately represented as in Fig. 41.

Assuming a linear interaction between the two stress components for critical buckling, which is the worst possible type of interaction, the factor λ_b against elastic critical buckling for a flat stiffener outstand hinged to the flange plate is given by:

$$\frac{\lambda_b \sigma_a}{G \left(\frac{t}{b}\right)^2} + \frac{\lambda_b \sigma_b}{\frac{4}{3} G \left(\frac{t}{b}\right)^2} = 1$$

$$\text{or } \lambda_b = \frac{G\left(\frac{t}{b}\right)^2 \frac{4\sigma_t}{3\sigma_t + \sigma_a}}{\sigma_t} \dots\dots (39a)$$

where $\sigma_t = \sigma_a + \sigma_b$ = stress at stiffener tip.

This is equivalent to multiplying σ_{cr} by the factor

$$\frac{4\sigma_t}{3\sigma_t + \sigma_a} \dots\dots (39b)$$

and comparing this modified value of σ_{cr} with σ_t .

8.2 Tee, Bulb-flat and Angle Stiffeners

The elastic critical buckling stress for uniformly compressed tee-type stiffener outstand flexurally restrained by the flange plate is given by equation (34), in which the three terms are respectively the contributions of the cross-sectional properties W , I_y and J . As discussed in the previous section, the stress gradient over the depth is allowed for, if the share contributed by the web towards these properties, and hence to σ_{cr} , is increased by the ratio given in (39b). But the shares contributed by the flange should not be increased, as the flange is subjected to the full value of σ_t . The contribution of the web towards I_y is negligible. But both the web and the flange contribute towards W and J , and so both the first and the third terms may be increased by a factor less than the value given in (39b).

As an approximation, it is suggested that only the third term is increased by the full value of the above factor in (39b), thus leading to:

$$\sigma_{cr} = m E F_1 + m E F_2 \left(\frac{d}{t_2}\right)^2 + E F_3 \left(\frac{t_2}{d}\right)^2 \frac{4\sigma_t}{3\sigma_t + \sigma_a} \dots (40)$$

where F_1 , F_2 and F_3 are given in Fig. 37, and m is given by equation (35).

9. DESIGN REQUIREMENTS FOR STIFFENER OUTSTANDS

It has been concluded in Section 3 that λ_b , i.e. σ_{cr}/σ_t should not be less than 2.25.

9.1 As a conservative first approximation, if only the third term in equation (40) is taken, then the span L and the number of half-waves will not influence this approximate value of σ_{cr} , and the following slenderness limit for the web of the stiffener may be stipulated:

$$\frac{d}{t_2} \dagger \left[\frac{E F_3}{2.25 \left(\frac{3}{4} \sigma_t + \frac{1}{4} \sigma_a \right)} \right]^{1/2} \dots \quad (41)$$

As a further safe approximation $\left(\frac{3}{4} \sigma_t + \frac{1}{4} \sigma_a \right)$ may be taken as the maximum stress in the stiffener σ_{max} . Noting that $F_3 = 0.385$ for flat section and 0.181 for equal-legged angles, this leads to:

$$\begin{aligned} \text{(a) for flats:} & \quad \frac{d}{t_2} \dagger 0.414 \sqrt{E/\sigma_{max}} \\ \text{(b) for equal-legged angles:} & \quad \frac{d}{t_2} \dagger 0.284 \sqrt{E/\sigma_{max}} \\ & \quad \text{or} \quad \frac{D}{t_2} \dagger 0.5 + 0.284 \sqrt{E/\sigma_{max}} \end{aligned}$$

where D is the overall width, and
 t_2 is the thickness of the legs.

9.2 When the torsional rigidity of the section is not adequate to satisfy (41), then the first and the second terms of equation (40) must be included; in this situation as a safe conservative approach m may be taken as $\left(\frac{t_2}{L} \right)^2$, which corresponds to neglecting the restraint offered by the flange plate. This approximation leads to:

$$\frac{d}{t_2} \dagger \left[\frac{F_3}{\frac{2.25 \sigma_t}{E} - \left(\frac{t_2}{L} \right)^2 F_1 - \left(\frac{d}{L} \right)^2 F_2} \cdot \frac{4\sigma_t}{3\sigma_t + \sigma_a} \right]^{1/2} \dots \quad (42)$$

9.3 When equation (42) is also not satisfied, then the restraint offered by the flange plate may be invoked by using the full equation (40), which leads to:

$$\frac{d}{t_2} \left\{ \left[\frac{F_3}{\frac{2.25 \sigma_t}{E} - m F_1 - m F_2 \left(\frac{d}{t_2}\right)^2} \cdot \frac{4\sigma_t}{3\sigma_t + \sigma_a} \right]^{1/2} \dots \right. \quad (43)$$

where m is given by equation (35).

9.4 In equation (43) σ_t and σ_a may be conservatively taken as the maximum stress in the stiffener σ_{max} . For flat section:

$$I_p = \frac{1}{3} t_2 d^3 \quad \text{and} \quad r_y = \frac{t_2}{2\sqrt{3}};$$

$$\text{hence} \quad \alpha = 3 \left(\frac{t_2}{d}\right)^3 \left(\frac{bt}{t_2^2}\right)$$

$$\beta = 12 \left(\frac{t_2}{d}\right)^3 \left(\frac{bt}{t_2^2}\right) \left(\frac{t}{b}\right)$$

$$\gamma = 12 \left(\frac{t_2}{d}\right)^5 \left(\frac{bt}{t_2^2}\right)$$

Substitution of the above in equation (35) leads to:

$$\left(\frac{t}{b}\right)^2 = 5.21 m^2 \left(\frac{t_2}{bt}\right) \left(\frac{d}{t_2}\right)^3 + 0.625 m + \frac{1}{10} \left(\frac{t_2}{d}\right)^2 \quad \dots \quad (44)$$

For a flat section, $F_1 = \pi^2/12$, $F_2 = 0$, $F_3 = 0.385$; taking $E = 205000 \text{ N/mm}^2$, equation (43) leads to:

$$m = 13.35 \times 10^{-6} \sigma_{max} - \frac{0.468}{(d/t_2)^2} \quad \dots \quad (45)$$

Hence when the torsional rigidity of the flat section is not big enough to produce its own contribution to the elastic critical stress equal to $2.25 \sigma_{max}$, i.e. when

$$\frac{d}{t_2} > 0.414 \sqrt{\frac{E}{\sigma_{max}}}$$

then the required value for m can be calculated from equation (45), and the upper limit for the $\left(\frac{b}{t}\right)$ ratio of the flange plate can be calculated from equation (44). This will then ensure that the flexural

restraint provided by the flange plate will be adequate to satisfy the criterion:

$$\sigma_{cr} \leq 2.25 \sigma_{max}$$

Taking σ_{max} as the yield stress, suitable graphs have been drawn in Fig. 42 giving the slenderness limitations of flat outstands for $\sigma_{ys} = 245$ and 355 N/mm^2 .

9.5 In addition to the above slenderness requirements of the web of the stiffener outstand, two further requirements should be stipulated, viz.

- (i) Slenderness of the flange of the tee-type stiffener outstand; the requirement for this can be taken to be the same as for a flat stiffener outstand. Neglecting warping rigidity EW , this requirement is shown in Section 9.1 to be:

$$\frac{b_1}{2t_1} \leq 0.414 \sqrt{E/\sigma_{max}}$$

where b_1 and t_1 are shown in Fig. 36

σ_{max} is the maximum calculated stress in the flange of the stiffener outstand.

- (ii) Slenderness of the web of the stiffener outstand when the denominator of the first term within the square-root sign in equations (42) or (43) is negative. In this case contributions of the warping rigidity EW and of the flexural rigidity EI_y to σ_{cr} , i.e. the sum of the first two terms in equation (40) is larger than $2.25 \sigma_t$. We can thus conclude that the dimensions of the flange of the outstand are large enough to give adequate support to the bottom edge of the web of the outstand against any tendency for lateral displacement. The slenderness requirement for the web of the outstand should then be the same as for the web of closed-type stiffeners derived in Section 10.

10. LOCAL BUCKLING OF CLOSED TYPE STIFFENERS

When the flange plate is stiffened by 'trough' type of stiffeners, the geometrical proportions of such stiffeners must be such as to produce negligible non-linearity in the axial load-shortening behaviour of such stiffeners. As pointed out in Section 1, residual stresses are rather unpredictable in either open or closed types of stiffeners, and hence no explicit allowance shall be made for residual stresses in the method given here.

10.1 Application of Large-Deflection Plate Theory

It is proposed that tolerances for out-of-plane imperfections in the walls of the trough-type stiffeners shall be the same as already suggested for flange plate panels. Hence the graph for strength and stiffness of residual-stress-free plates, i.e. Fig. 26b of Chapter 5, may be examined in order to obtain the dimensional limitations for the walls of closed stiffeners. It was observed that a slenderness limitation of:

$$S = \frac{b}{t} \sqrt{\frac{\sigma_{ys}}{E}} \not\leq 1.2 \quad \dots \quad (46)$$

produces a maximum fall in the strength/stiffness of 4.6% and also ensures a factor against elastic critical buckling of not less than 2.5. This fall in the strength/stiffener of 4.6% is higher than the 2.5% limit adopted for open type stiffeners. Frieze^[17] has shown that the load-shortening graphs of plates with all edges simply supported and with slenderness parameter $S \not\leq 1.2$ indicate a stable type of behaviour after the peak load is reached. However, tests at Manchester^[51] have shown that stiffened panels with slender flat stiffeners exhibit a violent fall-off of load after the peak stress is reached. In view of this stable behaviour of walls of closed type stiffeners it is considered that a maximum 4.6% fall in the strength/stiffness is acceptable and hence the flange of the trough stiffener, i.e. the horizontal bottom wall should satisfy the limitation $b_1/t_1 \not\leq 1.2 \sqrt{E/\sigma_{max}}$, when σ_{max} is the maximum calculated compressive stress in the bottom wall at ultimate load.

10.2 Effect of Variation of Stress in the Cross-Section

For the webs of the trough stiffener some allowance may be made for the fact that, due to flexure, the compressive stress may vary in the depth of the web. Assuming, as before, that the centroid of the combined stiffener section consisting of the trough stiffener and the girder flange plate is near the inner surface of the latter, the stress pattern on the trough may be assumed to be a combination of a uniform stress σ_a and a triangularly varying stress with the maximum value at the mid-plane of the bottom flange σ_b , as shown in Fig. 43.

The factor λ_b against critical buckling is given by the following approximate interaction relationship:

$$\frac{\lambda_b (\sigma_a + \frac{1}{2} \sigma_b)}{4\sigma_o} + \left[\frac{\lambda_b \cdot \frac{1}{2} \sigma_b}{24\sigma_o} \right]^2 = 1$$

where
$$\sigma_o = \frac{\pi^2 E}{12(1-\nu^2)} \left(\frac{t_2}{d}\right)^2$$

The solution for λ_b of the above quadratic equation is:

$$\lambda_b = \frac{-\frac{\sigma_b + \frac{1}{2} \sigma_b}{4\sigma_o} + \sqrt{\left[\frac{\sigma_a + \frac{1}{2} \sigma_b}{4\sigma_o}\right]^2 + \left[\frac{\sigma_b}{24\sigma_o}\right]^2}}{2 \left[\frac{\sigma_b}{48\sigma_o}\right]^2}$$

Taking the first two terms of the Binomial series,

$$\sqrt{\left[\frac{\sigma_a + \frac{1}{2} \sigma_b}{4\sigma_o}\right]^2 + \left[\frac{\sigma_b}{24\sigma_o}\right]^2} \approx \frac{\sigma_a + \frac{1}{2} \sigma_b}{4\sigma_o} + \frac{1}{2} \left[\frac{\sigma_b}{24\sigma_o}\right]^2 \frac{4\sigma_o}{\sigma_a + \frac{1}{2} \sigma_b}$$

and hence

$$\lambda_b \approx \frac{4\sigma_o}{\sigma_a + \frac{1}{2} \sigma_b}$$

i.e. for critical buckling a uniform compressive stress of $(\sigma_a + \frac{1}{2} \sigma_b)$ may be assumed on the web.

Aiming for the same factor of safety against critical buckling in the web as in the bottom flange of the trough, i.e. 2.5,

$$\frac{4\sigma_o}{\sigma_a + \frac{1}{2}\sigma_b} \dagger 2.5$$

which, after substituting for σ_o leads to:

$$\frac{d}{t_2} \dagger 1.7 \sqrt{\frac{E}{\sigma_t + \sigma_a}}$$

where σ_t is the stress at the outer edge of the web.

When the web of the trough stiffener is sloping, d must be taken as the actual width of the sloping web.

CHAPTER 10

BOX GIRDER TESTS FOR BEHAVIOUR OF STIFFENED COMPRESSION FLANGES

1. INTRODUCTION

An experimental programme of investigation into steel box girder behaviour was already under way, in the Engineering Structures Laboratories of Imperial College, at the time the Government appointed the Committee of Investigation into the Design and Erection of Steel Box Girder Bridges following the tragic events at Milford Haven and the Lower Yarra Crossing. It was almost immediately incorporated within the large-scale experimental programme established by the Committee of Investigation and was subsequently greatly extended beyond its original scope. The objective of this new programme was to collect as much experimental data on as many aspects of box girder behaviour as was possible within the limited amount of time available. The tests are, therefore, by no means an exhaustive study of all aspects of box girder behaviour but give some answers to the many questions which were posed by the Committee, and results of these tests were used to substantiate or modify the basis of certain of the methods contained within the clauses of the Committee's earlier appraisal^[54] rules and the final design documents^[3].

2. DESCRIPTION OF TESTS

2.1 Outline of Test Types

The tests were generally of two types: central point load tests on simply supported sections of box girders which simulated the conditions of high moment and shear which occur near the support region of a continuous structure, and pure moment tests which represent, in an idealised way, the conditions in the span region of a continuous girder. Of the eight models tested, three were of the pure moment type, four were centrally point loaded beam tests, and one was a modification of the latter type in which the model was subjected to both flexure and torsion.

As this thesis deals with the behaviour of the compression flange only, only those tests are described here in which the stiffened compression flange was critical, i.e. boxes 1, 2, 4 and 8. For ease of reference this original numbering of the boxes has been retained in this thesis.

These tests were conducted in 1971-72, when imperial units were still being used in the laboratory. In order to avoid redrafting of many drawings and graphs, imperial units of tonf for jack loads and inches for construction drawings and measured deflections have been retained.

[1 tonf = 9.964 KN; 1 inch = 25.4 mm.]

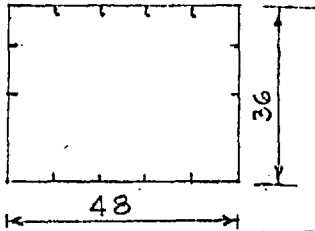
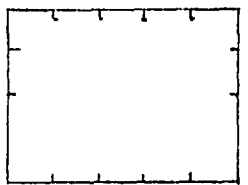
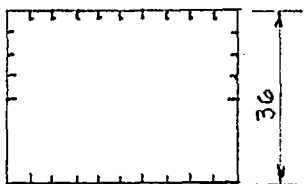
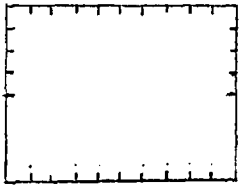
2.2 Description of Models

The models were approximately one quarter the size of those used in practice. Although the materials and fabrication procedure were representative of those used in full size box girder bridges, the relative sizes of welds were somewhat larger than would normally be employed. The material, mild steel similar to BS 4360, grade 43A, showed considerable scatter in its properties as derived from tensile test specimens. Tables 1a and 1b show the dimensions, properties and the relevant parameters of the critical components of these models.

2.3 Instrumentation

Deflections, including initial out-of-plane deformations and deflections under load, were measured on each model by a series of electrical deflection transducers. These were mounted on an inverted U-frame which straddled each girder and traversed the length of the models on a pair of rails. The rails, which were supported at three points on the flange, had fixed at regular intervals along their length a series of balls which were accurately levelled so that their uppermost points generated a plane under the weight of the U-frame. These balls also located the U-frame accurately at each of the sections chosen for measurements.

Weld-induced residual strains were measured over 2 in. and 4 in. gauge lengths between fixed points on the plate surface using a demountable mechanical Demec strain gauge. Recordings were taken at three stages of the fabrication: after cutting and butt welding of the component full length plates, after welding of the stiffeners to the plates, and after welding the stiffened plate components together to form the final model. Measurements were taken on both surfaces in order to obtain the mean strain, and temperature corrections were done by reference to gauge points marked on an unstressed plate.

| Model No. | Cross-section of model dimensions, in. | Component sizes and material properties | | | | |
|-----------|---|---|--|-------------------------------------|--|--|
| | | Component | Nominal size, in. | t, mm | σ_{ys} , N/mm ² | E, kN/mm ² |
| 1 |  | CF TF W LS TS D | 3/16 3/16 1/8 2 × 5/8 × 3/16L 3 × 2 × 1/4L 1/4 | 4.95 4.95 3.38 - - - | 247 247 273 329 314 255 | 201 201 215 201 195 199 |
| 2 |  | CF TF W LS TS | 3/16 3/16 1/8 2 × 5/8 × 3/16L 3 × 2 × 1/4L | 4.88 4.88 3.38 - - | 298 298 212 276 310 | 208 208 216 192 196 |
| 4 |  | CF TF W LS (CF), LS (W) LS (TF) TS | 3/16 3/16 3/16 2 × 5/8 × 3/16L 2 × 1/4 plate .4 × 2½ × 1/4L | 5.03 4.95 4.98 - - - | 221 216 281 287 304 304 | 207 208 215 199 207 201 |
| 8 |  | CF TF W LS TS | 3/16 3/16 1/8 1½ × 1/4 plate 3 × 1/4 plate | 4.72 4.67 3.17 - - | 276 366 252 312 294 | 208 208 216 210 208 |

| | | | | | |
|----|----------------|----|------------------------|---------|--|
| TF | Tension flange | CF | Compression flange | LS (CF) | Longitudinal stiffener on compression flange |
| W | Web | LS | Longitudinal stiffener | LS (TF) | Longitudinal stiffener on tension flange |
| D | Diaphragm | TS | Transverse stiffener | LS (W) | Longitudinal stiffener on web |

TABLE 1a: DIMENSIONS OF MODELS AND PROPERTIES OF MATERIALS

| <i>Model</i> | <i>Region of bridge</i> | <i>Critical components</i> | <i>Relevant parameters</i> | <i>Other features</i> |
|--------------|-------------------------|---|---------------------------------------|---|
| 1 | Intermediate support | (a) Largest web panels (b) Compression flange plate panels | (a) $b/t_w = 135$ (b) $b/t_f = 49$ | Flange stiffener $l/r = 49$; designed for simultaneous collapse of web and flange |
| 2 | Mid-span | Compression flange plate panels | $b/t_f = 51$ | Flange stiffener $l/r = 50$ |
| 4 | Mid-span | Compression flange stiffeners | $l/r = 45$ $b/t_f = 24$ | |
| 8 | Mid-span | Compression flange stiffeners | $l/r = 115$ $b/t_f = 26$ | Light transverse flange stiffeners given initial sinusoidal imperfections = span/310 and span/430 |

TABLE 1b: CRITICAL COMPONENTS OF MODELS AND RELEVANT PARAMETERS

Some 400 electrical resistance strain gauges, of rosette, cross and linear type, were used on each model to record the strains under load. The layout of the gauges and other relevant information on the instrumentation for each model are given in a series of reports [55].

2.4 Test Rigs

The central point load tests were carried out by applying hydraulic jack loading at one end of the model, providing the central reaction by means of bearings mounted on an overhead cross-beam, and resting the far end of the girder on bearings supported by concrete blocks on the laboratory floor. Thus the box was in the upside-down position in relation to the conditions at the support of a continuous girder. This position, Fig. 44, was adopted for ease of testing and observation of the critically compressed box components. Models so tested were fixed against longitudinal movement at the centre by means of stops each side of the radiused bearings.

Pure bending tests were carried out by applying jack loads to the extreme ends of special loading arms welded to each end of the box sections, Fig. 45. The arms were held down against vertical displacement at their junctions with the model. These holding down bolts had spherical bearing attachments which allowed rotation of the models in all directions. Although the system was self-stabilising, longitudinal and transverse movements of the girders were restricted by flexible stays anchored at one end to the loading arms and at the other end to the laboratory floor.

2.5 Material Properties

Yield stress and Young's Modulus for the critical components of the box were determined from tensile tests on coupons cut from surplus material. Straight, parallel-sided specimens $3/4$ in. wide \times 22 in. long were cut and prepared according to BS18. A 10 ton Amsler testing machine calibrated in accordance with BS1610 and conforming to grade A classification was used. Each test was conducted with a constant straining rate of approximately 300 micro-strains per minute. Thus the yield stresses obtained were the dynamic tensile yield stress values and are given in Table 1a.

In paragraph 3.3 of this chapter the collapse load of a box girder specimen is defined as the highest sustained value of the load reached in the whole test. Hence for correlation with this definition of the collapse load, static compressive yield stress values, rather than dynamic tensile values, should be used. Recent investigations^[56] have indicated that the ratio between the dynamic and the static tensile yield values is of the order of 1.04, when the dynamic test is conducted at approximately 300 micro-strains per minute, and the latter is taken as the lowest sustained value obtained after stopping the cross-heads for two minutes in the plastic phase. The investigations also indicated that the compressive yield stress can be expected to be approximately 5% higher than the tensile yield stresses, when both are conducted at the same strain rate.

It may be noted that the margin of error involved in using dynamic tensile yield stress values is not more than 1 per cent, and is considered acceptable.

3. TESTING PROCEDURE

3.1 Initial Measurements

Spot checks were made on residual strains before testing to ascertain if any redistribution of these strains had occurred during transportation and installation of the models. Initial out-of-plane deformations of the compression flanges and the webs were also measured and recorded at this stage. Subsequently, the actual dimensions of the model as fabricated, including the thicknesses of the component plates, were carefully recorded for use in the analysis of the test results.

3.2 Tests in Elastic Range

The first loading cycle in the testing of each model was restricted to loads well within the estimated ultimate capacity of the girder and was intended to provide information on the elastic behaviour of the model.

3.3 Tests to Collapse

Following the initial test in the elastic range, each model was loaded incrementally to collapse. During the early stages, loading was

controlled by predetermined increments of applied load while, in later stages, the applied deflections were increased incrementally by a strain control device located within the loading system. When each girder was nearing or beyond the collapse state, the load applied by the jacks for a constant overall girder deflection dropped from an instantaneous value to a lower sustained value over a period of time varying up to 45 min. This load fall-off was caused by the spread of plasticity and growth of buckles in critically stressed areas of the model. The instantaneous value of the load depended on the rate of load application as well as the imposed deformation; but the sustained value depended only on the latter. The highest value of the sustained load recorded in the whole test was taken to be the ultimate load of the model. After this load was reached, further increments of deflection were applied to each model to study its unloading characteristic. In some cases, it was possible to strengthen the girder after collapse had occurred in a particular element and re-test it until failure was reached in one or other of the remaining elements.

4. INITIAL IMPERFECTIONS

4.1 Out-of-Plane Deformations

Longitudinal and transverse initial deflection profiles of the compression flange and the webs of each girder were deduced from the transducer readings. For each girder the appropriate profiles of the compression flange are given separately at later sections.

It was noted that, in general, the longitudinal stiffeners bowed towards their outstand between transverse stiffeners, but that in some cases, notably in end bays, they deflected in the opposite direction. Plate panels were also generally deflected towards the surface to which the stiffeners were welded. The maximum curvature in the longitudinal direction occurred in the vicinity of the transverse stiffener welds. Away from these regions, the longitudinal profiles of the plate panels often showed small ripples superimposed on an otherwise gentle curve.

Table 2 gives the maximum values of measured transverse bows in the plate panels and the longitudinal stiffeners of the compression flange. Plate panel initial bows were not measured in models 4 and 8. Though the fabrication tolerances for prototype structures are not dir-

| Model | Initial plate panel bow*, effective over half-wave-length b | | | Initial stiffener bow measured over stiffener span L | | | |
|-------|---|--------------------------------------|-------------------------|--|--------------------------|--------------------------|--------------------|
| | from maximum observed value | from proposed tolerance in Chapter 5 | from Merrison tolerance | Panel | Average value in a panel | Maximum value in a panel | Merrison tolerance |
| 1 | $b/380$ | $b/250$ | $b/136$ | B-D | $-L/12400$ | $+L/1550$ | |
| | | | | D-I' | $+L/3100$ | | |
| | | | | I'-Q | $-L/7150$ | $-L/1630$ | |
| | | | | O-Q | $+L/15500$ | | |
| 2 | $b/330$ | $b/250$ | $b/136$ | A-C | $-L/2000$ | $+L/2280$ | |
| | | | | C-I | $-L/5280$ | | |
| | | | | I-O | $-L/3200$ | | |
| | | | | O-U | $-L/9250$ | $-L/1450$ | |
| | | | | U-W | $-L/1680$ | $-L/1200$ | |
| 4 | -- | $b/250$ | $b/139$ | A-C | $-L/1050$ | $+L/690$ | |
| | | | | C-I | $+L/1950$ | | |
| | | | | I-O | $+L/2280$ | $-L/510$ | |
| | | | | O-U | $+L/4920$ | | |
| | | | | U-W | $-L/660$ | | |
| 8 | -- | $b/250$ | $b/139$ | A-E | $+L/1770$ | $+L/930$ | |
| | | | | E-I | $+L/1500$ | $-L/610$ | |
| | | | | I-M | $-L/950$ | | |

*
+ the value indicated inward bow, i.e. towards the outstand
- the value indicated outward bow, i.e. away from the outstand

TABLE 2: SUMMARY OF MEASURED IMPERFECTIONS

ectly valid for smaller scale laboratory models, it can be seen from the table that the maximum plate panel bows were well within the tolerances proposed in Chapter 5. The Merrison Rules expression for plate tolerance includes the plate thickness in the denominator, i.e.

$$\Delta_p = \frac{2b}{30t} \left[1 + \frac{b}{5000} \right] - \text{all dimensions in mm.}$$

As the models were made with rather thin plates compared to actual box girders, this expression leads to rather high values.

It may, however, be noted that the maximum observed stiffener bows sometimes exceeded the Merrison tolerance, but the average bows in individual stiffened panels consisting of 4 or 9 stiffeners were well within the tolerances.

4.2 Residual Strains

A typical distribution of longitudinal compressive residual strains in the flange plate panels of model 2 is shown in Fig. 46a. Superimposed on the recorded distribution is the idealised residual strain pattern of the type assumed in Chapter 5 - a distribution which incidentally implies a discontinuity of strains. However, the assumption of a constant distribution of longitudinal compressive strains over the centre portion of the panel may be seen to be reasonable.

Figures 46b to 46d show typical distributions of average longitudinal compressive residual strains in the plate panels at corresponding cross-sections of models 2, 4 and 8. The only significant difference between the models was that there were twice as many stiffeners in the compression zone of models 4 and 8 compared with that in model 2. This difference is reflected in the increased magnitude of compressive residual strains in the former, consequent to the increased amount of welding. The residual strains measured in the webs suggest that both the level and distribution are governed to a large extent not only by the position, size and type of welds, but also by the sequence in which the stiffened flanges and webs are welded together.

In models 1 and 8 both longitudinal and transverse strains were measured near the central diaphragm and a transverse stiffener respectively, but in models 2 and 4 longitudinal strains only were measured away from any transverse welding.

Measured values of transverse strain were so irregular in distribution that no pattern could be established. Figure 46e shows the extent of variation in the readings in different strain gauges placed near one another in model 8.

5. WELDING RESIDUAL STRESSES

Average longitudinal compressive welding residual stresses in the compression flanges were calculated from an average value of the measured strains from one of the following two formulae as appropriate:

- (a) where both longitudinal and transverse strains, e_x and e_y respectively are available:

$$\sigma_R = \frac{E}{1 - \nu^2} (e_x + \nu e_y) \quad \dots \quad (1a)$$

- (b) where only longitudinal strains e are available:

$$\sigma_R = E e_x \quad \dots \quad (1b)$$

Theoretical values of compressive welding residual stresses were also calculated from the weld details and cross-section geometries of the compression flange. Manual intermittent welding was used to connect the longitudinal stiffeners to the flange plate, and MIG welding was used for the box corner welds; the coefficient for shrinkage force C for both welding was taken as 7.7 KN per sq. mm of weld area. The actual area of weld was estimated from several sections cut out from the relevant parts of the box after the completion of testing. The formulae used for calculating the theoretical residual stresses and the relevant data are given in Table 3, which also includes the experimental average values of the residual stresses obtained from the measured strains. It can be seen that the formula for predicting welding stresses, with the above value of the coefficient C for shrinkage force, is quite satisfactory. As only single-pass welds were used in the models, this validation of the formula should be considered to be limited to single-pass manual welds only.

| | | Unit | Model No. | | | |
|--|---------------|--------------------|-----------|-------|-------|-------|
| | | | 1 | 2 | 4 | 8 |
| Total flange area, | A_g | mm ² | 7226 | 7118 | 8787 | 7922 |
| Stiffener weld area, | W_s | mm ² | 9.5 | 11.0 | 11.0 | 11.0 |
| Stiffener weld length to gap ratio, r_1 | | - | 0.5 | 0.5 | 0.5 | 0.5 |
| No. of flange stiffener, | N | - | 4 | 4 | 9 | 9 |
| Box corner weld area, | W_c | mm ² | 15.8 | 15.8 | 25.8 | 19.4 |
| Ratio of web to flange thickness, r_2 | | - | 0.68 | 0.69 | 0.99 | 0.67 |
| Yield stress of flange plate, | σ_{ys} | kN/mm ² | 0.247 | 0.298 | 0.221 | 0.276 |
| Shrinkage force, F_s , due to stiffener welds, from formula below | | kN | 195.1 | 225.9 | 508.2 | 508.2 |
| Shrinkage force, F_c , due to box corner welds, from formula below | | kN | 144.8 | 114.0 | 199.7 | 178.9 |
| Longitudinal welding compressive stress: | | | | | | |
| (a) predicted value, σ_R , from formula below | | N/mm ² | 52.1 | 57.2 | 103.7 | 108.2 |
| (b) average experimental value, σ_R , obtained from measured strains from formula (1) | | N/mm ² | 58.4 | 52.2 | 122.9 | 107.0 |
| $F_s = 2CW_s N \frac{r_1}{1+r_1} \text{ kN}$ $F_c = 2CW_c \frac{1}{1+r_2} \text{ kN}$ $C = 7.7 \text{ kN/mm}^2, \text{ for manual weld}$ $\sigma_R = \frac{F_s \times 10^3}{A_g - \frac{F_s}{\sigma_{ys}}} + \frac{F_c \times 10^3}{A_g - \frac{F_c}{\sigma_{ys}}} \text{ N/mm}^2$ | | | | | | |

TABLE 3: COMPARISON BETWEEN PREDICTED AND MEASURED WELDING STRESSES

6. TEST DETAILS OF INDIVIDUAL MODELS

6.1 Model 1

The construction details of the model are shown in Figs 47a to 47c. Before testing, the initial geometrical imperfections of the plates and the stiffeners were determined at selected cross-sections shown in Fig. 48; the imperfection profiles at these cross-sections and the contour plots of the whole compression flange are given in Figs 49a to 49c.

While loading model 1 incrementally to collapse, the plate panels between longitudinal stiffeners in the compression flange began to show signs of buckling, just to one side of the central diaphragm, at a central point load of 90.0 tonf. At a load of 120.0 tonf, that is an average web shear stress, τ_a , of 97 N/mm^2 , the largest plate panels in the end web bays buckled in shear without any significant amplification of flange plate panel buckles. With little increase in load the middle web panels of the end bays also began to buckle and testing was terminated. Figure 50 shows diagrammatically the location of buckles in the web.

The fact that the web buckled in the area of least bending moment, rather than at the centre where the combined shear and direct stresses were greater, may be attributed to the combined effect of the stabilising influence of longitudinal tensile direct stresses upon shear buckling in the latter region, the relatively small in-plane restraint afforded by the end post compared with that due to continuity at the boundaries of the inner bays, and the presence of bearing stresses at the ends of the model.

At a load of 120.0 tonf in the second test, after strengthening the end bays, buckles were again visible in the largest of web plate panels but on this occasion of the intermediate web bays, Fig. 50. At a load of 132.0 tonf, that is nominal mid-plate flange stress, σ_a , of 201 N/mm^2 , the compression flange plate panels also showed significant buckling. With the application of the next load increment all four intermediate web bays collapsed and the load fell to a sustained value of 123.2 tonf. The intermediate bays were strengthened and the model was tested again.

In the third test at a maximum central point load of 128.0 tonf, that is $\sigma_a = 195 \text{ N/mm}^2$ and $\tau_a = 103 \text{ N/mm}^2$, failure occurred simultaneously in the flange on one side of the central diaphragm and in the web on the opposite side (Fig. 51). On the flange, the failure section was about one-third panel distance between the central diaphragm and the next transverse stiffener, near the former.

The entire loading history of the model during the three tests is shown in Fig. 52. Up to a central point load of approximately 90 tonf in the first test and 80 tonf in the second and the third test, the observed deflections were marginally less than those predicted by theory, when for the latter allowance is made for deflection caused by shear from the following equation:

$$\int \text{shear stress} \times \text{shear strain} \times dV = \Sigma P\Delta$$

where the left hand integral is extended over the whole volume of the box walls, and

P and Δ are the applied loads, and shear deflections at the location and in direction of the applied loads.

There was a small loss in the stiffness between 80 and 120 tonf central load in the second and the third tests, but a sharp fall-off of load occurred after the maximum load was reached in both these tests. The growth of load, curve 1, and of selected local and overall strains, curves 2 to 8, with overall deflection during this third test are shown in Figs 53a and 53b.

On the flange failure side the stiffeners failed at the same section at which plate collapse occurred by buckling in the direction of the outstand, namely, inwards. This caused flange stiffeners in the adjacent spans to move in the opposite direction and produced local lateral failure of the outstands near the transverse stiffeners. This latter phenomenon occurred only with loading beyond the peak value. The smallest web panels also buckled in line with the distorted flange panels causing the web-flange corners to collapse.

The webs on the opposite side of the diaphragm collapsed in a manner similar to that encountered in the two earlier tests. As further deformations were applied to the model beyond the ultimate load, bound-

aries of the web plate were pulled in as diagonal tension forces in the web panels became pronounced.

Figures 53a and 53b show that in the final test the overall load-deflection relationship, curve 1, was approximately linear up to a 120.0 tonf central load. Over this range the observed deflections were slightly less than those predicted using ordinary elastic beam theory in which allowance was made for shear deflections. The drooping nature of the relationship beyond peak load may be mainly attributed to the average stress-strain relationship of the compression flange after collapse. Curves 2, 3 and 4 of Fig. 53a show that stiffener collapse was precipitated almost immediately by plate panel collapse. Figure 54 confirms this by showing that longitudinal stiffeners buckled inwards at the same cross-section where flange plate panels failed.

Curves 5 and 6 of Fig. 53b show how strain in the longitudinal web stiffeners remained linear with load until the peak value was reached, whereas the out-of-plane deformation of the largest web panel was growing non-linearly with load from a relatively early stage. It is interesting to note that these web movements did not appear to affect the overall web stiffness. It was only after the peak load was reached that a significant increase in stiffener strains and movements occurred, thus confirming that collapse of the web was due to collapse of the individual panels. The growth of strains in the stiffeners beyond the ultimate load may be attributed to the axial compression arising from tension field action in the web panels, combined with the loss of effectiveness of the plate panels acting compositely with the stiffeners. As further deformations were applied to the girder the effect of these diagonal in-plane tensile forces was to exaggerate the rotations of the longitudinal stiffeners imposed by the buckling of adjacent panels in alternate directions.

6.2 Model 2

Model 2 was nominally of the same cross-section as model 1 (Tables 1a and 1b). The geometrical details of this model are shown in Figs 55a and 55b. The reference grid for initial deflection measurements and the longitudinal and transverse deflection profiles are given in Figs 56 to 57b. It may be noticed that the initial

deflections of longitudinal stiffeners between the cross frames were generally outwards, and were also of greater magnitude in the end bays A-C and U-W. While loading the model to collapse, buckling occurred in the flange plate panels between stiffeners adjacent to the welded transverse end frame at a jack load of 64.5 tonf, that is $\sigma_a = 206 \text{ N/mm}^2$. All flange panels, except for an internal one, deformed inwards (Fig. 58) while the adjacent web panels at the failed section buckled in a mode which maintained the angle between both elements. The longitudinal stiffeners of this end bay deflected away from the outstands while the adjacent bay moved in the opposite direction - a mode of buckling which conformed to that of the averaged initially deflected shape of the stiffeners. Figure 59 shows the gradual development of stiffener buckles in the end and the adjacent bays. Upon unloading significant residual buckles were observed, as shown in Fig. 59.

Subsequent examination of measured out-of-plane deflections indicated that those at several other sections had increased significantly at the measured peak load. Application of further deformations to the model caused a fall in sustained load. The end bay was stiffened as shown in Fig. 60 and the model was re-tested.

The growth of overall deflection and strains during the second test is shown in Fig. 61. At the same maximum nominal flange plate stress of $\sigma_a = 206 \text{ N/mm}^2$ flange plate buckling between stiffeners occurred at the centre of the stiffened bay adjacent to that which had previously collapsed (Figs 62a and 62b). As in the first test all the flange plate panels, except one, collapsed inwards, as shown in Fig. 63a, while the compression web panels at the same section again deformed in a compatible mode. Almost simultaneously with the visible formation of plate panel buckles, the longitudinal stiffeners deflected inwards with a hinge forming midway between transversals in line with the position of plate collapse, see Fig. 63b. As further deformations were applied a fall-off in sustained load occurred. Loss of stiffness in the bay in which the hinge formed caused the adjacent bays to introduce restraining moments at the transverse supports. Consequently, considerable compression was developed in the outstands of the longitudinal stiffeners at this location and they underwent local lateral buckling, see Fig. 63b.

During the first test the proximity of the flange plate buckles to the transverse fillet welds between flange plate and transverse end frame would suggest that the welds might have had a weakening effect on flange plate strength. One other possibility is that poor fit-up between the flange plate and that of the loading arm might have introduced a local eccentricity of loading in the plate. However, the results of the second test suggest that such effects were insignificant. The onset of local flange plate buckling occurred at 63.0 tonf jack load, that is $\sigma_{\alpha} = 201 \text{ N/mm}^2$, as may be seen from curves 2A, 2B, 2C and 2D of Fig. 61, whereas failure occurred at a stress of 206 N/mm^2 ; the corresponding plate panel deflections were of the order of plate thickness. (The elastic critical buckling stress, σ_{cr} , of this panel was 300 N/mm^2 .)

Longitudinal stiffener deflections, curve 3B, were small for loads up to those at which plate panel buckling commenced but increased at a faster rate beyond that point. Deformations applied to the model beyond this stage caused a fall-off in load similar to that encountered in the first model.

Load-deflection graphs for the two tests are shown in Figs 64a and 64b; Fig. 64a shows the deflection at the centre of the model over a length of 3.943 m observed during the first test, whereas Fig. 64b shows the central deflection over a length of 2.375 m observed during the second test. Also indicated in these figures are:

- (i) the theoretical deflections predicted by the simple bending theory taking the whole cross-section of the model as fully effective; and
- (ii) the deflection predicted by the simple bending theory, but ignoring the tensile yielded strips near the welds in the tension flange for calculating moment of inertia.

It would appear from these two figures that deflections can be predicted with reasonable accuracy by the simple beam theory taking full cross-sectional areas as effective.

6.3 Model 4

The slenderness ratio of the plate panels in the compression

flange of model 4 was made nominally half of that of models 1 and 2, by increasing the number of longitudinal stiffeners. The geometrical details are shown in Figs 65a and 65b. Details of the reference grid for deflection measurements are given in Fig. 56 and the initial deflection profiles in Figs 66a and 66b. Because of the close spacing of longitudinal stiffeners in the compression flange, it was difficult to measure the out-of-flatness of the flange plate panels; these data were not considered essential in view of the rather stocky proportions of the plate panels.

During the testing of this model, at a stage when the jack load reached 63.0 tonf, it was discovered that the amplifiers in the circuits of strain gauges and transducers had stopped functioning. Hence the model was unloaded, the amplifiers replaced and testing resumed again at a later date.

Buckling of the longitudinal stiffeners between transversals was first noticed at a jack load of 87.0 tonf, that is mid-plane flange plate stress $\sigma_{\alpha} = 216 \text{ N/mm}^2$. After applying further deformations to the model, collapse occurred at jack load of 92.5 tonf and flange plate stress of 230 N/mm^2 . The collapse mode was similar to the elastic critical buckling mode, namely, alternate bays deflecting in opposite directions between transverse stiffeners, see Fig. 67a, but it also followed closely the pattern of average stiffener initial deflections. In the end bays the longitudinal stiffeners deflected outwards, in conformity with the initial shape; at higher loads, the stiffener outstands consequently suffered lateral displacements, see Fig. 67b. Failure of the stiffened panels occurred without any noticeable buckling of the flange plate panels between the stiffeners. The gradual growth of the stiffener deflections, which closely followed the classical buckling mode throughout the test, is shown in Figs 68a to 68c.

The growth of transverse mid-plate strains up to collapse, curves 4A and 5A, Fig. 69, is consistent with the growth of Poisson's strains associated with the longitudinal strains, curves 2 and 3, in a laterally unrestrained plate. The transverse strains are approximately 0.3 times the longitudinal values, confirming that no significant large deflection or post-buckling effect was mobilised before reaching

collapse. However, it is interesting to note that the growth of longitudinal mid-plane strains at the centre of the flange plate panels, curves 4B and 5B, did deviate from linearity before any noticeable movement of the stiffeners, curve 6, occurred. Presumably, this was due to plastic redistribution of strains within the plate panels when the sum of the applied stress and the residual compressive stress present in the panels reached yield, and was directly responsible for the increasing loss in overall girder stiffness recorded beyond this stage.

The load-deflection graph for the model, Fig. 70, shows a stable plateau at peak load and indicates the model's capacity to sustain its collapse moment while undergoing further rotation. The maximum moment achieved was approximately 85% of the calculated plastic moment based on contributions from both web and flange, or 113% measured in terms of the flange capacity alone.

6.4 Model 8

All the models which previously failed by collapse of the compression flange had relatively stocky flange stiffeners even though in models 1 and 2 the flange plate panels were relatively slender. Therefore, model 8 was designed to study the failure of compression flanges in which both longitudinal and transverse stiffeners were slender while the plate panels were kept compact (see Tables 1a and 1b).

Figures 71a and 71b show the construction details of this model. In order to study the influence of initial imperfections on the behaviour of the transverse stiffeners, those at cross-sections E and I (Fig. 72) were predished; though the original intention was to impose a sinusoidal equal and opposite initial deflection pattern at those two cross-sections, the predishing actually achieved was towards the outstand at both the locations, of maximum magnitude of span/310 and span/430 at E and I respectively and of nearly sinusoidal pattern across the flange, as shown in Fig. 73b.

Figures 72 to 73b show the reference grid lines and the transverse and longitudinal initial deflection profiles.

6.4.1 Observations During Test

Referring to Fig. 74, up to a jack load of 31.0 tonf, that is mid-plane flange plate stress $\sigma_a = 88 \text{ N/mm}^2$, measured strains agreed satisfactorily with simple beam theory and measured girder deflections were marginally less than those similarly calculated. As the jack load and nominal flange stress increased to 46.0 tonf and 131 N/mm^2 respectively over the next two increments, only a slight loss of overall stiffness was noticeable although a marked departure of the recorded strains from simple beam theory values occurred at several locations. The next increment of deflection, which raised the jack load and the nominal flange stress to 51 tonf and 145 N/mm^2 , produced significant out-of-plane deformations of both the longitudinal stiffeners and the transverse stiffener E, see Figs 75a and 75b. It can be seen, by comparing Fig. 73a with Figs 75a and 75b, that the buckling mode followed closely the initially deflected shape of the compression flange. Considerable spalling of mill scale from the longitudinal stiffeners was observed in bay I-M, and the recorded strains confirmed that yielding of the stiffener outstands had occurred in this bay. The next increment produced the peak load of 55.5 tonf, that is $\sigma_a = 158 \text{ N/mm}^2$, and further magnified the already pronounced flange buckles. On completion of the test, local lateral buckling of the longitudinal stiffener outstand was observed to have occurred in bay I-M. Figures 76a and 76b show the deformed shape of the box at the completion of testing.

It can be shown that the load required to produce a nominal stress, as calculated by simple bending theory, at the centroid of the compression flange equal to the elastic critical buckling stress of the flange, is 55.4 tonf. This is almost identical to the maximum load sustained, i.e. 55.5 tonf. Therefore, in spite of the presence of large compressive residual stresses in the plate panels and pronounced initial deflections of the flange stiffeners, the flange not only sustained a load equal to the elastic critical load but also continued to maintain it, without fall-off, even when overall girder deflections were twice those producing flange buckling. It is clear, therefore, that there was a significant post-buckling (large deflection) contribution as the loads approached ultimate conditions. This behaviour is reflected in the growth of transverse strains, curves 4, 5, 6 and 7, Fig. 74. When the values of transverse strain are compared with

measured longitudinal strains, curves 2 and 3, it will be seen that up to a jack load of 46.0 tonf these strains were merely the transverse Poisson's strains associated with those applied longitudinally. Beyond that load, buckling of the stiffeners in panel I-M produced a fall-off in longitudinal strain, curve 3, but an increase in transverse strain, curve 5, at this section. This reflected the growth in transverse tensile stresses due to orthotropic behaviour of the flange, as the deflections of the stiffened flange bay became large. The effect of these transverse stresses was to restrict the growth of buckling in the failed panels. The more or less uniform distribution of longitudinal strains in the compression flange changed at the 51.0 tonf load level to a typical plate post-buckling distribution, that is, the stresses at the edges were higher than those measured in the centre of the flange.

Although it appears (Fig. 76a) that the flange may have collapsed by buckling over a wave length equal to that of the two bays A-E and E-I, it was in fact triggered by collapse of the stiffener outstands in compression in bay I-M. The longitudinal stiffeners in the two other bays were moving inwards in relation to the transverse stiffener E, but because this stiffener had a large initial deflection it was loaded by the vertical component of the in-plane compression of the longitudinal stiffeners framing into it. The vertical component of load on this stiffener was some $3\frac{1}{2}$ times that on the transverse stiffener I. This loading eventually caused the transverse stiffener at section E to collapse when deformations beyond those causing overall buckling were applied.

Figure 77 shows the load-deflection behaviour of the box observed during the test; also shown in this figure are the theoretical graphs based on (i) the whole of the girder cross-section taken as fully effective, and (ii) the yielded strips near welds in the tension flange taken as ineffective for computation of girder moment inertia; the observed deflections can be seen to fall within these two theoretically derived graphs.

The load deflection behaviour of the girder (see Fig. 77) showed onset of significant non-linearity at approximately 46 tons of jack load. The very slight kink in the load-deflection graph at a

jack load of 20 tons could possibly be attributed to the unavoidable experimental errors associated with the measurements of the transducers.

6.4.2 Reduction in Girder Stiffness due to Flange Stiffener Buckling

Because of the fairly high slenderness ratio of the flange stiffeners, it was considered probable that buckling of the compression flange stiffeners might have increased the girder deflections. So corrections were made to the deflections calculated by the conventional engineering beam theory, by incorporating a reduction factor K for the effective compression flange area, given by:

$$K = \frac{\sigma L/E}{\sigma L/E + \pi^2 \delta_p^2/4L}$$

where σ = centroidal applied stress on stiffener
 L = span of stiffener between transverse stiffeners
 δ_p = deflection of stiffeners due to jack load P , given by:

$$\delta_p = \delta_o \frac{P_{cr}}{P_{cr} - P} + e \left[\sec \frac{\pi}{2} \sqrt{P/P_{cr}} - 1 \right]$$

where δ_o = initial deflection of stiffeners
 P_{cr} = jack load to produce elastic critical stress at centroid of stiffener
 e = eccentricity of loading applied on the stiffener
 $= \frac{r^2}{h}$,

where r = radius of gyration of stiffener, and
 h = distance of stiffener centroid from girder neutral axis.

The above correction was found to be practically insignificant up to jack load of, say 30T; beyond this loading non-linearity of jack load vs. theoretical deflection started to develop, the slope finally being almost horizontal as the jack load approached P_{cr} . The theoretical value of P_{cr} was found to be 55.4T when the whole cross-section was considered fully effective, and 53.7T when the yielded strips in the tension flange were considered ineffective. By this approach it was possible to predict theoretically large girder deflections as the applied jack load gradually approached P_{cr} . The agreement

between the observed deflections and the theoretical deflections calculated in this manner is good. At low loading and also at loading approaching collapse load, observed deflections compared very satisfactorily with the theoretical ones calculated on the basis of the whole cross-section remaining effective; but in the intermediate loading stages the observed deflections were closer to the theoretical ones calculated with yielded strips on the tension flange taken as ineffective. It should, however, be mentioned that, as the measured yield stress of the tension flange plate was considerably higher than that of the compression flange and the web plates, the calculated loss of the effective tension flange area due to yielding at the welds was comparatively less than was the case with the other experimental boxes, and so the two graphs for the theoretical calculated deflections were quite close to each other.

6.4.3 *Behaviour of Intermediate Transverse Stiffeners on Compression Flange*

Measured initial transverse deflections of the compression flange at different cross-sections along the length of the box girder are shown in Fig. 73b. The deflection patterns at the intermediate transverse stiffener locations E and I were almost sinusoidal across the flange. The theoretical basis for the formula of effective loading on the cross-frames in Clause 2.9.2 of the Merrison Appraisal Rules^[54], as discussed in Appendix I of the Rules, is the assumption of sinusoidal initial deflection across the flange at all cross-sections, and the further assumption that alternate cross-frames have upwards and downwards initial deflections of equal magnitude. In spite of the departure of the initial deflections across the compression flange in spans A-E and I-M from the theoretical sinusoidal pattern (see Fig. 73b), it was considered reasonable to retain the assumption of sinusoidal deflection across the flange at all cross-sections for calculation of loads, etc., in the transverse stiffeners, with a maximum ordinate of 0.155 in. at section E and 0.110 in. at section I. In the longitudinal direction, however, as the initial deflections at the end cross-sections A and M were much smaller, and also as the deflections at E and I were not opposite in sign to each other, effective alternate up and down deflections were calculated for the two cross-frames at E and I separately, so

as to produce the same vertical component of force at the respective cross-frames due to longitudinal loading on the flange. These effective deflections were 0.05625 in. and 0.01625 in. respectively for cross-frames E and I, as shown in Fig. 78. Stresses at the tip of the outstand of the transverse stiffeners were calculated from the loading obtained from the formula in Clause 2.9.2. In using this formula some allowance was made for the notches in the transverse stiffener in calculating its effective moment of inertia. This method of treatment of the cross-frames is called Method 1, and the calculated and observed stresses are shown in Fig. 79. It can be seen that the agreement is extremely good for the critical cross-frame E, but not so good for the other cross-frame I, where actual stresses were 2 - 3 times the theoretical stresses. The comparison of calculated and observed further deflections of the cross-frame E due to applied load is also very good at higher loads, but for lower loads for this cross-frame and for the entire loading range for the cross-frame I, comparison is not realistic because of the likely margin of error in measuring the very small deflections involved.

In view of the very good agreement obtained for the critical cross-frame E in the above method, in spite of the assumptions involved, another variation of the same principles of cross-frame analysis as given in Appendix I of the Merrison Rules^[54] was tried. In this method, here called Method 2, the assumption of sinusoidal initial deflection across the flange at all cross-sections is retained; but instead of deriving effective alternate up and down deflections at successive cross-frames of a series of infinite number of frames, the actual measured magnitudes at locations A, E, I and M are retained, and also the theoretical flexural stiffnesses of a three-span system of longitudinal stiffeners are used.

The theoretical stresses at the tip of the outstand obtained from this method for the two cross-frames at E and I are also shown in Fig. 79; these stresses are very similar to the ones already calculated by Method 1, previously described, thus confirming the validity of the assumptions in the latter.

As already mentioned, agreement between the observed and the theoretical stresses is very satisfactory for cross-frame E, but observed stresses are considerably higher than theoretical stresses for cross-frame I.

CHAPTER 11

COMPARISON OF EXPERIMENTAL OBSERVATIONS WITH THEORY

1. IMPERIAL COLLEGE BOX TESTS

1.1 General

The observed collapse loads of box models 1, 2, 4 and 8 shall be compared with the values that can be predicted by application of the theory developed in the preceding chapters. The following general principles were adopted for applying the theory to the box tests:

1. An idealised bilinear plate stress-strain behaviour of the pattern shown in Fig. 22 was derived from the measured data of plate geometrical imperfections, welding residual compressive stress, yield stresses and Young's Moduli, with the help of the formulae given in Section 3 of Chapter 5.
2. From measured data of individual stiffener geometric imperfections between transverse supports, the average imperfection in each stiffened panel was calculated as shown in Table 2, Chapter 10, and the effective value of stiffener imperfection was then calculated from formula (13) in Chapter 8. For this purpose the test length of the models was assumed to be continued into the loading arms (see Fig. 45); but as imperfections were not measured in the loading arms they were taken as zero.
3. The additional eccentricity effects on flange stiffeners due to curvature of the whole box and the shift of centroid due to reduced effectiveness of flange plate were taken into account in accordance with Section 7 and 3.4 of Chapters 3 and 8 respectively.
4. Different Young's Modulus values in the various components of a box were allowed for by multiplying the appropriate dimension of each component by the ratio of its Young's Modulus to that of the compression flange plate; stresses calculated for the resultant effective sections had to be multiplied by the same ratio again to get true stresses.

5. When a box was subjected to several tests, i.e. several loading cycles, relaxation of welding residual stresses were investigated and taken into account for predicting its subsequent behaviour. Similarly, residual permanent deflections after a loading cycle were adopted as initial imperfections in the next loading cycle.
6. No shear lag effect was taken into account for collapse load calculations.
7. Reserve capacity in the web plate to resist further bending moment, after the compression flange stiffeners reached their predicted capacity, was approximately calculated and allowed for in the predicted strength of the whole box. This calculation was done on the basis of a linear stress distribution in the web, with yield stress on its edge attached to the compression flange.

1.2 Results of Application of Theory

The collapse load computations for the individual models highlighted some interesting features regarding their behaviour. These are described below.

1.2.1 *Box 1* - The worst flange plate panel imperfection was observed at section G and was approximately $b/640$, measured over a half-wavelength of b , i.e. the width of the plate panel. The flange stiffeners had also the worst inward imperfections in span D-I, near section G; the effective value of this imperfection was approximately $L/4630$, L being the span. The fact that the worst flange plate and flange stiffener imperfections coincided at section G explains why the flange buckled inwards at section G, causing the collapse of the box.

The first test of the box up to a jack load of 120 tonf could not have caused significant relaxation of residual stress in the compression flange, as the sum of the applied and the residual compression stress did not exceed yield stress.

The predicted jack load for collapse of flange plate panel near the central support, based on point B of the plate behaviour, (Fig. 22), and formulae given in the design rules in Section 3,

Chapter 5, is 132 tonf, which compares with the observed collapse loads of 132 tonf and 128 tonf in the second and the third tests respectively. The lower value in the third test may be attributed to larger residual deformations left after the second test. Operating on point A of the plate behaviour (Fig. 22) would have underestimated the strength by 11%. The mid-span regions of the flange stiffeners were not predicted to be critical from the theory, due to the sharp fall-off of bending moment. The web could not contribute any further to the bending resistance as the web buckled due to combined bending and shear.

1.2.2 *Box 2* - The end panels of this box were strengthened after the first test. Among the inner panels, the worst effective stiffener imperfection was inwards and equal to $L/3350$ in span C-I before the first test, and $L/429$ in span O-U as the residual imperfection after the first test. This latter figure was obtained as an average from deflection profiles of stiffeners S3 and S4 shown in Figs 80a and 80b; such profiles were not recorded for the other flange stiffeners. The average imperfections in the plate panels in span O-U varied from $b/444$ at section O to $b/1091$ mid-way between O and U; an average value of $b/640$ was adopted for calculation. No significant relaxation of residual compressive stresses could have occurred after the first test, for the same reason as given for Box 1 above. The stresses corresponding to points A and B of the plate behaviour in Fig. 22 were very close and hence point A was adopted for calculations. The predicted jack load for collapse was calculated to be 68.7 tonf and 64.5 tonf in the first and the second tests respectively, initiated by compression in flange plate. The lower value for the second test is due to the larger stiffener imperfection left after the first test. These results compare satisfactorily with the observed collapse loads of 64.5 tonf in both the tests. Failure in the first test occurred near the butt-welded transverse joint at the end of the experimental section of the box, which cannot, however, be predicted by the theory developed in the preceding chapters. The failure in the second test agrees with the prediction with respect to the magnitude of load and also the location and nature of the failure. Span I-O, which had an outward initial effective stiffener imperfection, was not predicted to be critical, but this span moved outwards as failure progressed

inwards in the adjacent span O-U. There was no reserve left in the web to sustain further bending moment, due to the lower yield stress of the web.

1.2.3 *Box 4* - Before the final collapse test reported in Chapter 10 was performed, this model was actually subjected to an earlier test with the jack load increasing up to 63 tonf. This test had to be terminated and the model unloaded, as the amplifiers in the circuits of strain gauges and transducers became faulty and gave incorrect readings on the data logger. No reliable data for strains and deflections could be obtained for this loading cycle. However, the jack load of 63 tonf represented an applied compressive stress in the flange plate of $.708 \sigma_{ys}$. As the flange plate had initial residual compressive stress of $.556 \sigma_{ys}$, this loading cycle must have produced considerable relaxation of the welding residual stresses; it can be shown that this will be reduced from $0.556 \sigma_{ys}$ to $0.292 \sigma_{ys}$ after the first loading cycle. Residual permanent imperfections of flange stiffeners after the first cycle could not be measured, but as the load in this cycle was not more than 0.68 times of the collapse load in the second test and as the stiffeners were not slender ($L/r = 45$), they could not have deflected substantially. Flange plate imperfections could not be measured at all, due to the close spacing of longitudinal stiffeners; from visual examinations it was evident that the flange plate imperfections were very small.

The effects of these small imperfections on such stocky plates ($b/t = 24.3$) must be very small. Hence it was deemed reasonable to ignore plate out-of-plane imperfections altogether, but to allow for the reduced welding residual stresses.

Outstand-initiated failure of the stiffeners was predicted by the formulae to be more critical than plate initiated failure, with effective outward initial imperfection of stiffeners in span U-W equal to $L/1235$. Because of the substantial difference in the stresses represented by points A and B of the plate behaviour, Fig. 22, viz. $0.292 \sigma_{ys}$, it was considered to be too conservative to adopt point A for plate secant stiffness and limiting stress. But adopting point B for plate behaviour for failure initiated by outstand in compression will also be too penalising; it will unduly reduce the plate effect-

ive width. This is because the plate will not be subjected to its compressive yield stress in this mode of buckling of the stiffener. Hence a trial method was adopted by using various points between A and B of the plate behaviour till agreement between the initially assumed and finally calculated stress values in the flange plate was obtained. The jack load corresponding to this mode of failure of the flange stiffener was calculated to be 82.2 tonf. In view of the higher yield stress of the web material, additional bending resistance of the compressive part of the web was approximately calculated to be 6.1 tonf, giving a total predicted jack load of 88.3 tonf for collapse of the box. Jack load to produce failure in the tension flange was calculated to be 83.1 tonf, possibly augmented by another 3.5 tons reserve capacity in the tensile half of the web; giving a total of 86.6 tonf. Actual failure load was observed to be 92.5 tonf. This higher observed value, compared with the predicted values, is almost certainly due to the spread of yielded zones in the web.

1.2.4 *Box 8* - For the same reasons as given for Box 4, plate panels between the longitudinal stiffeners were assumed to have no initial out-of-plane imperfections; the measured welding residual compressive stress of $0.388 \sigma_{ys}$ was, however, allowed for in the plate behaviour curve of Fig. 22. Because of the high slenderness ratio of the flange stiffeners, ($L/r = 115$), the Euler buckling load is the most important parameter in their strength as struts. Hence it was quite natural that calculations based on point A of the plate behaviour ($K_g = 1.0$) predicted higher strut strengths than values based on point B. Failure initiated by outstand in compression, with effective initial outward deflection of $L/1444$ in span I-M, was predicted by the formulae to be most critical; this was caused by a predicted jack load of 44.5 tonf. Additional moment capacity in the web was calculated to be 7.4 tonf, giving a total predicted failure jack load of 51.9 tonf.

Box 8 was further examined for benefit from orthotropic action in the flange. Due to orthotropic action, edge stiffeners carry more longitudinal stress than the central stiffeners, but are not subjected to additional flexural stresses due to buckling. In this instance the central stiffeners were found to be more critical, with a predicted jack load of 46.5 tonf for collapse, i.e. an improvement of 4.5% over

the collapse load of 44.5 tonf calculated for discrete struts. Taking the additional reserve of 7.1 tonf in the web into account, the total predicted jack load at failure is 53.6 tonf. This compares with 55.4 tonf observed.

1.3 Summary of Comparison

The results of the comparison between the predicted and the observed collapse loads for the four boxes are summarised below:

| <i>Box No.</i> | <i>Ratio</i> |
|----------------|----------------------------------|
| | <i>Predicted: Observed Loads</i> |
| 1 | 1.000 |
| 2 | 1.000 |
| 4 | 0.955 |
| 8 | 0.967 |

2. COMPARISON WITH OTHER EXPERIMENTAL RESULTS

2.1 General

A series of compression tests on single-span stiffened plate panels was done in Manchester, covering a wide range of slenderness and geometric imperfections of the flange plate, the stiffener outstand and the combined strut section; different levels of welding residual stresses were also covered by having otherwise identical pairs of specimens fabricated by intermittent and continuous welding. In some specimens high magnitudes of geometric imperfections were artificially produced. These geometric imperfections and residual stresses were measured and recorded, and also the axial shortening and growth of deflections of the specimen during loading tests. These tests have been fully reported in Reference [51].

The behaviour of these stiffened panels was predicted with respect to the ultimate strength, and also longitudinal shortening and deflection at the theoretical ultimate load, by applying the theory developed in the previous chapters.

The idealised bilinear load-shortening behaviour of the flange plate was derived from the formula in Section 3, Chapter 5, for the measured geometric imperfections and welding stress. For slender stiffener outstands, their loss of effectiveness was also calculated from the formula in Section 2, Chapter 9. For nominally flat flange plate panels, 5/8 of the actual measured maximum out-of-plane imperfections over a gauge length equal to the panel width was assumed as the amplitude of an equivalent idealised sinusoidal pattern over all the flange panels and along their entire lengths. For torsional imperfection of the stiffener outstands, the amplitude of the idealised critical mode of a single sinusoidal half-wave was taken as $\Delta_{sy} \cdot L/G$ when Δ_{sy} was the measured imperfection over a gauge length G , and L was the span. In the tests the point of application of the axial load was initially adjusted to produce no flexural stresses at very low load. It was assumed in the analysis that the point of application of axial load throughout the tests was through the theoretical centroid of the strut section at no load; it should be noted that this point is different from the centroid of the gross section, as an initially imperfect flange plate or slender outstand will have secant stiffness less than unity even at zero load - see formula (11), Chapter 5, and formula (24), Chapter 9. The shift of centroid of the effective section at higher loads was taken into account in predicting the strut behaviour; however, the modification factor of $\pm 1/2$ proposed to allow for continuity effects in multi-span struts was not used, as the test panels were single span. In many of the specimens, the eccentricity of applied loading due to the shift of centroid was much greater than the actual initial bow. Generally satisfactory correlation between predicted and observed deflections of these specimens at ultimate load proves the importance of this shift of centroid in the analysis of stiffened struts. Table 1 summarises the results of this comparison. Good agreement was found between the predicted and observed strengths. Axial shortening at ultimate load is sensitive to the axial stiffness of the combined cross-section; satisfactory agreement between the predicted and observed shortening prove the validity of the concept of bilinear load-shortening behaviour of the welded flange plate. A single effective width factor for both strength and stiffness of the flange plate will not be able to satisfactorily predict the amount of axial shortening.

Deflection at ultimate load is very sensitive to the magnitude of the initial strut imperfection and eccentricity of axial loading. This factor, and the fact that the strut is in a very unstable and gradually growing plastic state at the ultimate load, pose considerable difficulty in predicting the deflection at maximum load. In spite of these difficulties, the agreement between the observed and the predicted magnitudes is quite satisfactory, except for a few specimens; the reasons for the less than satisfactory correlation for these specimens are given in Section 2.3.

Satisfactory correlation of predicted and observed behaviour of specimens 3, 5, B11, B12, B22 and C3, which had slender stiffener outstands and low overall slenderness, prove the validity of the theory for strength of flat stiffener outstands developed in Chapter 9.

2.2 Method of Strut Analysis

The basic method adopted for the strut analysis was to first assume a point on the load-shortening curve of the flange plate, and calculate the strength of the strut based on plate stress and strain represented by this point; failure initiated by compression in either the flange plate or the outstand tip, or by tension in the outstand tip was investigated. For many specimens this point on the load-shortening curve was quite obvious, i.e. point A when the portion between A and B had a negative or a small positive slope, or point B when AB had a significant positive slope; but for slender struts it was sometimes necessary to investigate intermediate points between A and B, to get the maximum strength of the strut. For specimens with slender stiffeners, the analysis was restricted to longitudinal strain not exceeding yield strain of outstand, as the outstand would shed load dramatically beyond this strain.

2.3 Detailed Comments on Comparison with Test Results

- (i) For the specimens for which point at or near A of the load-shortening behaviour of flange plate was appropriate, i.e. specimens 4, 8, 11, D22, B21, B22, A22 and A23, the axial shortening and deflection were somewhat underestimated by the theory though the strength prediction was very good. The

reason is that the actual load-shortening behaviour of the flange plate is likely to be rounded, rather than have a sharp corner, at A, as the welding residual stresses in the plate would not strictly conform to the idealised rectangular pattern assumed in the theory.

- (ii) For specimens with high overall slenderness and continuous welding, i.e. specimens E21, E22 and E23, the theory underestimates the strut strength by 15 - 20%. This is due to the fact that the stress in the flange plate falls rapidly from the mid-span to the ends, as stress due to flexure of the strut is quite substantial in such slender struts. Hence the assumption in the theory of a single secant stiffness of the flange plate along the entire length of the strut leads to conservative prediction of the strut behaviour.
- (iii) For specimens with slender stiffener outstand and very slender flange plate connected by intermittent welding, i.e. specimens A11 and A12, the gap of 300 mm between adjacent weld attachments, which was twice the depth of the stiffener, caused sudden bursting of these attachments, and probably caused early failure. This must be the reason why these specimens failed at a lower load than the identical specimens with continuous welding. The theory, which does not allow for this phenomenon, overestimated the strength by approximately 10% and underestimated the shortening and deflection of these specimens.
- (iv) Tensile yielding of the outstand was predicted for specimen D23, and confirmed in the tests by the absence of any buckles either in the flange plate or in the outstand in the photograph of the failed specimens. For specimens D21, E21 E22 and E23 failure was predicted to be initiated simultaneously by tensile yielding of outstand while the flange plate stresses were beyond point A of the load-shortening behaviour. For specimens D11, D12 and E12, the predicted load for failure initiated by tensile yielding of the outstand was approximately only 12% higher than the predicted load for failure initiated by compression in the flange plate. These predictions of failure mechanism are supported by the presence of only moderate buckling of the flange plate panels at the collapse state of these specimens.

- (v) The failure of specimen 9 was predicted to be initiated by buckling of the flange plate, but it actually failed by torsional buckling of the stiffeners. This weakening of the stiffeners might have been caused by the gaps between the intermittent welds.
- (vi) Specimens C2 and A21 were predicted to fail at a load 25 and 35% less than actually observed. The high observed strengths are difficult to explain, particularly as they are even higher than that of C3, which is a much shorter strut of otherwise identical cross-section, and of A23, which had much smaller flange plate out-of-plane imperfection and also smaller overall stiffener bow, compared with C2 and A21 respectively.
- (vii) Agreement with respect to the axial shortening, magnitude of deflection and mode of buckling is very good for the remaining 20 out of the total 36 specimens.
- (viii) Agreement with respect to the collapse load is very good for most of these specimens; the mean and the standard deviation of the ratio

$$\frac{\text{predicted strength}}{\text{observed strength}}$$

was 0.961 and 0.09 respectively for the 36 specimens tested.

3. COMPARISON OF RECOMMENDED DESIGN RULES WITH EXPERIMENTAL RESULTS

3.1 Experimental collapse strengths of stiffened panels were collected from one hundred and five tests reported in various publications. These results were compared with the values that can be predicted from the design rules recommended in Chapter 12 and developed in the earlier chapters of this thesis. In many cases full details were not available regarding actual initial geometric imperfections and welding residual stresses in the models. The design rules, however, make some allowance for these imperfections, and the predicted strengths are thus the values that a designer will use for a practical design of similar geometric proportions. These tests cover 12 box girder tests, 48 stiffened panels with simply supported longitudinal edges and 45 stiffened panels with unsupported longitudinal edges. They also include 79 single-span tests and 26 tests on multi-span stiffeners. For the single-span tests, the proposed effectiveness factor of ± 0.5 for initial eccentricity on a continuous beam-column (see Section 3 of Chapter 8) has not been used for obvious reasons. The models in the Manchester series that had very high artificially imposed initial deformations have been excluded from this comparison, as the fabrication tolerances associated with the design rules were exceeded. The relevant details of these tests and a comparison between the observed and the predicted strengths are given in Table 2.

3.2 The mean and the standard deviation of the ratio of predicted to observed strengths are found to be 0.917 and 0.134 respectively for these 105 tests. These results are considered satisfactory and thus the proposed design rules are fully validated. These results are slightly inferior to those obtained by applying the basic theory to the whole Manchester series of tests (c.f. 0.961 mean and 0.09 standard deviation), but this can only be expected, as in the latter case the actual measured imperfections and welding stresses are taken into account.

3.3 In many of these specimens, the amount of welding, and the consequent residual compressive stresses, were considerably higher

than the magnitudes explicitly allowed for in the development of the design rules (see Section 5.1 of Chapter 5). In spite of this departure, satisfactory agreement was obtained over the whole series of 105 tests, and the predicted results were mostly on the safe side. This can be explained by the fact that the strength of welded plates, represented by point B in Fig. 22, is not sensitive to the actual level of welding compressive stress, when the latter is more than say 10 - 15 per cent of the yield stress. Hence it can be safely stated that the proposed design rules are valid for all welded stiffened compression panels, irrespective of the actual amount of welding.

| Specimen | o/a Slenderness L/r | Plate Slenderness b/t | Stiffener Slenderness d/t_2 | Welding Type* | Type of Imperfection* | Ultimate Load Squash Load | | Predicted Strength Observed Strength | Axial Shortening Length $\times 10^3 \leftarrow$ | | Maximum Deflection - mm | | |
|----------|--------------------------|----------------------------|----------------------------------|---------------|-----------------------|------------------------------|----------|---|--|----------|----------------------------|----------|-----|
| | | | | | | Predicted | Observed | | Predicted | Observed | Predicted | Observed | |
| 1 | 10 | 48 | 9.5 | C | D | .824 | .873 | .945 | 2.46 | 2.51 | Not Measured ↑ | | |
| 2 | 10 | " | 9.5 | H | D | .814 | .834 | .984 | 2.49 | 2.57 | | | |
| 3 | 11 | " | 16 | H | N | .848 | .853 | .994 | 1.34 | 1.20 | | | |
| 4 | 10 | " | 9.5 | H | N | .898 | .898 | 1.000 | 1.09 | 1.53 | | | |
| 5 | 11 | " | 16 | H | H | .822 | .813 | 1.012 | 1.34 | 1.26 | | | |
| 6 | 10 | " | 9.5 | C | N | .874 | .923 | .947 | 2.52 | 2.29 | | | |
| B11 | 10 | 70 | 16 | H | D | .630 | .631 | .999 | 1.63 | 1.86 | | | |
| B12 | 10 | " | 16 | H | N | .686 | .654 | 1.048 | 1.62 | 1.86 | | | |
| B21 | 10 | " | 16 | C | D | .598 | .670 | .892 | 1.71 | 2.62 | | | |
| B22 | 10 | " | 16 | C | N | .621 | .619 | 1.003 | 1.68 | 2.40 | | | |
| C3 | 11 | 46 | 16 | C | N | .787 | .772 | 1.019 | 1.43 | 1.53 | | | |
| 7 | 39 | 48 | 9.5 | C | N | .817 | .792 | 1.030 | 1.73 | 1.48 | | 5.74 | 5.9 |
| 8 | 39 | " | 9.5 | I | N | .844 | .852 | .991 | 1.10 | 1.47 | | 0.40 | 3.6 |
| 9 | 44 | " | 16 | H | N | .829 | .780 | 1.063 | 1.09 | 1.20 | | 0.69 | 1.2 |
| 10 | 44 | " | 16 | H | O | .653 | .720 | .906 | 0.87 | 1.09 | | 1.18 | 3.7 |
| 11 | 39 | " | 9.5 | H | O | .776 | .793 | .979 | 1.07 | 1.20 | 1.34 | 3.0 | |
| 12 | 39 | " | 9.5 | C | O | .772 | .793 | .973 | 1.63 | 1.64 | 6.44 | 6.5 | |
| 13 | 39 | " | 9.5 | H | D | .740 | .751 | .985 | 1.64 | 1.48 | 4.63 | 4.2 | |
| 14 | 39 | " | 9.5 | C | D | .763 | .832 | .916 | 1.62 | 1.80 | 4.77 | 4.7 | |
| 15 | 44 | " | 16 | I | T | .639 | .682 | .936 | 0.92 | 0.98 | 0.99 | 1.9 | |
| A11 | 41 | 70 | 16 | I | D | .604 | .546 | 1.107 | 1.49 | 1.96 | 1.17 | 11.5 | |
| A12 | 41 | " | 16 | I | N | .614 | .569 | 1.081 | 1.41 | 1.75 | 1.70 | 6.5 | |
| A21 | 41 | " | 16 | I | D | .416 | .643 | .646 | 1.31 | 2.29 | 2.79 | 9.0 | |
| A22 | 41 | " | 16 | C | O | .560 | .564 | .992 | 1.23 | 1.91 | 3.77 | 7.4 | |
| A23 | 41 | " | 16 | C | N | .621 | .618 | 1.004 | 1.38 | 2.84 | 3.87 | 5.4 | |
| C2 | 45 | 46 | 16 | C | N | .654 | .870 | .752 | 1.23 | 1.47 | 2.45 | 5.3 | |
| D11 | 94 | 46 | 6.7 | I | D | .606 | .632 | .958 | 1.03 | 1.20 | 6.59 | 6.5 | |
| D12 | 94 | " | 6.7 | I | N | .674 | .647 | 1.043 | 0.86 | 0.82 | 5.99 | 6.0 | |
| D21 | 94 | " | 6.7 | C | D | .534 | .573 | .932 | 1.21 | 1.53 | 11.23 | 10.0 | |
| D22 | 94 | " | 6.7 | C | N | .617 | .596 | 1.034 | 0.76 | 0.87 | 3.11 | 6.0 | |
| D23 | 94 | " | 6.7 | C | O | .406 | .432 | .940 | 0.61 | 0.76 | 9.54 | 11.5 | |
| E11 | 88 | 70 | 6.1 | I | D | .461 | .468 | .985 | 1.15 | 1.20 | 7.14 | 10.5 | |
| E12 | 88 | " | 6.1 | I | N | .475 | .474 | 1.003 | 1.14 | 1.09 | 10.30 | 6.5 | |
| E21 | 88 | " | 6.1 | C | D | .377 | .440 | .855 | 1.40 | 1.34 | 16.20 | 13.5 | |
| E22 | 88 | " | 6.1 | C | O | .277 | .334 | .829 | 0.98 | 1.42 | 14.77 | 15.0 | |
| E23 | 88 | " | 6.1 | C | N | .364 | .446 | .816 | 1.40 | 1.20 | 16.94 | 11.5 | |

TABLE 1: COMPARISON OF MANCHESTER TEST RESULTS WITH THEORY

* C - Continuous N - Nominally straight D - Flange plate dished
I - Intermittent O - Overall bow T - Stiffener outstand twisted

| (1) | (2) | (3) | (4) | (5) | (6) | (7) | (8) | (9) | (10) | (11) | (12) | (13) | (14) | (15) | (16) | (17) | (18) | (19) | (20) | |
|----------------------|-----------|---------|---------|------|------|---------|---------|-----------|---------|-----------------------|-----------------------------------|-----------------------------------|---------|----------------------------|-------------------------------|----------------------------|--|--|---------------------------------|-------|
| Source | Model No. | L mm | B mm | L.S. | L.E. | Plate | | Stiffener | | | | | r mm | σ_{ys} | | | σ_{su} Observed N/mm ² | $\frac{\sigma_{su}}{\sigma_{yca}}$ Observed | Ratio Pred./obs. Strength | |
| | | | | | | b mm | t mm | Shape | d mm | d _{cg} mm | A _s mm ² | I _O mm ² | | Plate N/mm ² | Stiffen. N/mm ² | Aver. N/mm ² | | | | |
| | | | | | | | | | | | | | | | | | | | | |
| Manchester [51] | 4 | 914 | 1524 | S | F | 457 | 9.52 | F | 152.5 | 76.2 | 2419 | 4,682,604 | 46.9 | 260 | 264 | 261 | 235 | .899 | 0.960 | |
| | 6 | " | " | " | " | " | " | " | " | " | " | " | " | " | " | " | 241 | .923 | 0.937 | |
| | 3 | " | " | " | " | " | " | " | " | " | 1451 | 2,808,087 | 41.5 | " | 270 | 263 | 225 | .857 | 0.979 | |
| | 8 | 1829 | " | " | " | " | " | " | " | " | 2419 | 4,682,604 | 46.9 | 262 | 261 | 262 | 223 | .852 | 0.878 | |
| | 7 | " | " | " | " | " | " | " | " | " | " | " | " | 255 | 268 | 260 | 206 | .792 | 0.924 | |
| | 9 | " | " | " | " | " | " | " | " | " | 1451 | 2,808,087 | 41.5 | 262 | 277 | 266 | 207 | .779 | 0.946 | |
| | B12 | 914 | " | " | " | " | 6.35 | " | " | " | " | " | " | 45.2 | 349 | 333 | 344 | 225 | .655 | 1.098 |
| | B22 | " | " | " | " | " | " | " | " | " | " | " | " | " | 352 | 344 | 349 | 216 | .618 | 1.168 |
| | C3 | " | " | " | " | " | 9.52 | " | " | " | " | " | " | 41.5 | 283 | 292 | 285 | 220 | .772 | 1.069 |
| | A12 | 1829 | " | " | " | " | 6.35 | " | " | " | " | " | " | 45.2 | 349 | 355 | 351 | 200 | .570 | 0.958 |
| | A23 | " | " | " | " | " | " | " | " | " | " | " | " | " | 334 | 324 | 331 | 209 | .632 | 0.893 |
| | E12 | " | " | " | " | " | " | " | " | 76.2 | 38.1 | 968 | 468,260 | 21.0 | 335 | 378 | 346 | 164 | .474 | 0.919 |
| | E23 | " | " | " | " | " | " | " | " | " | " | " | " | " | 330 | 369 | 340 | 152 | .447 | 0.993 |
| | D12 | " | " | " | " | " | 9.52 | " | " | " | " | " | " | 19.2 | 234 | 352 | 255 | 159 | .623 | 0.976 |
| | D22 | " | " | " | " | " | " | " | " | " | " | " | " | " | 244 | 287 | 252 | 151 | .599 | 0.940 |
| C2 | " | " | " | " | " | " | " | " | 152.5 | 76.2 | 1451 | 2,808,067 | 41.5 | 263 | 292 | 270 | 236 | .874 | 0.832 | |
| P.C.L. (London) [57] | TPA1 | 1143 | 1321 | C | S | 254 | 6.38 | b | 127 | 78 | 1226 | 1,968,775 | 48.1 | 279 | | | 251 | .900 | .897 | |
| | 2 | " | " | " | " | 317.5 | 6.10 | " | " | " | " | " | 46.8 | 312 | | | 211 | .676 | 1.047 | |
| | 3 | " | " | " | " | 254 | 6.32 | F | " | 63.5 | 1210 | 1,626,340 | 40.8 | 291 | | | 245 | .842 | 0.960 | |
| | 4 | " | " | " | " | 317.5 | 6.68 | " | " | " | " | " | 39.0 | 285 | | | 208 | .730 | 1.039 | |
| | TPB1 | " | " | " | " | 254 | 6.40 | b | " | 78 | 1226 | 1,968,775 | 48.1 | 280 | | | 247 | .882 | 0.914 | |
| | 2 | " | " | " | " | 317.5 | 6.27 | " | " | " | " | " | " | 46.8 | 325 | | | 228 | .702 | 1.007 |
| | 3 | " | " | " | " | 254 | 6.40 | F | " | 63.5 | 1210 | 1,626,340 | 40.8 | 313 | | | 248 | .792 | 1.020 | |
| | 4 | " | " | " | " | 317.5 | 6.30 | " | " | " | " | " | " | 39.4 | 298 | | | 216 | .725 | 1.019 |
| | TPC1 | " | " | " | " | 210 | 6.17 | b | " | 78 | 1226 | 1,968,775 | 49.3 | 282 | | | 265 | .940 | 0.839 | |
| | 2 | " | " | " | " | 254 | 6.25 | " | " | " | " | " | " | 48.3 | 287 | | | 251 | .875 | 0.912 |
| | 3 | " | " | " | " | 317.5 | 6.25 | " | " | " | " | " | " | 46.7 | 280 | | | 221 | .789 | 0.929 |
| | 4 | " | " | " | " | 210 | 6.30 | " | " | " | " | " | " | 49.3 | 293 | | | 263 | .898 | 0.931 |
| I.C. (London) [13] | 1 | 787 | 1219 | C | S | 244 | 4.95 | b | 51 | 29.5 | 295 | 74,962 | 14.6 | 247 | 329 | 263 | 201 | .764 | 0.893 | |
| | 2 | " | " | " | " | " | 4.88 | " | " | " | " | " | 14.7 | 298 | 276 | 294 | 224 | .762 | 0.845 | |
| | 4 | " | " | " | " | 122 | 5.03 | " | " | " | " | " | 17.6 | 221 | 304 | 235 | 202 | .860 | 0.893 | |
| | 8 | 1321 | " | " | " | " | 4.72 | F | 38 | 19.0 | 242 | 29,266 | 11.6 | 277 | 312 | 287 | 155 | .540 | 0.670 | |
| | 9 | 1574 | 2438 | " | " | 215 | 4.88 | " | 70 | 34.9 | 554 | 225,064 | 21.4 | 334 | 286 | 317 | 280 | .883 | 0.589 | |
| | 10 | " | " | " | " | " | 4.93 | " | " | " | " | " | " | " | 335 | 286 | 318 | 250 | .786 | 0.659 |
| Liege [22,49] | I | 1920 | 1600 | C | S | 200 | 4.20 | L | 45 | 28.7 | 327 | 66,255 | 15.8 | 401 | 377 | 394 | 197 | .500 | 0.476 | |
| | II | " | " | " | " | " | " | " | 65 | 39.6 | 470 | 202,018 | 23.6 | 387 | 418 | 385 | 246 | .640 | 0.736 | |
| | III | " | " | " | " | " | " | " | 75 | 53.7 | 706 | 392,898 | 32.1 | 388 | 392 | 337 | 269 | .800 | 0.743 | |
| | 4 | " | " | " | " | " | " | " | 100 | 65.9 | 1144 | 1,179,145 | 42.0 | 398 | 386 | 393 | 330 | .840 | 0.824 | |
| | 5 | 960 | " | " | " | " | " | " | 45 | 28.4 | 345 | 69,431 | 15.8 | 397 | 374 | 351 | 302 | .860 | 0.660 | |
| | 6 | " | " | " | " | " | " | " | " | 28.5 | 341 | 68,797 | " | " | " | 387 | 322 | .830 | 0.654 | |

Table 2: Comparison of Design Rules with Experimental Data
(For notations see footnote at the end of the table)

Contd./over

| (1) | (2) | (3) | (4) | (5) | (6) | (7) | (8) | (9) | (10) | (11) | (12) | (13) | (14) | (15) | (16) | (17) | (18) | (19) | (20) |
|-------------------------|------|------|------|-----|-----|------|------|------|-------|-------|---------|-----------|------|------|------|------|-------|-------|-------|
| Monash [27,58] | H | 3450 | 2440 | S | S | 533 | 9.85 | T | 152 | 91.8 | 1456 | 3,363,642 | 45.8 | | | 377 | 266 | .705 | 0.784 |
| | J | " | " | " | " | " | 9.95 | " | " | " | " | " | 45.7 | | | " | 235 | .623 | 0.870 |
| | K | " | " | C | " | " | 9.78 | " | " | " | " | " | 45.9 | | | 396 | 235 | .593 | 0.776 |
| | R | 1700 | 1220 | S | " | 457 | 9.95 | " | " | " | " | " | 47.8 | | | 377 | 271 | .719 | 0.954 |
| | S | " | - | " | - | " | 9.80 | " | " | " | " | " | 48.0 | | | " | 254 | .674 | 1.016 |
| | T | " | - | " | - | 610 | " | " | 102 | 61.9 | 896 | 909,647 | 25.4 | | | 340 | 170 | .500 | 1.114 |
| | U | " | - | " | - | " | 9.66 | " | " | " | 896 | " | 25.5 | | | 312 | 174 | .558 | 1.039 |
| | W | 3400 | - | " | - | 457 | 9.60 | " | 152 | 44.3 | 1456 | 3,363,642 | 48.2 | | | 400 | 249 | .622 | 1.050 |
| | M | 1730 | 1220 | " | - | 267 | 4.80 | " | 76 | 45.9 | 364 | 209,877 | 23.0 | | | 324 | 223 | .688 | 0.836 |
| Nagoya [60] | B11 | 921 | 766 | S | S | 192 | 6.13 | F | 60.0 | 30.0 | 350 | 104,940 | 16.3 | | | 341 | 284 | .830 | 0.884 |
| | B11R | 916 | 767 | " | " | " | 5.73 | " | 60.3 | 30.1 | 364 | 110,176 | 16.8 | | | " | 285 | .835 | 0.914 |
| | B12 | 920 | 765 | " | " | 191 | 6.00 | " | 72.3 | 36.1 | 434 | 188,967 | 20.7 | | | " | 308 | .903 | 0.915 |
| | B21 | 803 | 670 | " | " | 168 | 5.87 | " | 52.8 | 26.4 | 306 | 71,146 | 14.6 | | | " | 287 | .841 | 0.878 |
| | B24 | " | " | " | " | " | 6.02 | " | 83.4 | 41.7 | 663 | 384,312 | 26.6 | | | " | 362 | 1.061 | 0.797 |
| | B31 | 630 | 526 | " | " | 132 | 6.10 | " | 41.4 | 20.7 | 248 | 35,479 | 11.7 | | | " | 340 | .997 | 0.740 |
| | C11 | 1436 | 1200 | " | " | 240 | 5.85 | " | 82.9 | 41.4 | 478 | 273,942 | 22.8 | | | 271 | 152 | .561 | 1.321 |
| | C12 | 1434 | 1197 | " | " | " | 5.80 | " | 105.6 | 52.8 | 602 | 559,352 | 30.6 | | | " | 202 | .746 | 1.054 |
| | C14 | 1436 | 1198 | " | " | " | 5.93 | " | 126.8 | 63.4 | 1065 | 1,427,105 | 40.7 | | | " | 241 | .889 | 0.906 |
| | C21 | 1291 | 1076 | " | " | 215 | 5.87 | " | 75.7 | 37.8 | 447 | 213,284 | 21.2 | | | " | 217 | .803 | 0.920 |
| | C22 | " | " | " | " | " | 5.88 | " | 94.4 | 47.2 | 549 | 407,998 | 27.5 | | | " | 230 | .851 | 0.955 |
| | C24 | 1293 | 1074 | " | " | " | 5.84 | " | 114.9 | 57.4 | 954 | 1,049,197 | 37.0 | | | " | 251 | .926 | 0.890 |
| | C31 | 1148 | 958 | " | " | 192 | 5.93 | " | 65.0 | 32.5 | 392 | 138,228 | 18.2 | | | " | 186 | .686 | 1.039 |
| | C32 | 1147 | 959 | " | " | " | 6.00 | " | 85.0 | 42.5 | 497 | 299,386 | 24.9 | | | " | 222 | .819 | 1.005 |
| | C34 | 1152 | 960 | " | " | " | " | " | 102.0 | 51.0 | 816 | 707,472 | 32.7 | | | " | 239 | .883 | 0.948 |
| | C41 | 1003 | 840 | " | " | 168 | 5.87 | " | 57.0 | 28.5 | 344 | 93,059 | 16.2 | | | " | 218 | .805 | 0.888 |
| | C42 | 1004 | 838 | " | " | " | 5.73 | " | 75.0 | 37.5 | 439 | 206,016 | 22.3 | | | " | 272 | 1.003 | 0.815 |
| | C51 | 895 | 749 | " | " | 150 | 5.92 | " | 51.9 | 25.9 | 311 | 69,899 | 14.9 | | | " | 233 | .860 | 0.848 |
| | C61 | 2393 | 1197 | " | " | 239 | 5.99 | " | 110.0 | 55.0 | 906 | 913,953 | 34.5 | | | " | 228 | .844 | 0.858 |
| | C71 | 2160 | 1073 | " | " | 215 | 6.06 | " | 98.5 | 49.2 | 826 | 668,174 | 31.1 | | | " | 241 | .889 | 0.810 |
| | C81 | 1912 | 957 | " | " | 191 | 5.98 | " | 88.3 | 44.1 | 788 | 511,759 | 28.3 | | | " | 233 | .861 | 0.843 |
| | D11 | 1192 | 969 | " | " | 162 | 4.66 | " | 59.5 | 29.7 | 359 | 105,849 | 17.9 | | | " | 220 | .813 | 0.882 |
| | D12 | 1200 | 972 | " | " | " | 4.50 | " | 76.0 | 38.0 | 445 | 214,001 | 23.8 | | | " | 256 | .946 | 0.849 |
| D13 | 1190 | 965 | " | " | 161 | 4.68 | " | 89.0 | 44.5 | 530 | 349,547 | 28.4 | | | " | 258 | .953 | 0.865 | |
| D21 | 1022 | 862 | " | " | 144 | 4.71 | " | 52.0 | 26.0 | 315 | 71,007 | 15.7 | | | " | 231 | .855 | 0.843 | |
| D23 | 1028 | 860 | " | " | 143 | 4.55 | " | 79.6 | 39.8 | 473 | 249,657 | 25.6 | | | " | 274 | 1.011 | 0.866 | |
| D31 | 798 | 677 | " | " | 113 | 4.68 | " | 41.6 | 20.8 | 247 | 35,636 | 12.8 | | | " | 256 | .944 | 0.818 | |
| Dunferm line [61] | 1a | 1219 | 3200 | S | S | 610 | 8.00 | T | 153.7 | 110.3 | 2126 | 4,777,325 | 58.7 | 253 | 258 | 255 | 192 | .754 | 0.698 |
| | 2b | 1524 | " | " | " | 305 | 7.37 | " | 114.3 | 77.0 | 989 | 1,310,885 | 42.3 | 264 | 280 | 269 | 227 | .844 | 0.739 |
| | 3b | " | " | " | " | " | 6.40 | " | 77.2 | 48.9 | 506 | 310,069 | 23.9 | 256 | 227 | 250 | 151 | .604 | 1.017 |
| | 5 | " | " | " | " | 610 | 6.43 | " | 116.0 | 78.6 | 1008 | 1,376,410 | 37.0 | 252 | 235 | 249 | 176 | .708 | 0.698 |
| | 6 | 1219 | " | " | " | " | 6.32 | " | 76.2 | 48.4 | 492 | 293,020 | 18.4 | 261 | 246 | 259 | 125 | .482 | 0.994 |
| | 7 | 1524 | " | " | " | " | 6.30 | " | 115.1 | 78.2 | 975 | 1,305,579 | 36.6 | 293 | 310 | 298 | 185 | .621 | 0.739 |

Table 2: Contd. 2.

| | (1) | (2) | (3) | (4) | (5) | (6) | (7) | (8) | (9) | (10) | (11) | (12) | (13) | (14) | (15) | (16) | (17) | (18) | (19) | (20) |
|-------------------|-----|------|-----|-----|-----|-----|-------|-----|-----|-------|------|------------|------|------|------|------|------|------|-------|-------|
| Braunschweig [62] | 1 | 3450 | 740 | S | F | 460 | 7.00 | Tr | 198 | 128.2 | 3370 | 14,298,300 | 76.3 | 470 | 431 | 455 | 244 | .537 | 0.998 | |
| | 2 | " | " | " | " | " | " | " | " | " | " | " | " | 480 | 437 | 463 | 242 | .523 | 1.029 | |
| | 3 | " | " | " | " | " | " | " | " | " | " | " | " | 469 | 428 | 453 | 250 | .552 | 0.975 | |
| | 4 | 4920 | " | " | " | " | " | " | " | " | " | " | " | 395 | 385 | 391 | 200 | .511 | 1.268 | |
| | 5 | " | " | " | " | " | " | " | " | " | " | " | " | " | " | " | " | 198 | .506 | 1.281 |
| | 6 | 6396 | " | " | " | " | " | " | " | " | " | " | " | 311 | 348 | 326 | 159 | .488 | 0.910 | |
| | 7 | 3628 | 600 | C | " | 400 | 10.00 | | 250 | 157.8 | 4320 | 29,084,567 | 96.3 | 388 | 403 | 394 | 327 | .829 | 0.894 | |
| | 8 | " | " | S | " | " | " | " | " | " | " | " | " | 403 | 391 | 398 | 320 | .804 | 0.924 | |
| | 9 | 1814 | 300 | " | " | 200 | 5.00 | | 125 | 78.6 | 1098 | 1,845,872 | 48.1 | 394 | 382 | 389 | 289 | .743 | 0.999 | |
| | 10 | " | 700 | " | " | " | " | " | " | " | " | " | " | 389 | 377 | 384 | 276 | .718 | 1.036 | |
| | 11 | 4920 | 740 | " | " | 210 | 7.00 | | 150 | 95.7 | 2180 | 5,256,536 | 59.6 | 465 | 421 | 445 | 205 | .461 | 1.119 | |
| | 12 | " | " | " | " | " | " | " | " | " | " | " | " | 459 | 415 | 439 | 215 | .490 | 1.067 | |
| | 13 | " | " | " | " | " | " | " | " | " | " | " | " | 458 | 421 | 441 | 203 | .460 | 1.126 | |
| | 14 | 2640 | " | " | " | " | " | " | " | " | " | " | " | 396 | 394 | 395 | 312 | .790 | 0.975 | |
| | 15 | " | 883 | " | " | 533 | 10.00 | L | 152 | 92.6 | 1405 | 3,258,269 | 48.1 | 434 | 427 | 432 | 268 | .620 | 0.947 | |
| | 16 | 2600 | 740 | " | " | 460 | 7.00 | | 160 | 96.9 | 1461 | 3,760,737 | 57.0 | 459 | 436 | 451 | 242 | .537 | 1.001 | |
| | 17 | " | " | " | " | " | " | " | " | " | " | " | " | " | 440 | 452 | 248 | .548 | 0.978 | |
| | 18 | " | " | " | " | " | " | " | " | " | " | " | " | 462 | " | 454 | 253 | .557 | 1.052 | |
| | 19 | 4960 | " | " | " | " | " | " | " | " | " | " | " | 304 | 334 | 315 | 183 | .581 | 0.809 | |
| | 20 | 3450 | " | " | " | 210 | " | " | 110 | 69.5 | 1111 | 1,310,880 | 43.3 | 460 | 431 | 447 | 206 | .461 | 0.907 | |
| | 21 | " | " | " | " | " | " | " | " | " | " | " | " | 466 | 432 | 450 | 200 | .444 | 0.937 | |
| | 22 | " | " | " | " | " | " | " | " | " | " | " | " | " | 430 | 449 | 214 | .476 | 0.868 | |
| | 23 | 2640 | " | " | " | " | " | " | " | " | " | " | " | 398 | 390 | 394 | 278 | .705 | 0.818 | |

Notations:

L.S. Longitudinal structural arrangement; S stands for single span, C for spans continuous over several transverse stiffeners.

L.E. Longitudinal edge condition; S stands for edges simply supported against out-of-plane movement, F for free edges.

d_{cg} Depth of centroid of stiffening rib from the connected edge.

I_o Second moment of area of stiffening rib about its own centroid.

r Radius of gyration of the gross stiffener section, consisting of the stiffening rib and the flange plate.

σ_{ys} Yield stress, $\sigma_{y_{sp}}$ and $\sigma_{y_{ss}}$ relating to plate and stiffening rib respectively.

$$\sigma_{y_{sa}} \text{ Average yield stress} = \frac{bt \sigma_{y_{sp}} + A_s \sigma_{y_{ss}}}{bt + A_s}$$

d Stiffener overall depth

F Flat

B Bulb flat

L Angle

T Tee

Tr Trough

CHAPTER 12

DESIGN RULES AND TOLERANCES FOR LONGITUDINAL
STIFFENERS IN BOX GIRDER COMPRESSION FLANGES

1. INTRODUCTION

A method of design for longitudinal stiffeners in compression flanges of box girders is given in the previous chapters, taking into account the effects of various initial geometrical imperfections and welding residual stresses. An alternative simplified and conservative method of design is given here for the cases that satisfy the following limitations:

- (a) Fabrication tolerances given in Section 8 are met.
- (b) The geometrical restrictions given in Section 7 to prevent local instability of stiffeners are met.

1.2 Section 2 describes the simplified design method for longitudinal flange stiffeners, in a zone of approximately uniform bending moment of the box girder, treated as isolated struts. The effects of variation in the bending moment on the box girder and the effects of orthotropic action of the entire flange between webs of box girders and transverse flange stiffeners may be taken into account in accordance with Sections 3, 4 and 5. The effect of locally applied transverse loading directly above the stiffener may be allowed for in accordance with Section 6.

2. FLANGE STIFFENERS IN AN APPROXIMATELY UNIFORM BENDING MOMENT ZONE, TREATED AS ISOLATED STRUTS

2.1 The method described in this section is applicable to struts carrying uniform axial stress along their length.

From the bending moment and axial force, if any, due to factored loads acting on the gross section of the box girder, the longitudinal stress σ_a acting at the centroid of the gross stiffener section is obtained.

The gross stiffener section is defined to consist of the area of a stiffening rib A_s , and the flange plate of width b between the ribs, and thickness t .

2.2 Initial effective eccentricity of the applied longitudinal loading will be taken as:

$$\Delta = \delta_1 + \delta_2 + \delta_3 + \delta_4 ,$$

where

(i) $\delta_1 = \pm \frac{L}{750}$, being the spacing of transverse supports.

(ii) δ_2 is the additional eccentricity caused by the shift of the centroid due to the loss of stiffness of the flange plate, and is given by:

$$\delta_2 = \pm \frac{A_o}{2} \left[\frac{1}{A_e} - \frac{1}{A_g} \right] ,$$

where A_g is the gross area of the stiffener = $A_s + bt$

A_e is the effective area of the stiffener = $A_s + Kbt$

where K is given in Figs 26a and 26b for welded and stress free plates respectively

A_o is the moment of the area of the stiffening rib A_s about the mid-plane of the flange plate.

(iii) δ_3 is the additional eccentricity due to overall curvature of the box girder and is given by $\pm \frac{r^2}{2h}$ where r is the radius of gyration of the gross stiffener section, and h is the distance between the centroid of the gross stiffener section and the neutral plane of the gross box girder cross-section calculated

by taking both the bending moment and the axial force, if any, on the girder.

- (iv) δ_4 is the additional eccentricity due to any specified camber or curvature in the flange.

δ_4 will be taken as ± 0.5 times the maximum offset, measured from a base line of length L between adjacent transverse supports.

2.3 The stiffener should be checked in accordance with Clauses 2.4 to 2.6, taking

- (i) $P =$ axial force on the stiffener $= \sigma_a A_g$
 (ii) $M =$ maximum bending moment on the stiffener
 $= \frac{\pi^2}{L^2} E I_e \Delta (m - 1) ,$

where I_e is the moment of inertia of an effective stiffener section consisting of the area of the stiffening rib A_s and an associated area of flange width equal to $K.b$, and

$$m = \frac{1}{1 - \frac{PL^2}{\pi^2 EI_e}}$$

2.4 The maximum stress σ_{pm} at the mid-plane of the flange plate and σ_{om} at the tip of the stiffener outstand should be calculated from:

- (i) $\sigma_{pm} = \frac{KP}{A_e} + \frac{KM}{Z_p}$
 (ii) $\sigma_{om} = \frac{P}{A_e} - \frac{M}{Z_o} ,$

where K is given in Figs 26a and 26b

Z_p, Z_o are the section moduli, with respect to the mid-plane of the plate and the tip of the stiffener outstand respectively, of an effective stiffener section consisting of the area of the rib A_s and an associated area of flange width equal to $K.b$.

2.5 Plate-initiated failure of the stiffener will be checked by taking the maximum +ve value of Δ in Clause 2.2, and σ_{pm} shall not exceed:

$$\frac{\sigma_{au}}{\sigma_{ys}} \sqrt{(\sigma_{ys}^2 - 3\tau^2)}$$

where the ratio $\frac{\sigma_{au}}{\sigma_{ys}}$ is given in Figs 26a and 26b, and

τ is the shear stress in the flange plate due to torsion on the box girder, and

2.6 Outstand initiated failure of the stiffener shall be checked by taking both max +ve and -ve values of Δ in Clause 2.2, and neither the tensile nor the compressive value of σ_{om} shall exceed σ_{ys} .

(Note: σ_{om} is tensile when negative.)

2.7 Composite Steel-Concrete Compression Flange

When the structural concrete slab is itself designed adequately for the applied longitudinal stresses, and is adequately shear connected to the steel flange of the box girder, the resultant composite strut section does not require any further checks. The slenderness limitations on stiffener outstands given in Section 7 shall, however, be observed.

The bare stiffened steel flange will be checked in accordance with these rules for the loading applied to it before composite action is effective.

2.8 To satisfy the requirements given in Clauses 2.3 to 2.6 for flange stiffeners in an approximately uniform bending moment zone, not subjected to any locally applied transverse loading, and treated as isolated struts, suitable graphs are given in Figs 82a and 82b, which may be used in accordance with the following clauses to obtain directly the limiting values σ_{su} for the different modes of failure of the stiffener. The applied longitudinal stress σ_a defined in Clause 2.1 shall not exceed the lowest of these limiting values σ_{su} .

2.8.1 For the effective stiffener section consisting of the area of the stiffening rib A_s and the associated area of the flange = $K.b.t$, calculate:

- (i) r_e = radius of gyration about a horizontal axis through the centroid of the effective section.
- (ii) y_p and y_o = distances of the mid-plane of the flange plate and of the tip of the outstand respectively from the centroid of the effective section.

2.8.2 Failure initiated by plate in compression

- (a) From the graphs in Fig. 26 obtain:

$$\sigma_p = \frac{1}{K} \frac{\sigma_{au}}{\sigma_{ys}} \sqrt{(\sigma_{ys})^2 - 3\tau^2}$$

where τ is defined in Clause 2.5.

- (b) Calculate:

$$(i) \quad \lambda = \frac{L}{r_e} \sqrt{\frac{\sigma_p}{E}}, \quad \text{and}$$

$$(ii) \quad \eta = \frac{y_p \Delta}{r_e^2}, \quad \text{taking the highest positive value of } \Delta \text{ from Clause 2.2.}$$

- (c) From the graphs in Fig. 82a, obtain R .

$$(d) \quad \text{Calculate } \sigma_{su} = R \sigma_p \frac{A_e}{A_g}.$$

2.8.3 Failure initiated by outstand in compression

- (a) Calculate:

$$(i) \quad \lambda = \frac{L}{r_e} \sqrt{\frac{\sigma_{ys}}{E}}, \quad \text{and}$$

$$(ii) \quad \eta = - \frac{y_o \Delta}{r_e^2}, \quad \text{taking the highest negative value of } \Delta \text{ from Clause 2.2.}$$

Note: η will be positive, as Δ is negative.

(b) From the graphs in Fig. 82a, obtain R .

(c) Calculate $\sigma_{su} = R \sigma_{ys} \frac{A_e}{A_g}$.

2.8.4 Failure initiated by outstand yielding in tension

(a) Calculate:

$$(i) \quad \lambda = \frac{L}{r_e} \sqrt{\frac{\sigma_{ys}}{E}}$$

$$(ii) \quad \eta = -\frac{y_o \Delta}{r_e^2}, \quad \text{taking the highest positive value of } \Delta \text{ from Clause 2.2.}$$

(b) From the graphs in Fig. 82b obtain R .

(c) Calculate $\sigma_{su} = R \sigma_{ys} \frac{A_e}{A_g}$.

3. FLANGE STIFFENERS IN A VARYING MOMENT ZONE, TREATED AS ISOLATED STRUTS

3.1 The method given here is applicable to flange stiffeners subjected to a linearly varying longitudinal compressive stress pattern.

When the variation is not linear and/or when there is tension at one end, the same method may be applied by drawing a straight line envelope to the stress diagram avoiding any tension, as shown in Fig. 83.

σ_A and σ_B denote the higher and lower compressive longitudinal stresses at the two ends of the stiffener span L .

3.2 The stresses σ_{pm} and σ_{om} will be calculated in accordance with Clause 2.4 for each of the following two combinations of P and M :

$$(a) \quad (i) \quad P = \sigma_A \left[C_1 + \frac{\sigma_B}{\sigma_A} (1 - C_1) \right] A_g$$

$$(ii) \quad M = \frac{\pi^2}{L^2} EI_e \Delta (m - 1) C_2$$

where
$$m = \frac{1}{1 - \frac{\sigma_A A_g L^2}{C_3 \pi^2 EI_e}}$$

and C_1 , C_2 and C_3 are coefficients given in Fig. 28.

Where $0.75 < \frac{\sigma_B}{\sigma_A} < 1.0$, P and M may be approximately taken as:

$$\left[\frac{\sigma_B + \sigma_A}{2} \right] A_g \text{ and } \frac{\pi^2}{L^2} EI_e \Delta (m - 1)$$

respectively, with
$$m = \frac{1}{1 - \frac{(\sigma_A + \sigma_B) A_g L^2}{2\pi^2 EI_e}}$$

(b) (i) $P = \sigma_A A_g$

(ii) $M = \sigma_A A_g 2(\delta_2 + \delta_3)$, taking only +ve values of δ_2 and δ_3 .

3.3 The failure of the stiffener will be checked in accordance with Clauses 2.4 to 2.6, except that τ shall be taken as $(\tau_1 + \frac{1}{2} \tau_2)$, where τ_1 is the shear stress in the flange plate due to torsion on the box girder, and τ_2 is the maximum shear stress in the flange plate at the junction of the flange and the web of the box, due to shear force on the box girder.

4. FLANGE STIFFENERS IN AN APPROXIMATELY UNIFORM BENDING MOMENT ZONE, TREATED AS AN ORTHOTROPIC SYSTEM

4.1 The elastic critical buckling stress in longitudinal compression, σ_{cr}^* , of the orthotropic plate supported by the webs of the box girder and by the transverse stiffeners at spacing L , is given by:

$$\sigma_{cr}^* = \frac{\pi^2}{t + \frac{NA_s}{B}} \left[\frac{D_x}{L^2} + D_y \frac{L^2}{B^4} + \frac{2H}{B^2} \right]$$

where N is the number of stiffeners in the orthotropic plate

A_s is the area of each stiffening rib

B is the width between the box girder webs

$D_x = \frac{EI_e}{b}$, where I_e is defined in Clause 2.3 and b is the spacing of stiffeners

$$D_y = \frac{Et^3}{12(1 - \nu^2)}$$

$H = \frac{Gt^3}{6} + \frac{GJ_x}{2b} + \frac{\nu bt}{A_s + bt} D_y$, where J_x is the St. Venant torsion constant of the stiffener and is equal to:

(i) $\frac{\sum dt^3}{3}$ for open section, and

(ii) $\frac{4A^2}{\sum d/t}$ for closed sections

where d and t are width and thickness of component walls, and A is the area enclosed by the middle planes of the walls.

4.2 The following equation will be used to obtain the magnification m :

$$\sigma_a = \sigma_{cr}^* - \frac{\sigma_{cr}^*}{m} + \frac{E\Delta^2}{L^2} (m^2 - 1),$$

where σ_a and Δ have been defined in Clauses 2.1 and 2.2.

A convenient procedure for getting m is as follows:

Assume the first trial value for $m = m_1 = \frac{\sigma_{cr}^*}{\sigma_{cr}^* - \sigma_a}$

Calculate $\delta_m = \frac{\sigma_{cr}^*}{m_1^2} + \frac{2E\Delta^2 m_1}{L^2}$

$$\sigma_{a1} = \sigma_{cr}^* - \frac{\sigma_{cr}^*}{m_1} + \frac{E\Delta^2}{L^2} (m_1^2 - 1)$$

Next approximation for m is $m_2 = m_1 - \frac{\sigma_{a1} - \sigma_a}{\delta_m}$

and so on.

4.3 The longitudinal stresses σ_c^* and σ_e^* along the centre-line and the edge respectively of the orthotropic plate shall be obtained

from:

$$(i) \quad \sigma_c^* = \sigma_{cr}^* - \frac{\sigma_{cr}^*}{m} - \frac{E\Delta^2}{L^2} (m^2 - 1)$$

$$(ii) \quad \sigma_e^* = \sigma_{cr}^* - \frac{\sigma_{cr}^*}{m} + \frac{3E\Delta^2}{L^2} (m^2 - 1)$$

4.4 A stiffener along the centre-line and a stiffener near the longitudinal edge of the orthotropic plate shall be checked separately in accordance with Clauses 2.4 to 2.6 for the following forces and moments:

(a) Central Stiffener (i) $P = \sigma_c^* A_g$

(ii) $M = \frac{4\pi}{L^2} EI_e \Delta (m - 1)$

(b) Edge Stiffener (i) $P = \sigma_e^* A_g$

(ii) $M = \sigma_e^* A_g \Delta$

5. FLANGE STIFFENERS IN A VARYING MOMENT ZONE, TREATED AS AN ORTHOTROPIC SYSTEM

5.1 The stresses σ_A and σ_B shall be obtained in accordance with Clause 3.1.

5.2 The following equation shall be used to obtain the magnification m :

$$\sigma_A = C_3 \sigma_{cr}^* - \frac{C_3 \sigma_{cr}^*}{m} + \frac{E\Delta^2}{L^2} (m^2 - 1) ,$$

where σ_{cr}^* is defined in Clause 4.1
 C_3 is given in Fig. 28.

(See Clause 4.2 for a convenient procedure for getting m .)

5.3 The longitudinal stress σ_c^* in the mid-span region of the

central stiffener shall be obtained from:

$$\sigma_e^* = \left[C_3 \sigma_{cr}^* - \frac{C_3 \sigma_{cr}^*}{m} - \frac{E\Delta^2}{L^2} (m^2 - 1) \right] \left[C_1 + \frac{\sigma_B}{\sigma_A} (1 - C_1) \right]$$

and the central stiffener shall be checked in accordance with Clauses 2.4 to 2.6, taking

$$P = \sigma_e^* \cdot A_g$$

$$M = \frac{4\pi}{L^2} EI_e \Delta (m - 1) C_2$$

where m is obtained from Clause 5.2, and

C_1 and C_2 are given in Fig. 28.

5.4 The longitudinal stress σ_e^* at the heavily stressed end of a stiffener near the edge of the orthotropic plate shall be obtained from:

$$\sigma_{cr}^* = C_3 \sigma_{cr}^* - \frac{C_3 \sigma_{cr}^*}{m} + \frac{3E\Delta^2}{L^2} (m^2 - 1)$$

The stiffener will be checked in accordance with Clauses 2.4 to 2.6 for each of the following two combinations of P and M , taking $\tau = (\tau_1 + \frac{1}{2} \tau_2)$, where τ_1 and τ_2 are defined in Clauses 3.3:

(a) (i) $P = \sigma_e^* A_g$

(ii) $M = \sigma_e^* A_g 2(\delta_2 + \delta_3)$, taking only +ve values of δ_2 and δ_3 .

(b) (i) $P = \sigma_e^* A_g \left[C_1 + \frac{\sigma_B}{\sigma_A} (1 - C_1) \right]$

$$M = \sigma_e^* A_g \left[C_1 + \frac{\sigma_B}{\sigma_A} (1 - C_1) \right] \Delta C_2$$

where m is obtained from Clause 5.2, and

C_1 and C_2 are given in Fig. 28.

6. EFFECT OF LOCALLY APPLIED TRANSVERSE LOADING ON FLANGE

6.1 When loads are applied locally over a stiffened flange causing local transverse bending moment on one or a few of the stiffeners acting as beams between transverse supports, the methods given in Clauses 2.1 to 2.6 of Section 2, and Sections 3 to 5 may be applied, subject to the following modification.

6.2 Bending moments M_h and M_s in support and mid-span regions respectively in individual stiffeners due to locally applied loading should be calculated, taking into account lateral distribution of the load between adjacent stiffeners, continuity, etc., but ignoring the in-plane longitudinal loading on the flange. These moments shall be taken as positive when causing compression in the flange and tension in the outstand, and vice versa. The bending moment M in the stiffeners due to the effects of eccentricity of longitudinal loading, given in the previous sections, will then be increased or decreased by adding algebraically to it either the amount M_h or the amount $M_s \cdot m$, where m is the magnification factor defined in the previous sections. The maximum stresses will then be checked in accordance with Clauses 2.4 to 2.6.

6.3 It is permissible to redistribute the applied longitudinal stress σ_a over the entire width of the stiffened flange in such a manner that the stiffener subjected to high local bending moment carries a smaller proportion of the longitudinal applied stress, and thus the optimum strength of the entire width of the flange may be obtained.

7. SLENDERNESS LIMITATIONS ON STIFFENER COMPONENTS

7.1 Open type stiffeners, i.e. Flats, Bulb Flats, Tees, Angles:

Notations -

d, t_2, b, t are shown in Fig. 36

σ_{om} - maximum compressive stress at tip of stiffener outstand
(see Clause 2.4)

σ_{oa} - average compressive stress on effective stiffener

section ($= \frac{P}{A_e}$, see Clause 2.4)

I_p - polar moment of inertia of stiffener rib about its point of attachment with the flange plate; $I_p = I_x + I_y$, when the latter are the second moments of area of the stiffener rib about $x-x$ and $y-y$ axes respectively shown in Fig. 36;

r_y - radius of gyration of the stiffener rib about $y-y$ axis

J - St. Venant torsion constant of the stiffener rib and is approximately $\frac{1}{3} t_2^3 d (1 + K_1^3 K_2)$; (see Fig. 36 for K_1 and K_2)

F_1, F_2, F_3 - coefficients given in Fig. 37 for various ratios of K_1 and K_2 shown in Fig. 36

$$\alpha = \frac{bt t_2^2}{I_p} \quad \beta = \frac{bt}{A_s} \left(\frac{t}{b}\right)^2 \frac{t_2^4}{d^2 r_y^2}$$

$$\gamma = \frac{bt}{A_s} \frac{J}{I_p} \frac{t_2^4}{d^2 r_y^2}$$

7.1.1 (a) The ratio $\frac{d}{t_2}$ of the attached leg of the stiffener shall not exceed:

$$\sqrt{\frac{\frac{F_3}{2.25 \sigma_{om}} - m \left[F_1 + F_2 \left(\frac{d}{t_2}\right)^2 \right]}{E} \times \frac{4 \sigma_{om}}{3 \sigma_{om} + \sigma_{oa}}}$$

where $m = \frac{1}{50} \left[(\alpha^2 + 40\beta - 4\gamma)^{\frac{1}{2}} - \alpha \right]$, but not less than $\left[\frac{t_2}{L} \right]^2$

If, however, the denominator within the root sign in the above expression for limiting $\frac{d}{t_2}$ is negative, then $\frac{d}{t_2}$ shall not exceed:

$$1.7 \sqrt{\frac{E}{\sigma_{om} + \sigma_{oa}}}$$

7.1.1 (b) For plain flat sections the above formula leads approximately to:

$$\frac{d}{t_2} \dagger 0.83 \sqrt{\frac{E}{3 \sigma_{om} + \sigma_{oa}}}$$

7.1.1 (c) For the purpose of this check, (i) a bulb flat may be assumed to be equivalent to a tee section with flange of uniform thickness and of equal width and area to those of the bulb, and (ii) an angle section may be assumed to be equivalent to a tee section with flange dimensions identical to those of the unattached leg.

7.1.2 For the outstanding flange of a tee or an angle section, the ratio $\frac{\text{width of outstand}}{\text{thickness}}$ shall not exceed $0.415 \sqrt{\frac{E}{\sigma_{om}}}$.

7.2 Closed Type Stiffeners

The slenderness ratio of individual walls of closed type stiffeners shall satisfy the following requirements (see Fig. 43):

- (a) Bottom flange: $\frac{b_1}{t_1} \nlessgtr 1.20 \sqrt{\frac{E}{\sigma_{om}}}$
- (b) Side walls: $\frac{d}{t_2} \nlessgtr 1.70 \sqrt{\frac{E}{\sigma_{om} + \sigma_{oa}}}$

where σ_{om} and σ_{oa} are defined in Clause 7.1.

7.3 In Clauses 7.1 and 7.2, σ_{om} and σ_{oa} may both be conservatively taken as the yield stress of the outstand σ_{ys} .

8. FABRICATION TOLERANCE FOR STIFFENED COMPRESSION FLANGE

8.1 Stiffeners

- (a) Δ_{sx} is the geometrical imperfection of a stiffener measured in the vertical plane over the span L between transverse supports.

$$\Delta_{sx} \nlessgtr \frac{L}{900}$$

- (b) Δ_{sy} is the geometrical imperfection of the tip of the outstand of 'open' type stiffeners, measured in a horizontal plane over the gauge lengths L' defined below:

$$\Delta_{sy} \nlessgtr \frac{L'}{450} \sqrt{\frac{\sigma_{ys}}{245}}$$

where σ_{ys} is the characteristic yield stress in N/mm².

Δ_{sy} shall be separately measured and checked from the above formula for two values L' equal to L and $2b$, where b is the spacing between the stiffeners.

8.2 Plate Panels

- (a) Initial imperfection Δ_p of a plate panel between longitudinal supports is measured over a gauge length $G = 2 \times$ width of the plate panel between the longitudinal supports, along the longitudinal centre line of the panel.

$$\Delta_p \leq \frac{G}{250} \sqrt{\frac{\sigma_{ys}}{245}}$$

where σ_{ys} is the characteristic yield stress in N/mm^2 .

- (b) For closed type of stiffeners the above tolerance applies to each individual wall and $G = 2 \times$ width of the wall concerned.

CHAPTER 13

CONCLUSIONS

1. GENERAL

1.1 A complete analysis for the ultimate load behaviour of stiffened compression flanges, and a simple method for their design, have been developed. In this method of analysis and design, the various complex features associated with the stiffened compression flange have been satisfactorily dealt with.

1.2 It is shown in Chapter 3 that the longitudinal stiffeners can be treated as initially imperfect and/or eccentrically loaded struts, the cross-section of which consists of the stiffening section and the associated flange plate. But the influence of initial out-of-flatness and welding residual stresses on the behaviour of the flange plate must be taken into account in the following manner:

- (i) a reduced effective width of the flange plate, representing the reduction in its axial stiffness, must be taken for the sectional properties of the strut;
- (ii) the material yield stress of the flange plate must be replaced by its reduced compressive strength.

1.3 The load-shortening behaviour of the flange plate between adjacent stiffeners is obtained in Chapters 4 and 5 by applying the large-deflection theory for thin plates, in conjunction with an idealised residual stress pattern caused by welding. It is shown that this behaviour can be represented by two straight lines, one for the elastic phase and the other the post-elastic phase. The reduction coefficients for stiffness and strength, appropriate to the levels of out-of-flatness and welding stresses, are derived for incorporation in the strut analysis as described in the previous paragraph.

1.4 The restraining influence of the entire orthotropically stiffened flange on the buckling behaviour of the individual stiffeners is accounted for in the strut analysis by using an appropriate express-

ion for the magnification of the initial out-of-straightness of the strut. In Chapter 6 this expression is derived from the large-deflection theory for flexure of orthotropic plates. It has thus been possible to retain the simplicity of the concept of an isolated strut, at the same time making use of the additional restraint from orthotropic action.

1.5 The benefit of reduction in longitudinal stress in zones of rapidly falling bending moment on the box girder is quantified in Chapter 7. The simple device of taking the applied stress at $0.4 L$ from the heavily stressed end of the stiffener span is shown to be satisfactory, though over-conservative in certain situations. For more economical results, suitable coefficients are given for incorporation in the analysis for uniformly compressed struts.

1.6 The benefit of continuity of the flange stiffeners over transverse supports is studied in Chapter 8 by applying the three-moment theorem for beam-columns. When the initial imperfections in the adjacent spans are not in the alternately up and down sinusoidal mode, their influence on the buckling behaviour of a continuous strut is shown to be considerably less than in the case where the initial imperfections are in the critical buckling mode. Suitable reduction coefficients are derived for effective values of these imperfections. It is also shown that such 'non-sympathetic' imperfection pattern may cause a change in the sign of the bending moment within a stiffener span - a phenomenon that cannot be predicted by analysing only one span. It may be unsafe if this aspect is ignored in the design of continuous struts of unsymmetrical cross-sections, such as the longitudinal stiffeners in a box girder flange.

1.7 The analysis of the flange stiffeners presented in this thesis requires that premature local buckling of the stiffener outstand is prevented. Geometrical limitations are derived in Chapter 9 for this purpose. It is also shown that slender stiffener outstands may need flexural restraint from the flange plate, which must be stocky enough for this purpose; suitable criteria are developed in this chapter.

1.8 In Chapters 10 and 11 the analytical theories developed in the preceding chapters have been comprehensively verified with available test data, and have also been used to explain in detail the entire behaviour of four box girders tested to collapse.

1.9 Chapter 12 provides simple design rules and related workmanship tolerances developed from these theories. A comprehensive comparison of results from these rules with test data from various sources confirm the reliability and economy of these rules.

2. FURTHER WORK

This investigation does not deal with (i) the effect of shear lag on the ultimate strength of box girders, (ii) the design of transverse stiffeners in the compression flange, and (iii) the evaluation of local bending moments due to wheel loads.

It is, however, considered that further theoretical work based on the application of non-linear elasto-plastic methods to stiffened plates, and supported by suitable experiments, would be useful for evaluating the influence of the following aspects on the post-elastic behaviour of stiffened compression flanges:

- (i) the effects of shear lag;
- (ii) the interaction of axial compression and local wheel loading;
- (iii) the non-linear torsional buckling behaviour of stiffener outstands.

REFERENCES

1. Inquiry into the Basis of Design and Method of Erection of Steel Box Girder Bridges: Interim Report. HMSO, London; 1971.
2. Inquiry into the Basis of Design and Method of Erection of Steel Box Girder Bridges: Report of the Committee. HMSO, London; 1973.
3. Inquiry into the Basis of Design and Method of Erection of Steel Box Girder Bridges: Interim Design and Workmanship Rules: Parts I to IV. HMSO, London; 1973.
4. Column Research Council. Guide to Design Criteria for Metal Compression Members. John Wiley & Sons, 1966.
5. Moxham, K.E. Buckling Tests on Individual Welded Steel Plates in Compression. Cambridge University Report CUED/C - Struct/TR3 (1971).
6. Ractliffe, A.T. The Strength of Plates in Compression. PhD Thesis, Cambridge University, 1970.
7. Moxham, K.E. Theoretical Prediction of the Strength of Welded Steel Plates in Compression. Cambridge University Report CUED/C - Struct/TR2 (1971).
8. Williams, D.G. Some Examples of the Elastic Behaviour of Initially Deformed Bridge Panels. Civil Engineering and Public Works Review, October 1971.
9. Rockey, K.C. and Skaloud, M. The Ultimate Load Behaviour of Plate Girders in Shear. The Structural Engineer, January 1972.
10. Ostapenko, A., Chern, C. and Parsanejad, S. Ultimate Strength Design of Plate Girders. Developments in Bridge Design and Construction (Ed: Rockey, Bannister and Evans). Crosby Lockwood, 1971.
11. Porter, D.M., Rockey, K.C. and Evans, H.R. The Collapse Behaviour of Plate Girders Loaded in Shear. The Structural Engineer, August 1975.
12. G. Maunsell & Partners. Report on Parametric Study of Web Panels. Department of the Environment, London, 1972.

13. Dowling, P.J., et al. Experimental and Predicted Collapse Behaviour of Rectangular Steel Box Girders. Steel Box Girder Bridges. The Institution of Civil Engineers, London, 1973.
14. Rockey, K.C., Evans, H.R. and Porter, D.M. The Ultimate Load Capacity of Stiffened Webs Subjected to Shear and Bending. Steel Box Girder Bridges. The Institution of Civil Engineers, London, 1973.
15. Crisfield, M.A. Large-deflection Elasto-plastic Buckling Analysis of Plates Using Finite Elements. Report LR593, 1973; Transport and Road Research Laboratory, Crowthorne.
16. Harding, J.E., Hobbs, R.E. and Neal, B.G. Ultimate Load Behaviour of Plates Under Combined Direct and Shear In-plane Loading. Steel Plated Structures (Ed: Dowling, Harding and Frieze), Crosby Lockwood Staples, London.
17. Frieze, P.A., Dowling, P.J. and Hobbs, R.E. Ultimate Load Behaviour of Plates in Compression. Steel Plated Structures (Ed: Dowling, Harding and Frieze), Crosby Lockwood Staples, London.
18. Edwards, L.S. Sensitivity of Stiffened Compression Panels to Geometrical Imperfections. Imperial College, London, December 1974.
19. Moolani, F.M. Ultimate Load Behaviour of Steel Box Girder Stiffened Compression Flanges. PhD Thesis, University of London, 1976.
20. Little, G.H. Stiffened Steel Compression Panels - Theoretical Failure Analysis. The Structural Engineer, December 1976.
21. Basu, A.K., et al. Elastic Post-buckling Behaviour of Discretely Stiffened Plates. Stability of Steel Structures: European Convention for Constructional Steelwork, Liege, April 1977.
22. Massonnet, C. and Maquoi, R. New Theory and Tests on the Ultimate Strength of Stiffened Box Girders. Steel Box Girder Bridges. The Institution of Civil Engineers, London, 1973.

23. Winter, G. Strength of Thin Steel Compression Flanges. Transactions of the American Society of Civil Engineers, vol. 112, 1947.
24. Faulkner, D., et al. Synthesis of Welded Grillages to Withstand Compression and Normal Loads. Journal of Computers and Structures, vol. 3, 1973.
25. Dwight, J.B. and Little G.H. Stiffened Steel Compression Flanges - A Simpler Approach. The Structural Engineer, December 1976.
26. Rubin, H. Longitudinally Stiffened and Compressed Plates of Box Girders. ECCS Commission 8, Working Group 3 Document.
27. Murray, N.W. Analysis and Design of Stiffened Plates for Collapse Load. The Structural Engineer, March 1975.
28. Horne, M.R. and Narayanan, R. An Approximate Method for the Design of Stiffened Steel Compression Panels. Proceedings of The Institution of Civil Engineers: Research & Theory, September 1975.
29. Viridi, K.S. Inelastic Column Behaviour: Its Application to Composite Columns in Biaxial Bending and Stiffened Plates in Compression. PhD Thesis, University of London, November 1973.
30. Beer, H. and Schulz, G. Bases Théoriques des Courbes Européennes de Flambement. Construction Metallique No. 3, 1970.
31. Dwight, J.B. Use of Perry Formula to Represent the New European Strut Curves. Cambridge University Report CUED/C-Struct/TR30 (1972).
32. Koiter, W.T. and Kuiken, G.D.C. The Interaction Between Local Buckling and Overall Buckling on the Behaviour of Built-up Columns. Rpt. No. 447, Laboratory of Engineering Mechanics, Delft, May 1971.
33. Thompson, J.M.T. and Hunt, G.W. A General Theory of Elastic Stability. John Wiley & Sons, London.
34. Bulson, P.S. The Stability of Flat Plates. Chatto & Windus, London.

35. Marguerre, K. and Treffitz, E. Über die Tragfähigkeit eines langbelasteten Plattenstreifens nach Überschreiten der Beullast. Zeitung f.a. Math. u Mech. Vol. 17, 1937.
36. Yamaki, N. Post-buckling Behaviour of Rectangular Plates with Small Initial Curvature Loaded in Edge Compression. Journal of Applied Mechanics, September 1959.
37. Stein, M. Loads and Deformations of Buckled Rectangular Plates. NASA Technical Report R-40, 1959.
38. Hemp, W.S. The Theory of Flat Panels Buckled in Compression. ARC Technical Report R & M No. 2178. HMSO London, 1945.
39. Coan, J.M. Large-deflection Theory for Plates with Small Initial Curvature Loaded in Edge Compression. Journal of Applied Mechanics, Vol. 18, June 1951.
40. Cox, H.L. The Buckling of Plates and Shells. Pergamon Press, 1963.
41. Walker, A.C. The Post-buckling Behaviour of Simply-supported Square Plates. Aeronautical Quarterly, Vol. 20, August 1969.
42. Dawson, R.G. and Walker, A.C. Post-buckling of Geometrically Imperfect Plates. Proceedings of the American Society of Civil Engineers, January 1972.
43. Sparkes, S.R., Chapman, J.C. and Pippard, A.J.S. Experiments on the Flexure of Rectangular Box Girders of Thin Steel Plating. Colston Papers: Engineering Structures. Butterworths 1949.
44. Falconer, B.H. and Chapman, J.C. Compressive Buckling of Stiffened Plates. The Engineer, June 5 and 12, 1953.
45. Dwight, J.B. and Moxham, K.E. Welded Steel Plates in Compression. The Structural Engineer, February 1969.
46. Young, B.W., et al. Residual Stress Measurements and Tolerances. Steel Box Girder Bridges. The Institution of Civil Engineers, London, 1973.
47. Bridges Engineering Division, Department of Transport: Report on Deformation in Steel Box Girder Bridges.

48. Maquoi, R. Etude Théorique et Expérimentale de la Résistance Post-critique des Semelles. Comprimées Raidies des Ponts Métalliques en Caisson. PhD Thesis, University of Liège.
49. Ritz, W. Über Eine Neue Methode zur Lösung Gewisser Variationsprobleme der Mathematischen Physik. Zeit. f. Reine und Angewandte Mathematik. 1909.
50. Timoshenko, S.P. and Gere, J.M. Theory of Elastic Stability. McGraw-Hill Book Co.
51. Horne, M.R. and Narayanan, R. Ultimate Load Capacity of Longitudinally Stiffened Panels. Simon Engineering Laboratories, University of Manchester. January and July 1974.
52. Measurement of Residual Stresses and Imperfections. CIRIA Research Project 183. (Report not yet published.)
53. Bleich, F. Buckling Strength of Metal Structures. McGraw-Hill Book Co.
54. Committee of Investigation into the Design and Erection of Steel Box Girder Bridges. Interim Design Appraisal Rules. Department of the Environment, 1972.
55. Guile, P.J.D. and Dowling, P.J. Steel Box Girders. CESLIC Reports BGI, BG3, BG5 and BGI8. Imperial College, London, 1971-72.
56. Recommended Standard Practices for Structural Testing of Steel Models. Supplementary Report 254. Transport and Road Research Laboratory, Crowthorne, 1977.
57. Dorman, A.P. and Dwight, J.B. Tests on Stiffened Compression Plate Panels. Steel Box Girder Bridges. The Institution of Civil Engineers, London, 1973.
58. Murray, N.W. Buckling of Stiffened Panels Loaded Axially and in Bending. The Structural Engineer, August 1973.
59. Walker, A.C. and Murray, N.W. Analysis for Stiffened Plate Panel Buckling. Monash University Report No. 2, 1974.
60. Fukumoto, et al. Ultimate Compressive Strength of Stiffened Plates. Proceedings of the ASCE Speciality Conference on Metal Bridges, St. Louis, 1974.

61. Smith, C.S. Compressive Strength of Welded Steel Ship Grillates. Transactions of the Royal Institution of Naval Architects, Vol. 117, 1975.
62. Barbré, R., et al. Traglastversuche an Ausschnitten Gedrückter Gurte Mehrerer Hohlkastenbrücken. Institut für Stahlbau. Technische Universität Braunschweig. Hamburg, 1976.

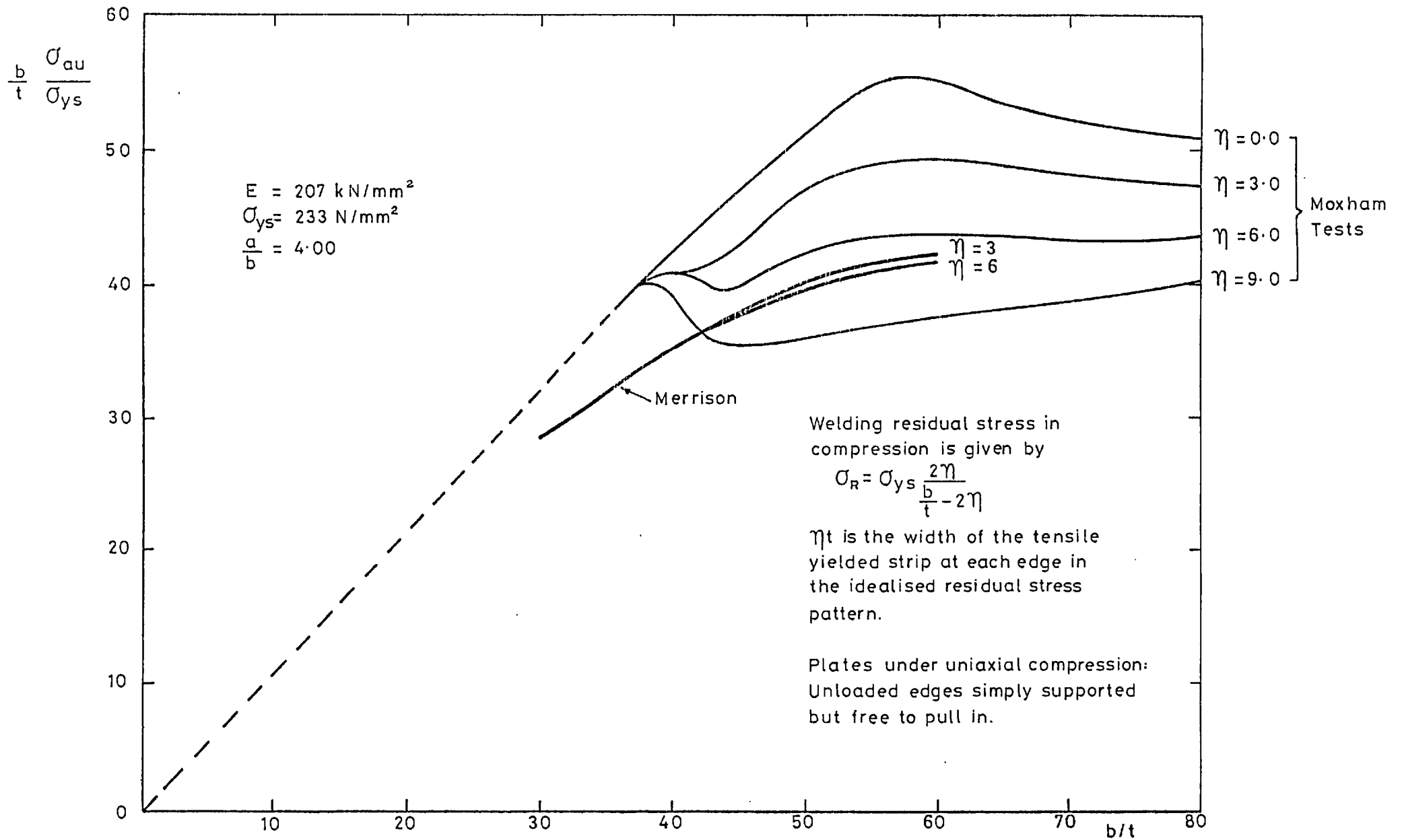


Fig 1. Comparison of collapse strength predicted by Merrison and observed in Moxham's tests.

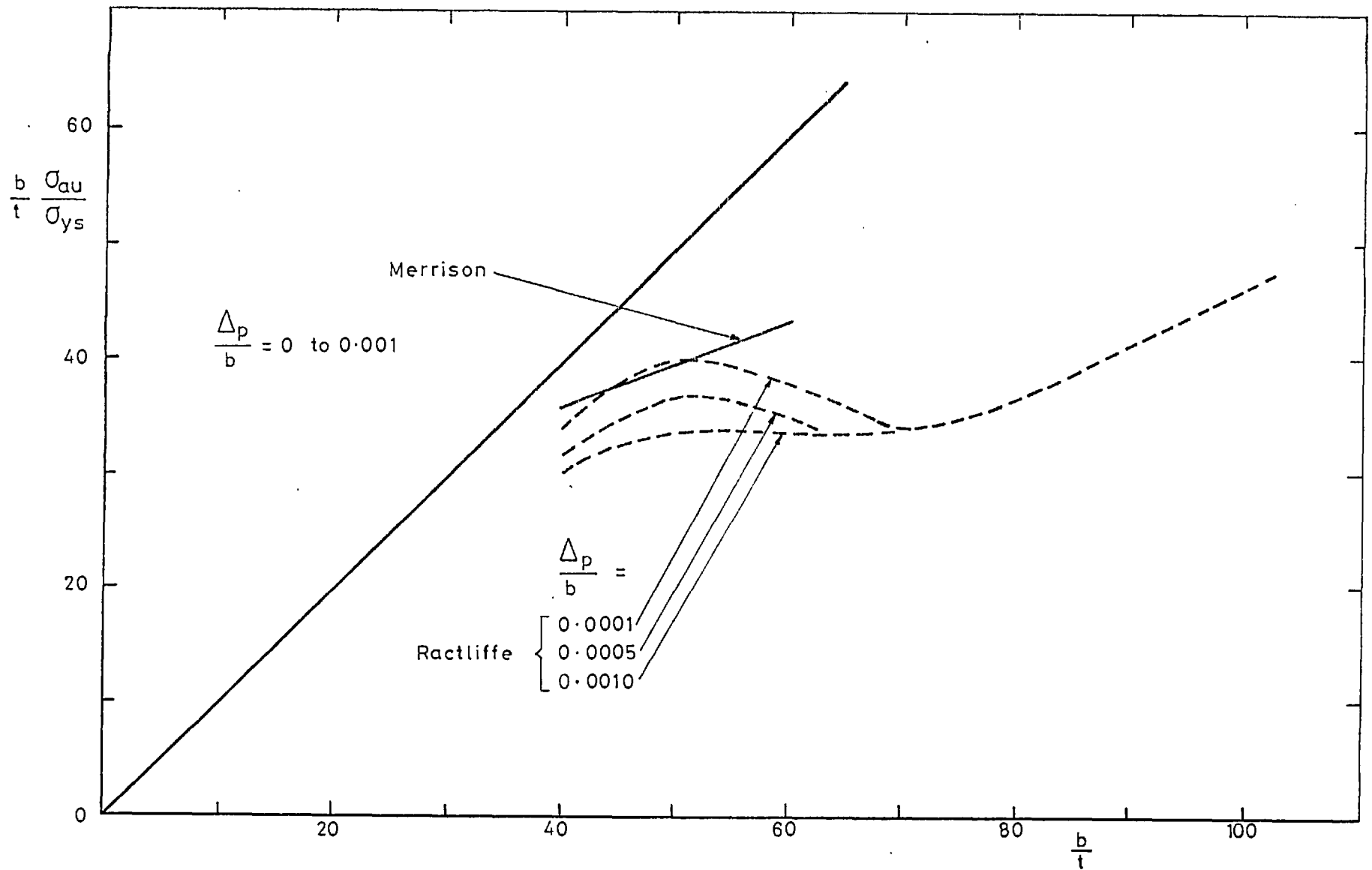


Fig. 2. Comparison of theoretical collapse strength between Merrison and Ractliffe. $\sigma_{ys} = 247 \text{ N/mm}^2$, $\eta = 3$. Plates under uniaxial compression, with unloaded edges held straight.

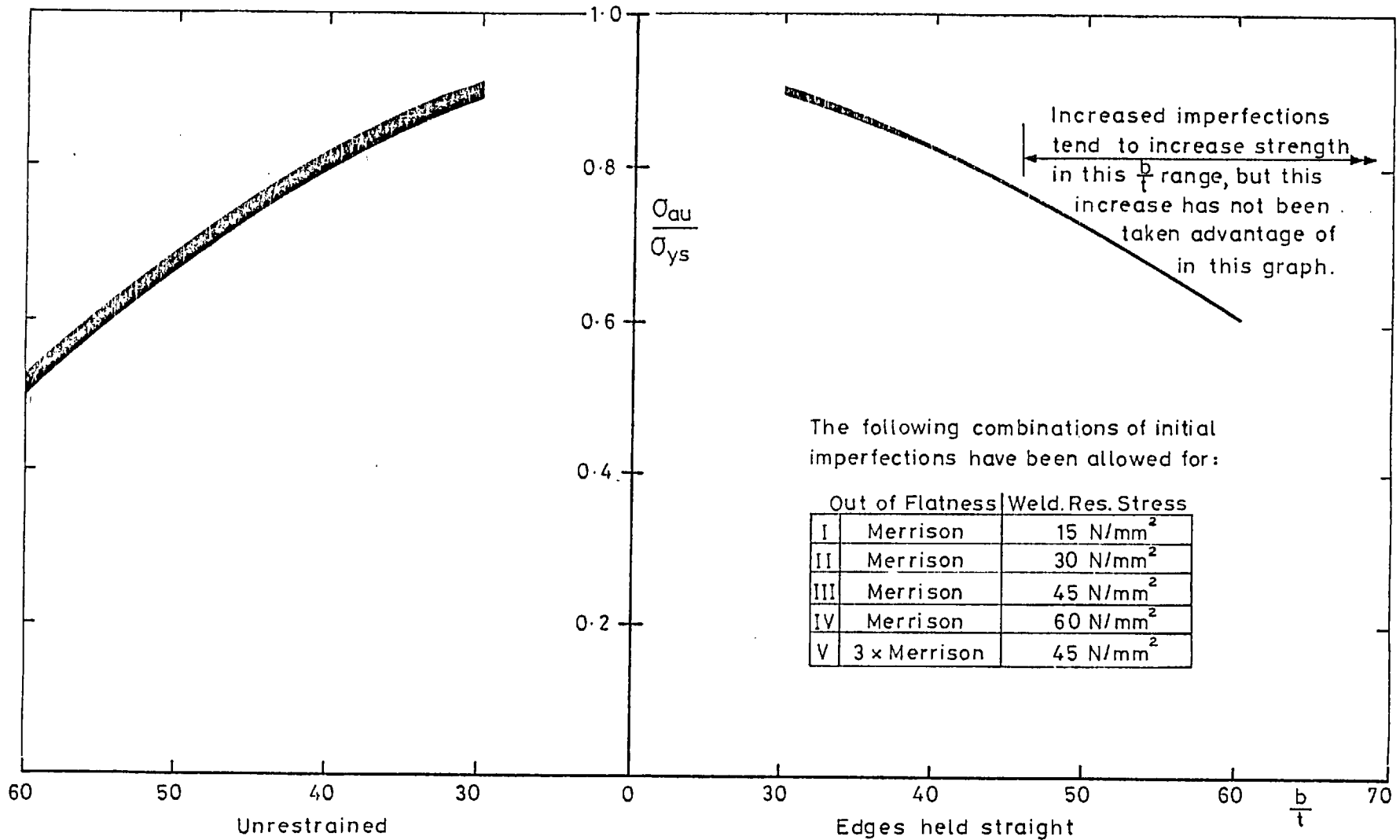


Fig.3 Band width for $\frac{\sigma_{au}}{\sigma_{ys}}$ in Merrison Rules for plates under uniaxial compression (HYS, $\sigma_{ys} = 355 \text{ N/mm}^2$) for changes in initial imperfections.

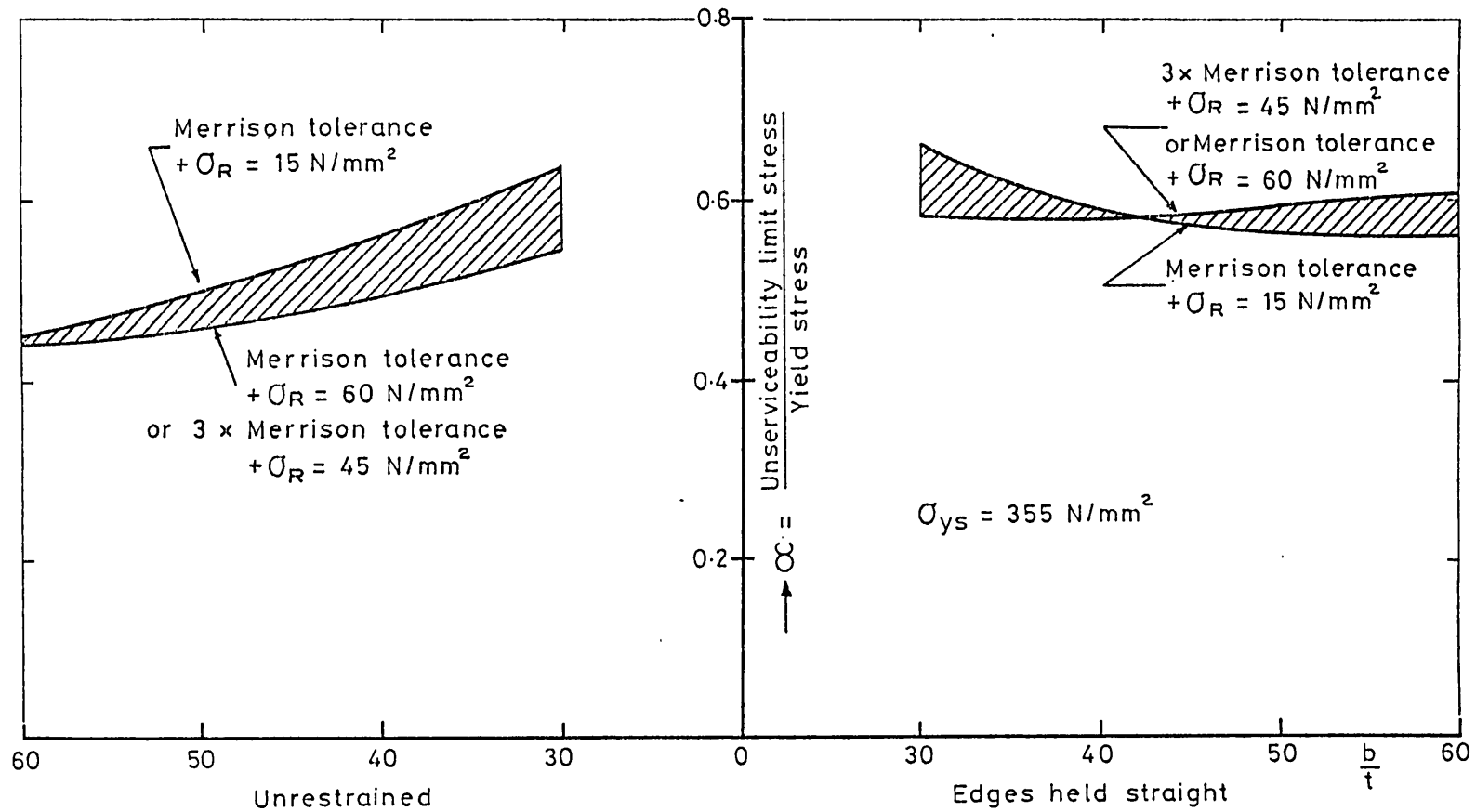


Fig. 4 Band width for unserviceability limit in Merrison Rules for plates under uniaxial compression due to changes in initial imperfections

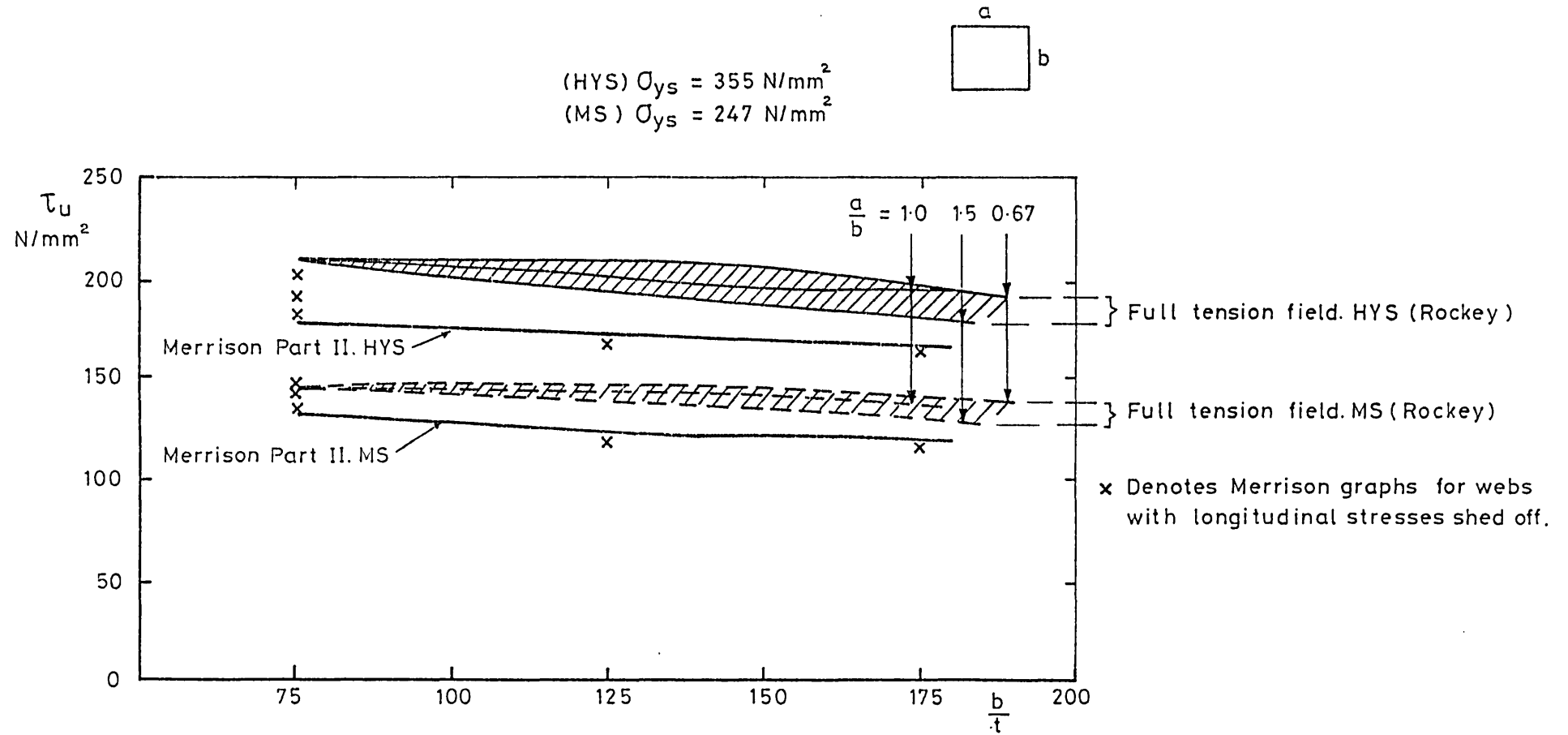


Fig. 5 Comparison of ultimate shear capacity of fully restrained webs given by the Merrison Rules and the tension - field model of Rockey

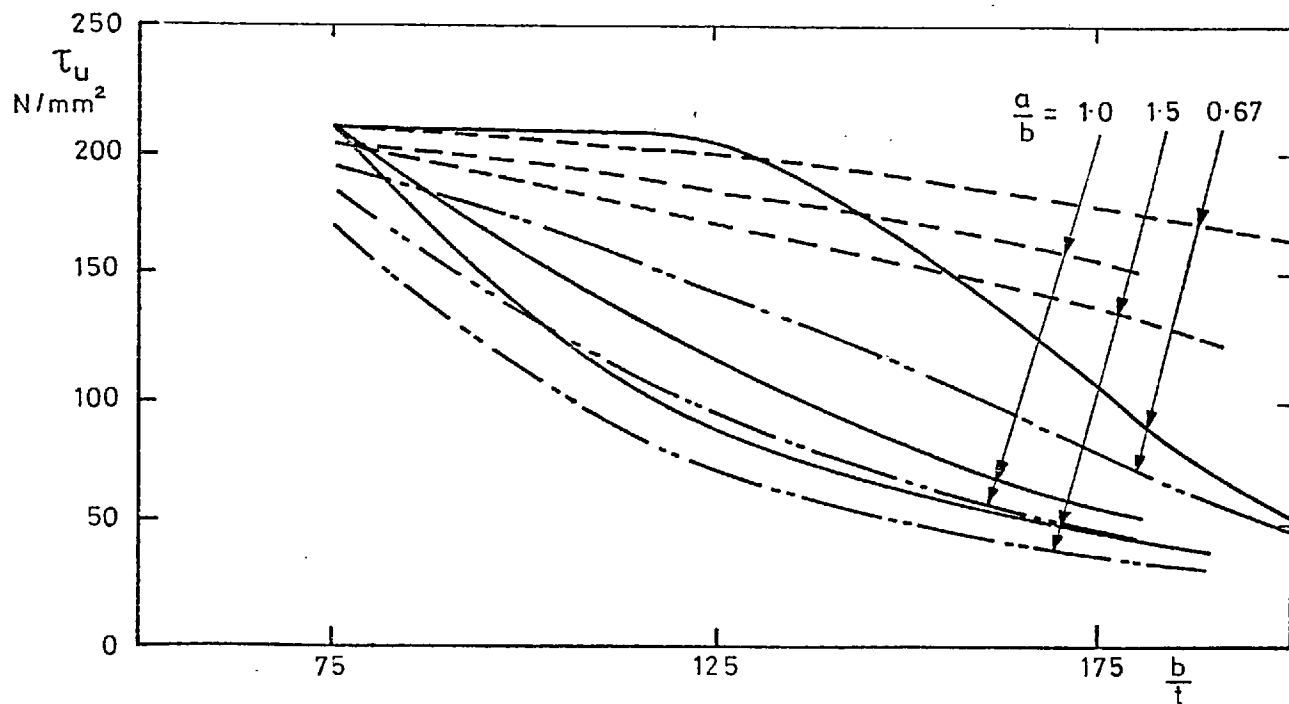
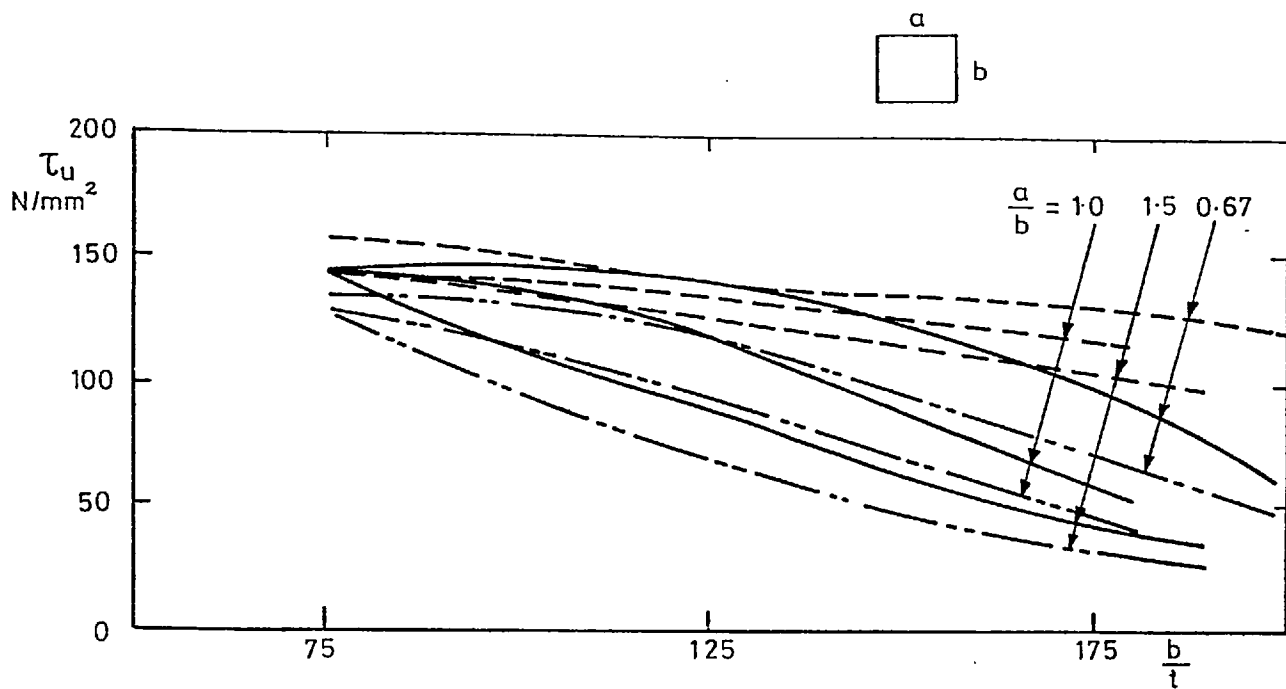


Fig. 6b HYS ($\sigma_{ys} = 355 \text{ N/mm}^2$)

Comparison of ultimate shear capacity of 'Unrestrained' webs given by the Merrison Rules, Rocky model and Ostapenko model.

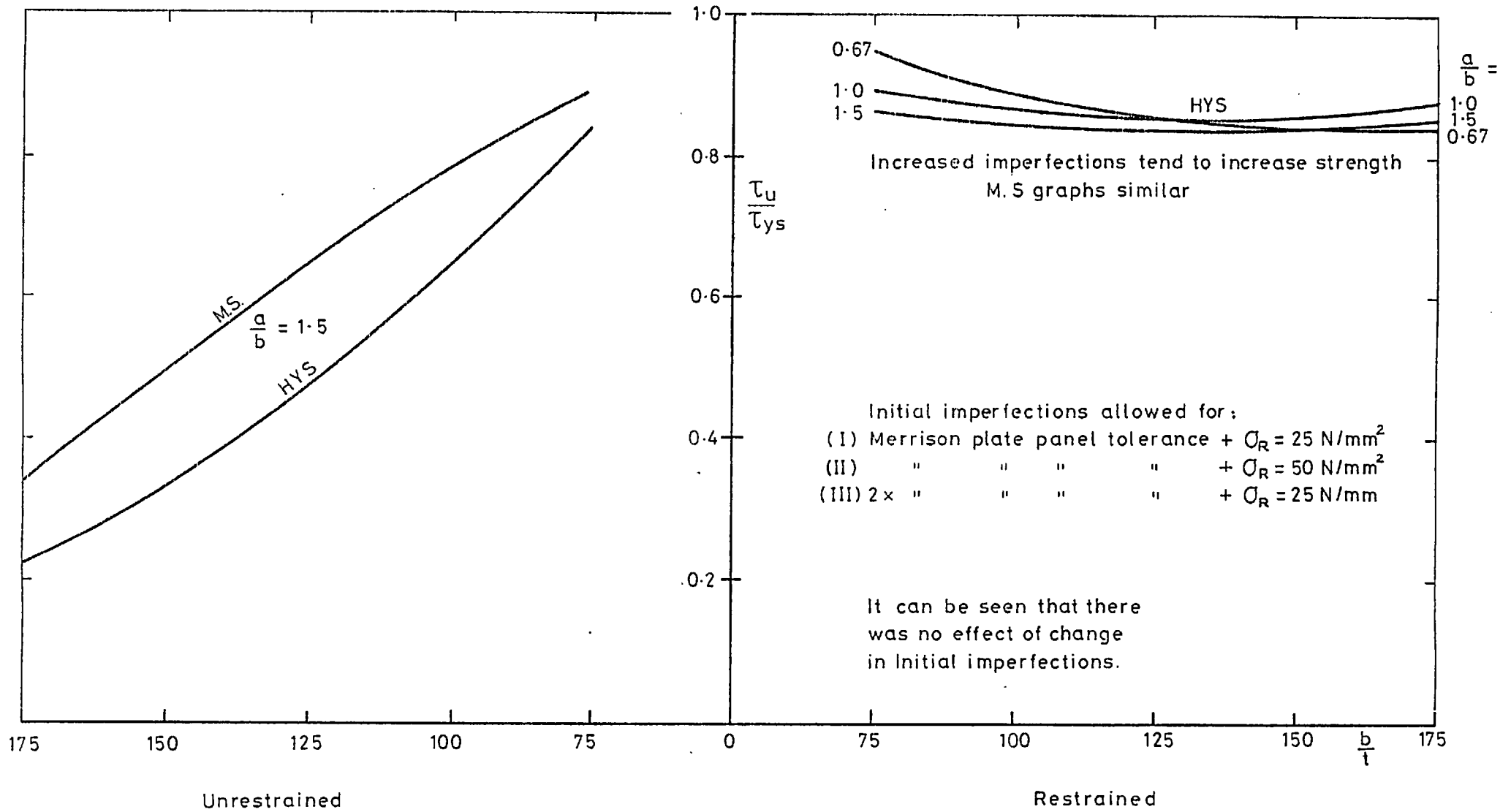


Fig.7 Band width for $\frac{\tau_u}{\tau_{ys}}$ in Merrison Rules for pure shear for changes in initial imperfections

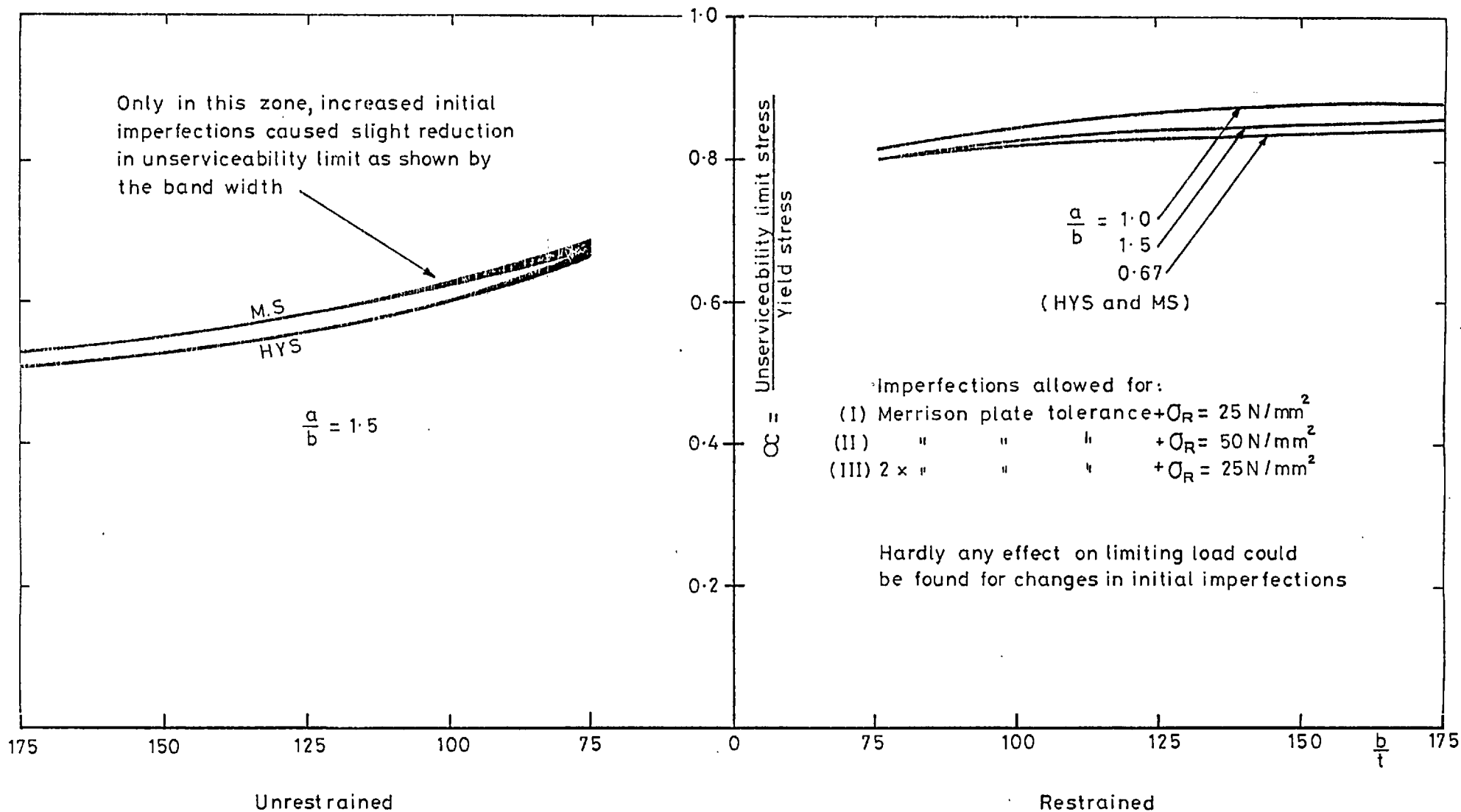


Fig.8 Band width for unserviceability limit in Merrison Rules for pure shear due to changes in initial imperfections.

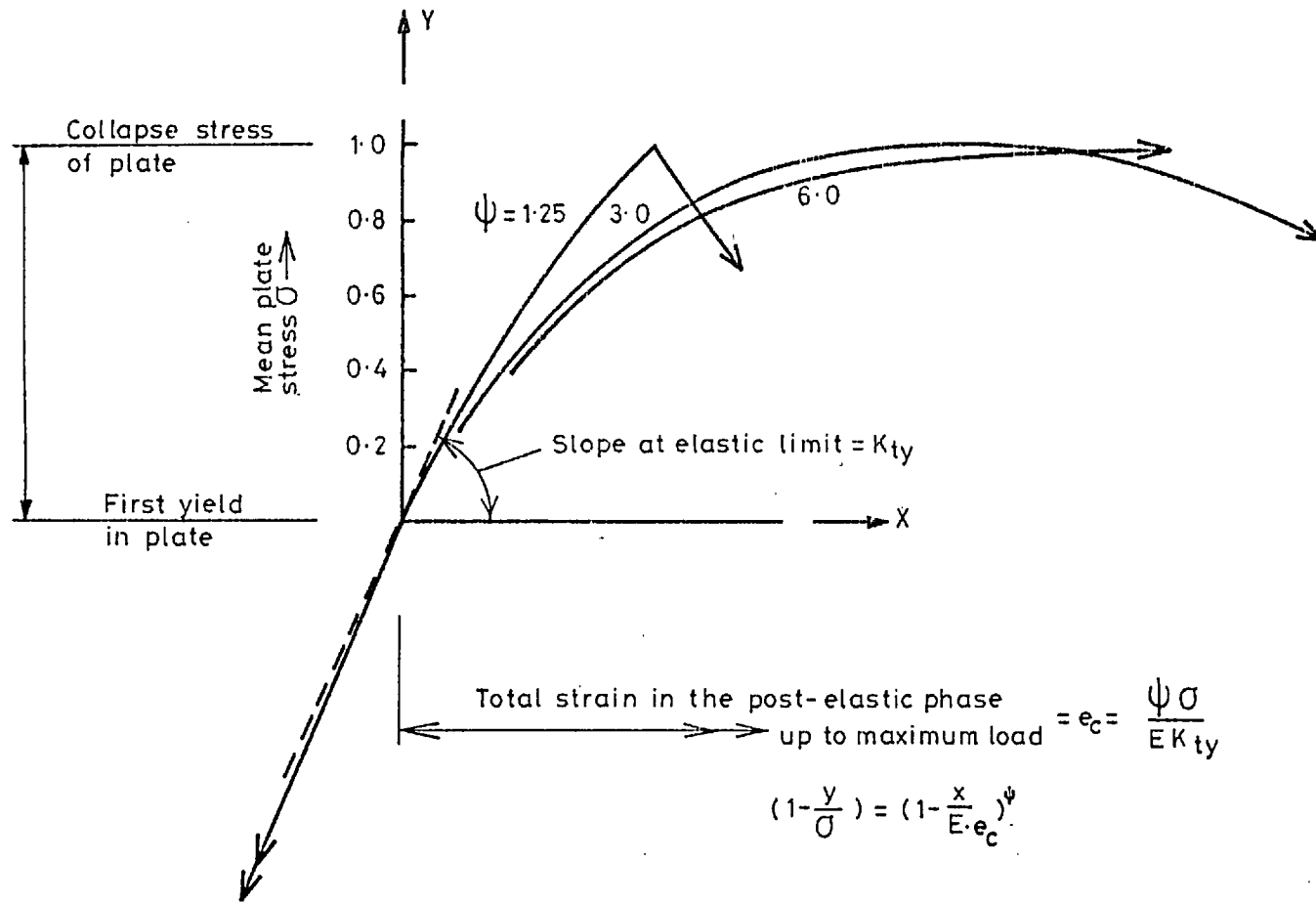


Fig. 9 Hypothetical load - end shortening behaviour of plate

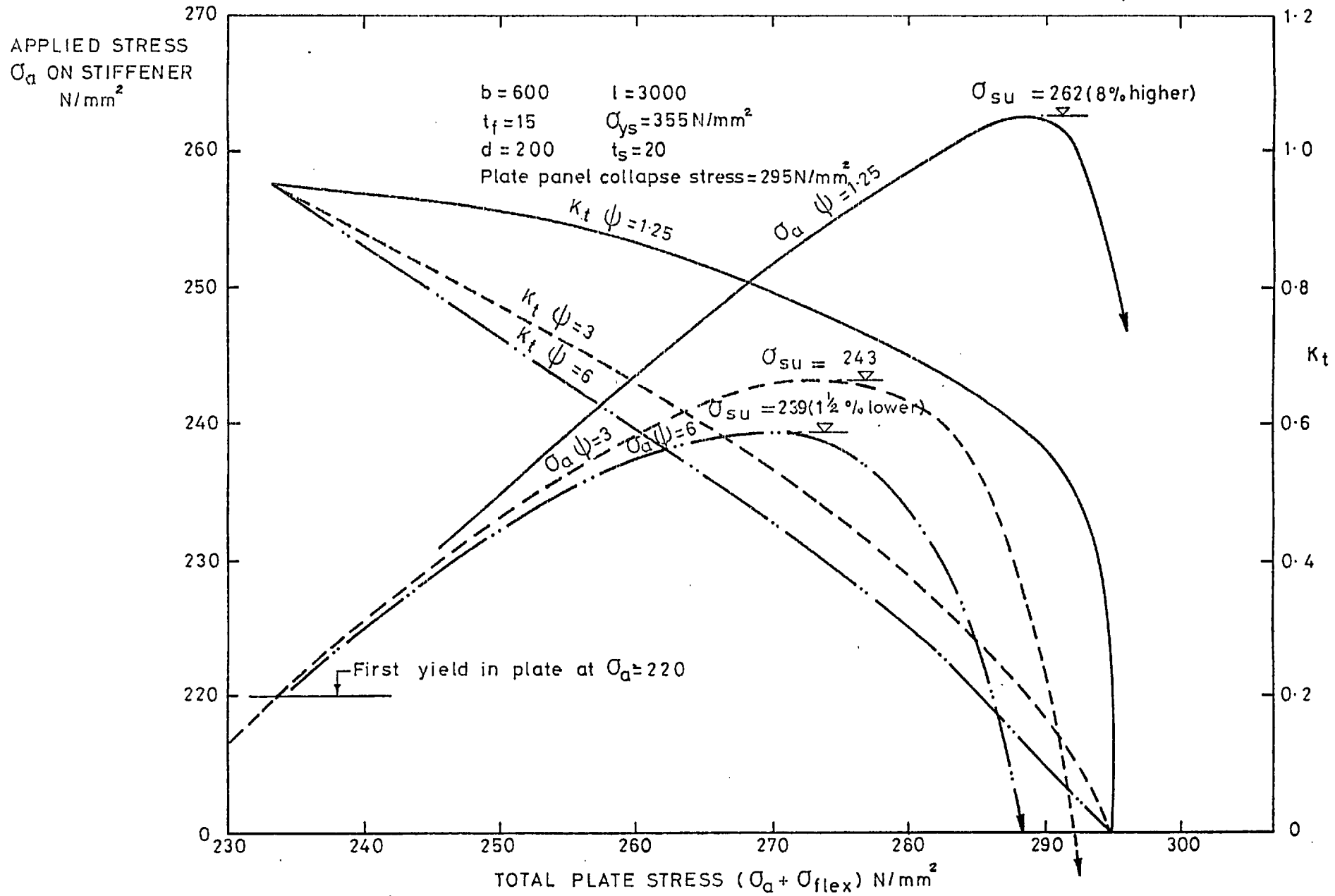


Fig.10 Variation in stiffener collapse stress for different types of plate load-deformation behaviour in post-elastic phase.

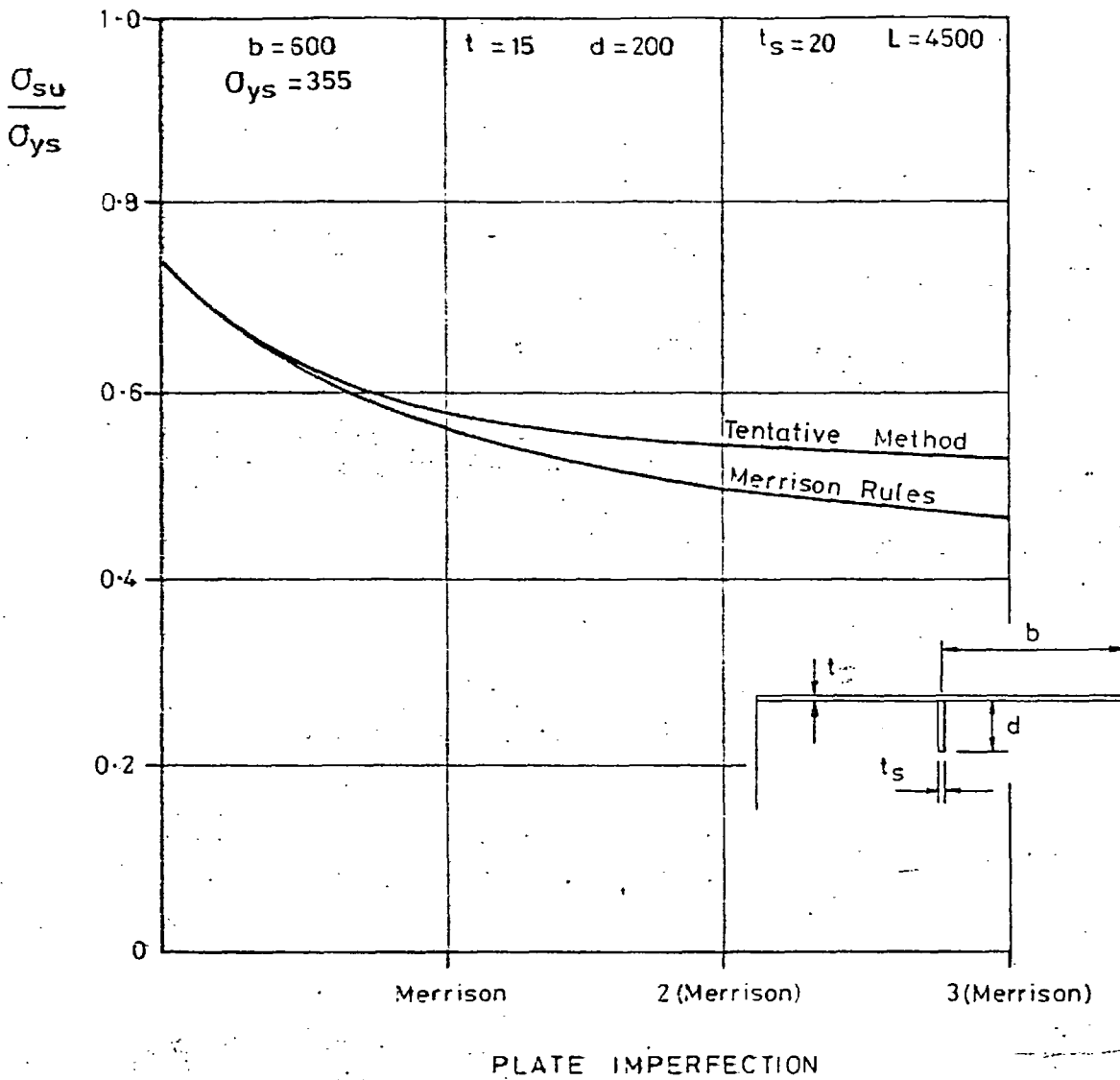
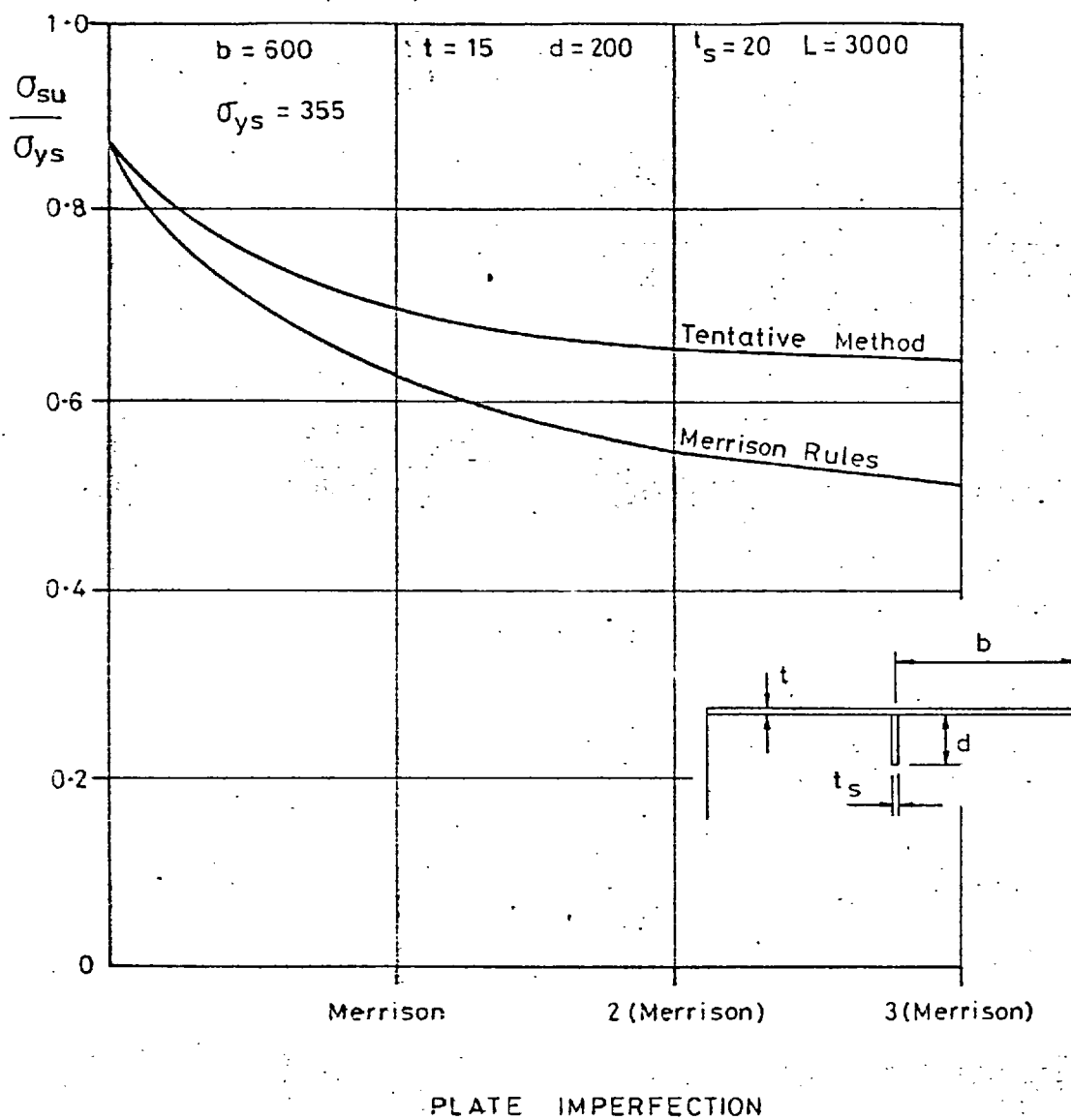


Fig.11a Sensitivity of stiffener strength on initial imperfections of flange plate



Welding residual stress $\cdot 27 = 0.076 \sigma_{ys}$

Fig.11b Sensitivity of stiffener strength on initial imperfections of flange plate.

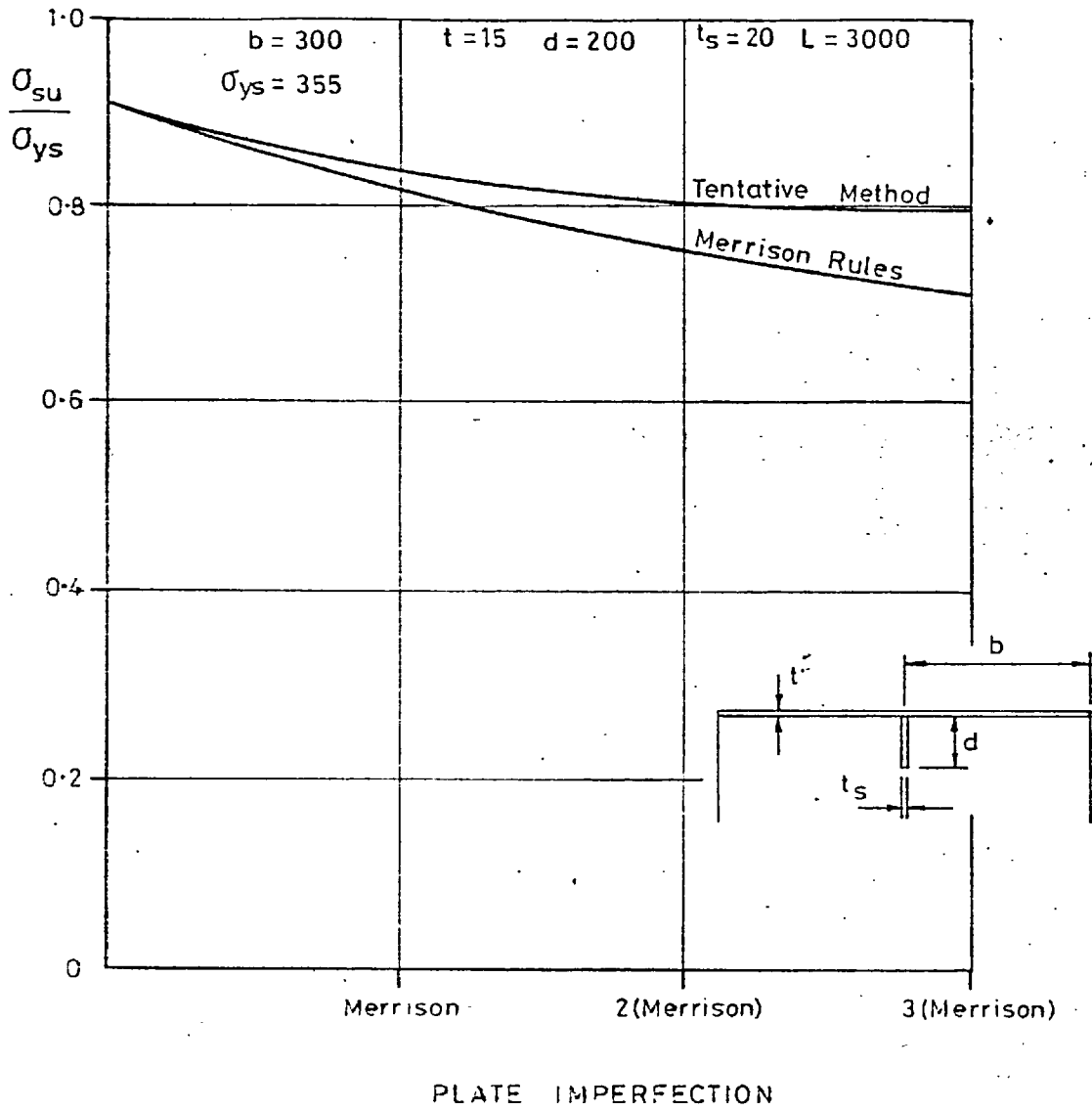


Fig 11c Sensitivity of stiffener strength on initial imperfections of flange plate

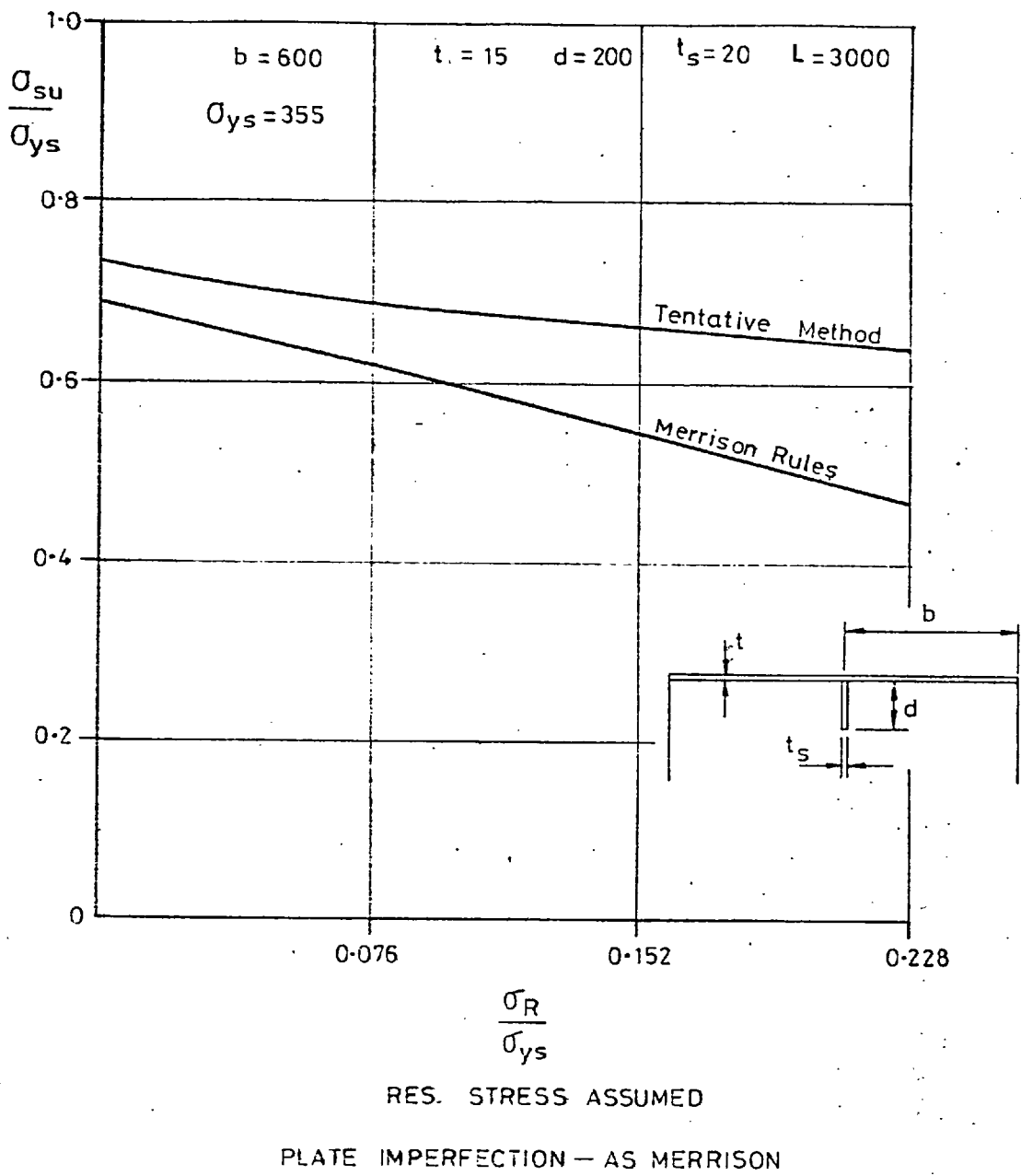


Fig.11d Sensitivity of stiffener strength on initial imperfections of flange plate

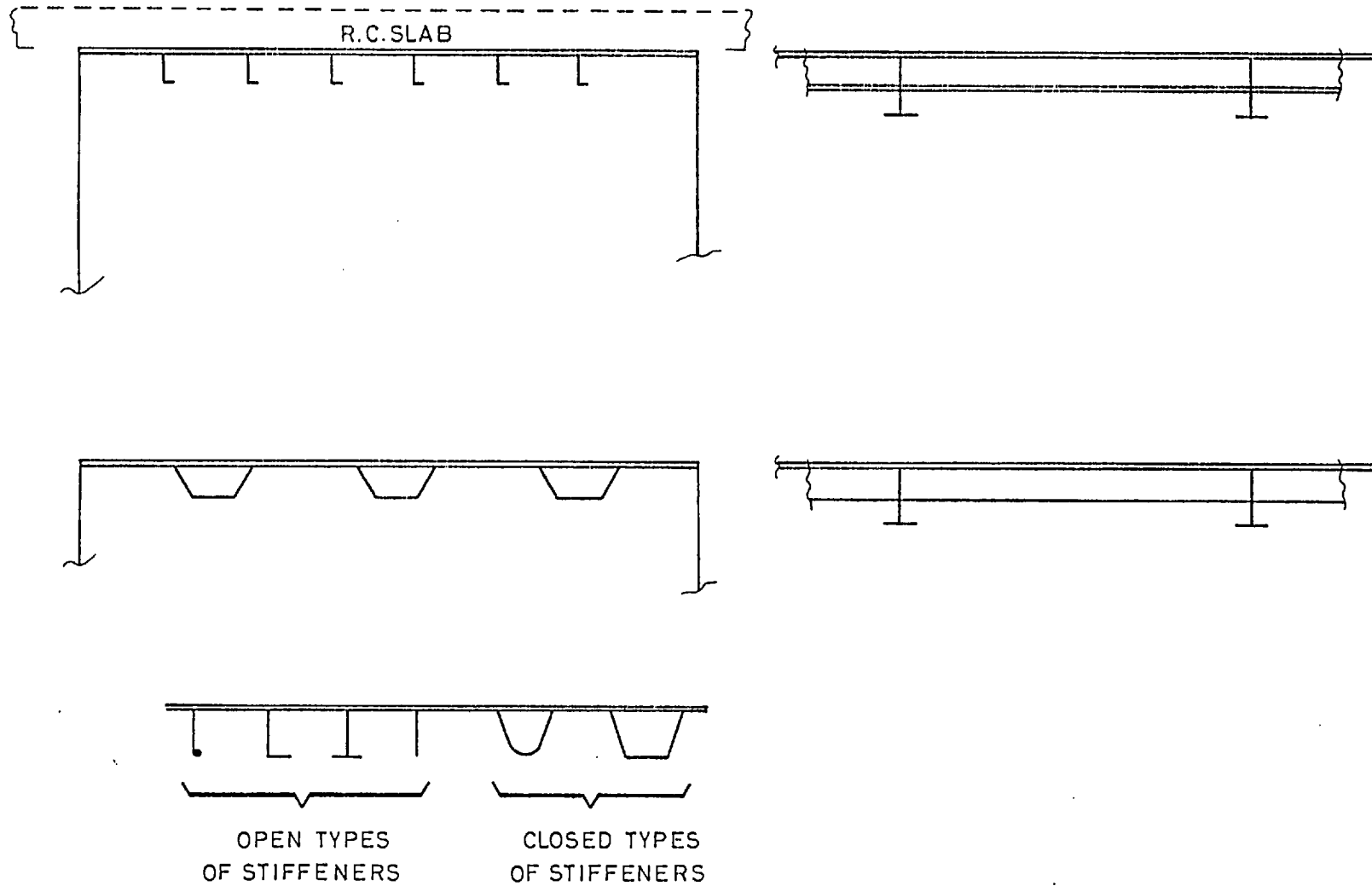


Fig.12 Typical construction details of compression flange of box girders

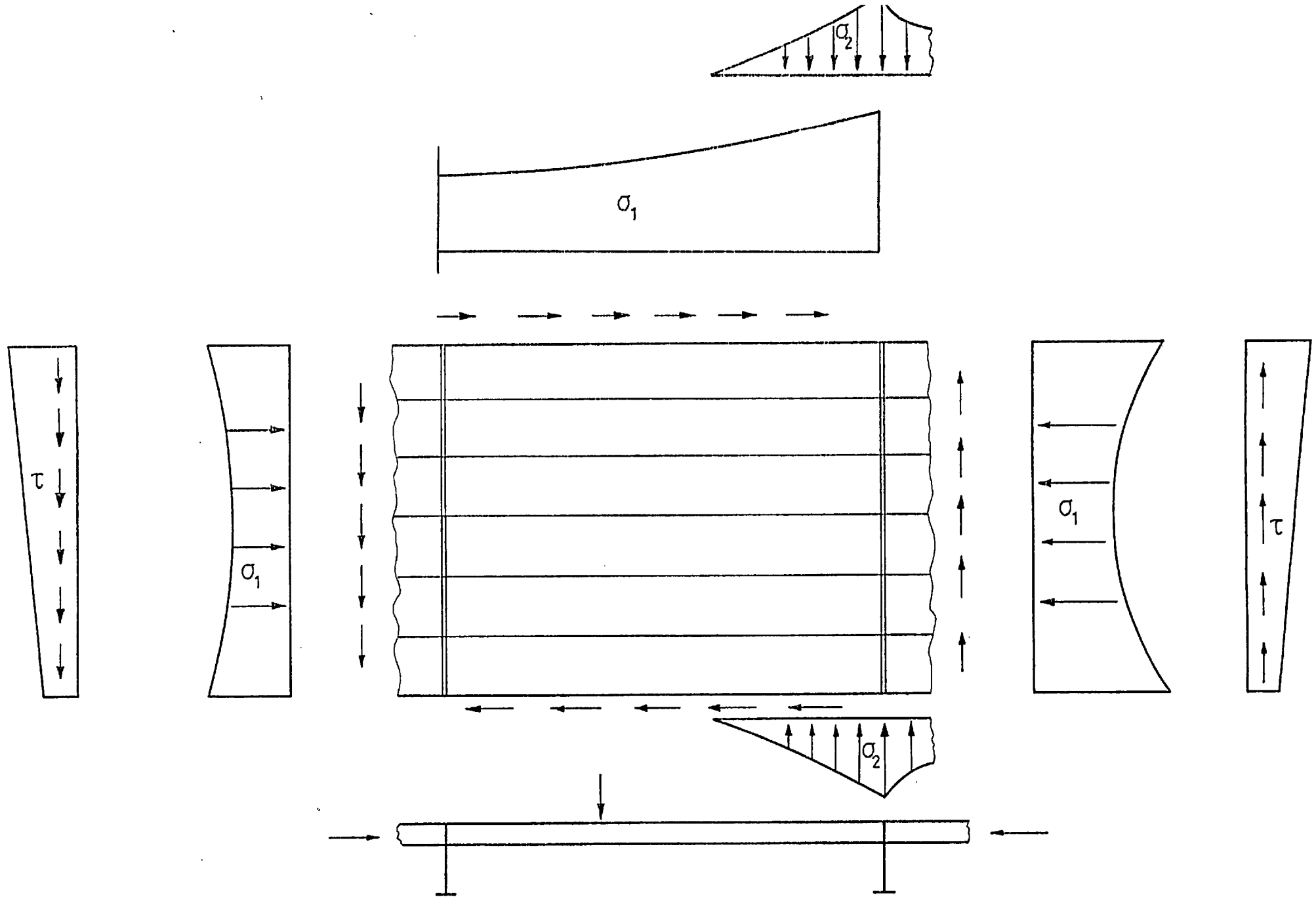


Fig 13. Stress system on compression flange of box girders

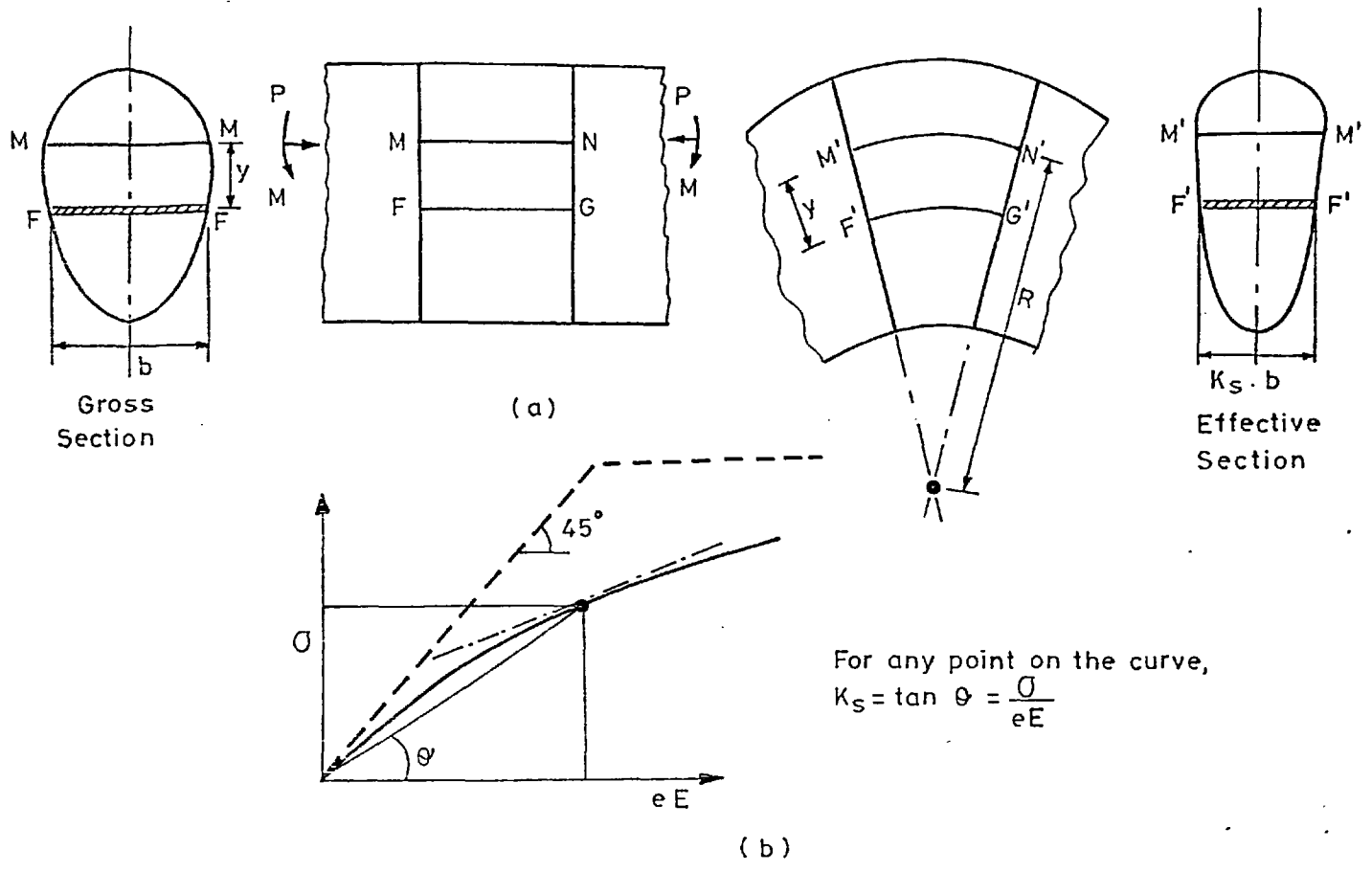
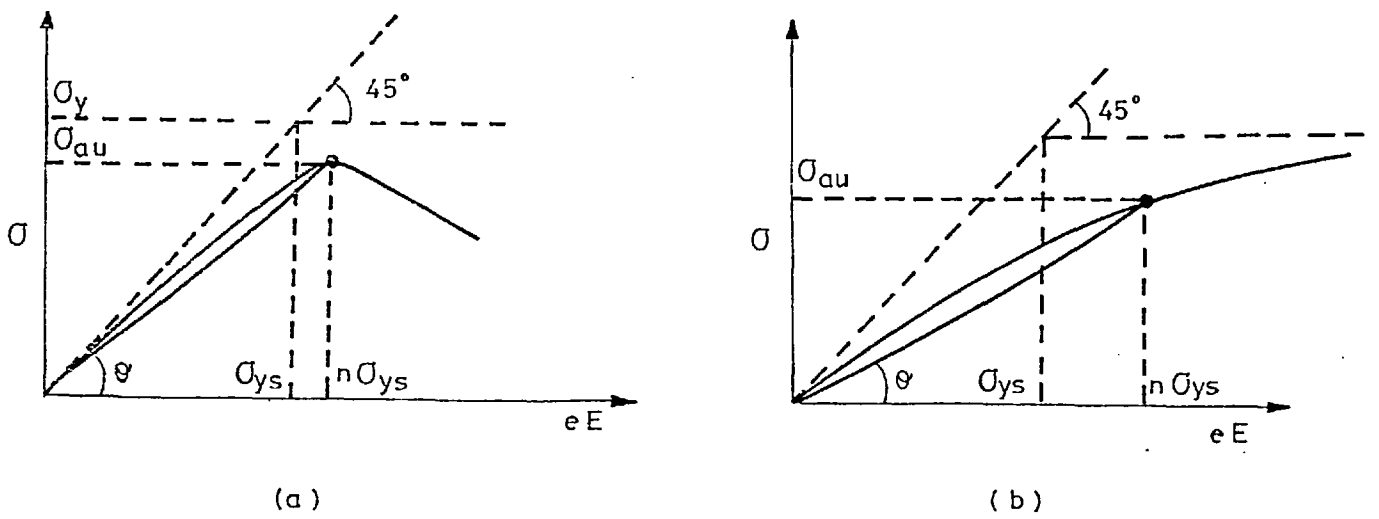


Fig.14 Non-linear behaviour of stiffener components



$$K_{SU} = \tan \theta \frac{\sigma_{au}}{n\sigma_{ys}}$$

Fig.15 Non-linear behaviour of flange plate

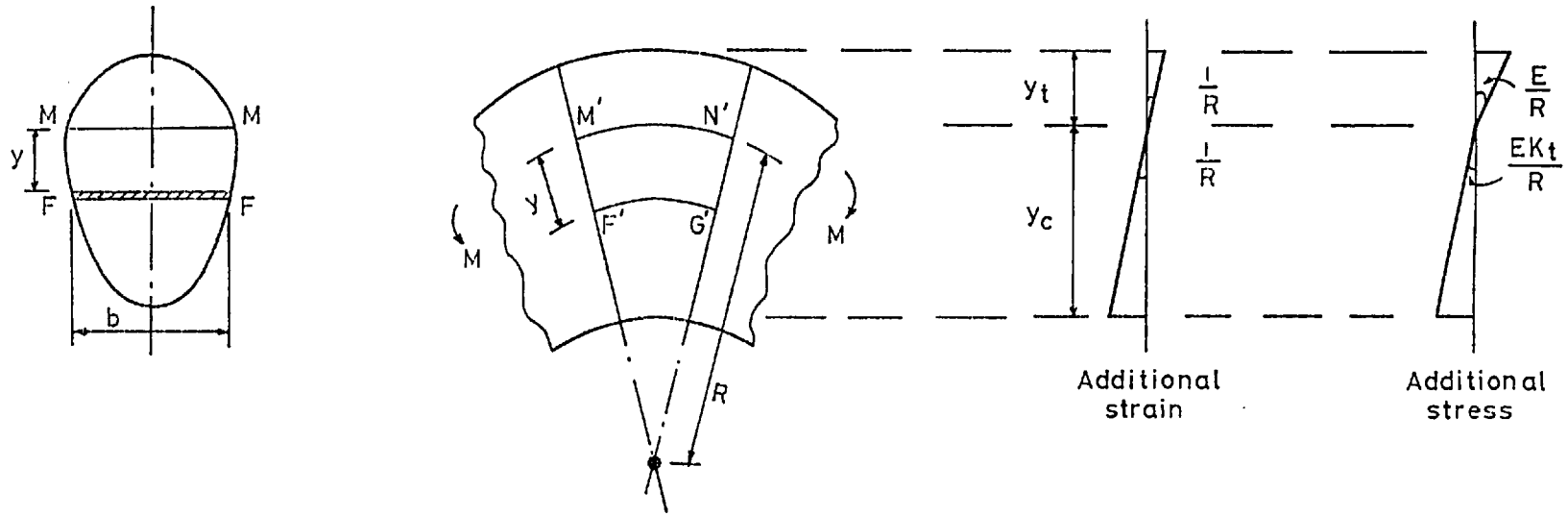


Fig. 16

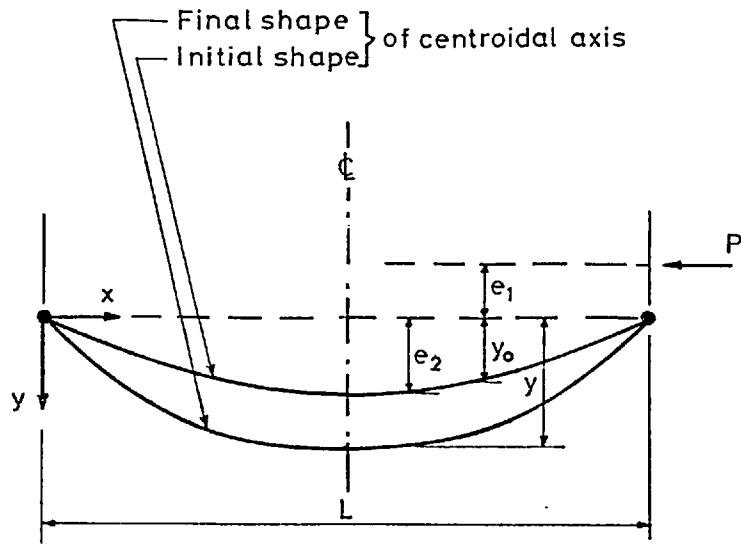


Fig.17a Eccentrically loaded imperfect strut

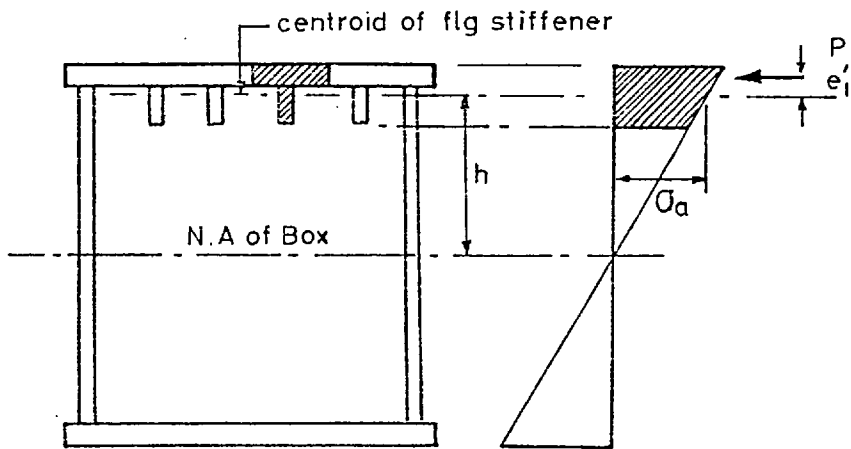


Fig.17b Curvature of box girder

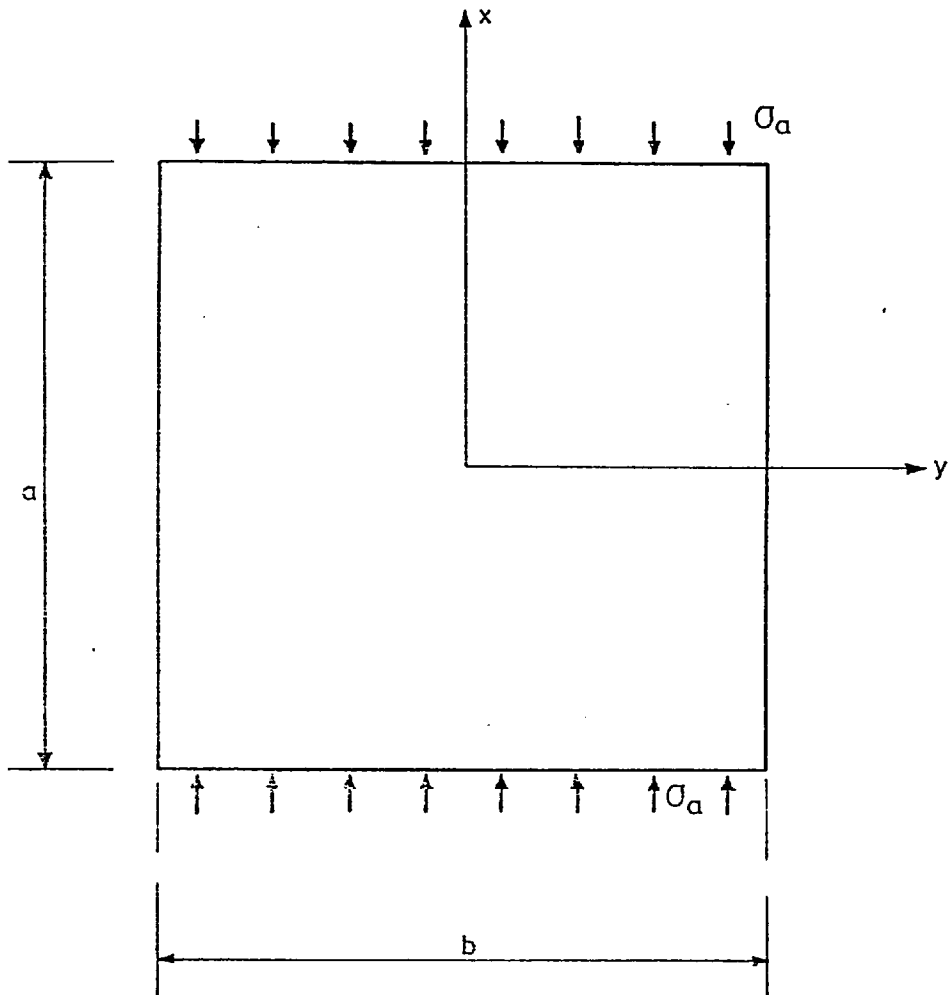


Fig 18 Geometry and co-ordinate axes of plate

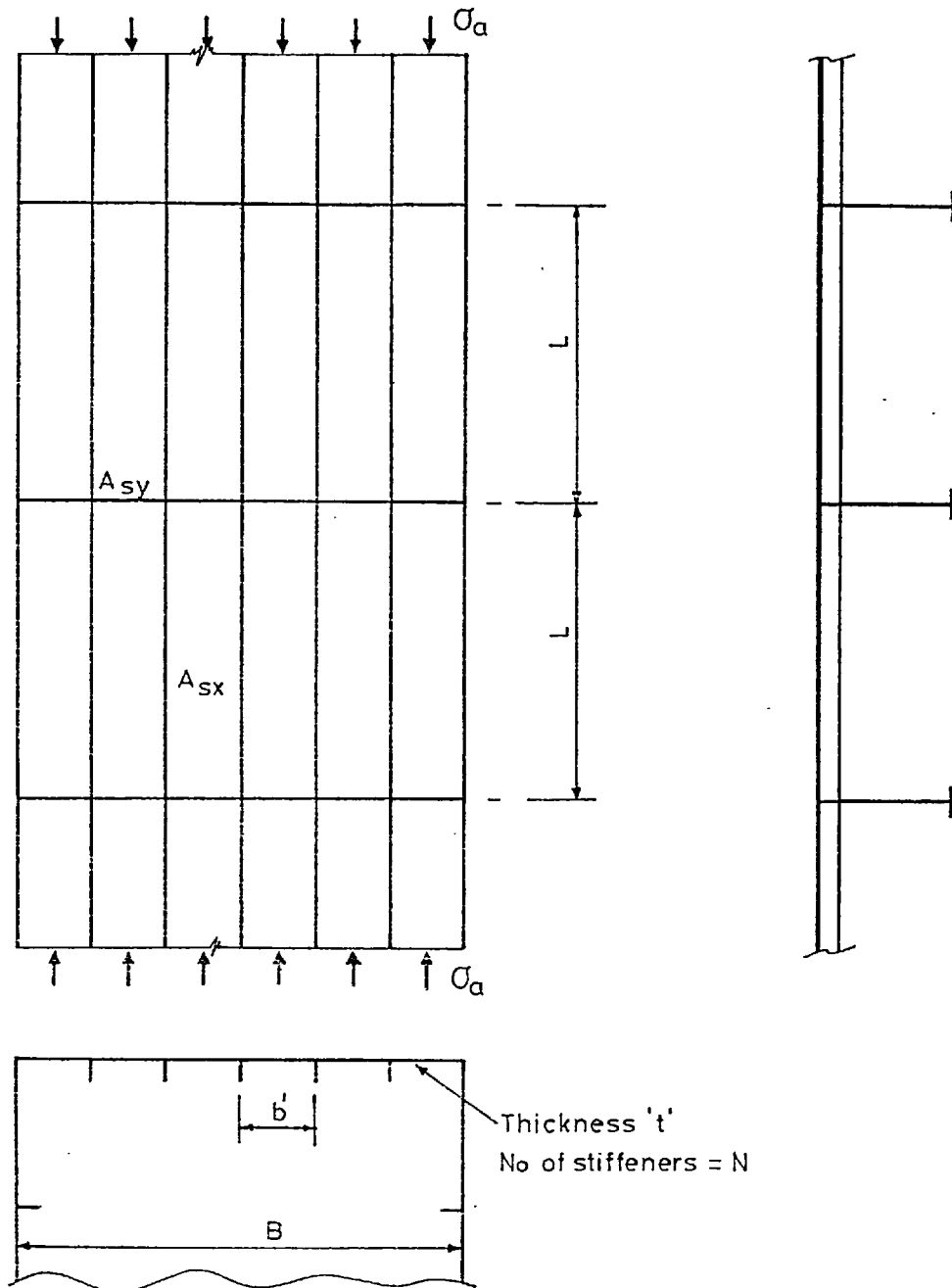


Fig 19. Stiffened compression flange

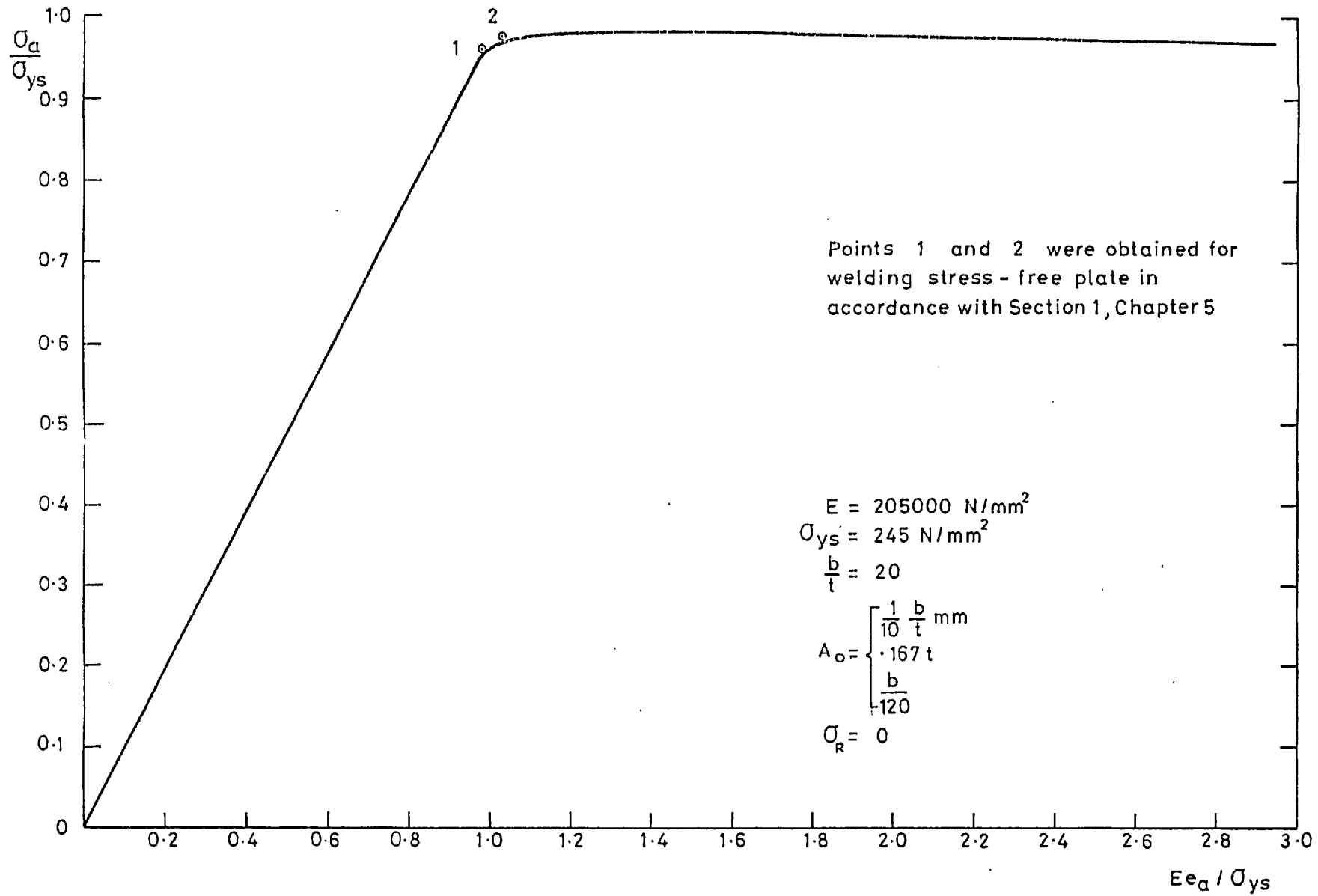


Fig 20a. Average stress - strain curves for plate
in compression with constrained edges

[Obtained from ref (17)]

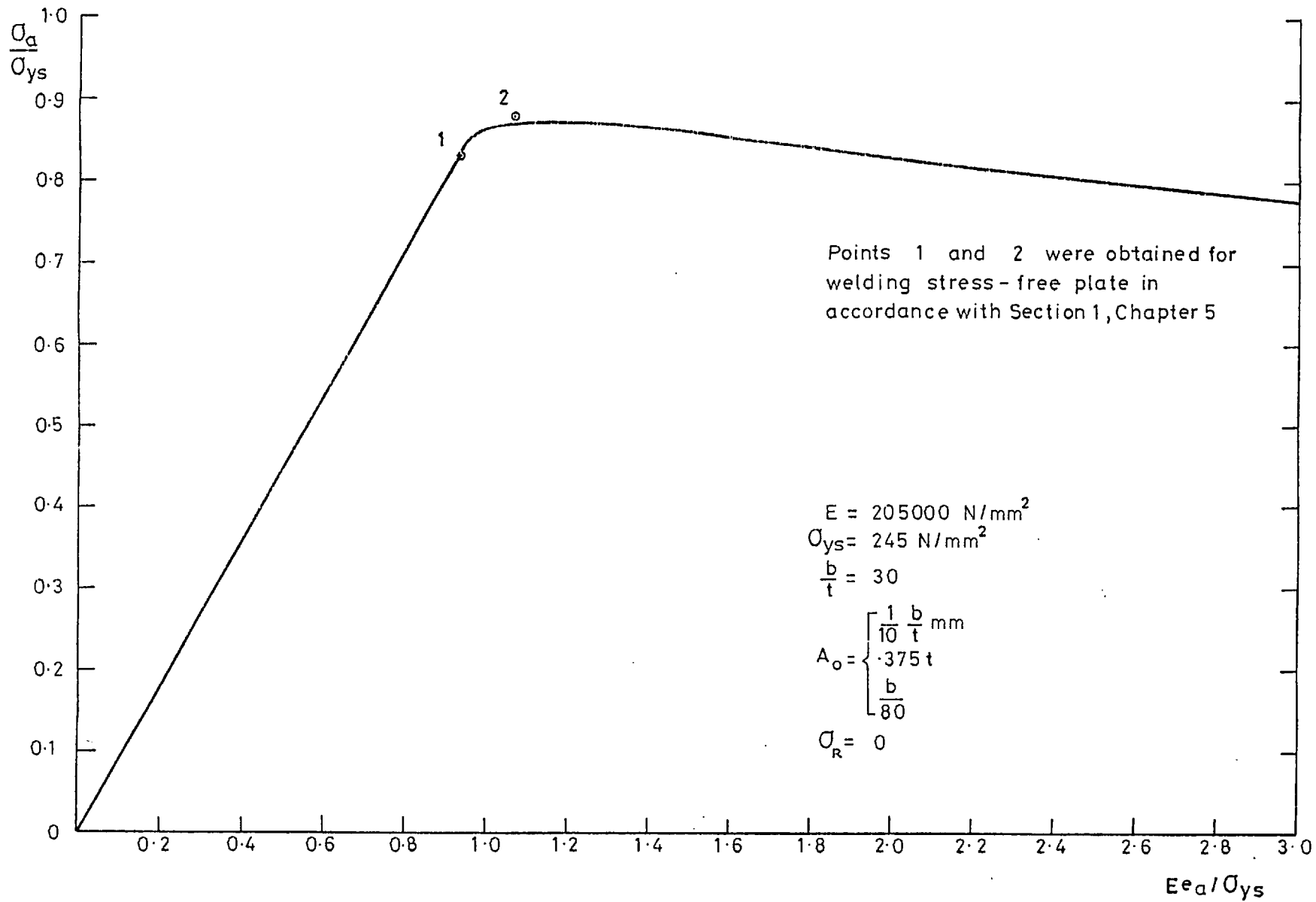


Fig 20b. Average stress-strain curves for plate
in compression with constrained edges

[Obtained from ref (17)]

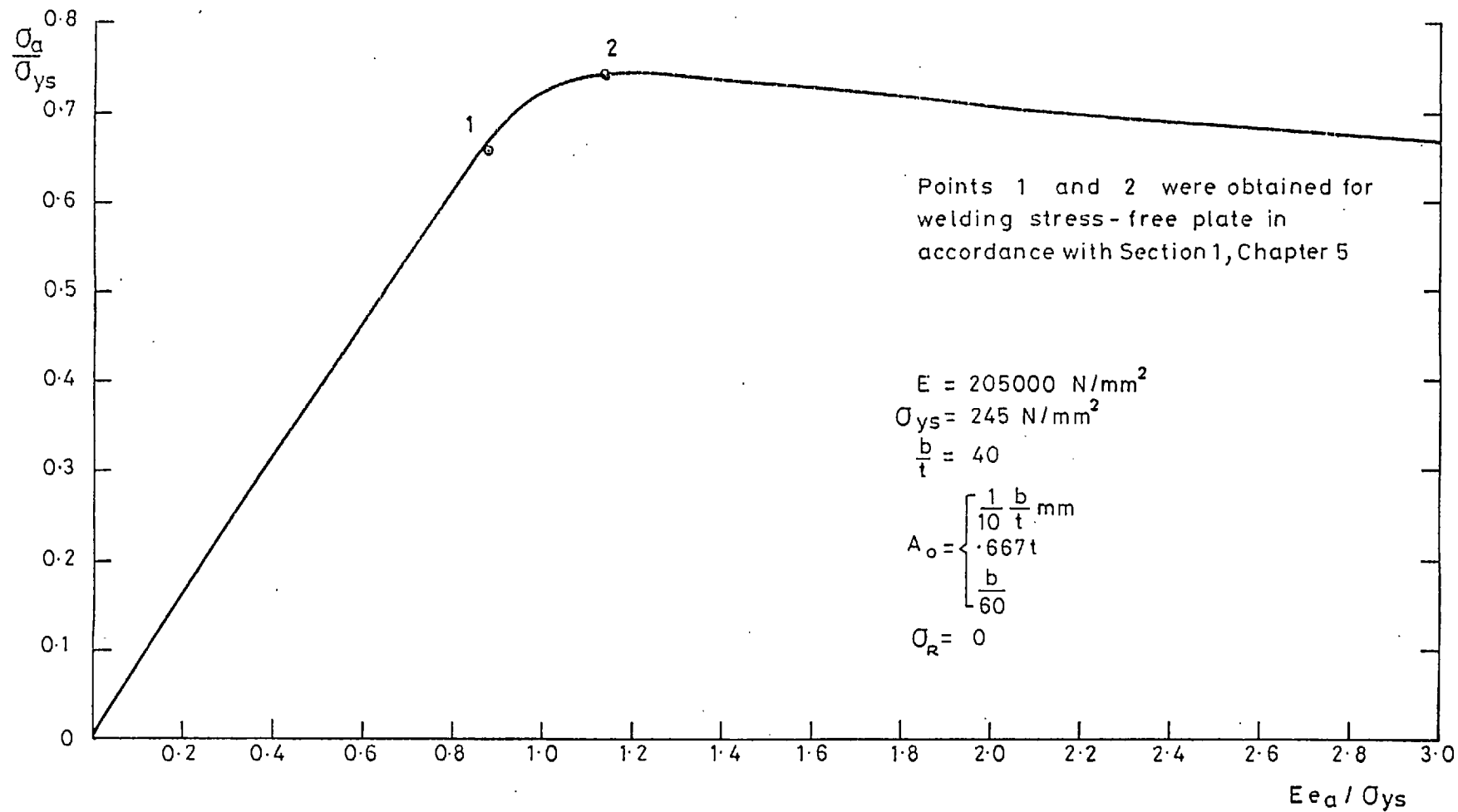


Fig 20c. Average stress-strain curves for plate in compression with constrained edges

[Obtained from ref (17)]

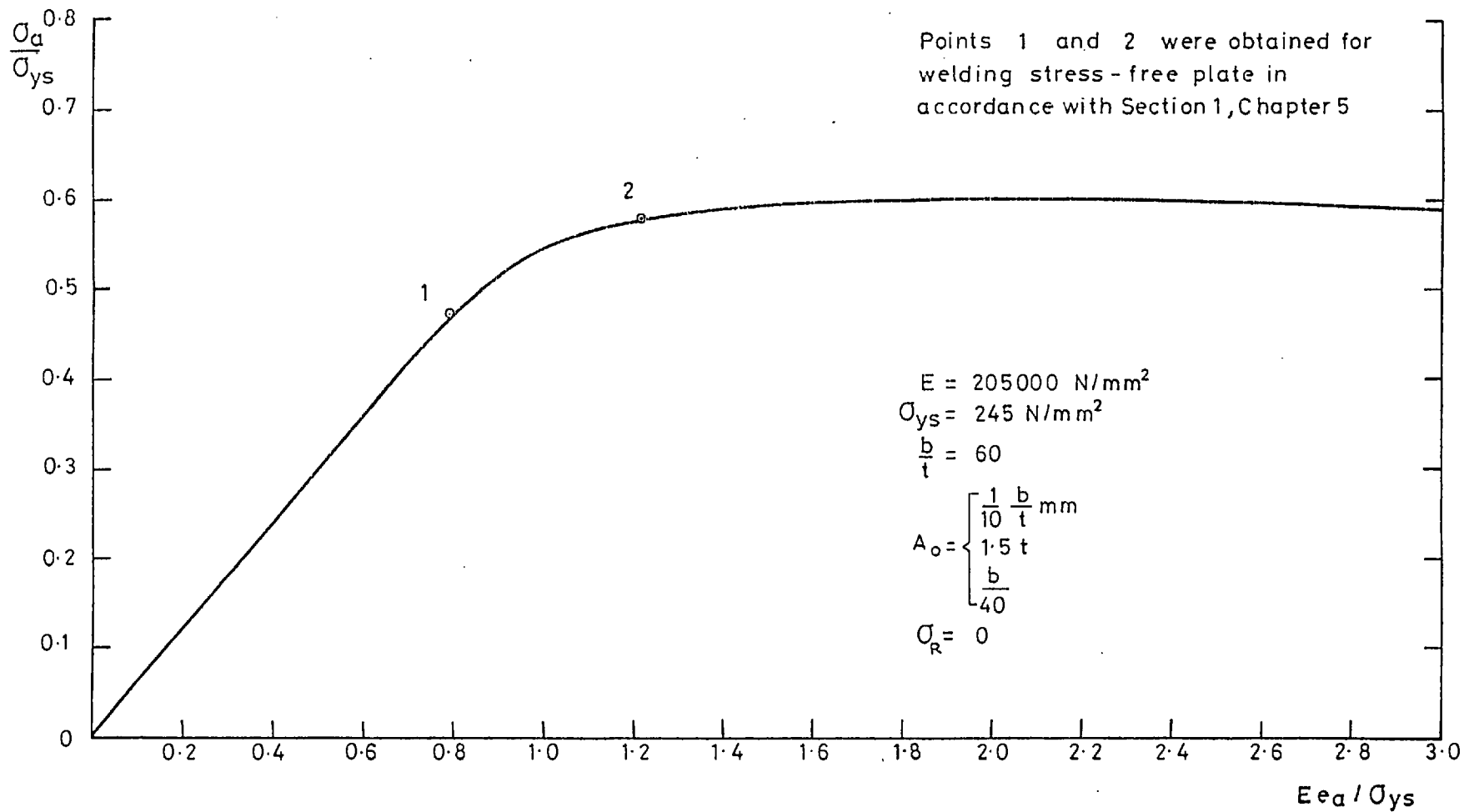


Fig 20d. Average stress-strain curves for plate in compression with constrained edges. [Obtained from ref (17.)]

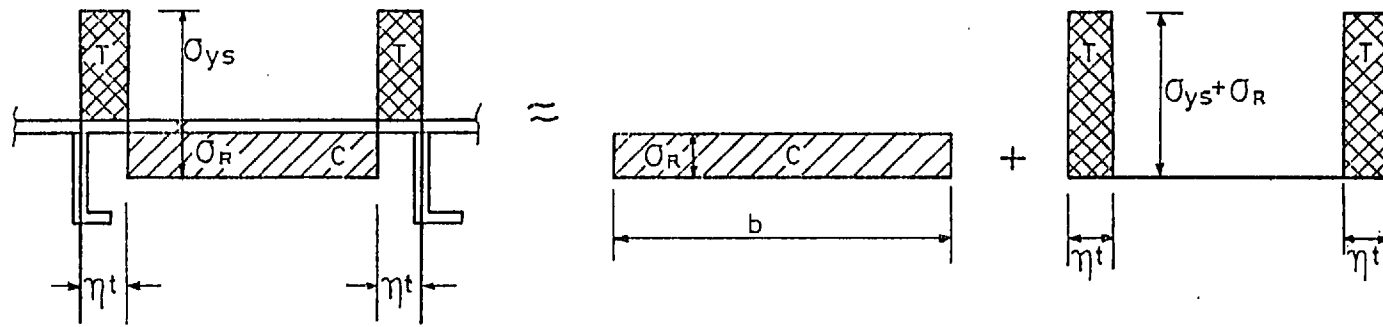


Fig. 21 Welding residual stress pattern

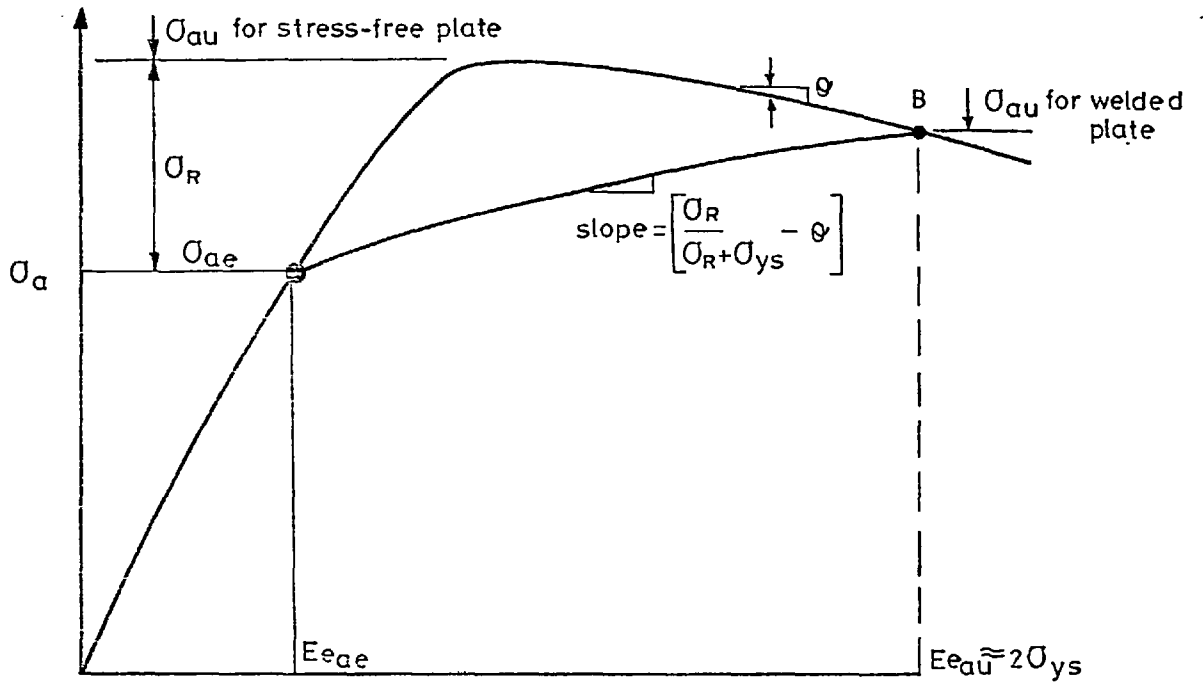


Fig.22 Load - shortening behaviour of welded flange plate

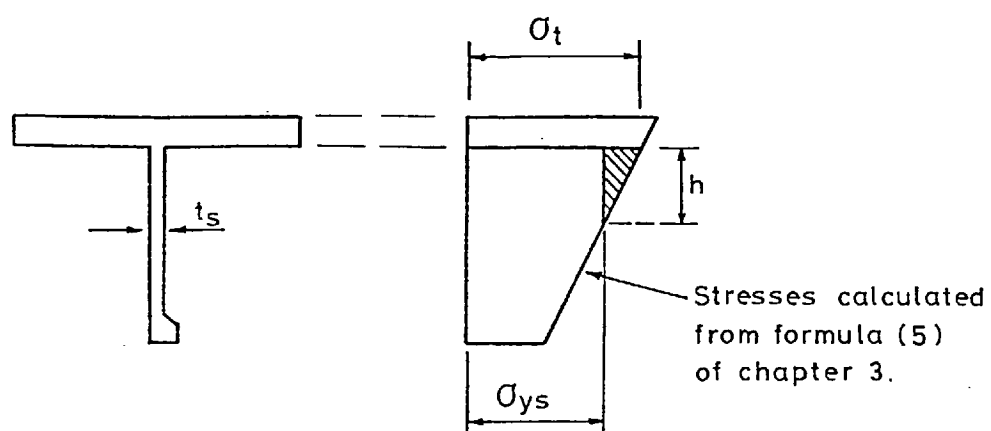


Fig. 23 Compressive yielding in outstand

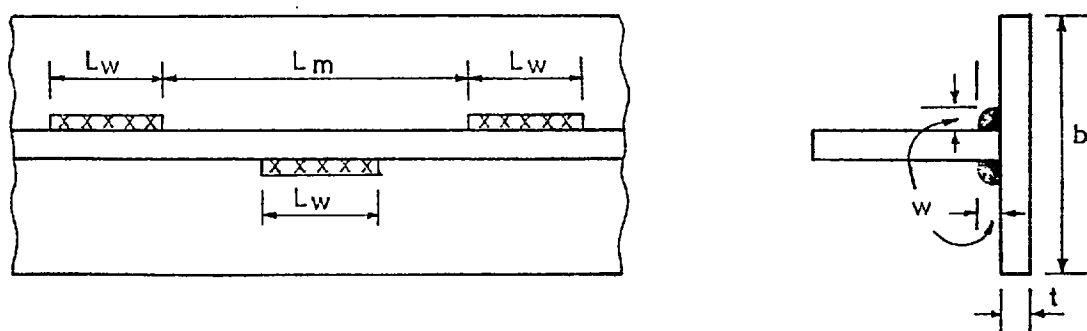


Fig. 24 Intermittent welding

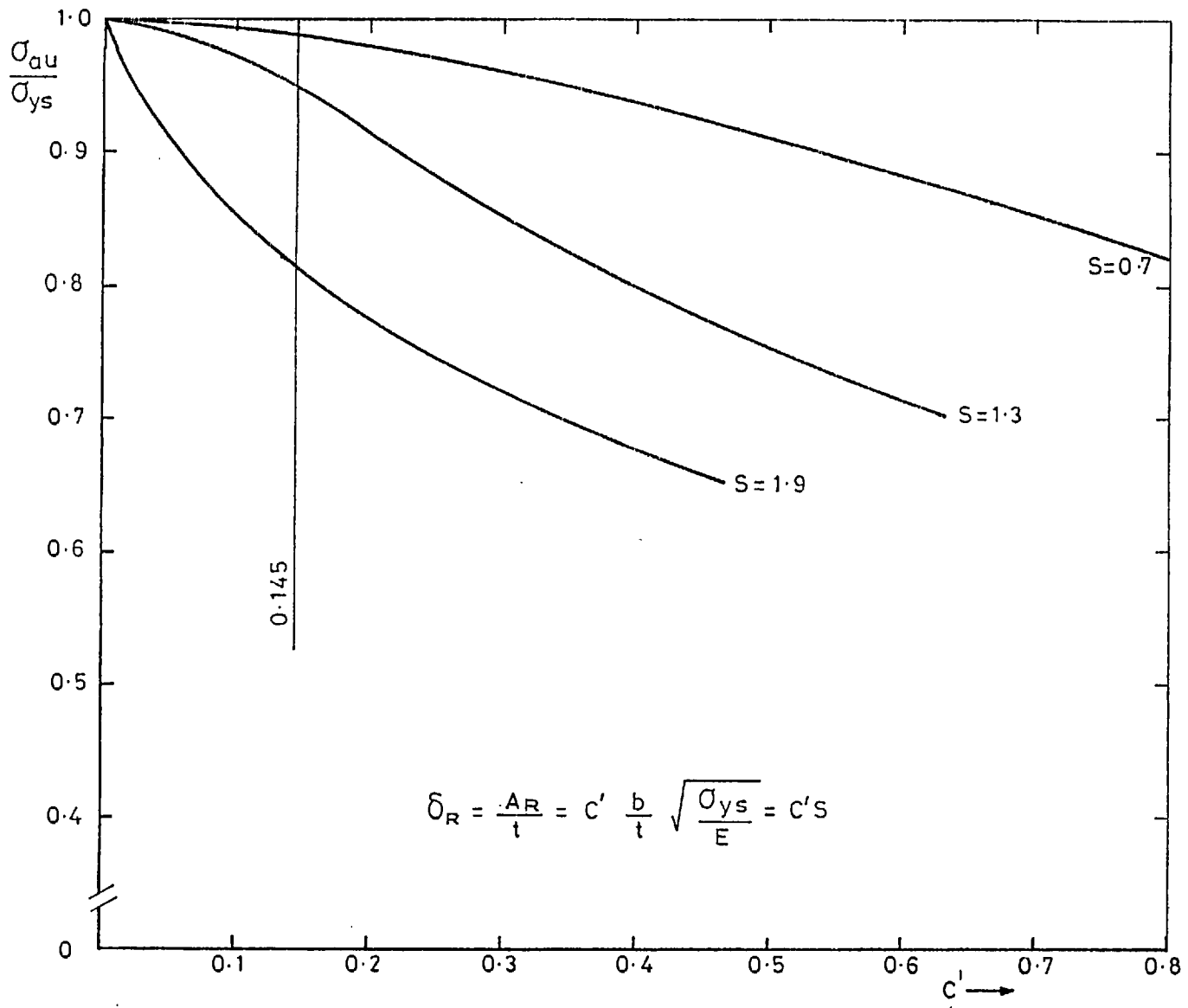
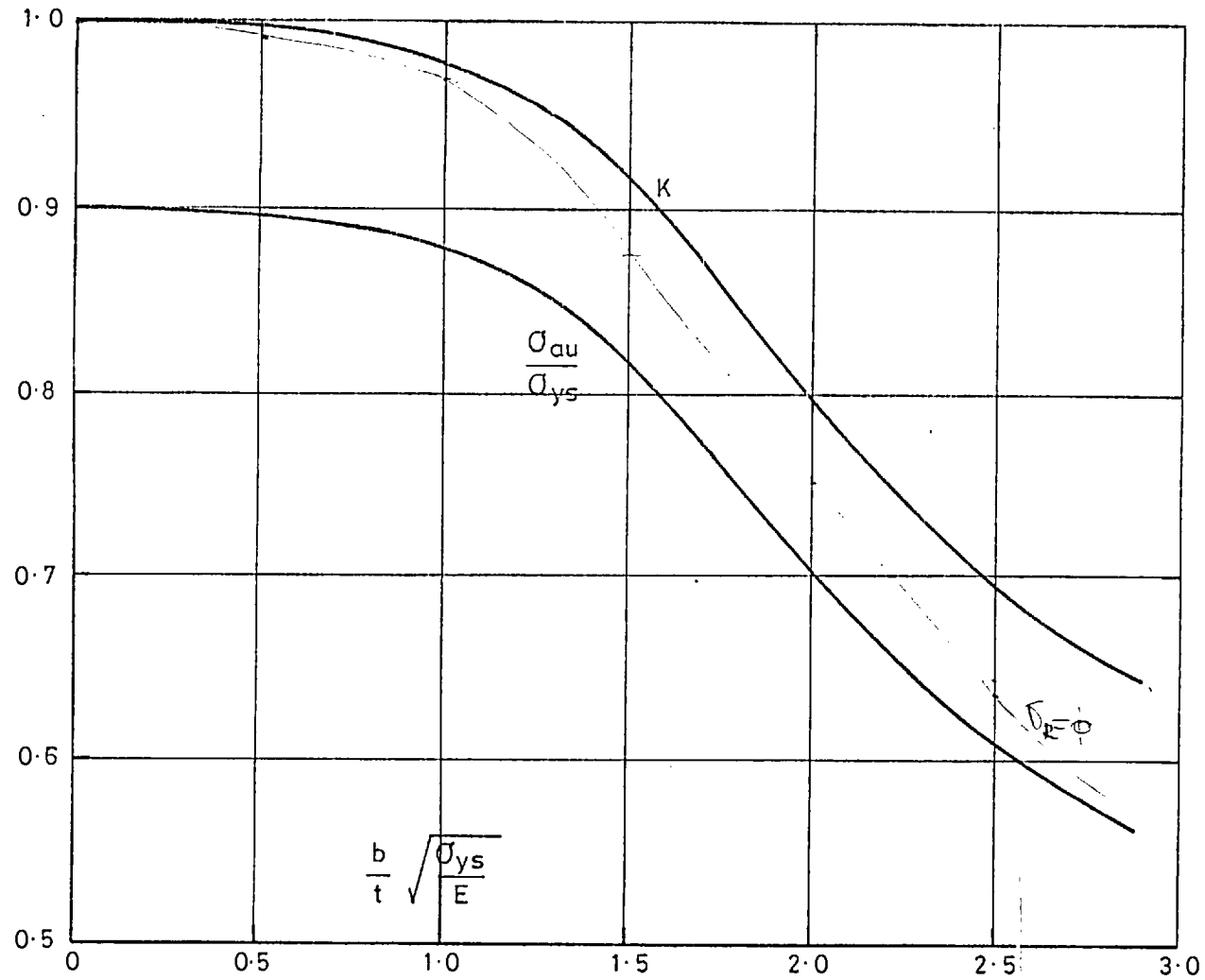


Fig.25 Sensitivity of plate strength to imperfection



Use $\frac{b_1}{t}$ or $\frac{b_2}{t}$, whichever is larger for closed type stiffeners (see fig.81)

Fig.26a: Curves for welded plates

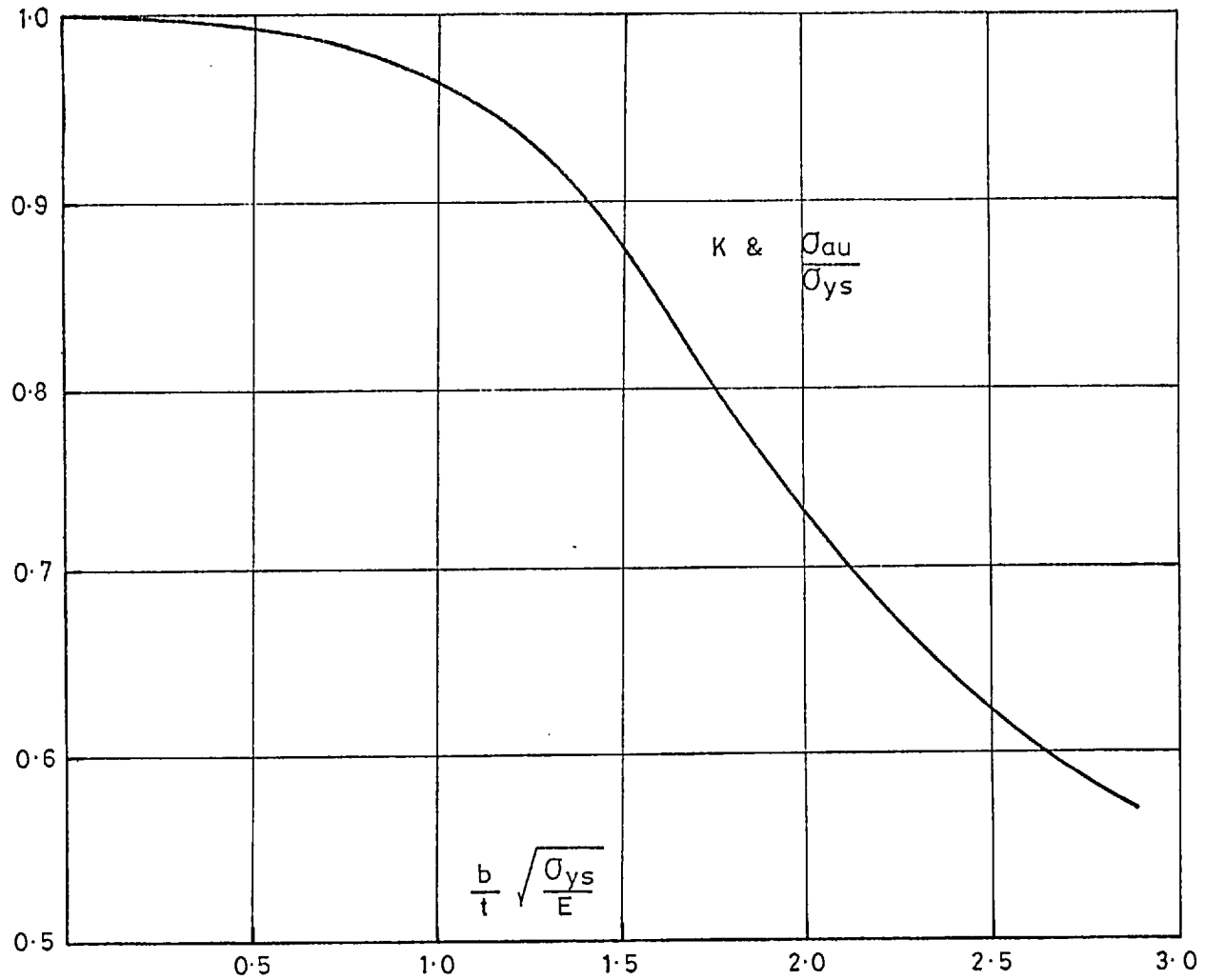


Fig. 26 b Curve for residual stress-free plates

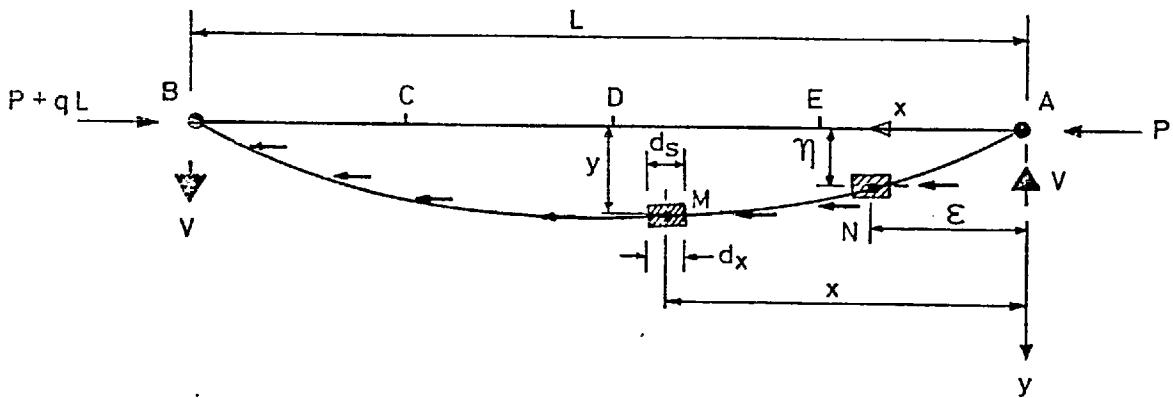


Fig.27 Strut subjected to varying axial load

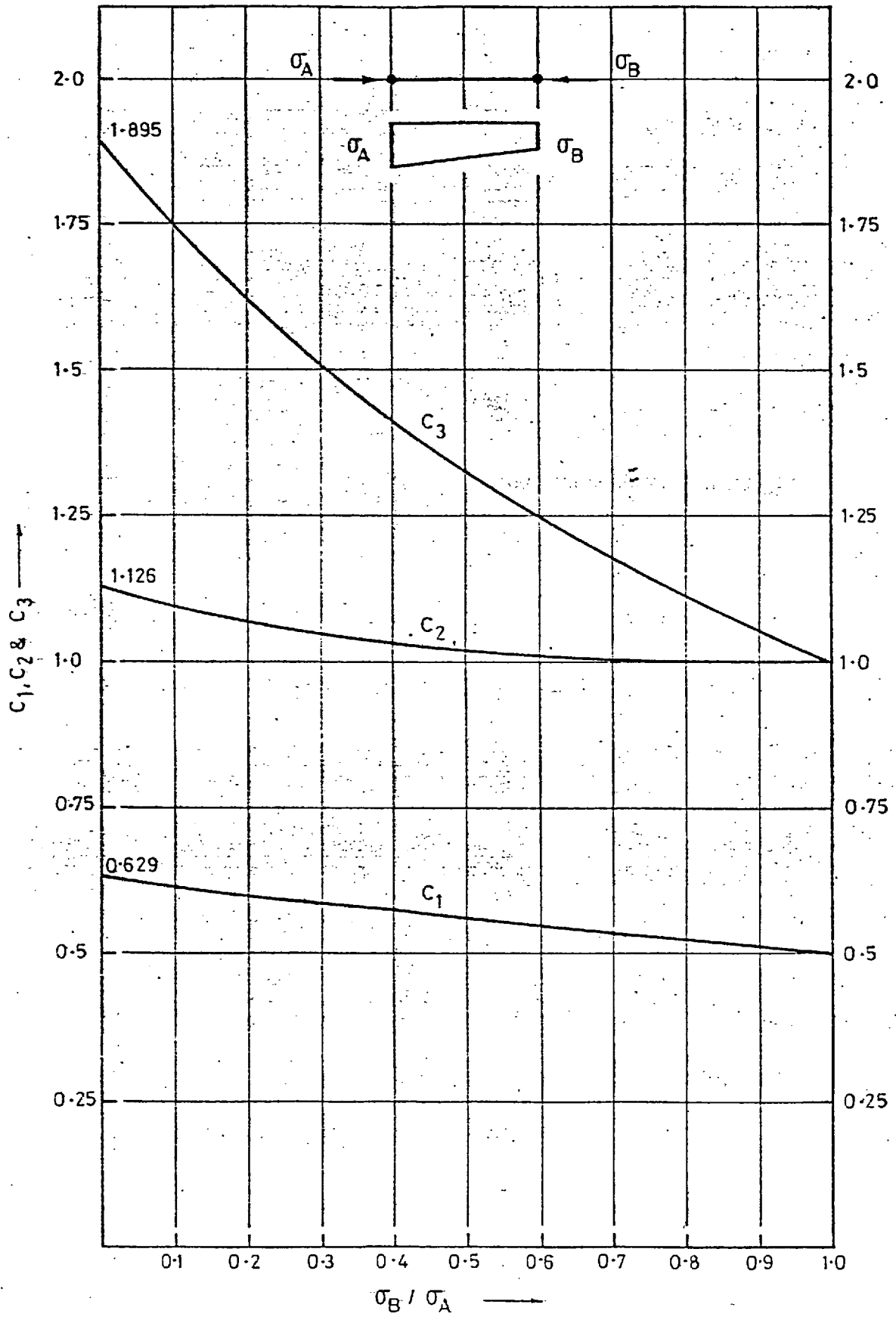


Fig 28 Coefficients for moment gradient

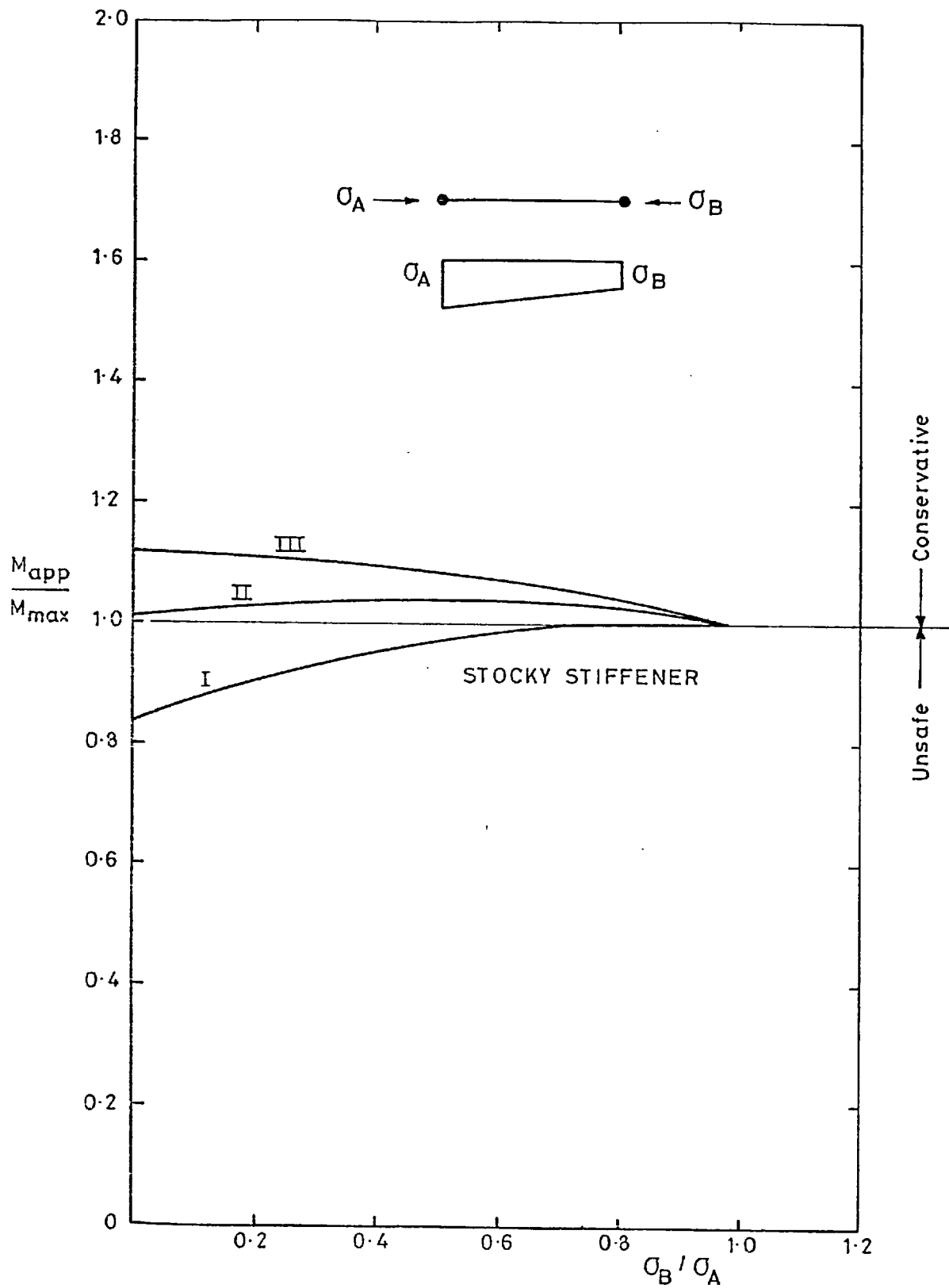


Fig. 29a. Accuracy of a simplified approach

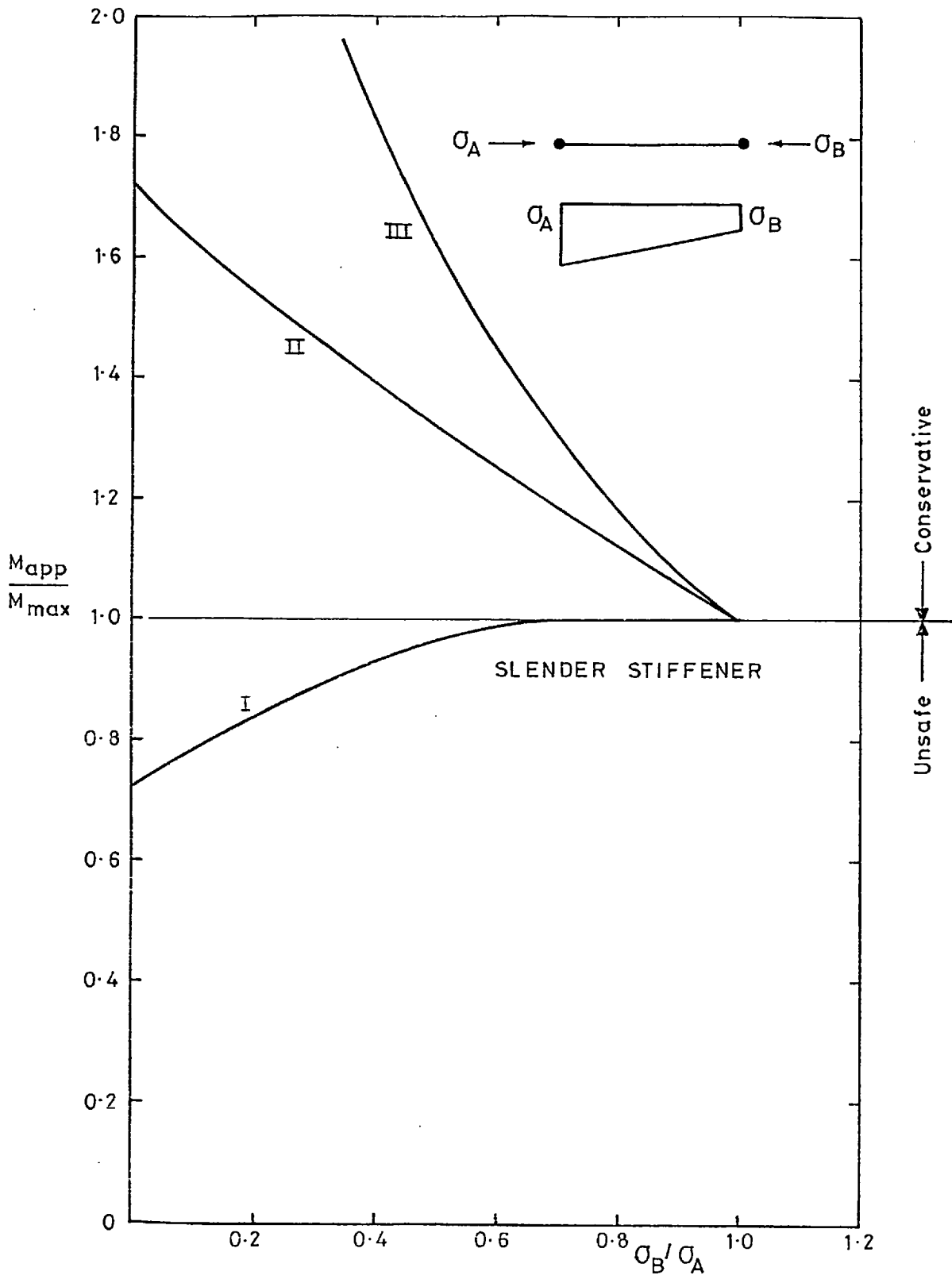


Fig. 29b. Accuracy of a simplified approach

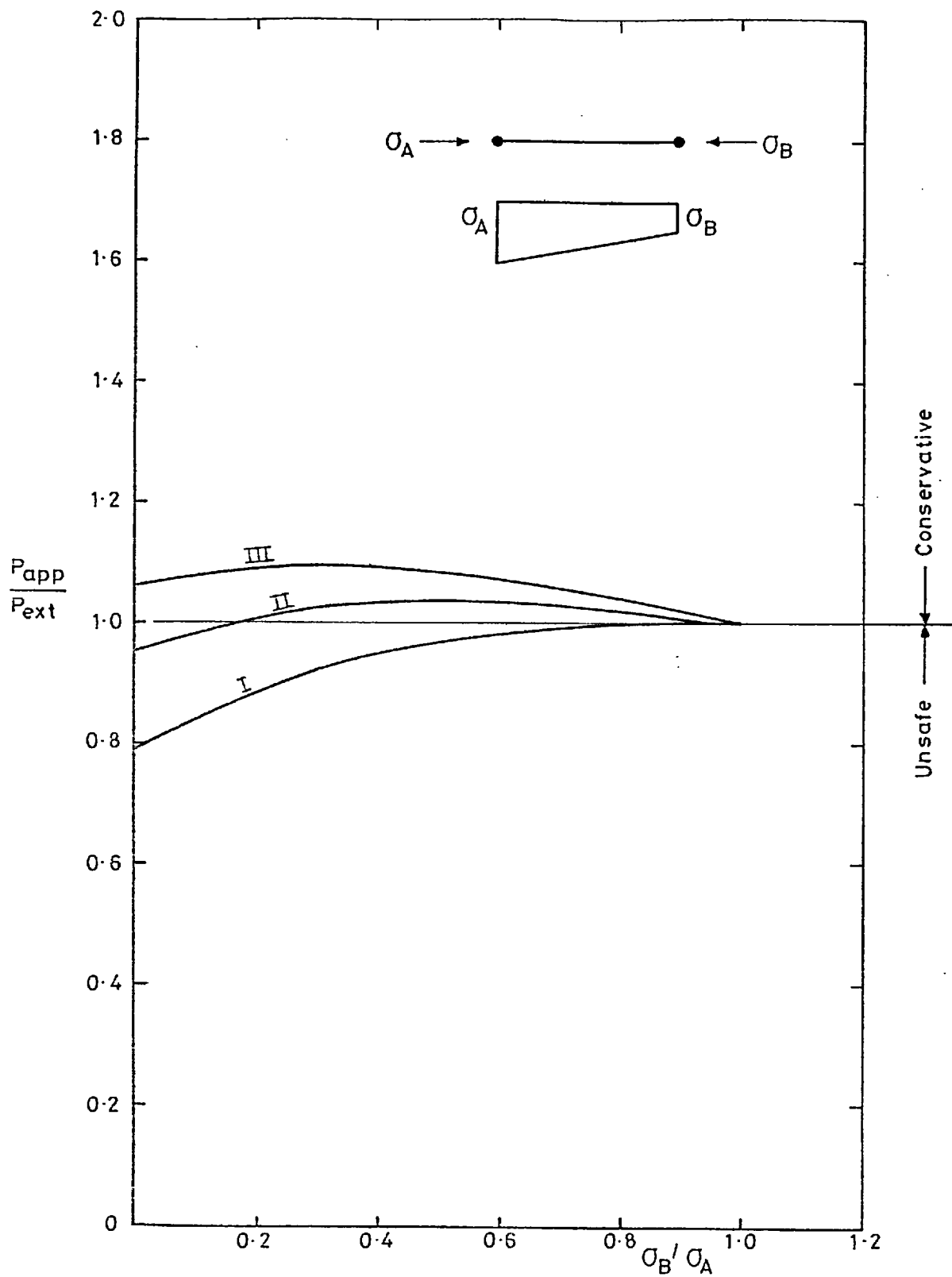


Fig. 29c. Accuracy of a simplified approach

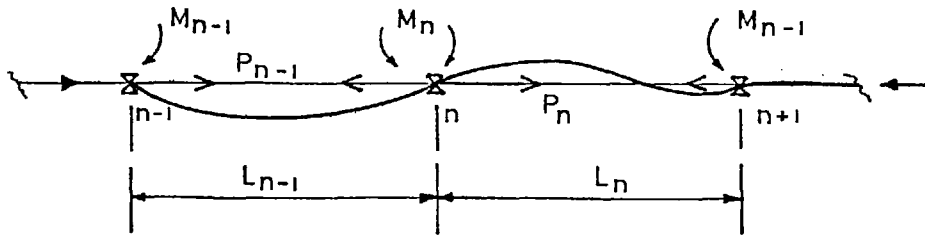
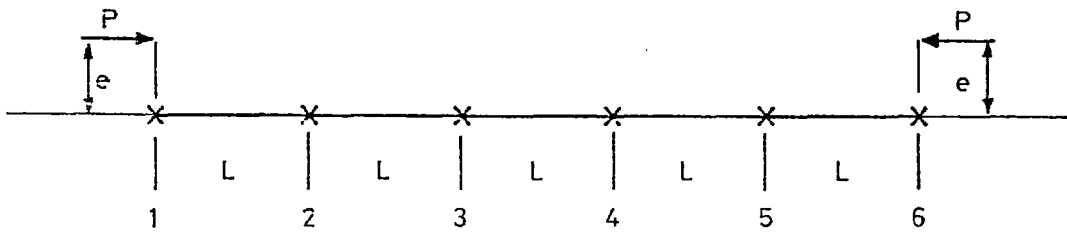
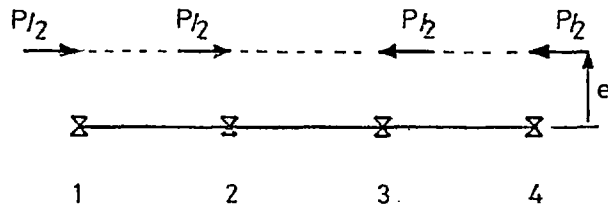


Fig.30 Continuous beam-column



(a)



(b)

Fig.31 Continuous beam - column subjected to eccentric axial load

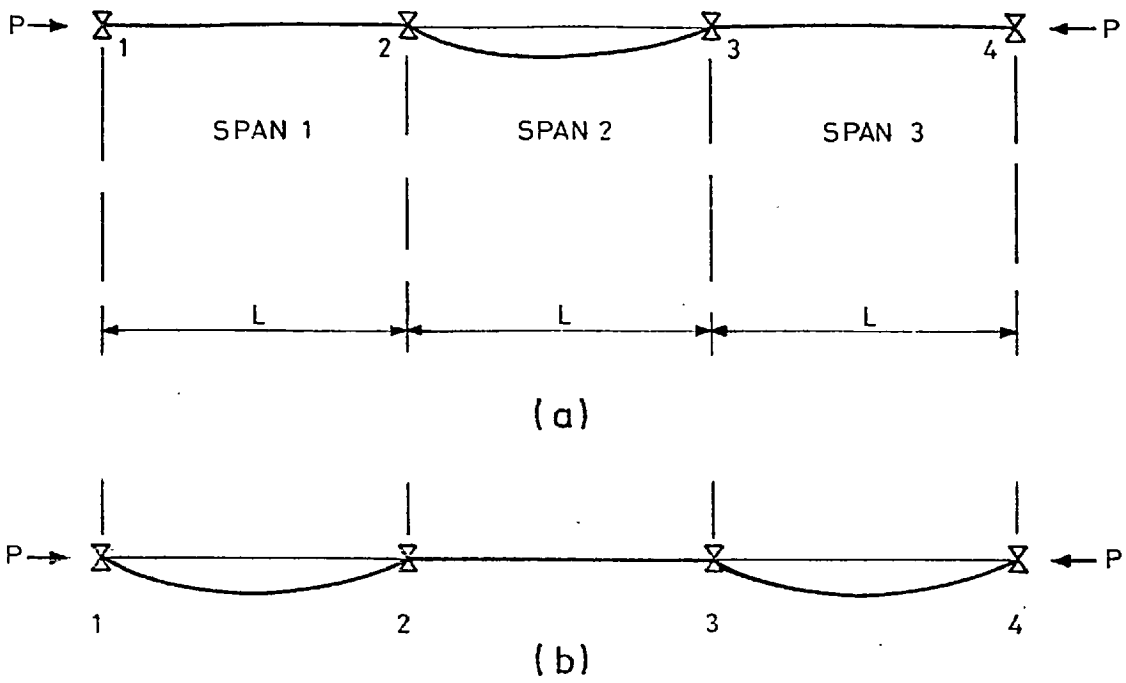


Fig.32 Continuous beam - column with random imperfections

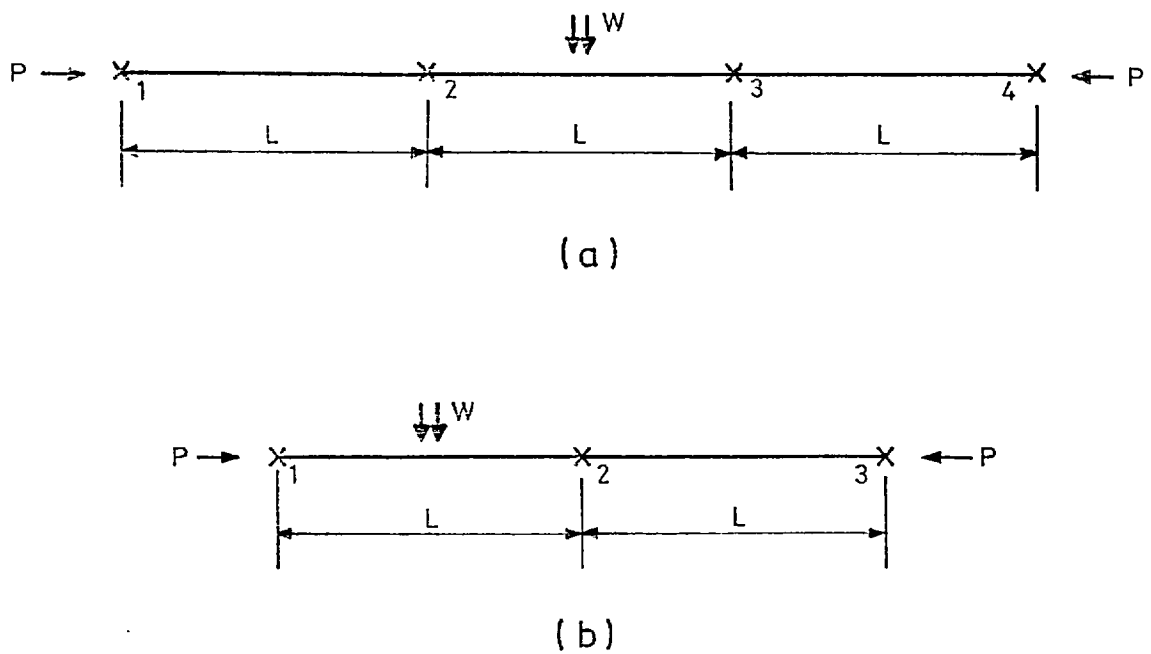


Fig.33 Continuous beam-columns subjected to local transverse load

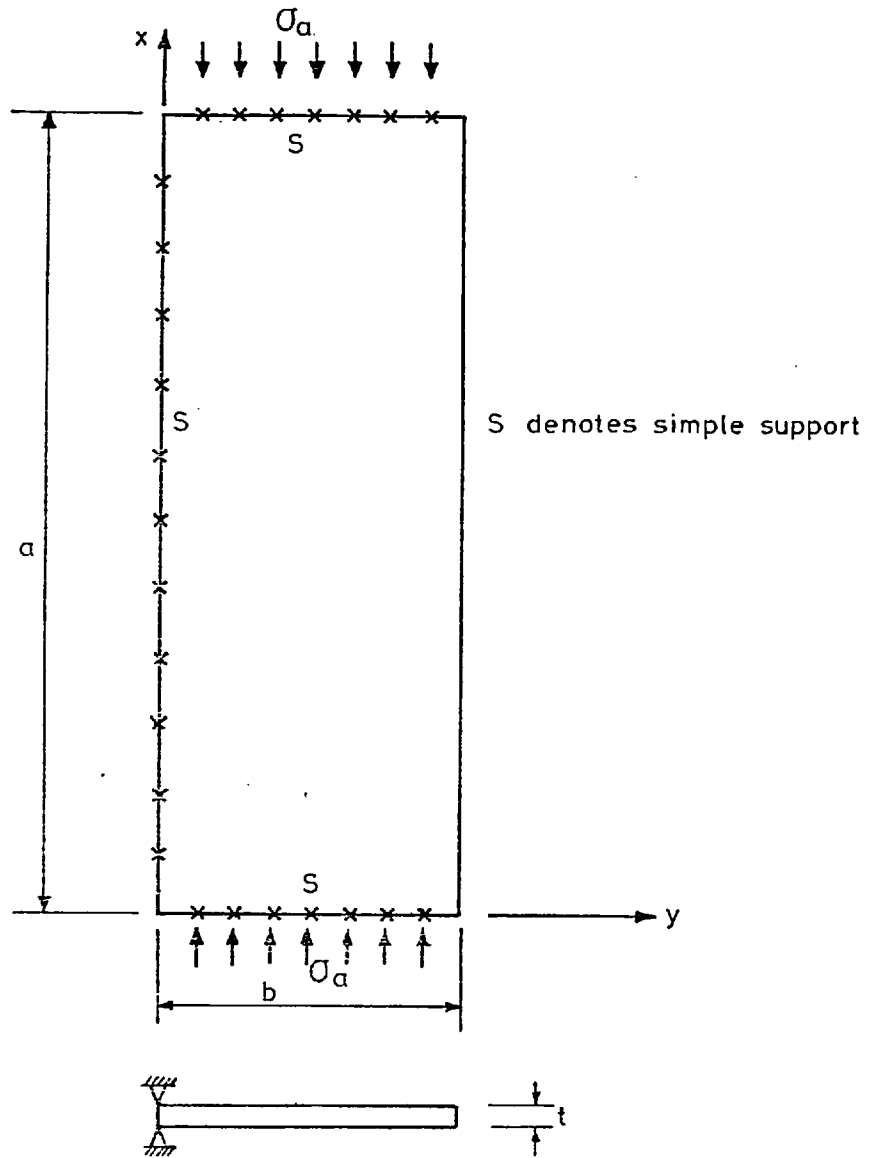


Fig.34 Plate panel supported on three edges

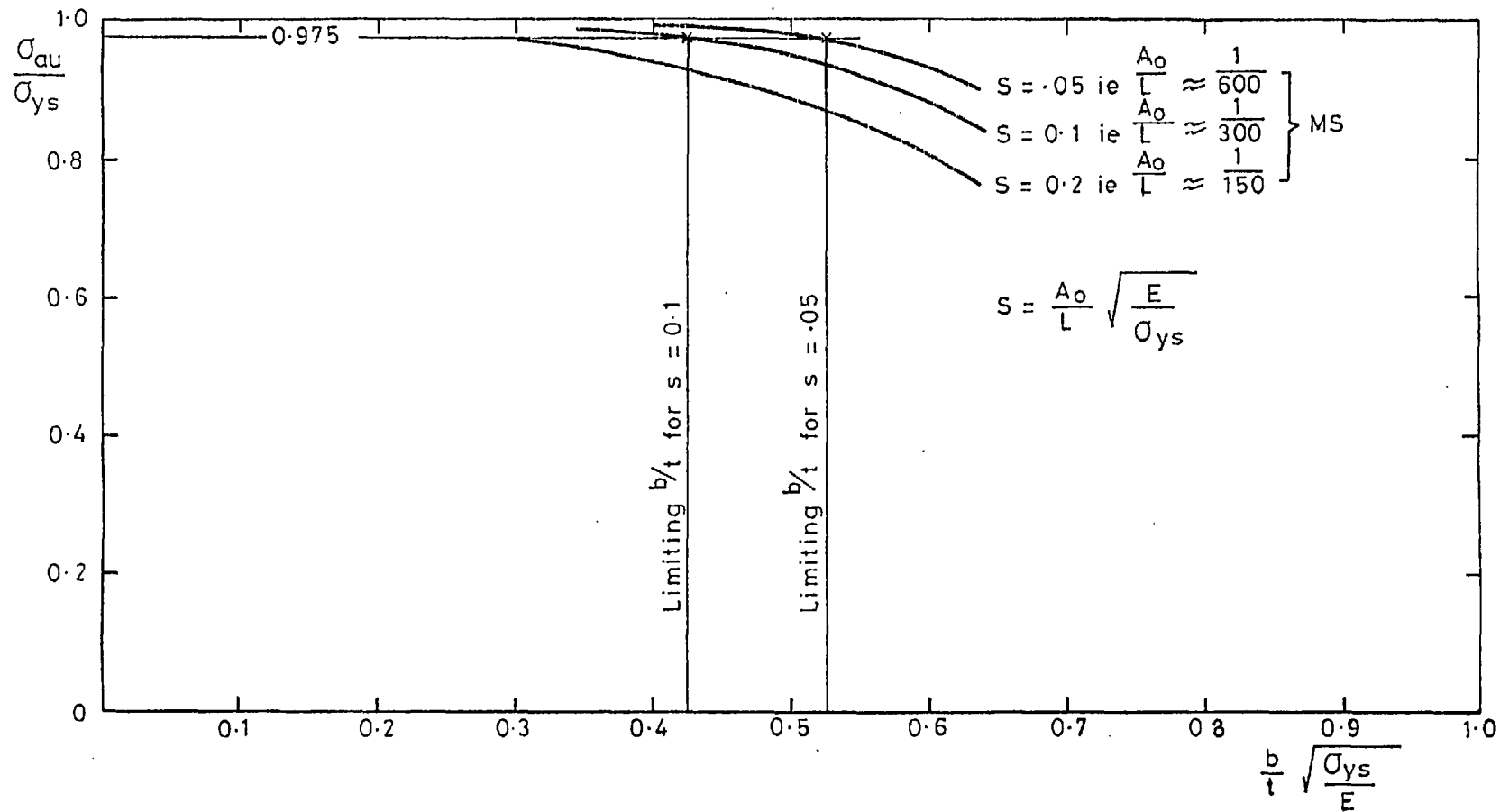
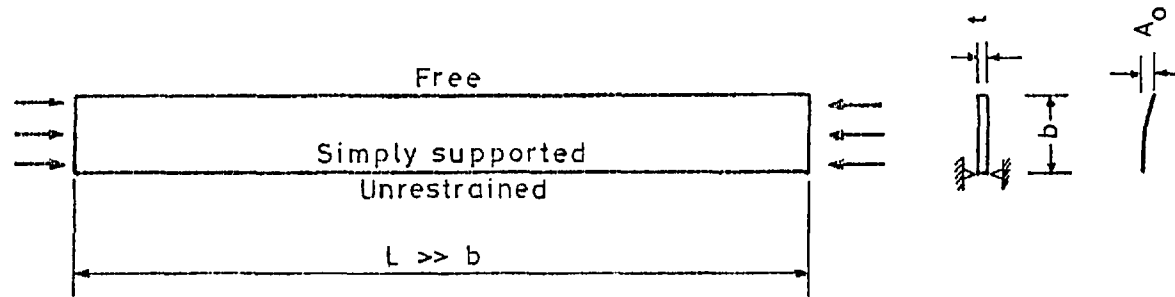


Fig.35 Strength sensitivity of flat stiffeners to initial imperfection

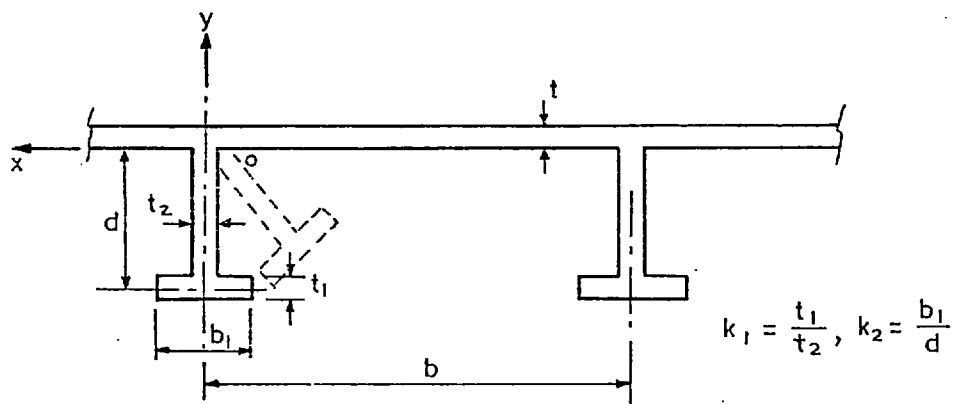


Fig.36 Torsional buckling of tee-type outstand.

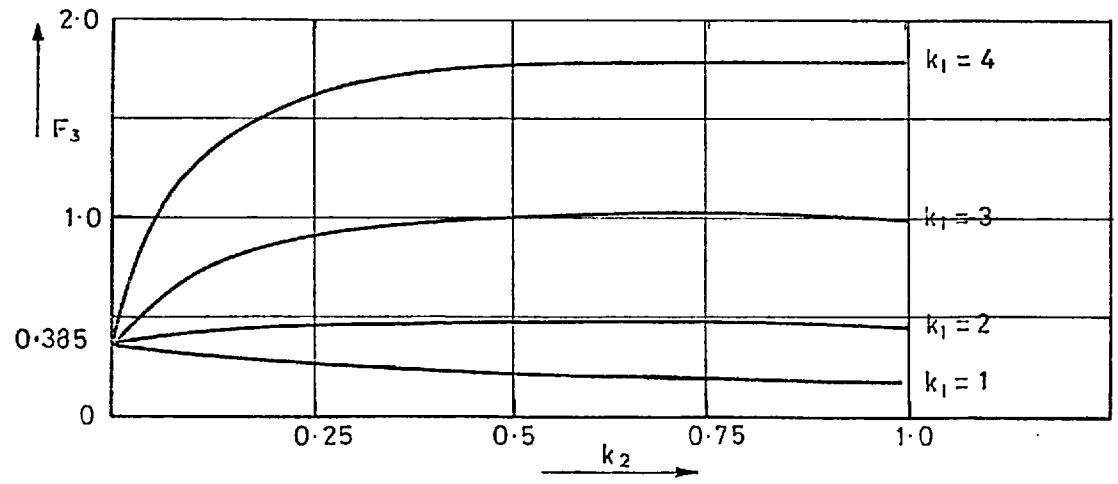
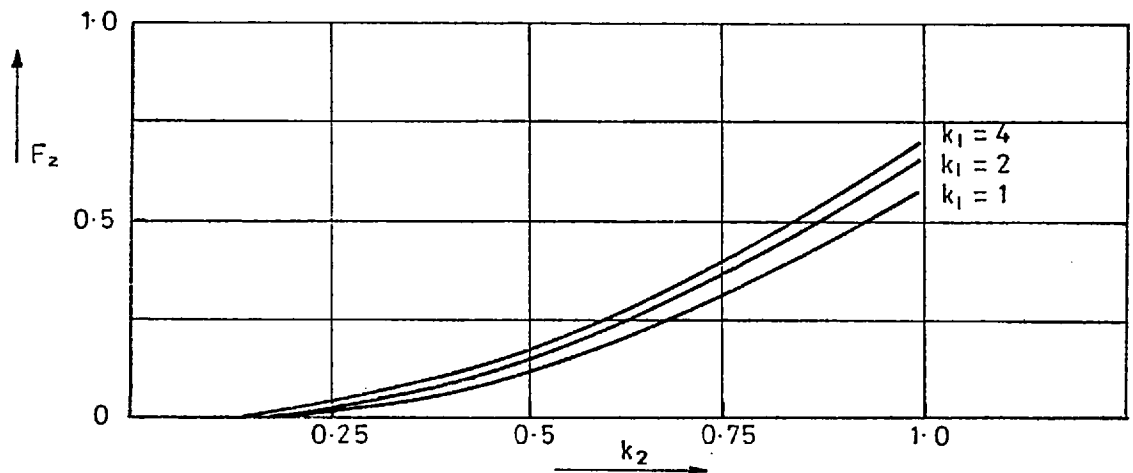
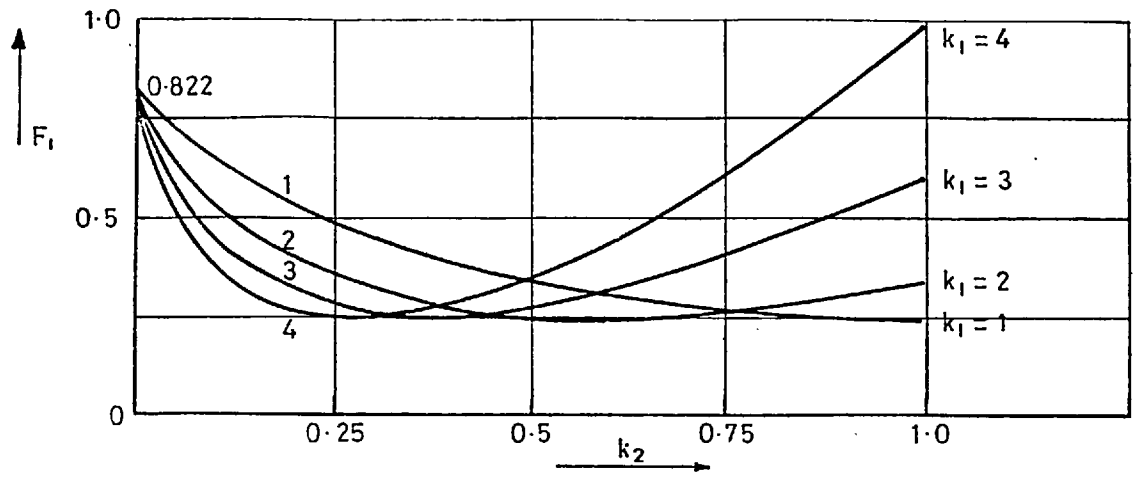


Fig. 37 Coefficients for torsional buckling

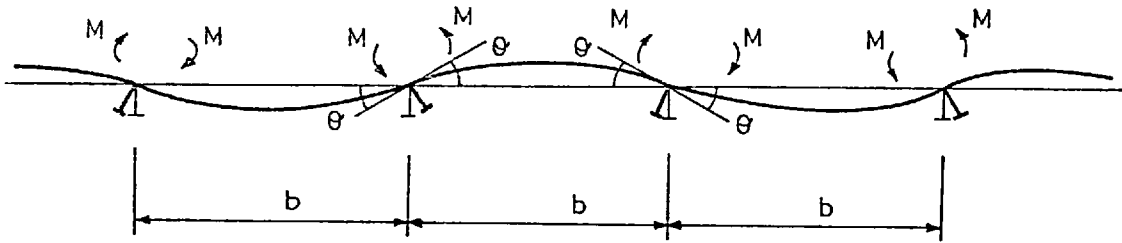


Fig. 38 Restraint by flange plate

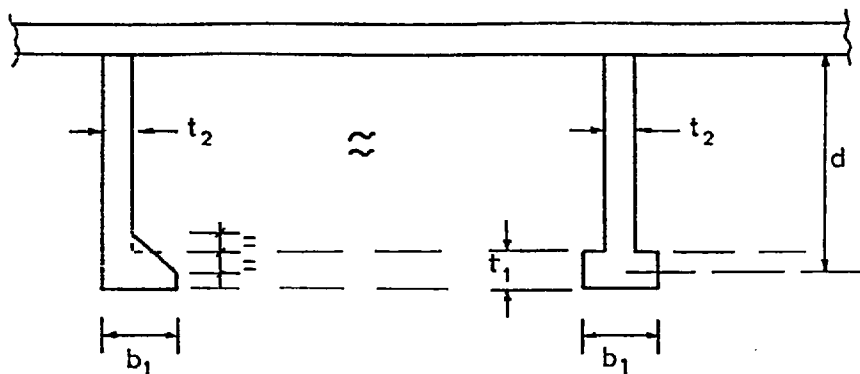


Fig.39a. Bulb flat stiffener

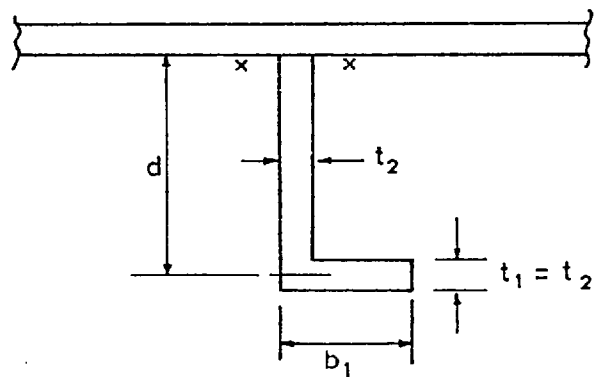


Fig.39b Angle stiffener

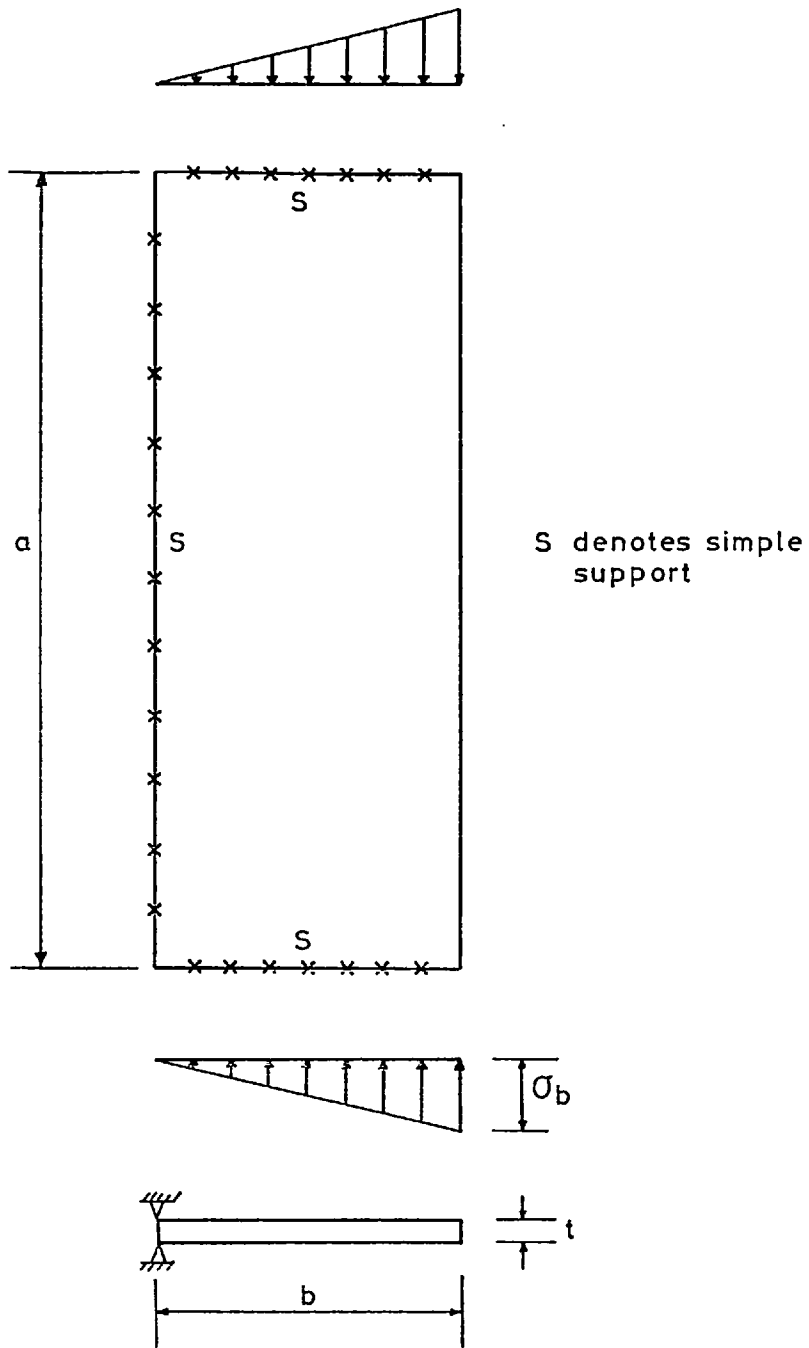


Fig. 40 Varying longitudinal stress on outstand

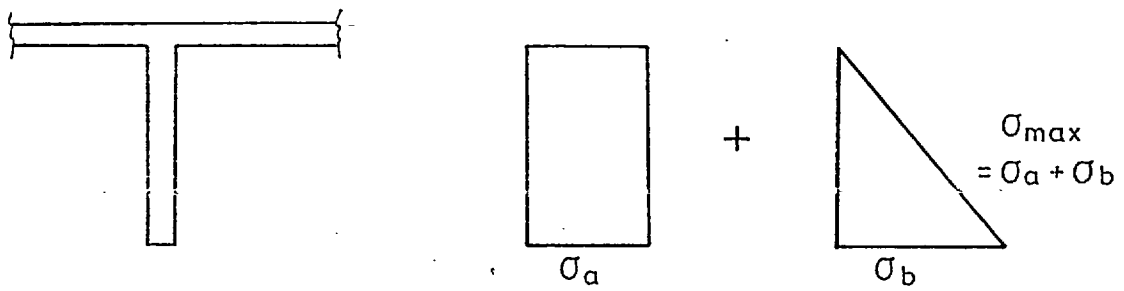


Fig.41 Varying axial stress on flat outstand

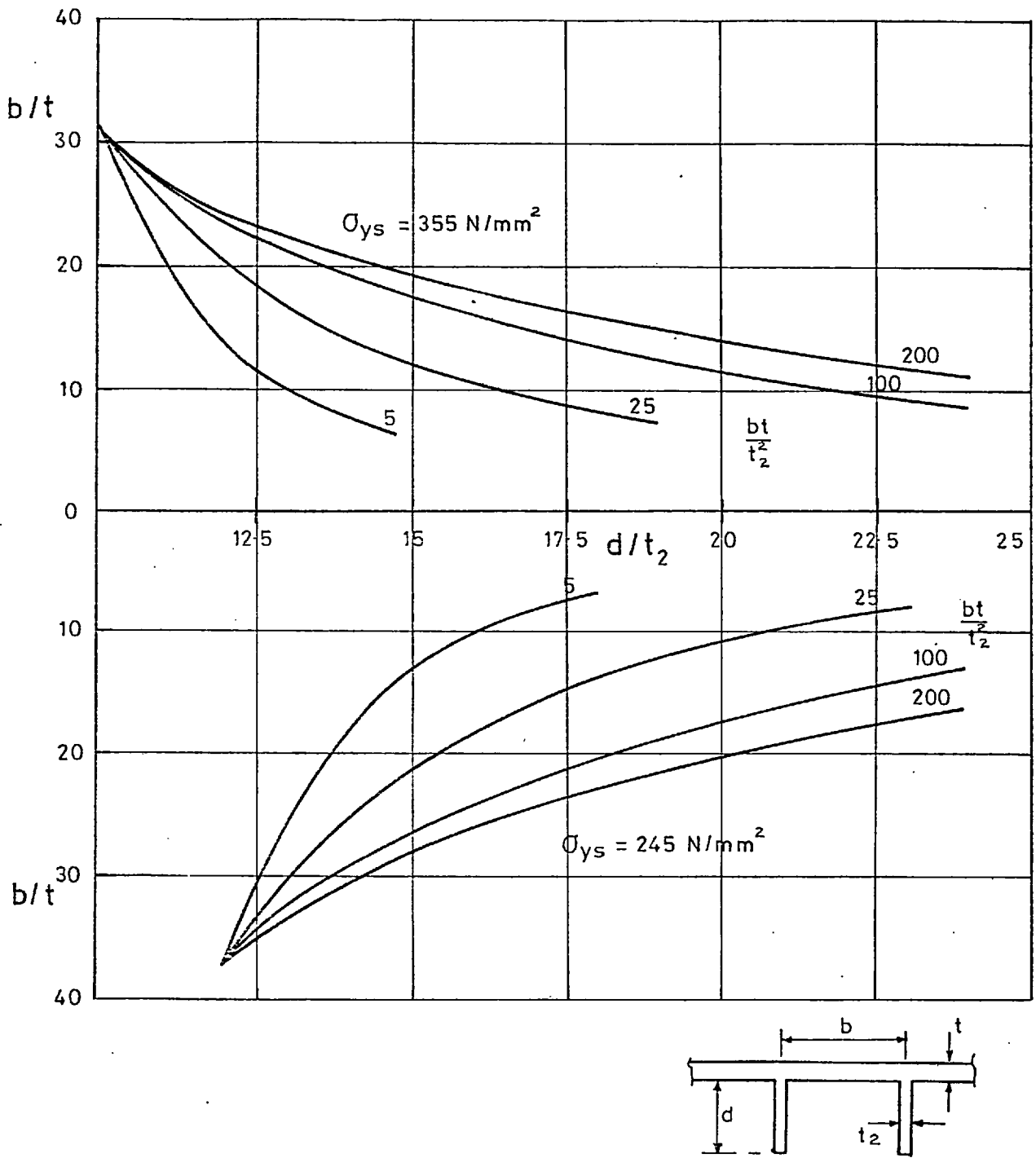


Fig.42 Torsional buckling of flat outstand

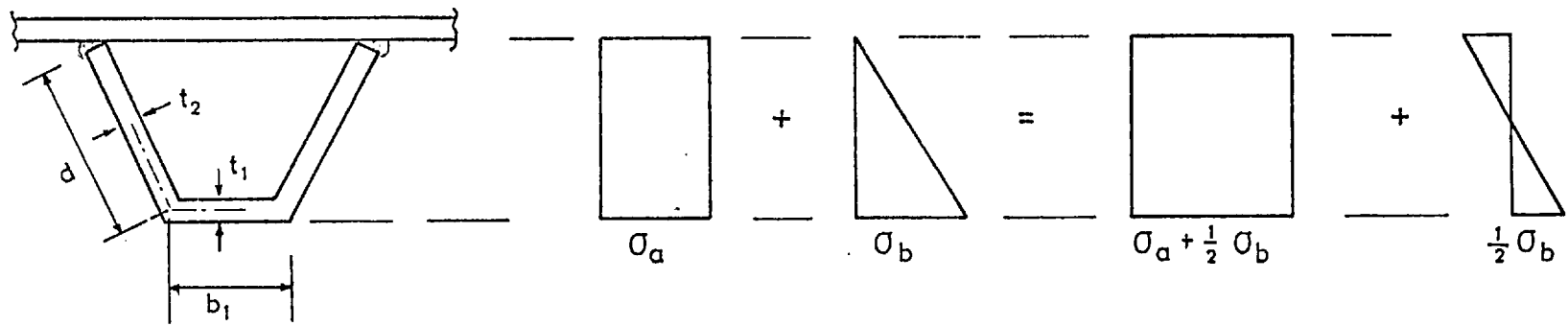
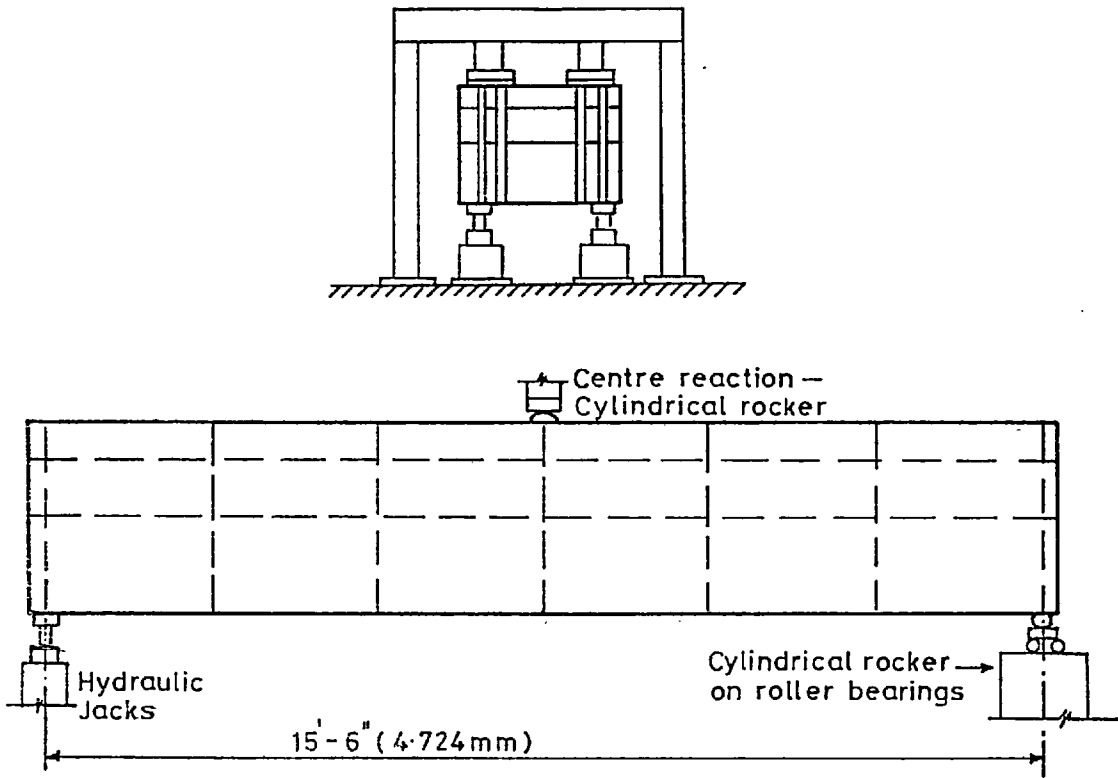


Fig.43 Closed stiffeners



TEST RIG FOR MODEL 1. INSERT SHOWS TRANSVERSE LOCATIONS OF JACKS AND CENTRAL BEARINGS

Fig.44 Diagram of rig used for point load tests

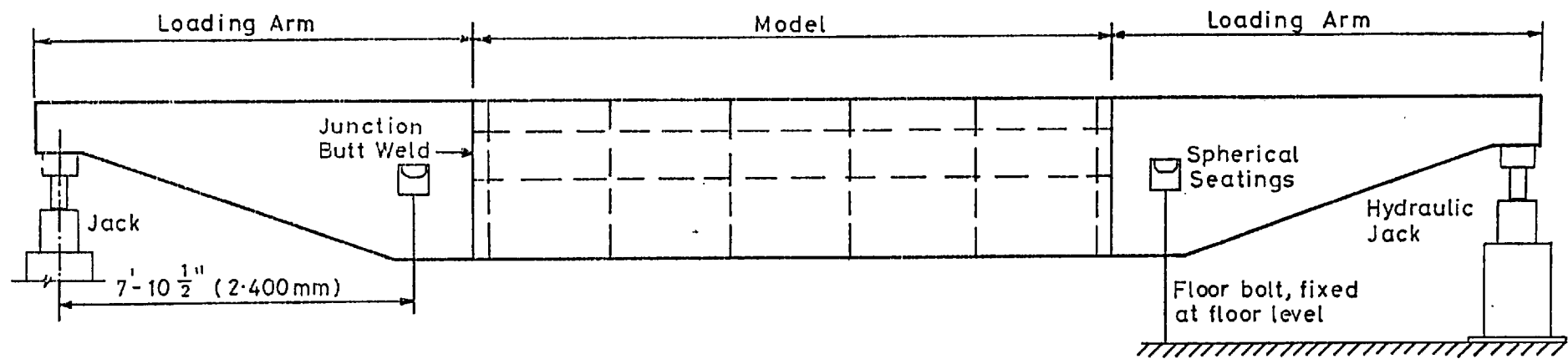


Fig. 45 Diagram of rig used to apply pure moment – Models 2,4 & 8

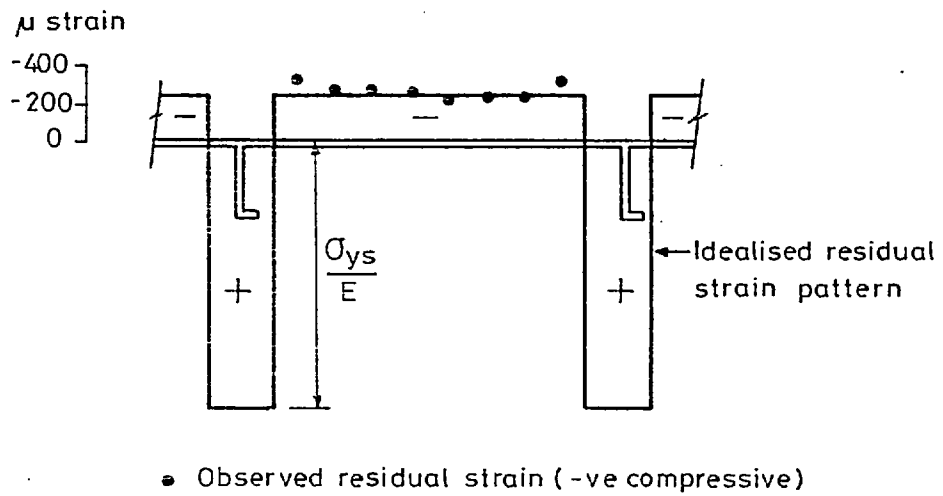


Fig. 46a. Typical distribution of longitudinal residual strain in a compression flange panel of Model 2.

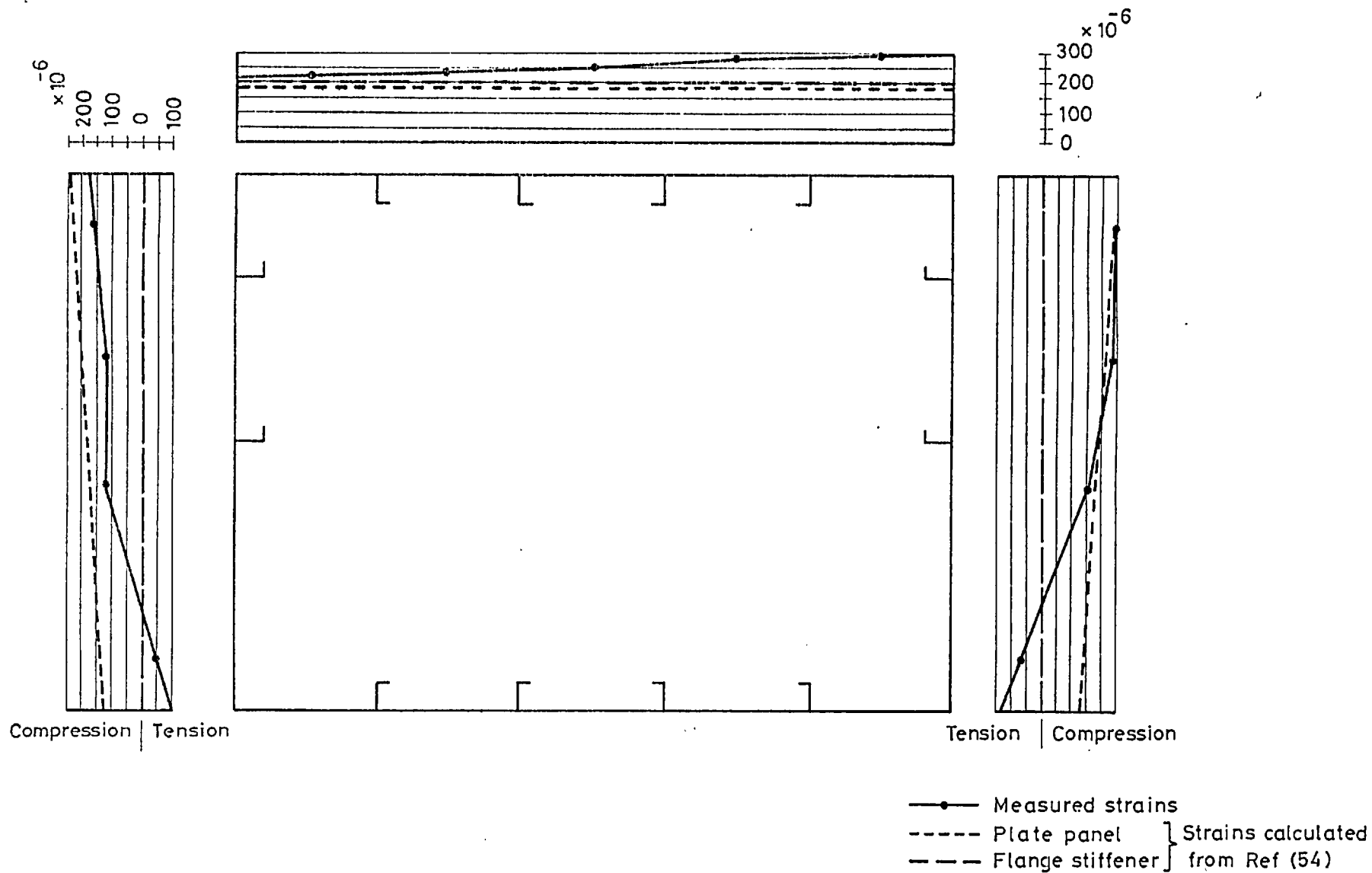


Fig46b. Measured welding residual strains - Model 2.

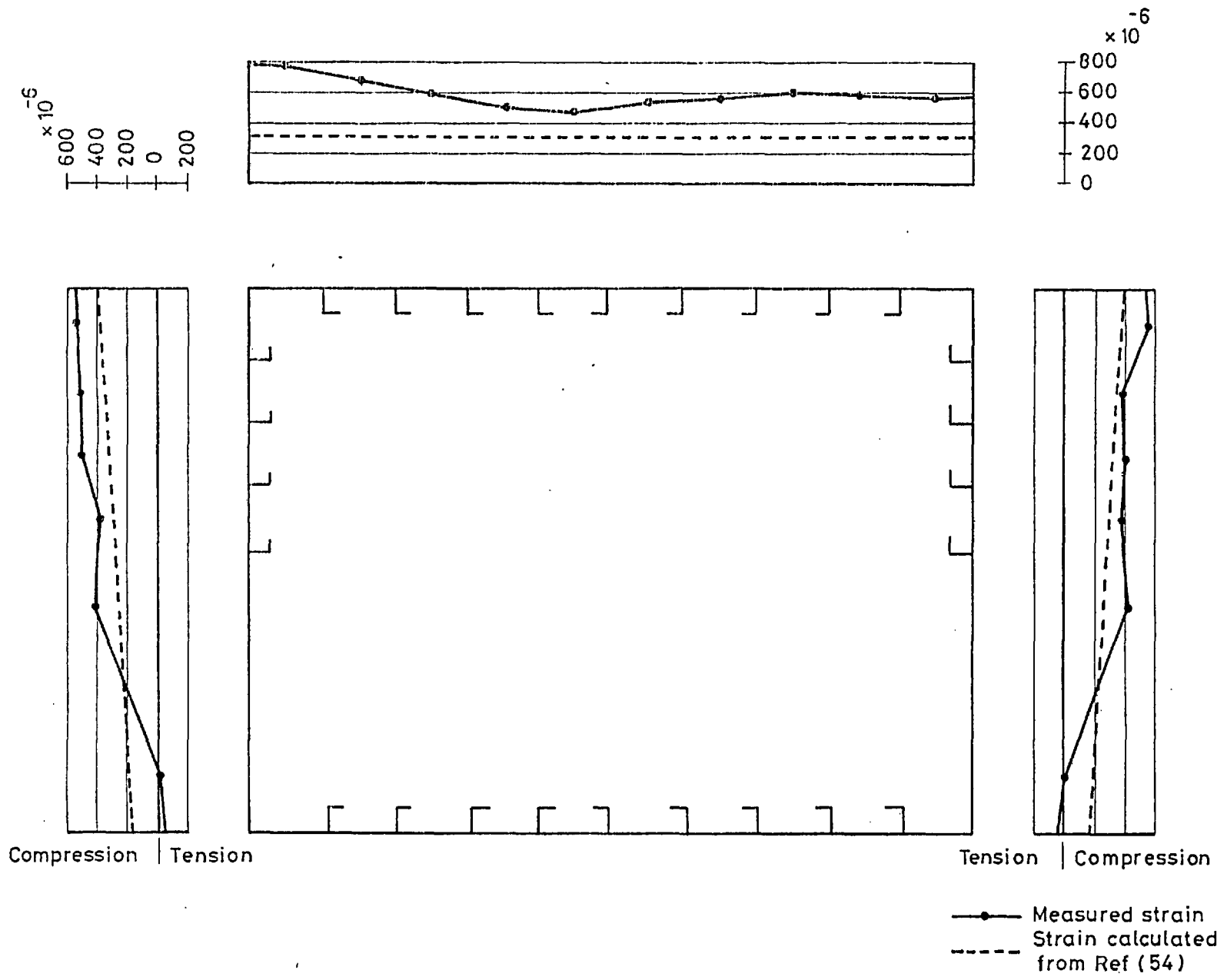


Fig 46c. Measured welding residual strains - Model 4

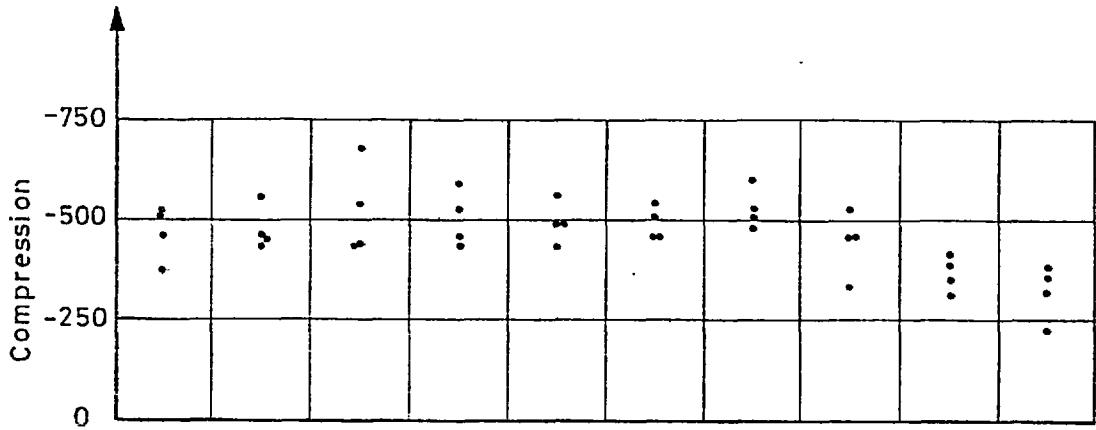


Fig 46d. Measured average longitudinal strains on compression flange ($\times 10^{-6}$) - Model 8

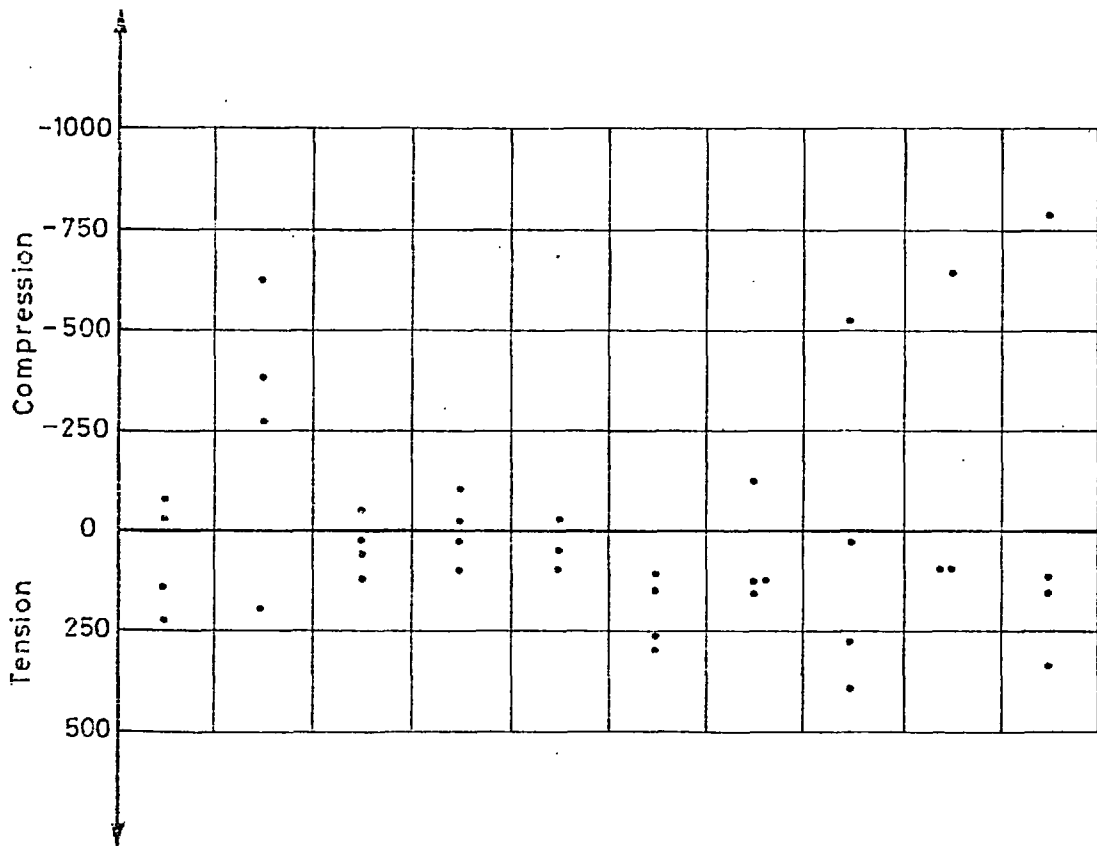
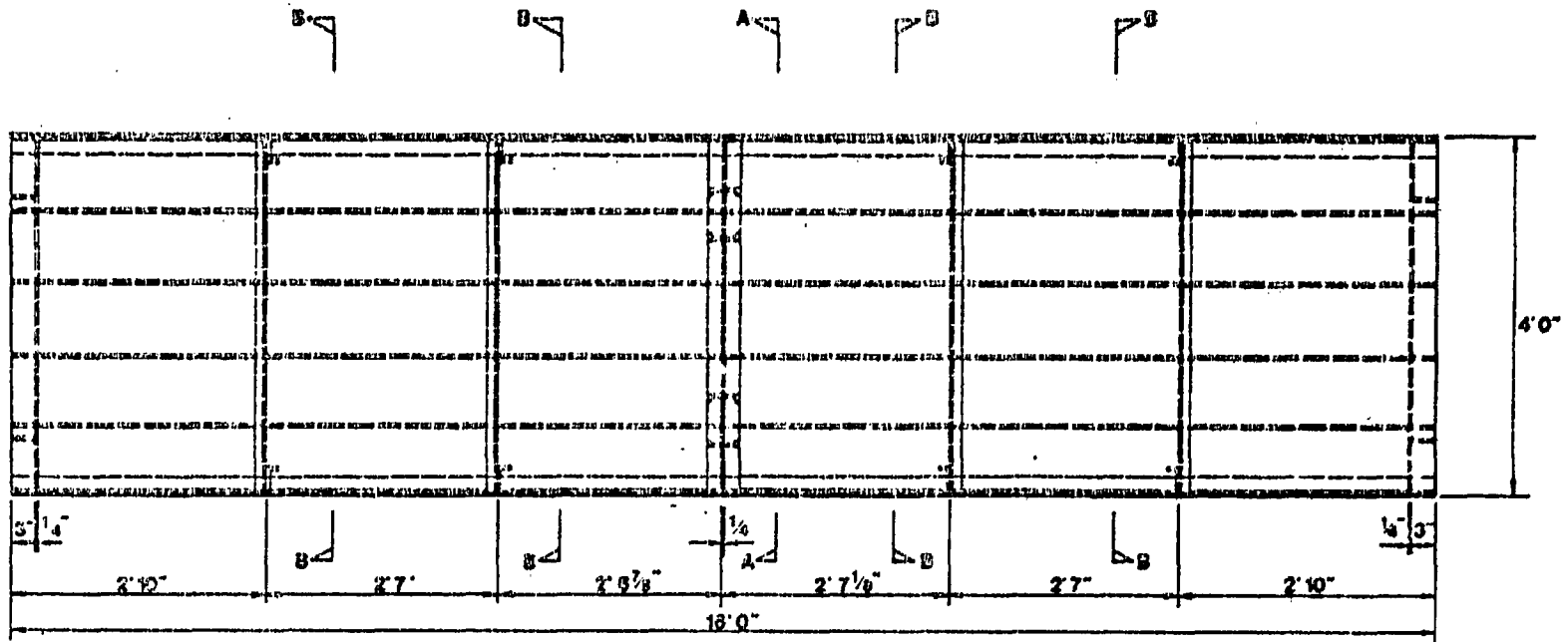
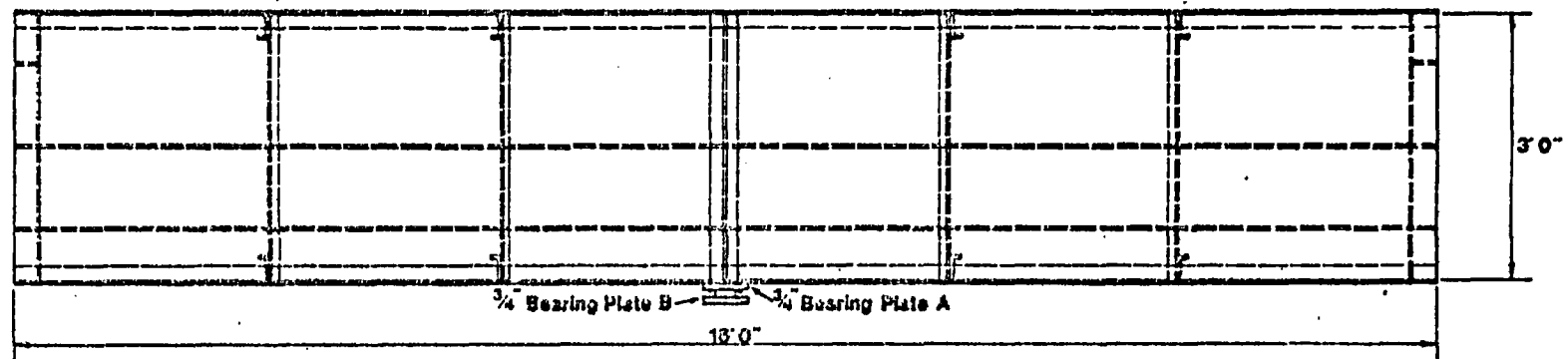


Fig 46e Measured transverse strains on compression flange ($\times 10^{-6}$) - Model 8

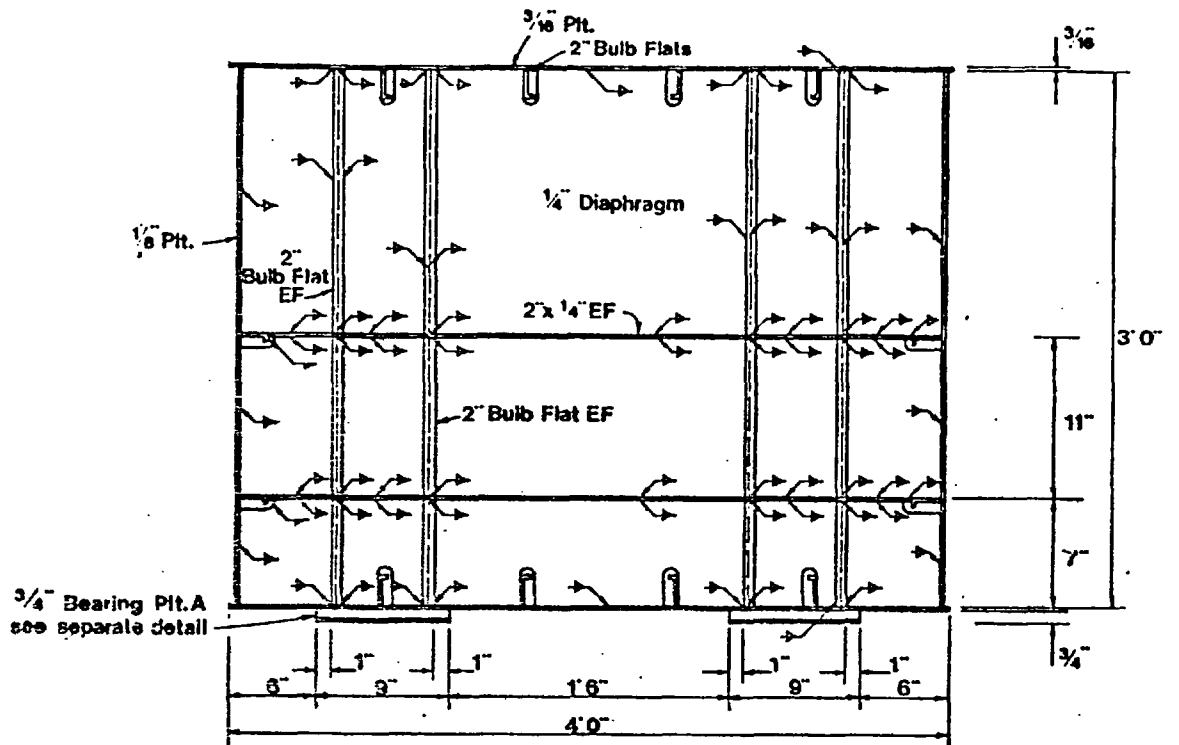


PLAN ON TOP

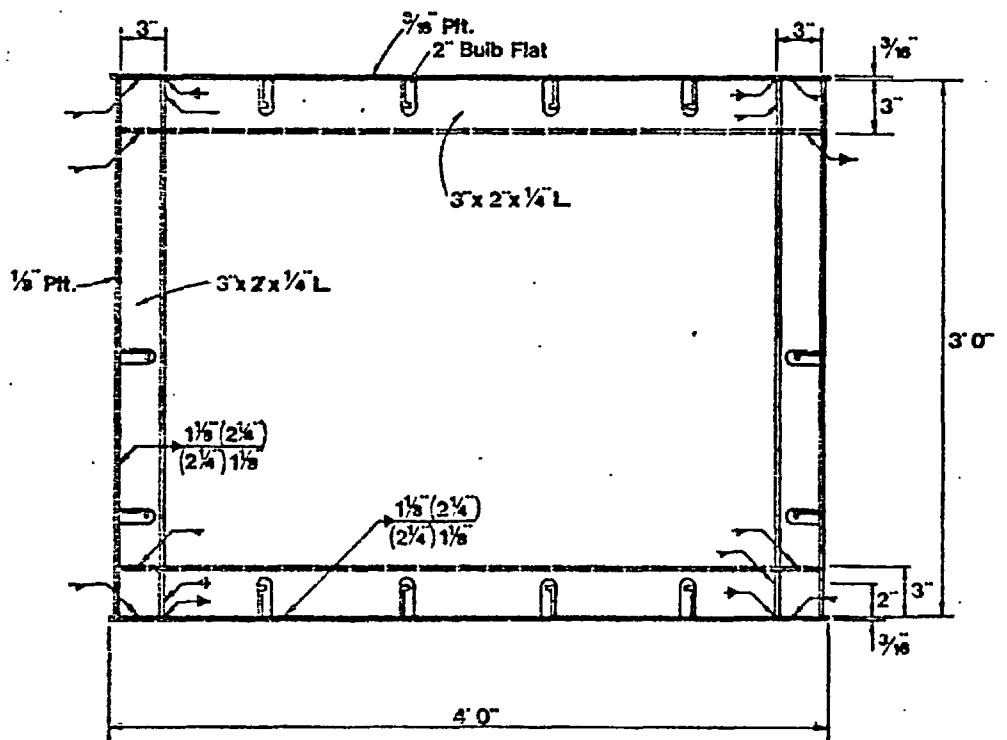


SIDE ELEVATION

Fig. 47 a Model 1: Plan and elevation



SECTION A-A



SECTION B-B

Fig. 47.b
Model 1: Details of diaphragm and internal cross-frame

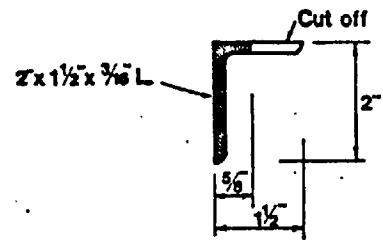
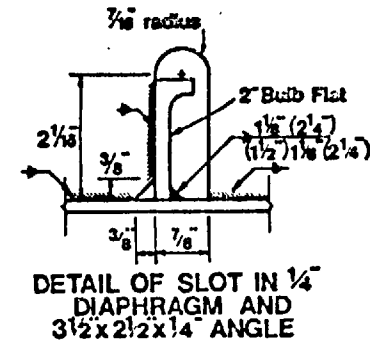
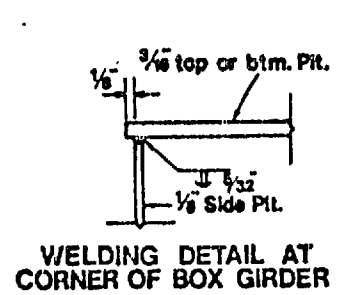
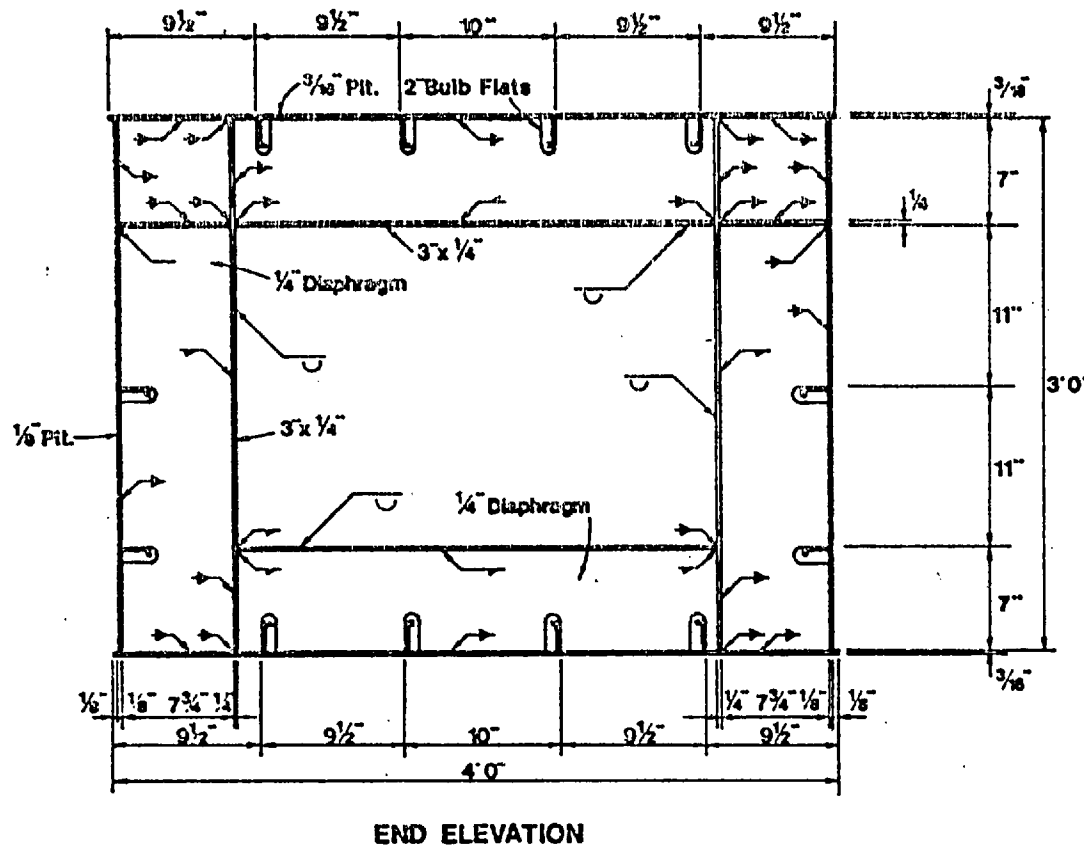
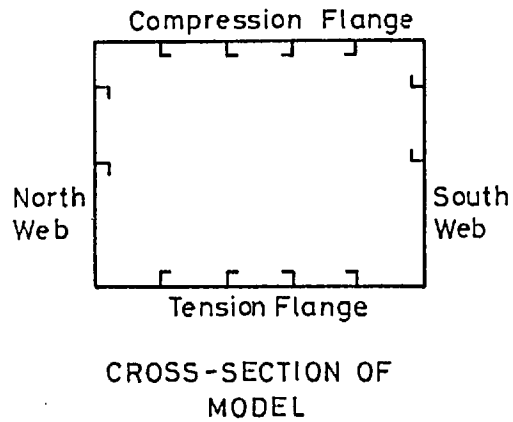
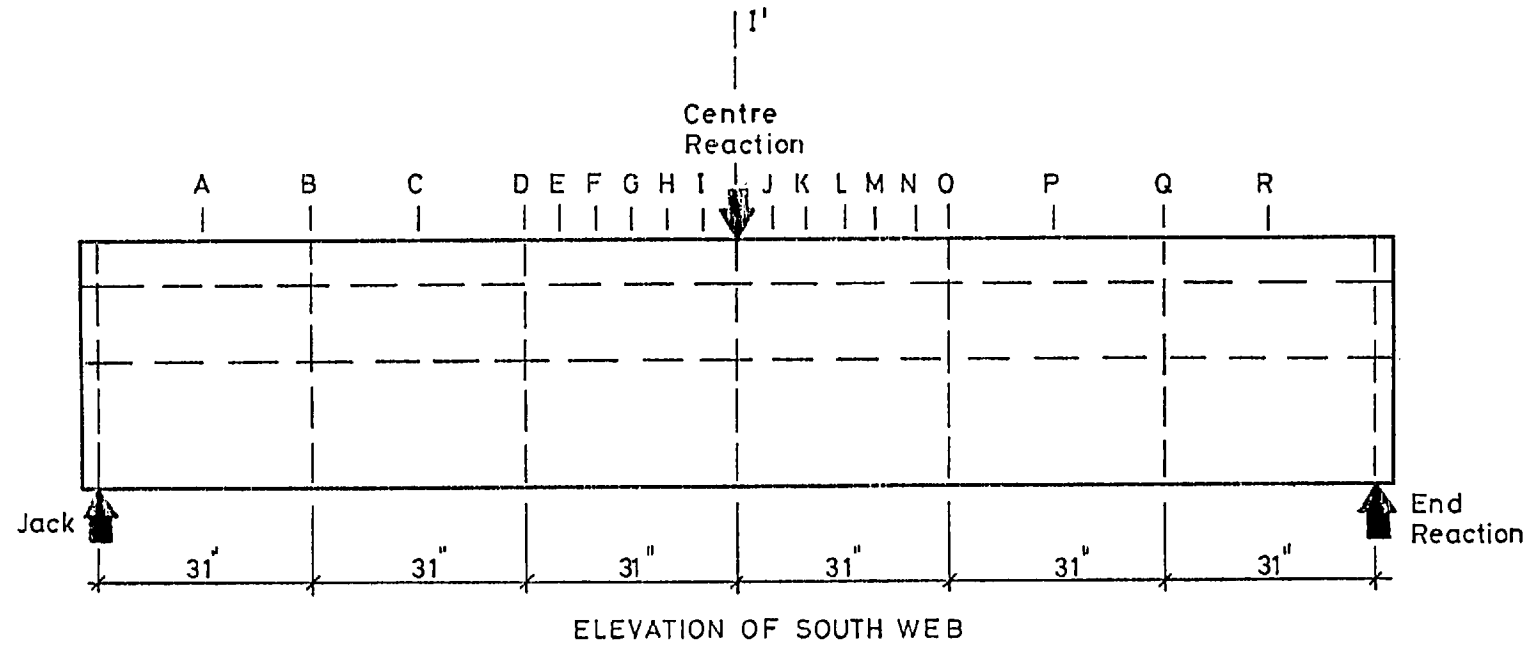


Fig. 47-c Model 1: End cross-frame



Note:
Letters A to R indicate
locations along the model.
All grid lines within panels
are at equal distances

Fig. 48 Details of reference grid - Model 1.

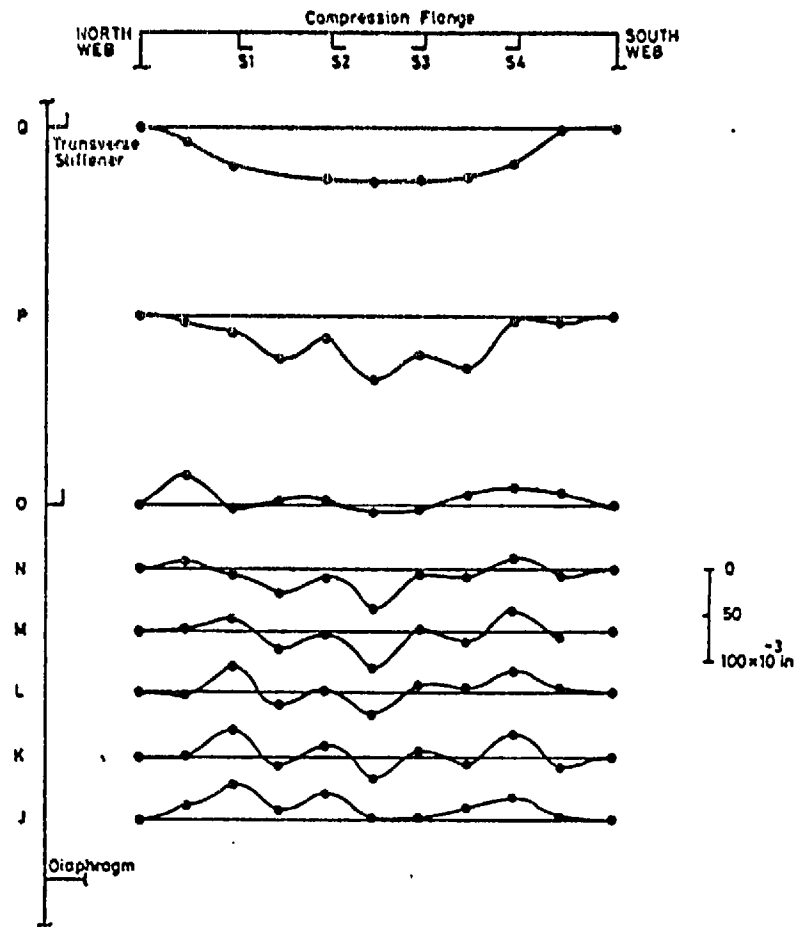
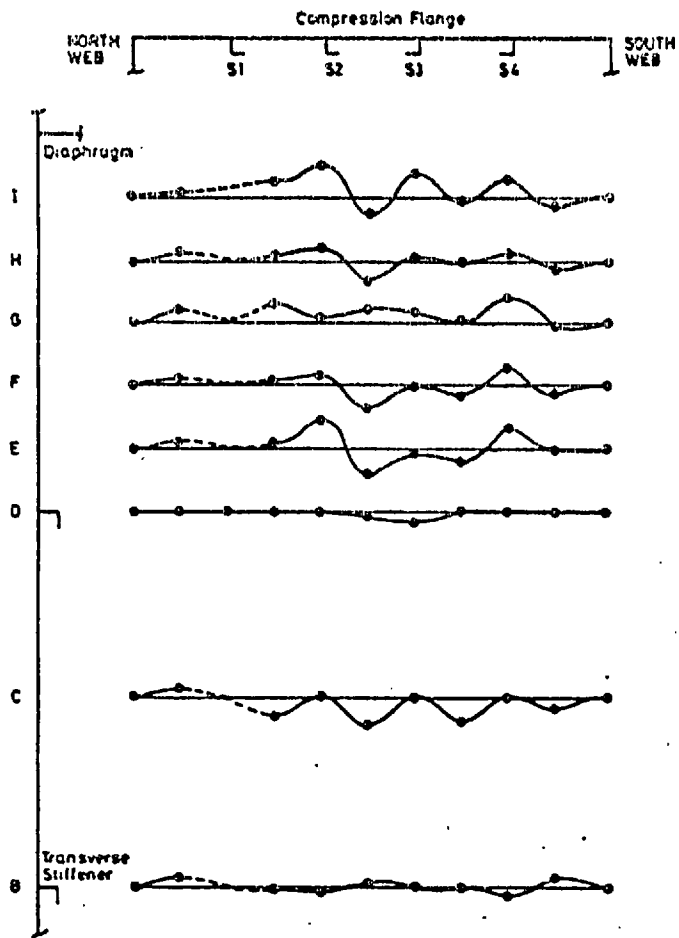


Fig. 49a. Model 1: Transverse initial deflection profiles of compression flange

Compression Flange (West)

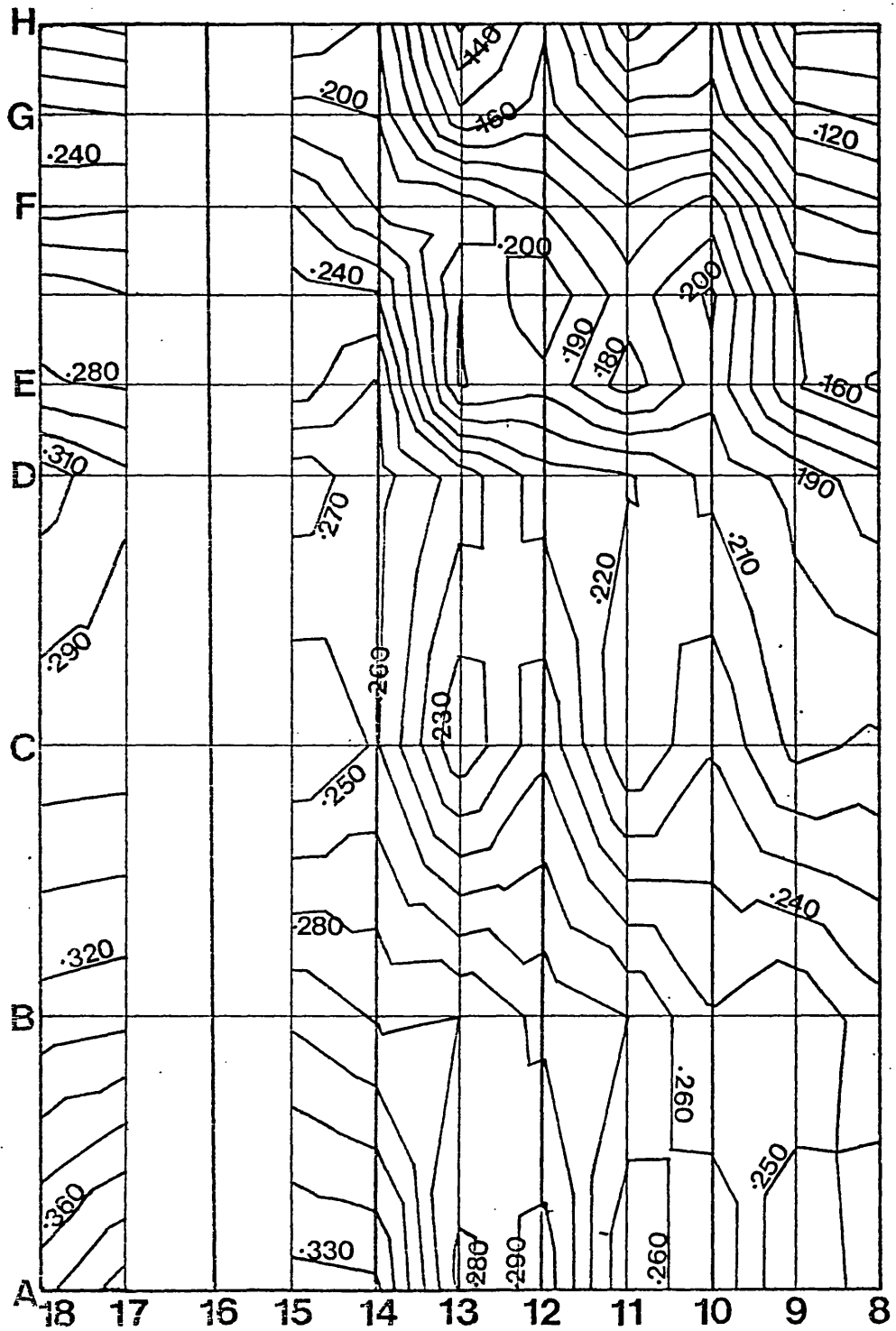


Fig.49b. Model 1. Initial distortions.

Compression Flange (East)

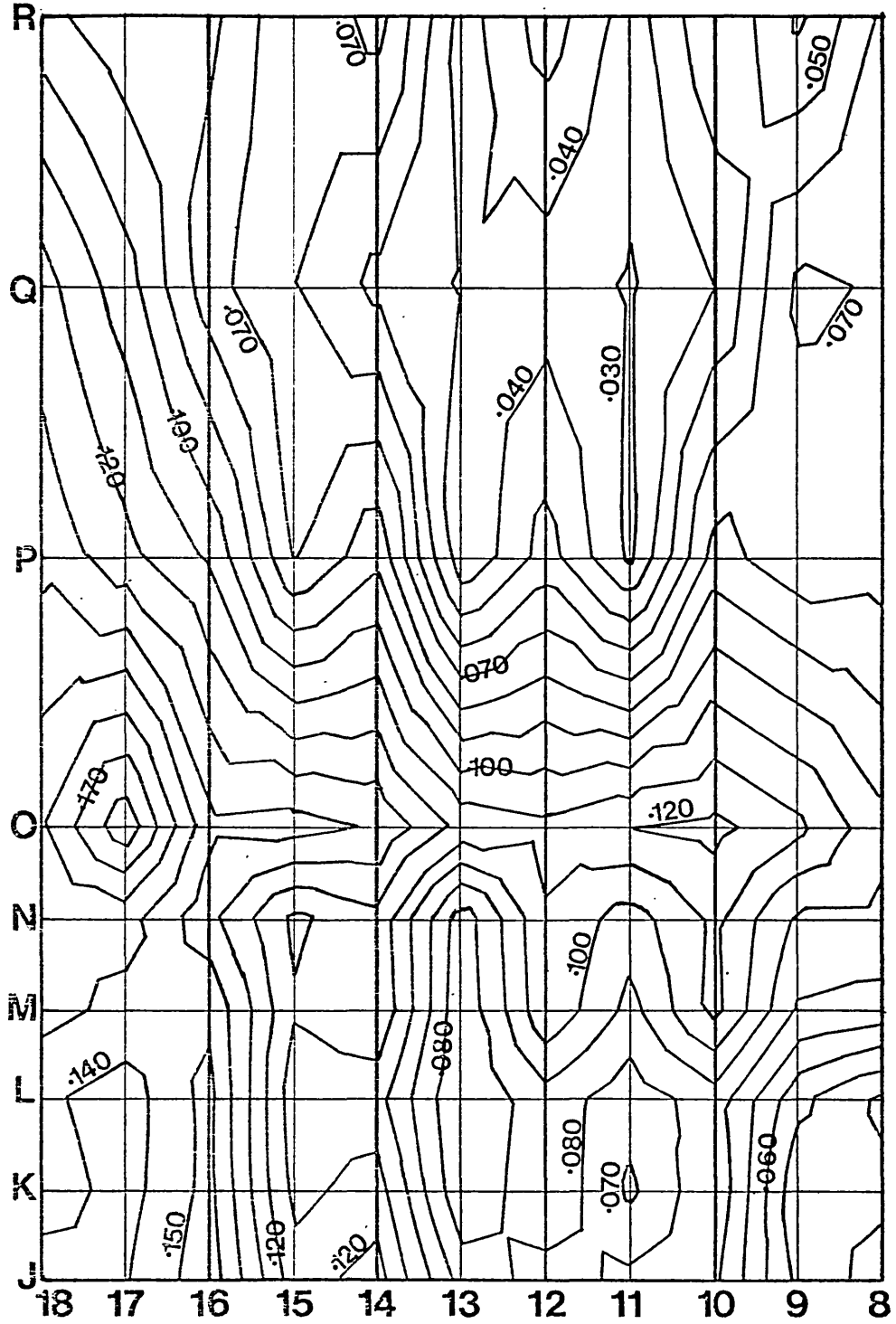


Fig.49c. Model 1. Initial distortions

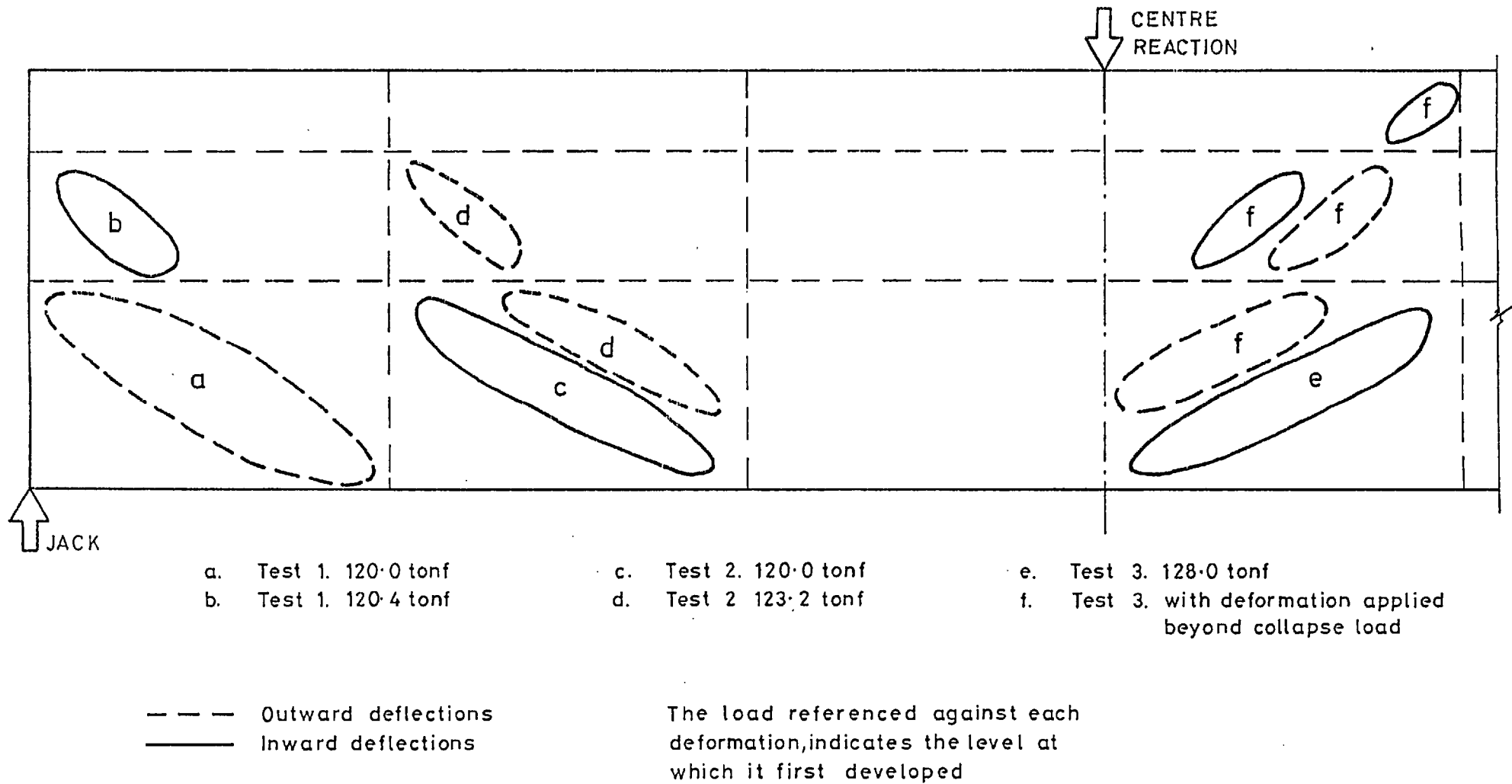


Fig. 50. Development of shear buckles during the three ultimate load tests—Model.1.

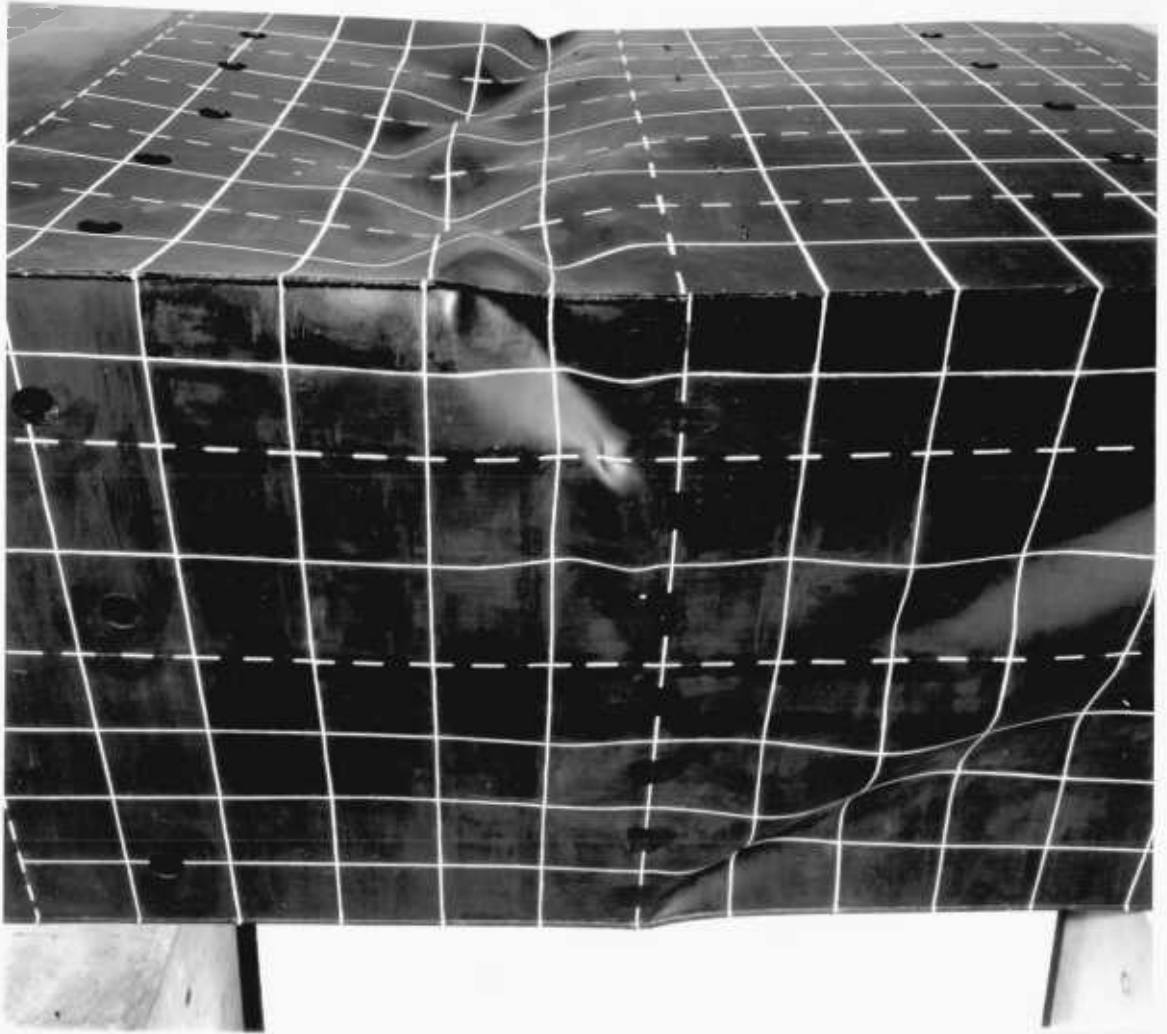


Fig. 51 Model 1 - showing buckling of the compression flange and the web near the central point load position.

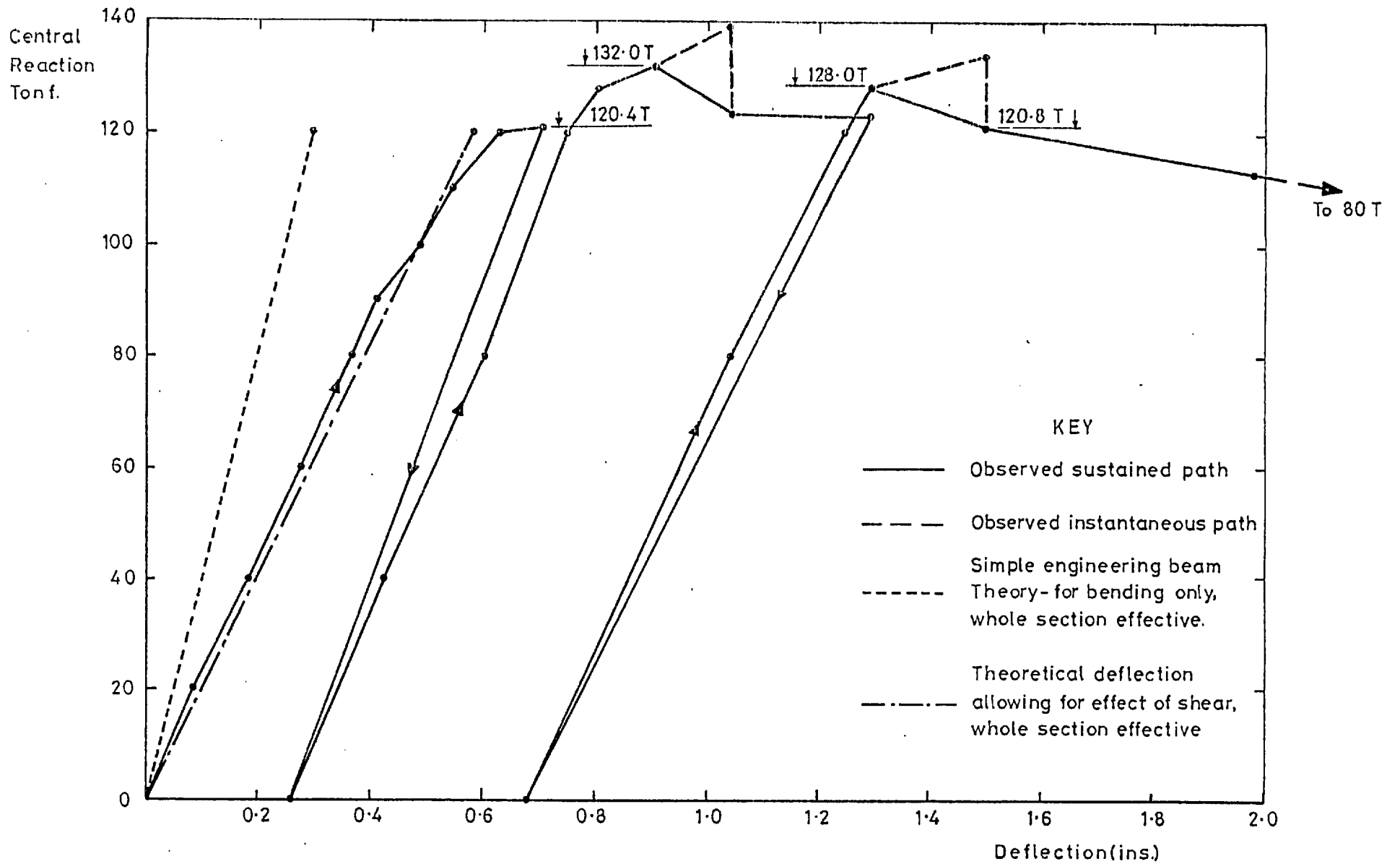
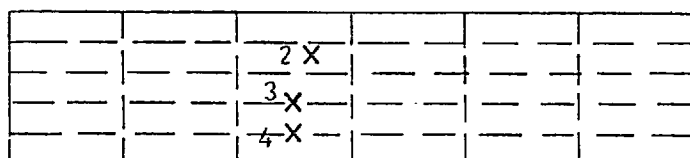
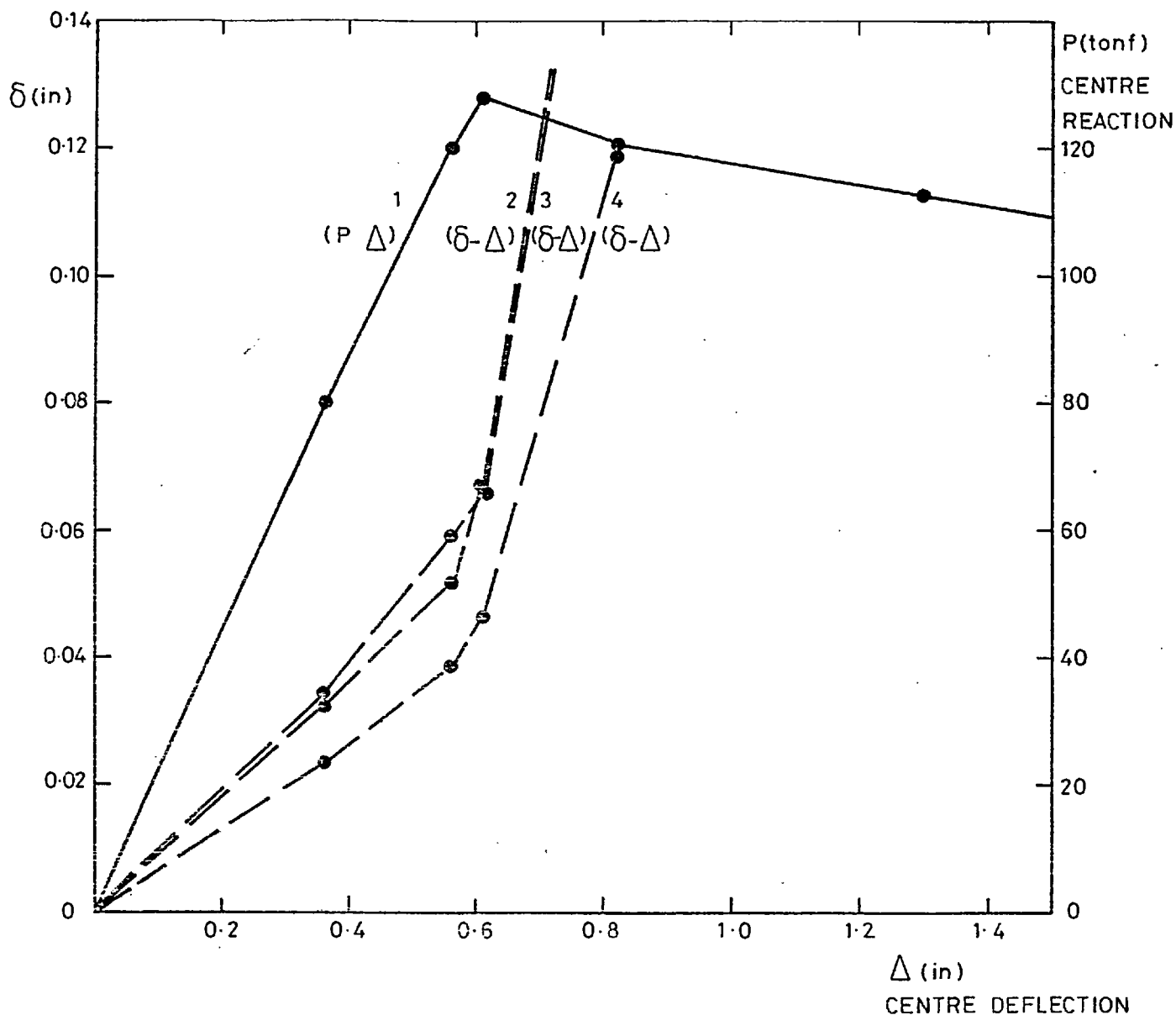


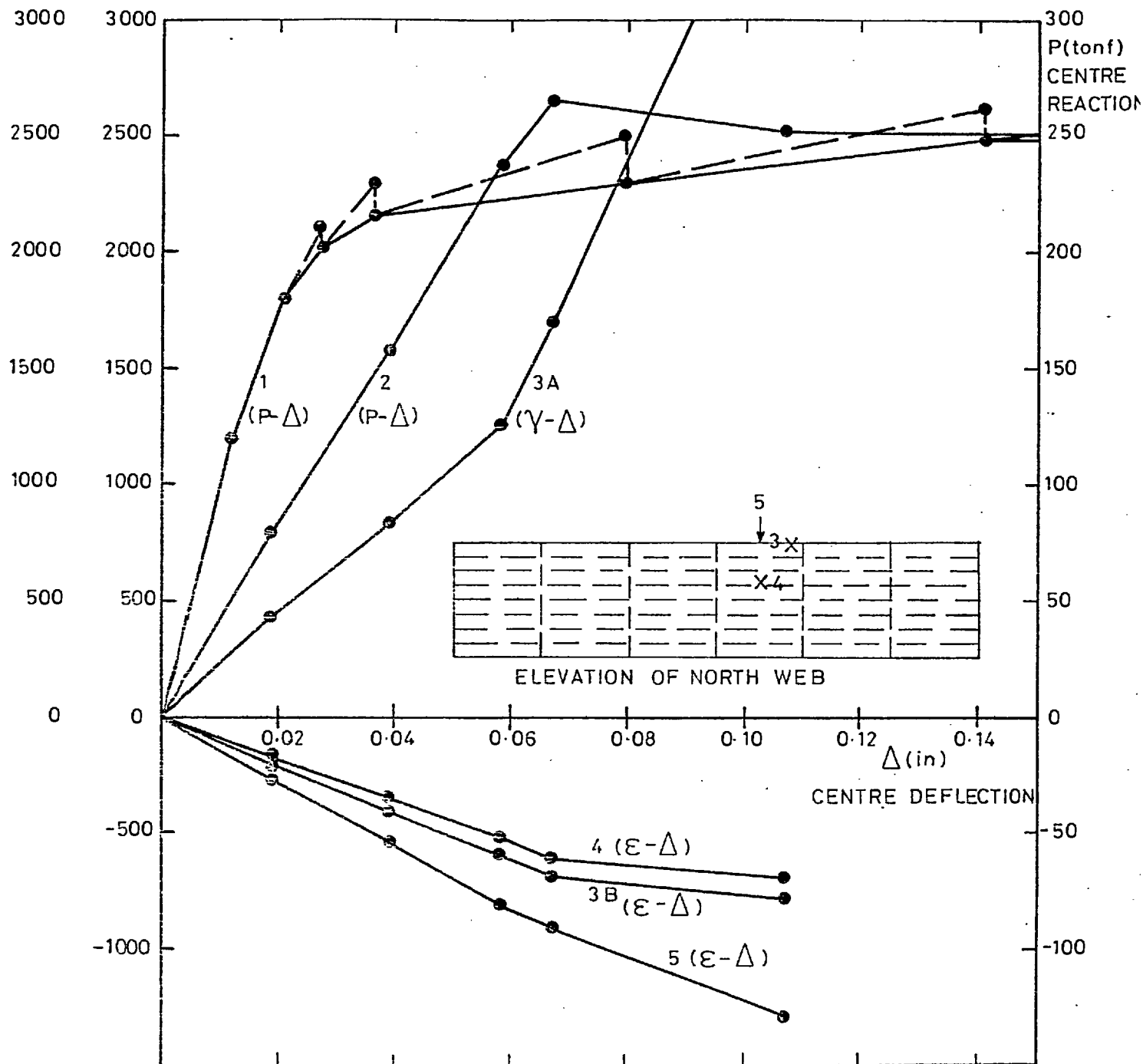
Fig. 52 Load-deflection curve - Model 1.



PLAN OF COMPRESSION FLANGE

- CURVE 1. LOAD-DEFLECTION RELATIONSHIP
- CURVE 2. PLATE PANEL OUT-OF-PLANE DEFORMATION AT LOCATION 2
- CURVE 3. STIFFENER OUT-OF-PLANE DEFLECTION AT LOCATION 3.
- CURVE 4. STIFFENER OUT-OF-PLANE DEFLECTION AT LOCATION 4.

Fig 53a. Model 1. Compression flange. Growth of deflections and strains with load.



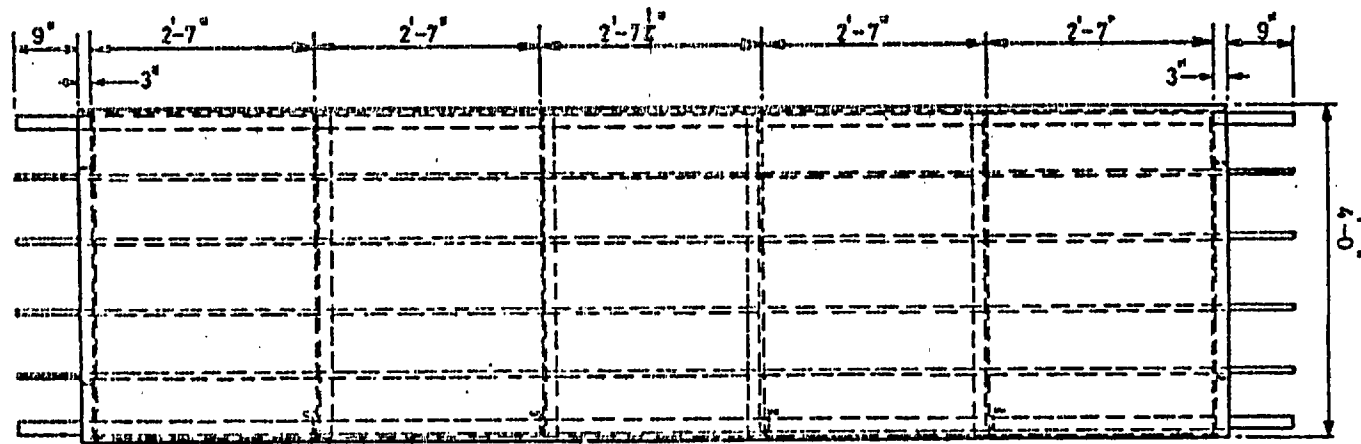
- CURVE 1. OVERALL LOAD-DEFLECTION RELATIONSHIP (TEST 1) SHOWING BOTH INSTANTANEOUS (DASHED) AND SUSTAINED (FULL) PATHS
- CURVE 2. OVERALL LOAD-DEFLECTION RELATIONSHIP (TEST 2)
- CURVE 3A. MID-PLANE SHEAR STRAIN AT LOCATION 3 (TEST 2)
- CURVE 3B. MID-PLANE STRAIN AT LOCATION 3 (TEST 2)
- CURVE 4. MID-PLANE STRAIN AT LOCATION 4 (TEST 2)
- CURVE 5. MID-PLANE STRAIN AT CENTRE FLANGE STIFFENER LOCATION 5 (TEST 2)

Note. The variation in stiffness between Test 1 and 2 (Curves 1 and 2) is due to adopting a different length of base line for the two tests.

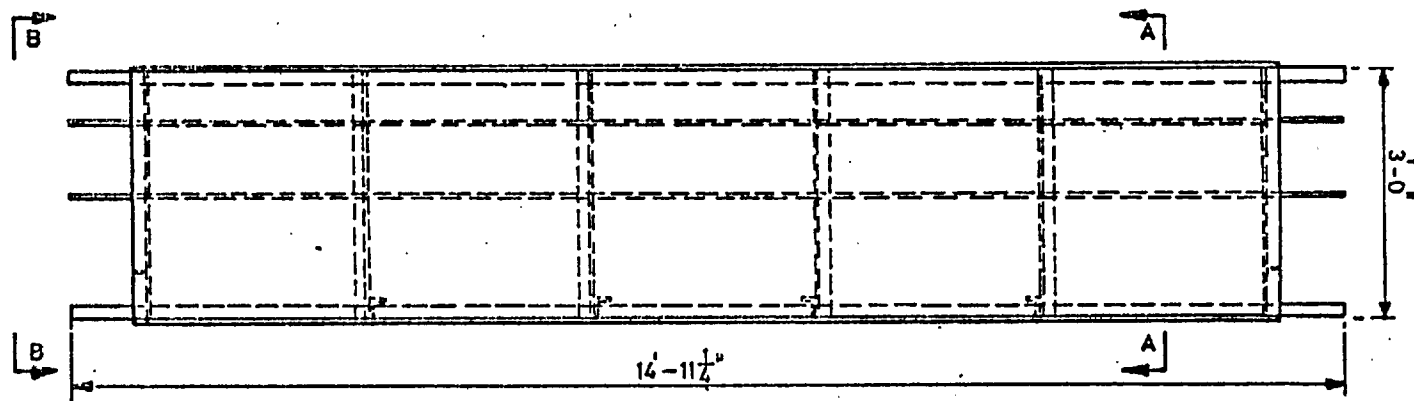
Fig 53b. Growth of deflections and strains with load. Model 1.



Fig. 54 Model 1 - an inside view of the model

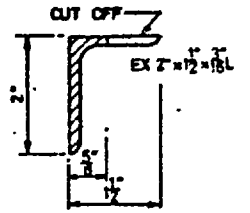
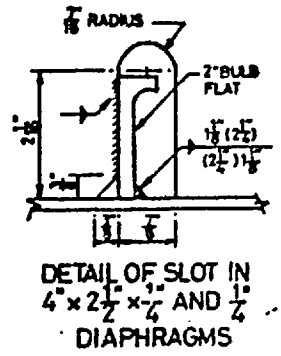
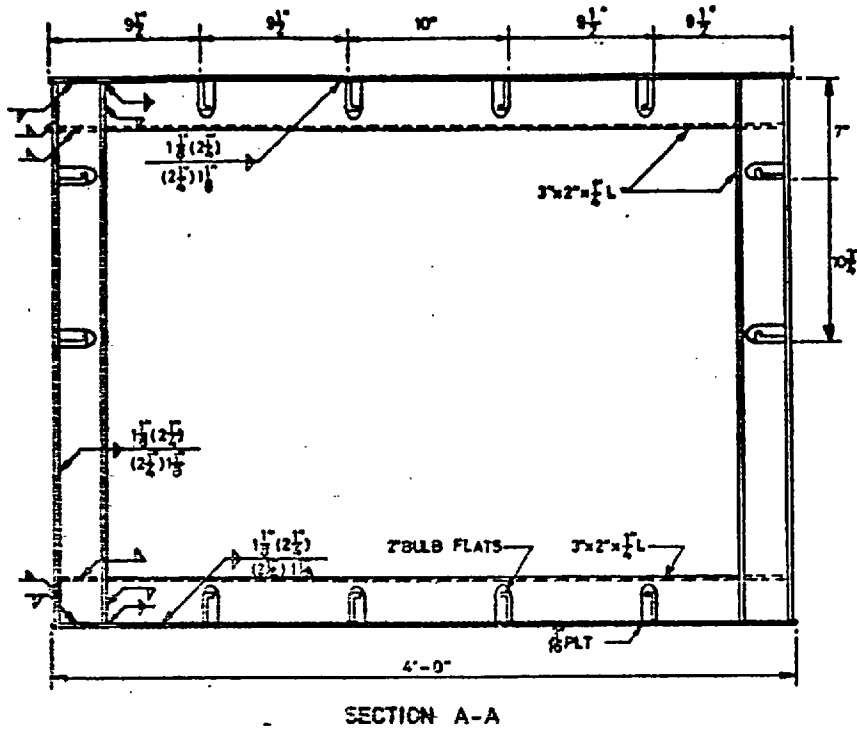


PLAN OF COMPRESSION FLANGE



SIDE ELEVATION

Fig. 55 a. Model 2: Plan and elevation



note: Bulb flat shown shaded.

DETAIL OF 2" BULB FLAT

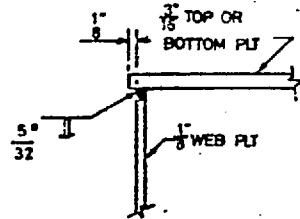
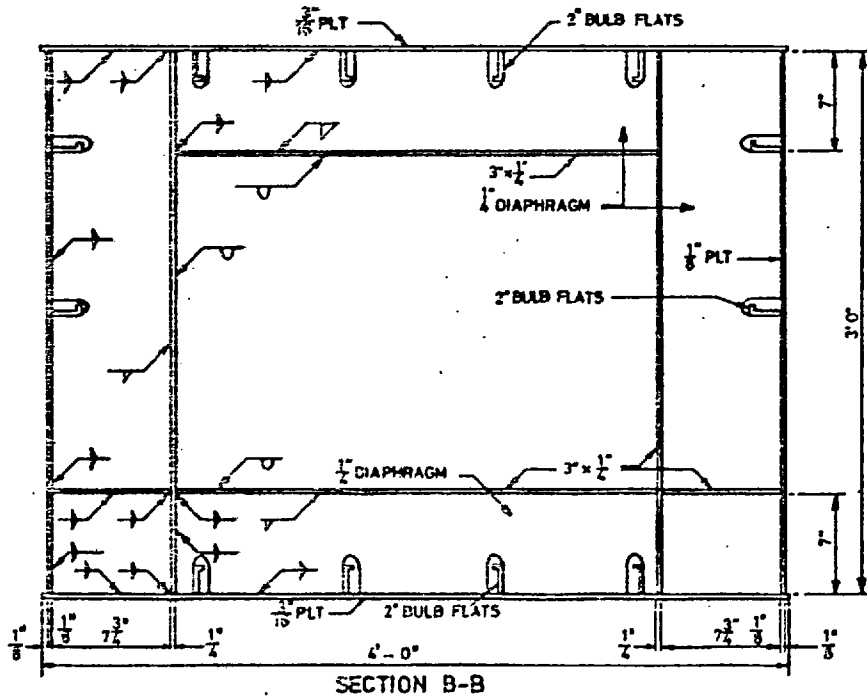
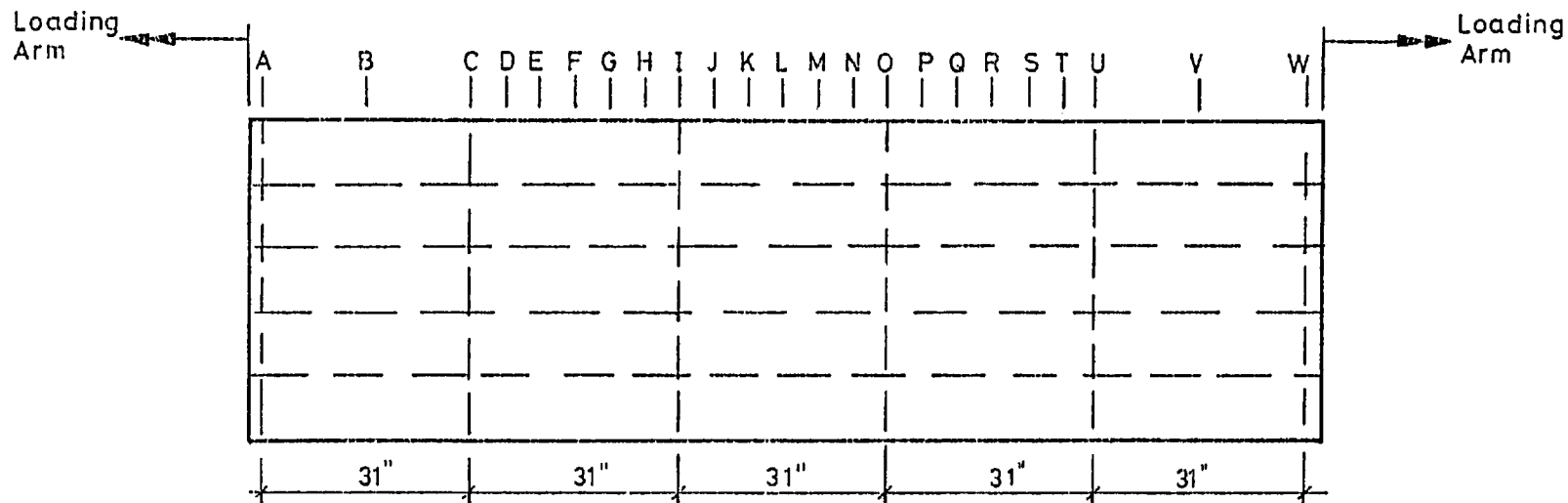
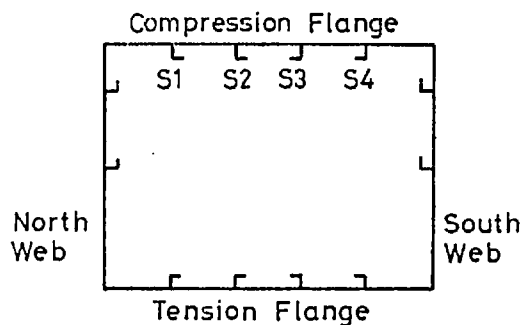


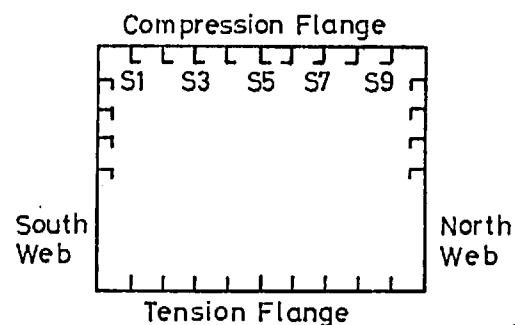
Fig. 55b.
Model 2: Cross-sections



PLAN OF MODEL 2. COMPRESSION FLANGE



CROSS-SECTION OF MODEL 2.
(viewed from end A)



CROSS-SECTION OF MODEL 4.
(viewed from end A)

Notes:
Overall plan dimensions of Model 4. similar to Model 2.
Letters A to W indicate locations along the model.
All grid lines within panels are at equal distances

Fig. 56 Details of reference grid - Models 2. and 4.

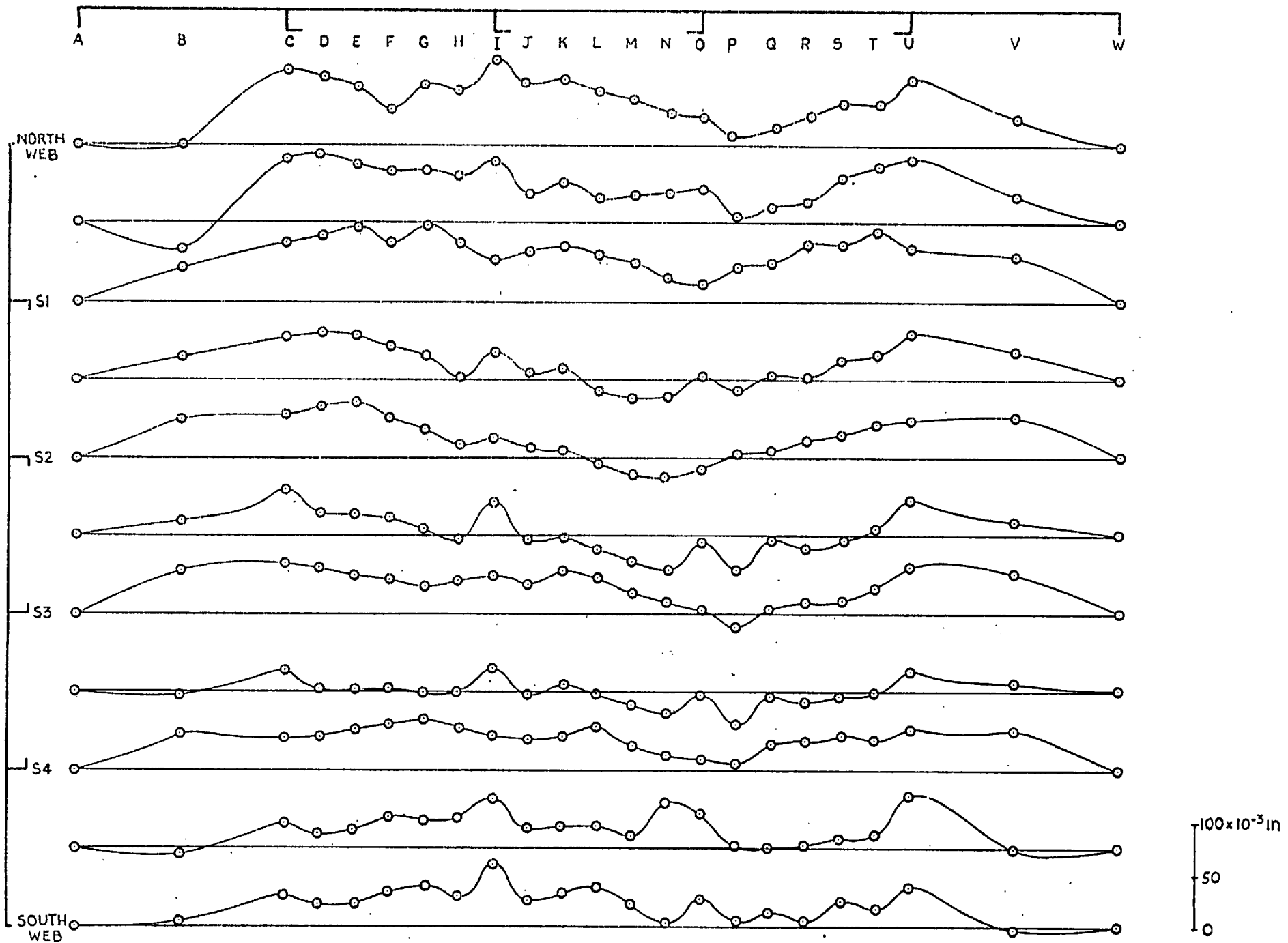


Fig 57a Model 2: Longitudinal initial deflection profiles of compression flange

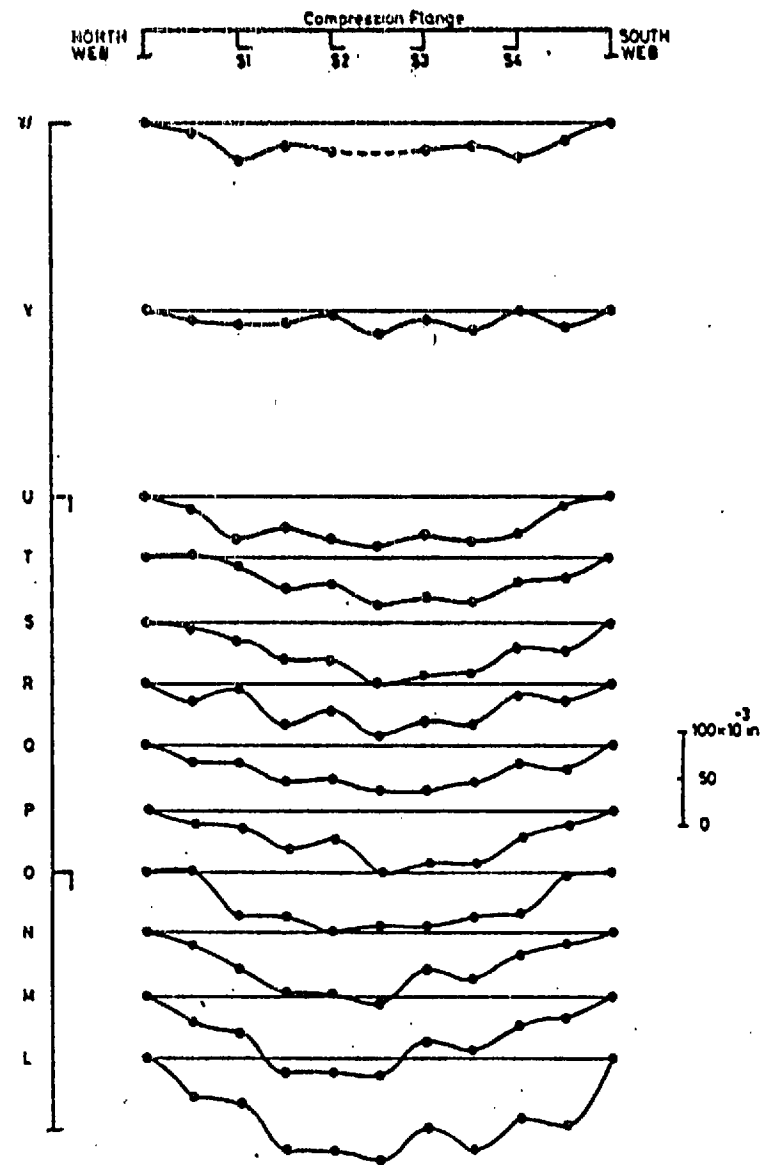
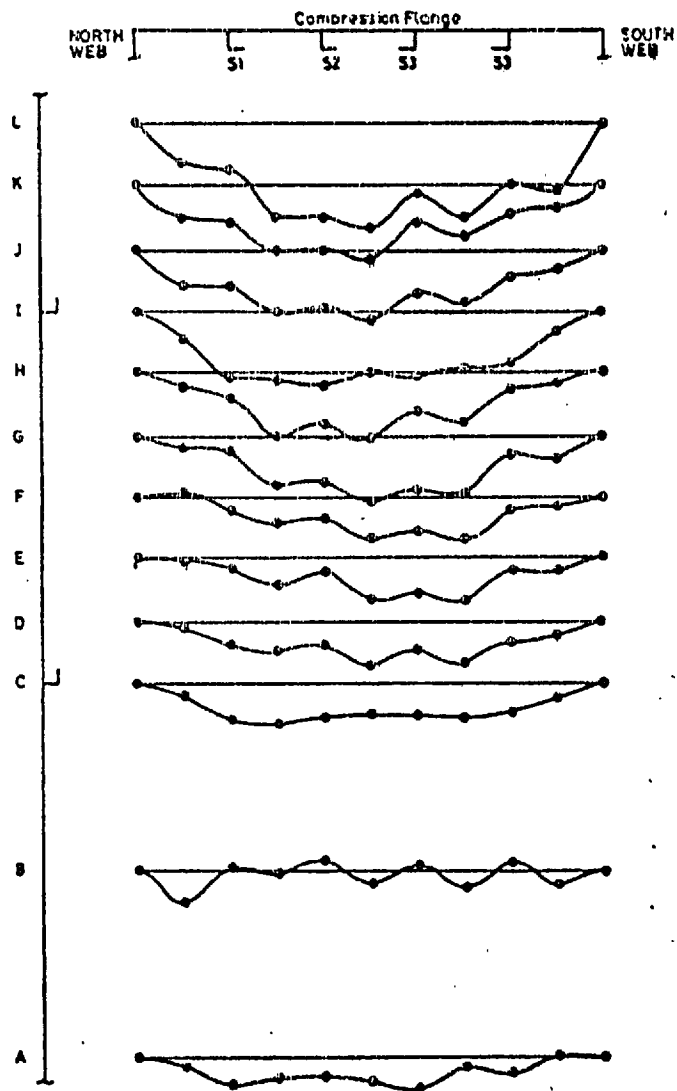
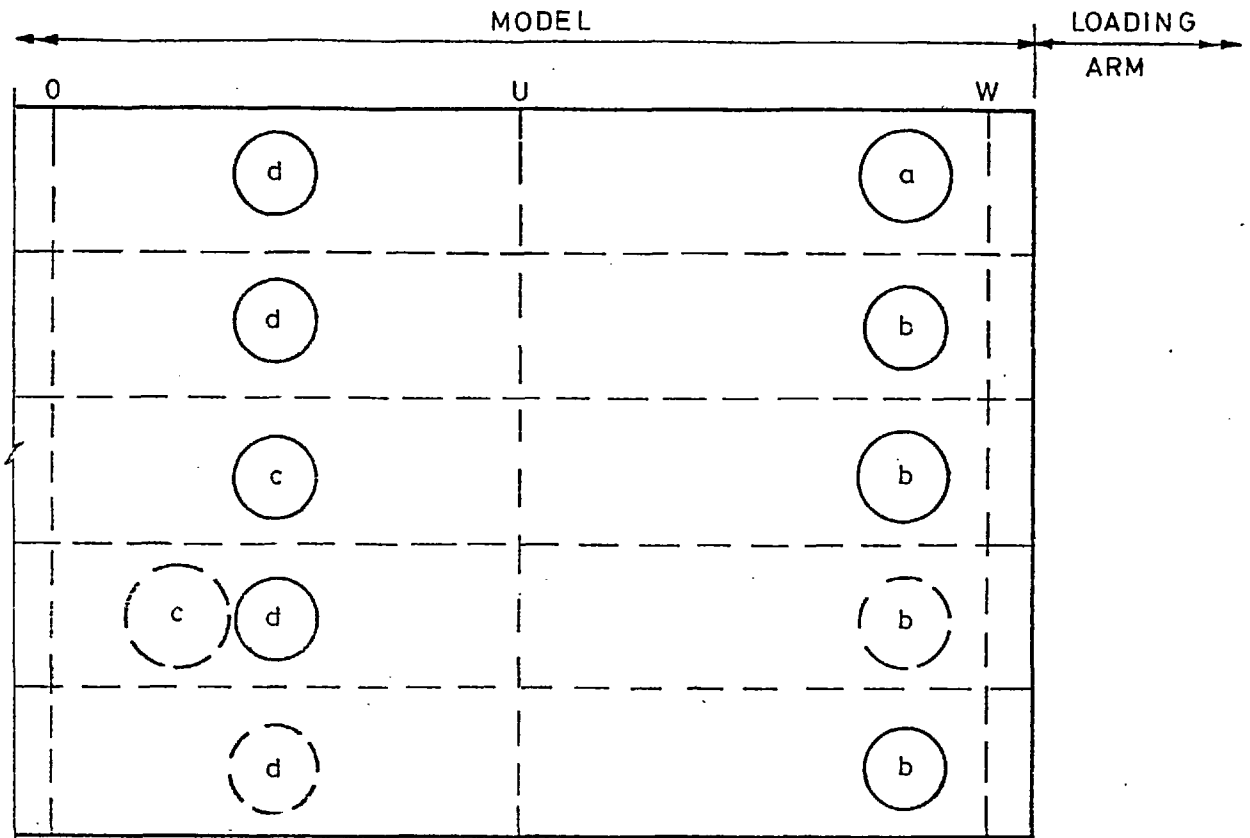


Fig. 57b.
Model 2: Transverse initial deflection profiles of compression flange



a. Test 1, 58.5 tonf
b. Test 1, 60.5 tonf

c. Test 2, 59.0 tonf
d. Test 2, 60.5 tonf

Fig.58 Model 2. Development of compression flange plate panel buckles during the two collapse load tests: the dashed lines indicate outward deflections, the full lines inwards. The load referenced against each deformation indicates the level at which it first developed.

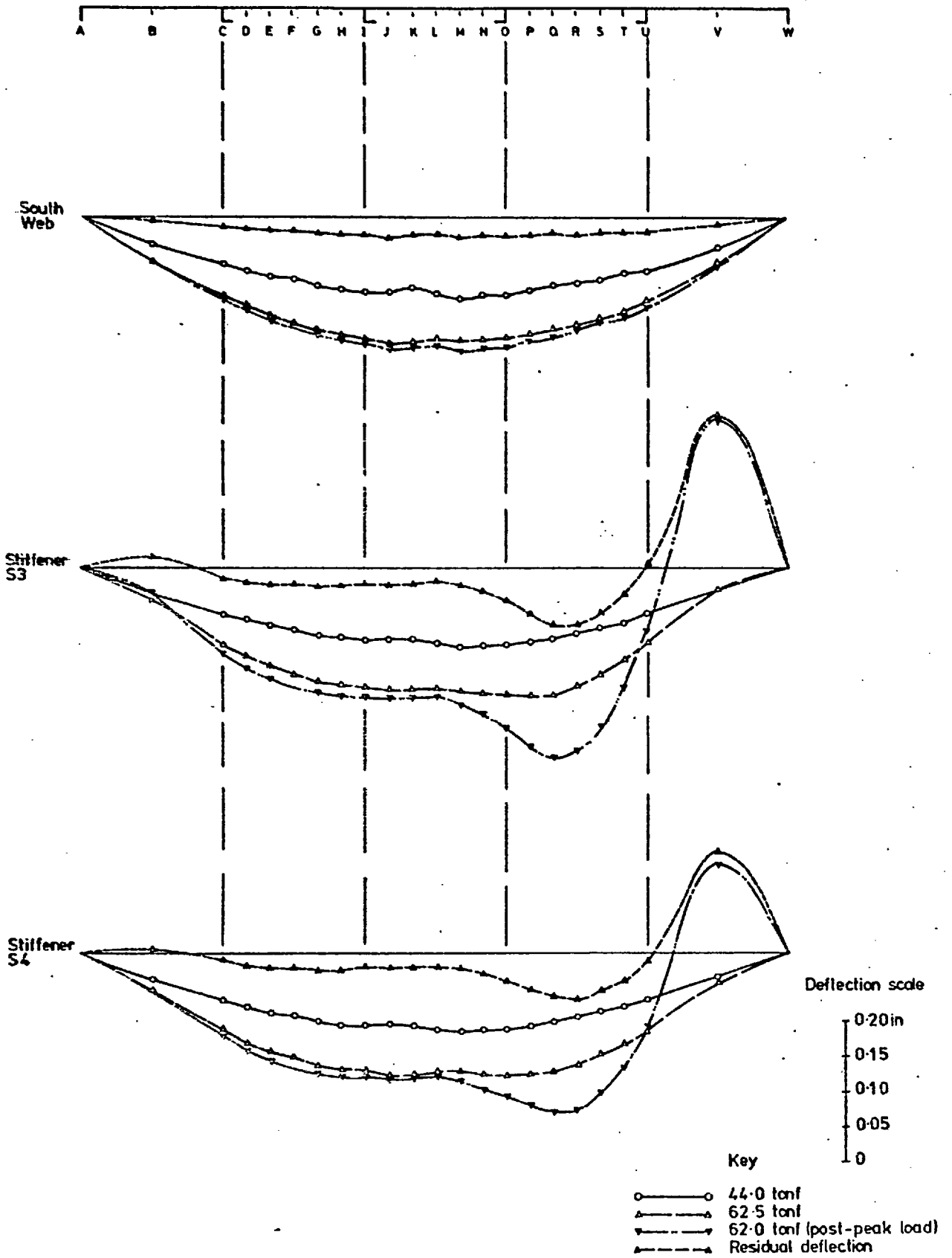


Fig. 59
 Model 2: Longitudinal deflections (Relative to Initial Shape)
 in the first test

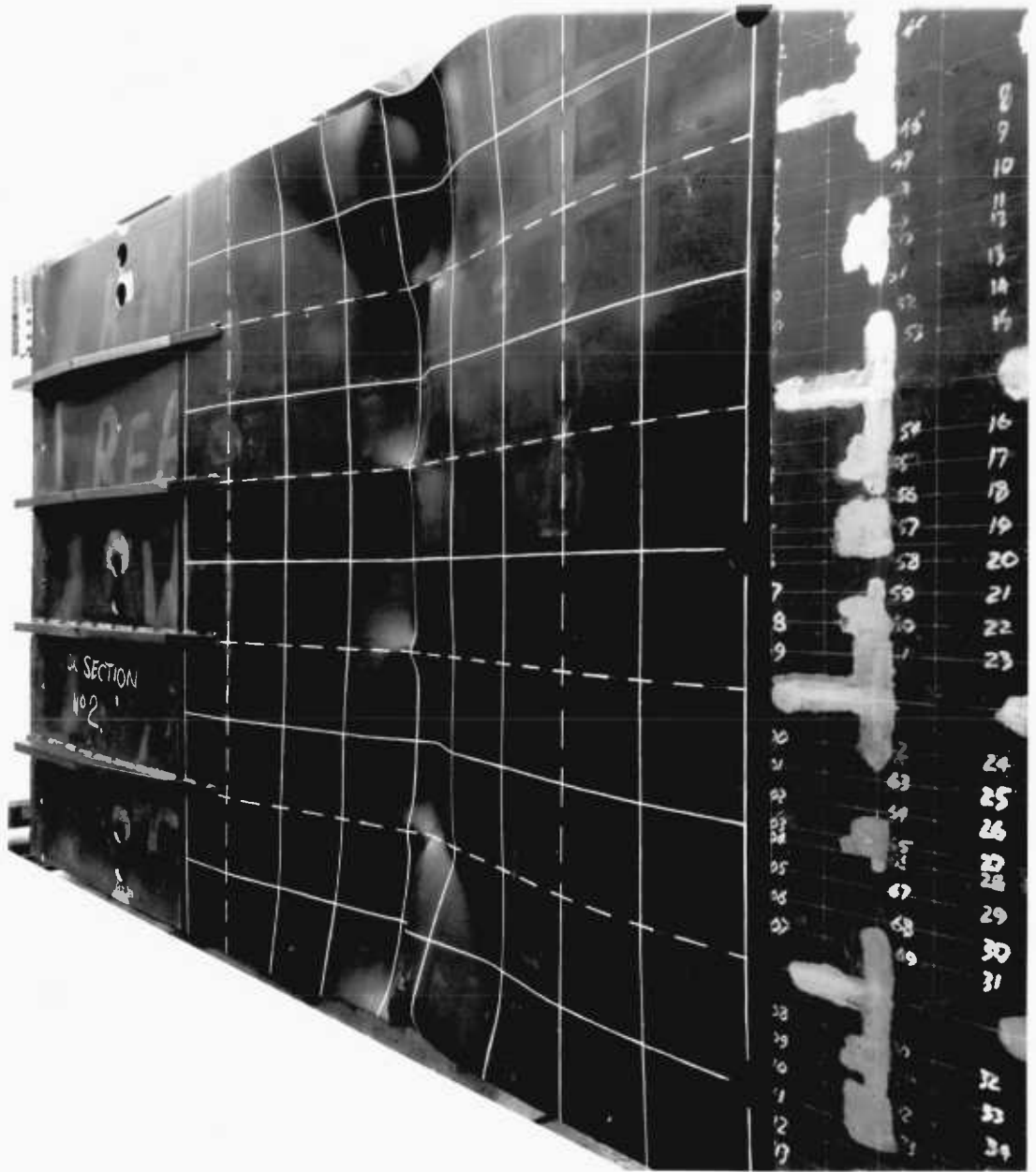
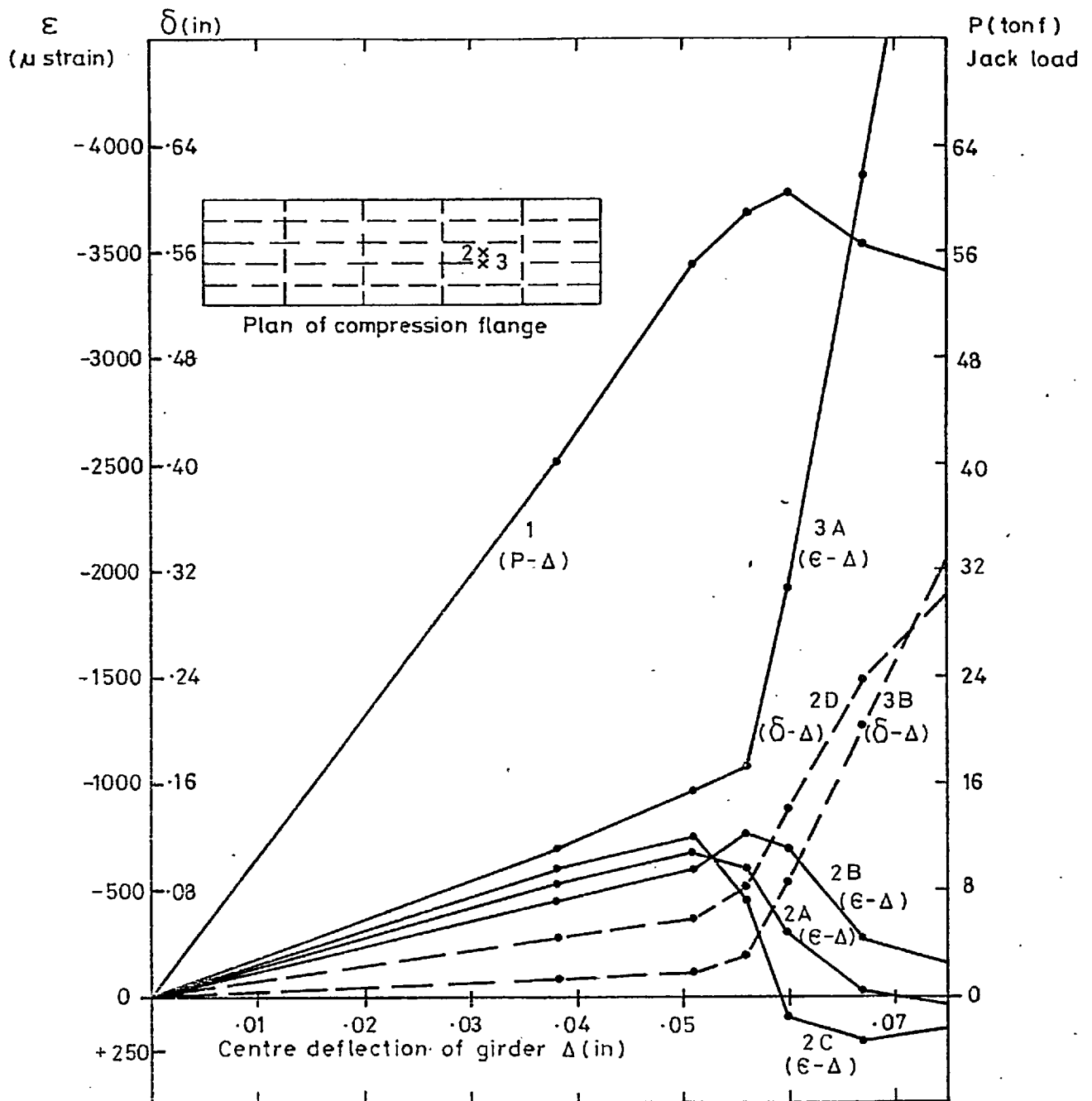


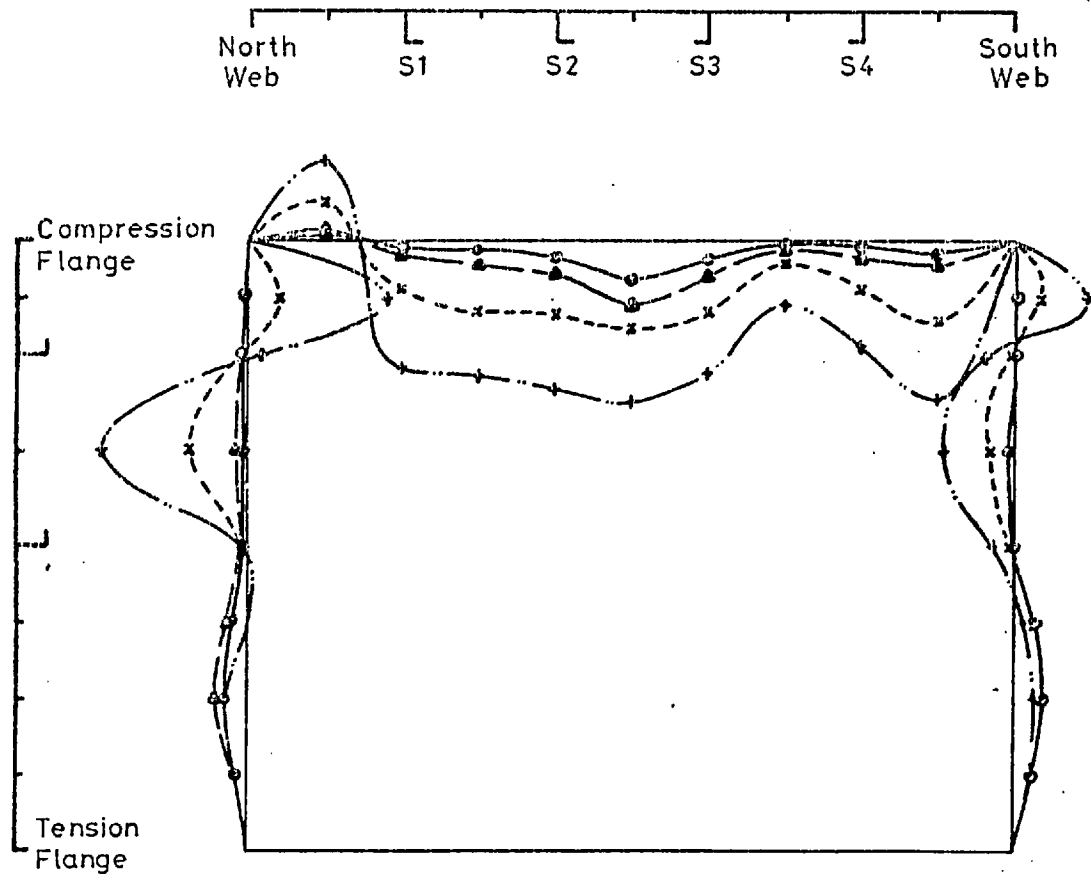
Fig. 60 Model 2 - showing buckles in the compression flange after the second collapse test. After first collapse in the panel adjacent to the end cross-frame, this bay was stiffened as shown. Stiffener locations are indicated by dashed lines.



CURVE 1 OVERALL LOAD-DEFLECTION RELATIONSHIP
 CURVE 2A MID-PLANE STRAIN AT LOCATION 2.
 CURVE 2B INNER SURFACE STRAIN AT LOCATION 2.
 CURVE 2C OUTER SURFACE STRAIN AT LOCATION 2.
 CURVE 2D PLATE PANEL OUT-OF-PLANE DEFORMATION AT LOCATION 2.
 CURVE 3A MID-PLANE STRAIN AT LOCTION 3.
 CURVE 3B STIFFENER OUT-OF- PLANE DEFLECTION AT LOCATION 3.

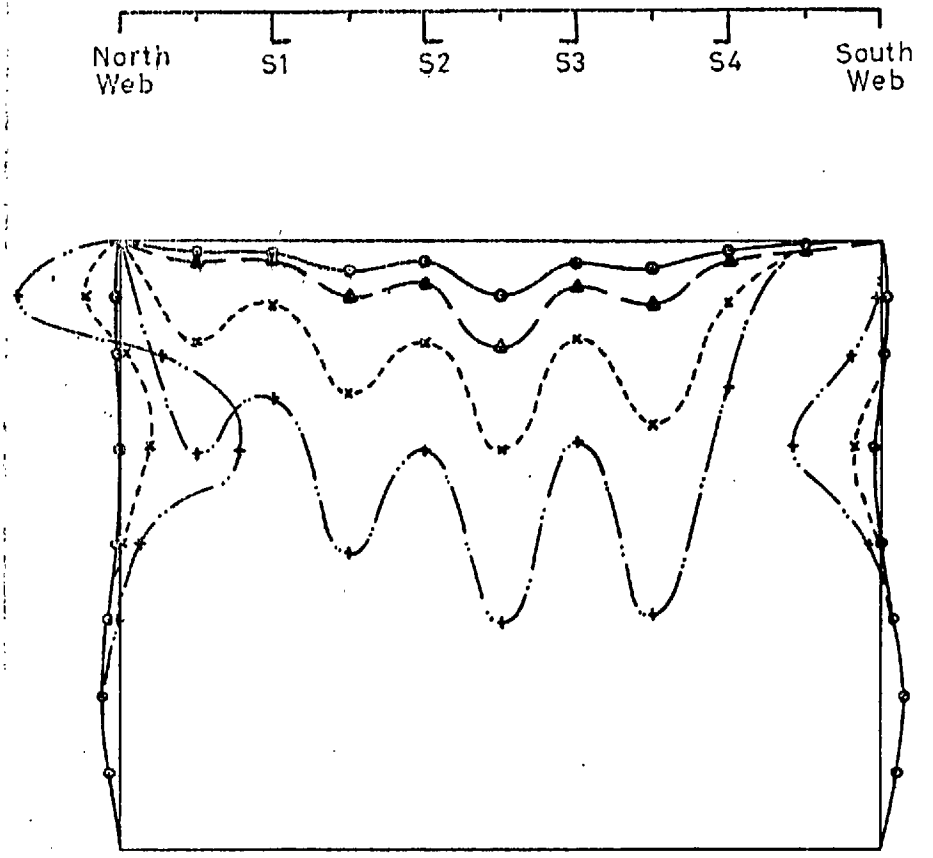
Note : DATUM LOAD WAS 4.0 tonf. THUS TOTAL LOAD ON MODEL IS $(P+4)$ tonf

Fig.61 Growth of deflections and strains with load - Model 2. Test.2.



SECTION Q

- 44.0 tonf
- △— 63.0 tonf
- - - x - - - 64.5 tonf
- · - · - 60.5 tonf (post - peak load)



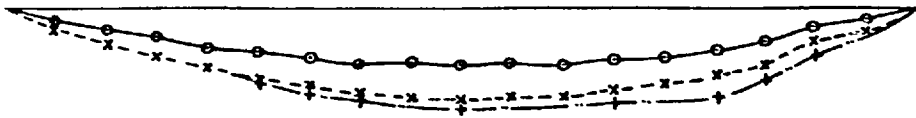
SECTION R

0
100
200
300
400
500
× 10 in

Fig62a. Test 2-Measured transverse deflections. Model 2

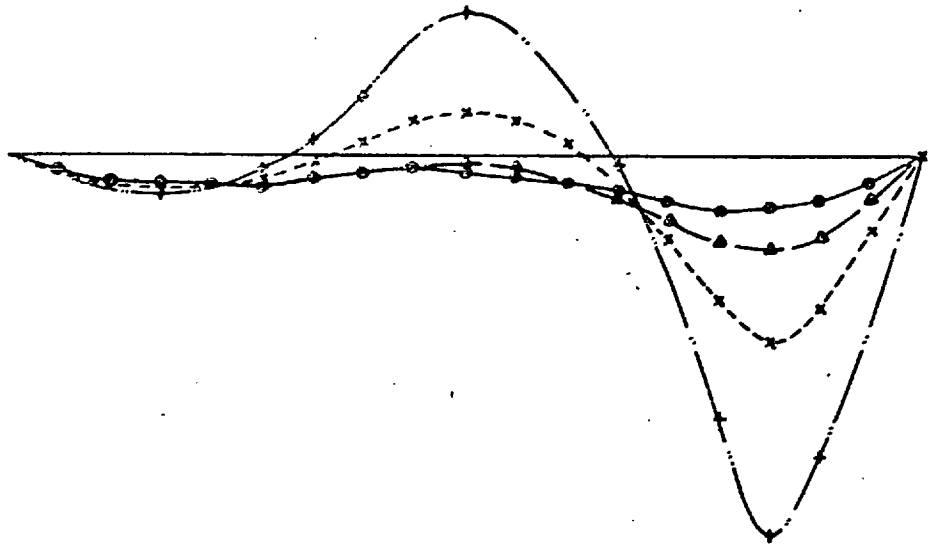
C D E F G H I J K L M N O P Q R S T U

South Web



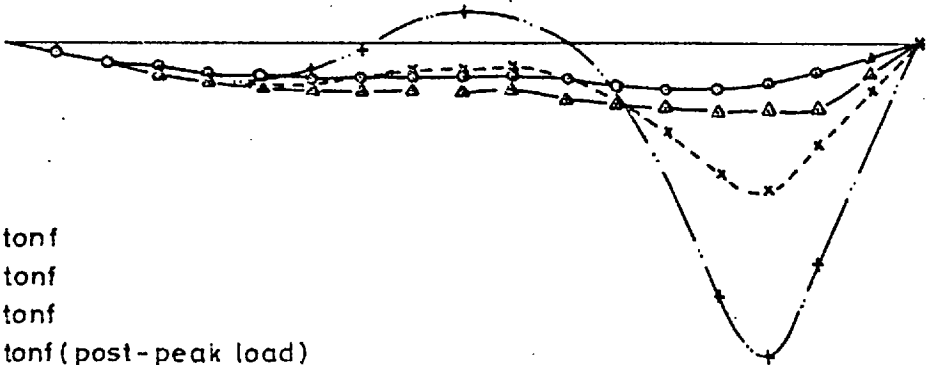
0
50
 $100 \times 10^{-3} \text{ in}$

Stiffener S3



-100
-50
0
50
100
150
200
 $250 \times 10^{-3} \text{ in}$

Stiffener S4



0
50
100
150
 $200 \times 10^{-3} \text{ in}$

- KEY
- 44.0 tonf
 - △—△ 63.0 tonf
 - x—x 64.5 tonf
 - +—+ 60.5 tonf (post-peak load)

Fig 52b Test 2-Measured longitudinal deflections. Model 2.

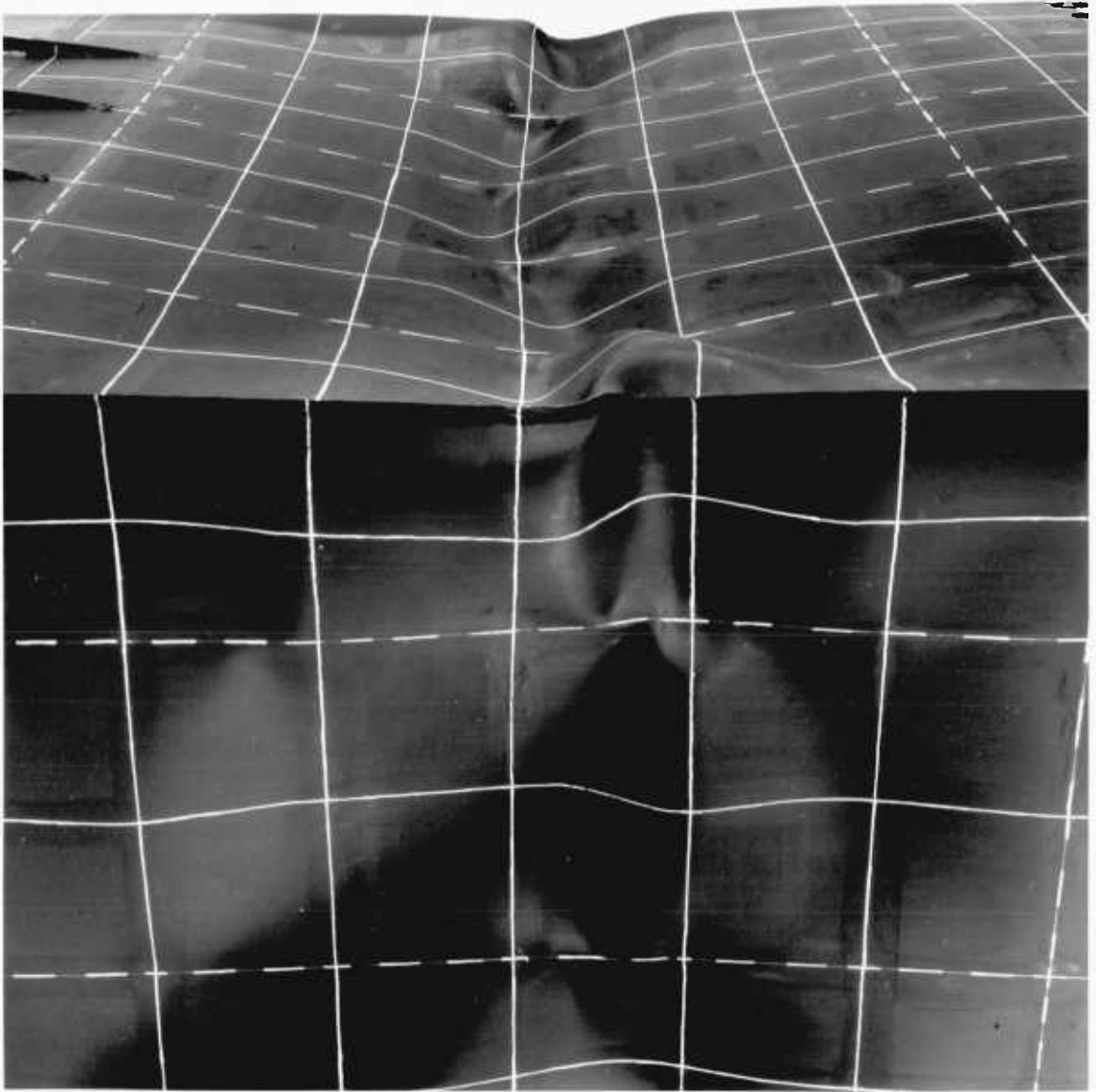


Fig. 63a Model 2 - a close-up view showing the mid-span regions of the compression flange and north web, after second test.

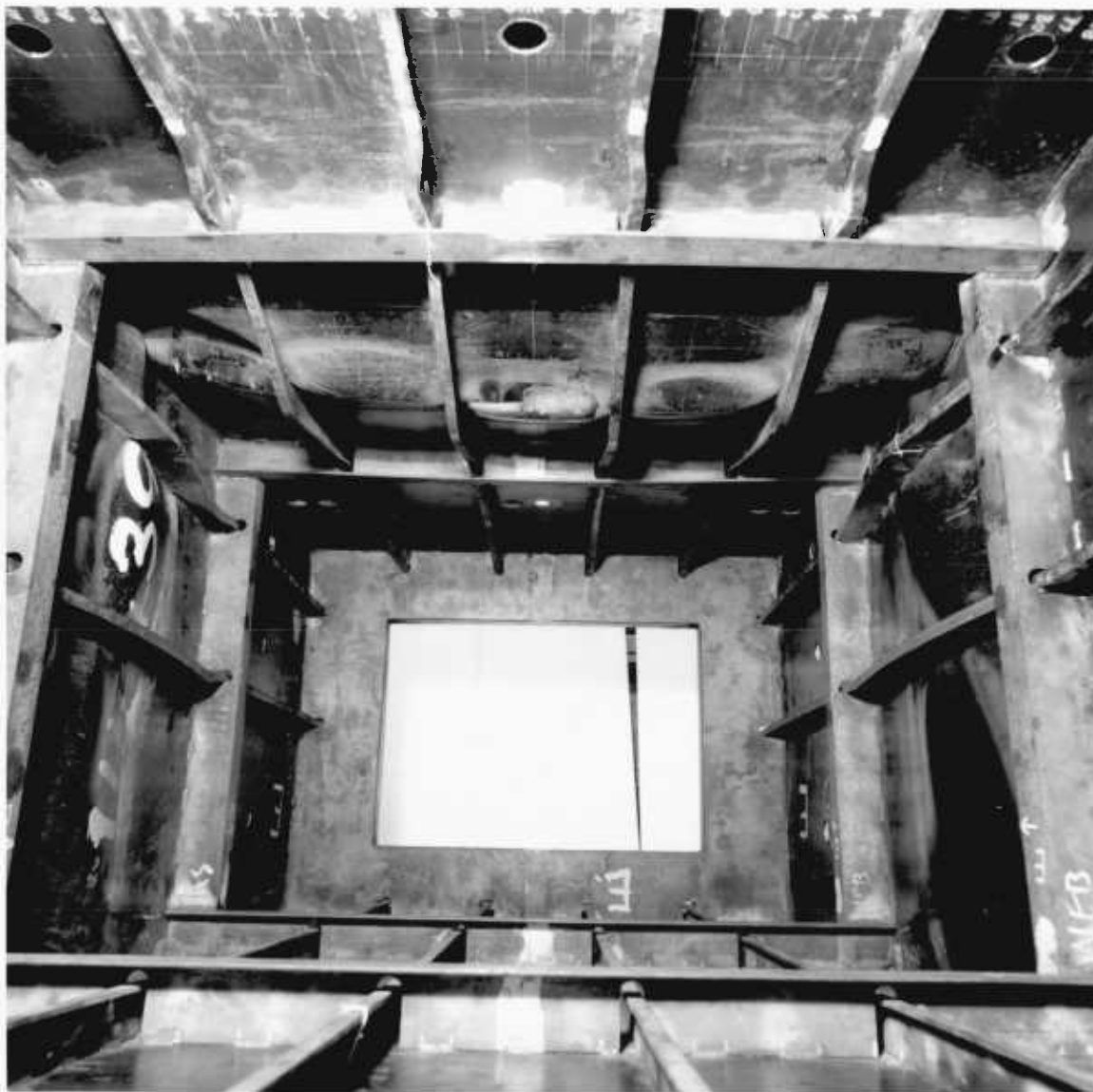


Fig. 63b Model 2 - showing the interior of the model (from end C) after collapse. Note the lateral buckling of longitudinal stiffeners close to the transversals, in the bay adjacent to the critical one.

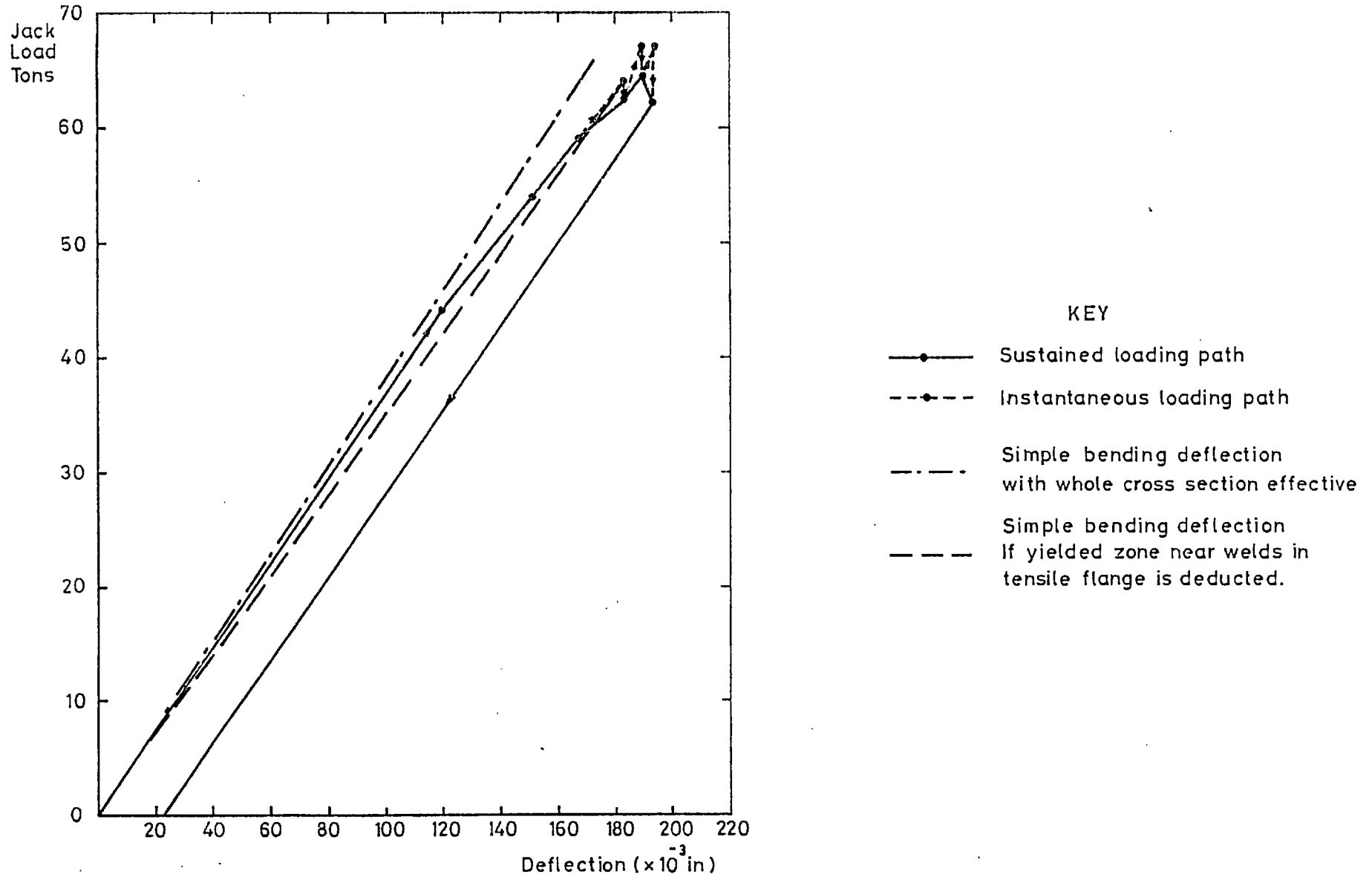


Fig. 64a. Test 1. Load - deflection curve - Model 2.

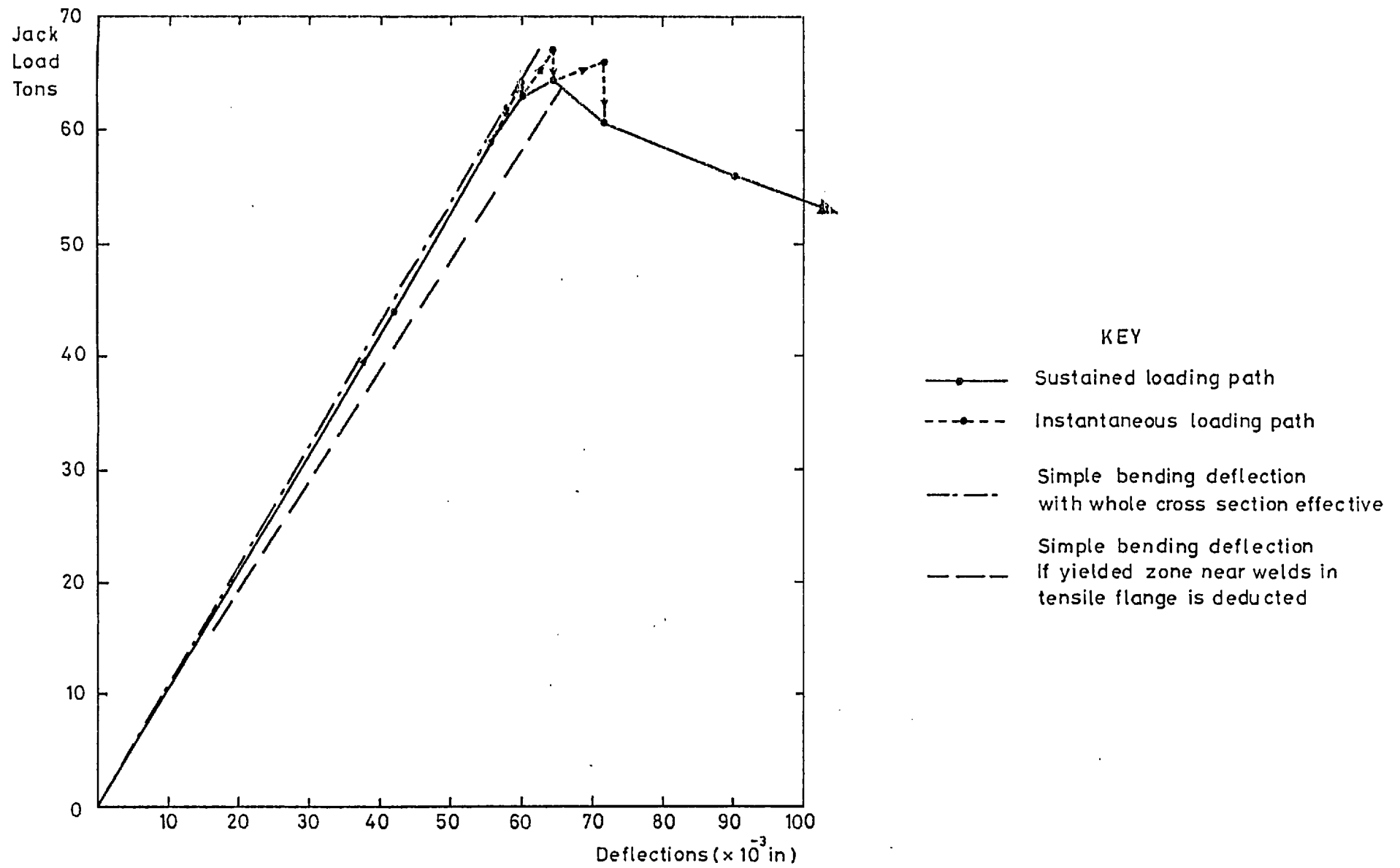
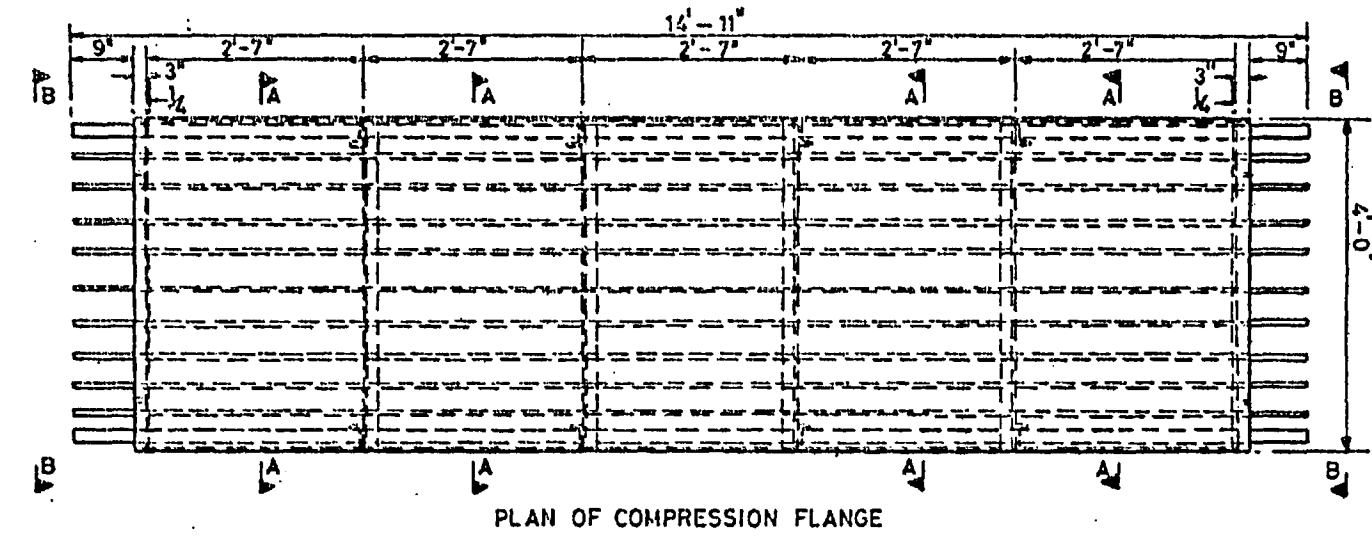
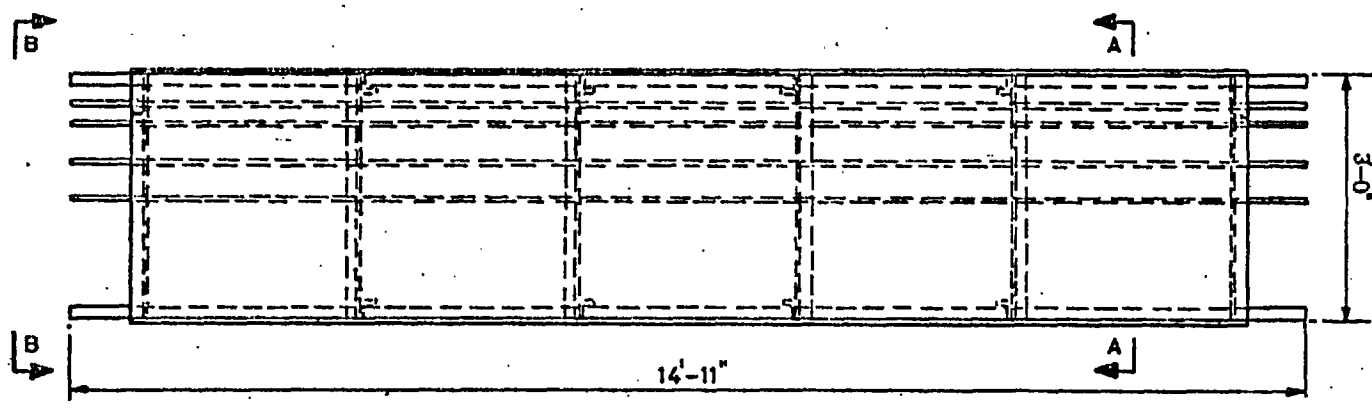


Fig. 64b. Test 2. Load - deflection curve - Model 2.



PLAN OF COMPRESSION FLANGE



SIDE ELEVATION

Fig.65a. Model 4: Plan and elevation

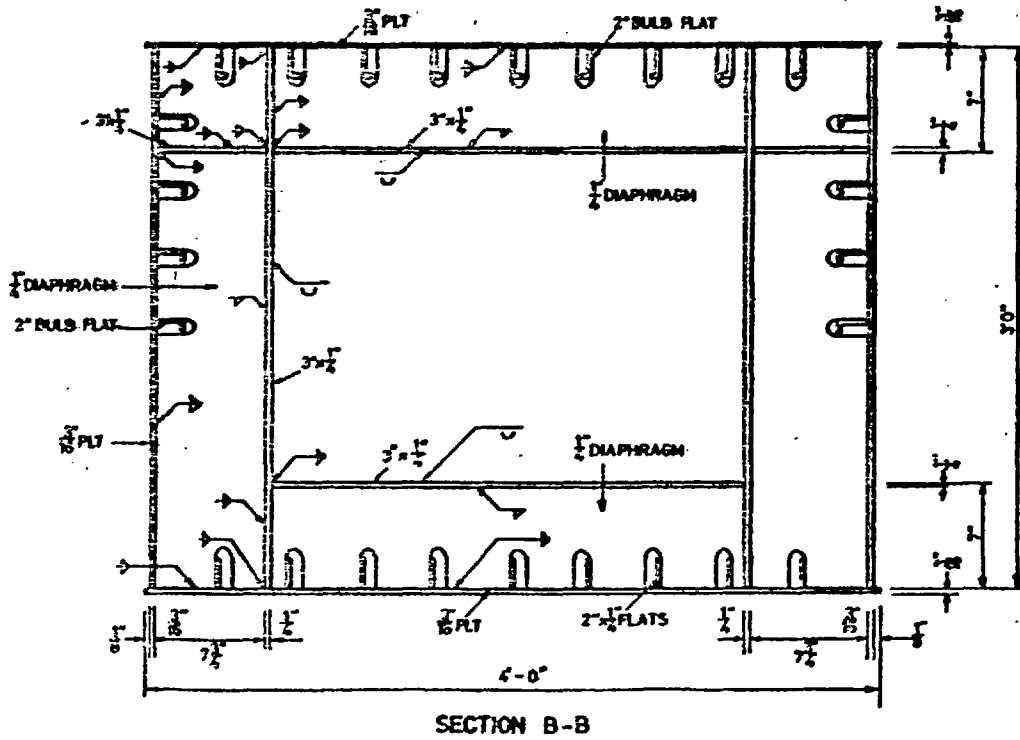
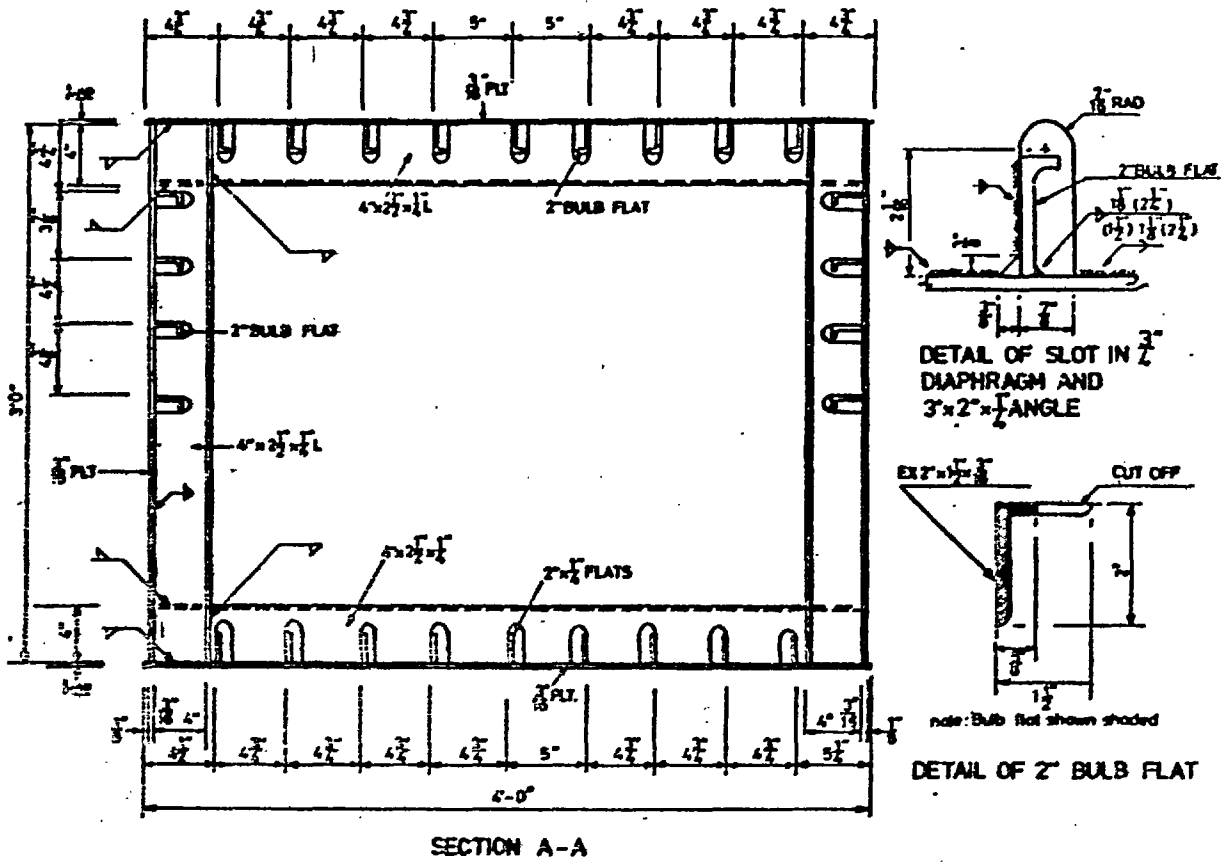


Fig.65 b. Model 4: Cross-sections

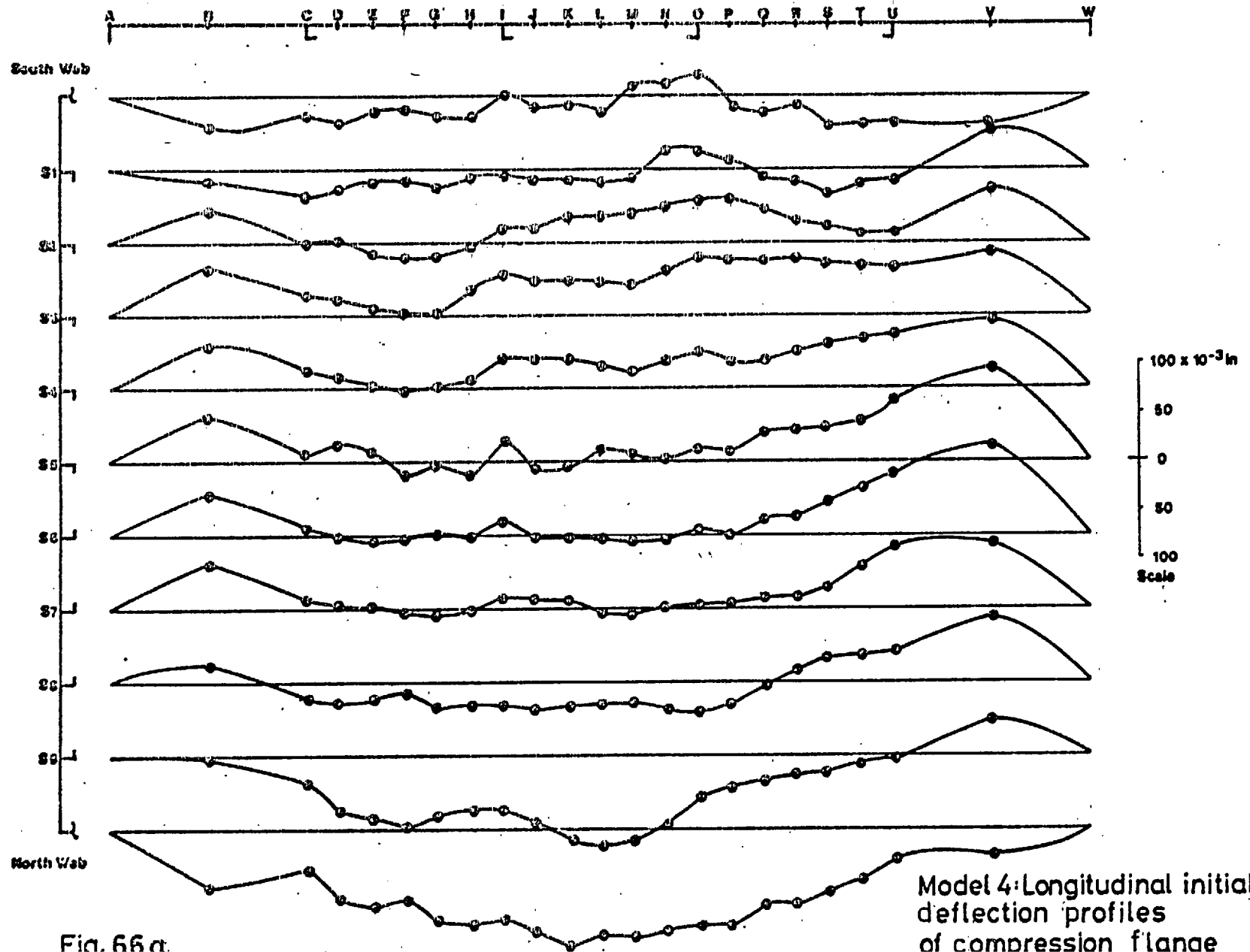


Fig. 66a.

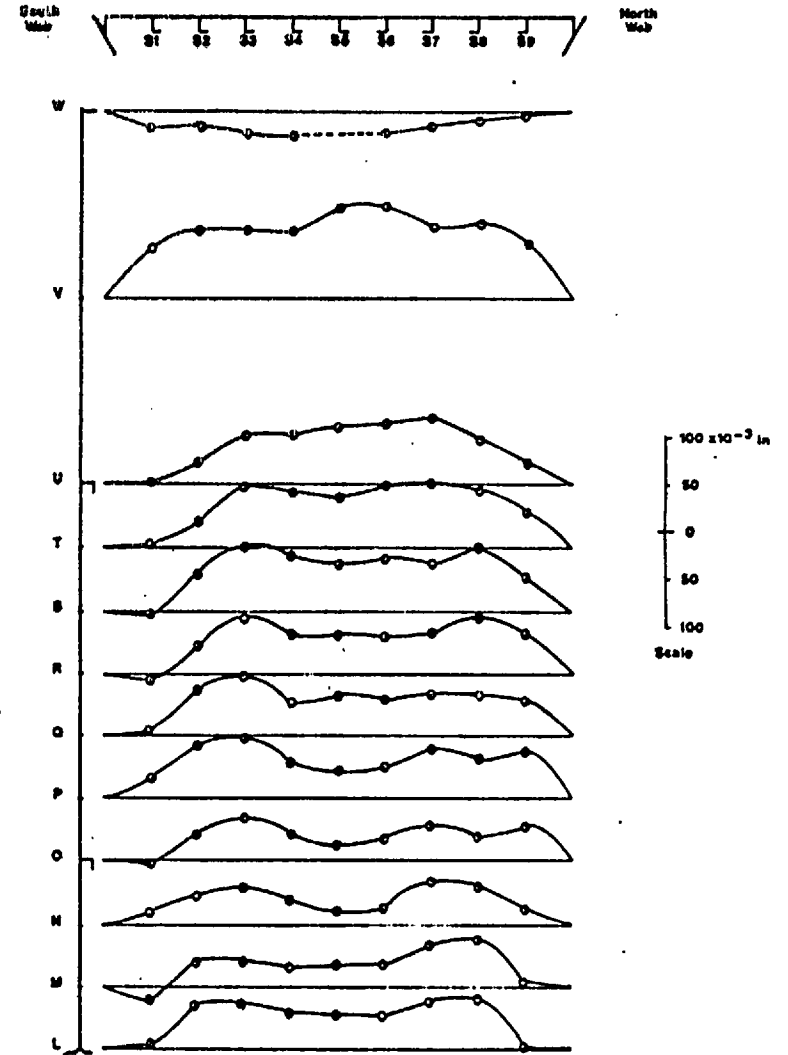
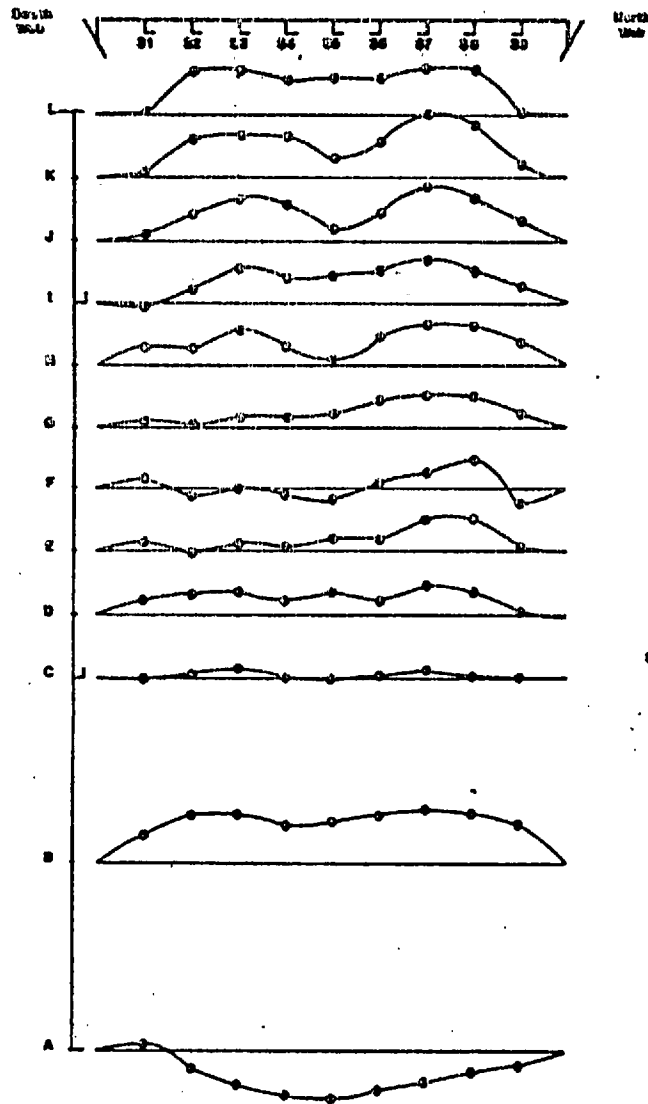


Fig. 66 b.
 Model 4: Transverse initial deflection profiles of compression flange

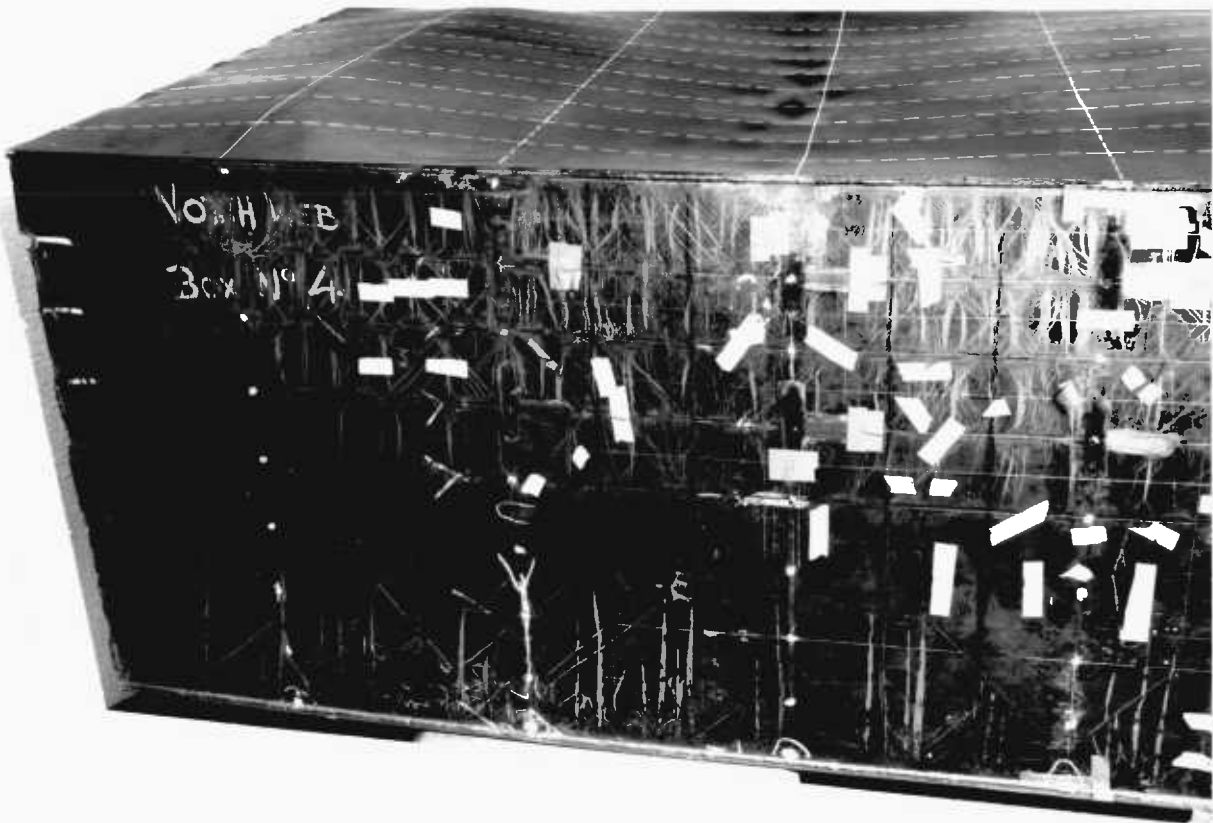


Fig. 67a Model 4 - showing part of the compression flange after the test to failure. Stiffener locations are indicated by dashed lines.

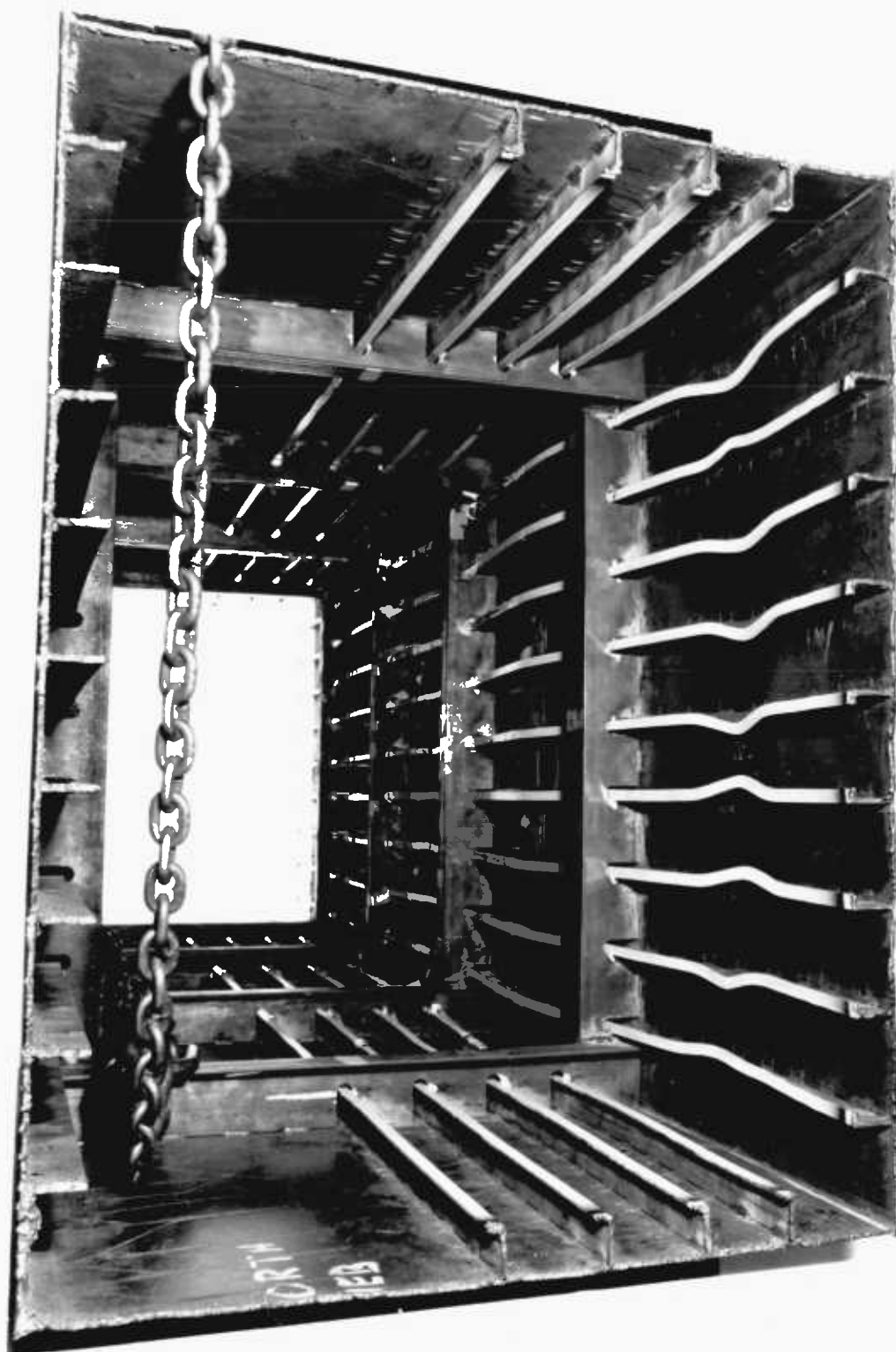


Fig. 67b Model 4 - an interior view of the model after failure.

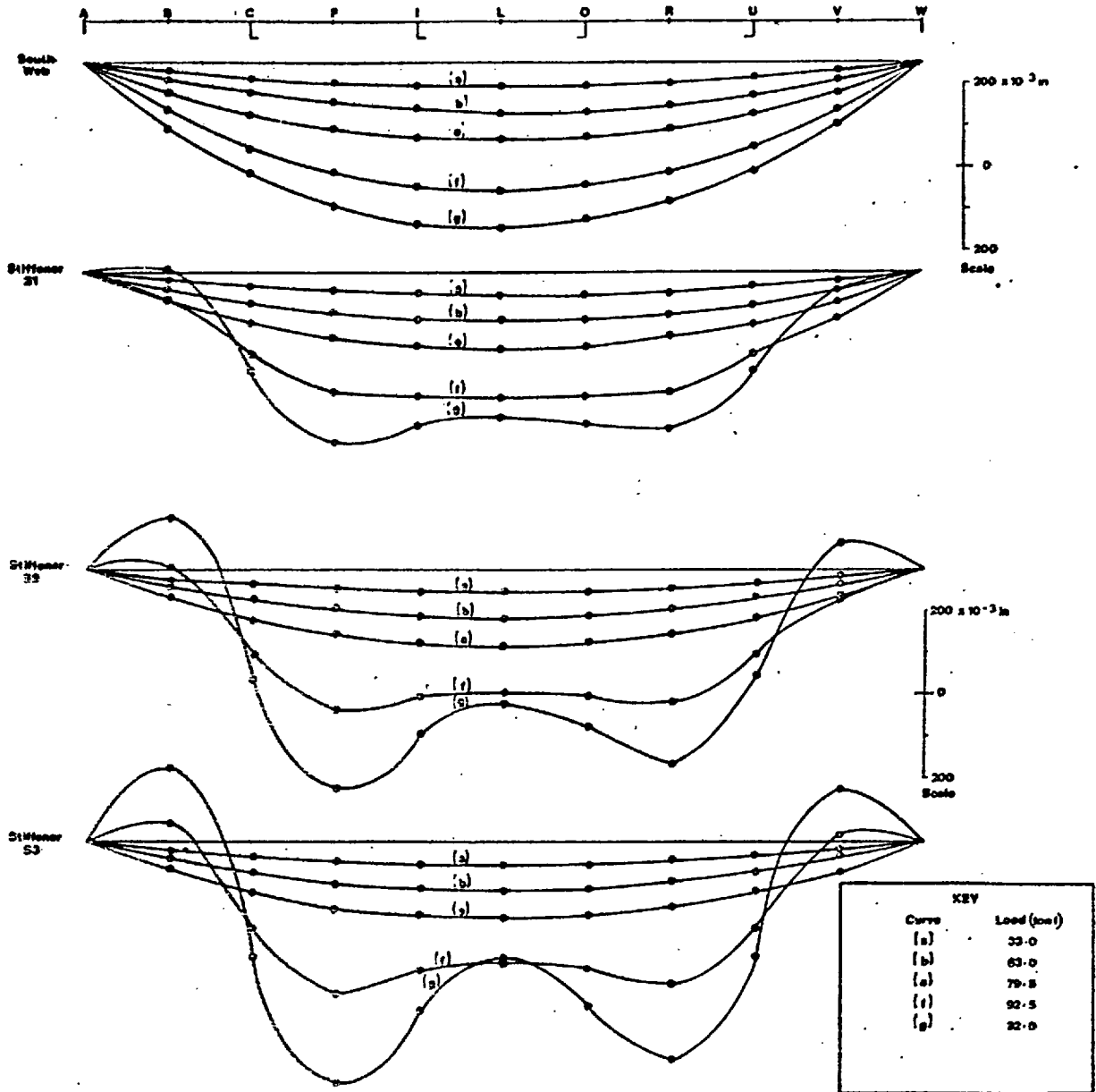


Fig. 68 a Model 4: Longitudinal deflections (Relative to Initial Shape)

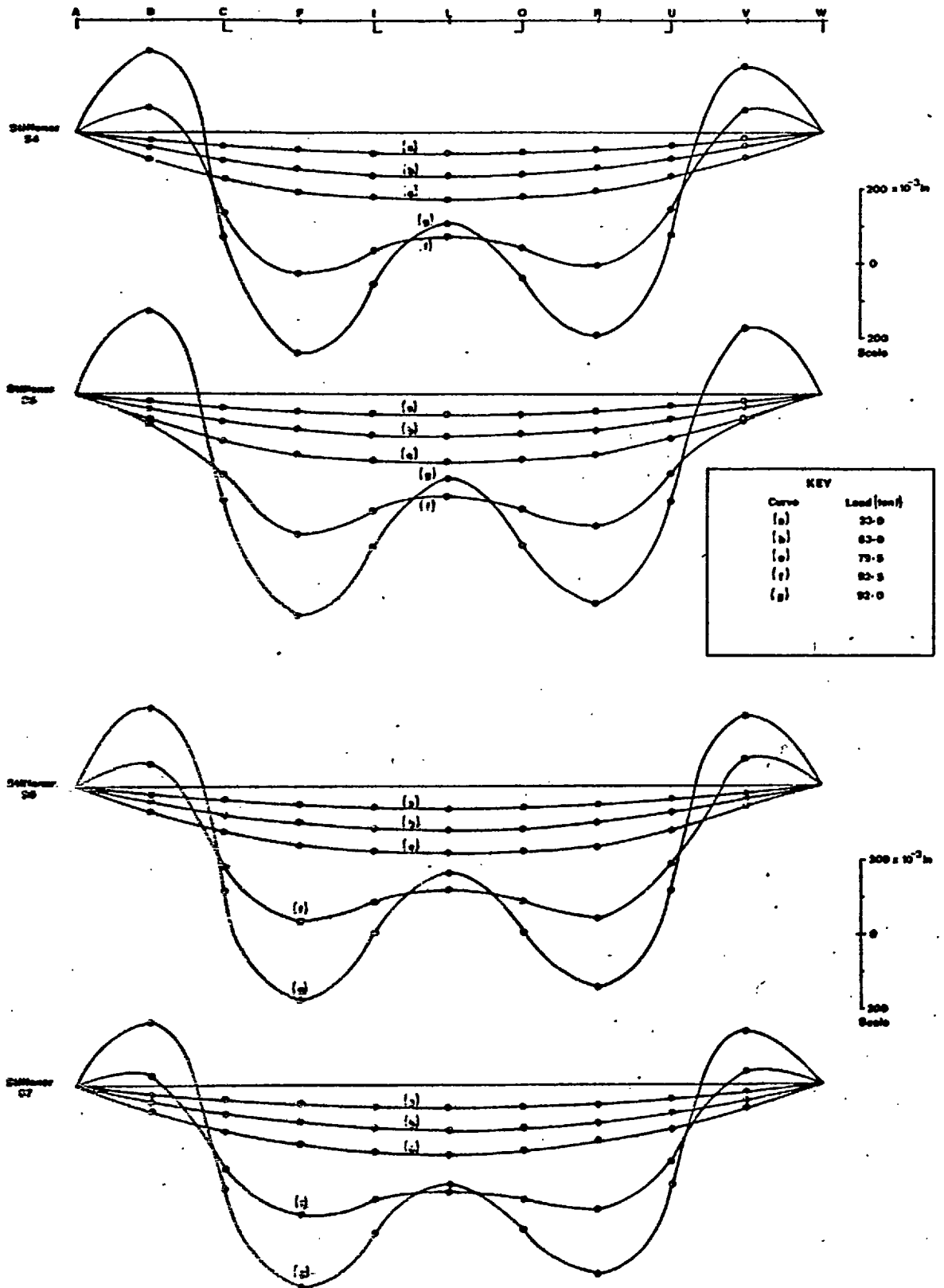


Fig. 58b. Model 4: Longitudinal deflections (Relative to Initial Shape)

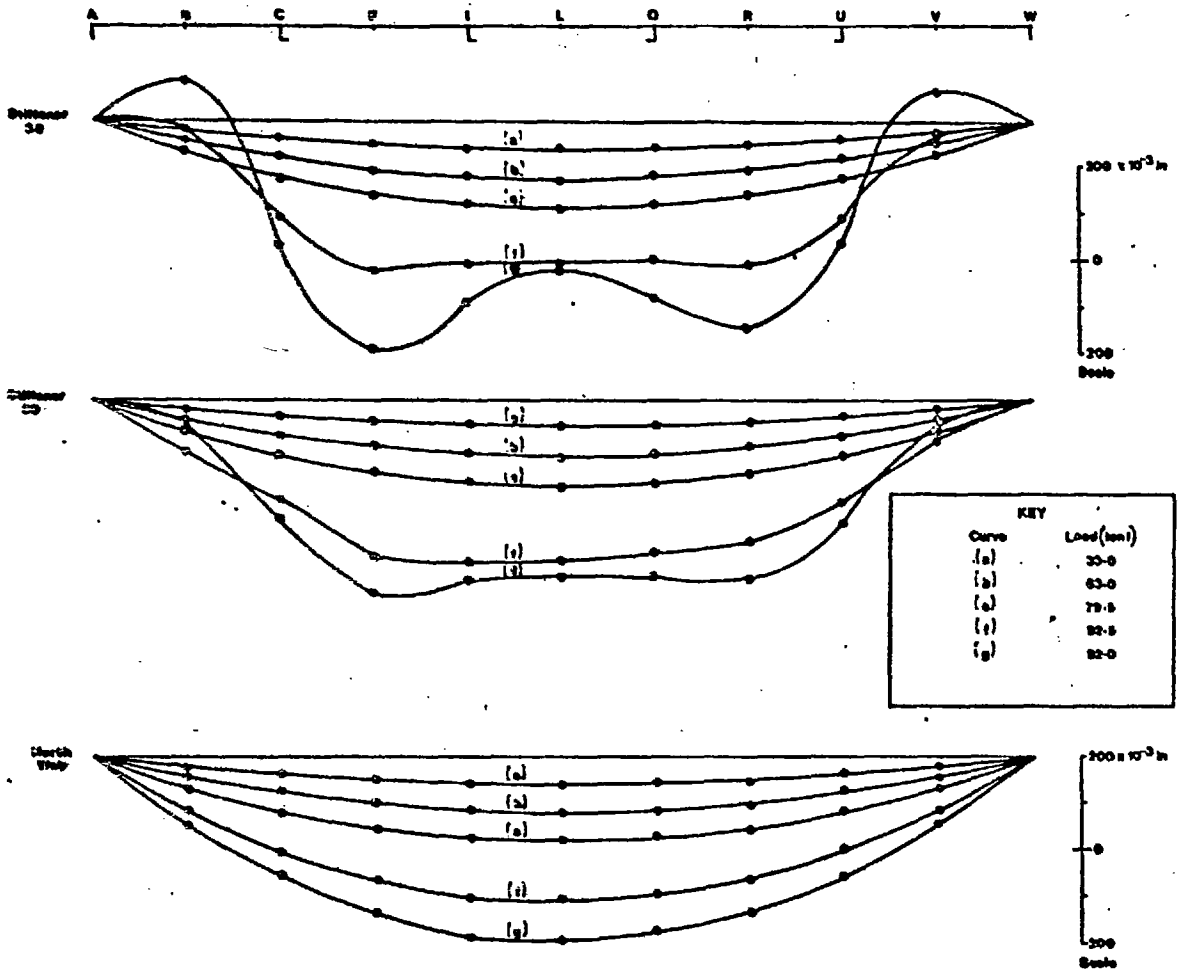
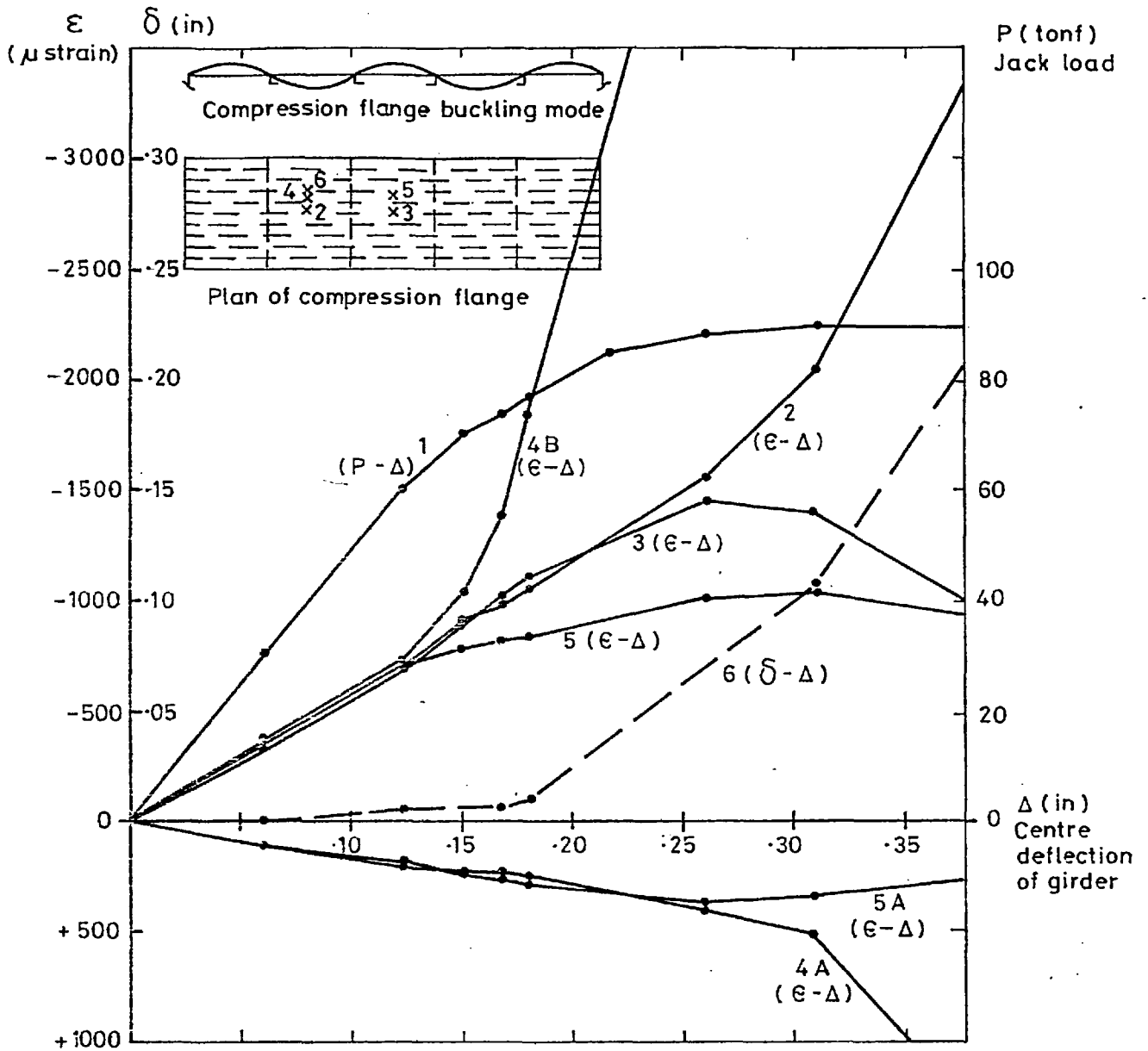


Fig. 68c Model 4: Longitudinal deflections.
(Relative to Initial Shape)



- CURVE 1 OVERALL LOAD - DEFLECTION RELATIONSHIP
 CURVE 2 MID-PLANE STRAIN AT LOCATION 2.
 CURVE 3 MID-PLANE STRAIN AT LOCATION 3.
 CURVE 4A TRANSVERSE MID-PLANE STRAIN AT LOCATION 4.
 CURVE 4B MID-PLANE STRAIN AT LOCATION 4.
 CURVE 5A TRANSVERSE MID-PLANE STRAIN AT LOCATION 5.
 CURVE 5B MID-PLANE STRAIN AT LOCATION 5.
 CURVE 6 STIFFENER OUT-OF-PLANE DEFLECTION AT LOCATION 6.

Note: DATUM LOAD WAS 3 tonf. THUS TOTAL LOAD ON MODEL IS $(P+3)$ tonf

Fig. 69 Growth of deflections and strains with load - Model 4.

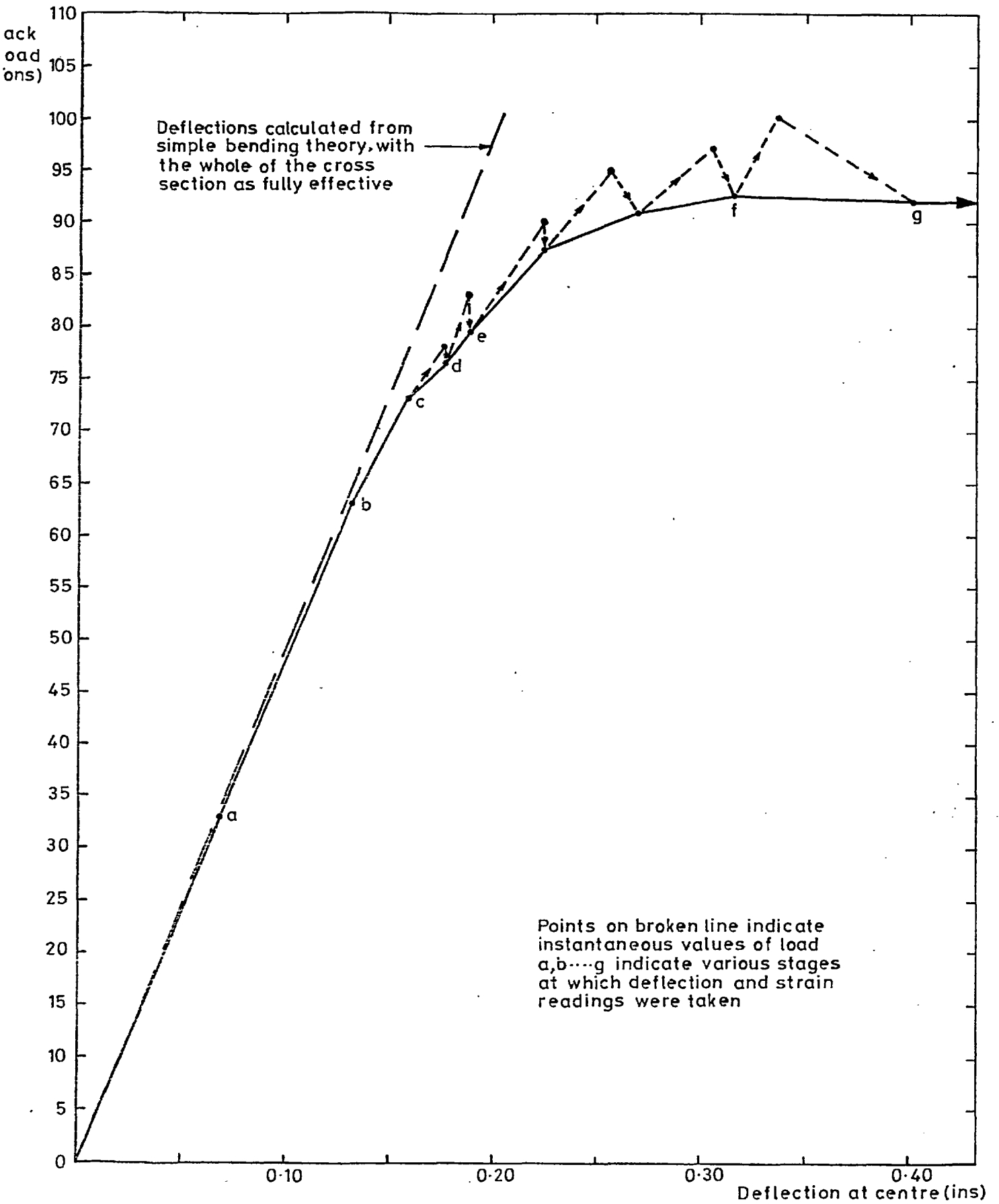
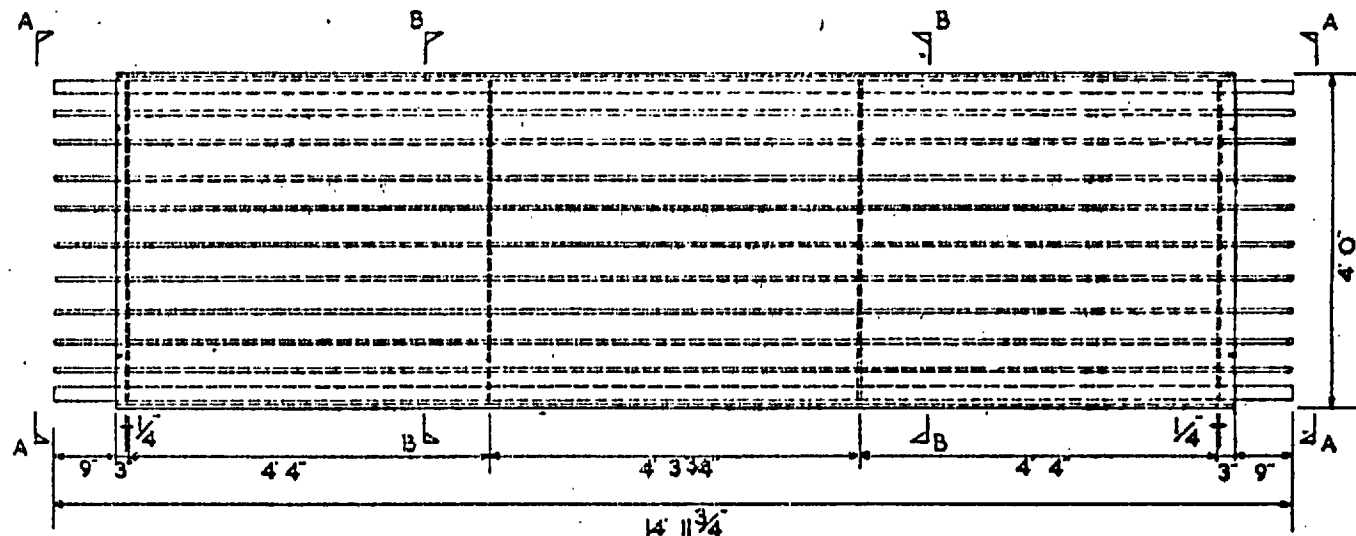
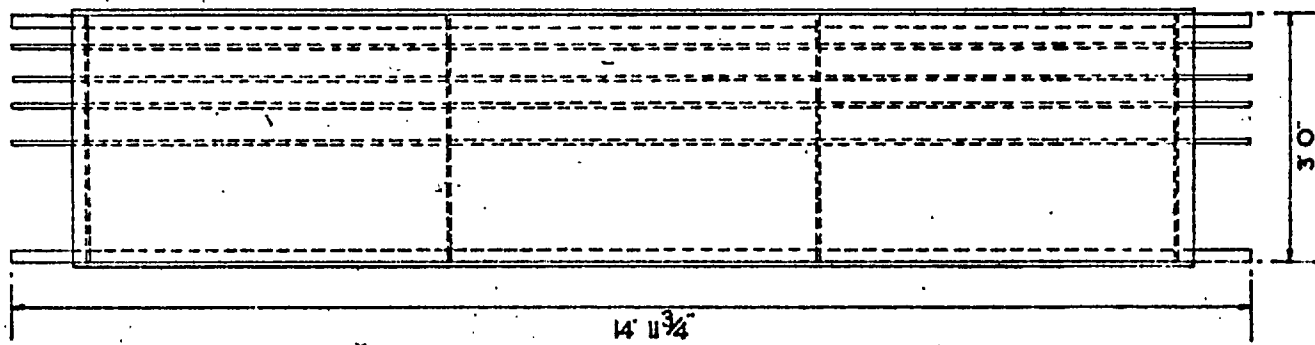


Fig. 70 Load-deflection curve - Model 4.

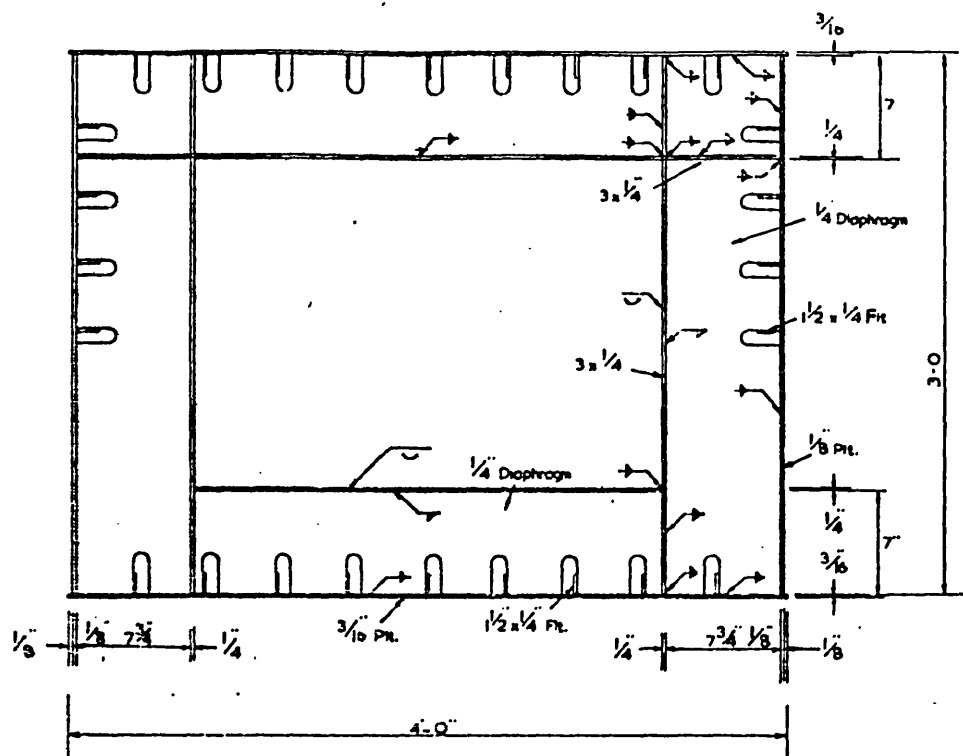


PLAN OF COMPRESSION FLANGE



SIDE ELEVATION

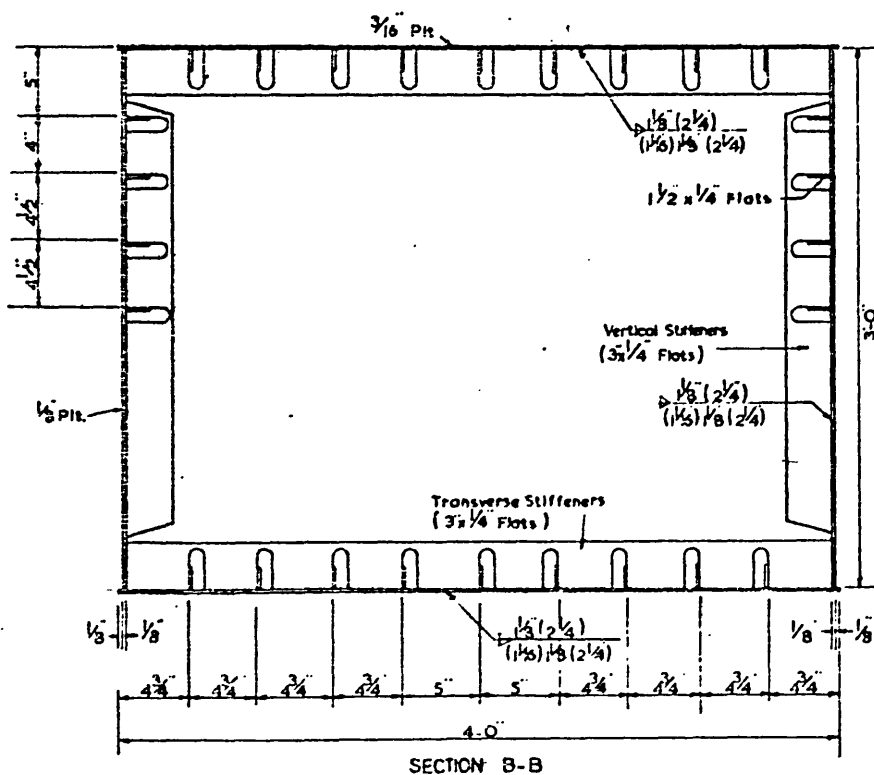
Fig. 71.a Model 8: Plan and elevation



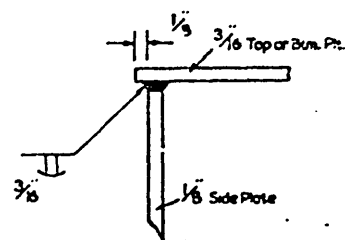
NOTES

- 1 Unless noted otherwise all welds are $\frac{1}{8}$ " fillet welds (measured across throat).
- 2 $1\frac{1}{2}$ " x $1\frac{1}{2}$ " Flats are continuous throughout the length of the model

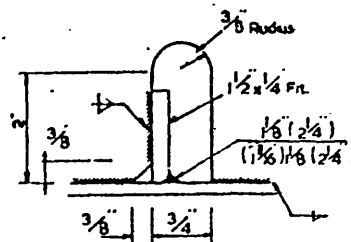
SECTION A-A



SECTION B-B

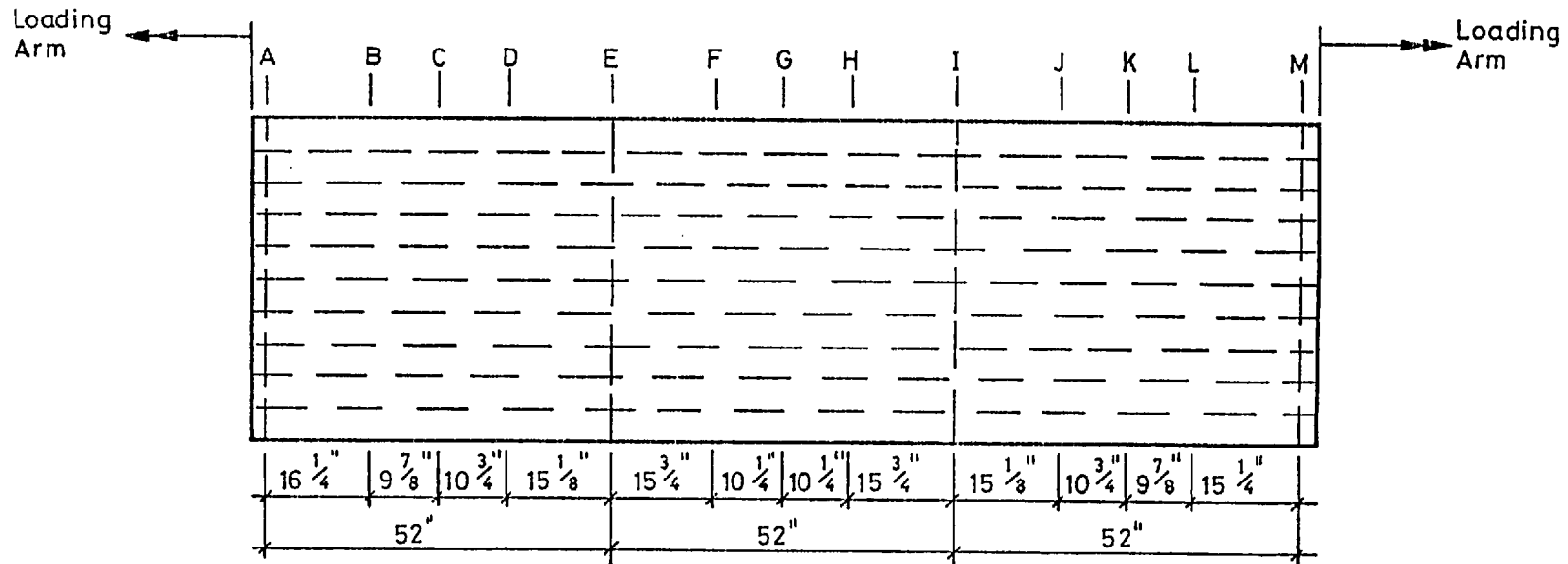


WELDING DETAIL AT CORNER OF BOX GIRDER

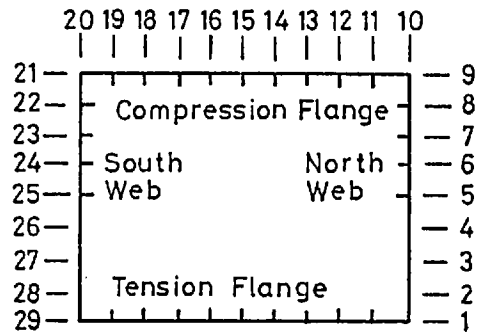


DETAIL OF SLOT IN $\frac{1}{4}$ " DIAPHRAGM, VERTICAL AND TRANSVERSE STIFFENERS

Fig. 71b Model 8: Cross - sections



PLAN OF COMPRESSION FLANGE



CROSS SECTION OF MODEL 8
(viewed from end A)

Note:
Letters A to M indicate
locations along the model

Fig. 72 Details of reference grid - Model 8

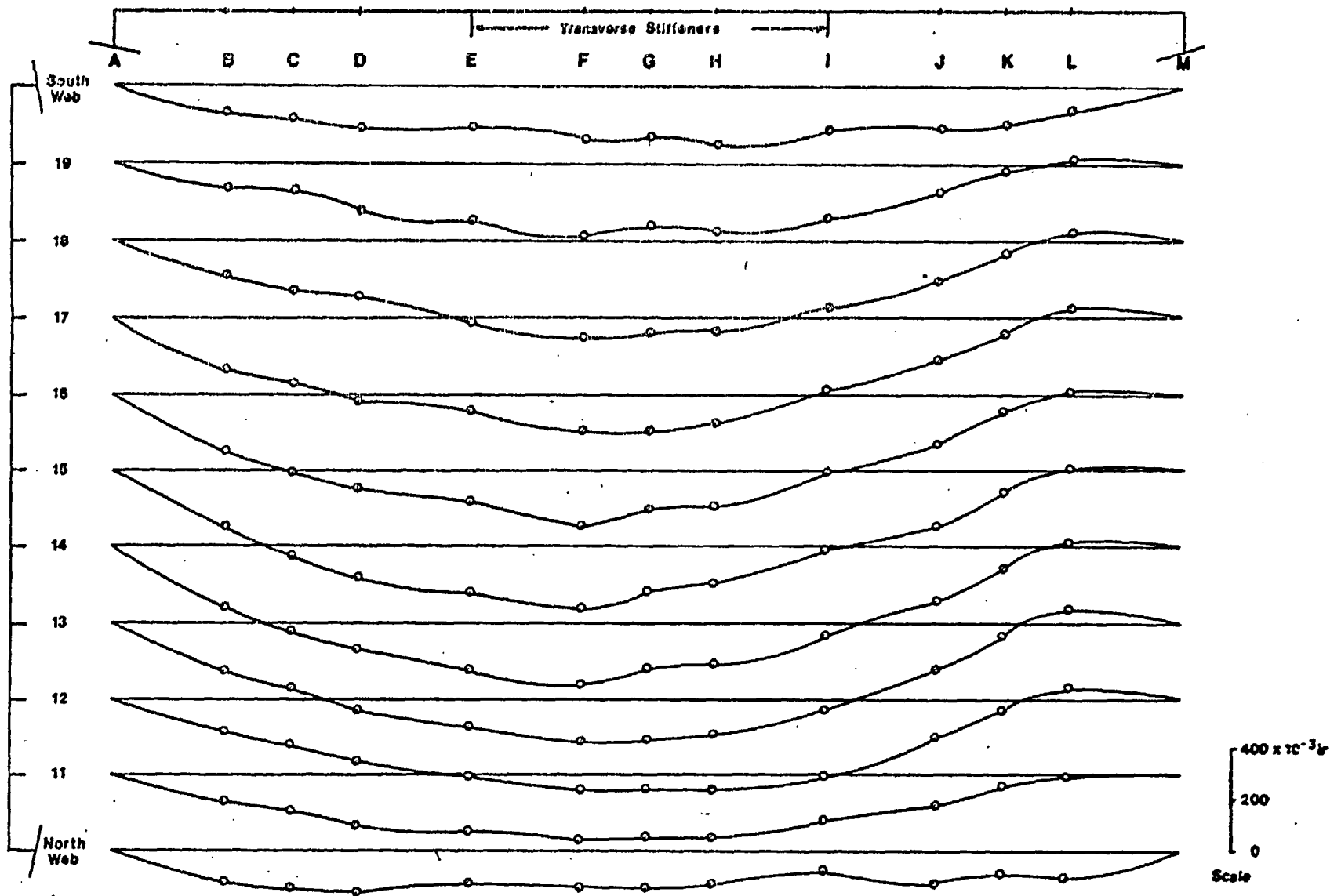


Fig.73a. Model 8: Longitudinal initial deflection profiles of compression flange

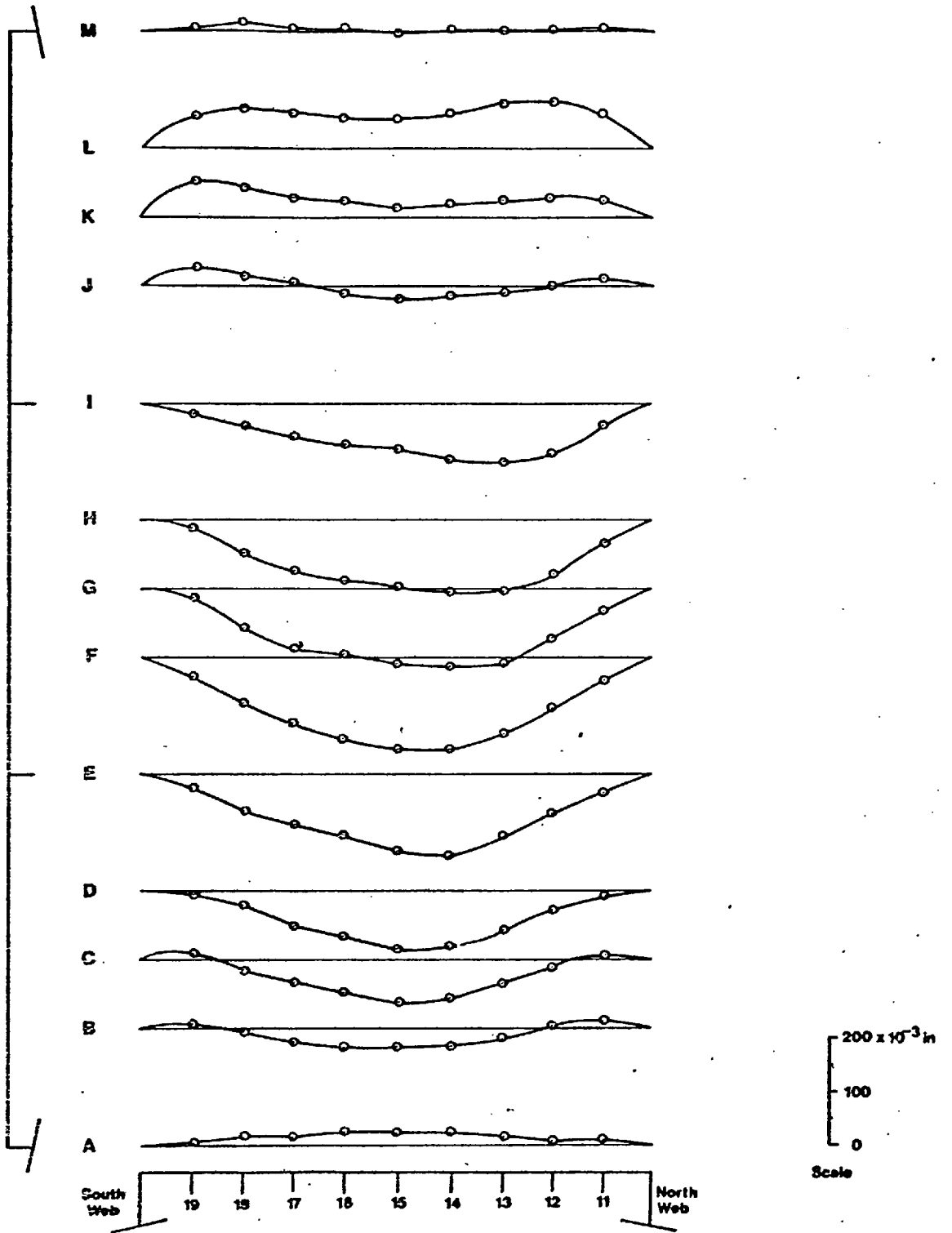
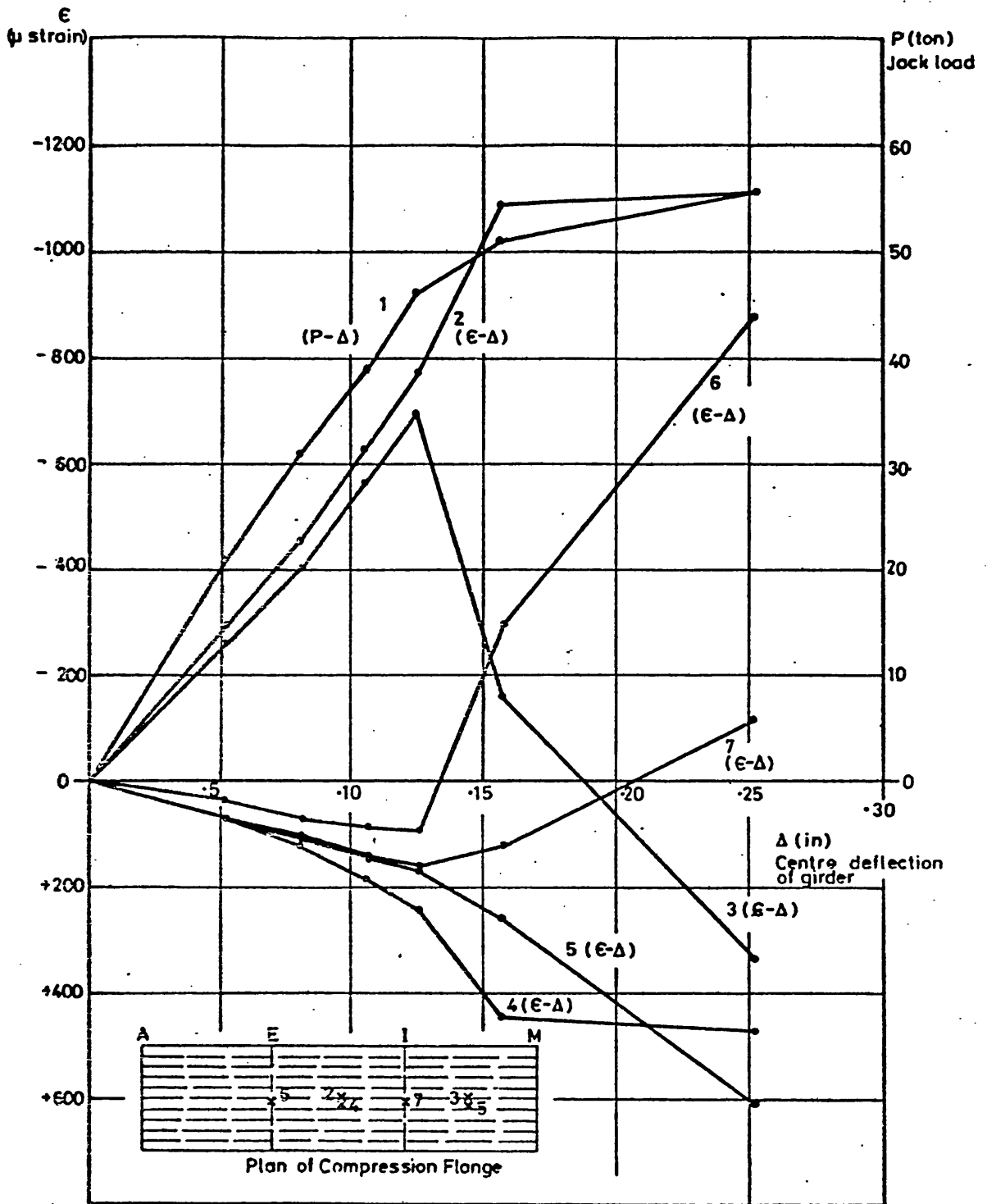


Fig. 73b. :
Model 8: Transverse initial deflection profiles of compression flange



- CURVE 1 OVERALL LOAD-DEFLECTION RELATIONSHIP
- CURVE 2 MID-PLANE STRAIN AT LOCATION 2
- CURVE 3 MID-PLANE STRAIN AT LOCATION 3
- CURVE 4 TRANSVERSE MID-PLANE STRAIN AT LOCATION 4
- CURVE 5 TRANSVERSE MID-PLANE STRAIN AT LOCATION 5
- CURVE 6 TRANSVERSE MID-PLANE STRAIN AT LOCATION 6
- CURVE 7 TRANSVERSE MID-PLANE STRAIN AT LOCATION 7

Fig. 74 Model 8. Growth of deflections and strains with load.

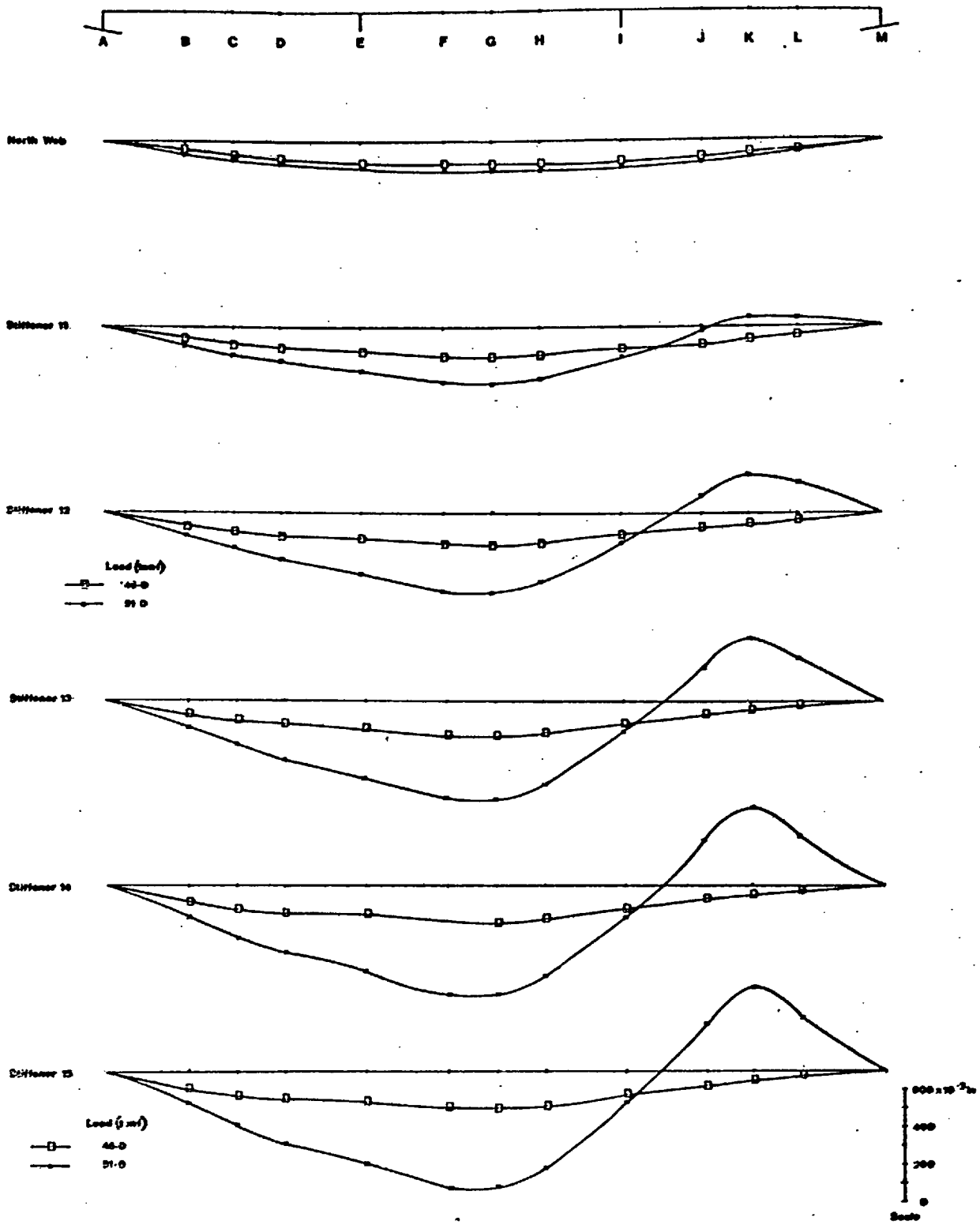


Fig.75a. Model 8: Longitudinal deflections (Relative to Initial Shape)

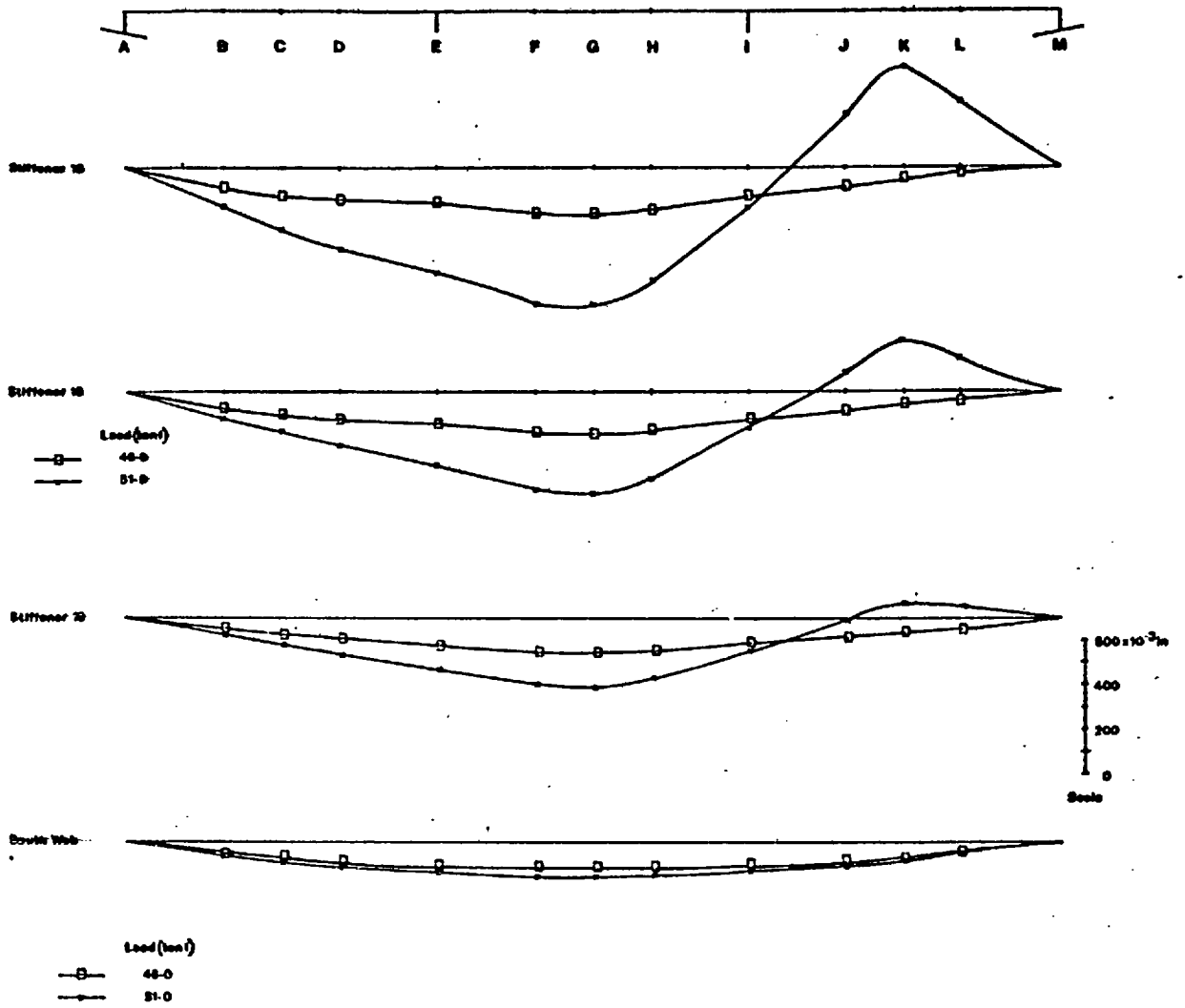


Fig.75b Model 8: Longitudinal deflections (Relative to Initial Shape)

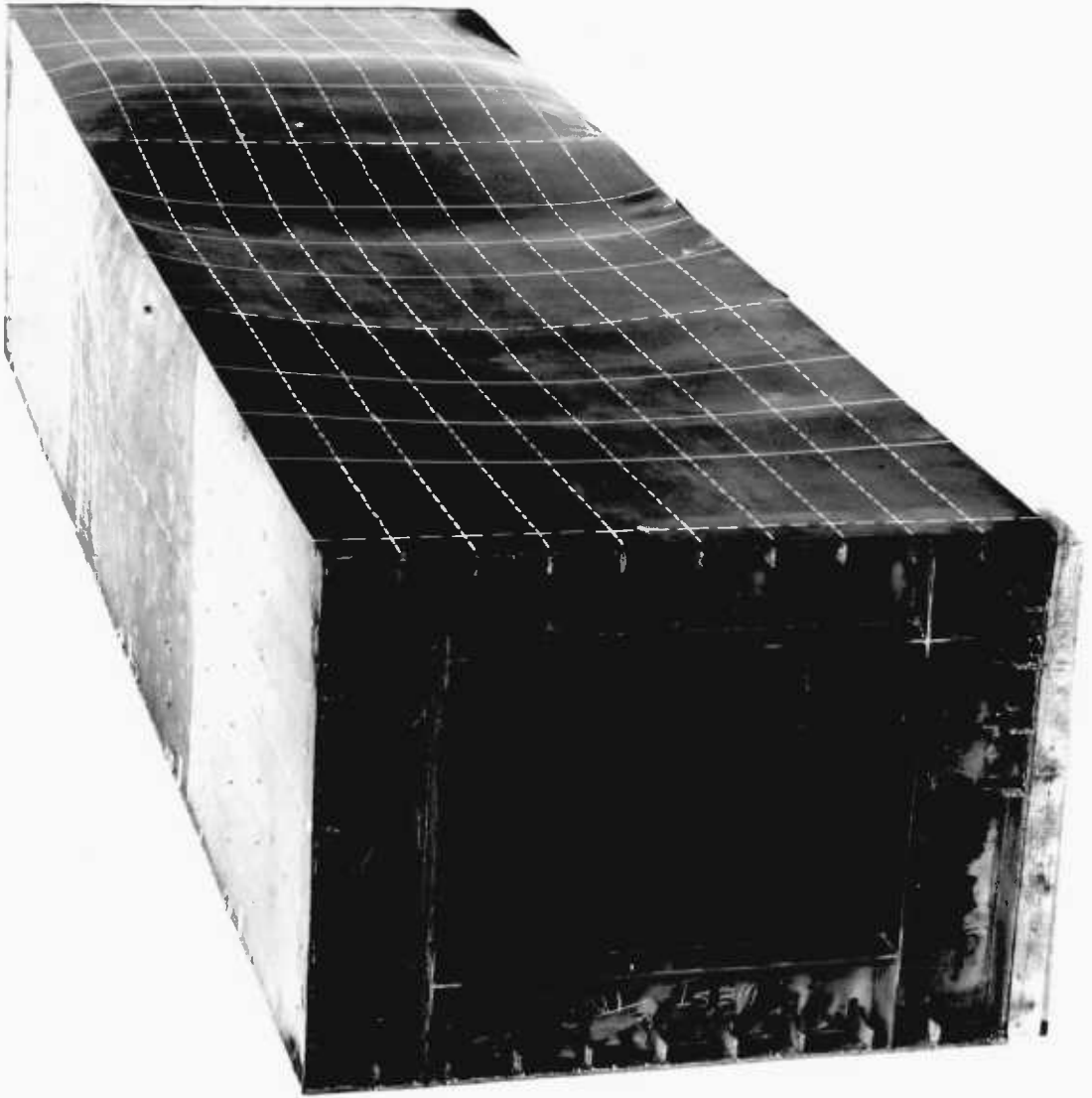


Fig. 76a Model 3 - showing overall buckled shape of the flange after the collapse test.

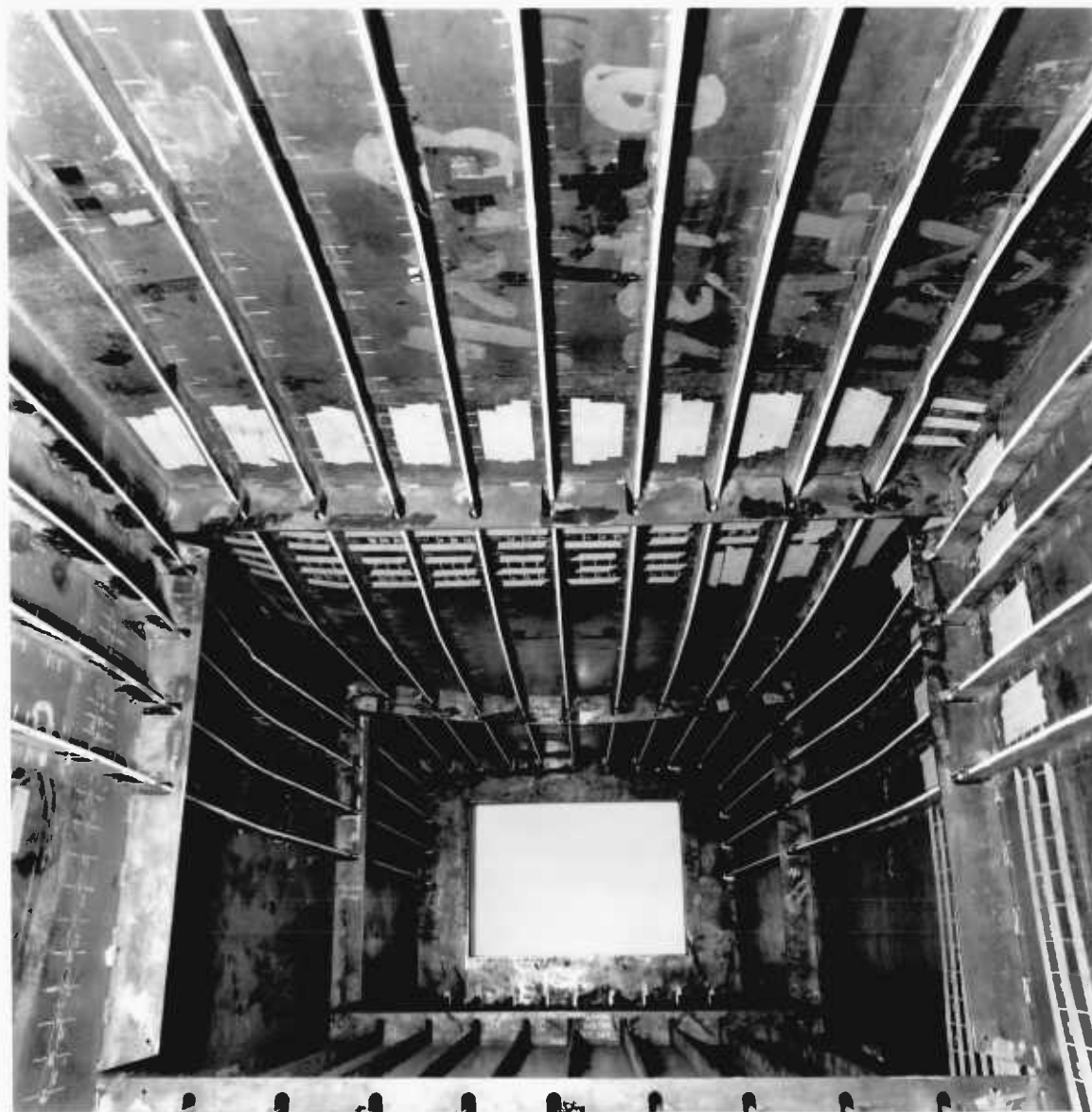


Fig. 76b Model 8 - showing the inside of the model (from end M) after failure. The compression flange is at the top of the picture.

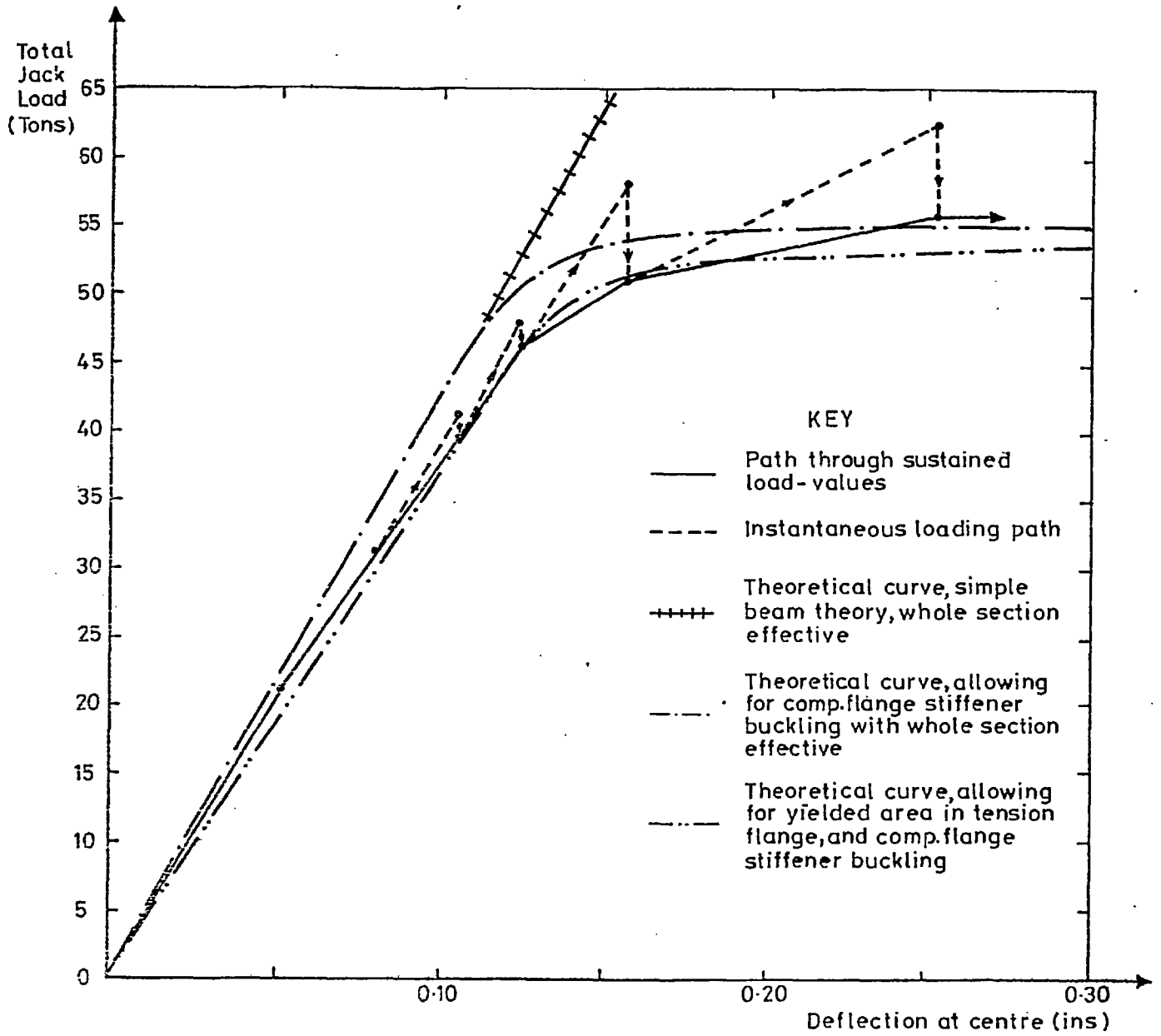


Fig.77 Load-deflection behaviour - Model. 8

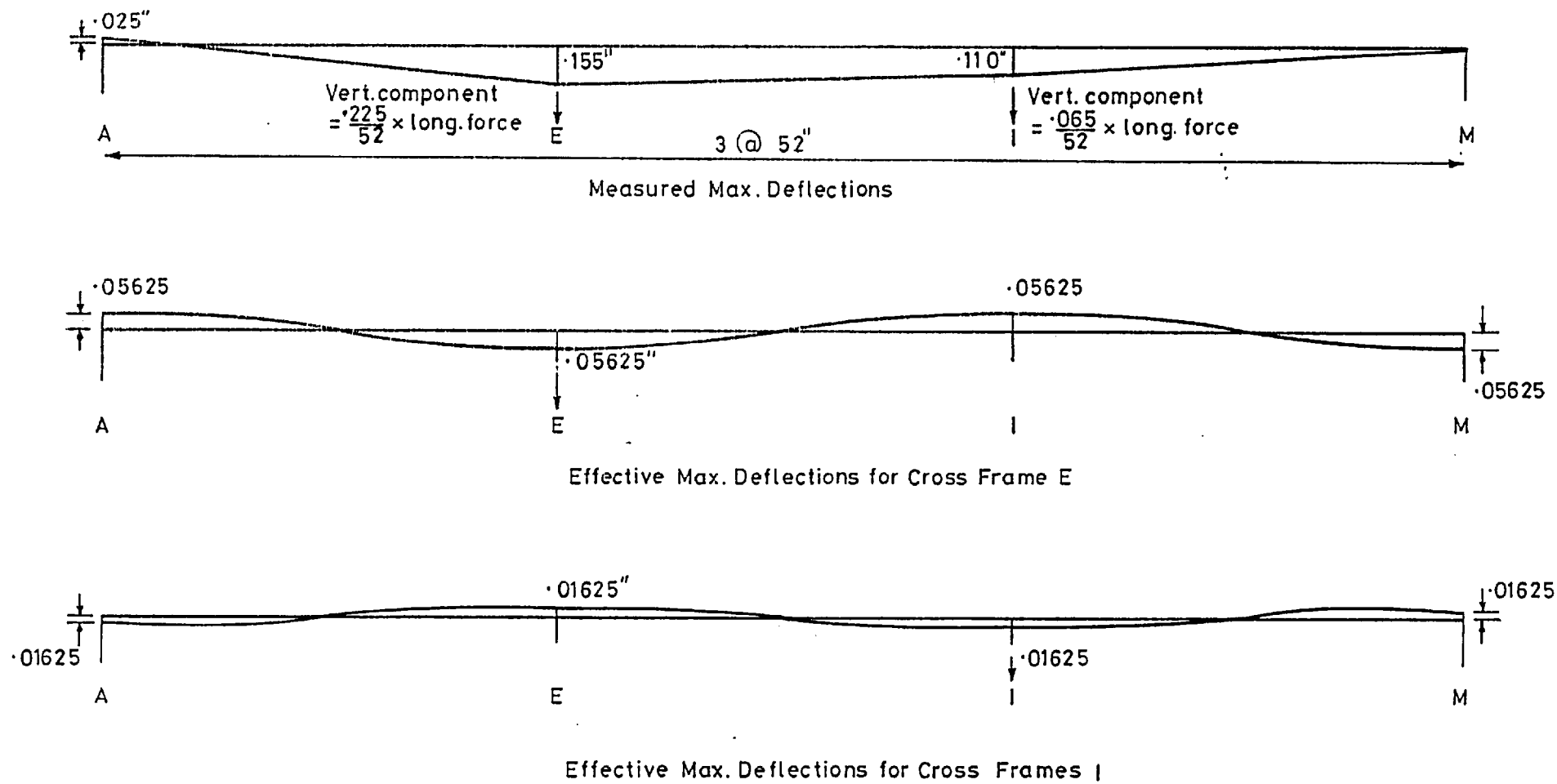


Fig.78 Initial deflections of cross-frames - Model 8.

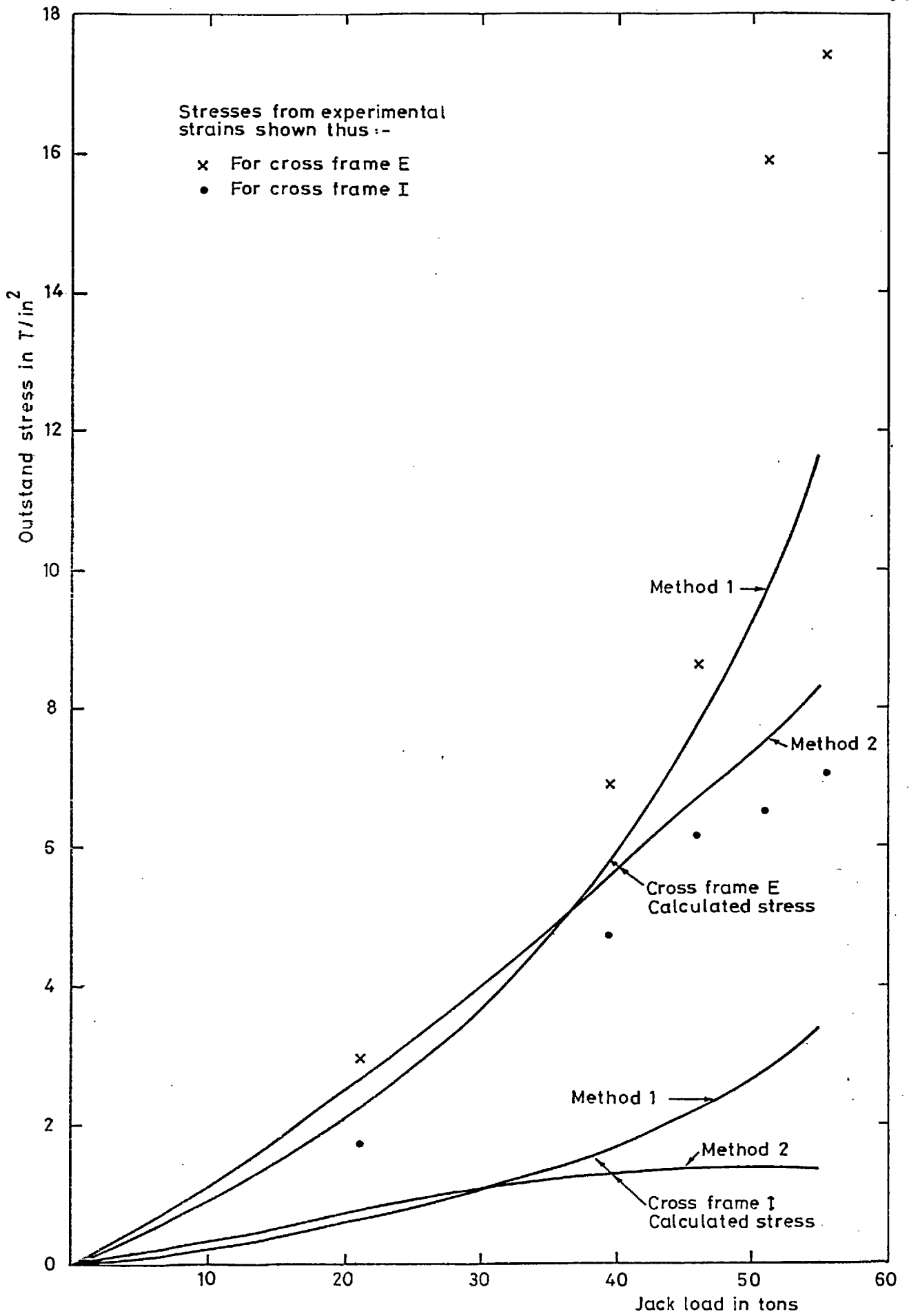


Fig 79. Stresses at tip of outstand of transverse stiffeners - Model 8.

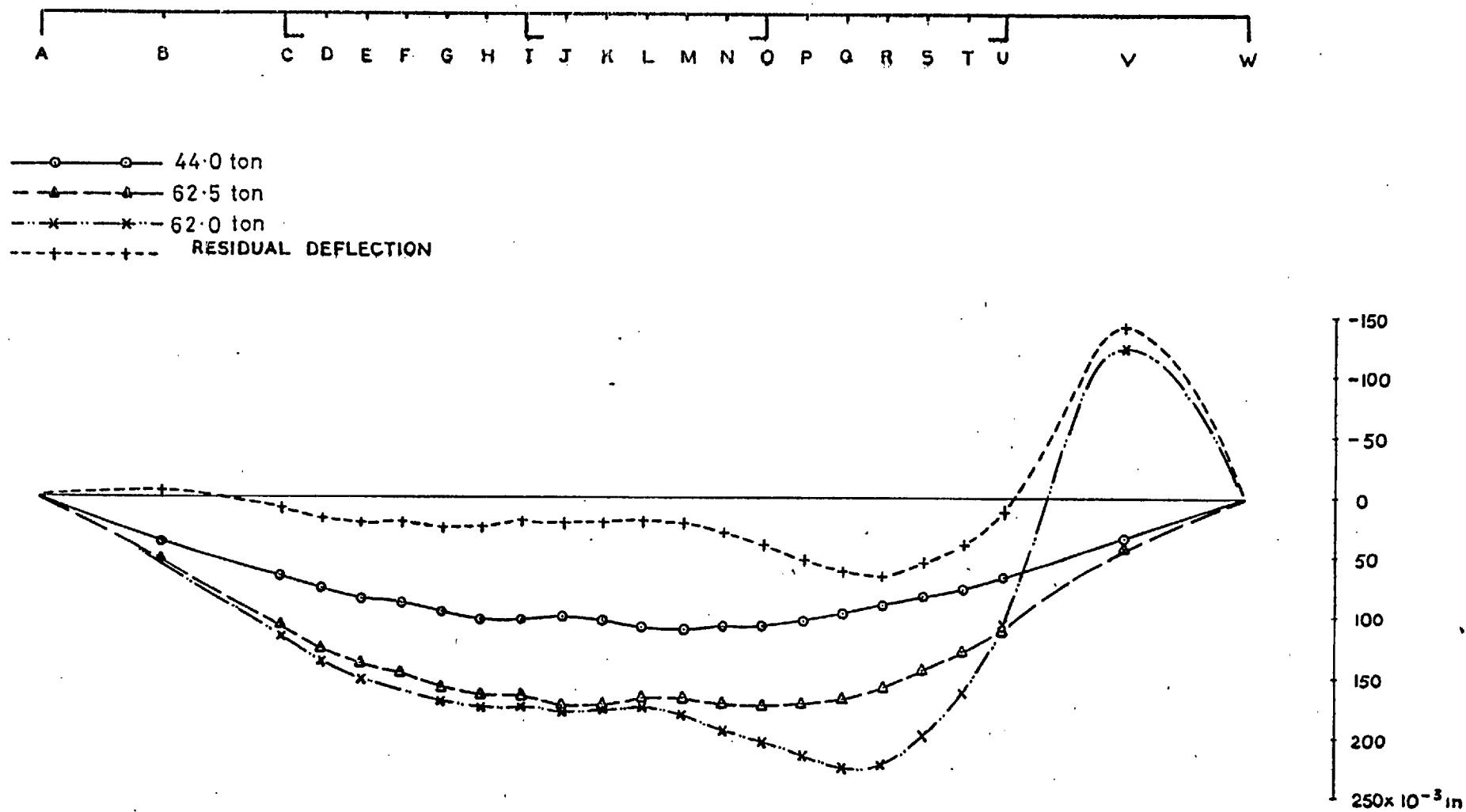


Fig 80a Test 1 - Observed deflection of stiffener S4. Model 2.

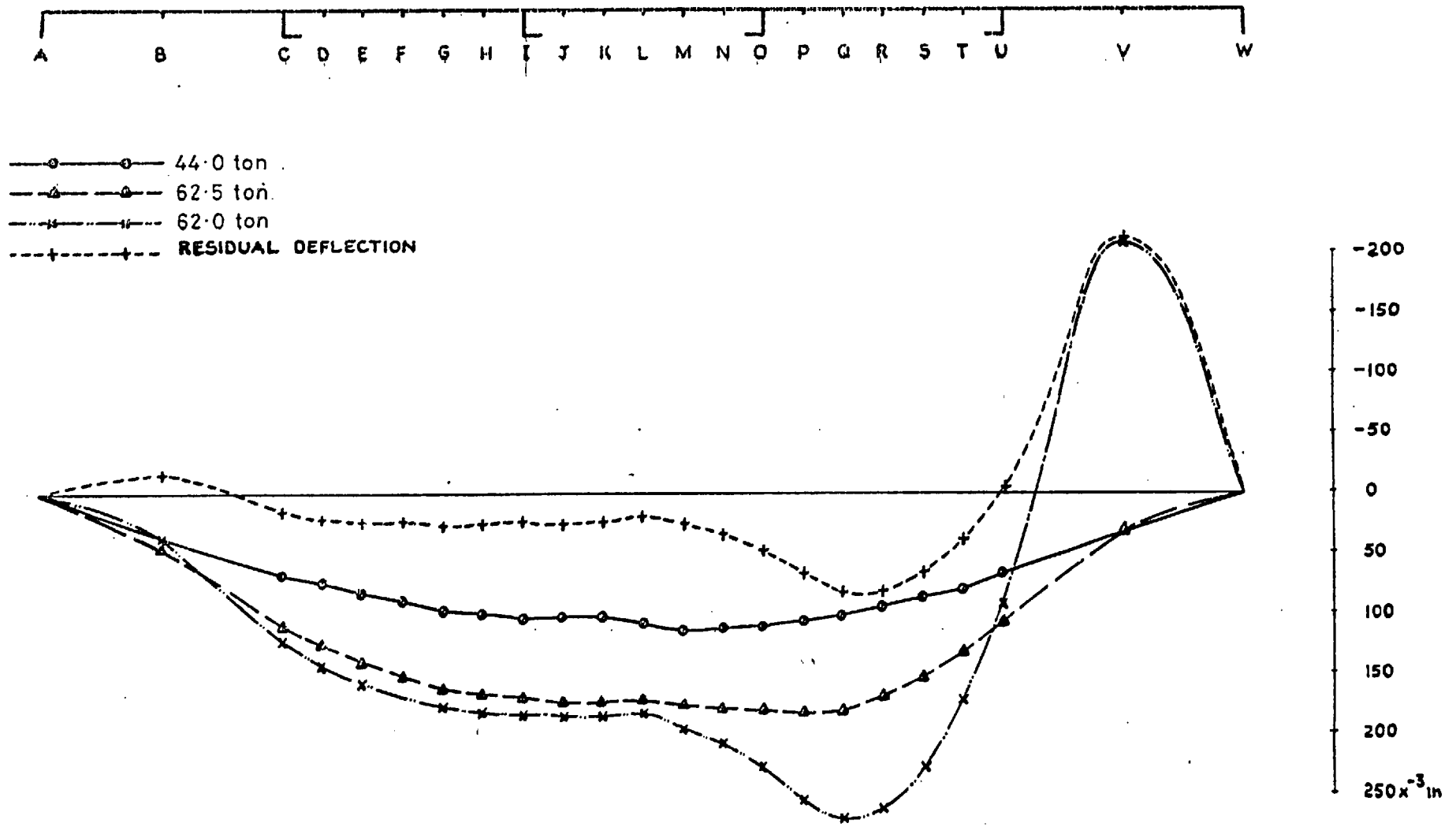


Fig80b Test1-Observed deflection of stiffener S3. Model 2.

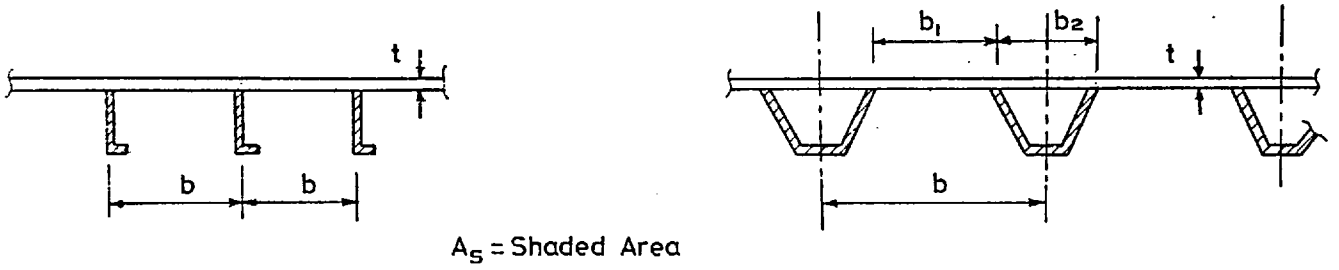


Fig 81. Geometry of stiffened compressive flange

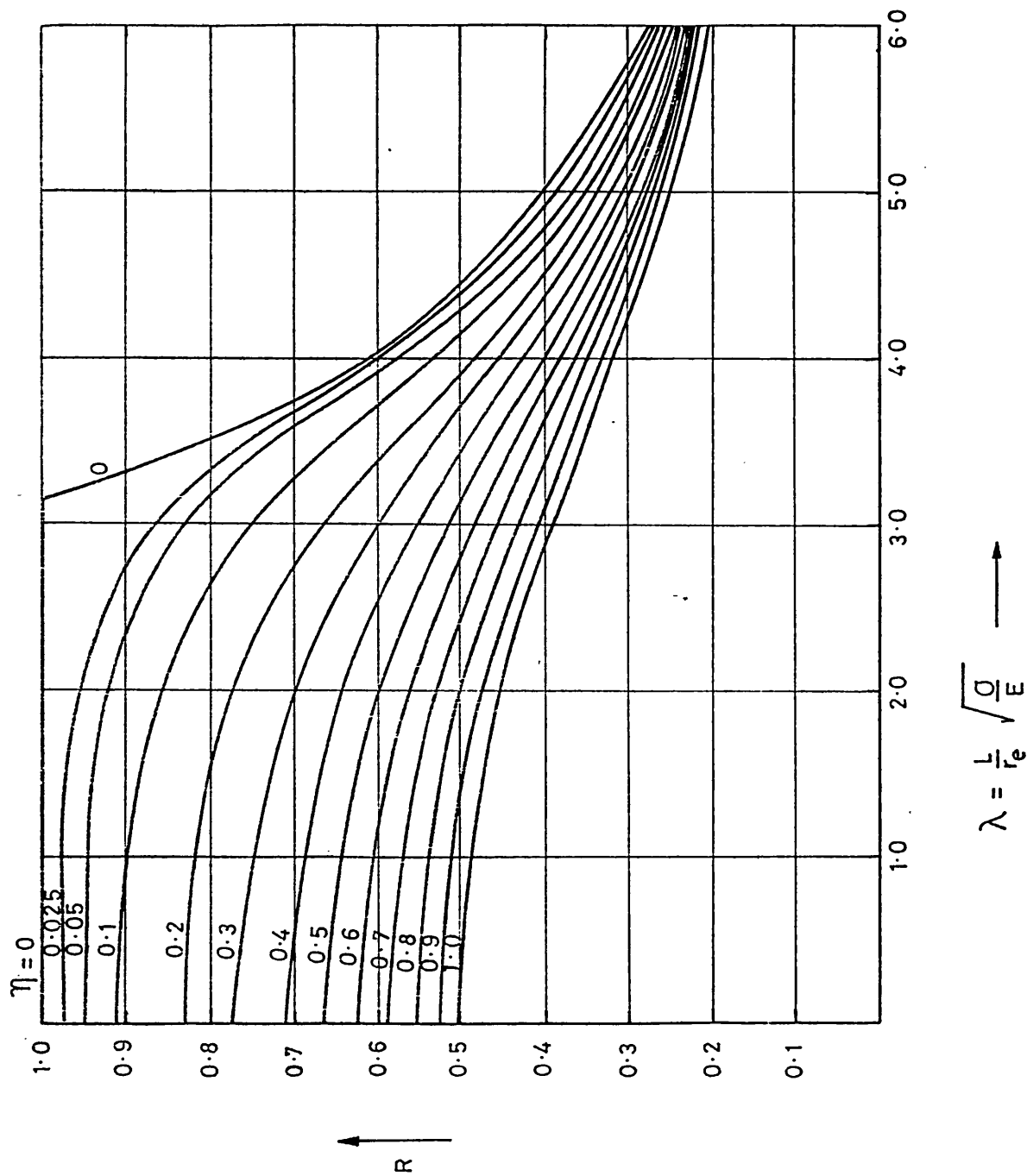


Fig 82a. Strut curves for compression yielding

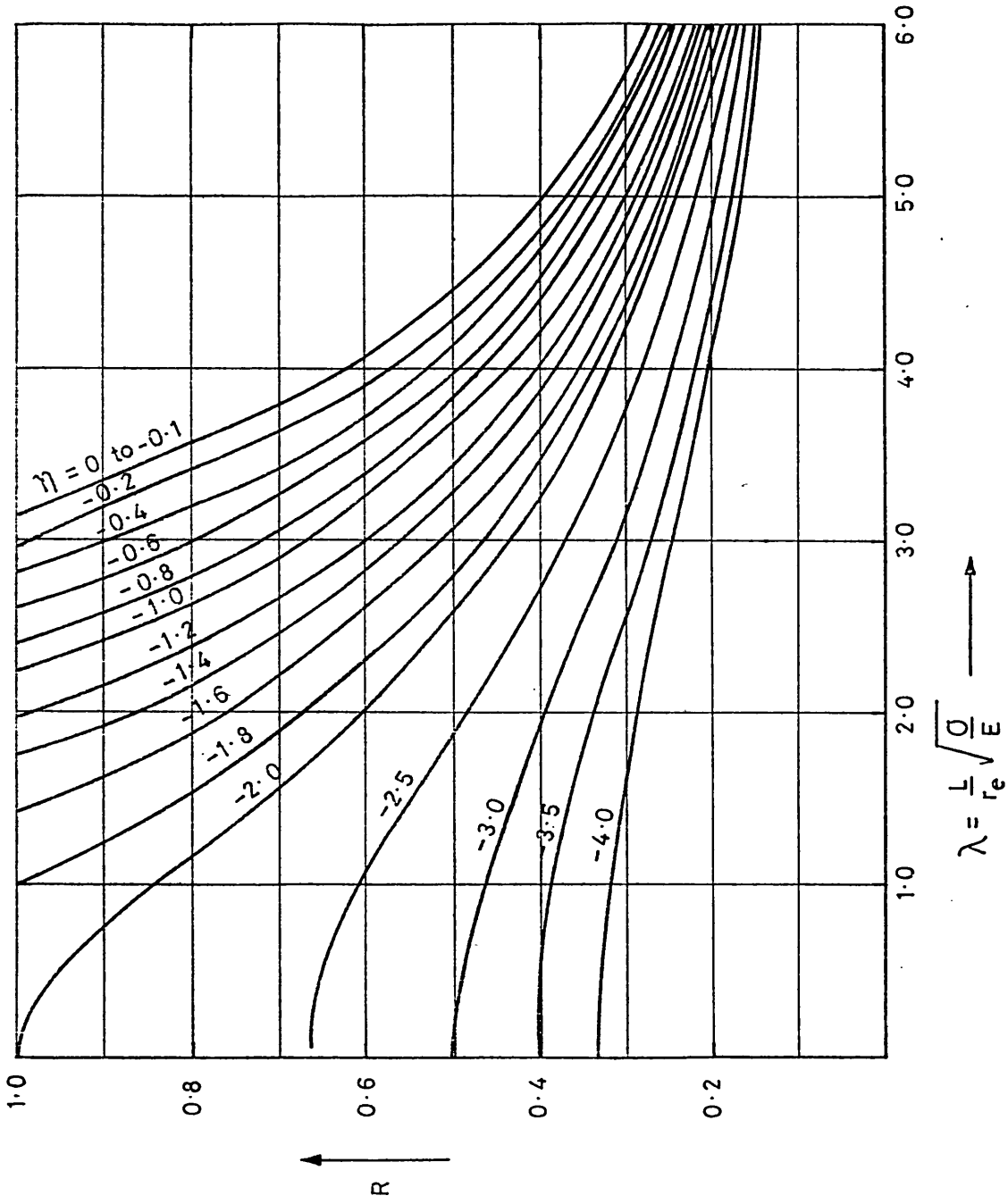


Fig 82b Curves for unsymmetrical strut for tensile yielding

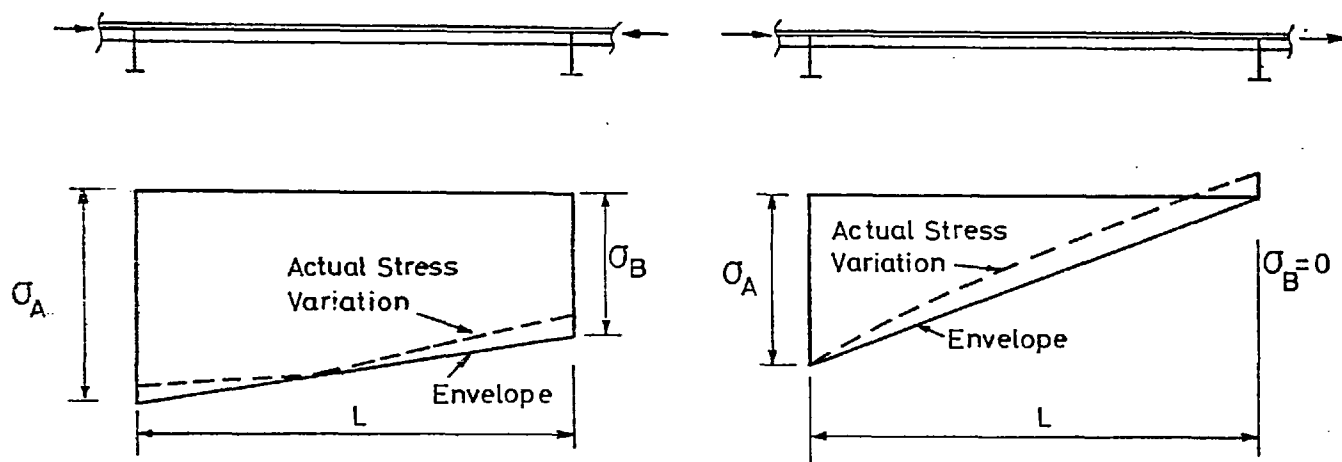


Fig83. Varying axial load in flange stiffener